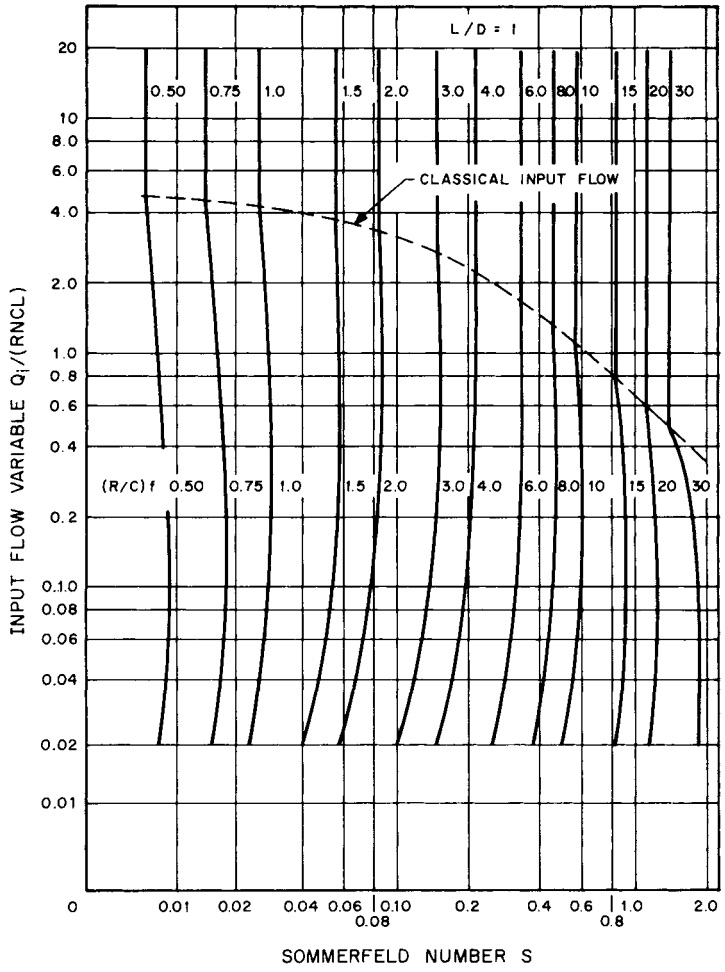

FIGURE 19.15 Inlet flow variable versus Sommerfeld number for parametric values of friction variable; $L/D = 1$, full journal bearing. *(From Connors [19.9].)*

1. Select a value of $Q_i/(RCNL)$.
2. Assume a viscosity value.
3. Compute the Sommerfeld number.
4. Use the $Q_i/(RCNL)$ and S values to find $J\rho C^*(T_a - T_i)/P$ in Fig. 19.16.
5. Calculate the mean film temperature T_a.
6. Increment μ and repeat the process from step 3 until there are sufficient points to establish an intersection with the lubricant's μ versus T data. This intersection represents the operating point for the given $Q_i/(RNCL)$.
7. Increment the input flow variable, and return to step 2.

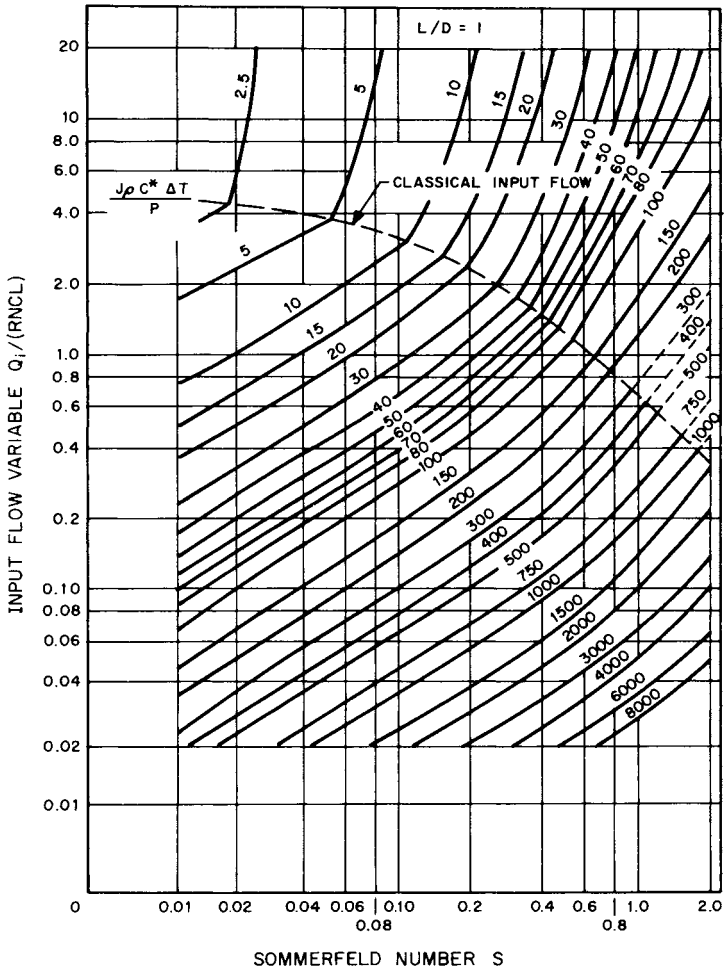

FIGURE 19.16 Inlet flow variable versus Sommerfeld number for parametric values of temperature-rise variable; $L/D = 1$, full journal bearing. *(From Connors [19.9].)*

For $Q_i/(RCNL) = 1$, the following sets of data were obtained by performing this calculation procedure:

$$\mu = \begin{cases} 1.5 \times 10^{-6} \text{ reyn} \\ 3.0 \times 10^{-6} \text{ reyn} \\ 6.0 \times 10^{-6} \text{ reyn} \end{cases} \qquad S = \begin{cases} 0.12 \\ 0.24 \\ 0.48 \end{cases}$$

$$\frac{J\rho C^*(T_a - T_i)}{P} = \begin{cases} 32 \\ 60 \\ 115 \end{cases} \qquad T_a = \begin{cases} 126.8°\text{F} \\ 150.2°\text{F} \\ 196.2°\text{F} \end{cases}$$

Using these and the lubricant μ versus T relation as presented in Table 19.16, we find the operating point to be

$$T_a = 155°\text{F} \qquad \mu = 3.2 \times 10^{-6} \text{ reyn}$$

Hence, $S = 0.256$. Also from Fig.19.14 we obtain $h_0/C = 0.52$, and so $h_0 = 0.00208$. Further, from Fig. 19.15, $(R/C)(f) = 5$, and so $f = 0.01$, which allows us to calculate the power loss to be 0.857 horsepower (hp). Assuming other values of $Q_i/(RCNL)$ permits Fig. 19.17 to be drawn. The Raimondi-Boyd value corresponding to $Q_i \to \infty$ is also presented.

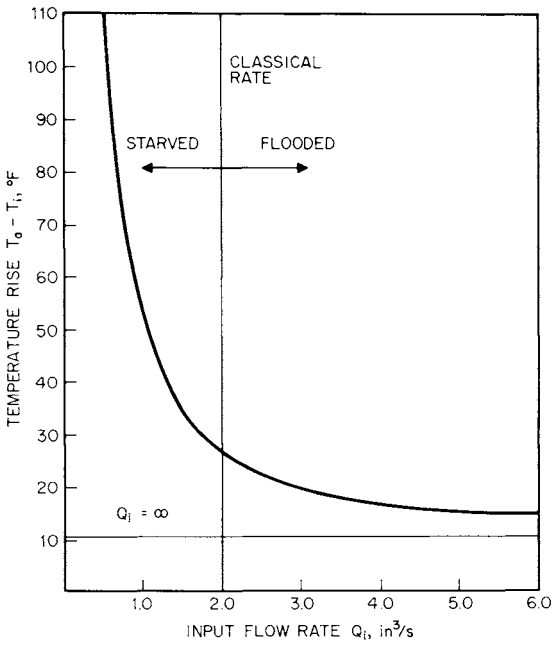

FIGURE 19.17 Lubricant temperature rise versus lubricant input flow rate (Example 3).

In Sec. 19.5.4 it was shown that

$$(T_a - T_i)_{\text{conduction}} = (1 - \lambda)(T_a - T_i)_{\text{no conduction}}$$

where λ = ratio of heat conduction to heat generation rate and is assumed to be a constant. By using this idea, a new operating point for a given $Q_i/(RCNL)$ can be determined. For example, with $\lambda = 0.25$ and $Q_i/(RCNL) = 1$, we find that $T_a = 147°\text{F}$, $h_0 = 0.0023$, and HP = 0.960 hp.

19.6.3 Optimization

In designing a journal bearing, a choice must be made among several potential designs for the particular application. Thus the designer must establish an optimum design criterion for the bearing. The design criterion describes the designer's objective, and numerous criteria can be envisioned (e.g., minimizing frictional loss, minimizing the lubricant temperature rise, minimizing the lubricant supply to the bearing, and so forth).

The search for an optimum bearing design is best conducted with the aid of a computer. However, optimum bearing design can also be achieved graphically. Moes and Bosma [19.10] developed a design chart for the full journal bearing which enables the designer to select optimum bearing dimensions. This chart is constructed in terms of two dimensionless groups called X and Y here. The groups include two quantities of primary importance to the bearing designer: minimum film thickness h_0 and frictional torque M_j; the groups do not contain the bearing clearance. The dimensionless groups are

$$X \equiv \frac{h_0}{R}\left(\frac{P}{2\pi N\mu}\right)^{1/2} \qquad Y \equiv \frac{M_j}{WR}\left(\frac{P}{2\pi N\mu}\right)^{1/2} \tag{19.15}$$

Both X and Y can be written in terms of the Sommerfeld number. Recalling that $h_0 = C(1 - \varepsilon)$ and $S = (\mu N/P)(R/C)^2$, we can easily show that

$$X = \frac{1-\varepsilon}{\sqrt{2\pi S}} \qquad \text{and} \qquad Y = \frac{M_j}{WC}\frac{1}{\sqrt{2\pi S}}$$

Figure 19.18 is a plot of full journal bearing design data on the XY plane. In the diagram, two families of curves can be distinguished: curves of constant L/D ratio and curves of constant ε. Use of this diagram permits rather complicated optimization procedures to be performed.

Example 4. Calculate the permissible range of minimum film thickness and bearing clearance that will produce minimum shaft torque for a full journal bearing operating under the following conditions:

$\mu = 5 \times 10^{-6}$ reyn $\qquad D = 4$ in

$N = 1800$ rev/min $\qquad L = 3$ in

$W = 1800$ lbf

Solution. As a first step, we calculate the largest h_0 for the given conditions. This is easily accomplished by locating the coordinates on Fig. 19.18 corresponding to the maximum X for $L/D = \frac{3}{4}$, or

$$\begin{Bmatrix} X \\ Y \\ \varepsilon \end{Bmatrix} = \begin{Bmatrix} 0.385 \\ 4.0 \\ 0.54 \end{Bmatrix} \qquad \text{at } X = X_{\max}$$

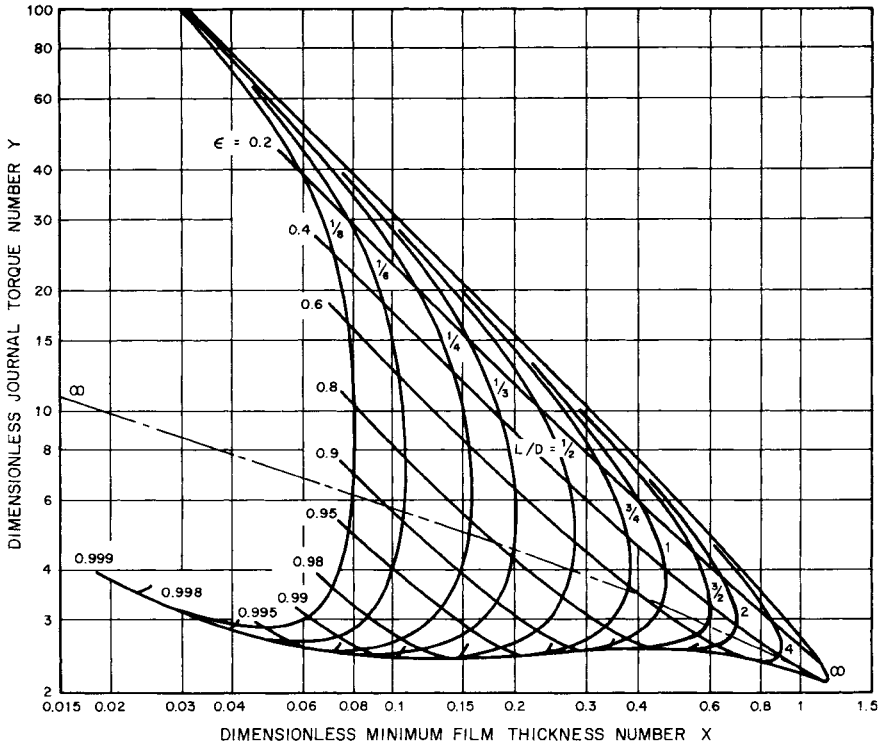

FIGURE 19.18 Optimization chart for full journal bearings. *(From Moes and Bosma [19.10].)*

Thus, from Eq. (19.15),

$$h_0 = 1.93 \times 10^{-3} \text{ in} \qquad \text{and} \qquad M_j = 36.1 \text{ in} \cdot \text{lbf}$$

The clearance is calculated from $C = h_0/(1 - \varepsilon) = 4.2 \times 10^{-3}$ in.

Next the coordinates on Fig. 19.18 corresponding to the minimum shaft torque (minimum value of Y at $L/D = \frac{3}{4}$) are located at

$$\begin{Bmatrix} X \\ Y \\ \varepsilon \end{Bmatrix} = \begin{Bmatrix} 0.18 \\ 2.5 \\ 0.97 \end{Bmatrix} \qquad \text{at } Y = Y_{\min}$$

Thus, from Eq. (19.15),

$$h_0 = 9.02 \times 10^{-4} \text{ in} \qquad \text{and} \qquad M_j = 22.6 \text{ in} \cdot \text{lbf}$$

The clearance for this case is calculated to be 3.01×10^{-2} in.

Thus the two optima (largest film thickness and smallest shaft torque) do not coincide. Thus, a compromise clearance value must generally be selected. Figure 19.19 is a plot of recommended minimum clearance for given shaft speed and diameter, which can be used as a helpful guide in this process.

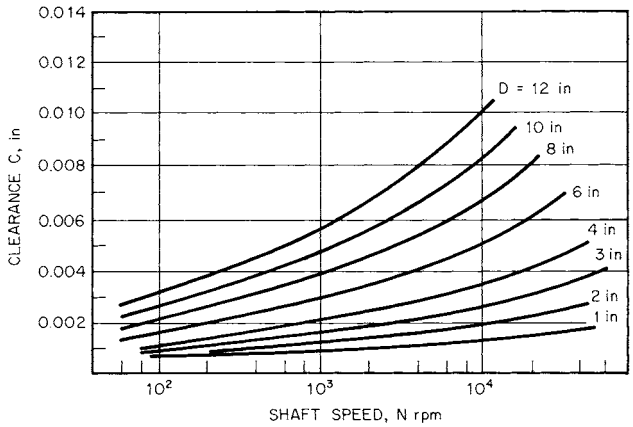

FIGURE 19.19 Recommended minimum clearance versus journal speed for a given journal diameter.

Example 5. Determine the bearing length and clearance for a full journal bearing operating steadily with minimum friction loss for the following conditions:

$\mu = 17.83 \times 10^{-6}$ $W = 1500$ lbf

$N = 4800$ rev/min $D = 6$ in

and a minimum allowable film thickness of

$$(h_0)_{\min} = 4.4 \times 10^{-4}$$

Solution. Because both X and Y contain the bearing length L, a new set of dimensionless groups not containing L must be developed. This pair is easily seen to be

$$U = (X)\left(\frac{L}{D}\right)^{1/2} = \frac{h_0}{R}\left(\frac{W}{2\pi\mu N D^2}\right)^{1/2} \tag{19.16}$$

$$V = (Y)\left(\frac{L}{D}\right)^{1/2} = \frac{M_j}{WR}\left(\frac{W}{2\pi\mu N D^2}\right)^{1/2} \tag{19.17}$$

For the given information, the smallest value of U (termed $U_{\min}$ because the smallest value of h_0 is used) can be directly calculated from Eq. (19.16):

$$U_{\min} = 0.10 \qquad \text{Thus,} \qquad X \geq (0.10)\left(\frac{D}{L}\right)^{1/2}$$

Selected L/D values permit an array of X values to be calculated. This in turn permits the minimum values of Y (that is, $Y_{\min}$) to be read from Fig. 19.18. Then corresponding $V_{\min}$ values can be calculated from Eq. (19.17). Table 19.17 contains the results of this operation.

TABLE 19.17 Summary of Calculated Results for Example 5

L/D	X	$Y_{\min}$	$V_{\min}$
1/4	0.2	No solution	
1/3	0.173	3.20	1.85
1/2	0.414	2.43	1.72
3/4	0.115	2.40	2.08
1	0.100	2.40	2.40

Next a cubic equation is fitted to the $V_{\min}$ data, and we find

$$V_{\min} = 4.057 - 11.927\frac{L}{D} + 18.742\left(\frac{L}{D}\right)^2 - 8.472\left(\frac{L}{D}\right)^3 \qquad (19.18)$$

The optimum value of L/D for a minimum friction loss can be found by differentiation, which yields the optimum bearing length:

$$L = 0.464D = 2.78 \text{ in}$$

The frictional loss can be calculated by inserting the optimum L/D ratio in the cubic equation:

$$V_{\min} = (Y)\left(\frac{L}{D}\right)^{1/2} = 1.712$$

Thus, $Y = 2.513$, and the eccentricity ratio is read from Fig. 19.18 as $\varepsilon \cong 0.98$. Finally the optimum bearing clearance is calculated to be $C = 2.2 \times 10^{-2}$ in.

19.7 GAS-LUBRICATED JOURNAL BEARINGS

Gas-lubricated journal bearings have been employed in a wide variety of modern industrial applications. For example, they are used in dental drills, high-speed machine tools, digital-computer peripheral devices, high-speed turbomachines, and navigational instruments.

Gas bearings produce very little friction even at high speeds; hence, they have low frictional losses and generate minimal amounts of heat. In addition, gas lubri-

cants are chemically very stable over a wide range of temperatures; they neither freeze nor boil; they are nonflammable; and they do not contaminate bearing surfaces. Gas bearings also have low noise characteristics.

On the negative side, gas bearings do not have much load-carrying capacity and have large startup wear. Also, because the gas film thickness is quite small, gas bearings require superior surface finish and manufacture. Great care must be exercised with the journal alignment. Further, thin films offer very little cushion or damping capacity; consequently, gas bearings are prone to certain vibrational instabilities.

19.7.1 Limiting Gas Bearing Solutions

The compressible-flow Reynolds equation, Eq. (19.7), is too complex to permit a general analytical solution, and numerical methods have been used to obtain gas bearing information. However, considerable insight can be gained by considering solutions for limiting cases. Besides the limiting geometric problems of long and short bearings, two other limiting classes of problems are important: gas films with low bearing numbers and gas films with high bearing numbers. The former pertain to low-speed, high-loading applications, and the latter pertain to very-high-speed, light-loading applications. Some bearing performance parameters for gas films with low and high bearing numbers are shown in Table 19.18.

TABLE 19.18 Long Gas Journal Bearing Performance Parameters, Limiting Cases, Long-Bearing Theory

Performance parameter	Low bearing number	Large bearing number
$\frac{p}{p_a}$	$\frac{1 + \Lambda\varepsilon \sin\theta(2 + \varepsilon\cos\theta)}{(2+\varepsilon)^2(1+\varepsilon\cos\theta)^2}$	$\frac{\sqrt{1 + 3\varepsilon^2/2}}{1 + \varepsilon\cos\theta}$
$\frac{W_R}{p_a DL}$	0	$\frac{\pi}{2}\left(1 + \frac{3\varepsilon^2}{2}\right)^{1/2}[(1-\varepsilon^2)^{-1/2} - 1]$
$\frac{W_T}{p_a DL}$	$\frac{\pi\varepsilon\Lambda}{(2+\varepsilon^2)\sqrt{1-\varepsilon^2}}$	0
ϕ	$\frac{\pi}{2}$	0
$\frac{F_j}{\mu UL}\frac{C}{R}$	$\frac{4\pi(1+2\varepsilon^2)}{(2+\varepsilon^2)\sqrt{1-\varepsilon^2}}$	$\frac{2\pi}{\sqrt{1-\varepsilon^2}}$
$\left(\frac{R}{C}\right)(f)$	$\frac{1+2\varepsilon^2}{3\varepsilon}$	$\frac{2\mu UR}{C^2 P_a\sqrt{(1+3\varepsilon^2/2}(1-\sqrt{1-\varepsilon^2})}$

19.7.2 Stability Considerations

The journal bearing of a rotating machine cannot be treated separately. It is part of a complex dynamic system, and its design can influence the dynamic behavior of the entire system. Bearing damping controls vibration amplitude and tolerance to any imbalance and, to a large extent, determines whether the rotor will be dynamically stable. A bearing running in an unstable mode can lose its ability to support load, and rubbing contact can occur between the bearing and the shaft surfaces.

Rotor bearing instabilities are particularly troublesome in gas-lubricated bearings; the film is considerably thinner in gas bearings than in liquid-lubricated bearings and so does not possess the damping capacity. We can differentiate between two forms of dynamic instability: *synchronous whirl* and *half-frequency whirl* (also called fractional-frequency whirl and film whirl).

Synchronous Whirl. A rotating shaft experiences periodic deflection (forced vibration) because of the distribution of load, the method of shaft support, the degree of flexibility of the shaft, and any imbalance within the rotating mass. This deflection causes the journal to orbit within its bearings at the rotational speed. When the frequency of this vibration occurs at the natural frequency (or critical speed) of the system, a resonance condition exists. In this condition, the amplitude of vibration (size of the journal orbit) increases and can cause bearing failure. Because the shaft rotational speed and the critical speed coincide, this form of instability is termed *synchronous whirl.*

Since stable operation occurs on either side of the critical speed, the bearing system must be designed so that critical speeds do not exist in the operating speed range. This can be accomplished by making the critical speeds either very large or very small. Large critical speeds can be established by increasing the bearing stiffness by reducing the bearing clearance. Lower critical speeds can be established by increasing the shaft flexibility. The instability can also be suppressed by mounting the bearing in a flexible housing which introduces additional system damping.

Half-Frequency Whirl. A deflected rotating shaft has its center whirl, or orbit, around the center of the bearing. When the whirl speed Ω is equal to or somewhat less than half the rotational speed of the shaft, ω, the hydrodynamic capacity of the bearing to support a load is diminished and, in fact, may fall to zero. With any subsequent rotational speed increase, the whirl amplitude will increase, and the bearing and journal may come into violent contact. This form of self-activated vibrational instability is called *half-frequency* or *half-speed whirl.* Because the whirl speed for gas bearings is generally less than the rotational speed, the instability is also termed *fractional-frequency whirl.* Figure 19.20 is a map for assessing the stability of a full journal bearing.

Half-speed whirl may be suppressed by altering the circumferential symmetry of the bearing. This can be accomplished by providing axial grooves in the bearing surface, by dividing the circumference into a number of sections, or lobes, or by using tilting pads. Also, introducing more damping into the system through the use of flexible housing mounts can be helpful.

19.7.3 Cylindrical Ungrooved Gas Journal Bearings

Complete plain cylindrical journal bearings are generally used in applications that require support of a fixed, unidirectional load. Self-excited whirl instability is a com-

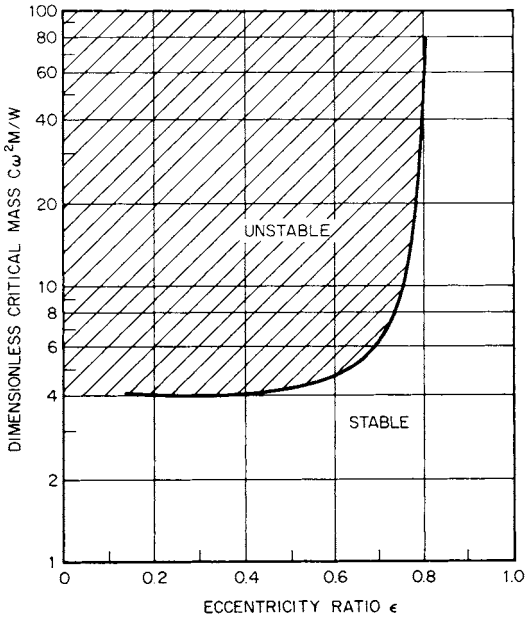

FIGURE 19.20 Bearing stability for full journal bearing, $L/D = 1$.

mon problem with high-speed rotor systems supported by this type of bearing. However, if the load is sufficiently large to have an eccentricity ratio on the order of 0.8, whirl problems are reduced (refer to Fig. 19.20).

Ungrooved cylindrical gas bearings have been analyzed by Raimondi [19.11]. Performance characteristics were developed numerically and presented in the form of various design charts for L/D ratios of ½, 1, and 2. Figures 19.21 to 19.23 are a sampling of these charts for an L/D ratio of 1.

A porous journal bearing is a plain cylindrical journal bearing with a porous liner that is fixed in the bearing housing (Fig. 19.24). An externally pressurized gas is supplied to the outer surface of the liner and flows through the porous material into the bearing clearance space.

The steady performance of a self-acting porous gas bearing of finite length has been determined by Wu [19.12]. Table 19.19 shows a sample of these performance data. The data are applicable for a particular porous linear thickness ratio (0.083) and for particular combinations of the *slip coefficient* α (dependent on the structure of the porous material), the *permeability* k (a physical property of the porous material), and bearing dimensions R and C.

Example 6. For the following conditions

$D = 0.5$ in $\quad N = 47\,000$ rev/min

$L = 0.5$ in $\quad \mu = 2.6 \times 10^{-9}$ reyn (air at 80°F)

$C = 2 \times 10^{-4}$ in $\quad p_a = 40$ psi

$W = 6.1$ lbf

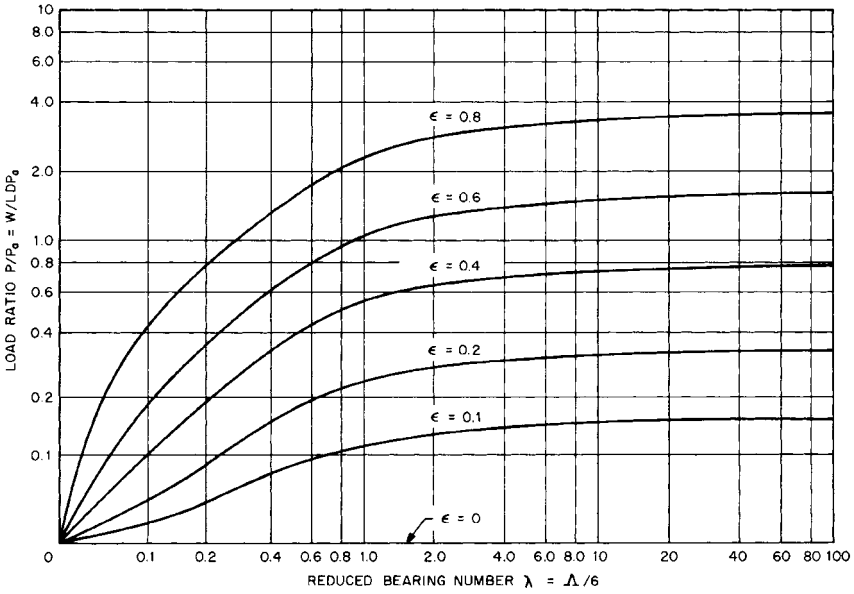

FIGURE 19.21 Load ratio versus reduced bearing number of an ungrooved cylindrical gas bearing; $L/D = 1$. *(From Raimondi [19.11].)*

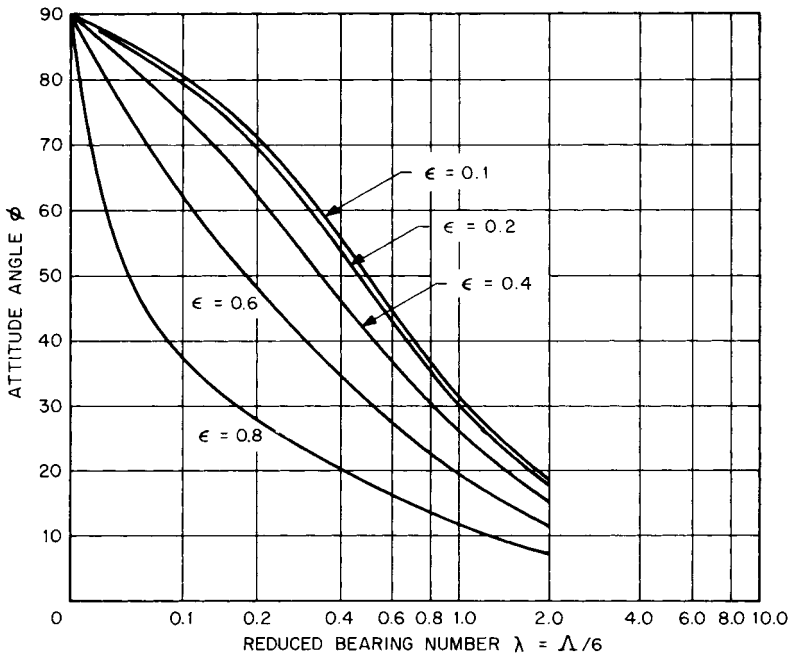

FIGURE 19.22 Attitude angle versus reduced bearing number of an ungrooved cylindrical gas bearing; $L/D = 1$. *(From Raimondi [19.11].)*

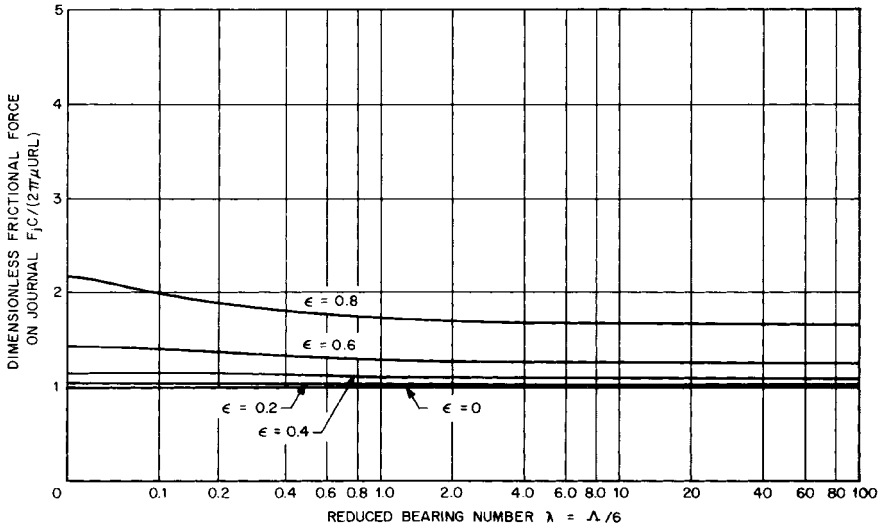

FIGURE 19.23 Dimensionless journal frictional force versus reduced bearing number of an ungrooved cylindrical gas bearing; $L/D = 1$. *(From Raimondi [19.11].)*

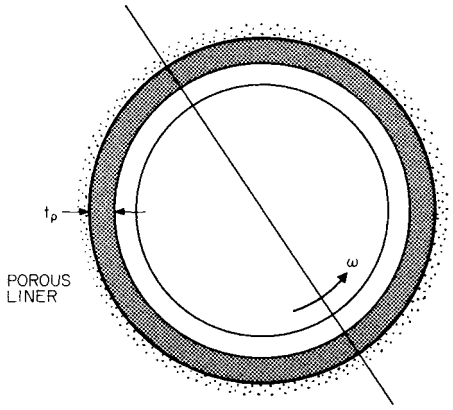

FIGURE 19.24 Porous journal bearing.

compare the performance of a porous gas bearing to that of a solid wall bearing. The porous bearing material is ceramic 0.021 in thick with a permeability $k = 1.33 \times 10^{-12}$ in^2 and a slip coefficient $\alpha = 0.3$.

Solution. Since $L/D = 1$, $t_p/R \cong 0.083$, $\beta = \alpha C/k \cong 50$, and $\Omega = 12kR/C^3 \cong 0.5$, the data of Table 19.19 may be used. The bearing number is

$$\Lambda = \frac{6\mu\omega}{p_a}\left(\frac{R}{C}\right)^2 = 3.0$$

TABLE 19.19 Gas-Lubricated Bearing Performance Data, $L/D = 1$, $t_p/R = 0.083$, $\Omega = 0.5$, $\beta = 50$

ε	Λ	$\frac{P}{p_a}$	ϕ, deg	$\left(\frac{R}{C}\right)(f)$
0.2	0.6	0.039	80.563	8.1034
	1.2	0.0756	72.109	8.3784
	3.0	0.1594	52.470	9.9199
	6.0	0.2272	34.402	13.8773
	12.0	0.2662	20.290	23.6302
	50.0	0.2959	7.602	88.4725
	100.0	0.3054	5.014	171.9223
	∞	0.3264	0	∞
0.4	0.6	0.0853	77.245	4.0835
	1.2	0.1638	66.670	4.2517
	3.0	0.3441	46.382	5.0012
	6.0	0.5067	30.262	6.7025
	12.0	0.6164	17.806	10.9197
	50.0	0.6982	6.424	39.9776
	100.0	0.7188	4.164	77.6340
	∞	0.7746	0	∞
0.6	0.6	0.1500	70.129	2.8072
	1.2	0.2872	56.903	2.8961
	3.0	0.6102	37.598	3.3003
	6.0	0.9322	24.537	4.2078
	12.0	1.1854	14.488	6.4992
	50.0	1.3774	4.962	23.0667
	100.0	1.4186	3.122	44.7611
	∞	1.5603	0	∞
0.8	0.6	0.2547	61.657	2.2908
	1.2	0.4995	47.468	2.2971
	3.0	1.1050	31.147	2.4980
	6.0	1.7837	20.348	2.9210
	12.0	2.3907	12.272	4.2374
	50.0	2.8736	4.046	14.4249
	100.0	2.9640	2.436	27.9331
	∞	3.4193	0	∞

SOURCE: Ref. [19.12].

The load ratio is

$$\frac{P}{p_a} = \frac{W/(LD)}{p_a} = 0.61$$

Entering Table 19.18 with these values, we find

$$\varepsilon = 0.6 \qquad \phi = 37.598 \qquad \left(\frac{R}{C}\right)(f) = 3.3003$$

For the same values we can find from Figs. 19.21 to 19.23 for the solid wall bearing $\varepsilon = 0.54$, $\phi = 33.7°$, and

$$\frac{F_j C}{2\pi\mu URL} = 1.18$$

From the last value, we may compute for comparative purposes

$$\left(\frac{R}{C}\right)(f) = 3.038$$

Thus the porous bearing operates at a larger eccentricity ratio (which indicates better stability) but has larger frictional loss. On the other hand, for a given ε, the porous bearing has a lower load capacity compared to the solid wall bearing. This loss of load capacity becomes more severe as the eccentricity ratio is increased.

19.7.4 Axially Grooved Gas Journal Bearings

The addition of axial slots, or grooves, in the bearing surface can produce several positive effects. Feed grooves can reduce frictional heating and energy losses. The grooves, in effect, turn the surface into a number of partial arc bearings, which can reduce the tendency for half-frequency whirl instability. What is more, grooving a bearing leads to only a slight increase in the manufacturing costs. Although a variety of grooving arrangements can be envisioned, three or four equally spaced axial grooves are typically employed. Feed grooves of 30° to 60° extent are commonly used. However, bearing stability decreases with increase in the groove size.

Castelli and Pirvics [19.13] presented tabular design data for axially grooved gas bearings. The subtended angle of each groove was taken to be 5°. Figures 19.25 and 19.26 are sample design chart data for a gas bearing with three grooves and an L/D ratio of 2.

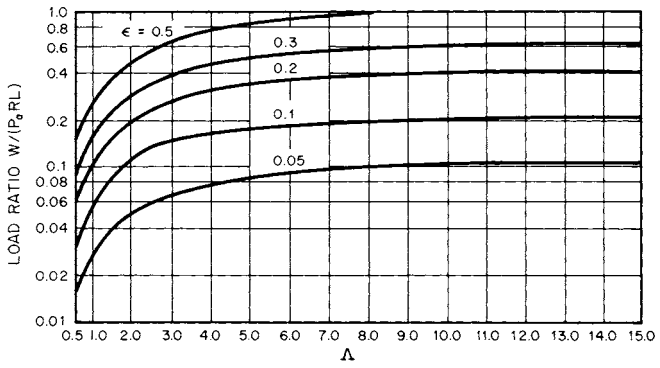

FIGURE 19.25 Load ratio versus compressibility number for an axial-groove gas bearing, $L/D = 2$; three evenly spaced axial grooves—first groove 60° clockwise from load line. *(From Castelli and Pirvics [19.13].)*

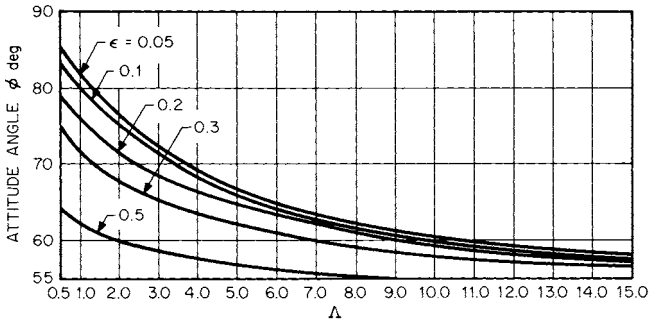

FIGURE 19.26 Attitude angle versus compressibility number for an axial-groove gas bearing, $L/D = 2$; three evenly spaced axial grooves—first groove 60° clockwise from load line. *(From Castelli and Pirvics [19.13].)*

19.7.5 Noncircular Gas Journal Bearings

For low eccentricity ratios, a noncircular gas bearing has superior stability properties but inferior load capacity when it is compared with a circular gas bearing. At higher eccentricity ratios, the load-carrying capacity of the noncircular gas bearing exceeds that of the circular gas bearing. For applications where load capacity is not an issue (e.g., in vertical-shaft cases), use of a noncircular gas bearing minimizes stability concerns that exist at the lower eccentricity ratios.

Pinkus [19.14] has investigated the performance of elliptical and three-lobe gas bearings. It was found that the direction of load application is important to the performance of a noncircular gas bearing. In fact, load-carrying capacity can be optimized by rotating the bearing relative to the load line. The rotation is generally clockwise anywhere from a few degrees to 25°. Table 19.20 presents a comparison of expected eccentricity ratios for given values of S and Λ for circular, elliptical, and three-lobe gas bearings. Higher values of ε required by the noncircular bearings over the ε for the circular bearing at the same Sommerfeld number indicate a lower load capacity. Pinkus also presented envelopes of operation. Figure 19.27 is a plot of Som-

TABLE 19.20 Eccentricity Ratio versus Sommerfeld and Bearing Numbers for Circular, Elliptical, and Three-Lobe Noncircular Gas Bearings

Bearing number Λ	Sommerfeld number S	Eccentricity ratio ε				
		Circular	Elliptical central loading	Elliptical optimum loading	Three-lobe central loading	Three-lobe optimum loading
1	0.365	0.2	0.54	0.525	0.55	0.545
1	0.162	0.4	0.59	0.56	0.615	0.605
1	0.0866	0.6	0.67	0.635	0.70	0.685
1	0.0381	0.8	0.815	0.77	0.84	0.815
3	0.365	0.25	0.57	0.535	0.595	0.57
3	0.162	0.475	0.65	0.59	0.68	0.645
3	0.0860	0.655	0.75	0.685	0.80	0.755

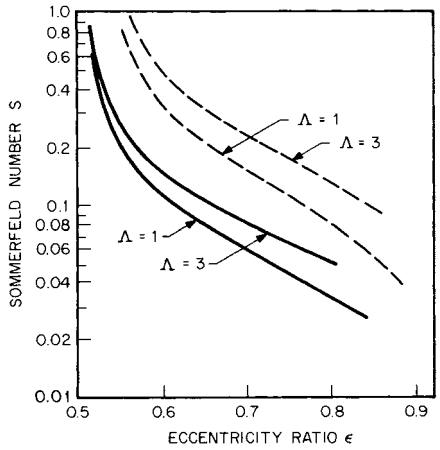

FIGURE 19.27 Sommerfeld number versus eccentricity ratio for a noncentrally loaded elliptical gas bearing, $L/D = 1$. *(From Pinkus [19.14].)*

merfeld number versus the eccentricity ratio for a noncentrally loaded elliptical gas bearing. The upper set of curves represents the largest ε for a given S at a particular Λ, and it would be used in an attempt to avoid stability problems. The lower set of curves represents the optimum loading conditions.

19.8 HYDROSTATIC JOURNAL BEARING DESIGN

Hydrostatic journal bearings (also called *externally pressurized* bearings) offer large radial load-carrying capacities at all rotational speeds (including zero). They exert very little friction and have controllable stiffness. The principal disadvantage of hydrostatic journal bearings is the cost of the pressurized lubricant supply system. These bearings are widely used in the machine-tool industry.

19.8.1 Classification of Bearings and Components

There are basically three types of hydrostatic journal bearings: the single-pad, the multipad, and the multirecess. The various types are depicted in Table 19.21.

The main components of a hydrostatic journal bearing are the pad and the lubricant supply system. The pad consists of a recess, or pocket, region and the surrounding land material. The recess is generally deep compared with the film thickness: typically the depth is taken to be 20 times the radial clearance. In sizing the recess, the land width is reduced as much as practical; however, if the land width is too small, edge effects can become significant. These effects can be avoided if the land width is taken to be greater than 100 times the clearance.

Pressurized lubricant is provided to each bearing recess through the supply system. This system may be as simple as a direct line between the recess and the supply pump. Bearings using such simple systems are termed *noncompensated hydrostatic*

TABLE 19.21 Types of Hydrostatic Journal Bearings

Type		Comments
Single-pad journal bearing		1. Included angle less than 180°. 2. Normally used to support unidirectional loads. 3. May have multiple recesses. 4. Lubricant flow and pad design based on a maximum load applied to a uniform film equaling minimum radial clearance $R_B - R_j$.
Multipad journal bearing	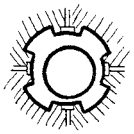	1. Included angle of each pad is less than 180°. 2. Used for rotating, oscillating, or reversing radial loads. 3. Two opposed pads can be used for reversing loads. 4. If angular variation of the load is less than 80°, a two-pad journal bearing may be used. 5. Bearing stiffness is reduced if load is directed between pads. 6. Axial grooves provide cooling capability at high rotational speeds.
Multirecess journal bearing	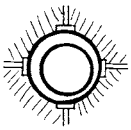	1. No pressure-reducing grooves between recesses. 2. Usually contains four or more recesses. 3. Used for rotating and reversing loads. 4. Does not require as much flow per recess as multipad type. 5. Circumferential flow from high-pressure pockets to lower-pressure pockets evens pressure distribution around bearing.

bearings and are frequently used to lift highly loaded journals prior to rotation. In that context they are termed *oil lifts.*

In order for a single pump to deliver lubricant to more than one pad or recess, restrictors (or compensating devices) are required in each supply line. Restrictors limit the flow to each pad, thereby permitting all pads to become activated. Without compensating devices, pad imbalance would occur. Restrictors, then, are used to control the operation of a hydrostatic bearing.

There are three common types of restrictors: the capillary tube, the orifice plate, and the flow control valve. Table 19.22 compares these devices. This table was pre-

pared from a comprehensive series of papers on hydrostatic bearing design by Rippel [19.15]. In addition to flow-load control, the resistor affects the stiffness of the bearing. Bearing stiffness is related to the ability of the bearing to tolerate any changes in the applied load.

19.8.2 Design Parameters

For hydrostatic journal bearings at low rotational speeds, the primary design parameters are maximum load, lubricant flow rate, and stiffness. Of secondary importance are considerations of frictional horsepower and lubricant temperature rise.

The load-carrying capacity of a hydrostatic journal bearing is generally written as

$$W = a_f A_p p_r \tag{19.19}$$

where a_f = pad load coefficient, A_p = projected bearing area, and p_r = recess pressure. The pad load coefficient is dimensionless and physically represents the ratio of the average lubricant pressure in the pad to the lubricant pressure supplied to the pad. O'Donoghue and Rowe [19.16] give equations for a_f for both multirecess and multipad bearings.

The lubricant flow rate may be determined from

$$Q = q_f \frac{h^3 p_r}{\mu} \tag{19.20}$$

where q_f = flow factor for a single pad. The flow factor depends on the geometry and land widths of the bearing.

Journal bearing stiffness expresses the ability of the bearing to accommodate any changes in the applied load. Stiffness is proportional to the slope of the bearing load versus film thickness curve, or

$$s = -\frac{dW}{dh} \tag{19.21}$$

Stiffness will depend on the method of flow control (capillary tube, etc.) and the amount of circumferential flow. O'Donoghue and Rowe [19.16] provide a detailed derivation of the journal bearing stiffness and have developed equations for both multipad and multirecess bearings.

19.8.3 Design Procedures

A variety of design procedures are available for hydrostatic bearings. Some are based on experimental findings, whereas others are based on numerical solutions of the Reynolds equation.

Many existing methods incorporate numerous charts and tables which clearly place a limit on the methods; in order to use these procedures, the appropriate reference must be consulted. Alternatively, O'Donoghue and Rowe [19.16] have developed a general approximate method of design that does not require the use of various design charts. The method is strictly valid for thin land bearings, and many of the parameters are conservatively estimated. The following is a condensation of this design procedure for a multirecess bearing:

TABLE 19.22 Comparison of Three Types of Flow Resistors

	Initial cost	Fabrication and installation costs	Reliability	Availability	Ability to remain unclogged	Serviceability	Life	Flow relationship	Restrictions	Notes
Capillary tube	4†	3	5	5	1	4	5	$Q = k_c \frac{P_s - P_r}{\mu}$ $k_c = \pi D_c^4 / 128 L_c$	$L_c > 20 D_c$ $R_e = \frac{4\rho Q}{\pi D_c \mu} < 2000$	1. Laminar flow device. 2. Hypodermic needle tubing can generally be used. 3. To prevent clogging $D_c > 0.025$ in.
Sharp-edged orifice	5	2	5	5	3	4	4	$Q = k_0 (P_s - P_r)^{1/2}$ $k_0 = \frac{C_D \pi D_0^2}{2\sqrt{2\rho}}$	$C_D = f(R_e)$ $R_e = \frac{\sqrt{2\rho(P_s - P_r)} D_0}{\mu}$ $C_D \sim 0.6$ for $R_e > 15$ and $D_0 / D_{\text{line}} < 0.1$	1. Turbulent flow device. 2. To prevent clogging, $D_0 > 0.020$ in.
Flow control valve	1	4	2	5	5	2	2	$Q = k_v$ k_v = constant		1. Relatively expensive. 2. Flow is maintained at constant value.

†Rating numbers: 5 is high (best); 1 is low (worst).

Design Specification

1. Set the maximum load W.
2. Select the number of recesses n (typically $n = 4$, but $n = 6$ for high-precision bearings).
3. Select a pressure ratio p_r/p_s (a design value of 0.5 is recommended).

Bearing Dimensions

1. Calculate the bearing diameter $D = \sqrt{W/50}$ in.
2. Set width $L = D$.
3. Calculate the axial-flow land width a (refer to Fig. 19.28; recommended value: $a = L/4$).

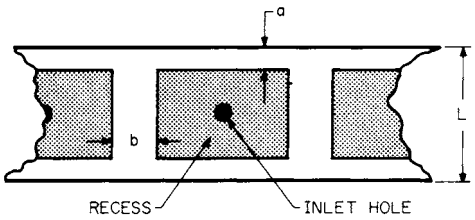

FIGURE 19.28 Hydrostatic pad geometry.

4. Calculate the circumferential land width b [refer to Fig. 19.28; recommended value: $b = \pi D/(4n)$].
5. Calculate the projected pad area $A_p = D(L - a)$.
6. Calculate the recess area for one pad only: $A_r = (\pi D - nb)(L - a)/n$.
7. Calculate the effective frictional area: $A_f = (\pi DL/n) - 0.75A_f$.

Miscellaneous Coefficients and Parameters

1. Establish a design value of film thickness h_d (recommended value: 50 to 10 times larger than the machinery tolerance on h).
2. Calculate the circumferential flow factor $\gamma = na(L - a)/(\pi Db)$; for recommended values of D, L, a, and b: $\gamma = \frac{3}{4}(n/\pi)^2$.
3. Compute the design dimensionless stiffness parameter $\bar{s}$ from Table 19.23 depending on the method of flow control selected.
4. Calculate the flow factor $q_f = \pi D/(6an)$.

Performance Parameters

1. Calculate the minimum supply pressure $p_{s,\min} = 2W/(a_f A_p)$ [recommended: $a_f = \bar{s}$ (capillary tube at design Table 19.23)].

TABLE 19.23 Dimensionless Stiffness at Design Condition for Multirecess Bearing

$$\bar{s} = \frac{C_1}{1 + C_{2\gamma}}$$

Number of recesses n	Capillary tube		Sharp-edged orifice		Flow control valve		Recommended value of γ†
	C_1	C_2	C_1	C_2	C_1	C_2	
3	0.27	0.75	0.36	1.0	0.54	1.5	0.68
4	0.96	0.50	1.28	0.67	1.91	1.01	1.22
5	1.03	0.35	1.38	0.46	2.13	0.69	1.90
6	1.08	0.25	1.43	0.33	2.15	0.50	2.74

†SOURCE: Ref. [19.16].

2. Calculate the stiffness $s = p_s A_p \bar{s}/h_d$ (if this value is too low, either D and/or p_s must be increased).
3. Calculate the minimum running clearance $h_0 = h_d - W/s$.
4. Determine the flow rate $Q = (nq_f p_s h^3 d)/(2\mu)$. A calculated value of viscosity can be used:

$$\mu = \frac{60 P_s h^2 d \sqrt{q_f/(2A_f)}}{\pi D N} \qquad \text{reyn}$$

REFERENCES

19.1 G. G. Hirs, "The Load Capacity and Stability Characteristics of Hydrodynamic Grooved Journal Bearings," *ASLE Transactions,* vol. 8, 1965, pp. 296–305.

19.2 E. R. Booser, "Plain-Bearing Materials," *Machine Design,* June 18, 1970 (bearings reference issue), pp. 14–20.

19.3 V. Hopkins, "Self-Lubricating Bearing Materials—A Review," *Assessment of Lubricant Technology,* ASME, 1972, pp. 21–26.

19.4 A. W. J. DeGee, "Selection of Materials for Lubricated Journal Bearings," *Wear,* vol. 36, 1976, pp. 33–61.

19.5 B. R. Reason and I. P. Narang, "Rapid Design and Performance Evaluation of Steady State Journal Bearings—A Technique Amendable to Programmable Hand Calculators," *ASLE Transactions,* vol. 25, no. 4, 1982, pp. 429–449.

19.6 J. Shigley and C. R. Mischke, *Mechanical Engineering Design,* 5th ed., McGraw-Hill, New York, 1989, pp. 498–507.

19.7 A. A. Raimondi and J. Boyd, "A Solution for the Finite Journal Bearing and Its Application to Analysis and Design," I, II, and III, *ASLE Transactions,* vol. 1, 1958, pp. 159–174, 175–193, and 194–209, respectively.

19.8 A. Seireg and S. Dandage, "Empirical Design Procedure for the Thermodynamic Behavior of Journal Bearings," *ASME Journal of Lubrication Technology,* vol. 104, April 1982, pp. 135–148.

19.9 H. J. Connors, "An Analysis of the Effect of Lubricant Supply Rate on the Performance of the 360° Journal Bearing," *ASLE Transactions,* vol. 5, 1962, pp. 404–417.

19.10 H. Moes and R. Bosma, "Design Charts for Optimum Bearing Configurations: 1—The Full Journal Bearing," *ASME Journal of Lubrication Technology,* vol. 93, April 1971, pp. 302–306.

19.11 A. A. Raimondi, "A Numerical Solution for the Gas Lubricated Full Journal Bearing of Finite Length," *ASLE Transactions,* vol. 4, 1961, pp. 131–155.

19.12 E. R. Wu, "Gas-Lubricated Porous Bearings of Finite Length—Self-Acting Journal Bearings," *ASME Journal of Lubrication Technology,* vol. 101, July 1979, pp. 338–348.

19.13 V. Castelli and J. Pirvics, "Equilibrium Characteristics of Axial-Grooved Gas-Lubricated Bearings," *ASME Journal of Lubrication Technology,* vol. 89, April 1967, pp. 177–196.

19.14 O. Pinkus, "Analysis of Noncircular Gas Journal Bearings," *ASME Journal of Lubrication Technology,* vol. 87, October 1975, pp. 616–619.

19.15 H. C. Rippel, "Design of Hydrostatic Bearings," *Machine Design,* parts 1 to 10, Aug. 1 to Dec. 5, 1963.

19.16 J. P. O'Donoghue and W. B. Rowe, "Hydrostatic Bearing Design," *Tribology,* vol. 2, February 1969, pp. 25–71.

CHAPTER 20
LUBRICATION

A. R. Lansdown, M.Sc., Ph.D.
Director, Swansea Tribology Centre
University College of Swansea
Swansea, United Kingdom

20.1 FUNCTIONS AND TYPES OF LUBRICANT

Whenever relative movement takes place between two surfaces in contact, there will be resistance to movement. This resistance is called the *frictional force,* or simply *friction.* Where this situation exists, it is often desirable to reduce, control, or modify the friction.

Broadly speaking, any process by which the friction in a moving contact is reduced may be described as *lubrication.* Traditionally this description has presented no problems. Friction reduction was obtained by introducing a solid or liquid material, called a *lubricant,* into the contact, so that the surfaces in relative motion were separated by a film of the lubricant. Lubricants consisted of a relatively few types of material, such as natural or mineral oils, graphite, molybdenum disulfide, and talc, and the relationship between lubricants and the process of lubrication was clear and unambiguous.

Recent technological developments have confused this previously clear picture. Friction reduction may now be provided by liquids, solids, or gases or by physical or chemical modification of the surfaces themselves. Alternatively, the sliding components may be manufactured from a material which is itself designed to reduce friction or within which a lubricant has been uniformly or nonuniformly dispersed. Such systems are sometimes described as "unlubricated," but this is clearly a matter of terminology. The system may be unconventionally lubricated, but it is certainly not unlubricated.

On the other hand, lubrication may be used to modify friction but not specifically to reduce it. Certain composite brake materials may incorporate graphite or molybdenum disulfide, whose presence is designed to ensure steady or consistent levels of friction. The additives are clearly lubricants, and it would be pedantic to assert that their use in brake materials is not lubrication.

This introduction is intended only to generate an open-minded approach to the processes of lubrication and to the selection of lubricants. In practice, the vast majority of systems are still lubricated by conventional oils or greases or by equally ancient but less conventional solid lubricants. It is when some aspect of the system makes the use of these simple lubricants difficult or unsatisfactory that the wider interpretation of lubrication may offer solutions. In addition to their primary function of reducing or controlling friction, lubricants are usually expected to reduce wear and perhaps also to reduce heat or corrosion.

In terms of volume, the most important types of lubricant are still the liquids (oils) and semiliquids (greases). Solid lubricants have been rapidly increasing in importance since about 1950, especially for environmental conditions which are too severe for oils and greases. Gases can be used as lubricants in much the same way as liquids, but as is explained later, the low viscosities of gases increase the difficulties of bearing design and construction.

20.2 SELECTION OF LUBRICANT TYPE

A useful first principle in selecting a type of lubrication is to choose the simplest technique which will work satisfactorily. In very many cases this will mean inserting a small quantity of oil or grease in the component on initial assembly; this is almost never replaced or refilled. Typical examples are door locks, hinges, car-window winders, switches, clocks, and watches.

This simple system is likely to be unsatisfactory if the loads or speeds are high or if the service life is long and continuous. Then it becomes necessary to choose the lubricant with care and often to use a replenishment system.

The two main factors in selecting the type of lubricant are the speed and the load. If the speed is high, then the amount of frictional heating tends to be high, and low-viscosity lubricants will give lower viscous friction and better heat transfer. If the loads are high, then low-viscosity lubricants will tend to be expelled from the contact. This situation is summarized in Fig. 20.1.

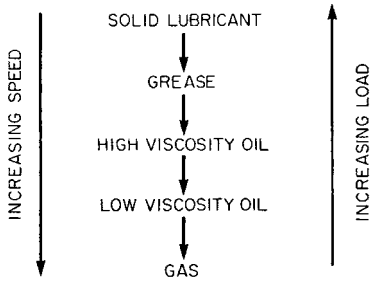

FIGURE 20.1 Effect of speed and load on choice of lubricant type. *(From Ref. [20.1].)*

It is difficult to give precise guidance about the load and speed limits for the various lubricant types, because of the effects of geometry, environment, and variations within each type, but Fig. 20.2 gives some approximate limits.

Some other property of the system will sometimes restrict the choice of lubricant type. For example, in watches or instrument mechanisms, any lubricant type could meet the load and speed requirements, but because of the need for low friction, it is normal to use a very low-viscosity oil. However, for open gears, wire ropes, or chains, the major problem is to prevent the lubricant from being thrown off the moving parts, and

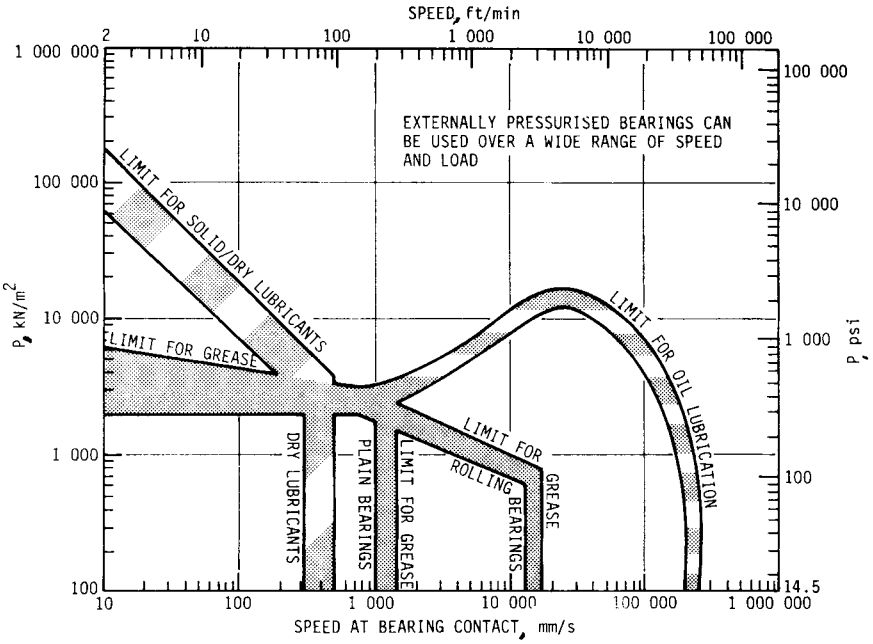

FIGURE 20.2 Speed and load limitations for different types of lubricants. *(From Ref. [20.2].)*

it is necessary to use a "tacky" bituminous oil or grease having special adhesive properties.

In an existing system the geometry may restrict the choice of lubricant type. Thus, an unsealed rolling bearing may have to be lubricated with grease because oil would not be retained in the bearing. But where the lubrication requirements are difficult or particularly important, it will usually be essential to first choose the lubricant type and then design a suitable system for that lubricant. Some very expensive mistakes have been made, even in high technology such as aerospace engineering, where systems that could not be lubricated have been designed and built.

20.3 LIQUID LUBRICANTS: PRINCIPLES AND REQUIREMENTS

The most important single property of a liquid lubricant is its viscosity. Figure 20.3 shows how the viscosity of the lubricant affects the nature and quality of the lubrication. This figure is often called a *Stribeck curve,* although there seems to be some doubt as to whether Stribeck used the diagram in the form shown.

The expression $\eta N/P$ is known as the *Sommerfeld number,* in which η is the lubricant viscosity, N represents the relative speed of movement between the counterfaces of the bearing, and P is the mean pressure or specific load supported by the bearing. Of these three factors, only the viscosity is a property of the lubricant. And if N and P are held constant, the figure shows directly the relationship between the coefficient of friction μ and the lubricant viscosity η.

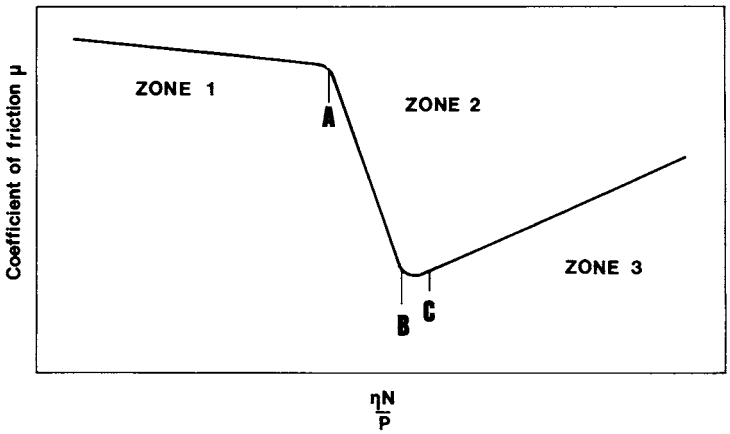

FIGURE 20.3 Effect of viscosity on lubrication.

The graph can be conveniently divided into three zones. In zone 3, the bearing surfaces are fully separated by a thick film of the liquid lubricant. This is, therefore, the zone of *thick-film* or *hydrodynamic lubrication,* and the friction is entirely viscous friction caused by mechanical shearing of the liquid film. There is no contact between the interacting surfaces and therefore virtually no wear.

As the viscosity decreases in zone 3, the thickness of the liquid film also decreases until at point *C* it is only just sufficient to ensure complete separation of the surfaces. Further reduction in viscosity, and therefore in film thickness, results in occasional contact between asperities on the surfaces. The relatively high friction in asperity contacts offsets the continuing reduction in viscous friction, so that at point *B* the friction is roughly equal to that at *C.*

Point *C* is the ideal point, at which there is zero wear with almost minimum friction, but in practice the design target will be slightly to the right of *C,* to provide a safety margin.

With further reduction in viscosity from point *B,* an increasing proportion of the load is carried by asperity contact, and the friction increases rapidly to point *A.* At this point the whole of the bearing load is being carried by asperity contact, and further viscosity reduction has only a very slight effect on friction.

Zone 1, to the left of point *A,* is the zone of *boundary lubrication.* In this zone, chemical and physical properties of the lubricant other than its bulk viscosity control the quality of the lubrication; these properties are described in Sec. 20.5.

Zone 2, between points *A* and *B,* is the zone of mixed lubrication, in which the load is carried partly by the film of liquid lubricant and partly by asperity interaction. The proportion carried by asperity interaction decreases from 100 percent at *A* to 0 percent at *C.*

Strictly speaking, Fig. 20.3 relates to a plain journal bearing, and *N* usually refers to the rotational speed. Similar patterns arise with other bearing geometries in which some form of hydrodynamic oil film can occur.

The relationship between viscosity and oil-film thickness is given by the Reynolds equation, which can be written as follows:

$$\frac{\partial}{\partial x}\left(h^3\frac{\partial P}{\partial x}\right)+\frac{\partial}{\partial z}\left(h^3\frac{\partial P}{\partial z}\right)=\eta\left(6U\frac{\partial h}{\partial x}+6h\frac{\partial U}{\partial x}+12V\right)$$

where h = lubricant-film thickness
P = pressure
x, z = coordinates
U, V = speeds in directions x and z

Fuller details of the influence of lubricant viscosity on plain journal bearings are given in Chap. 19.

In nonconformal lubricated systems such as rolling bearings and gears, the relationship between lubricant viscosity and film thickness is complicated by two additional effects: the elastic deformation of the interacting surfaces and the increase in lubricant viscosity as a result of high pressure. The lubrication regime is then known as *elastohydrodynamic* and is described mathematically by various equations.

For roller bearings, a typical equation is the Dowson-Higginson equation:

$$h_{\min} = \frac{2.65(\eta_o U)^{0.7} R^{0.43} \alpha^{0.54}}{E^{0.03} p^{0.13}}$$

where η_o = oil viscosity in entry zone
R = effective radius
α = pressure coefficient of viscosity

Here U represents the speed, p a load parameter, and E a material parameter based on modulus and Poisson's ratio.

For ball bearings, an equivalent equation is the one developed by Archard and Cowking:

$$h_{\min} = \frac{1.4(\eta_o U \alpha)^{0.74} E^{0.074}}{R^{0.74} p^{0.074}}$$

For such nonconformal systems, a diagram similar to Fig. 20.3 has been suggested in which zone 2 represents elastohydrodynamic lubrication. It is difficult to think of a specific system to which the relationship exactly applies, but it may be a useful concept that the lubricant-film thickness and the friction in elastohydrodynamic lubrication bridge the gap between thick-film hydrodynamic lubrication and boundary lubrication.

A form of microelastohydrodynamic lubrication has been suggested as a mechanism for asperity lubrication under boundary conditions (see Sec. 20.5). If this suggestion is valid, the process would probably be present in the zone of mixed lubrication.

Where full-fluid-film lubrication is considered necessary but the viscosity, load, speed, and geometry are not suitable for providing full-fluid-film separation hydrodynamically, the technique of *external pressurization* can be used. Quite simply, this means feeding a fluid into a bearing at high pressure, so that the applied hydrostatic pressure is sufficient to separate the interacting surfaces of the bearing.

Externally pressurized bearings broaden the range of systems in which the benefits of full-fluid-film separation can be obtained and enable many liquids to be used successfully as lubricants which would otherwise be unsuitable. These include aqueous and other low-viscosity process fluids. Remember that the lubricant viscosity considered in Fig. 20.3 and in the various film-thickness equations is the viscosity under the relevant system conditions, especially the temperature. The viscosity of all liquids decreases with increase in temperature, and this and other factors affecting viscosity are considered in Sec. 20.4.

The viscosity and boundary lubrication properties of the lubricant completely define the lubrication performance, but many other properties are important in service. Most of these other properties are related to progressive deterioration of the lubricant; these are described in Sec. 20.6.

20.4 LUBRICANT VISCOSITY

Viscosity of lubricants is defined in two different ways, and unfortunately both definitions are very widely used.

20.4.1 Dynamic or Absolute Viscosity

Dynamic or *absolute viscosity* is the ratio of the shear stress to the resultant shear rate when a fluid flows. In SI units it is measured in pascal-seconds or newton-seconds per square meter, but the centimeter-gram-second (cgs) unit, the centipoise, is more widely accepted, and

$$1 \text{ centipoise (cP)} = 10^{-3} \text{ Pa} \cdot \text{s} = 10^{-3} \text{ N} \cdot \text{s/m}^2$$

The centipoise is the unit of viscosity used in calculations based on the Reynolds equation and the various elastohydrodynamic lubrication equations.

20.4.2 Kinematic Viscosity

The *kinematic viscosity* is equal to the dynamic viscosity divided by the density. The SI unit is square meters per second, but the cgs unit, the centistoke, is more widely accepted, and

$$1 \text{ centistoke (cSt)} = 1 \text{ mm}^2/\text{s}$$

The centistoke is the unit most often quoted by lubricant suppliers and users.

In practice, the difference between kinematic and dynamic viscosities is not often of major importance for lubricating oils, because their densities at operating temperatures usually lie between 0.8 and 1.2. However, for some fluorinated synthetic oils with high densities, and for gases, the difference can be very significant.

The viscosities of most lubricating oils are between 10 and about 600 cSt at the operating temperature, with a median figure of about 90 cSt. Lower viscosities are more applicable for bearings than for gears, as well as where the loads are light, the speeds are high, or the system is fully enclosed. Conversely, higher viscosities are selected for gears and where the speeds are low, the loads are high, or the system is well ventilated. Some typical viscosity ranges at the operating temperatures are shown in Table 20.1.

The variation of oil viscosity with temperature will be very important in some systems, where the operating temperature either varies over a wide range or is very different from the reference temperature for which the oil viscosity is quoted.

The viscosity of any liquid decreases as the temperature increases, but the rate of decrease can vary considerably from one liquid to another. Figure 20.4 shows the

TABLE 20.1 Typical Operating Viscosity Ranges

Lubricant	Viscosity range, cSt
Clocks and instrument oils	5–20
Motor oils	10–50
Roller bearing oils	10–300
Plain bearing oils	20–1500
Medium-speed gear oils	50–150
Hypoid gear oils	50–600
Worm gear oils	200–1000

change of viscosity with temperature for some typical lubricating oils. A graphical presentation of this type is the most useful way to show this information, but it is much more common to quote the viscosity index (VI).

The *viscosity index* defines the viscosity-temperature relationship of an oil on an arbitrary scale in comparison with two standard oils. One of these standard oils has

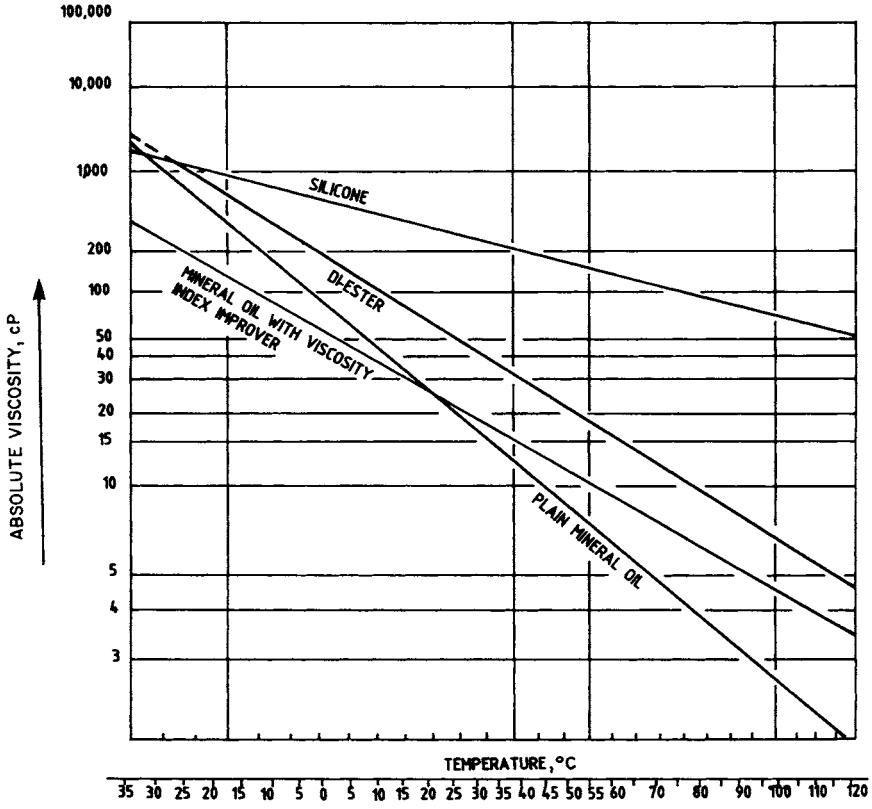

FIGURE 20.4 Variation of viscosity with temperature.

a viscosity index of 0, representing the most rapid change of viscosity with temperature normally found with any mineral oil. The second standard oil has a viscosity index of 100, representing the lowest change of viscosity with temperature found with a mineral oil in the absence of relevant additives.

The equation for the calculation of the viscosity index of an oil sample is

$$\text{VI} = \frac{100(L - U)}{L - H}$$

where U = viscosity of sample in centistokes at 40°C, L = viscosity in centistokes at 40°C of oil of 0 VI having the same viscosity at 100°C as the test oil, and H = viscosity at 40°C of oil of 100 VI having the same viscosity at 100°C as the test oil.

Some synthetic oils can have viscosity indices of well over 150 by the above definition, but the applicability of the definition at such high values is doubtful. The viscosity index of an oil can be increased by dissolving in it a quantity (sometimes as high as 20 percent) of a suitable polymer, called a *viscosity index improver.*

The SAE viscosity rating scale is very widely used and is reproduced in Table 20.2. It is possible for an oil to satisfy more than one rating. A mineral oil of high viscosity index could meet the 20W and 30 criteria and would then be called a 20W/30 multigrade oil. More commonly, a VI improved oil could meet the 20W and 50 criteria and would then be called a 20W/50 multigrade oil.

Note that the viscosity measurements used to establish SAE ratings are carried out at low shear rate. At high shear rate in a bearing, the effect of the polymer may

TABLE 20.2 1977 Table of SAE Oil Ratings

SAE no.	Maximum viscosity at −18°C, cP	Viscosity at 100°C, cSt	
		Minimum	Maximum
Engine oils			
5W	1 250	3.8	
10W	2 500	4.1	
20W†	10 000	5.6	
20	.....	5.6	<9.3
30	.....	9.3	<12.5
40	.....	12.5	<16.3
50	.....	16.3	<21.9
Gear oils			
75	3 250		
80	21 600		
90	.....	14	<25
140	.....	25	<43
250	.....	43	

†15W may be used to identify 20W oils which have a maximum viscosity of 5000 cP.

disappear, and a 20W/50 oil at very high shear rate may behave as a thinner oil than a 20W, namely, a 15W or even 10W. In practice, this may not be important, because in a high-speed bearing the viscosity will probably still produce adequate oil-film thickness.

Theoretically the viscosity index is important only where significant temperature variations apply, but in fact there is a tendency to use only high-viscosity-index oils in the manufacture of high-quality lubricant. As a result, a high viscosity index is often considered a criterion of lubricant quality, even where viscosity index as such is of little or no importance.

Before we leave the subject of lubricant viscosity, perhaps some obsolescent viscosity units should be mentioned. These are the *Saybolt viscosity* (SUS) in North America, the *Redwood viscosity* in the United Kingdom, and the *Engler viscosity* in continental Europe. All three are of little practical utility, but have been very widely used, and strenuous efforts have been made by standardizing organizations for many years to replace them entirely by kinematic viscosity.

20.5 BOUNDARY LUBRICATION

Boundary lubrication is important where there is significant solid-solid contact between sliding surfaces. To understand boundary lubrication, it is useful to first consider what happens when two metal surfaces slide against each other with no lubricant present.

In an extreme case, where the metal surfaces are not contaminated by an oxide film or any other foreign substance, there will be a tendency for the surfaces to adhere to each other. This tendency will be very strong for some pairs of metals and weaker for others. A few guidelines for common metals are as follows:

1. Identical metals in contact have a strong tendency to adhere.
2. Softer metals have a stronger tendency to adhere than harder metals.
3. Nonmetallic alloying elements tend to reduce adhesion (e.g., carbon in cast iron).
4. Iron and its alloys have a low tendency to adhere to lead, silver, tin, cadmium, and copper and a high tendency to adhere to aluminum, zinc, titanium, and nickel.

Real metal surfaces are usually contaminated, especially by films of their own oxides. Such contaminant films commonly reduce adhesion and thus reduce friction and wear. Oxide films are particularly good lubricants, except for titanium.

Thus friction and wear can usually be reduced by deliberately generating suitable contaminant films on metallic surfaces. Where no liquid lubricant is present, such a process is a type of dry or solid lubrication. Where the film-forming process takes place in a liquid lubricant, it is called boundary lubrication.

Boundary lubricating films can be produced in several ways, which differ in the severity of the film-forming process and in the effectiveness of the resulting film. The mildest film-forming process is adsorption, in which a layer one or more molecules thick is formed on a solid surface by purely physical attraction. Adsorbed films are effective in reducing friction and wear, provided that the resulting film is sufficiently thick. Figure 20.5 shows diagrammatically the way in which adsorption of a long-chain alcohol generates a thick film on a metal surface even when the film is only one molecule thick.

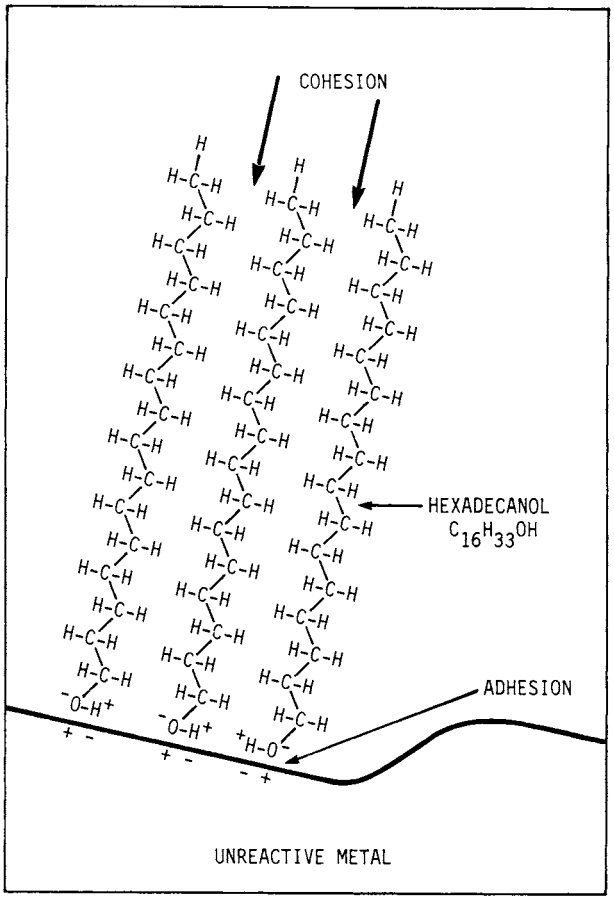

FIGURE 20.5 Representation of adsorption of a long-chain alcohol. *(From Ref. [20.3].)*

Mineral oils often contain small amounts of natural compounds which produce useful adsorbed films. These compounds include unsaturated hydrocarbons (olefines) and nonhydrocarbons containing oxygen, nitrogen, or sulfur atoms (known as asphaltenes). Vegetable oils and animal fats also produce strong adsorbed films and may be added in small concentrations to mineral oils for that reason. Other mild boundary additives include long-chain alcohols such as lauryl alcohol and esters such as ethyl stearate or ethyl oleate.

Adsorbed boundary films are removed fairly easily, either mechanically or by increased temperature. A more resistant film is generated by chemisorption, in which a mild reaction takes place between the metal surface and a suitable compound. Typical chemisorbed compounds include aliphatic ("fatty") acids, such as oleic and stearic acids. A chemisorbed film is shown diagrammatically in Fig. 20.6.

Even more resistant films are produced by reaction with the metal surface. The reactive compounds usually contain phosphorus, sulfur, or chlorine and ultimately

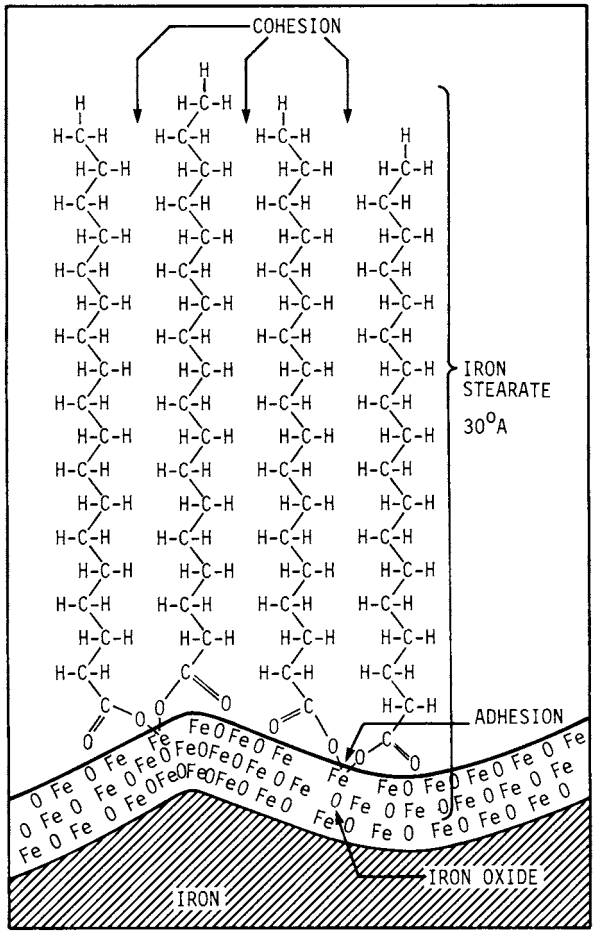

FIGURE 20.6 Representation of chemisorption of a long-chain aliphatic acid. *(From Ref. [20.3].)*

produce films of metal phosphide, sulfide, or chloride on the sliding surface. These reactive additives are known as *extreme-pressure,* or EP, additives.

The processes by which modern boundary lubricant additives generate surface films may be very complex. A single additive such as trixylyl phosphate may be initially adsorbed on the metal surface, then react to form a chemisorbed film of organometallic phosphate, and finally, under severe sliding or heating, react to form metal phosphate or phosphide.

All these boundary lubricant compounds have corresponding disadvantages. As a general rule, they should be used only where the conditions of use require them. The mild, adsorbed compounds have the least undesirable side effects. They are more readily oxidized than the usual mineral-base oils and, as a result, have a higher tendency to produce corrosive acidic compounds and insoluble gums or lacquers. However, these effects are not serious, and mild antiwear additives are widely used

in small quantities where sliding conditions are not severe, such as in hydraulic fluids and turbine oils.

The stronger chemisorbed additives such as fatty acids, organic phosphates, and thiophosphates are correspondingly more reactive. They are used in motor oils and gear oils. Finally, the reactive sulfurized olefines and chlorinated compounds are, in fact, controlled corrodents and are used only where the sliding conditions are very severe, such as in hypoid gearboxes and in metalworking processes.

Boundary lubrication is a very complex process. Apart from the direct film-forming techniques described earlier, there are several other effects which probably make an important contribution to boundary lubrication:

1. *The Rehbinder effect* The presence of surface-active molecules adjacent to a metal surface decreases the yield stress. Since many boundary lubricants are more or less surface-active, they can be expected to reduce the stresses developed when asperities interact.
2. *Viscosity increase adjacent to a metal surface* This effect is controversial, but it seems probable that interaction between adsorbed molecules and the free ambient oil can result in a greaselike thickening or trapping of oil molecules adjacent to the surface.
3. *Microelastohydrodynamic effects* The interaction between two asperities sliding past each other in a liquid is similar to the interaction between gear teeth, and in the same way it can be expected to generate elastohydrodynamic lubrication on a microscopic scale. The increase in viscosity of the lubricant and the elastic deformation of the asperities will both tend to reduce friction and wear. However, if the Rehbinder effect is also present, then plastic flow of the asperities is also encouraged. The term *microrheodynamic lubrication* has been used to describe this complex process.
4. *Heating* Even in well-lubricated sliding there will be transient heating effects at asperity interactions, and these will reduce the modulus and the yield stress at asperity interactions.

Boundary lubrication as a whole is not well understood, but the magnitude of its beneficial effects can be easily seen from the significant reductions in friction, wear, and seizure obtained with suitable liquid lubricants in slow metallic sliding.

20.6 DETERIORATION PROBLEMS

In theory, if the right viscosity and the right boundary properties have been selected, then the lubrication requirements will be met. In practice, there is one further complication—the oil deteriorates. Much of the technology of lubricating oils and additives is concerned with reducing or compensating for deterioration.

The three important types of deterioration are oxidation, thermal decomposition, and contamination. A fourth long-term effect is reaction with other materials in the system, which is considered in terms of compatibility. Oxidation is the most important deterioration process because over a long period, even at normal atmospheric temperature, almost all lubricants show some degree of oxidation.

Petroleum-base oils produced by mild refining techniques oxidize readily above 120°C to produce acidic compounds, sludges, and lacquers. The total oxygen uptake is not high, and this suggests that the trace compounds, such as aromatics and

asphaltenes, are reacting, and that possibly in doing so some are acting as oxidation inhibitors for the paraffinic hydrocarbons present. Such mildly refined oils are not much improved by the addition of antioxidants.

More severe refining or hydrogenation produces a more highly paraffinic oil which absorbs oxygen more readily but without producing such harmful oxidation products. More important, however, the oxidation resistance of such highly refined base oils is very considerably improved by the addition of suitable oxidation inhibitors.

Most modern petroleum-base oils are highly refined in order to give consistent products with a wide operating-temperature range. Antioxidants are therefore an important part of the formulation of almost all modern mineral-oil lubricants.

The commonly used antioxidants are amines, hindered phenols, organic phosphites, and organometallic compounds. One particularly important additive is zinc diethyl dithiophosphate, which is a very effective antioxidant and also has useful boundary lubrication and corrosion-inhibition properties.

If no oxygen is present, lubricants can be used at much higher temperatures without breaking down. In other words, their thermal stability is greater than their oxidative stability. This effect can be seen for mineral oils in Table 20.3. To prevent contact of oxygen with the oil, the system must be sealed against the entry of air or purged with an inert gas such as nitrogen. Some critical hydraulic systems, such as those in high-speed aircraft, are operated in this way.

In high-vacuum systems such as spacecraft or electron microscopes, there is no oxygen contact. But in high vacuum an increase in temperature tends to vaporize the

TABLE 20.3 Range of Temperature Limits in Degrees Celsius for Mineral Oils as a Function of Required Life

Oil condition	Life, h				
	1	10	10^2	10^3	10^4
Thermal stability limit; insignificant oxygen present	415 to 435	385 to 405	355 to 375	320 to 340	290 to 310
Limit dependent on amount of oxygen present and presence or absence of catalysts	190 to 415	170 to 385	140 to 355	155 to 320	90 to 290
Limit imposed by oxidation where oxygen supply is unlimited; for oils containing antioxidants	175 to 190	155 to 170	125 to 140	100 to 115	80 to 90
Limit imposed by oxidation where oxygen supply is unlimited; for oils without antioxidants	155 to 165	130 to 140	95 to 110	65 to 80	35 to 50
Lower temperature limit imposed by pour point; varies with oil source, viscosity, treatment, and additives	−65 to 0	−65 to 0	−65 to 0	−65 to 0	−65 to 0

SOURCE: Ref. [20.2].

oil, so that high thermal stability is of little or no value. It follows that oxidative stability is usually much more important than thermal stability.

Compatibility of lubricating oils with other materials in the system is complex, and Table 20.4 lists some of the possible problems and solutions. Compatibility problems with synthetic lubricants are even more complicated; these are considered further in the next section.

20.7 SELECTING THE OIL TYPE

So far most of the information in this chapter has been related to mineral oils. For almost 150 years the availability, good performance, variety, and cheapness of mineral oils have made them the first choice for most applications. They still represent over 90 percent of total lubricant use, but many other liquids are used successfully as lubricants and can provide special features which make them the best choice in particular situations.

Table 20.5 shows the most important types of lubricating oil and their advantages and disadvantages as compared with mineral oils. The natural oils comprise a wide variety of compounds of vegetable or animal origin, consisting mainly of organic esters. They all have better low-friction and boundary lubrication properties than mineral oils, but lower thermal and oxidative stability. Before mineral oils became generally available, natural oils and fats were the most common lubricants, and several are still widely used because their properties make them particularly suitable for special applications, as shown in Table 20.6.

The diesters were the first synthetic lubricating oils to be used in large quantities. Their higher thermal and oxidative stability made them more suitable than mineral

TABLE 20.4 Examples of Compatibility Problems and Possible Solutions

Problem	Solution
1. Attack by mineral oils on natural rubber	Change to nitrile rubber or neoprene
2. Attack by synthetic oils on natural rubber, nitrile, or other rubber	Change to suitable rubber for specific oil, e.g., Viton, resin-cured butyl, or EPR
3. Attack by synthetic oils on plastics or paints	Change to resistant plastics such as PTFE, polyimide, polysulfone, or polyphenylene sulfide
4. Corrosion by dissolved water	Use rust-inhibitor additives such as sulfonates
5. Corrosion by acidic degradation products	Use corrosion inhibitors such as ZDDP, or increase antioxidants to reduce degradation
6. Corrosion by additives of copper alloys or mild steel	Use less powerful EP additives, or change to corrosion-resistant metals
7. Corrosion by synthetic oils	Change to more resistant metals or platings

TABLE 20.5 Advantages and Disadvantages of Main Nonmineral Oils

Oil type	Comparison with mineral oils	
	Advantages	Disadvantages
1. Vegetable oil	Good boundary lubrication; does not cause carburization of steel in metalforming	Decomposes readily to give high viscosity or sludges and lacquers
2. Diesters, hindered esters	Higher temperature stability; high viscosity index	Some attack on rubbers and plastics
3. Polyglycol	Miscibility with water; decomposes without producing solid degradation products	Low maximum temperature
4. Silicones	High temperature stability; resistance to chemicals	Poor boundary lubrication for steel on steel
5. Phosphate ester	Fire resistance; very good boundary lubrication	Attack on rubbers and plastics; poor temperature stability
6. Chlorinated diphenyls	Fire resistance; chemical stability; boundary lubrication	Poor viscosity index; attack on plastics and copper alloys
7. Fluorocarbon	Excellent temperature and chemical stability	Price; poor viscosity index

TABLE 20.6 Some Uses of Natural Oils and Fats

Oil type	Uses
1. Rapeseed oil	*a.* To reduce friction in plain bearings where oil-film thickness is inadequate by addition of 5% to 10% to mineral oil
	b. In metal forming to give low friction and EP properties without staining or carburizing
	c. Has been used as lubricant in continuous casting
2. Castor oil	*a.* As low-viscosity hydraulic fluid for compatibility with natural rubber
	b. To give low viscous drag and good boundary lubrication in racing car engines and early aircraft engines
3. Tallow	*a.* For low friction in metal forming
4. Sperm oil	*a.* For outstanding boundary lubrication in metal cutting especially in sulfurized form; now virtually obsolete because of whale protection laws

oils for gas-turbine lubrication, and by about 1960 they were almost universally used for aircraft jet engines. For the even more demanding conditions of supersonic jet engines, the more complex ester lubricants such as hindered phenols and triesters were developed.

Phosphate esters and chlorinated diphenyls have very low-flammability characteristics, and this has led to their wide use where critical fire-risk situations occur, such as in aviation and coal mining. Their overall properties are mediocre, but are sufficiently good for use where fire resistance is particularly important.

Other synthetic fluids such as silicones, chlorinated silicones, fluorinated silicones, fluorinated hydrocarbon, and polyphenyl ethers are all used in relatively small quantities for their high-temperature stability, but all are inferior lubricants and very expensive compared with mineral oils.

Several types of water-containing fluid are used in large quantities, and these are listed in Table 20.7. They are used almost entirely to provide either fire resistance or superior cooling.

Mineral oils can be considered as the normal, conventional oils, and alternative types are used only when they can offer some particular advantage over mineral oils. Table 20.8 summarizes the selection of oil type in relation to the special properties required.

It is difficult to give precise high-temperature limits for the use of specific oil types, because the limiting temperature depends on the required life and the amount of degradation which is acceptable. Even for water-containing lubricants, the upper temperature limit may be from 50 to 85°C depending on the required life, the degree of ventilation, and the amount of water loss which is acceptable. Table 20.9 summarizes the temperature limits for a few synthetic oils, but the limits shown should be considered only approximate.

Serious incompatibility problems can occur with lubricating oils, especially with nonmetallic materials such as rubber seals and hoses. Table 20.10 lists some satisfactory and unsatisfactory materials for use with various lubricants.

TABLE 20.7 Some Water-Containing Lubricants

Oil type	Applications
1. Invert emulsions (water in mineral oil)	Used as hydraulic fluids for fire resistance, e.g., in coal mining. Good lubricating properties.
2. Dilute emulsions (5% mineral oil in water)	Used for fire resistance and cheapness where good lubrication properties not needed (e.g., roof jacks in coal mining).
3. "Soluble" oils (about 1% oil in water)	Used for their good cooling properties in metal cutting and grinding operations.
4. Water/Polyglycol	Used for fire resistance where increased viscosity and lack of solid degradation products are required.
5. "Synthetic" Coolants (solutions of boundary additives in water)	Used for excellent cooling and stability in metal cutting operations.

TABLE 20.8 Choice of Oil Type for Specific Properties

Property required	Choice of oil type
1. Wide range of viscosities	Mineral oil; silicone; polyglycol
2. Good boundary lubrication	Natural oil or fat; mineral oil with suitable additives; ester; phosphate ester
3. Long life	Mineral oil; silicone; fluorocarbon; ester; polyphenyl ether
4. High temperature stability	Polyphenyl ether; fluorocarbon; silicone; ester
5. Fire resistance	Emulsions; fluorocarbon; fluorosilicone; chlorinated biphenyl; phosphate ester
6. Cheapness	Emulsions; mineral oil

20.8 LUBRICATING GREASES

Lubricating greases are not simply very viscous oils. They consist of lubricating oils, often of quite low viscosity, which have been thickened by means of finely dispersed solids called thickeners. The effect of the thickeners is to produce a semirigid structure in which the dispersion of thickener particles is stabilized by electric charges. The liquid phase is firmly held by a combination of opposite electric charges, adsorp-

TABLE 20.9 Range of Temperature Limits in Degrees Celsius for Some Synthetic Oils as a Function of the Required Life

Name of lubricant; type of limit	Life, h				
	1	10	10^2	10^3	10^4
Polyphenyl ethers; thermal stability limit	545	520	490	455	425
Polyphenyl ethers; oxidation limit	350	330	305	280	260
Silicones; thermal stability limit	280 to 290	260 to 275	240 to 260	220 to 245	200 to 230
Esters and silicones; oxidation limit	225 to 260	215 to 245	200 to 240	185 to 220	175 to 210
Phosphate esters; thermal and oxidative limit	160	145	130	110	100
Polyphenal ethers; pour-point limit	0	0	0	0	0
Silicones and esters; pour-point limit	−60	−60	−60	−60	−60

SOURCE: Ref. [20.2].

TABLE 20.10 Some Compatible and Incompatible Materials for Different Oil Types

Oil type	Rubbers and plastics	
	Satisfactory	Unsatisfactory
1. Natural oils	Most rubbers, including natural rubber; most plastics	SBR rubber; highly plasticized polyethylene and polypropylene
2. Mineral oil	Nitrile rubber; neofrene; Viton; EPR; most unplasticized plastics	Natural rubber; SBR; highly plasticized plastics; polyurethanes
3. Esters	High nitrile; Viton; nylons; PPS; polyethersulfones	Natural rubber; SBR; low nitrile; polyacrylates; polyurethanes
4. Silicones	High nitrile; Viton; nylons; PPS	Natural rubber; silicone rubber; plasticized plastics
5. Phosphate ester	Resin-cured butyl rubber; EPR; PPS	Most other rubbers; many plastics

tion, and mechanical trapping. As a result, the whole grease behaves as a more or less soft solid, and there is only a very slight tendency for the oil to flow out of the grease.

Greases can probably be made from any type of lubricating oil, but in practice the majority are based on mineral oils, and only a few other base oils are of any real importance. Diesters have been used to produce greases for higher and lower temperatures than greases based on mineral oils are suitable for. Silicones are used for higher temperatures again, and fluorinated hydrocarbons for even higher temperatures; both these types are also used because of their chemical inertness, but the total quantities are relatively small. Phosphate esters have been used for fire resistance, and vegetable oils for compatibility with foodstuffs; but, again, the quantities are very small.

The most commonly used thickeners are soaps, which are salts of organic acids with calcium, sodium, lithium, or aluminum. The soaps take the form of fibrous particles which interlock to give a high level of stiffness at low soap concentrations. Many other substances which have been used as grease thickeners tend to be more spherical and have to be used at higher concentrations than soaps to achieve the same degree of thickening.

Most of the additives used in lubricating oils are also effective in greases. And some, such as the solid lubricants graphite and molybdenum disulfide, are much more effective in greases than in oils.

Table 20.11 lists some of the many different components which may be used in greases. The possible combinations of these components, and their different proportions, lead to an infinite range of grease formulations. In practice, a typical grease consists of a mineral oil in which are dispersed about 10 percent of a soap thickener, about 1 percent of antioxidant, and small amounts of other additives such as corrosion inhibitors, antiwear or extreme-pressure agents, and structure modifiers.

The most important physical characteristic of a grease is its relative hardness or softness, which is called *consistency.* Consistency is assessed by measuring the dis-

TABLE 20.11 Some Components Used in Grease Manufacture

Base oils	Thickeners	Additives
Mineral oils	Sodium soap	Antioxidants
Silicones	Lithium soap	EP additives
Diesters	Aluminum soap	Corrosion inhibitors
Chlorinated silicone	Lithium complex	Metal deactivators
Fluorocarbons	Aluminum complex	Tackiness additives
Phosphate esters	Bentonite clay	Water repellants
	PTFE	Structure modifiers
	Indanthrene dye	

tance in tenths of a millimeter to which a standard metal cone penetrates the grease under a standard load; the result is known as the *penetration.* A widely used classification of greases is that of the American National Lubricating Grease Institute (NLGI), and Table 20.12 shows the relationship between NLGI number and penetration.

TABLE 20.12 NLGI Grease Classification

NLGI number	Worked penetration at 25°C
000	445–475
00	400–430
0	355–385
1	310–340
2	265–295
3	220–250
4	175–205
5	130–160
6	85–115

The consistency of a grease varies with temperature, and there is generally an irregular increase in penetration (softening) as the temperature increases. Eventually a temperature is reached at which the grease is soft enough for a drop to fall away or flow from the bulk of the grease; this is called the *drop point.* The drop point is usually taken to be the maximum temperature at which the grease can be used in service, but several factors confuse this situation:

1. The drop point is measured in a standard apparatus which bears no resemblance to any service equipment, so that the correlation with service use may be poor.
2. Some greases will never give a drop point because chemical decomposition begins before the thickener structure breaks down.
3. A grease may be a satisfactory lubricant above its drop point, although then it will behave like an oil rather than a grease.

4. Some greases can be heated above their drop points and will again form a grease when cooled, although normally the re-formed grease will be markedly inferior in properties.

At high temperature greases will decompose thermally or oxidatively in the same way as lubricating oils. In addition, the grease structure may break down, as explained previously, or the thickener itself may decompose. Table 20.13 depicts the general effects of temperature on lubricating greases.

A grease behaves as an extreme form of non-Newtonian fluid, and its viscous properties change when it is sheared in a feed line or a bearing. Occasionally the viscosity increases with small shear rates, but more commonly the viscosity decreases as the shear rate increases, until eventually the viscosity reaches that of the base oil. For this reason, the viscosity of the base oil may be important if the grease is to be used in high-speed equipment.

The mechanism by which a grease lubricates is more complicated than that for an oil, and it depends partly on the geometry of the system. Some part of the total grease fill distributes itself over the contacting surfaces and is continually sheared in the same way as an oil. This part of the grease performs the lubricating function, giving either hydrodynamic lubrication or boundary lubrication according to the load, speed, and effective viscosity.

The remainder of the grease is swept out of the path of the moving parts and remains almost completely static in the covers of a bearing or the upswept parts of a gearbox. Because of the solid nature of the grease, there is virtually no circulation or exchange between the static, nonlubricating portion and the moving, lubricating portion.

In a plain bearing or a closely fitting gearbox, a high proportion of the grease fill is being continuously sheared at the contacting surfaces. In a roller bearing or a spa-

TABLE 20.13 Temperature Limits in Degrees Celsius for Greases as a Function of Required Life

Grease; type of limit	Life, h				
	1	10	10^2	10^3	10^4
Synthetic greases; oxidation limit with unlimited oxygen present	275 to 285	255 to 265	225 to 240	200 to 225	175 to 200
Synthetic greases; drop-point limit with inorganic thickeners	250	250	250	250	250
Mineral-oil greases; upper limit imposed by drop point depends on thickener; oxidation dependent on amount of oxygen present	80 to 200	80 to 200	80 to 200	80 to 200	80 to 200
Mineral greases; oxidation limit with unlimited oxygen	185 to 200	160 to 175	135 to 150	110 to 125	85 to 100
Mineral greases; lower limit imposed by high torque	−50 to −10	−50 to −10	−50 to −10	−50 to −10	−50 to −10
Synthetic greases; lowest limit imposed by high torque	−70 to −80	−70 to −80	−70 to −80	−70 to −80	−70 to −80

SOURCE: Ref. [20.2]

cious gearbox, a small proportion of the grease is continuously sheared and provides all the lubrication, while the larger proportion is inactive.

If a rolling bearing or gearbox is overfilled with grease, it may be impossible for the surplus to escape from the moving parts. Then a large quantity of grease will be continuously sheared, or "churned," and this causes a buildup of temperature which can severely damage the grease and the components. It is, therefore, important with grease lubrication to leave a void space which is sufficient to accommodate all the surplus grease; in a ball bearing, this could be more than 60 percent of the total space available.

The static grease which is not involved in lubrication may fulfill two useful functions: It may provide a very effective seal against the ingress of dust or other contaminants, and it can prevent loss of base oil from the grease fill. In addition, the static grease may form a reservoir from which to resupply the lubricated surfaces if the lubricating portion of the grease becomes depleted.

If the void space in the system is large, i.e., in a large bearing or gearbox, then usually it is desirable to use a stiffer grease to avoid the surplus grease "slumping" into the moving parts and being continuously churned. The advantages and disadvantages of grease lubrication are summarized in Table 20.14.

The selection of a grease for a specific application depends on five factors: speed, load, size, temperature range, and any grease feed system. For average conditions of speed, load, and size with no feed system, an NLGI no. 2 grease would be the normal choice, and such a grease with a mineral-oil base is sometimes known as a multipurpose grease. The effect of the various factors on selection can then be summarized in a few paragraphs.

1. *Speed* For high speeds, a stiffer grease, NLGI no. 3, should be used except in plain bearings, where no. 2 would usually be hard enough. For lower speeds, a softer grease such as no. 1 or no. 0 should be used.

TABLE 20.14 Advantages and Disadvantages of Grease Lubrication

Advantages
1. Maintain effective lubricant film on surfaces during a shutdown
2. Provide useful squeeze-film lubrication
3. Give effective sealing of rolling bearings
4. Maintain a reserve supply of lubricant in the vicinity of the bearing
5. Reduce contamination problems compared with oil
6. Provide an effective carrier for solid lubricants for antiseize or highly loaded situations
Disadvantages
1. Ineffective cooling
2. Limitations on bearing speed
3. Possible incompatibility with other similar greases
4. Lower oxidation resistance
5. Poorer storage stability

2. *Load* For high loads, it may be advantageous to use EP additives or molybdenum disulfide. Because higher loads will lead to higher power consumption and therefore higher temperature, a stiffer grease such as no. 3 or a synthetic-base oil may help.
3. *Size* For large systems, use a stiffer grease, no. 3 or no. 4. For very small systems, use a softer grease, such as no. 1 or no. 0.
4. *Temperature range* The drop point should be higher than the maximum predicted operating temperature. For sustained operation at higher temperatures, a synthetic-base oil may be necessary. For very high temperatures, about 230°C, one of the very expensive fluorocarbon greases may be required.
5. *Feed systems* If the grease is to be supplied through a centralized system, usually it is desirable to use one grade softer than would otherwise be chosen (i.e., use a no. 0 instead of a no. 1 or a no. 00 instead of a no. 0). Occasionally a particular grease will be found unsuitable for a centralized feed because separation occurs and the lines become plugged with thickener, but this problem is now becoming less common.

20.9 SOLID LUBRICANTS

Any solid material can act as a solid lubricant provided that it shears readily and smoothly when interposed between sliding surfaces. Some of the wide range of solids which can be used are listed in Table 20.15.

TABLE 20.15 Materials Used as Solid Lubricants

Layer-lattice compounds	
Molybdenum disulfide	Graphite
Tungsten diselenide	Tungsten disulfide
Niobium diselenide	Calcium fluoride
Graphite fluoride	
Polymers	
PTFE	PTFCE
PVF_2	FEP
Acetal	Polyimide
Polyphenylenesulfide	Polysulfones
Metals	
Silver	Gold
Tin	Lead
Barium	Gallium
Other inorganics	
Boron nitride	Molybdenum trioxide

There are many other desirable properties, including the following:

1. Ability to adhere to one or both of the bearing surfaces to ensure retention in the contact area
2. Chemical stability over the required temperature range in the particular environment
3. Sufficient resistance to wear
4. Nontoxicity
5. Easy application
6. Economy

Most of the available materials are eliminated by these requirements, and in practice almost all solid lubrication in engineering is provided by three materials—graphite, molybdenum disulfide, and polytetrafluoroethylene (PTFE).

Solid lubricants can be used in several different forms, such as loose powder, adhering powder, bonded film, or solid block. In the form of a solid block, the material is often called a *dry* bearing material rather than a solid lubricant.

20.9.1 Graphite

Graphite is probably the oldest known of the three main solid lubricants, and it has ceased to be the dominant one since about 1950. It is a grayish black crystalline form of carbon in which the atoms are arranged hexagonally in monatomic layers. The strong chemical bonds between the carbon atoms give strength to the layers, so that they resist bending or fracture and can carry useful loads. The bonds between the layers are relatively weak, and so the layers slide easily over each other and can be easily separated.

When graphite is used as a lubricant, the crystals orient themselves so that the layers are parallel to the bearing surfaces. The layers then adhere fairly well to the bearing surfaces, but slide easily over each other to give low friction.

The low shearing forces, and therefore the low friction, are not an inherent property of the graphite but are strongly influenced by the presence of moisture or certain other adsorbents. If graphite is used in a very dry atmosphere, the crystal layers have quite high interlayer bonding forces, and the friction and wear are high.

The biggest advantage of graphite over molybdenum disulfide and PTFE is its electrical conductivity, and it is almost universally used as a component in electric brushes. Its coefficient of friction varies from 0.05 at high loads to 0.15 at low loads, and these low values are maintained to over 500°C in air.

In block form, graphite has quite high structural integrity. It is commonly used in an impure form as graphitized carbon, in which the degree of crystallization can vary from 30 to over 80 percent of that of crystalline graphite. The frictional and structural properties and abrasiveness vary with the purity and degree of graphitization, and graphite technology is complex.

Graphite can be used in block form, as free powder, or as a coating deposited from dispersion in a liquid. It adheres readily to many solid surfaces, but probably its strength of adhesion is generally lower than that of molybdenum disulfide.

20.9.2 Molybdenum Disulfide

Molybdenum disulfide has also been known as a solid lubricant for centuries, but because it is similar in appearance, it has often been confused with graphite. Its use

has increased enormously since about 1950, and for high-technology applications it is now generally preferred to graphite. In crude form, molybdenum disulfide is found naturally, sometimes in very large quantities, as molybdenite, the most common ore of molybdenum.

Like graphite, molybdenum disulfide is a dark gray crystalline material with a hexagonal layer-lattice structure. The bond strengths within the layers are very high, whereas those between layers are very low. The load-carrying capacity normal to the crystal planes is therefore high, and the shear strength parallel to the crystal layers is very low.

Unlike graphite, molybdenum disulfide does not require the presence of adsorbed moisture or other vapors to give low interplanar strength. Its low friction is therefore an inherent property which is maintained in high vacuum and in dry atmospheres.

Molybdenum disulfide starts to oxidize significantly above 350°C in oxygen and 450°C in air, but the main oxidation product is molybdic oxide, which is itself a fair high-temperature lubricant. In high vacuum the disulfide is said to be stable to 1000°C, and it outgasses (evaporates) very slowly, so that it has been widely used in space.

The adhesion to metals and many other solid surfaces is excellent, and durable coatings can be produced on metal surfaces by burnishing (a coating of loose powder is rubbed into the surface to give a very thin, shiny, and strong film). The powder may be applied free or from dispersion in a volatile liquid. Durable coatings can also be obtained by sputtering, but this technique is expensive and is not widely used.

Bonded coatings are widely used, in which molybdenum disulfide powder is incorporated in almost any effective adhesive, including many polymers, natural resins, or molten solids. The performance of the softer bonded coatings is also improved if they are carefully burnished before use. The coefficient of friction of burnished films varies from 0.02 to about 0.12. But for bonded films the friction depends on the nature of the binder and the percentage composition, and it can vary from 0.02 to about 0.3.

Molybdenum disulfide is often added to oils or greases to give high load-carrying capacity, especially at low running speeds. There is also strong evidence that the addition of up to 2 percent to vehicle engine oils produces a small but significant fuel savings without any apparent disadvantages.

At one time molybdenum disulfide suffered considerable criticism, especially for reported corrosion of steels and aluminum. Some of this may have been due to its use in conjunction with graphite. Some was certainly caused by failure to understand that solid lubricants, unlike oils and greases, do not normally protect against corrosion. It is probably fair to say that molybdenum disulfide is now well understood and that, when properly used, it is a very valuable solid lubricant.

20.9.3 Polytetrafluoroethylene

Abbreviated PTFE, polytetrafluoroethylene is a polymer produced from ethylene in which all the hydrogen atoms have been replaced by fluorine atoms. This fluorination produces a material of very high chemical stability and low intermolecular bond strength, while the polymerization of an ethylene-type molecule gives long, straight molecular chains.

The result is a white solid which consists of masses of parallel long-chain molecules that slide easily past one another. This leads to the same sort of low shear strength parallel to the chains which is found in molybdenum disulfide and to a high

load-carrying capacity normal to the chains, but significantly lower than that of molybdenum disulfide.

PTFE is often used in the form of solid components, occasionally in bonded coatings, and very rarely as free powder. In addition, it has been used very successfully in composites, and two types are particularly effective.

The coefficient of friction of pure PTFE varies from 0.02 at high load to about 0.1 at low load. It is a rather soft solid, so that its load-carrying capacity is limited and its wear rate is high. It therefore needs reinforcement for use in highly loaded bearings. One successful form of reinforcement is to incorporate the PTFE in the pores of a sintered metal, especially bronze. In one composite, further reinforcement is obtained by dispersing fine particles of lead in the PTFE.

A second, and probably even more successful, form of reinforcement is by means of strengthening fibers. Glass fiber or carbon fiber can be incorporated in solid PTFE components, but the resulting high structural strength is obtained at the cost of an increase in the coefficient of friction to between 0.06 and 0.2. An alternative technique is to interweave PTFE fibers and reinforcing fibers of glass, metal, rayon, or other synthetics. Some of the resulting composites have outstanding strength with low wear rate and low friction.

PTFE can be used in air to about 250°C, but in high vacuum it outgasses slowly, and so it is used in spacecraft only in well-shielded locations.

Because of its high chemical stability, PTFE can be used safely in oxygen systems and in many types of chemical plants. It is nontoxic in almost all situations and is therefore used in the pharmaceutical and food industries, even in situations where low friction is not required, and as the nonstick lubricant in domestic cooking utensils.

20.9.4 Miscellaneous Solid Lubricants

Other solid lubricants are used to a relatively minor degree, in situations where they have specific advantages. They can be classified in three broad categories: inorganics, polymers, and metals.

The inorganics include a number of materials similar to molybdenum disulfide, known generally as the lubricating dichalcogenides. None of these occurs naturally, and the synthetic materials are relatively expensive. Tungsten disulfide has a higher oxidation temperature, and both tungsten disulfide and tungsten diselenide oxidize more slowly than molybdenum disulfide. Niobium diselenide has better electrical conductivity and has been used in electric contact brushes, but in fact molybdenum disulfide composites have been shown to be equally satisfactory.

Other inorganics have been used for their much higher temperature limits, and these include molybdic oxide, boron nitride, graphite fluoride, and calcium fluoride.

The low friction and chemical inertness of PTFE make it difficult to bond to other materials, and two other fluorinated polymers have been recommended for their better bonding behavior: polyvinylfluoride (PVF_2) and polytrifluorochloroethylene (PTFCE). But in both cases the advantages of better bonding and slightly higher structural strength are offset by higher friction.

For higher temperatures, polyimide, polysulfones, and polyphenylene sulfide can be used unlubricated. Other polymers, such as nylons, acetals, and phenolics, are occasionally used unlubricated where sliding speeds are low, but they require lubrication by oil, grease, or water for really useful performance.

Silver, gold, and tin have useful antigalling properties in slow sliding, but metallic coatings are mainly used as lubricants only in high vacuum, where silver, gold, barium, gallium, and lead have all been used successfully.

20.10 GAS LUBRICATION

Gases can be used to provide full-fluid-film lubrication in the same ways as liquids in hydrodynamic and externally pressurized bearings. The physical laws governing behavior are the same for both liquids and gases, but the very low viscosities of gases lead to considerable practical differences in their use, especially in self-pressurizing, or "gas-dynamic," bearings:

1. Operating speeds are much higher to compensate for low viscosity.
2. Surface finish and precision must be better because of the much smaller lubricant-film thickness.
3. Lubricant flow rate is higher for the same pressure differential.
4. Load-carrying capacity is generally low.

As a result, gas bearings tend to be small, high-speed, and lightly loaded, with tight tolerances and high-quality surface finishes. The overall design and manufacturing cost is high, and they are mainly used in high-technology applications.

Any gas or vapor can be used provided that it is chemically stable under the operating conditions and does not attack any of the system materials. If no chemical change takes place, there is no upper temperature limit to the use of a gas, and the viscosity increases as temperature increases.

Air is the most common gas used in gas lubrication. Nitrogen or helium may be used where inertness is important. Otherwise, any gas which is available can be used, especially if it is available at high enough pressure for external pressurization.

Some of the advantages of gas lubrication are high precision, very low friction, cleanliness, and ready availability of lubricant. The greatest potential advantage is the wide temperature range. In theory, it should be possible to design a gas bearing to operate from −250 to +2000°C. The corresponding disadvantages include the demanding design and construction requirements, the low load-carrying capacity, and the need for a very clean gas supply. Examples of important applications of gas bearings are dentists' air-turbine drills, high-precision grinding spindles, and inertial gyroscopes.

20.11 LUBRICANT FEED SYSTEMS

In many lubricated components, no feed system is needed, because the initial lubricant fill is sufficient to last the required life. A feed system becomes necessary when the lubricant must be replaced or replenished, for one of the following reasons:

1. The temperature is too high, so that the lubricant must be removed and replaced by a fresh charge of cooler lubricant.
2. Lubricant becomes depleted by leakage or creepage and must be topped up.
3. Lubricant decomposes and must be replaced with a fresh charge.
4. Lubricant becomes contaminated and must be replaced with clean material.

Where the rate of loss or deterioration is relatively low, it will be sufficient to provide a facility for occasional topping up by means of an oil can or a grease gun, provided that access to the lubricated component is available. Where this occasional manual topping up is not adequate, a lubricant feed system will be needed. It is

beyond the scope of this chapter to describe the whole range and design of lubricant feed systems available. It is only possible to give a brief description of the main types and the factors involved in selecting them.

20.11.1 Internal Circulation

One obvious way to reduce oil temperature, slow down the increase in contamination, and increase the life is simply to increase the quantity of oil supplied in the initial fill. This requires an increase in the volume of space available for oil or, in other words, the creation of an oil reservoir or sump adjacent to the lubricated bearings or gears.

Circulation of the oil can be ensured by arranging for the moving parts to dip below the surface of the oil. But they should not be completely submerged because the resulting viscous drag and churning of the oil lead to excessive power consumption and heating. For slow-moving components this problem is not serious, but for high speeds the depth of immersion is critical, and the following guidelines are useful:

1. Gears should be immersed to twice the tooth height. In a vertical train, the oil level should be just below the shaft of the lowest gear.
2. Rolling bearings should be immersed to halfway up to the lowest rollers or balls.
3. Crankshafts should be immersed so that the oil level is just above the big-end bearings at their lowest point.
4. The oil level should be higher for slow operation than for higher-speed systems.

Oil is carried by the partly submerged components to contacting surfaces and is also spread by splashing. Where transfer by these two mechanisms is inadequate, the oil feed can be improved by the use of rings or disks, as shown in Fig. 20.7. Both operate by providing a larger surface with higher peripheral speed to transfer the oil, but they do not cause excessive viscous drag because they are both uniform in shape.

Disks have an advantage over rings in that they can be designed to propel oil axially as well as radially, and this is particularly useful for bearing lubrication. Usually plain bearings cannot be adequately lubricated by partial immersion in oil unless the oil flow is augmented by a ring or a disk. If a weir is incorporated, part of the splashed oil can be trapped and directed to critical locations.

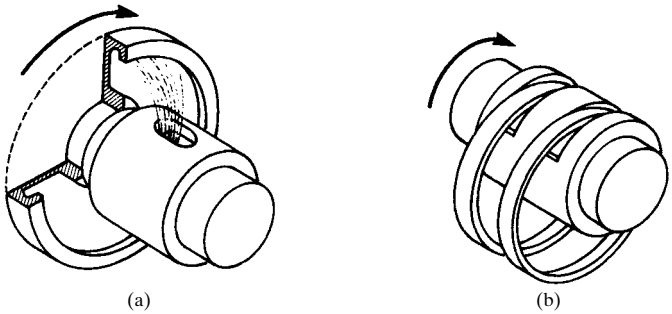

(a) (b)

FIGURE 20.7 Ring and disk lubrication. (*a*) Disk; (*b*) ring. *(From Ref. [20.1].)*

20.11.2 Topping Up Systems

Where the main problem is loss of oil by leakage or creep, it may be sufficient to set up a wick or drip feed to provide a small-scale supply. Wicks or pads consist of porous or permeable materials such as felt which transfer oil by capillary action to the bearing surfaces. The pads may form a path from a reservoir to the bearing or may simply contain a small initial oil fill to increase the quantity available and feed it slowly to the bearing. This latter approach is commonly used in small electric motors.

Drip feeds consist of small reservoirs mounted above the bearing or gears and equipped with a feed tube with some form of flow regulation and usually a sight glass. They can be used to provide a much higher flow rate than a wick.

20.11.3 Centralized Total-Loss Systems

Wick and drip feeds are examples of total-loss systems, in which no attempt is made to collect the oil after feeding it to the bearings or gears. Far more sophisticated total-loss systems can be used to supply oil or grease to a number of separate components.

The requirements of centralized total-loss systems are basically very simple. A typical system consists of a reservoir, a single pump to pressurize a manifold, and a number of controllers, each regulating the feed to a single lubrication point. Alternatively, the flow to several lines may be controlled by a multipiston pump, in which individual single-cylinder piston pumps are operated by cams on a common camshaft immersed in the lubricant. The number of outlets can vary from one to several hundred.

The main advantage of centralized total-loss systems is that they reduce the labor required where a large number of components need relubricating. They are also valuable where the lubrication points are not readily accessible. Their disadvantages are that they do not provide any form of cooling or removal of contaminants, and there is no recovery of used lubricant.

20.11.4 Oil Mist or Fog Systems

One type of total-loss system which has become widely used in recent years is oil mist or fog, in which fine droplets of oil are carried by a stream of air from a reservoir to a bearing or gears. The mist or fog of oil in air is produced by passing the airstream through the reservoir at low speed and low pressure. The oil is usually formulated to have low surface tension. The resulting dispersion of oil droplets is passed through steel, copper, or plastic pipes to the vicinity of the lubricated component. Passage through fine nozzles, or reclassifiers, then increases the linear flow rate to something over 45 meters per second (m/s) and thus causes the oil droplets to coalesce, producing a flow of liquid oil to the lubrication point.

Oil mist and fog systems have two advantages over other total-loss systems in that the oil supply rate can be very low, resulting in a clean system, and the airflow gives a significant amount of cooling.

20.11.5 Oil-Circulation Systems

The most sophisticated centralized systems are those in which the lubricant is collected after use and returned to the reservoir for recirculation. The basic require-

ments of such a system are a reservoir, a pump, possibly a flow divider or proportioner, feed lines, and return lines.

In practice a full-circulation system is likely to be more complex and to include many of or all the following components:

Multiple or divided reservoirs
Heaters
Coolers
Oil-level warning devices
Full-flow filtration to protect the pump
Bypass filtration
Pressure switches and alarms
Water separators
Chip detectors
Sampling points
Sight glass

Circulation systems give a high degree of control over the quality and quantity of oil supplied to each component, enabling the cleanliness and the temperature of the oil to be controlled. Their only disadvantage is their complexity and therefore their cost.

20.12 LUBRICANT STORAGE

The storage of lubricants, like that of any other class of goods, depends first on making rational decisions about the number of varieties and the quantities which it is necessary to store. The special factors which then need to be considered in storing lubricants are as follows:

1. Lubricants are an integral part of the precision components in which they are used. They must therefore be treated as precision components and protected carefully against contamination by dirt, water, or other materials. Never store them in the open.
2. Because most lubricants are liquids, they have no characteristic shapes, and it is very easy to use the wrong lubricant in a machine. This is always undesirable and sometimes catastrophic. So it is important to label lubricant containers carefully and to control their issue and use.
3. Some lubricants deteriorate in storage, and it is important to use supplies in proper rotation and ensure that storage lives are not exceeded.
4. Many lubricants are flammable, and special precautions are necessary to reduce fire risk.
5. Lubricants are slippery, and spillages can cause accidents. Floor gratings and drainage channels should be supplied, and absorbent powders or granules kept available to absorb spilled oil.
6. Oil drums are very convenient and satisfactory containers for storing lubricants, but water can collect in the recessed top and enter even through sealed apertures to contaminate the contents. Drums should always be stored horizontally and never upright.

REFERENCES

20.1 A. R. Lansdown, *Lubrication: A Practical Guide to Lubricant Selection,* Pergamon, New York, 1982.

20.2 M. J. Neale (ed.), *The Tribology Handbook,* 2d ed., Butterworth, London, 1996.

20.3 D. Godfrey, "Boundary Lubrication," in P. M. Ku (ed.), *Interdisciplinary Approach to Friction and Wear,* NASA SP-181, 1968.

CHAPTER 21
SEALS

R. Bruce Hopkins, Ph.D., P.E.
The Hopkins Engineering Co., P.C.
Cedar Falls, Iowa

21.1 ELASTOMERIC SEAL RINGS

Seal rings of the O-ring type are used as both static and dynamic seals. Static seals serve the same purpose as gaskets; that is, they provide a seal between two members that are not intended to undergo relative motion. Dynamic seals, however, are used where rotating or reciprocating motion is intended to occur.

O-rings are molded to the size of the elastomeric material with a circular cross section, as shown in Fig. 21.1*a*. The *size* is designated by the cross-sectional diameter *w* and the nominal inside diameter (ID). The standard sizes specified in SAE J120a are summarized in Table 21.1. The first size number in a group is associated with the minimum inside diameter, and the last size number is associated with the maximum inside diameter. Some manufacturers provide additional sizes that extend the range of inside diameters for a particular cross-section size. The nominal inside diameters were selected to provide dynamic seals in cylinder bores dimensioned in inches and common fractions of inches. Either SAE J120a or manufacturers' recommendations should be consulted to obtain the recommended compression of the cross section. The compression is different for static and dynamic applications.

The rectangular-section ring in Fig. 21.1*b* is manufactured by cutting lengths from a tube of molded material. The standard sizes listed in SAE J120a are summarized in Table 21.2. The first size number in a group is associated with the minimum inside diameter, and the last size number is associated with the maximum inside diameter. Rectangular-section rings are suitable for static applications with pressures up to 1500 psi [10.3 newtons per square millimeter (N/mm^2)].

The standard shape of groove for sealing rings is shown in Fig. 21.2. The actual groove dimensions depend on the type and size of the seal ring cross section and the nature of the application. Recommended groove dimensions are provided in SAE J120a and in the manufacturers' literature. Because elastomeric materials are almost incompressible, it is necessary to provide sufficient volume for the seal ring in the groove. The recommended groove dimensions do so.

For static seals, a finish on surfaces contacted by the seal ring that is rougher than 32 μin (0.8 μm) may lead to leakage. Because rough finishes accelerate seal wear in dynamic seals, a surface finish of 5 to 16 μin (0.13 to 0.4 μm) is preferred. Friction is

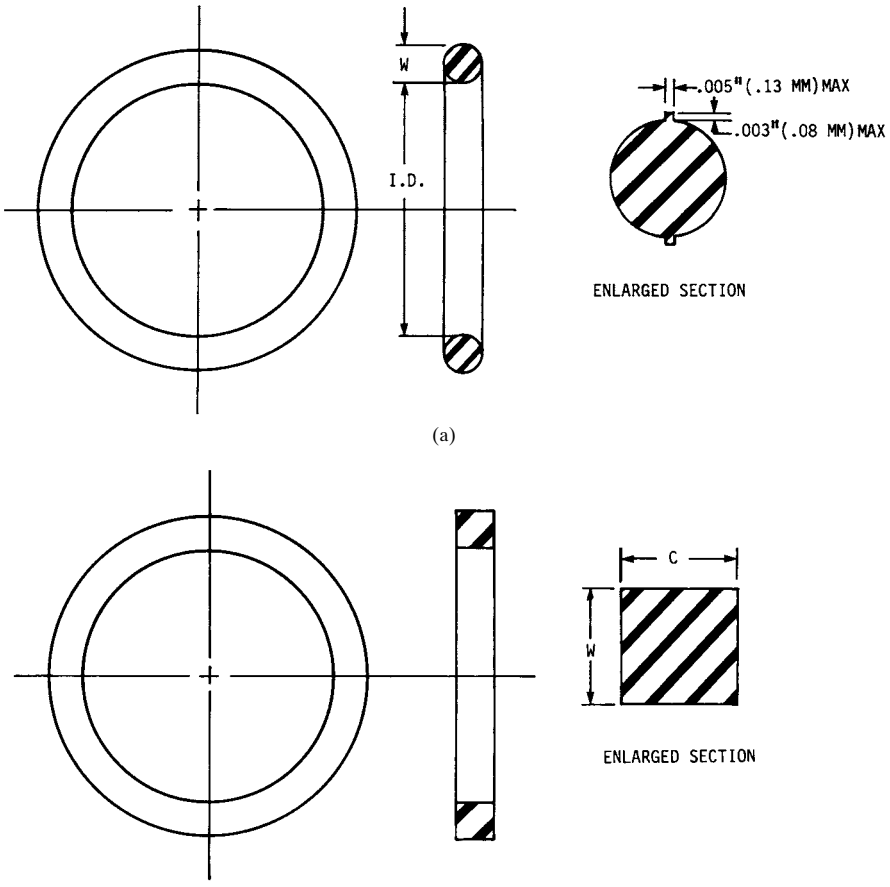

FIGURE 21.1 Seal rings. (*a*) O-ring; (*b*) rectangular-section ring.

TABLE 21.1 Standard Sizes of O-Rings

Size no.	*w*, in	Actual ID, in	
		Minimum	Maximum
006 to 045	0.070 ± 0.003	0.114 ± 0.005	3.989 ± 0.015
110 to 163	0.103 ± 0.003	0.362 ± 0.005	5.987 ± 0.023
210 to 281	0.139 ± 0.004	0.734 ± 0.006	14.984 ± 0.060
325 to 349	0.210 ± 0.005	1.475 ± 0.010	4.475 ± 0.010
425 to 460	0.275 ± 0.006	4.475 ± 0.015	15.475 ± 0.015

TABLE 21.2 Standard Sizes of Rectangular-Section Rings

Size no.	*w*, in	*c*, in	Actual ID, in	
			Minimum	Maximum
R006 to R045	0.066 ± 0.004	0.066 ± 0.003	0.114 ± 0.005	3.989 ± 0.015
R110 to R163	0.099 ± 0.004	0.099 ± 0.003	0.362 ± 0.005	5.987 ± 0.023
R210 to R281	0.134 ± 0.004	0.134 ± 0.004	0.734 ± 0.006	14.984 ± 0.060
R325 to R349	0.203 ± 0.005	0.203 ± 0.005	1.475 ± 0.010	4.475 ± 0.015
R425 to R460	0.265 ± 0.005	0.265 ± 0.005	4.475 ± 0.015	15.475 ± 0.030

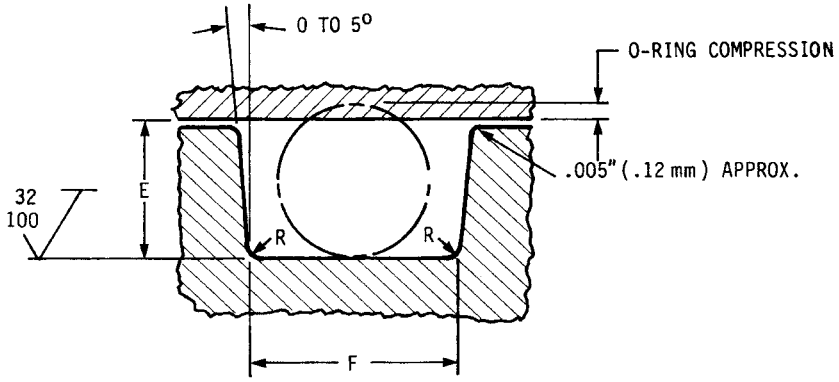

FIGURE 21.2 Shape of groove for seal rings.

reduced with the smoother finish, but surfaces smoother than 5 μin (0.13 μm) may not be satisfactory for reciprocating motion.

A static seal ring application in which the joint is subject to internal pressure only is shown in Fig. 21.3*a*. The groove design in Fig. 21.3*b* is for a joint subject to external pressure or internal vacuum only. It is generally advisable in these applications to use as large a seal ring cross section as possible because the tolerance on the groove depth is greater with larger cross sections. This requires less precise machining and tends to reduce manufacturing costs.

O-rings are also used as static seals for hydraulic tube fittings that are screwed into tapped holes. Recommended machining dimensions are provided in SAE J514 (July 2001).

Elastomeric sealing rings are most commonly made of nitrile (Buna N) compounds. These compounds are low in cost and are compatible with alcohol, gasoline, hydraulic fluids, lubricating oils, and water. They also are suitable for temperatures ranging from –67 to 257°F (–55 to 125°C). For resistance to higher temperatures or compatibility with other fluids, other compounds are employed. Among these compounds are butyl, ethylene propylene, neoprene, fluorocarbon, silicone, and polyurethane.

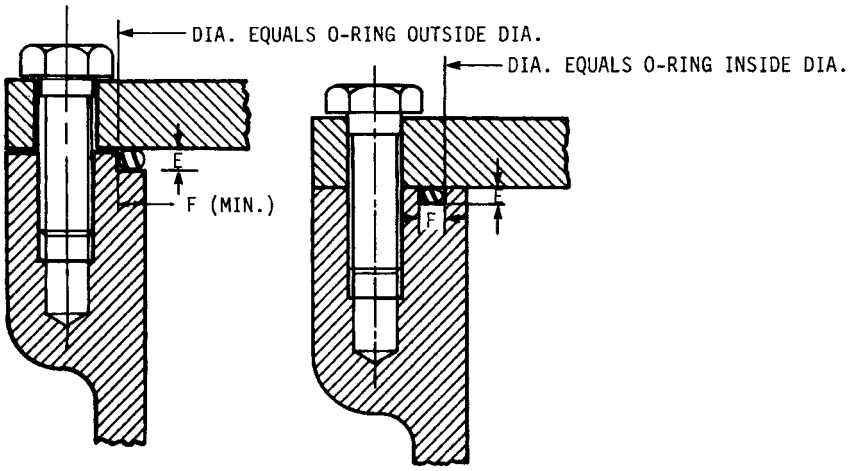

FIGURE 21.3 Static O-ring seals. (*a*) Joint subject to internal pressure only; (*b*) joint subject to external pressure.

21.2 SEALS FOR ROTARY MOTION

Seals are required on rotating shafts to retain working fluids, to retain lubricants, and to exclude dirt. The selection of a seal type depends on fluid pressure, shaft speed, and whether any leakage can be permitted. There are many variations of the basic seal types that are available from various manufacturers.

21.2.1 O-Rings

Attempts to use O-rings as seals for rotating shafts have not always been successful because the elastomers shrink when heated. If an O-ring is under tension, friction between the ring and the shaft generates heat that makes the ring shrink. Contraction of the ring creates additional heat, and failure occurs rapidly.

O-rings have been used successfully on rotating shafts when they are installed under compression by using a smaller-than-normal groove diameter in the housing. Satisfactory life can then be obtained at shaft speeds up to 750 feet per minute (ft/min) [3.8 meters per second (m/s)] and sealed pressures up to 200 psi (1.38 N/mm^2). Recommended O-ring cross sections are 0.139 in (3.53 mm) for speeds up to 400 ft/min (2.0 m/s), 0.103 in (2.62 mm) for speeds from 400 to 600 ft/min (2.0 to 3.0 m/s), and 0.070 in (1.78 mm) for speeds exceeding 600 ft/min (3.0 m/s) [21.1].

21.2.2 Radial Lip Seals

A section through a radial lip seal is shown in Fig. 21.4. This type is used primarily for retention of lubricants and exclusion of dirt. It is suited for conditions of low lubricant pressure, moderate shaft speeds, less-than-severe environmental conditions,

and situations where slight leakage may be permitted. Radial lip seals are compact, effective, inexpensive, and easily installed.

The outer case is held in the bearing housing by an interference fit. The garter spring provides a uniform radial force to maintain contact between the elastomeric sealing lips and the shaft. Lubricant leakage is reduced when hydrodynamic sealing lips are used. Such lips have very shallow grooves molded into the primary sealing lip to pump lubricant out of the contact area. Hydrodynamic sealing lips are manufactured for rotation in one direction only or for rotation in either direction.

Sealing lips are most commonly made of nitrile (Buna N) rubber compounds because of their compatibility with greases, lubricating oils, and hydraulic fluids. The nitrile compounds have poor to fair compatibility with extreme-pressure (EP) additives used in some gear lubricants. A polyacrylate or fluoroelastomer compound is a better choice with EP lubricants.

Radial lip seal terminology is presented in SAE J111 (October 2002), and recommendations for applications are made in SAE J946 (October 2002). One of the purposes of the secondary sealing lip shown in Fig. 21.4 is to exclude dust. That lip, however, leads to higher seal temperatures because of the additional friction, and the higher temperatures lead to earlier seal failure. Dual lip seals are not recommended for shaft speeds exceeding 150 ft/min (0.76 m/s) [21.2].

A minimum hardness of Rockwell C 30 is recommended for the portions of shafts that contact the sealing lips in order to prevent scoring of the shaft. If the shaft may be damaged in handling, a minimum hardness of Rockwell C 45 will provide protection against damage. A hard surface can be provided for soft shafts by use of a hardened wear sleeve of thin steel that is held in place by an interference fit.

Radial lip seals function best with carbon-, alloy-, or stainless-steel shafts or nickel-plated surfaces. Use with aluminum alloys, brass, bronze, magnesium, zinc, or similar metals is not recommended. Shaft surface texture should be in the range of 10 to 20 μin (0.25 to 0.50 μm). This condition can best be met by plunge grinding.

This type of seal is limited to sealing pressures of 3 psig (0.02 N/mm^2 gauge) at shaft speeds exceeding 2000 ft/min (10.2 m/s) and 7 psig (0.05 N/mm^2 gauge) at speeds up to 1000 ft/min (5.1 m/s). When pressures exceed these limits, a mechanical face seal is preferable.

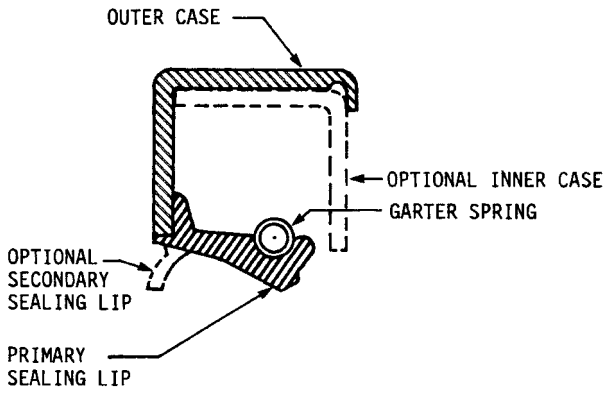

FIGURE 21.4 Cross section of radial lip seal.

21.2.3 Face Seals

Whereas a radial lip seal contacts the shaft circumference, a face seal acts against a surface perpendicular to the shaft axis. The seal may be mounted in a housing and seal against a shoulder or collar on the shaft. The seal also may be mounted on the shaft and seal against a surface on the housing. Some elastomeric face-sealing elements are loaded by mechanical springs, whereas others are not.

Elastomeric face seals (Fig. 21.5*a*) are used to retain lubricants. For high-speed applications, the lubricant should be on the side where centrifugal force throws the lubricant into the sealing area. These seals have the disadvantage of requiring rather precise location with respect to the sealing surface in order to provide the proper force on the seal. The sealing surface must be flat and smooth, with a surface finish of 10 to 20 μin (0.25 to 0.50 μm). Less rigid control of surface flatness is required for low speeds.

Mechanical face seals are used in situations where a radial lip seal or elastomeric face seal will not be satisfactory. Abrasive conditions, such as those encountered by earth-moving machinery and mining machinery, may dictate the use of a mechanical face seal. A mechanical seal is frequently used in the automotive coolant pump (Fig. 21.5*b*), in which the pressure is relatively low. Here, the stationary spring-loaded seal ring contacts a flat surface on the rotor.

If the seal in Fig. 21.5*b* were used with high-pressure fluid, a high axial sealing force would result. Friction between the rotor and stator could possibly cause overheating of the seal elements. Consequently, a balanced mechanical face seal, such as in Fig. 21.5*c,* is used for higher pressures. These seals are proportioned so that much of the force due to pressure is balanced. This leaves a small net force to provide contact between rotor and stator.

Another type of face seal, Fig. 21.6, is used to seal lubricants in rotating elements of machines that operate in environments where water, mud, or dust must be excluded. The seal consists of two hardened steel rings with lapped sealing surfaces that are forced together by surrounding elastomeric rings. The seal surfaces are tapered so that the point of contact moves inward as wear occurs. The seal rings do not contact the shaft that they surround; instead, one seal ring is driven by the rotating component through the elastomeric ring.

21.2.4 Metal Sealing Rings

Cast-iron sealing rings are used in hydraulic applications where oil must be introduced through a rotating shaft (Fig. 21.7). A typical application is to operate a clutch in an automatic transmission for a motor vehicle. Ring cross-sectional dimensions are similar to those for engine piston rings of the same outside diameter. Information on designing to accommodate these rings is provided in SAE J281 (Sept. 1980) and SAE J1236 (May 1995).

21.2.5 Compression Packings

The stuffing box (Fig. 21.8) is used to seal fluids under pressure with either rotating or reciprocating shafts. Sealing between the packing and the shaft occurs as a result of axial movement of the gland when the nuts are tightened. Friction between the packing and the shaft causes wear, and so periodic tightening of the nuts is required.

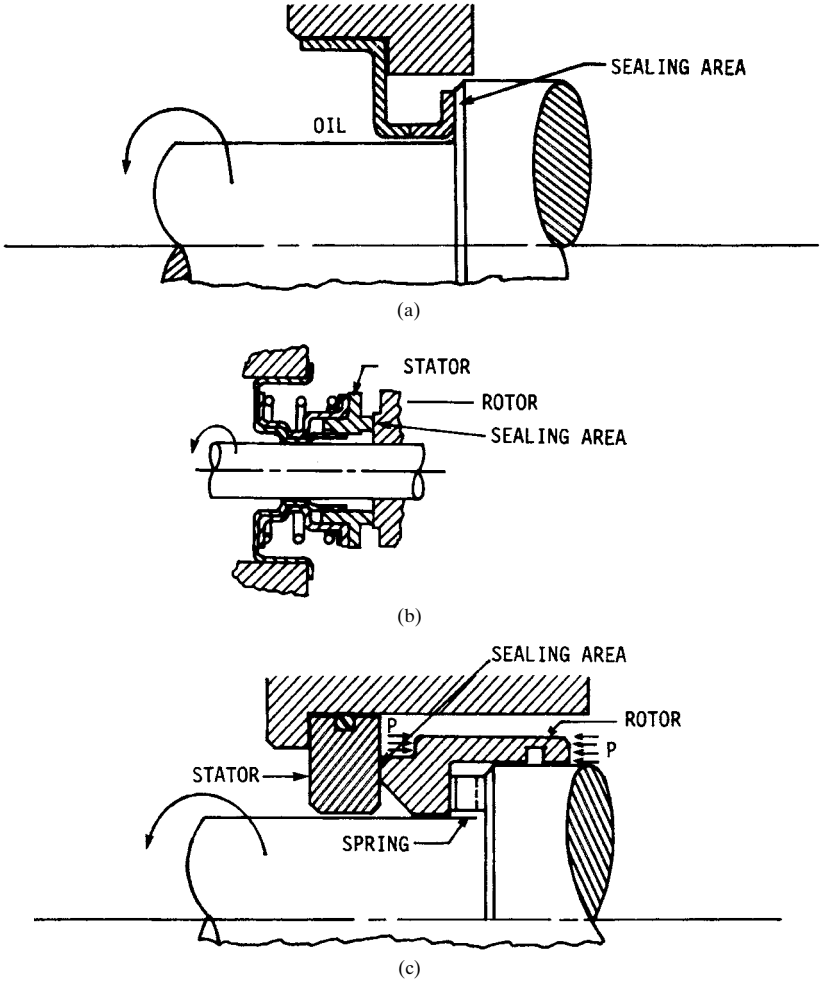

FIGURE 21.5 Face seals. (*a*) Housing-mounted elastomeric seal; (*b*) mechanical seal for engine coolant pump; (*c*) balanced mechanical seal.

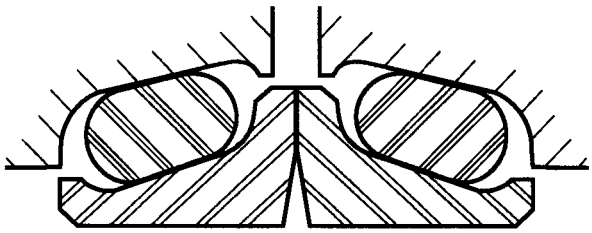

FIGURE 21.6 Cross section of a face seal for severe operating environments.

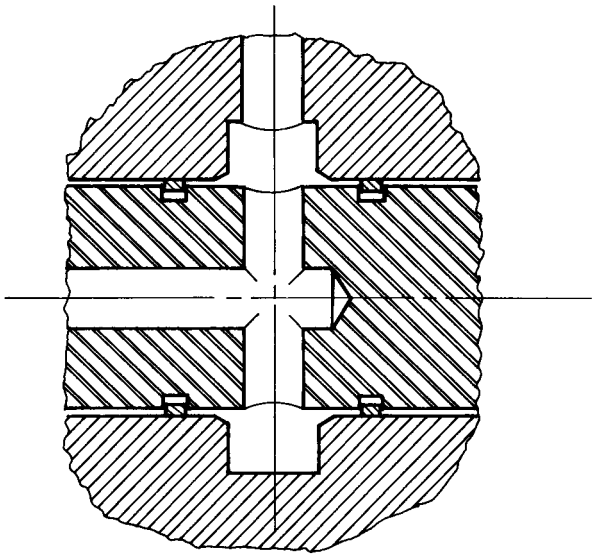

FIGURE 21.7 Metal seal ring application on a rotating shaft.

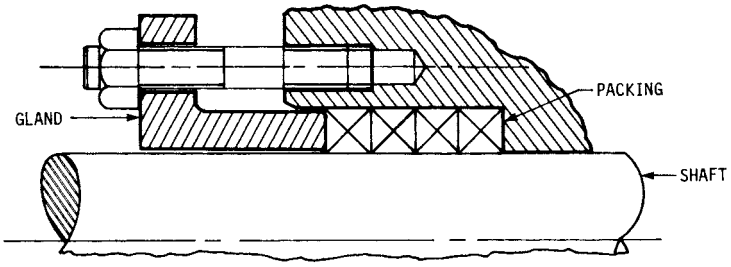

FIGURE 21.8 Stuffing box for a rotating shaft.

Packing material is usually obtained in straight lengths of square or rectangular cross section. Pieces are cut off and formed into rings that fit the stuffing box. The choice of packing material depends on the fluid to be sealed. Available packing materials include artificial fibers, asbestos, cotton, graphite, jute, leather, and metals. The metal packings are used for temperature conditions where the other materials are inadequate. The metal packings are formed from foil which is compressed into the proper packing shape.

In the design of stuffing boxes, small clearances are provided between the shaft and surrounding parts. The small clearances minimize extrusion of the packing into the clearance spaces.

Valve stems undergo a helical motion rather than a rotary motion when the valve is opened or closed. Investigations into the prevention of valve leakage and wear of valve stems resulted in a procedure for establishing packing dimensions for valve stems [21.3].

21.2.6 Noncontacting Seals

Frictional losses occur with sealing methods that utilize physical contact between a rotating and a stationary part. With high rubbing velocities, friction losses may be a significant factor. Those losses can be eliminated by using a seal that does not require physical contact. A noncontacting seal, however, cannot prevent leakage completely, although it does reduce it to a tolerable level.

One method of achieving a low leakage rate is to provide a very small clearance between the shaft and the surrounding housing or bushing. The longer the low-clearance passage, the greater the reduction in leakage.

A type of noncontacting seal called the *labyrinth seal* (Fig. 21.9) is used on such machines as large blowers and steam turbines. It can be used to retain lubricant in the bearings or to seal the working fluid in the machine. Effectiveness of the seal depends on small clearances between the seal and the shaft. In sealing the working fluid, the small clearances create a series of pressure drops between the working fluid and the atmosphere.

Labyrinth seals are usually made from a relatively soft metal such as aluminum or bronze so that the shaft is not damaged if contact between shaft and seal occurs. The simplest type is shown in Fig. 21.9, but other types are also used.

21.3 SEALS FOR RECIPROCATING MOTION

Some of the sealing methods used for rotary motion are also satisfactory for reciprocating motion. O-rings, compression packings, metal sealing rings, and some additional types are used to seal reciprocating rods, shafts, and pistons.

21.3.1 O-Rings

The O-ring is used extensively because of the low installed cost and effectiveness as a seal. It is well adapted to sealing reciprocating motion as well as for use as a static seal. Figure 21.10 shows applications on a piston and piston rod as well as a static seal application. Many such applications are for hydraulic cylinders in which the hydraulic oil acts as the lubricant for the O-rings.

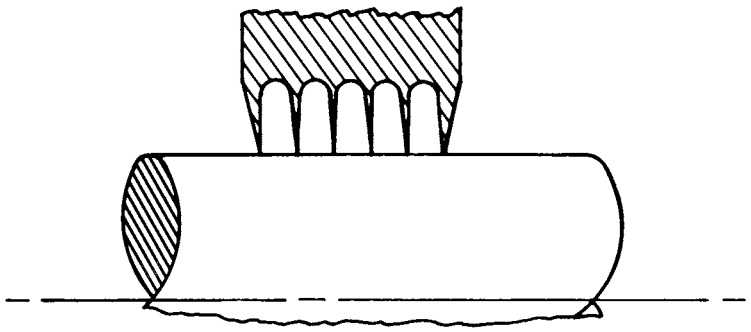

FIGURE 21.9 Labyrinth type of noncontacting seal.

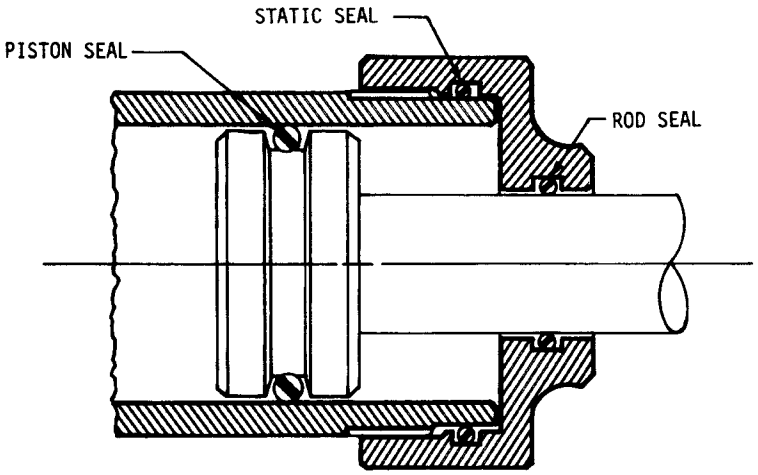

FIGURE 21.10 Applications of O-rings as a static seal and as seals for reciprocating motion.

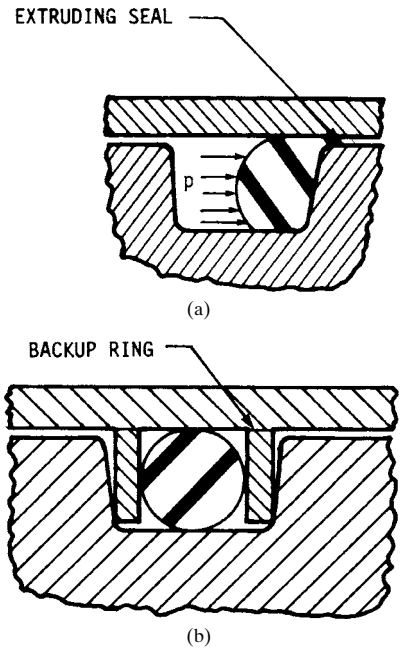

FIGURE 21.11 (*a*) Extrusion of O-ring into clearance space due to pressure. (*b*) Use of backup ring to prevent extrusion.

Rectangular-section rings are not suited for reciprocating motion and are used only in static applications. The shape of the groove for circular-section O-rings for sealing reciprocating motion is the same as that for static applications (Fig. 21.2). The recommended groove depth *E*, however, is slightly different for reciprocating motion. Recommended dimensions are available in SAE J120a and in the manufacturers' literature.

An O-ring must seal the clearance space between the reciprocating and stationary parts, for example, between the piston and the cylinder in Fig. 21.10. The amount of clearance that can be permitted depends on the pressure differential across the O-ring and the ring hardness. If the clearance is too great, the O-ring is extruded into the clearance space (Fig. 21.11*a*). The reciprocating motion then tears away small pieces of the O-ring, which results in a leaking seal and contamination of the working fluid by the O-ring particles.

The pressure limitations of O-rings can be overcome by the use of backup rings (Fig. 21.11*b*) or other devices that prevent O-ring extrusion. Backup rings are made from leather, plastics, or metal. The metal rings are split like a piston ring for radial compression during assembly into the cylinder.

Recommendations on the combination of clearance and pressure for which backup rings are required vary to some extent among the various O-ring suppliers. Figure 21.12 provides one such recommendation [21.4]. In this figure, if the combination of fluid pressure and maximum gap falls to the right of a hardness curve, backup rings are required. If a piston or rod can be forced to one side of the bore, the maximum gap is the difference between the two diameters. If, however, the radial position of the piston or rod is restrained, as by bearings, the radial clearance is the maximum gap.

Both the compression of the O-ring cross section to effect a seal and fluid pressure acting on the seal cause friction forces that oppose reciprocating motion. Information for estimating friction factors is provided in Fig. 21.13 [21.4]. The friction factor due to compression of the cross section can be obtained from Fig. 21.13*a*. The seal compression is expressed as a percentage of the O-ring cross section. The friction factor is multiplied by the circumference of the surface where relative motion occurs to obtain the friction force. For a piston, the circumference of the cylinder bore is used; for a piston rod, the rod circumference applies.

The friction factor for pressure differential across the O-ring is obtained from Fig. 21.13*b*. That factor is multiplied by the projected area of the O-ring to obtain the friction force. For an O-ring in a piston, the projected area is the product of the diameter of the ring cross section and the circumference of the cylinder bore. The total estimated friction force is the sum of the friction forces due to compression and fluid pressure.

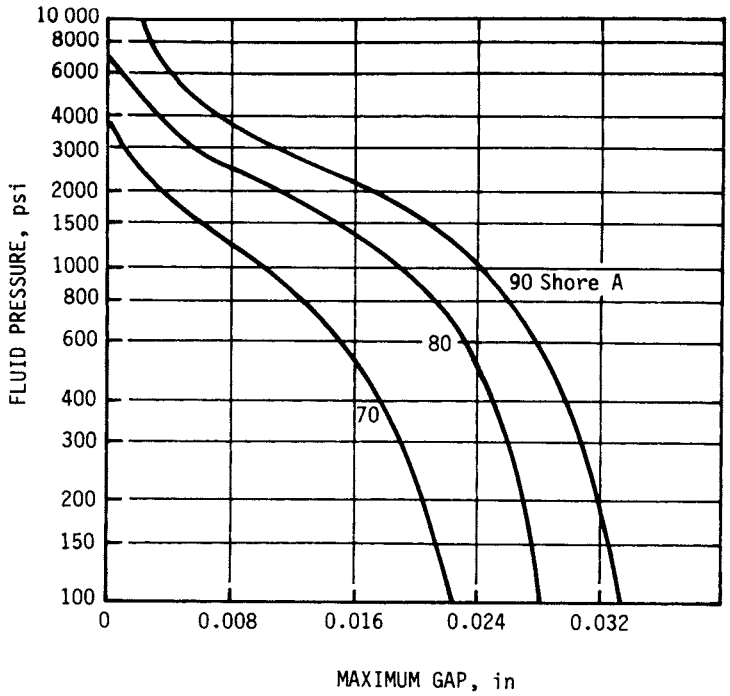

FIGURE 21.12 Extrusion limits for O-rings. *(From Ref. [21.4].)*

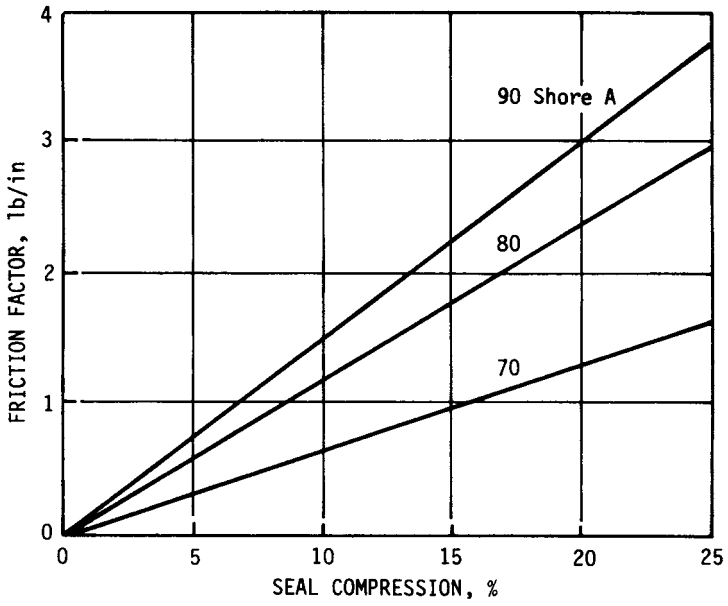

(a)

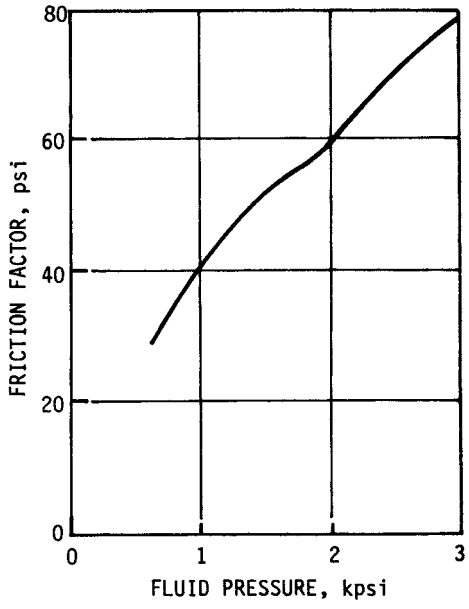

(b)

FIGURE 21.13 O-ring friction factors due to (*a*) compression of the cross section and (*b*) fluid pressure. *(From Ref. [21.4].)*

The finish of rubbing surfaces should be 8 to 16 μin (0.2 to 0.4 μm) for O-rings with a hardness of 70 Shore A. For rougher surfaces, a higher O-ring hardness should be used to ensure reasonable life.

O-rings may be damaged if they are forced over sharp corners during assembly. The addition of chamfers to corners is an inexpensive method of reducing damage. Serious damage to O-rings occurs if they are forced to pass over a hole in a cylinder wall while under pressure. If this occurs, the O-ring expands into the hole and must later be forced back into the groove. This action tends to shear pieces off the ring and thus destroy its ability to seal.

21.3.2 Lip Packings

Cup packings, U-seals, V-ring packings, and other forms of lip packings are used primarily to seal reciprocating motion. The packing material is usually leather, solid rubber, or fabric-reinforced rubber, although other compounds are available for difficult applications. An advantage of leather packings is a low coefficient of friction, on the order of 0.006 to 0.008 depending on the tanning process. Low friction increases the life of a packing because less heat is generated.

Cup packings (Fig. 21.14) were one of the first types of piston seals for hydraulic and pneumatic applications. The fluid pressure expands the cup outward against the cylinder wall and thus seals the piston in the cylinder. This action requires that a double-acting cylinder have two packings in order to seal the pressure in both directions of operation. The inner portion of the piston in Fig. 21.14 is a boss to prevent excessive tightening of the washer against the cup. If the cup is crushed against the piston, good sealing will not be obtained.

Figure 21.15 shows elastomeric U-seals on a double-acting piston. This type of seal is also used on piston rods. They have approximately the same pressure limitations as O-rings, and backup rings are required for higher pressures. When a U-seal is made of leather, a filler is required between the lips to prevent collapse of the seal.

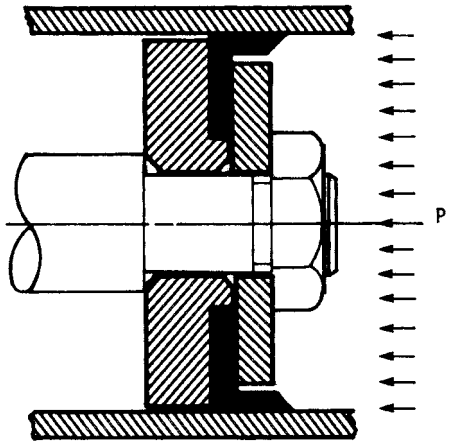

FIGURE 21.14 Cup packing for single-acting cylinder.

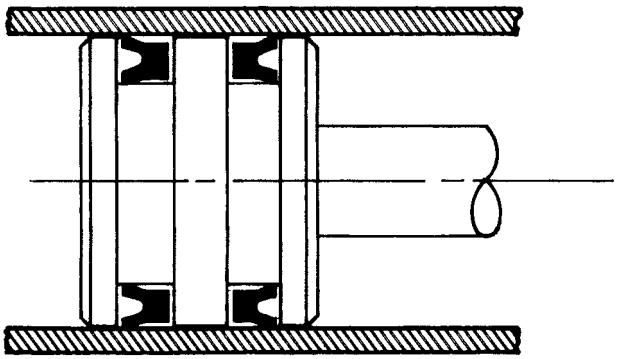

FIGURE 21.15 U-seals for a double-acting piston.

Rod scrapers are used on piston rods of hydraulic cylinders that are exposed to harsh environments. The purpose is to exclude mud, dust, and ice from the cylinder. A typical rod scraper is composed of a polyurethane element bonded to a metal shell which is pressed into the end cap of the cylinder. Molybdenum disulfide is sometimes added to the polyurethane to reduce friction. A rod scraper added to the end cap of a cylinder is shown in Fig. 21.16. The sealing lip is pointed outward to remove foreign material when the piston rod is retracted.

The chief use of the V-ring packing (Fig. 21.17) is for sealing piston rods or reciprocating shafts, although it can also be used to seal pistons. The ability to seal fluids under pressure depends on the type of packing material and number of packings used. The V-ring packing is considered superior to other lip types for sealing high pressures, especially above 50 000 psi (345 N/mm^2).

The V shape of the packing is obtained through the adapters that support the rings. Fluid pressure then expands the packing against the shaft and housing to seal

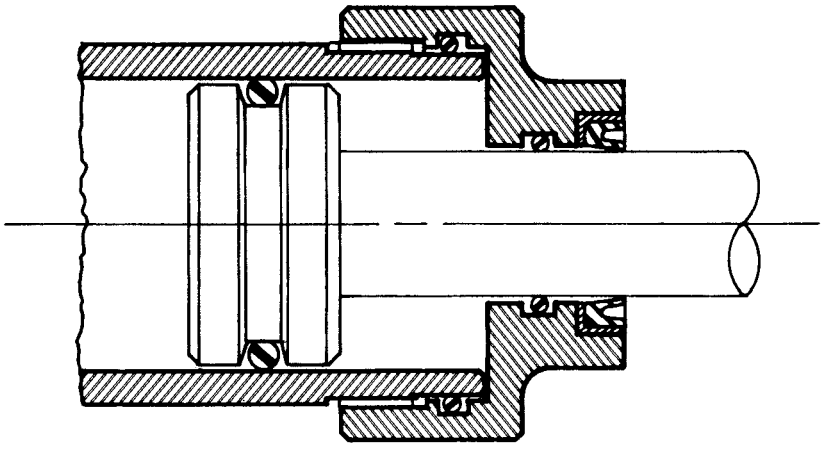

FIGURE 21.16 Rod scraper on piston rod.

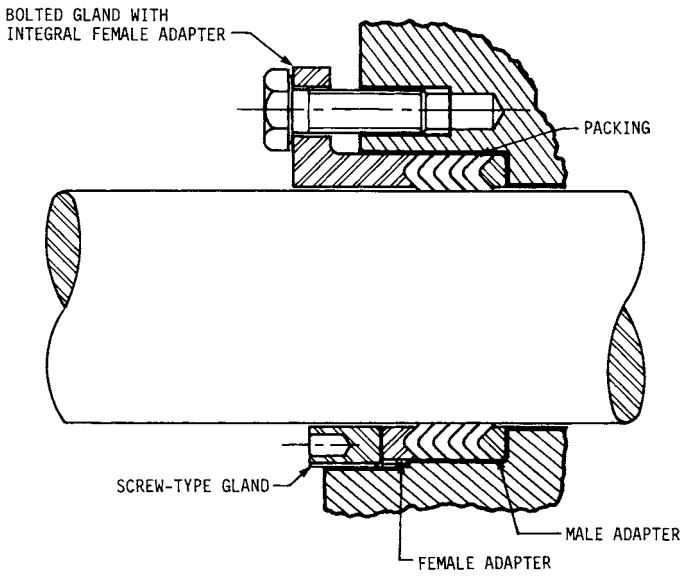

FIGURE 21.17 V-ring packing for a reciprocating shaft.

the fluid. A continuous packing provides better sealing than a series of split rings, although the latter are easier to install and remove.

21.3.3 Piston Rings

Piston rings for automotive engine applications are made of gray cast iron. The rings are used to seal gases in the cylinder and to restrict oil to the crankcase.

Piston rings must be split for assembly over the piston. This requires shaping the ring so that it will provide a uniform radial force against the cylinder wall. Piston ring manufacturers have developed methods of attaining this objective.

REFERENCES

21.1 Leonard J. Martini, "Sealing Rotary Shafts with O-Rings," *Machine Design,* May 26, 1977, pp. 97–99.

21.2 Bert Robins, "Radial Lip Seals—Are Two Too Many?" *Power Transmission Design,* October 1982, pp. 73, 74.

21.3 L. I. Ezekoye and J. A. George, "Valve Packings that Don't Leak," *Machine Design,* Jan. 20, 1977, pp. 142, 143.

21.4 Wes J. Ratelle, "Seal Selection: Beyond Standard Practice," *Machine Design,* Jan. 20, 1977, pp. 133–137.

SEALS

P · A · R · T · 6

FASTENING, JOINING, AND CONNECTING

CHAPTER 22
BOLTED AND RIVETED JOINTS

John H. Bickford
Vice President, Manager of the Power-Dyne Division, Retired
Raymond Engineering Inc.
Middletown, Connecticut

SYMBOLS AND UNITS

A	Cross-sectional area, in^2 (mm^2)
A_B	Cross-sectional area of the body of a bolt, in^2 (mm^2)
A_r	Cross-sectional area of the body of the rivet, in^2 (mm^2)
A_S	Cross-sectional area of the tensile stress area of the threaded portion of a bolt, in^2 (mm^2)
A_1, A_2, A_3, etc.	Cross-sectional areas of individual fasteners, in^2 (mm^2)
b	Number of shear planes which pass through the fastener; and/or the number of slip surfaces in a shear joint
d	Nominal diameter of the bolt, in (mm)
E	Modulus of elasticity, psi (MPa)
F	Force, lb (kN)
F_B	Tension in a bolt, lb (kN)
F_b	Primary shear force on a bolt, lb (kN)
F_B(max)	Maximum anticipated tension in the bolt, lb (kN)
F_{BY}	Tension in a bolt at yield, lb (kN)
F_C	Clamping force on the joint, lb (kN)
F_C(min)	Minimum acceptable clamping force on a joint, lb (kN)
F_J(min)	Minimum anticipated clamping force on the joint, lb (kN)

F_n	Reaction moment force seen by the nth bolt in an eccentrically loaded shear joint, lb (kN)
F_{PA}	Average preload in a group of bolts, lb (kN)
F_P(max)	Maximum anticipated initial preload in a bolt, lb (kN)
F_P(min)	Minimum anticipated initial preload in a bolt, lb (kN)
F_{PT}	Target preload, lb (kN)
F_{TR}	Maximum external transverse load on the joint, per bolt, lb (kN)
F_r	External shear load on the rivet, lb (kN)
F_T(max)	Maximum acceptable tension in a bolt, lb (kN)
F_X	External tension load on a joint, lb (kN)
F_1, F_2, F_3, etc.	Secondary shear or reaction moment forces seen by individual bolts in an eccentric joint, lb (kN)
H	Distance between the centerline of the bolt holes nearest to the edge of a joint or splice plate and that edge, in (mm)
k_B	Stiffness of a bolt or rivet, lb/in (kN/mm)
k_G	Stiffness of a gasket, lb/in (kN/mm)
k_J	Stiffness of the joint members, lb/in (kN/mm)
k_T	Stiffness of gasketed joint, lb/in (kN/mm)
K	Nut factor
l_G	Grip length of the fasteners, in (mm)
L	Distance between the bolt and the nearest edge of the connected part, or to the nearest edge of the next bolt hole, measured in the direction of the force on the joint, in (mm)
L_B	Effective length of the body of a bolt (the length of body in the grip plus one-half the thickness of the head, for example), in (mm)
L_S	Effective length of the threaded portion of a bolt [the length of the threads within the grip plus one-half the thickness of the nut(s), for example], in (mm)
m	Number of fasteners in the joint
M	Moment exerted on a shear joint by an external force, lb · in (N · m)
n	Number of threads per inch
N	Number of cycles achieved in fatigue life test
P	Pitch of the threads, in (mm)
P_S	Scatter in preload anticipated from bolting tool used for assembly (expressed as a decimal)
P_Z	Percentage loss (expressed as a decimal) in initial preload as a result of short-term relaxation and/or elastic interactions
r	Radial distance from the centroid of a group of fasteners to a fastener, in (mm)
r_n	Radial distance to the nth fastener, in (mm)

BOLTED AND RIVETED JOINTS

r_s	Bolt slenderness ratio (l_G/d)
r_1, r_2, r_3, etc.	Radial distance of individual fasteners, in (mm)
R_{JB}	Stiffness ratio (k_J/k_B)
R_S	Slip resistance of a friction-type joint, lb (kN)
S	Ratio of the ultimate shear strength of the bolt material to its ultimate tensile strength
S_u	Minimum ultimate tensile strength, psi (MPa)
S_{YB}	Yield strength of the bolt, psi (MPa)
t	Thickness of a joint or a splice plate, in (mm)
t_J	Total thickness of a joint, in (mm)
T	Torque, lb · in (N · m)
W	Width of a joint plate, in (mm)
x	Coordinate distance, in (mm)
$\bar{x}$	Coordinate distance to the centroid of a bolt group, in (mm)
x_1, x_2, x_3, etc.	x coordinates for individual fasteners, in (mm)
y	Coordinate distance, in (mm)
$\bar{y}$	Coordinate distance to the centroid of a bolt group, in (mm)
y_1, y_2, y_3, etc.	y coordinates for individual fasteners, in (mm)
Δ	Incremental change or variation
λ	Ratio of shear stress in a bolt to the ultimate tensile strength
μ_S	Slip coefficient of a friction-type joint
σ	Stress, psi (MPa)
σ_B	Bearing stress, psi (MPa)
σ(max)	Maximum tensile stress imposed during fatigue tests, psi (MPa)
σ_T	Allowable tensile stress, psi (MPa)
σ_T(max)	Maximum acceptable tensile stress in a bolt, psi (MPa)
σ^2	Statistical variance (standard deviation squared)
σ_O^2	Statistical variance of the tension errors created by operator variables
σ_T^2	Statistical variance of the tension errors created by tool variables
τ	Shear stress, psi (MPa)
τ_A	Allowable shear stress, psi (MPa)
τ_B	Shear stress in a bolt, psi (MPa)
ϕ	Ratio of tensile stress in a bolt to the ultimate tensile strength

Joints are an extremely important part of any structure. Whether held together by bolts or rivets or weldments or adhesives or something else, joints make complex structures and machines possible. Bolted joints, at least, also make disassembly and reassembly possible. And many joints are critical elements of the structure, the thing most likely to fail. Because of this, it is important for the designer to understand joints. In this chapter we will deal specifically with bolted and riveted joints, starting with a discussion of joints loaded in shear (with the applied loads at right angles to

the axes of the fasteners) and continuing with tension joints in which the loads are applied more or less parallel to the axes of fasteners. As we shall see, the design procedures for shear joints and tension joints are quite different.

22.1 SHEAR LOADING OF JOINTS

Now let us look at joints loaded in shear. I am much indebted, for the discussion of shear joints, to Shigley, Fisher, Higdon, and their coauthors ([22.1], [22.2], [22.3]).

22.1.1 Types of Shear Joints

Shear joints are found almost exclusively in structural steel work. Such joints can be assembled with either rivets or bolts. Rivets used to be the only choice, but since the early 1950s, bolts have steadily gained in popularity.

Two basic types of joint are used, *lap* and *butt,* each of which is illustrated in Fig. 22.1. These are further defined as being either (1) friction-type joints, where the fasteners create a significant clamping force on the joint and the resulting friction between joint members prevents joint slip, or (2) bearing-type joints, where the fasteners, in effect, act as points to prevent slip.

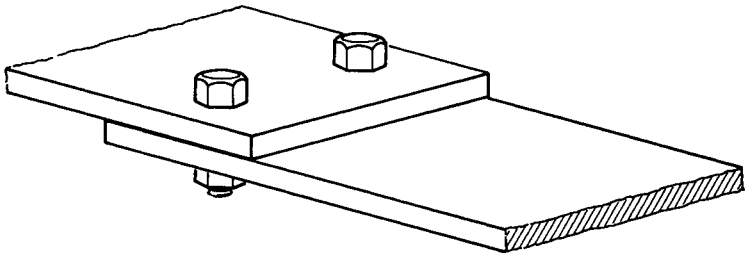

(a)

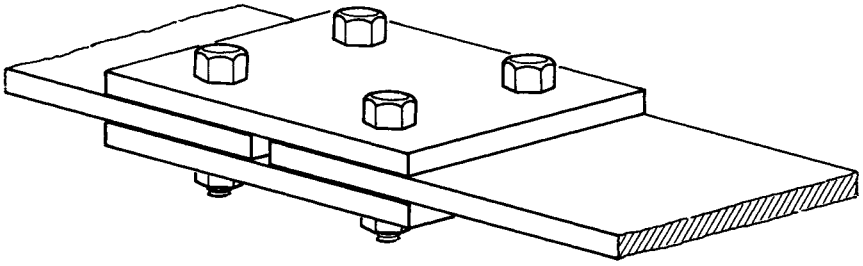

(b)

FIGURE 22.1 Joints loaded in shear. (*a*) Lap joint; (*b*) butt joint.

Only bolts can be used in friction-type joints, because only bolts can be counted on to develop the high clamping forces required to produce the necessary frictional resistance to slip. Rivets or bolts can be used in bearing-type joints.

22.1.2 Allowable-Stress Design Procedure

In the *allowable-stress design procedure,* all fasteners in the joint are assumed to see an equal share of the applied loads. Empirical means have been used to determine the maximum working stresses which can be allowed in the fasteners and joint members under these assumptions. A typical allowable shear stress might be 20 percent of the ultimate shear strength of the material. A factor of safety (in this case 5:1) has been incorporated into the selection of allowable stress.

We should note in passing that the fasteners in a shear joint do not, in fact, all see equal loads, especially if the joint is a long one containing many rows of fasteners. But the equal-load assumption greatly simplifies the joint-design procedure, and if the assumption is used in conjunction with the allowable stresses (with their built-in factors of safety) derived under the same assumption, it is a perfectly safe procedure.

Bearing-type Joints. To design a successful bearing-type joint, the designer must size the parts so that the fasteners will not shear, the joint plates will not fail in tension nor be deformed by bearing stresses, and the fasteners will not tear loose from the plates. None of these things will happen if the allowable stresses are not exceeded in the fasteners or in the joint plates. Table 22.1 lists typical allowable stresses specified for various rivet, bolt, and joint materials. This table is for reference only. It is always best to refer to current engineering specifications when selecting an allowable stress for a particular application.

Here is how the designer determines whether or not the stresses in the proposed joint are within these limits.

Stresses within the Fasteners. The shear stress within a rivet is

$$\tau = \frac{F}{bmA_r} \tag{22.1}$$

The shear stress within each bolt in the joint will be

$$\tau = \frac{F}{A_T} \tag{22.2}$$

A bolt can have different cross-sectional areas. If the plane passes through the unthreaded body of the bolt, the area is simply

$$A_B = \frac{\pi d^2}{4} \tag{22.3}$$

If the shear plane passes through the threaded portion of the bolt, the cross-sectional area is considered to be the tensile-stress area of the threads and can be found for Unified [22.4] or metric [22.5] threads from

TABLE 22.1 Allowable Stresses

Material	Source	Comments	Allowable stress		
			Tension kpsi (MPa)	Shear kpsi (MPa)	Bearing† kpsi (MPa)
ASTM A325 bolts	1	Used in bearing-type joints with slotted or standard holes, and			†
		some threads in shear planes	....	21.0 (145)	
		no threads in shear planes	....	30.0 (207)	
ASTM A325 bolts	1	Used in friction-type joints with standard holes and surfaces of			†
		clean mill scale	....	17.5 (52)	
		blast-cleaned carbon or low-alloy steel	....	27.5 (190)	
		blast-cleaned inorganic zinc rich paint		29.5 (203)	
ASTM A490 bolts	1	Bearing-type joints with slotted or standard holes, and			†
		some threads in shear planes	....	28.0 (193)	
		no threads in shear planes	....	40.0 (276)	
ASTM A490 bolts	1	Friction-type joints with standard holes and surfaces of			†
		clean mill scale	....	22.0 (152)	
		blast-cleaned carbon or alloy steel	....	34.5 (238)	
		blast-cleaned inorganic zinc-rich paint		37.0 (255)	
ASTM SA193 Grade B7 at an operating temperature of	2	Used for bolts‡			
−20°F	...	.....	18.8–25 (130–172)		
+650°F	...	.....	18.8–25.0 (130–172)		
+850°F	...	.....	16.3–17.0 (112–117)		
+1000°F	...	.....	4.5 (31)		

TABLE 22.1 Allowable Stresses (*Continued*)

Material	Source	Comments	Allowable stress		
			Tension kpsi (MPa)	Shear kpsi (MPa)	Bearing† kpsi (MPa)
ASTM SA31 rivets	3	Used in SA515 plate	....	9 (62)	18 (124)
ASTM A502-1 rivets	3	Used in A36 plate		13 (93)	401 (276)
ASTM A36 joint material	4		22 (152)	14.5 (100)	48.6 (335)
58-kpsi ultimate tensile steel: joint material	5	Joint length 25 in (with A325 bolts) Joint length 80 in (with A325 bolts)	....	23.2 (160) 29 (200)	
100-kpsi ultimate tensile strength steel: joint material	6	Joint length 20 in (with A490 bolts) Joint length 90 in (with A490 bolts)	....	50 (345) 40 (276)	
ASTM A440 joint material	7	Based on a safety factor of 2.48:1 (S_u/σ_T)	25.4–28.2 (175–194)		
ASTM A514 joint material	7	Based on a safety factor of 2:00:1 (S_u/σ_T)	50–65 (345–448)		
ASTM A515 joint material	3	Stress in net section	14 (95)		

†The allowable bearing stress for either A325 or A490 bolts is either $LS_u/2d$ or $1.5S_u$, whichever is least.
‡The stress allowed depends on the diameter of the bolts. The material cannot be through-hardened, so larger sizes will support less stress.

SOURCES:

1. "Structural Joints Using ASTM A325 or A490 Bolts." AISC specification, April 14, 1980, pp. 4–5.
2. "ASME Boiler and Pressure Vessel Code," Sec. VIII, Div. I, American Society of Mechanical Engineers, New York, 1977. Table UCS-23, pp. 208–209.
3. Archie Higdon, Edward H. Ohlsen, William B. Stiles, John A. Weese, and William F. Riley, *Mechanics of Materials,* 3d ed., John Wiley and Sons, New York, 1978, p. 632.
4. John W. Fisher, "Design Examples for High Strength Bolting," *High Strength Bolting for Structural Joints,* Bethlehem Steel Co., Bethlehem, Pennsylvania, 1970, p. 52.
5. John W. Fisher and John H. A. Struik, *Guide to Design Criteria for Bolted and Riveted Joints,* John Wiley and Sons, New York, 1974, p. 124.
6. Ibid., p. 127.
7. Ibid., p. 123.

Unified:
$$A_S = \frac{\pi}{4}\left(d - \frac{0.9743}{n}\right)^2 \tag{22.4}$$

Metric:
$$A_S = \frac{\pi}{4}(d - 0.9382P)^2$$

Here is an example based on Fig. 22.2. The bolts are ASTM A325 steel, $m = 5$ bolts, $F = 38\,250$ lb (170.1 kN), $d = \frac{3}{4}$ in (19.1 mm), $b = 2$ (one through the body of each bolt, one through the threads), and $n = 12$ threads per inch (2.12 mm per thread).

The total cross-sectional area through the bodies of all five bolts and then through the threads is

$$5A_B = \frac{5\pi(0.75)^2}{4} = 2.209 \text{ in}^2 \ (1425 \text{ mm}^2)$$

$$5A_S = \frac{5\pi}{4}\left(0.75 - \frac{0.9743}{12}\right)^2 = 1.757 \text{ in}^2 \ (1133 \text{ mm}^2)$$

The shear stress in each bolt will be

$$\tau = \frac{F}{A_T} = \frac{38\,250}{2.209 + 1.757} = 9646 \text{ psi } (66.5 \text{ MPa})$$

which is well within the shear stress allowed for A325 steel bolts (Table 22.1).

Tensile Stress in the Plate. To compute the tensile stress in the plates (we will assume that these are made of A36 steel), we first compute the cross-sectional area of a row containing the most bolts. With reference to Figs. 22.2 and 22.3, that area will be

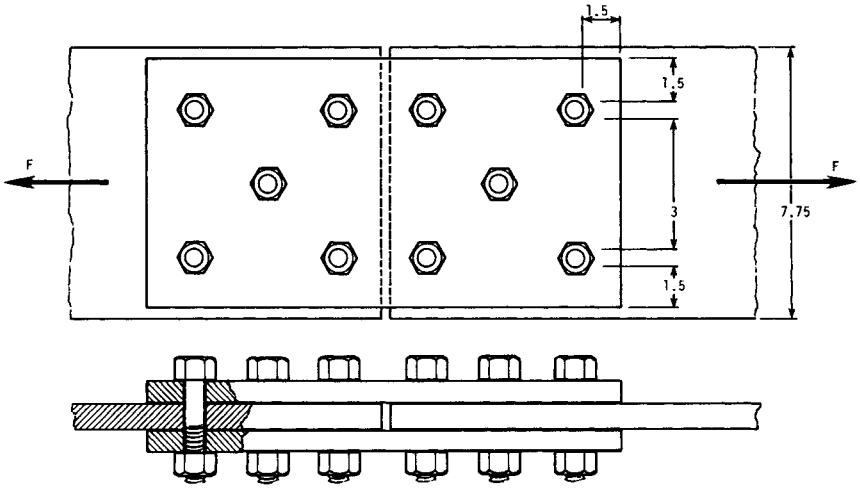

FIGURE 22.2 Shear joint example. The joint and splice plates here are each ¾ in (19.1 mm) thick. Dimensions given are in inches. To convert to millimeters, multiply by 25.4.

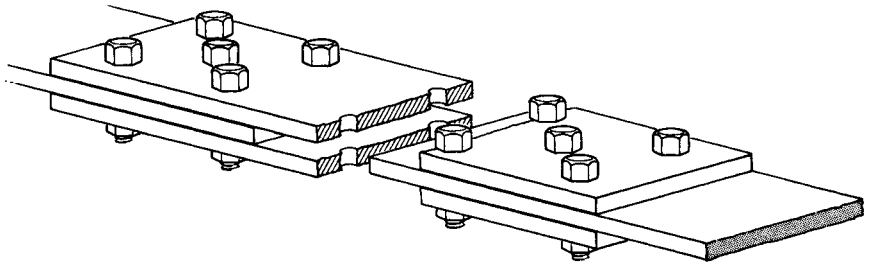

FIGURE 22.3 Tensile failure of the splice plates. Tensile failure in the plates occurs in the cross section intersecting the most bolt holes.

$$A = 0.75(1.5) + 0.75(3) + 0.75(1.5) = 4.5 \text{ in}^2 \ (2903 \text{ mm}^2)$$

The stress in two such cross sections (there are two splice plates) will be

$$\sigma = \frac{F}{A} = \frac{38\,250}{(4.5)2} = 4250 \text{ psi } (29.3 \text{ MPa})$$

These plates will not fail; the stress level in them is well within the allowable tensile-stress value of 21.6 kpsi for A36 steel. In some joints we would want to check other sections as well, perhaps a section in the splice plate.

Bearing Stresses on the Plates. If the fasteners exert too great a load on the plates, the latter can be deformed; bolt holes will elongate, for example. To check this possibility, the designer computes the following (see Fig. 22.4):

$$\sigma_B = \frac{F}{mdl_G}$$

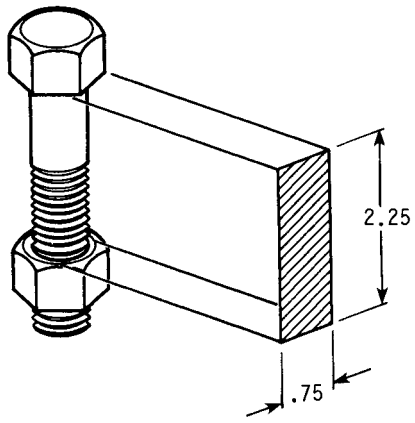

FIGURE 22.4 The bearing area of a bolt. The dimensions given are those used in the example in the text for the joint shown in Fig. 22.2. Dimensions are in inches. Multiply by 25.4 to convert to millimeters.

For our example, $l_G = 2.25$ in (57.2 mm), $m = 5$, and $d = 0.75$ in (19.1 mm). Then

$$\sigma_B = \frac{38\,250}{5(0.75)(2.25)} = 4533 \text{ psi } (31.3 \text{ MPa})$$

Note that the allowable bearing stresses listed in Table 22.1 are greater than the allowable shear stresses for the same plate material.

Tearout Stress. Finally, the designer should determine whether or not the fasteners will tear out of a joint plate, as in the lap joint shown in Fig. 22.5. In the example shown there are six shear areas. The shear stress in the tearout sections will be

$$\tau = \frac{100\,000}{6(0.75)(2)} = 11\,111 \text{ psi } (76.6 \text{ MPa})$$

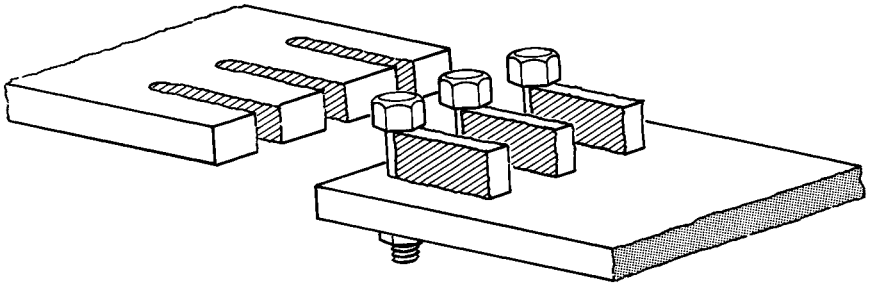

FIGURE 22.5 Tearout. The pieces torn from the margin of the plate can be wedge-shaped as well as rectilinear, as shown here.

where $F =$ 100 kip (445 kN)
$H =$ 2 in (50.8 mm)
$t =$ ¾ in (19.1 mm)

Friction-type Joints. Now let us design a friction-type joint using the same dimensions, materials, and bolt pattern as in Fig. 22.1, but this time preloading the bolts high enough so that the friction forces between joint members (between the so-called faying surfaces) become high enough to prevent slip under the design load.

Computing Slip Resistance. To compute the slip resistance of the joint under a shear load, we use the following expression (from Ref. [22.6], p. 72):

$$R_S = \mu_S F_{PA} bm \tag{22.5}$$

Typical slip coefficients are tabulated in Table 22.2. Note that engineering specifications published by the AISC and others carefully define and limit the joint surface conditions that are permitted for structural steel work involving friction-type joints. The designer cannot arbitrarily paint such surfaces, for example; if they are painted, they must be painted with an approved material. In most cases they are not painted. Nor can such surfaces be polished or lubricated, since these treatments would alter the slip coefficient. A few of the surface conditions permitted under current specifications are listed in Table 22.2. Further conditions and coating materials are under investigation.

To continue our example, let us assume that the joint surfaces will be grit blasted before use, resulting in an anticipated slip coefficient of 0.493. Now we must estimate the average preload in the bolts. Let us assume that we have created an average preload of 17 kip in each of the five bolts in our joint. We can now compute the slip resistance as

$$R_S = \mu_S F_{PA} bm = 0.493\ (17\ 000)(2)(5)$$

$$= 83\ 810 \text{ lb } (373 \text{ kN})$$

Comparing Slip Resistance to Strength in Bearing. The ultimate strength of a friction-type joint is considered to be the lower of its slip resistance or bearing strength. To compute the bearing strength, we use the same equations we used earlier. This time, however, we enter the allowable shear stress for each material and

TABLE 22.2 Slip Coefficients

Surfaces	Source	Typical slip coefficient μ_S
Free of paint or other applied finish, oil, dirt, loose rust or scale, burrs, or defects. Tight mill scale permitted	1	0.45
Clean mill scale	2	0.35
Hot dip galvanized	2	0.16
Hot dip galvanized, wire brushed	2	0.3–0.4
Grit blasted	3	0.331–0.527
Sand blasted	3	0.47
Metallized zinc sprayed (hot) onto grit blasted surface	4	0.422

SOURCES:
1. Specification BS 4604: Part 1: 1970, British Standards Institution, London, 1970.
2. *High Strength Bolting for Structural Joints,* Bethlehem Steel Co., Bethlehem, Pennsylvania, 1970, p. 14.
3. John W. Fisher and John H. A. Struik, *Guide to Design Criteria for Bolted and Riveted Joints,* John Wiley and Sons, New York, 1974, p. 78.
4. Ibid., p. 200.

then compute the force which would produce that stress. These forces are computed separately for the fasteners, the net section of the plates, the fasteners bearing against the plates, and tearout. The least of these forces is then compared to the slip resistance to determine the ultimate design strength of the joint. If you do this for our example, you will find that the shear strength of the bolts determines the ultimate strength of this joint.

22.2 ECCENTRIC LOADS ON SHEAR JOINTS

22.2.1 Definition of an Eccentric Load

If the resultant of the external load on a joint passes through the centroid of the bolt pattern, such a joint is called an *axial shear joint.* Under these conditions, all the fasteners in the joint can be assumed to see an equal shear load.

If the resultant of the applied load passes through some point other than the centroid of the bolt group, as in Fig. 22.6, there will be a net moment on the bolt pattern. Each of the bolts will help the joint resist this moment. A joint loaded this way is said to be under an *eccentric shear load.*

22.2.2 Determine the Centroid of the Bolt Group

To locate the centroid of the bolt group, we arbitrarily position xy reference axes near the joint, as shown in Fig. 22.7. We then use the following equations to locate the centroid within the group (Ref. [22.1], p. 360):

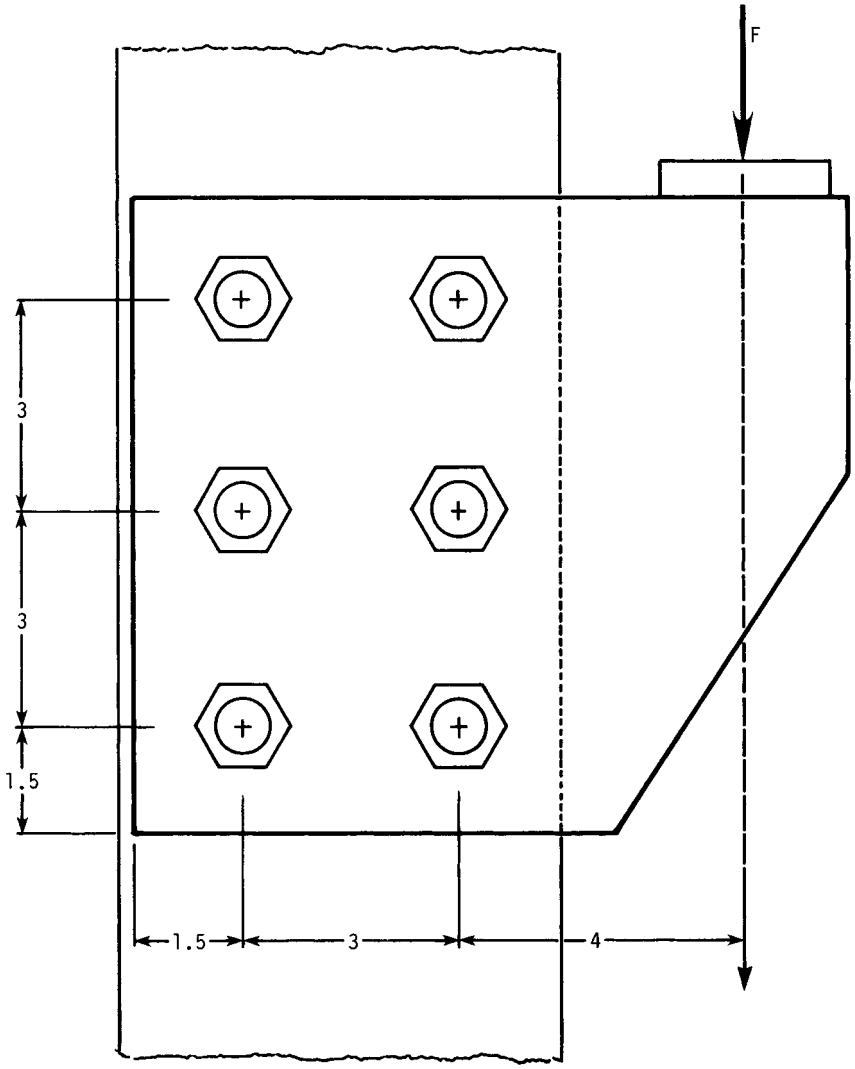

FIGURE 22.6 Eccentrically loaded shear joint. For the example used in the text, it is assumed that the bolts are ¾—12 × 3, ASTM A325; the plates are made of A36 steel; the eccentric applied load F is 38.25 kip (170 kN).

$$\bar{x} = \frac{A_1x_1 + A_2x_2 + \cdots + A_6x_6}{A_1 + A_2 + \cdots + A_6}$$

$$\bar{y} = \frac{A_1y_1 + A_2y_2 + \cdots + A_6y_6}{A_1 + A_2 + \cdots + A_6} \tag{22.6}$$

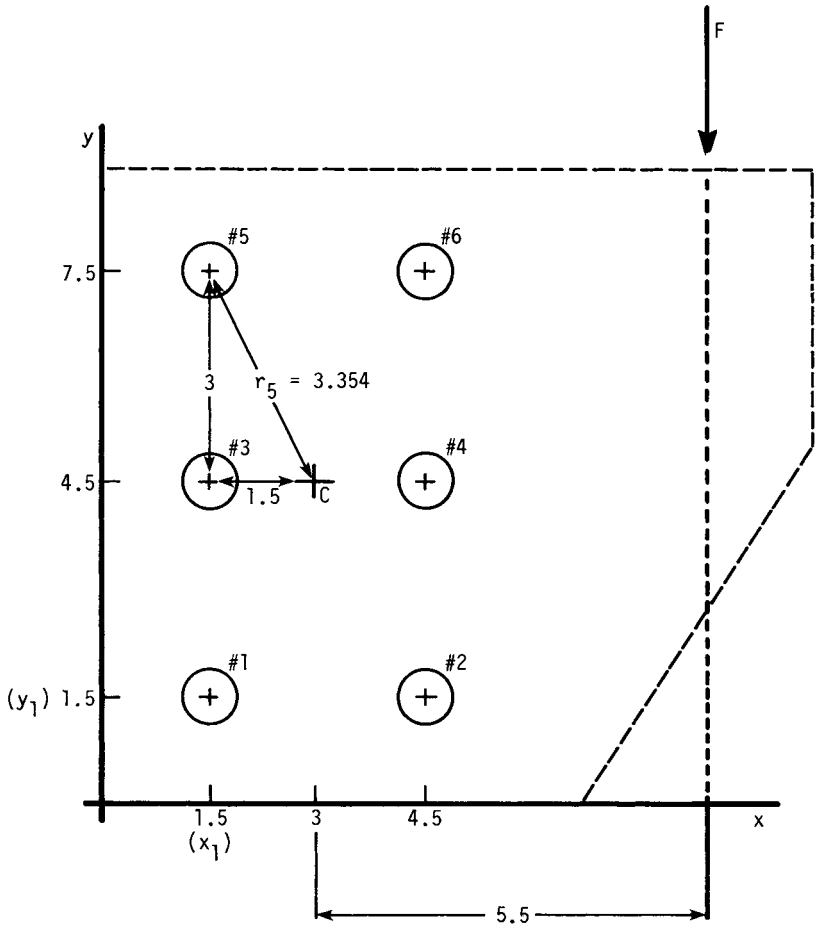

FIGURE 22.7 The centroid of a bolt pattern. To determine the centroid of a bolt pattern, one arbitrarily positions coordinate axes near the pattern and then uses the procedure given in the text. I have used the edges of the splice plate for the x and y axes in this case. Multiply the dimensions shown (which are in inches) by 25.4 to convert them to millimeters.

For the joint shown in Fig. 22.6 we see, assuming that $A_1 = A_2 = \text{etc.} = 0.442$ in^2 (285 mm^2),

$$\bar{x} = \frac{0.442(1.5 + 4.5 + 1.5 + 4.5 + 1.5 + 4.5)}{6(0.442)} = 3 \text{ in } (76.2 \text{ mm})$$

Similarly, we find that $\bar{y} = 4.5$ in (114.3 mm).

22.2.3 Determining the Stresses in the Bolts

Primary Shear Force. We compute the primary shear forces on the fasteners as simply (see Fig. 22.8)

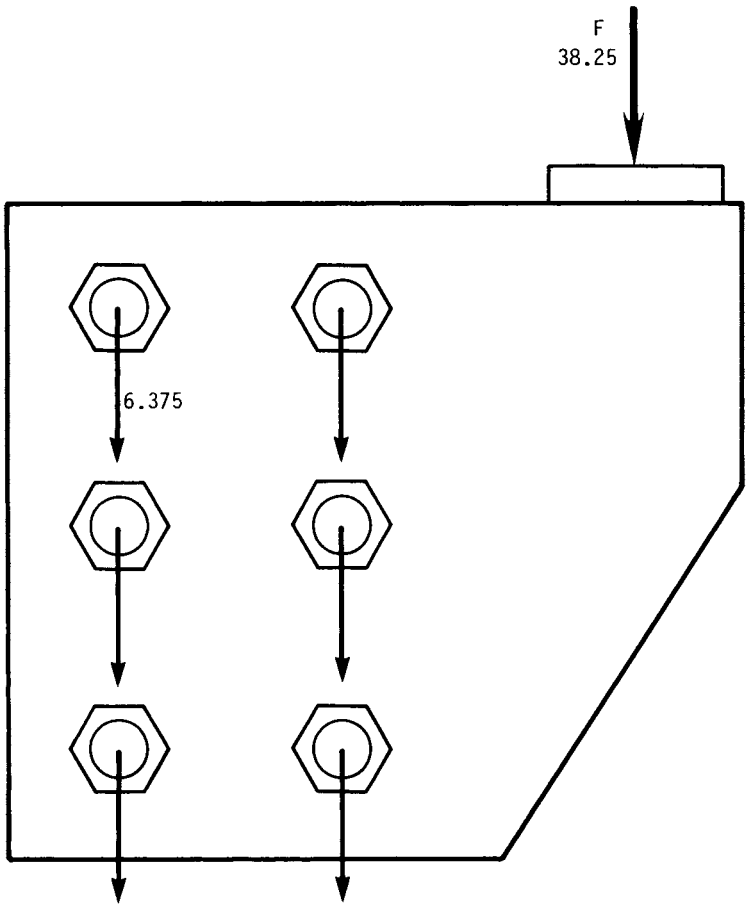

FIGURE 22.8 Primary shear forces on the bolts. The primary forces on the bolts are equal and are parallel. Forces shown are in kilopounds; multiply by 4.448 to convert to kilonewtons.

$$F_b = \frac{F}{m} = \frac{38\,250}{6} = 6375 \text{ lb } (28.4 \text{ kN})$$

Secondary Shear Forces. We next determine the reaction moment forces in each fastener using the two equations (Ref. [22.1], p. 362):

$$M = F_1 r_1 + F_2 r_2 + \cdots + F_6 r_6 \tag{22.7}$$

$$\frac{F_1}{r_1} = \frac{F_2}{r_2} = \frac{F_3}{r_3} = \cdots = \frac{F_6}{r_6} \tag{22.8}$$

Combining these equations, we determine that the reaction force seen on a given bolt is

$$F_n = \frac{Mr_n}{r_1^2 + r_2^2 + \cdots + r_6^2} \tag{22.9}$$

Let us continue our example. As we can see from Fig. 22.7, we have an external force of 38 250 lb (170.1 kN) acting at a distance from the centroid of 5.5 in (140 mm). The input moment, then, is 210 kip · in (23.8 N · m). The radial distance from the centroid to bolt 5 (one of the four bolts which are most distant from the centroid) is 3.354 in (85.2 mm). The reaction force seen by each of these bolts is (see Fig. 22.9)

$$F_5 = \frac{210\,375(3.354)}{4(3.354)^2 + 2(1.5)^2} = 14\,255 \text{ lb } (63.4 \text{ kN})$$

Combining Primary and Secondary Shear Forces. The primary and secondary shear forces on bolt 5 are shown in Fig. 22.9. Combining these two forces by vectorial means, we see that the total force F_{R5} on this bolt is 12 750 lb (56.7 kN).

Let us assume that there are two slip planes here—that one of them passes through the body of the bolt and the other passes through the threads as in the ear-

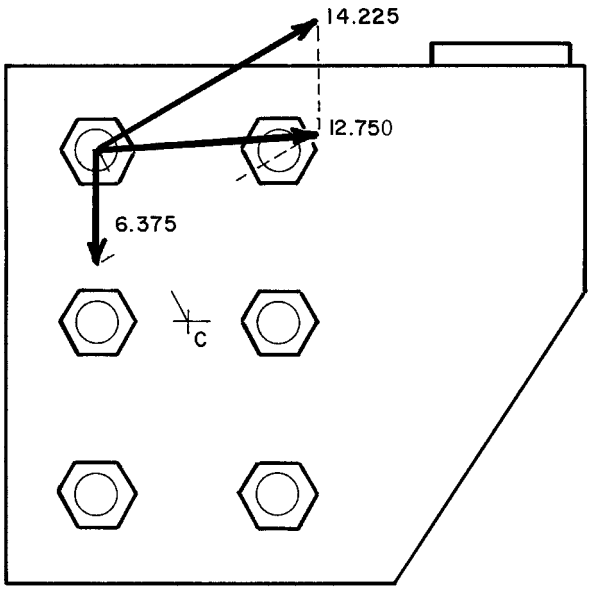

FIGURE 22.9 Combining primary and shear forces. I have selected one of the four *most distant* bolts to calculate the secondary shear force, 14.255 kip (63.4 kN), which has a line of action at right angles to the radial line connecting the bolt to the centroid. The resultant of primary and secondary forces on this bolt is 12.750 kip (56.7 kN).

lier example illustrated in Fig. 22.2. The shear area of bolt 5, therefore, is (see Sec. 22.1.2 for the equations) 0.793 in^2 (511 mm^2).

We can now compute the shear stress within this bolt:

$$\tau = \frac{F_{R5}}{A_5} = \frac{12\,750}{0.793} = 16\,078 \text{ psi}$$

This is less than the maximum shear stress allowed for A325 steel bolts (see Table 22.1), and so the design is acceptable.

It is informative to compare these results with those obtained in Sec. 22.1.3, where we analyzed a joint having similar dimensions, the same input load, and one less bolt. The axial load in the earlier case created a shear stress of only 9646 psi (66.5 MPa) in each bolt. When the same load is applied eccentrically, passing 5.5 in from the centroid, it creates 16 078/9646 times as much stress in the most distant bolts, even though there are more bolts this time to take the load. Be warned!

22.3 TENSION-LOADED JOINTS: PRELOADING OF BOLTS

In the joints discussed so far, the bolts or rivets were loaded in shear. Such joints are usually encountered in structural steel work. Most other bolted joints in this world are loaded primarily in tension—with the applied loads more or less parallel to the axis of the bolts.

The analysis of tension joints usually centers on an analysis of the tension in the fasteners: first with the initial or *pre*load in the fasteners when they are initially tightened, and then with the working loads that exist in the fasteners and in the joint members when external forces are applied to the joint as the product or structure is put into use. These working loads consist of the preload plus or minus some portion of the external load seen by the joint in use.

Because clamping force is essential when a joint has to resist tension loads, rivets are rarely used. The following discussion, therefore, will focus on bolted joints. The analytical procedure described, however, could be used with riveted joints if the designer is able to estimate the initial preload in the rivets.

22.3.1 Preliminary Design and Calculations

Estimate External Loads. The first step in the design procedure is to estimate the external loads which will be seen by each bolted joint. Such loads can be static, dynamic, or impact in nature. They can be created by weights such as snow, water, or other parts of the structure. They can be created by inertial forces, by shock or vibration, by changes in temperature, by fluid pressure, or by prime movers.

Fastener Stiffness. The next step is to compute the stiffness or spring rate of the fasteners using the following equation:

$$k_B = \frac{A_S A_B E}{L_S A_B + L_B A_S} \tag{22.10}$$

Example. With reference to Fig. 22.10, $A_S = 0.232$ in^2 (150 mm^2), $L_B = 2.711$ in (68.9 mm), $A_B = 0.307$ in^2 (198 mm^2), $E = 30\ (10)^6$ psi (207 GPa), and $L_S = 1.024$ in (26 mm). Thus

$$k_B = \frac{0.232(0.307)(30 \times 10^6)}{1.024(0.307) + 2.711(0.232)} = 2.265 \times 10^6 \text{ lb/in } (0.396 \text{ N/mm})$$

Stiffness of a Nongasketed Joint. The only accurate way to determine joint stiffness at present is by experiment. Apply an external tension load to a fastener in an actual joint. Using strain gauges or ultrasonics, determine the effect which this external load has on the tension in the bolt. Knowing the stiffness of the bolt (which must be determined first), use joint-diagram techniques (which will be discussed soon) to estimate the stiffness of the joint.

Although it is not possible for me to give you theoretical equations, I can suggest a way in which you can make a rough estimate of joint stiffness. This procedure is based on experimental results published by Motosh [22.7], Junker [22.8], and Osgood [22.9], and can be used only if the joint members and bolts are made of steel with a modulus of approximately 30×10^6 psi (207 GPa).

First compute the slenderness ratio for the bolt (l_G/d). If this ratio is greater than 1/1, you next compute a stiffness ratio R_{JB} using the empirical equation

$$R_{JB} = 1 + \frac{3(l_G)}{7d} \tag{22.11}$$

The final step is to compute that portion of the stiffness of the joint which is loaded by a single bolt from

$$k_J = R_{JB} k_B$$

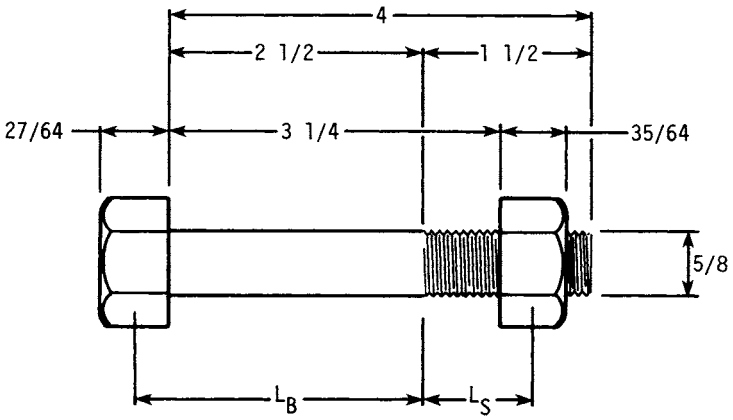

FIGURE 22.10 Computing the stiffness of a bolt. The dimensions given are those used in the example in the text. This is a ⅜—12 × 4, SAE J429 Grade 8 hexagon-head bolt with a 3.25-in (82.6-mm) grip. Other dimensions shown are in inches. Multiply them by 25.4 to convert to millimeters.

If the slenderness ratio l_G/d falls between 0.4 and 1.0, it is reasonable to assume a stiffness ratio R_{JB} of 1.0. When the slenderness ratio l_G/d falls below 0.4, the stiffness of the joint increases dramatically. At a slenderness ratio of 0.2, for example, R_{JB} is 4.0 and climbing rapidly (Ref. [22.6], pp. 199–206).

Example. For the bolt shown in Fig. 22.10 used in a 3.25-in (82.6-mm) thick joint,

$$R_{JB} = \frac{3(3.25)}{7(0.625)} = 3.23$$

Since we computed the bolt stiffness earlier as 2.265×10^6 lb/in (396 kN/mm), the joint stiffness will be

$$k_J = 3.23(2.265 \times 10^6) = 7.316 \times 10^6 \text{ lb/in } (1280 \text{ kN/mm}).$$

Stiffness of Gasketed Joints. The procedure just defined allows you to determine the approximate stiffness of a nongasketed joint. If a gasket is involved, you should use the relationship

$$\frac{1}{k_T} = \frac{1}{k_J} + \frac{1}{k_G} \tag{22.12}$$

You may have to determine the compressive stiffness of the gasket by making an experiment or by contacting the gasket manufacturer, since very little information has been published on this subject (but see Chap. 25). A few typical values for pressure-vessel gasket materials are given in Table 22.3, but these values should be used for other gaskets with caution.

Note that the stiffness of a gasket, like the stiffness of everything else, depends on its cross-sectional area. The values given in Table 22.3 are in terms of pressure or stress on the gasket versus deflection, not in terms of force versus deflection. Before you can combine gasket stiffness with joint stiffness, therefore, you must determine how large an area of the gasket is loaded by a single bolt (total gasket area divided by the number of bolts). This per-bolt area is multiplied by stress to determine the stiffness in terms of force per unit deflection. For example, the compressed asbestos gasket listed in Table 22.3 has a total surface area of 11.2 in^2 (7219 mm^2). If it is clamped by eight bolts, the per-bolt area is 1.4 in^2 (903 mm^2). The stiffness is listed in Table 22.3 as 6.67×10^2 ksi/in (181 MPa/mm). In force terms, per bolt, this becomes 6.67×10^5 (1.4) = 9.338×10^5 lb/in (1.634×10^2 kN/mm).

The stiffness values given in Table 22.3 are for gaskets in use, after initial preloading. Gaskets exhibit a lot of hysteresis. Their stiffness during initial compression is a lot less (generally) than their stiffness as they are unloaded and reloaded. As long as the usage cycles do not take the stress on the gasket above the original assembly stress, their behavior will be repetitive and elastic, with only a little hysteresis, as suggested by Fig. 22.11. And when analyzing the effect of loads on joint behavior, we are interested only in how the gaskets act as they are used, not in their behavior during assembly.

22.3.2 Selecting the Target Preload

Our joint will perform as intended only if it is properly clamped together by the fasteners. We must, therefore, select the preload values very carefully.

TABLE 22.3 Gasket Stiffness

Source	Gasket	Dimensions, in (mm)				Stiffness kpsi/in (MPa/mm)
		ID	OD	w	t	
1	Spiral-wound, asbestos-filled (300-lb class)	5 (127)	5.75 (146)	0.375 (9.52)	0.175 (4.45)	4.71×10^2 (127.6)
1	Spiral-wound asbestos-filled (600-lb class)	4.75 (121)	5.75 (146)	0.5 (12.7)	0.175 (4.45)	6.95×10^2 (188.3)
1	Compressed asbestos	4 (102)	5.5 (140)	0.75 (19)	0.062 (1.59)	6.67×10^2 (180.7)
2	Flat stainless steel double-jacketed asbestos-filled	6.5 (191)	7.5 (216)	0.5 (12.7)	0.125 (3)	43.3×10^2 (1176)
2	Solid oval ring-style 950 soft iron	5.438 (138)	6.314 (160)	0.469 (9.7)	0.688 (14.3)	27.5×10^2 (747)

SOURCE:

1. H. D. Raut, André Bazergui, and Luc Marchand, "Gasket Leakage Behavior Trends: Results of 1977–79 PVRC Exploratory Gasket Test Program," *Welding Research Council Bulletin* no. 271, WRC, New York, October 1981, Figs. 16 and 18.
2. André Bazergui and Luc Marchand, "PVRC Milestone Gasket Tests—First Results," report submitted to the Special Commission on Bolted Flanged Connections of the Pressure Vessel Research Committee of the Welding Research Council, September 1982, Figs. 12 and 13.

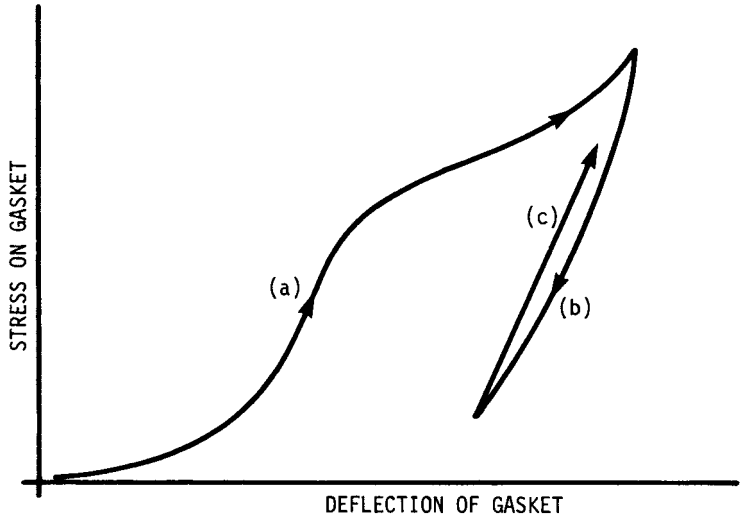

FIGURE 22.11 Typical stress versus deflection characteristics of a spiral-wound, asbestos-filled gasket during (*a*) initial loading, (*b*) unloading, and (*c*) reloading.

Acceptable Upper Limit for the Tension in the Bolts. In general, we always want the greatest preload in the bolts which the parts (bolts, joint members, and gasket) can stand. To determine the maximum acceptable tension in the bolt, therefore, we start by determining the yield load of each part involved in terms of bolt tension. The force that will cause the bolt material to yield is

$$F_{BY} = S_{YB} A_S \tag{22.13}$$

Let us begin an example using the joint shown in Fig. 22.12. We will use the bolt illustrated in Fig. 22.10. Let us make the joint members of ASTM A441 steel. The yield strength of our J429 Grade 8 bolts is 81 kpsi (558 MPa), worst case. For the bolts, with $A_S = 0.232$ in^2 (150 mm^2),

$$F_{BY} = 81 \times 10^3 \, (0.232) = 18.8 \times 10^3 \text{ lb } (83.6 \text{ kN})$$

For the joint, we determine the yield load of that portion of the joint which lies under the head of the bolt or under the washer (using the distance across flats of the head or nut to compute the bearing area). If our joint material is ASTM A441 steel

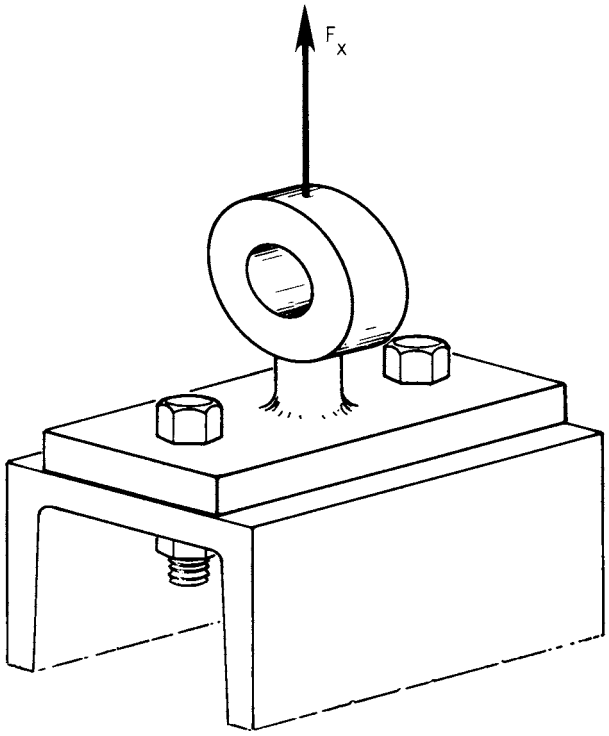

FIGURE 22.12 Joint loaded in tension. This is the joint analyzed in the text. The bolts used here are those shown in Fig. 22.10.

with a yield strength of 40 kpsi (276 MPa), we would find that a *bolt* force of 27.6 kip (122 kN) would yield the joint. We take the lesser of the joint or bolt yield loads, 18.8×10^3 lb (83.6 kN) as the yield load of the system.

Next, since we are planning to tighten these fasteners by applying torque to the nuts, we subtract 10 percent from the yield strength of the fastener to allow for the torsional stresses which will be developed in the fastener as it is tightened. If we were planning to use a high-pressure lubricant on the threads, we might subtract only 2 to 4 percent for torsion. Since no lube will be used in our example, we subtract 10 percent, making the upper limit 16.9×10^3 lb (75.2 kN).

This will remain our upper limit unless the fasteners will also be subjected to shear stress; or unless code limits, stress corrosion problems, or the desire for a safety factor forces us to reduce it further. We will assume, in our example, that they do not.

Before continuing, however, let us see what we would have to do if the bolts *did* see a combined tension and shear load. This might happen, for example, in a bearing-type joint in which we planned to preload (tension) the bolts to a significant percentage of yield. There are other types of joint, of course, which are subjected to both tensile and shear loads in use. Any shear load on the bolt will "use up" part of the strength of the bolt, leaving less capacity for tensile loads (Ref. [22.6], p. 226).

Under these conditions, the maximum acceptable tensile stress in a bolt can be determined using any of the static failure theories of Chap. 28. Here, we select the equation

$$\left(\frac{\lambda}{S}\right)^2 + \phi^2 = 1 \tag{22.14}$$

where S = the ratio of the shear strength to the tensile strength (typically 0.6) for bolt steels. Equation (22.14) is a form of the maximum-shear-stress theory.

Acceptable Lower Limit for the Clamping Force on the Joint. When we are computing the maximum acceptable forces, we focus on the joint, because its behavior can be seriously affected if the interface forces become too small. The joint, for example, might leak, it might vibrate loose, or it might have a short fatigue life. To determine the lower acceptable limit, we must consider each potential failure mode separately, estimate the minimum preload required to control that particular problem, and then select the *highest* of these several minimum requirements to establish the minimum for the system.

This is one of the more difficult steps of our procedure. In fact, we may be able to determine the acceptable minimum preload only by making fatigue or vibration tests or the like. (We will consider fatigue problems at length in Sec. 22.5.) There are some rules of thumb, however, which we can apply.

If our joint is a friction-type shear joint, or if it will be subjected to transverse vibration, we want a minimum preload which will prevent joint slip under the maximum anticipated shear load. This load is

$$F_C(\min) \geq \frac{F_X}{S} \tag{22.15}$$

If we are dealing with a foundation bolt or something where it is only necessary to avoid separation of the joint members, the minimum acceptable preload can be zero. If we are dealing with a gasketed joint, we will have to worry about the minimum acceptable gasket pressure required to keep that gasket from leaking.

Example. Let us assume for our ongoing example that we are concerned only about separation of the joint members. Minimum acceptable clamping force, therefore, is zero.

Select an Initial Preload Target. We now, rather arbitrarily, select an initial preload target that is somewhere between the acceptable minimum and acceptable maximum bolt tensions which we computed earlier. Let us try 60 percent of the acceptable maximum of 16.9 kip (75.2 kN) or, in our example, 10.1×10^3 lb (45.1 kN).

22.3.3 Estimating Actual Upper Limit on Bolt Tension

We must now determine whether or not the tension we will actually develop in any bolt will exceed the maximum acceptable tension, given our preliminary target preload and a consideration of the tools, lubricants, and procedures we are planning to use during assembly. We must also consider the effects of the external tension loads which will be placed on this joint after assembly.

Tool Errors. We can select many different types of assembly tools. Each choice carries with it certain accuracy implications; some tools can produce preload in the fasteners with far greater precision than can other tools. Table 22.4 lists some of the many possibilities. We will assume for our example that we are going to use a manual torque wrench and must face a potential scatter in preload for a given torque of ±30 percent.

Operator Problems. Even if we used perfect tools, we would see some scatter in the resulting preload because of operator problems. Are the operators skilled, properly trained, or tired? Do they care about their work? Are the bolts readily accessible?

Let us assume for purposes of our example that the operators will contribute an estimated ±10 percent additional scatter in preload. We do not just add this 10 percent to the 30 percent we assigned to the torque wrench when we assess the combined impact of tools and operators. We use the statistician's method for combining the variances of two variables, as follows:

$$\sigma^2 = \sigma_T^2 + \sigma_O^2 \tag{22.16}$$

In our example this suggests that the combined variance will be

$$\sigma^2 = 30^2 + 10^2 = 1000$$

giving us a ±3 sigma "deviation" (square root of the variance) of ±31.6 percent.

We have selected a target preload of 10.1×10^3 lb. Consideration of tool and operator scatter gives us

$$F_P(\max) = F_{PT} + 0.316F_{PT} = 13.3 \times 10^3 \text{ lb (59.2 kN)}$$

$$F_P(\max) = F_{PT} - 0.316F_{PT} = 6.91 \times 10^3 \text{ lb (30.7 kN)}$$

Effects of External Tension Load. Now let us see what happens when an external tension load is placed on the preloaded joint. Although it is difficult to do this in

TABLE 22.4 Tool Accuracy

Control parameter and type of tool	Source	Reported scatter in preload, %
Torque control with		
1. Power wrench	1	±23 to 28
2. Hand wrench	2	±21 to 81
3. Hand wrench	3	−20. 4 to 99
4. Hand wrench plus torque multiplier	4	±70 to150
5. Dial or click wrench	4	±60 to80
6. Wrench with electronic readout	4	±40 to60
7. Hand wrench	2	±12
8. Air-powered tool with torque feedback	5	±20
9. Hand wrench in laboratory conditions	6	±30
10. Air tool with one shot clutch	7	±30
11. Stall torque air tool	7	±35
12. Hand wrench	7	±30
Torque-turn control with		
13. Yield control system (computer-controlled air tool)	8	±8
14. Turn-of-the-nut procedure used in structural steel work	9	±15
15. Logarithmic rate method (LRM†) controlled air tool	11	±2.2 to 2.6
16. Turn-of-the nut	6	±15
Miscellaneous methods		
17. Strain-gauged load washers	10	±15
18. Strain-gauged bolts	10	±1
19. Swaged lockbolts	10	±5
20. Bolt heaters	12	±15
21. Air-powered impact wrench	5	±50
22. Manual slug wrench	3	−48 to + 50
23. Air-powered impact wrench	4	−300 to +150
24. Hydraulic tensioners controlled by "large vernier gauge readout"	4	±20
25. Torque-time control on air tool	5	±11
26. Operator feel	6	±35
27. Fastener elongation	6	±3 to 5
28. Ultrasonic control of preload		±1 to10

†Trademark of Rockwell International

SOURCES:

1. Robert J. Finkelston and P. W. Wallace, "Advances in High Performance Mechanical Fastening," SAE Paper No. 800451, 1980, p. 6.
2. Results of tests conducted privately.
3. Roly Laird, "The Nuts and Bolts of Preventing Failure Where Pressure Is Hot," *Engineer* (GB), vol. 245, no. 6330, July 21, 1977, p. 37.
4. Steven F. Aaronson, "Analyzing Critical Joints," *Machine Design,* January 21, 1982, p. 95.
5. *Investigation of Threaded Fastener Structural Integrity,* Southwest Research Institute, San Antonio, Texas, October 1977, p. 3.
6. *Fastener Standards,* 5th ed., Industrial Fastener Institute, Cleveland, Ohio, 1970, p. N-12.
7. Edwin Rodkey, "Making Fastened Joints Reliable—Way to Keep 'em Tight," *Assembly Engineering,* March 1977, pp. 24–27.
8. Robert J. Finkeltson, "Optimized Bolt Tightening Takes to the Field," SPS Laboratories, Jenkintown, PA., March 1981.
9. E. Donald, "Fatigue-Indicating Fasteners; A New Dimension in Quality Control," *Fastener Technology,* March 1979.
10. Larry D. Mercer, "How Swaged Lockbolts Optimize Fastener Preload," National Design Engineering Conference, Chicago, Ill., 1982.
11. S. Eshghy, "Tension by Ultrasonic Stretch," privately published, June 1982.
12. Carl Osgood, "How Elasticitiy Influences Bolted-Joint Design," *Machine Design,* March 1972, p. 106.

practice, we usually assume that a tension load is applied between the head of the fastener and the nut or tapped hole at the other end. Such a load would have a *worst-case effect* on the tension in the fasteners and on the clamping force on joint members, so this assumption is a safe and conservative one.

Any such tension load, no matter how small, will add to the tension in the bolts, increasing the length of the bolts slightly and thereby reducing the clamping force on the joint interface.

Not all the external load applied to the bolt is seen by the bolt, however. Part of the external load merely replaces part of the outward force which the joint initially exerted on the bolts that were clamping it. This can be illustrated by what engineers call a *joint diagram,* such as that shown in Fig. 22.13. Note that the external load applied to the bolt is equal to the sum of the changes which occur in the bolt and joint. It is equal, in other words, to the increase in tension in the fasteners plus the decrease in compressive load in the joint. We say that one part of the external load has been "absorbed" by the bolts; the rest has been absorbed by the joint (Ref. [22.6], pp. 199*ff*).

The relative stiffness or spring rate of bolt and joint determines how much of the load each will absorb. In Fig. 22.13 the joint stiffness is 3.23 times that of the bolt, as determined by our previous calculation of the stiffness ratio R_{JB} for the bolt in Fig. 22.10. The joint, therefore, will absorb approximately seven-tenths of any applied external tension load.

We should note in passing that the effects of an external *compressive* load can also be illustrated by a joint diagram, such as that shown in Fig. 22.14. This time the tension in the bolt is reduced and the compression in the joint is increased simultaneously by the single external load. The portions absorbed by fasteners and joint are again proportional to their relative stiffness.

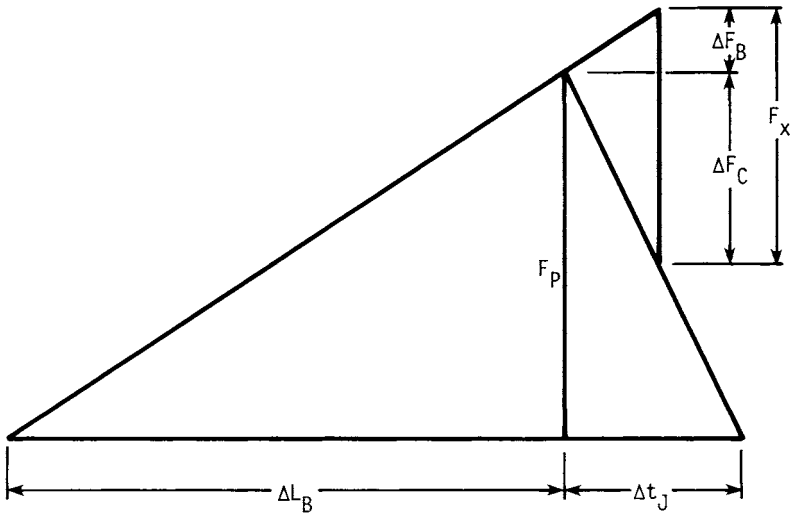

FIGURE 22.13 Joint diagram for a joint loaded in tension. A joint diagram consists of two force-elongation diagrams, one for the bolt and one for the joint material loaded by that bolt put front-to-front (Ref. [22.6], pp. 199–206). It illustrates the combined elastic behavior of bolt and joint.

BOLTED AND RIVETED JOINTS

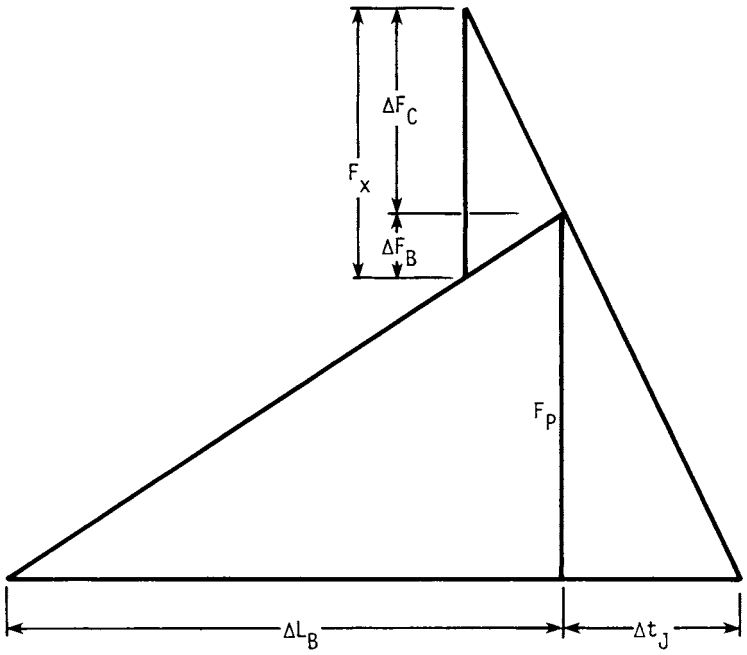

FIGURE 22.14 Joint diagram for a joint loaded in compression.

Note that *any* external compression or tension load will alter both the tension in the fasteners and the compression in the joint. This is contrary to the widely held belief that there will be no such change in either member until and unless the external tensile load exceeds the preload in magnitude.

If the external tensile load exceeds the initial preload, then all clamping force will have been removed from the joint and the bolts will see, in its entirety, any additional tension load placed on that joint.

One nice feature of the joint diagram is that it allows us to derive expressions which define joint behavior, such as the following:

$$k_B = \frac{F_P}{\Delta L_B} \qquad k_J = \frac{F_P}{\Delta t_j} \tag{22.17}$$

$$\Delta F_B = F_x\left(\frac{k_B}{k_J + k_B}\right) \tag{22.18}$$

$$\Delta F_C = F_x\left(1 - \frac{k_B}{k_J + k_B}\right) \tag{22.19}$$

Let us continue the example we started in Fig. 22.12 by assuming an external tensile load of 10 kip (44.5 kN) per bolt has been placed on the system and computing the estimated effect of the external load on the bolt tension:

$$F_B = 5000\left[\frac{2.265 \times 10^6}{(7.316 + 2.265) \times 10^6}\right] = 1182 \text{ lb } (5.26 \text{ kN})$$

Estimated Maximum Tension in the Bolts. We can now combine all the effects which we have studied to determine the maximum anticipated tension in the bolts under the worst-case situation:

$$F_B(\max) = F_P(\max) + \Delta F_B$$

$$F_B(\max) = 13.3 \times 10^3 + 1.182 \times 10^3 = 14.5 \times 10^3 \text{ lb } (64.5 \text{ kN})$$

So our anticipated maximum is less than the acceptable maximum preload of 16.9×10^3 lb (75.2 kN). We can therefore continue with our analysis. Note that if the anticipated maximum had exceeded the acceptable maximum, we would have had to lower our target preload somewhat and try again.

22.3.4 Estimating Actual Lower Limit on the Clamping Force

To determine the lower limit on clamping force, we follow a procedure similar to that used for determining the maximum tension to be expected in the fasteners, this time subtracting, not adding, from target preload the tool and operator scatter and that portion of the external load which reduces the clamping force on the joint members (ΔF_C in Fig. 22.13). When considering the lower limit, we must also consider one other effect: the short-term relaxation of the joint following or during initial tightening.

Relaxation Effects.

Embedment Relaxation. When joint and fastener are first assembled, especially if we are dealing with new parts, they contact each other only on the microscopically rough high spots of their contact surfaces. These high spots will be loaded past the yield point and will creep and flow when first placed under load until enough additional surface area has been brought into play to stabilize the process. Other plastic flow can occur in thread roots, in the head-to-body fillet, and even in some whole threads, causing further relaxation. All these effects are lumped together under the term *embedment relaxation.* Typically they will lead to a loss of 2 to 10 percent of initial preload in the first few seconds or minutes after initial tightening. Let us assume a 5 percent loss of our ongoing example.

Elastic Interactions in the Joint. Achieving perfect initial preload is not our only problem when we tighten a multibolt joint. When we tighten the first fasteners, we stretch them and partially compress the joint. When we subsequently tighten other fasteners in the same joint, we further compress the joint. Because this act allows previously tightened fasteners to contract a little, it reduces the tension in those fasteners even if we achieved perfect *initial* preload in each when we first tightened it.

The effect a fastener has on a previously tightened fastener is illustrated in Fig. 22.14. The new fastener applies a compressive load to the joint which had been previously preloaded by the first bolt.

Estimating Minimum Clamping Force. Elastic interactions can be a special problem in large-diameter and/or gasketed joints. Since our example is neither, and involves only two bolts, we will assume that these interactions cost us, worst case,

only 25 percent of initial preload in that bolt tightened first. Worst-case minimum clamping force in the vicinity of that bolt, therefore, becomes

$$F_C(\min) = F_P(\min) - F_X\left(1 - \frac{k_B}{k_J + k_B}\right) - F_P(\min)P_Z$$

$$F_C(\min) = 6.91 \times 10^3 - 5000\left[1 - \frac{2.265 \times 10^6}{(7.316 + 2.265) \times 10^6}\right] \qquad (22.20)$$

$$- 6.91 \times 10^3(0.05 + 0.25) = 1019 \text{ lb } (4.53 \text{ kN})$$

So our computed anticipated minimum is greater than the zero minimum acceptable clamping force determined earlier. If it had not been acceptable, we would, of course, have had to readjust our target preload and/or select more accurate tools and/or revise our design.

22.3.5 Achieving a Desired Preload

In most cases we will try to achieve our target preload by using a wrench of some sort to apply torque to the nut or to the head of the bolt, accepting the resulting scatter in preload which this implies. We will discuss the torque-preload relationship at length in the next section. First, however, let us take a brief look at some of our other options for tightening bolts.

Hydraulic Tensioners and Bolt Heaters. On large bolts we do not have to use a wrench. We can use a hydraulic tensioner which exerts a pure tension on the bolt, grabbing a few threads which stick out past the nut. Once the tool has stretched the bolt by the desired amount, the nut is run down to retain the tension. Then the tool lets go. At first glance this sounds like a perfect answer to some of the torquing and friction uncertainties we shall consider in Sec. 22.4, but there are other problems. The amount of preload retained by the fastener's nut is never the same as the preload introduced by the tool, because the nut must embed itself in the joint to pick up the loads originally supported by the much larger feet of the tensioner. This *elastic recovery loss* can equal 10 to 80 percent of the initial tension, depending on whether the fastener is relatively long (smaller loss) or short, and depending on how much torque was applied to the nut when it was run down (more torque, less loss).

Hydraulic tensioners, however, are superb tools when it comes to preloading large fasteners. They can be gang-driven from a single hydraulic pump and so can tighten several fasteners simultaneously with the same initial tension in each. This can be a very important feature when you are tightening large joints, especially if they are gasketed.

Tensioners also eliminate the galling problems often encountered when we attempt to torque large fasteners (3 in in diameter or more). The male and female threads are not turned relative to each other under heavy contact pressure with the tensioner. So tensioners have a place, but they do not provide perfect control of bolt preload.

Another nonwrench sometimes used to preload large fasteners is a bolt heater. This is inserted in an axial hole running down the center of the bolt. The bolt gets longer as it gets hot. When it is hot, the nut is run down against the joint to retain the increase in length produced by the heat. Since this is a crude way to preload bolts,

the process must be controlled by other means. Dial gauges or micrometers are usually used to measure the net change in length of the bolts after they have cooled. If they have been stretched too much or too little, the bolts must be reheated and the nuts run down again. The process takes skill but is widely used on large fasteners (again 3 in or so and larger).

Microprocessor-Controlled Torque-Turn Tools. Hydraulic tensioners and bolt heaters make it possible to tighten fasteners without suffering the uncertainties of the torque-preload relationship, but they can be used only on large-diameter fasteners. For smaller ones, we need something else. One relatively new approach—microprocessor-controlled tools—measures both applied torque and the turn of the nut to monitor and/or control fastener preload. Most of the presently available systems are designed for automatic or semiautomatic assembly in mass-production operations (automotive, primarily), but there are manual versions of some of them. They can control preload to ±2 to 5 percent if the joints are relatively soft (preload builds up smoothly as the bolts are tightened) and reasonable control is maintained over fastener dimensions and lubricity.

Some of these systems are designed to tighten every fastener to the yield point. This provides good preload accuracy (control is based on the act of yield rather than the torque-friction-preload relationship). But not all joints can be tightened safely to the yield point of the fastener. Although there is considerable debate on this point, many designers feel that yield-point tightening can lead to fatigue failure or rupture unless future external loads can be predicted and controlled.

Turn-of-the-Nut Control. There is one place where tightening to or past the yield point is the norm; structural steel joints have been tightened this way for half a century using a carefully designed process called *turn-of-the-nut.* The fastener is first tightened to 60 to 80 percent of yield by the application of torque (usually with an air-powered impact wrench). The location of one corner of the nut is then noted, and a wrench is used to give the nut a specified half turn or so (depending on the size of the fastener and whether or not it is being used on a flat or tapered joint member). This amount of turn always takes the bolt beyond yield. Since external loads can be predicted, however, and are generally static rather than dynamic, the process is a safe and effective way to control preload.

Ultrasonic Control of Preload. Ultrasonic instruments are sometimes used instead of torque and/or turn-of-the-nut to control preload (Ref. [22.6], p. 157). This technology has been used in a few aerospace applications for nearly a decade and is just starting to emerge in the commercial marketplace.

Presently available instruments send bursts of sound through the fastener and measure the time it takes for these wavefronts to travel through the fastener, echo off the far end, and return to the transducer. As the fastener is tightened, the time required for this round trip increases because the fastener gets longer, and so the path length is increased. Also, the velocity of the sound waves decreases as the stress level increases.

Microprocessors in the instruments sort out the change-in-length effect from the velocity effect and display either the change in length of the fastener or the average stress level in the tensile-stress area of the threads. Either of these quantities can be used to estimate fastener preload with better accuracy than is possible with torque or torque-turn controls.

One advantage of ultrasonics is that it can also be used in some cases to measure residual or working loads in the fasteners, as well as initial loads. You can use it to

detect the effects of elastic interactions, for example, and therefore to compensate for such interactions. You can measure residual loads days or even years after initial tightening, which is never possible with torque and/or turn means.

Ultrasonics can be used with any sort of wrench, as well as with tensioners or heaters, to tighten fasteners.

22.4 BOLT TORQUE REQUIREMENTS

22.4.1 The Problem

Although torque is the most common way to tighten a fastener, it is not a very good way, usually, to control the preload developed within the fastener. As we saw in Table 23.4, we must expect to see a scatter of ±30 percent or worse in the preload we achieve if we are using torque tools to tighten the fasteners. This scatter is acceptable in most applications, however. We compensate for it by overdesign, using larger bolts than might otherwise be necessary, for example.

Many factors affect this scatter in preload. These include such things as the finish on nuts, bolts, and joint members; the age, temperature, quantity, condition, and type of the lubricants used, if any; the speed with which the fasteners are tightened; the fit between male and female threads; the size of the holes and their perpendicularity with respect to joint surfaces; and the hardness of all parts. There is no way in which we can control or predict all the variables in a given situation, and so we must always expect and accept a considerable scatter in preload results when we use torque to control the tightening operation.

22.4.2 Selecting the Correct Torque

Having said all this, we must still select an appropriate torque to produce, or attempt to produce, the target preload we have established for our design. Our best bet is to use the so-called short-form torque equation to make an estimate. This equation is

$$T = KdF_{PT} \tag{22.21}$$

The nut factor K is an experimental constant, a *bugger factor,* if you will, which defines the relationship which exists between applied torque and achieved preload in a given situation. The only way to determine what K should be in your application is to make some actual experiments in which you measure both torque *and* preload and compute the mean K and the scatter in K. If accuracy is not a big concern or you are merely trying to select the proper size of wrench or determine the approximate preloads you will achieve, then it is safe to use a nut factor listed in Table 22.5.

22.5 FATIGUE LOADING OF BOLTED AND RIVETED JOINTS

When a bolt or joint member suddenly and unexpectedly breaks, it has probably failed because of fatigue. This is certainly one of the most common modes of failure for bolted joints. The designer, therefore, should learn how to cope with it.

TABLE 22.5 Nut Factors

Lubricant or coating on the fastener	Source	Nut factor	
		Reported mean	Reported range
1. Cadmium plate	1	0.194–0.246	0.153–0.328
2. Zinc plate	5	0.332	0.262–0.398
3. Black oxide	1	0.163–0.194	0.109–0.279
4. Baked on PTFE	1	0.092–0.112	0.064–0.142
5. Molydisulfide paste	2	0.155	0.14–0.17
6. Machine oil	2	0.21	0.20–0.225
7. Carnaba wax (5% emulsion)	2	0.148	0.12–0.165
8. 60 Spindle oil	2	0.22	0.21–0.23
9. As received steel fasteners	3	0.20	0.158–0.267
10. Molydisulfide grease	3	0.137	0.10–0.16
11. Phosphate and oil	3	0.19	0.15–0.23
12. Copper-based anti seize compound	3	0.132	0.08–0.23
13. As received steel fasteners	4	0.20	0.161–0.267
14. Plated fasteners	4	0.15	
15. Grease, oil, or wax	4	0.12	

SOURCES:

1. Values given are typical results from a very large and unpublished set of experiments on ASTM A193 B7 studs treated with various coatings. The tests were made in 1979–1980. Mean values for K varied with the diameter of the studs tested and the torques applied in various test series.
2. Kazuo Maruyama, Makoto Masuda, and Nobutoshi Ohashi, "Study of Tightening Control Methods for High Strength Bolts," *Bulletin of the Research Laboratory Precision Machine Selection,* Tokyo Institute of Technology, N46, September 1980, pp. 27–32.
3. John H. Bickford, *An Introduction to the Design and Behavior of Bolted Joints,* Marcel Dekker, Inc., New York, 1981, p. 429.
4. *Fastener Standards,* 5th ed., Industrial Fastener Institute, Cleveland, Ohio, 1970, p. N-16.
5. Edwin Rodkey, "Making Fastened Joints Reliable—Ways to Keep 'em Tight," *Assembly Engineering,* March 1977, p. 24.

22.5.1 Spotting a Fatigue Problem

It is usually easy to diagnose a fatigue failure. Here are the clues:

1. *Cyclic Loads* Fatigue failures always occur under cyclic tension loads.
2. *No Advance Warning* Fatigue failure is always sudden and almost always unexpected. The parts do not neck-down or wear out before they fail.
3. *Appearance of the Break Surface* If you examine the surface of a part which has failed in fatigue, you will usually find that a section of the surface is smooth, sometimes almost polished. Another portion of the surface, surrounding the first, may be a little rougher but is still basically smooth. The remainder of the surface will be very rough indeed.
4. *Typical Failure Points* The parts tend to fail at points of high stress concentration. Figures 22.15 and 22.16 show the most common failure points.

22.5.2 Estimating Fatigue Life

Many factors affect the fatigue life of any machine part, including fasteners. Such things as shape, heat treatment, surface finish, the mean load stress, the magnitude of

load excursions, and the material all play a role. If you know the basic strength of the part, however, you can use the methods of Chap. 29 to estimate fatigue strength or endurance limit. Table 22.6 gives you the strength information you will need to do this for fasteners. You will find other information pertinent to the fatigue of joint members in Chaps. 32 and 29.

The term *proof strength* in Table 22.6 deserves explanation. It is common to test the strength of fasteners by applying tension loads to them. The *proof load* of a given fastener is the highest tensile force which can be applied to it without causing a permanent set to the fastener. The *proof strength* can then be determined by dividing the proof load by the tensile-stress area of the threads [Eq. (22.4)].

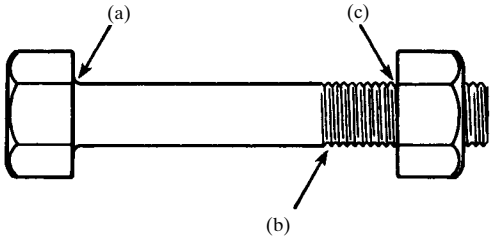

FIGURE 22.15 Typical failure points of a bolt. (*a*) Failure at head fillet; (*b*) failure at thread runout; (*c*) failure at first thread to engage the nut.

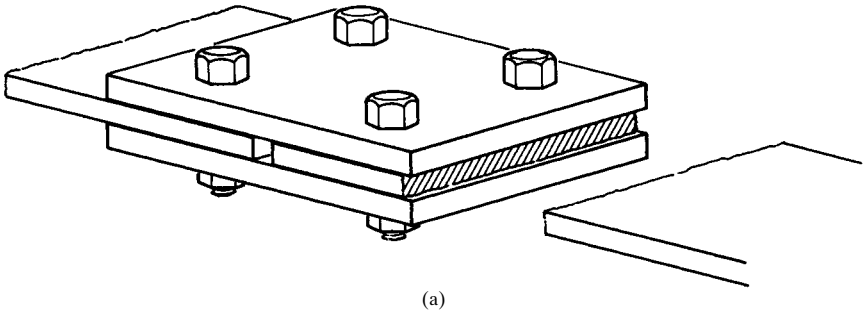

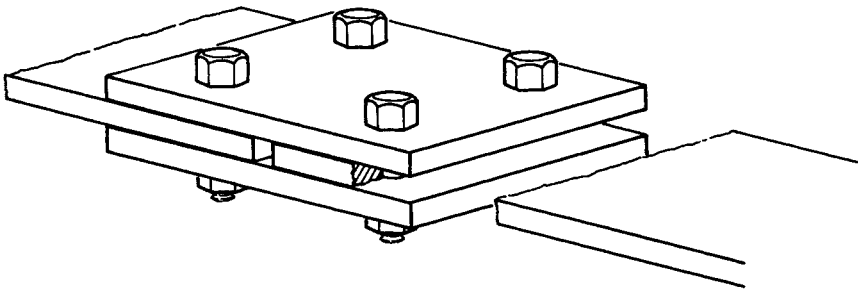

FIGURE 22.16 Typical fatigue failures in joints loaded in shear. (*a*) Failure occurs in the gross cross section, near the place where the splice plates and joint plates meet, in a friction-type joint; (*b*) failure occurs in a net cross section, through a line of bolts, in a bearing-type joint.

TABLE 22.6 Specifications and Identification Markings for Bolts, Screws, Studs, Sems,[a] and U Bolts[b]

SAE grade	ASTM grade	Metric grade[c]	Nominal diameter in	Proof strength,[d] kpsi	Tensile strength,[d] kpsi	Yield strength,[d,e] kpsi	Core hardness Rockwell min/max	Grade identification marking	Products[f]	Material
1	A307	4.6	¼ thru 1½	33	60	36	B70/B100	None	B, Sc, St	Low- or medium-carbon steel
2	...	5.8	¼ thru ¾	55	74	57	B80/B100	None	B, Sc, St	Low- or medium-carbon steel
		4.6	Over ¾ thru 1½	33	60	36	B70/B100	None	B, Sc, St	Low- or medium-carbon steel
4	...	8.9	¼ thru 1½	65[g]	115	100	C22/C32	None	St	Medium-carbon, cold-drawn steel
5	A449 or A325 Type 1	8.8	¼ thru 1	85	120	92	C25/C34		B, Sc, St	Medium-carbon steel, Q&T
		7.8	Over 1 thru 1½	74	105	81	C19/C30		B, Sc, St	Medium-carbon steel, Q&T
		8.6	Over 1½ to 3	55	90	58	...		B, Sc, St	Medium-carbon steel, Q&T
5.1	...	8.8	No. 6 thru ⅝	85	120	...	C25/C40		Se	Low- or medium-carbon, Q&T
		8.8	No. 6 thru ½	85	120	...	C25/C40		B, Sc, St	Low- or medium-carbon, Q&T

5.2	A325	8.8	¼ thru 1	85	120	92	C26/C36		B, Sc	Low-carbon martensite steel, fully killed, fine-grained, Q&T
7[h]	Type 2 ...	10.9	¼ thru 1½	105	133	115	C28/C34		B, Sc	Medium-carbon alloy steel, Q&T
8	A354 Grade	10.9	¼ thru 1½	120	150	130	C33/C39		B, Sc, St	Medium-carbon alloy steel, Q&T
8.1	BD ...	10.9	¼ thru 1½	120	150	130	C31/C38	None	St	Elevated temperature drawn steel-medium carbon alloy or G15410
8.2	...	10.9	¼ thru 1	120	150	130	C35/C42		B, Sc	Low-carbon martensite steel, fully killed, fine-grained, Q&T
...	A574	12.9	0 thru ¼	140	180	160	C39/C45	12.9	SHCS	Alloy steel, Q&T
		12.9	⅜ thru 1¼	135	170	160	C37/C45	12.9	SHCS	Alloy steel, Q&T

[a]Sems = screw and washer assemblies.
[b]Compiled from ANSI/SAE J429j; ANSI B18.3.1-1978; and ASTM A307, A325, A354, A449, and A574.
[c]Metric grade is *xx.x*, where *xx* is approximately $0.01S_u$ in MPa and *.x* is the ratio of the minimum S_y to S_u.
[d]Multiply the strengths in kilopounds per square inch by 6.89 to get strength in megapascals.
[e]Yield strength is stress at which a permanent set of 0.2% of gauge length occurs.
[f]B = bolt, Sc = screws, St = studs, Sc = Sems, and SHCS = socket head cap screws.
[g]Entry appears to be in error but conforms to the standard ANSI/SAE J429j.
[h]Grade 7 bolts and screws are roll threaded after heat treatment.

SOURCE: From Joseph E. Shigley and Charles R. Mischke, *Mechanical Engineering Design*, 5th ed., McGraw-Hill, 1989; reproduced by permission of the authors and the publisher.

22.5.3 Reducing Fatigue Problems

There are a lot of things you can do to minimize fatigue problems.

Material and Part Selection and Care. Materials with higher tensile strengths tend to have better fatigue lives than those with lower tensile strengths, at least up to an ultimate tensile strength of 200 kpsi (1379 MPa) or so. It also helps to select a material having low-notch sensitivity.

Avoid decarburization of the parts. Decarburization can weaken part surfaces and make it much easier for initial cracks to form.

Make sure that nut faces and the undersurface of the bolt head are perpendicular to the axis of the bolt threads and that the holes are perpendicular to the surfaces of the joints [22.10]. Two degrees of angularity can reduce fatigue life to only 25 percent of normal.

Lubricate the threads [22.10]. If nothing else, this can reduce corrosion problems, and corrosion is a main source of initial cracks.

If using fasteners with a tensile strength above 150 kpsi (1034 MPa), do *not* use lubricants containing sulfides, since these can contribute to stress-corrosion cracking, which will accelerate fatigue failure [22.11].

Grit blast the surfaces of joints loaded in shear before assembling because anything which increases the slip resistance improves fatigue life ([22.2], p. 120).

Prevent Crack Initiation. Polish, but do not hard coat, bolt surfaces, or shot peen the surfaces, or roll bolt threads after heat treatment. Do anything and everything possible to avoid corrosion of bolts or joint members (see Chap. 35).

Reduce Load Excursions. Even if the magnitude of external loads imposed on a joint are beyond the designer's control, there are many things which he or she can do to reduce the variations in load seen by a given joint. And these variations, or *load excursions,* are a key issue. We always want to keep the ratio between minimum load and maximum load seen by the parts as close to unity as possible.

Some say the minimum bolt tension should always be more than half the maximum bolt tension. Others recommend a preload that is at least two to three times the magnitude of the worst-case external load to be applied to the joint. Because of the large number of variables involved, such rules will apply only to certain applications. Nevertheless, they give you an idea of the importance of minimizing load excursions.

It helps to increase the ratio between the stiffness of the joint and the stiffness of the bolt (k_J/k_B) so that the joint will absorb a larger percentage of the applied load excursions. There are many ways to do this. For examples, see Fig. 22.17*a* and *b.* Reducing the body of the bolt to nine-tenths of the nominal diameter is sometimes recommended.

It helps to compensate for initial preload loss and relaxation effects by retightening the bolts after they have relaxed. By the same token, try to avoid vibration loss of preload by providing damping and/or by periodic retightening of the nuts and/or by using special vibration-resistant fasteners.

Reduce Stresses in Parts. Make sure there are at least three threads above and below the faces of the nut (Fig. 22.17*c*). Do not let the thread run-out point coincide with the shear plane of the joint (Fig. 22.17*d*). Roll the threads instead of cutting

BOLTED AND RIVETED JOINTS

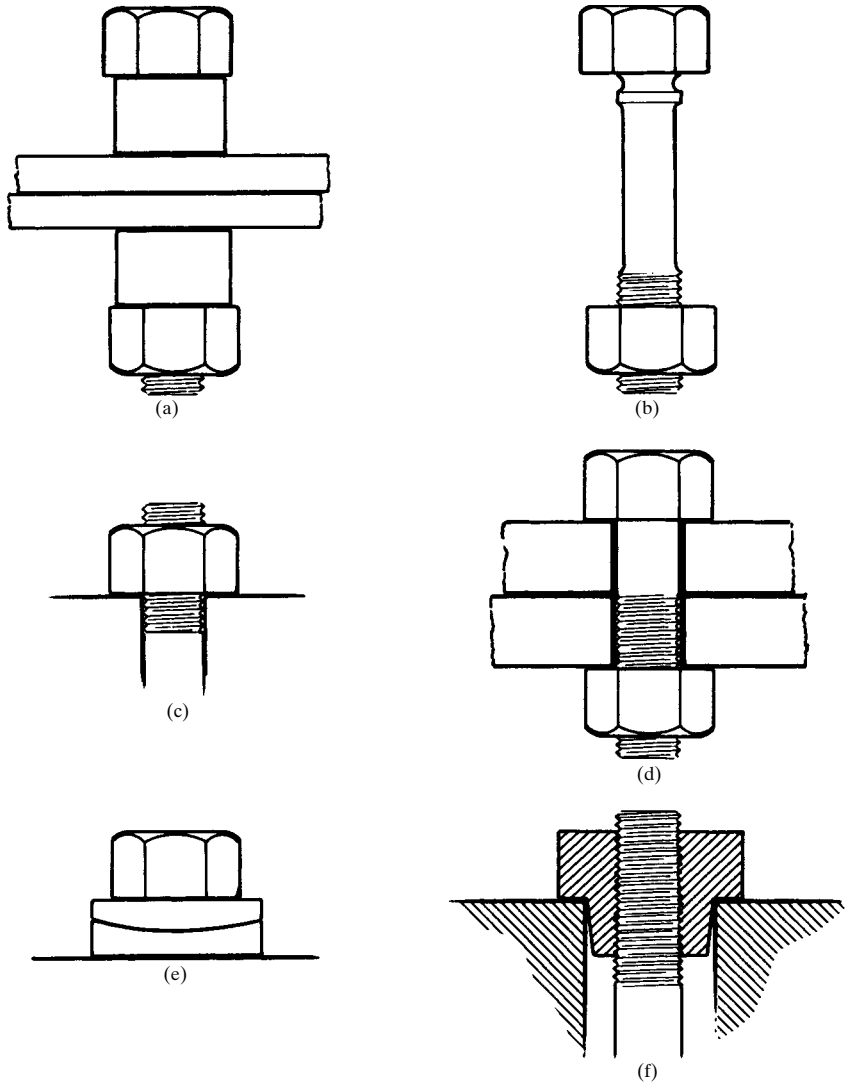

FIGURE 22.17 Ways to improve the fatigue life of bolts. (*a*) Use collars to increase the length-to-diameter ratio of the bolts; (*b*) turn down the body of a bolt to reduce its stiffness; (*c*) make sure that there are at least three threads above and below a nut to reduce thread stress concentrations; (*d*) it also helps to avoid the situation, shown here, where thread run-out coincides with a shear plane in the joint, or (*e*) to use spherical washers to help a bolt adjust to bending loads, or (*f*) to use tension nuts to reduce thread stress levels. All figures shown are improvements except (*d*).

them, and if possible, roll them after heat treatment instead of before [22.12]. Use a large root radius in the threads.

Use a large head-to-body fillet, and use elliptical fillets instead of round fillets [22.13]. Use spherical washers to minimize bending effects (Fig. 22.17*e*). Use Class 2 threads instead of Class 3. Use tension nuts for a smoother stress transition in the bolts (Fig. 22.17*f*). Use nuts that are longer than normal. Make sure the thread-to-body run-out is smooth and gradual.

22.6 PROGRAMMING SUGGESTIONS FOR JOINTS LOADED IN TENSION

Figure 22.18 shows the flowchart of a computer program which might be used to design bolted joints loaded in tension. We start by entering dimensions, strengths, external loads, and the like. Next, we compute the cross-sectional areas of the bolt and the stiffness of bolt and joint members. The program assumes that the joint is not gasketed.

Next, we compute the maximum acceptable tension in the bolt, basing this either on a code or specification limit or on the yield strength of the bolt. If the bolts are to see a combination of tension and shear loads, the acceptable upper limit of tension must, of course, be reduced.

The next step is to determine the acceptable lower limit on the clamping force in the joint. This will usually be a more complicated procedure than suggested by the flowchart. If gaskets are involved, for example, it would be necessary to calculate minimum clamping force using the procedures and equations of the ASME Boiler and Pressure Vessel Code, or the like. If all we are concerned about is transverse slip or total separation, we could use the equations shown in the flowchart.

We complete the definition of our design specifications by computing a target preload and then printing out the upper and lower acceptable limits, the force required to yield the bolt, and the target preload. It is useful to know these things if we need to revise the target preload at a later point in the program.

Having determined the acceptable upper and lower limits, we now take a series of steps to estimate the actual limits we will achieve in practice based on our target preload and estimates of such things as tool scatter and joint relaxation. During this part of the procedure we also introduce the estimated effects of the external tension loads on the joint, assuming linear joint behavior. The equations used here are derived from the joint diagram in Fig. 22.13.

We compute the anticipated upper limit on bolt tension first, and then we compute the anticipated lower limit on clamping force. We compare them, one at a time, to the acceptable limits. We recycle, choosing a new target preload, if the anticipated limits fall outside of the acceptable limits. In some cases we will not be able to satisfy our specifications merely by modifying the target preload; we may have to choose new joint dimensions to enlarge the range between upper and lower limits or choose more accurate tools to reduce the range between the upper and lower limits anticipated in practice.

When our conditions are satisfied, we complete the program by computing the torque required to aim for the target preload. Then we print out the final values of the parameters computed.

BOLTED AND RIVETED JOINTS

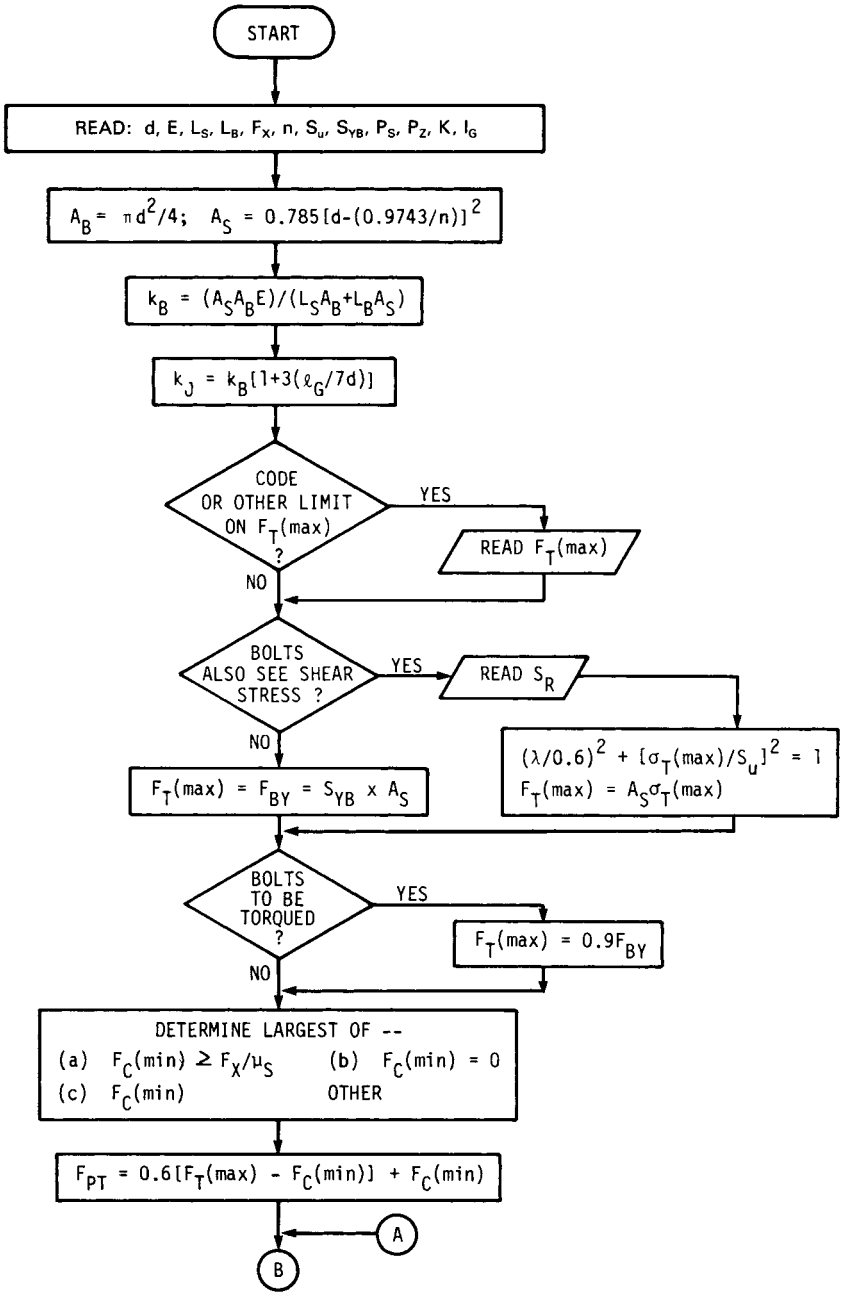

(a)

FIGURE 22.18 Flowchart describing a computer program which could be used to design non-gasketed joints loaded in tension. Chart continues on next page.

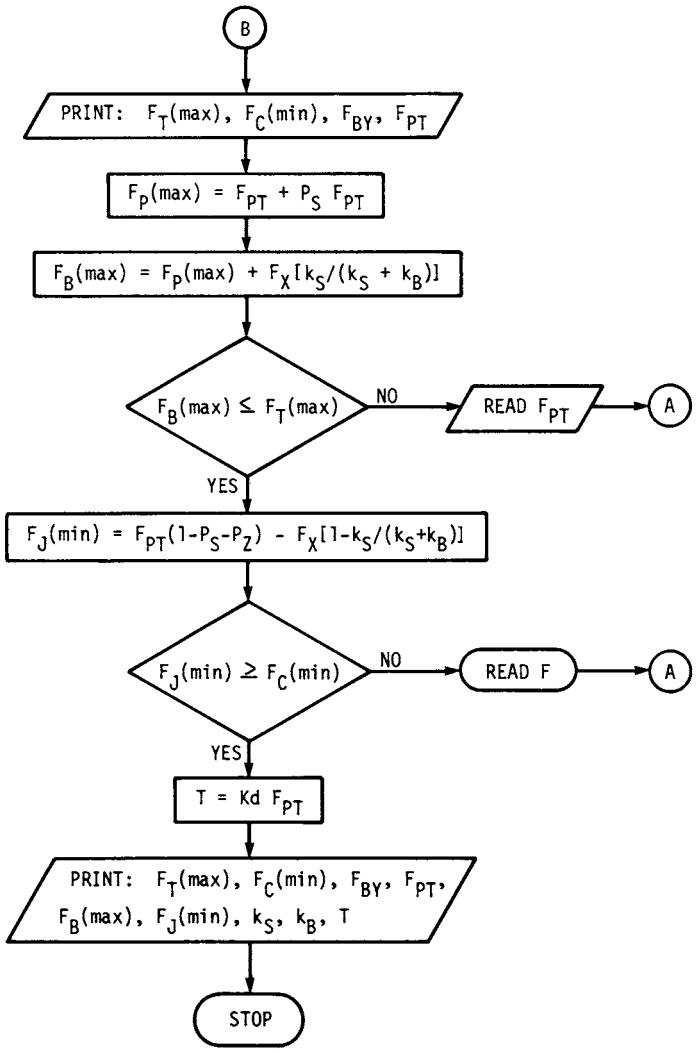

(b)

FIGURE 22.18 *(Continued)*

REFERENCES

22.1 Joseph E. Shigley and Charles R. Mischke, *Mechanical Engineering Design,* 5th ed., McGraw-Hill Book Company, New York, 1989.

22.2 Goeffrey L. Kulak, John W. Fisher, and John H. A. Struik, *Guide to Design Criteria for Bolted and Riveted Joints,* 2d ed., John Wiley & Sons, New York, 1987.

22.3 Archie Higdon, Edward H. Ohlsen, William B. Stiles, John A. Weese, and William F. Riley, *Mechanics of Materials,* 3d ed., John Wiley & Sons, New York, 1978.

BOLTED AND RIVETED JOINTS

22.4 ANSI Specification B1.1-1974, "Screw Threads," American Society of Mechanical Engineers, New York, 1974, p. 80.

22.5 Specifications BS 3643: Part 2: 1981, "ISO Metric Screw Threads," British Standards Institute, London, 1981, p. 10.

22.6 John H. Bickford, *An Introduction to the Design and Behavior of Bolted Joints,* 2d ed., Marcel Dekker, New York, 1990, p. 106.

22.7 Nabil Motosh, "Determination of Joint Stiffness in Bolted Connections," *Trans. ASME,* August 1976, p. 859.

22.8 G. H. Junker, "Principle of the Calculation of High Duty Bolted Joints: Interpretation of VDI Directive 2230," Unbrako Technical Thesis, SPS, Jenkintown, Pa., 1974, p. 8.

22.9 Carl C. Osgood, *Fatigue Design,* Wiley-Interscience, New York, 1970, p. 196.

22.10 Joseph Viglione, "Nut Design Factors for Long Life," *Machine Design,* August 1965, p. 138.

22.11 "Degradation of Threaded Fasteners in the Reactor Coolant Pressure Boundary of PWR Plants," U.S. Nuclear Regulatory Commission, Washington, D.C., June 1982, p. 2.

22.12 Edwin Rodkey, "Making Fastened Joints Reliable—Ways to Keep 'em Tight," *Assembly Engineering,* March 1977, pp. 24–27.

22.13 "Thread Forms and Torque Systems Boost Reliability of Bolted Joints," *Product Engineering,* December 1977, p. 38.

CHAPTER 23
THREADED FASTENERS

Joseph E. Shigley
Professor Emeritus
The University of Michigan
Ann Arbor, Michigan

This chapter is intended to cover the description, uses, materials, and sizes of threaded fasteners. The amount of data available concerning this subject is extremely large, so the intent here is to provide the information necessary for the usual machine-design task of selecting such fasteners. The data contained in this chapter have been compiled in part from the standards listed in Ref. [23.1].

23.1 SCREW THREADS

Standard screw threads consist of the *Unified inch series* and the *metric series.* Two profiles have been standardized in the metric series; these are called the M and MJ profiles. Figure 23.1 shows that both the Unified and metric M threads utilize the same profile.

The metric MJ profile has a rounded fillet at the root of the external thread and a larger minor diameter of both the internal and external threads. This profile is used for applications requiring a high fatigue strength and is also employed in aerospace applications.

The Unified-series profile, shown in Fig. 23.1, is designated as UN. Another unified profile, designated as UNR, has a rounded root on the external thread.

Unified thread standards are based on the nominal size (major diameter) and the number of threads per inch. The three standards *coarse* (UNC), *fine* (UNF), and *extra fine* (UNEF) are listed in Table 23.1 and are called the *standard series.* Typical specifications would be written

¼–20 UNC or ¼–20 UNRC

Both these designations specify a nominal size of ¼ in and 20 threads per inch.

A *constant-pitch* unified series consisting of 4, 6, 8, 12, 16, 20, 28, and 32 threads per inch has also been standardized. These are used mostly for sizes over 1 in, and 8 UN, 12 UN, and 16 UN are the preferred pitches.

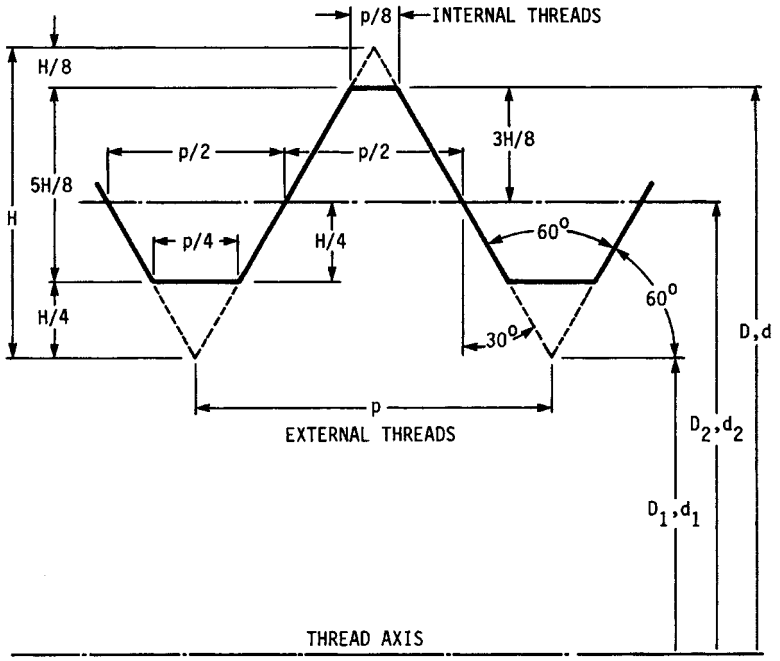

FIGURE 23.1 Basic thread profile for Unified (UN) and metric (M) threads (ISO 68). $D(d)$ = basic major diameter of internal (external) thread; $D_1(d_1)$ = basic minor diameter of internal (external) thread; $D_2(d_2)$ = basic pitch diameter of internal (external) thread; p = pitch; $H = 0.5\sqrt{3}p$.

As shown in Table 23.2, the metric series consists of a coarse thread and, often, several fine threads. These are specified by giving the size or major diameter and the pitch (see Fig. 23.1). Typical specifications would be written

$$\text{M } 70 \times 1.5 \qquad \text{or} \qquad \text{MJ } 70 \times 1.5$$

which specifies a major diameter of 70 mm and a pitch of 1.5 mm.

Unified threads may be further designated as UN A for external threads and UN B for internal threads. The tolerance classes are 1A, 2A, and 3A for external threads and 1B, 2B, and 3B for internal threads. Class 2 is for general use, class 3 is a tight fit used where great accuracy is required, and class 1 is a loose fit which permits very easy assembly and allows the possibility of nicks on the threads.

Metric threads utilize the international tolerance grades (see Chap. 27).

23.1.1 Choosing the Pitch

The Unified coarse-thread series (UNC or UNRC) and the metric coarse-thread series (M or MJ) provide the most resistance to internal thread stripping. Consequently, coarse threads should be used for materials such as brass, cast iron, aluminum, and other lower-strength materials. However, the coarse-thread series are

TABLE 23.1 Standard Series of UN and UNR Screw Threads†

Nominal size	Basic major diameter	Threads per inch		
		Coarse, UNC	Fine, UNF	Extra-fine, UNEF
0	0.0600		80	
1	0.0730	64	72	
2	0.0860	56	64	
3	0.0990	48	56	
4	0.1120	40	48	
5	0.1250	40	44	
6	0.1380	32	40	
8	0.1640	32	36	
10	0.1900	24	32	
12	0.2160	24	28	32
1/4	0.2500	20	28	32
5/16	0.3125	18	24	32
3/8	0.3750	16	24	32
7/16	0.4375	14	20	28
1/2	0.500	13	20	28
9/16	0.5625	12	18	24
5/8	0.6250	11	18	24
3/4	0.7500	10	16	20
7/8	0.8750	9	14	20
1	1.0000	8	12	20
1 1/8	1.1250	7	12	18
1 1/4	1.2500	7	12	18
1 3/8	1.3750	6	12	18
1 1/2	1.5000	6	12	18

†All dimensions in inches.

TABLE 23.2 Standard Diameter-Pitch Combinations for Metric M Screw Threads†

Basic major diameter			Pitch	
Preferred	First option	Second option	Coarse	Fine
1.6	...	...	0.35	
2	...	...	0.4	
2.5	...	...	0.45	
3	...	...	0.5	
	3.5	...	0.6	
4	...	...	0.7	
5	...	...	0.8	
6	...	...	1	

TABLE 23.2 Standard Diameter-Pitch Combinations for Metric M Screw Threads† (*Continued*)

Basic major diameter			Pitch	
Preferred	First option	Second option	Coarse	Fine
8	...	...	1.25	1
10	...	...	1.5	1.25 or 0.75
12	...	...	1.75	1.25 or 1
	14	...	2	1.5 or 1.25‡
	15	...	...	1
16	...	...	2	1.5
	...	17	...	1
	18	...	...	1.5
20	...	...	2.5	1.5 or 1
	22	...	2.5§	1.5
24	...	...	3	2
	...	25	...	1.5
	27	...	3¶	2
30	...	...	3.5	2 or 0.5
	33	...	...	2
	...	35¶	...	1.5
36	...	...	4	2
	39	...	...	2
	...	40	...	1.5
42	...	...	4.5	2
	45	...	...	1.5
48	...	...	5	2
	...	50	...	1.5
	...	55	...	1.5
56	...	...	5.5	2
	60	...	...	1.5
64	...	...	6	2
	...	65	...	1.5
	...	70	...	1.5
72	...	...	6	2
	...	75	...	1.5
80	...	...	6	1.5
	85	...	...	2
90	...	...	6	2
	95	...	...	2
100	...	...	6	2
	105	...	...	2
110	...	...	...	2
	120	...	...	2
	130	...	...	2
140	...	...	...	2
	150	...	...	2
160	...	...	...	3
	170	...	...	3
180	...	...	...	3
	190	...	...	3
200	...	...	...	3

†All dimensions in millimeters.
‡Only for engine spark plugs.
§Only for high-strength structural steel bolts.
¶Only for nuts for bearings.

also widely used with other materials because mass-produced fasteners are usually made with coarse threads and hence are the most economical. The coarse-thread series should also be used whenever fast assembly is needed or when dropping or handling the fasteners may damage the threads by causing nicks or dents.

The Unified fine-thread series (UNF or UNRF) and metric fine-thread series (M and MJ) find their greatest use where a high fastener strength is required and where vibration may be a problem. The shallow depth of thread, and hence larger minor diameter, increases the strength of the external member. It also permits a smaller wall thickness for the internal member.

Extra-fine-series screw threads are useful for thin nuts, on thin-wall tubing, and where parts may require a very fine adjustment.

23.1.2 Pipe Threads

The profile of pipe threads is similar to the UN profile except that there is a taper of 1 on 16 based on the outside diameter. The last few threads will be imperfect because of the taper and the chamfer on the thread-cutting die. Table 23.3 gives the basic dimensions of Unified-inch-series standard pipe threads.

23.2 BOLTS

The symbols used to indicate the dimensions of square and hex bolt heads are shown in Fig. 23.2. See Table 23.4 for head dimensions. The washer or bearing face shown in Fig. 23.2*b* is standard for the *heavy structural hex bolt* (Table 23.4) and for the *finished hex bolt.* A finished hex bolt is identical to a hex cap screw (see Table 23.13). The basic thread length for bolts is

$$L_T = \begin{cases} 2D + 0.25 & L \le 6 \\ 2D + 0.50 & L > 6 \end{cases} \tag{23.1}$$

TABLE 23.3 Basic Dimensions of Standard Pipe Threads†

Nominal pipe size	Outside diameter	Threads per inch	Thread length on OD (approx.)
$\frac{1}{16}$	0.3125	27	0.261
$\frac{1}{8}$	0.405	27	0.264
$\frac{1}{4}$	0.540	18	0.402
$\frac{3}{8}$	0.675	18	0.408
$\frac{1}{2}$	0.840	14	0.534
$\frac{3}{4}$	1.050	14	0.546
1	1.315	$11\frac{1}{2}$	0.683
$1\frac{1}{4}$	1.660	$11\frac{1}{2}$	0.707
$1\frac{1}{2}$	1.900	$11\frac{1}{2}$	0.723
2	2.375	$11\frac{1}{2}$	0.757
$2\frac{1}{2}$	2.875	8	1.138
Over $2\frac{1}{2}$	. . . . .	8	

†All dimensions in inches.

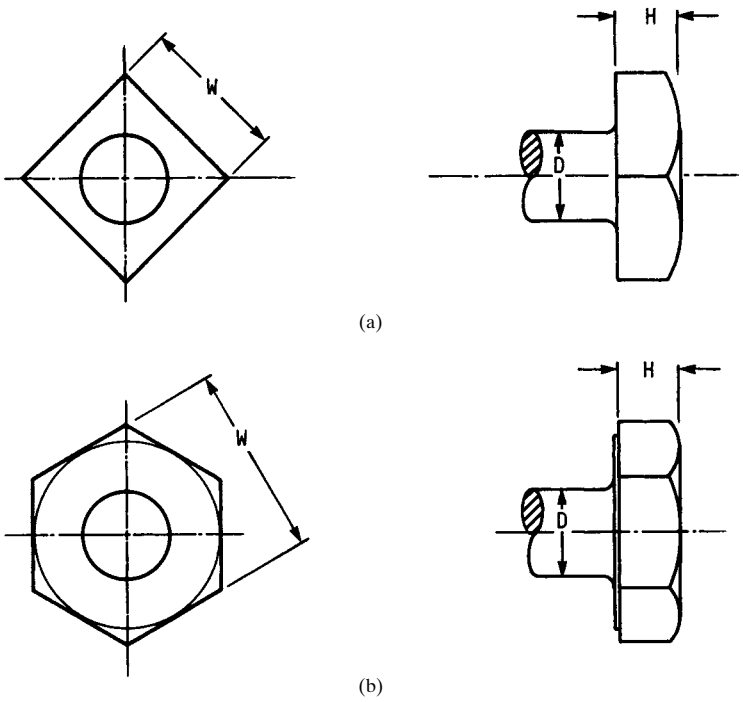

FIGURE 23.2 Bolt heads. (*a*) Square; (*b*) hex; the washer or bearing face is used only on heavy hex structural bolts.

where L = bolt length, measured under the head, and L_T = thread length, in inches.

Head dimensions for metric hex bolts are listed in Table 23.5. The heavy hex structural bolt is the only one of these with a bearing face. The thread length is

$$L_T = \begin{cases} 2D + 6 & L \le 125 \quad D \le 48 \\ 2D + 12 & 125 \le L \le 200 \\ 2D + 25 & L > 200 \end{cases} \tag{23.2}$$

Here L and L_T are in millimeters.

Standards for bolt materials and the corresponding head markings are listed in Tables 23.6, 23.7, and 23.8. The property class number in Table 23.8 is a code derived from the tensile strength S_{ut} and the yield strength S_y. If we designate the class number by the symbol $X.Y$, then $X = S_{ut}/100$ and $Y = S_y/S_{ut}$. Bolts in metric sizes are normally manufactured to SAE and ASTM specifications too. For fillet dimensions, see Tables 23.9 and 23.10.

Typical heads for *round-head* or *carriage bolts* are shown in Fig. 23.3, and head dimensions are given in Tables 23.11 and 23.12. Other standard bolts are step bolts, which have a square neck with a larger-diameter head, and several countersunk-head bolts with and without square necks. The bolts listed in Table 23.12 are the only round-head metric bolts that are standardized at this writing. Round-head bolts are made to the same material specifications as hex bolts and use the same head markings.

TABLE 23.4 Dimensions of Square- and Hex-Head Bolts (Inch Series)

Nominal size	Head type							
	Square		Regular hex†		Heavy hex‡		Structural hex	
	W	*H*	*W*	*H*	*W*	*H*	*W*	*H*
1/4	3/8	11/64	7/16	11/64				
5/16	1/2	13/64	1/2	7/32				
3/8	9/16	1/4	9/16	1/4				
7/16	5/8	19/64	5/8	19/64				
1/2	3/4	21/64	3/4	11/32	7/8	11/32	7/8	5/16
5/8	15/16	27/64	15/16	27/64	1 1/16	27/64	1 1/16	25/64
3/4	1 1/8	1/2	1 1/8	1/2	1 1/4	1/2	1 1/4	15/32
7/8	1 5/16	19/32	1 5/16	37/64	1 7/16	37/64	1 7/16	35/64
1	1 1/2	21/32	1 1/2	43/64	1 5/8	43/64	1 5/8	39/64
1 1/8	1 11/16	3/4	1 11/16	3/4	1 13/16	3/4	1 13/16	11/16
1 1/4	1 7/8	27/32	1 7/8	27/32	2	27/32	2	25/32
1 3/8	2 1/16	29/32	2 1/16	29/32	2 3/16	29/32	2 3/16	27/32
1 1/2	2 1/4	1	2 1/4	1	2 3/8	1	2 3/8	15/16

†Also available in standard sizes up to 4 in.
‡Also available in standard sizes up to 3 in.

TABLE 23.5 Dimensions of Metric Hex Bolts (Metric Series)†

Nominal diameter	Thread pitch	Type of bolt					
		Regular‡		Heavy		Structural	
		W	*H*	*W*	*H*	*W*	*H*
M5	0.8	8	3.58				
M6	1	10	4.38				
M8	1.25	13	5.68				
M10	1.5	16	6.85				
M12	1.75	18	7.95	21	7.95		
M14	2	21	9.25	24	9.25		
M16	2	24	10.75	27	10.75	27	10.75
M20	2.5	30	13.40	34	13.40	34	13.40
M22	2.5	..	.....	..	.....	36	14.90
M24	3	36	15.90	41	15.90	41	15.90
M27	3	..	.....	..	.....	46	17.90
M30	3.5	46	19.75	50	19.75	50	19.75
M36	4	55	23.55	60	23.55	60	23.55

†Head dimensions are maximum. All dimensions in millimeters.
‡Also available in standard sizes to 100 mm.

TABLE 23.6 SAE Grade Markings for Steel Bolts

SAE grade no.	Size range incl.	Proof strength,† kpsi	Tensile strength,† kpsi	Material	Head marking
1	¼–1½			Low- or medium-carbon steel	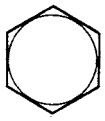
2	¼–¾ ⅞–1½	55 33	74 60		
5	¼–1 1⅛–1½	85 74	120 105	Medium-carbon steel, Q & T	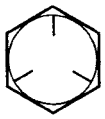
5.2	¼–1	85	120	Low-carbon martensite steel, Q & T	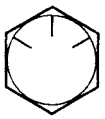
7	¼–1½	105	133	Medium-carbon alloy steel, Q & T‡	
8	¼–1½	120	150	Medium-carbon alloy steel, Q & T	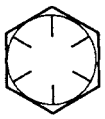
8.2	¼–1	120	150	Low-carbon martensite steel, Q & T	

†Minimum values.
‡Roll threaded after heat treatment.
SOURCES: See "Helpful Hints," by Russell, Burdsall & Ward Corp., Mentor, Ohio 44060; and Chap. 22.

TABLE 23.7 ASTM Grade Markings for Steel Bolts

ASTM designation	Size range incl.	Proof strength,† kpsi	Tensile strength,† kpsi	Material	Head marking
A307	¼ to 4			Low-carbon steel	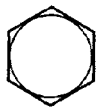
A325 type 1	½ to 1 1⅛ to 1½	85 74	120 105	Medium-carbon steel, Q & T	
A325 type 2	½ to 1 1⅛ to 1½	85 74	120 105	Low-carbon martensite steel, Q & T	
A325 type 3	½ to 1 1⅛ to 1½	85 74	120 105	Weathering steel, Q & T	
A354 grade BC				Alloy steel, Q & T	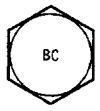
A354 grade BD	¼ to 4	120	150	Alloy steel, Q & T	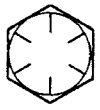
A449	¼ to 1 1⅛ to 1½ 1¾ to 3	85 74 55	120 105 90	Medium-carbon steel, Q & T	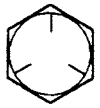
A490 type 1	½ to 1½	120	150	Alloy steel, Q & T	
A490 type 3				Weathering steel, Q & T	

†Minimum values.

SOURCES: See "Helpful Hints," by Russell, Burdsall & Ward Corp., Mentor, Ohio 44060; and Chap. 22.

TABLE 23.8 Metric Mechanical-Property Classes for Steel Bolts, Screws, and Studs

Property class	Size range incl.	Proof strength, MPa	Tensile strength, MPa	Material	Head marking
4.6	M5–M36	225	400	Low- or medium-carbon steel	
4.8	M1.6–M16	310	420	Low- or medium-carbon steel	
5.8	M5–M24	380	520	Low- or medium-carbon steel	
8.8	M16–M36	600	830	Medium-carbon steel, Q & T	
9.8	M1.6–M16	650	900	Medium-carbon steel, Q & T	
10.9	M5–M36	830	1040	Low-carbon martensite steel, Q & T	
12.9	M1.6–M36	970	1220	Alloy steel, Q & T	

SOURCES: "Helpful Hints," by Russell, Burdsall & Ward Corp., Mentor, Ohio 44060; see also Chap. 22 and SAE standard J1199, and ASTM standard F568.

TABLE 23.9 Under-the-Head Fillet Radii for Hex Bolts (Inch Series)

Size	Regular and heavy		Heavy structural	
	Maximum	Minimum	Maximum	Minimum
$\frac{1}{4}$–$\frac{1}{2}$	0.03	0.01	0.031	0.009
$\frac{5}{8}$–$\frac{7}{8}$	0.06	0.02	0.062	0.021
1–1$\frac{1}{2}$	0.09	0.03	0.093	0.062

TABLE 23.10 Under-the-Head Fillet Radii for Hex Bolts (Metric Series)†

Size	Regular and heavy (min.)	Heavy structural (min.)
M5	0.2	
M6	0.3	
M8–M10	0.4	
M12–M16	0.6	0.6
M20–M22	0.8	0.8
M24	0.8	1.0
M27	. .	1.2
M30	1.0	1.2
M36	1.0	1.5

†All dimensions in millimeters.

23.3 SCREWS

23.3.1 Hexagon Head

Hex screw heads resemble those shown in Fig. 23.2*b,* and they all have a washer or bearing face. Basic dimensions of the *cap screw* and the *heavy screw* in the inch series are given in Table 23.13. Three metric series are standardized. These are the *cap screw,* the *formed screw,* which has an indentation in the head, and the *heavy screw;* see Table 23.14 for basic dimensions of these. Hex screws are made to the same material specifications as bolts and utilize the same head markings (see Tables 23.6, 23.7, and 23.8). Use Eq. (23.1) or (23.2) to determine the basic length of thread.

23.3.2 Sockets and Keys

Figure 23.4 illustrates the standard hex and spline socket, and the products in Fig. 23.5 illustrate the variety. Socket screws are driven with a socket key, as in Fig. 23.4*c,* or with a length of hex or spline stock, called a *bit.* The bit is used for driving by inserting it into a standard socket wrench or power driver. Dimensions of standard keys are given in Tables 23.15, 23.16, and 23.17. Metric splines have not as yet been standardized.

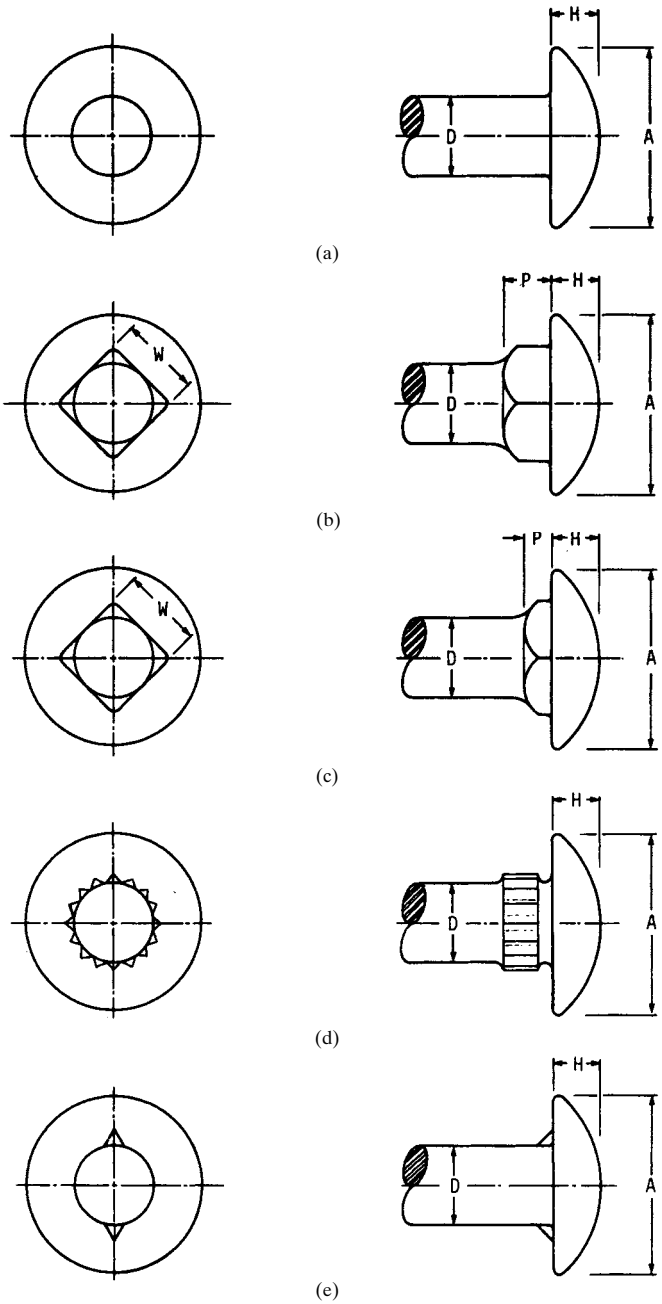

FIGURE 23.3 Some types of round-head bolts. (*a*) Plain; (*b*) regular square-neck; (*c*) short square-neck; (*d*) rib-neck; (*e*) fin-neck.

TABLE 23.11 Some Basic Dimensions of Round-Head Bolts (Inch Series)†

Nominal size	Max. head diameter A	Max. head height H	Max. square width W‡
No. 10	0.469	0.114	0.199
$\frac{1}{4}$	0.594	0.145	0.260
$\frac{5}{16}$	0.719	0.176	0.324
$\frac{3}{8}$	0.844	0.208	0.388
$\frac{7}{16}$	0.969	0.239	0.452
$\frac{1}{2}$	1.094	0.270	0.515
$\frac{5}{8}$	1.344	0.344	0.642
$\frac{3}{4}$	1.594	0.406	0.768
$\frac{7}{8}$	1.844	0.469	0.895
1	2.094	0.531	1.022

†Short square-neck and rib-neck bolts are standardized only to $\frac{3}{4}$ in; fin-neck bolts are standard only to $\frac{1}{2}$ in.
‡Not applicable to plain, rib-neck, or fin-neck bolts.

TABLE 23.12 Some Basic Dimensions of Round-Head Short Square-Neck Metric Bolts

Nominal size	Thread pitch	Max. head diameter A	Max. head height H	Max. square width W
M6	1	14.2	3.6	6.48
M8	1.25	18.0	4.8	8.58
M10	1.5	22.3	5.8	10.58
M12	1.75	26.6	6.8	12.70
M14	2	30.5	7.9	14.70
M16	2	35.0	8.9	16.70
M20	2.5	43.0	10.9	20.84

23.3.3 Socket-Head Cap Screws

Figure 23.6*a* illustrates a *socket-head cap screw,* and Fig. 23.6*c* shows a *flat countersunk-head cap screw. Socket button-head cap screws* resemble Fig. 23.8*a,* but have a hex or spline driving socket instead of the slot. Head dimensions for these, in inch and metric sizes, are given in Tables 23.18 to 23.23 inclusive.

Thread-length formulas are

$$L_T = 2D + 0.50 \text{ in} \qquad L_T = 2D + 12 \text{ mm} \tag{23.3}$$

Shorter cap screws are threaded full length.

Alloy-steel cap screws, in both inch and metric sizes, should contain an alloying element, such as chromium, nickel, molybdenum, or vanadium, in such quantities as to ensure that a hardness range of 36 to 45 R_C is achieved.

TABLE 23.13 Basic Dimensions of Hex Cap Screws (Finished Hex Bolts) and Heavy Hex Screws (Inch Series)

Nominal size	Fillet radii		Fastener type			
			Hex cap screw		Heavy hex screw	
	Maximum	Minimum	*W*	*H*	*W*	*H*
$\frac{1}{4}$	0.025	0.015	$\frac{7}{16}$	$\frac{5}{32}$		
$\frac{5}{16}$	0.025	0.015	$\frac{1}{2}$	$\frac{13}{64}$		
$\frac{3}{8}$	0.025	0.015	$\frac{9}{16}$	$\frac{15}{64}$		
$\frac{7}{16}$	0.025	0.015	$\frac{5}{8}$	$\frac{9}{32}$		
$\frac{1}{2}$	0.025	0.015	$\frac{3}{4}$	$\frac{5}{16}$	$\frac{7}{8}$	$\frac{5}{16}$
$\frac{9}{16}$	0.045	0.020	$\frac{13}{16}$	$\frac{23}{64}$		
$\frac{5}{8}$	0.045	0.020	$\frac{15}{16}$	$\frac{25}{64}$	$1\frac{1}{16}$	$\frac{25}{64}$
$\frac{3}{4}$	0.045	0.020	$1\frac{1}{8}$	$\frac{15}{32}$	$1\frac{1}{4}$	$\frac{15}{32}$
$\frac{7}{8}$	0.065	0.040	$1\frac{5}{16}$	$\frac{35}{64}$	$1\frac{7}{16}$	$\frac{35}{64}$
1	0.095	0.060	$1\frac{1}{2}$	$\frac{39}{64}$	$1\frac{5}{8}$	$\frac{39}{64}$
$1\frac{1}{8}$	0.095	0.060	$1\frac{11}{16}$	$\frac{11}{16}$	$1\frac{13}{16}$	$\frac{11}{16}$
$1\frac{1}{4}$	0.095	0.060	$1\frac{7}{8}$	$\frac{25}{32}$	2	$\frac{25}{32}$
$1\frac{3}{8}$	0.095	0.060	$2\frac{1}{16}$	$\frac{27}{32}$	$2\frac{3}{16}$	$\frac{27}{32}$
$1\frac{1}{2}$	0.095	0.060	$2\frac{1}{4}$	$1\frac{15}{16}$	$2\frac{3}{8}$	$\frac{15}{16}$

TABLE 23.14 Basic Dimensions of Metric Hex Screws†

Nominal diameter	Thread pitch	Type of screw			Height *H*	Fillet radius§
		Cap‡ *W*	Formed‡ *W*	Heavy‡ *W*		
M5	0.8	8	8	. .	3.65	0.2
M6	1	10	10	. .	4.15	0.3
M8	1.25	13	13	. .	5.50	0.4
M10	1.5	16	16	. .	6.63	0.4
M12	1.75	18	18	21	7.76	0.6
M14	2	21	21	24	9.09	0.6
M16	2	24	24	27	10.32	0.6
M20	2.5	30	30	34	12.88	0.8
M24	3	36	36	41	15.44	0.8
M30	3.5	46	. .	50	19.48	1.0
M36	4	55	. .	60	23.38	1.0

†All dimensions in millimeters.
‡Maximum.
§Minimum.

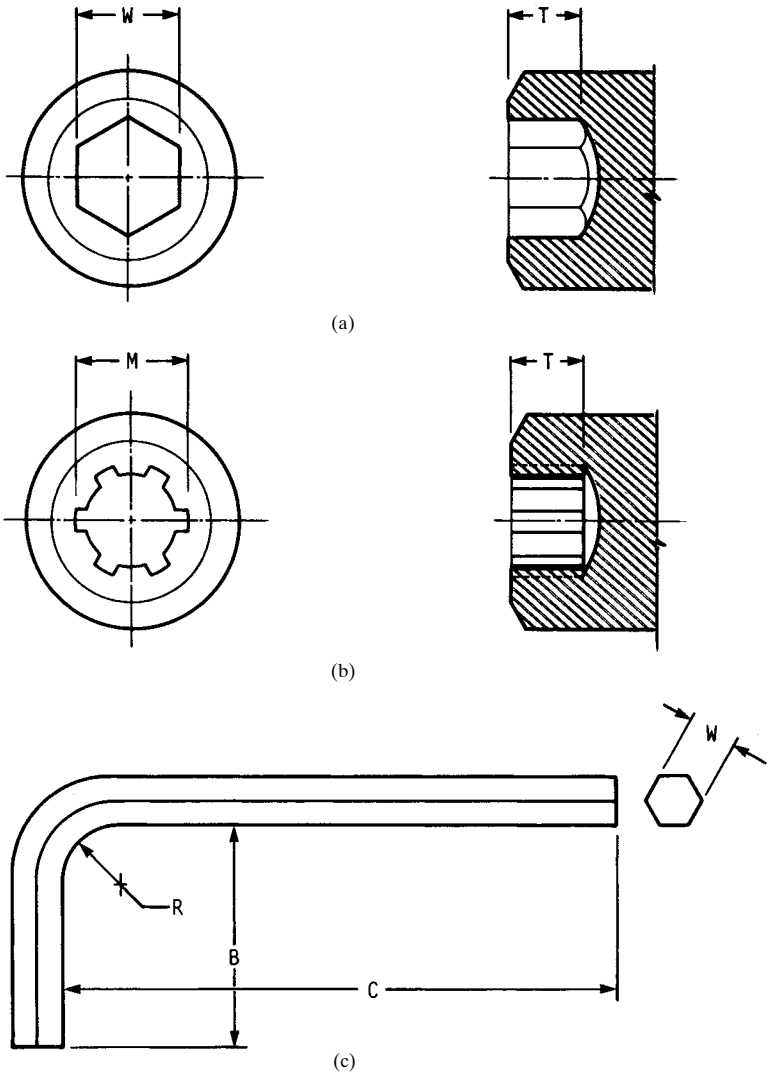

FIGURE 23.4 Standard socket shapes. (*a*) Forged hex socket; (*b*) forged spline; (*c*) hex-socket key.

23.3.4 Shoulder Screws

The nominal size D_S shown for the shoulder screw in Fig. 23.6*b* is related to the maximum and minimum shoulder diameters by the relation

$$D_S(\text{max}) = D_S - 0.002 \qquad D_S(\text{min}) = D_s - 0.004 \tag{23.4}$$

Sizes, in the inch series, are tabulated in Table 23.24.

FIGURE 23.5 Hex-socket fasteners. From left to right, the parts are identified as a low socket-head cap screw, a button-head socket cap screw, a socket shoulder screw, a socket set screw, a socket-head cap screw, a socket flat-head cap screw, a hexagon key, a dowel pin, and a socket pressure plug. *(Holo-Krome Company.)*

TABLE 23.15 Hex-Socket Key Sizes (Inch Series)

Nominal width W	Short arm B		Long arm C	
	Maximum	Minimum	Shorts†	Longs†
0.028	0.312	0.125	1.312	2.688
0.035	0.438	0.250	1.312	2.766
0.050	0.625	0.438	1.750	2.938
1/16	0.656	0.469	1.844	3.094
5/64	0.703	0.516	1.969	3.281
3/32	0.750	0.562	2.094	3.469
7/64	0.797	0.609	2.219	3.656
1/8	0.844	0.656	2.344	3.844
9/64	0.891	0.703	2.469	4.031
5/32	0.938	0.750	2.954	4.219
3/16	1.031	0.844	2.844	4.594
7/32	1.125	0.938	3.094	4.969
1/4	1.219	1.031	3.344	5.344
5/16	1.344	1.156	3.844	6.094
3/8	1.469	1.281	4.344	6.844
7/16	1.594	1.406	4.844	7.594
1/2	1.719	1.531	5.344	8.344
9/16	1.844	1.656	5.844	9.094
5/8	1.969	1.781	6.344	9.844
3/4	2.219	2.031	7.344	11.344
7/8	2.469	2.281	8.344	12.844
1	2.719	2.531	9.344	14.344

†Maximum.

TABLE 23.16 Spline-Socket Key Sizes (Inch Series)

Nominal size M	Short arm B		Long arm C	
	Maximum	Minimum	Shorts†	Longs†
0.033‡	0.312	0.125	1.312	
0.048	0.438	0.250	1.312	
0.060	0.625	0.438	1.750	
0.072	0.656	0.469	1.844	
0.096	0.703	0.516	1.969	
0.111	0.750	0.562	2.094	
0.133	0.797	0.609	2.219	3.656
0.145	0.844	0.656	2.344	3.844
0.168	0.891	0.703	2.469	4.031
0.183	0.938	0.750	2.594	4.219
0.216	1.031	0.844	2.844	4.594
0.251	1.125	0.938	3.094	4.969
0.291	1.219	1.031	3.344	5.344
0.372	1.344	1.156	3.844	6.094
0.454	1.469	1.281	4.344	6.844
0.595	1.719	1.531	5.344	8.344
0.620	1.844	1.656	5.844	9.094
0.698	1.844	1.656	5.844	
0.790	1.969	1.781	6.344	

†Maximum.
‡This size has only four splines.

TABLE 23.17 Basic Maximum Dimensions of Metric Hex Keys†

Nominal size W	Short arm B	Long arm C	
		Shorts	Longs
0.7	5.5	34	62
0.9	9	34	62
1.3	13.5	44	84
1.5	14	45	90
2	16	50	100
2.5	18	56	112
3	20	63	126
4	25	70	142
5	28	80	160
6	32	90	180
8	36	100	200
10	40	112	224
12	45	125	250
14	56	140	280
17	63	160	320
19	70	180	360
22	80	200	400
24	90	224	448
27	100	250	500

†All dimensions in millimeters.

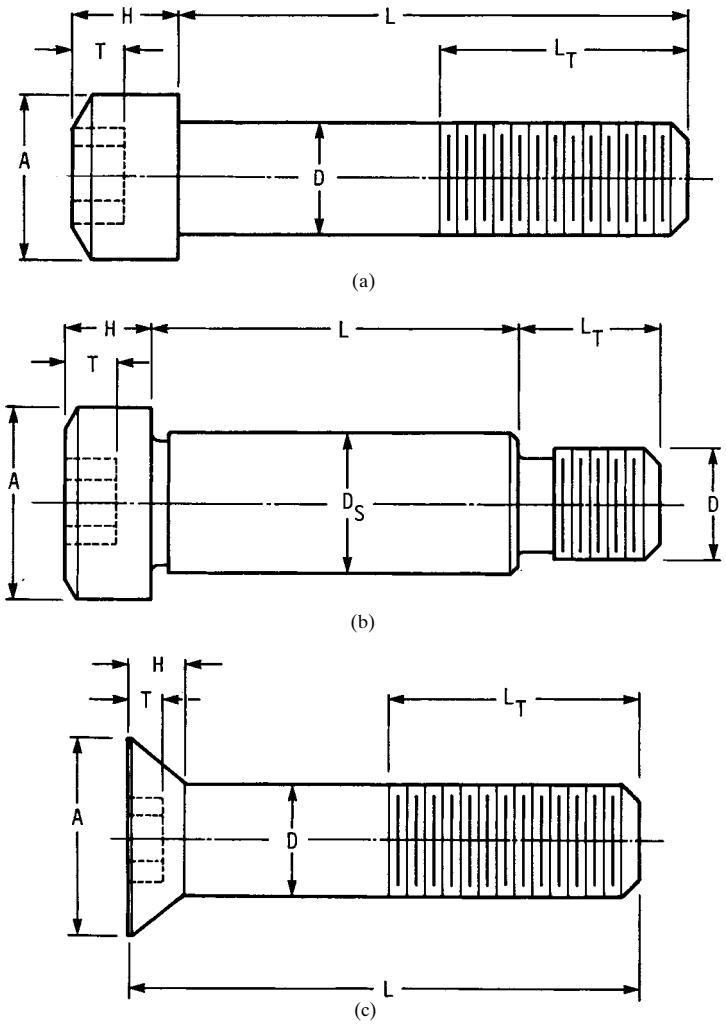

FIGURE 23.6 Socket screws. (*a*) Cap screw; (*b*) shoulder screw; (*c*) flat-head screw.

The maximum and minimum shoulder diameters for metric sizes are

$$D_S(\max) = D_S - \begin{cases} 0.013 & D_S \le 10 \\ 0.016 & 10 < D_S \le 20 \\ 0.020 & D_S > 20 \end{cases}$$

$$D_S(\min) = D_S - \begin{cases} 0.049 & D_S \le 10 \\ 0.059 & 10 < D_S \le 20 \\ 0.072 & D_S > 20 \end{cases} \tag{23.5}$$

TABLE 23.18 Basic Dimensions of Socket-Head Cap Screws (Inch Series)

Nominal size D	Max. head diameter A	Max. head height H	Hex size W	Spline size M	Socket depth† T
0	0.096	0.060	0.050	0.060	0.025
1	0.118	0.073	1/16	0.072	0.031
2	0.140	0.086	5/64	0.096	0.038
3	0.161	0.099	5/64	0.096	0.044
4	0.183	0.112	3/32	0.111	0.051
5	0.205	0.125	3/32	0.111	0.057
6	0.226	0.138	7/64	0.133	0.064
8	0.270	0.164	9/64	0.168	0.077
10	0.312	0.190	5/32	0.183	0.090
1/4	0.375	0.250	3/16	0.216	0.120
5/16	0.469	0.312	1/4	0.291	0.151
3/8	0.562	0.375	5/16	0.372	0.182
7/16	0.656	0.438	3/8	0.454	0.213
1/2	0.750	0.500	3/8	0.454	0.245
5/8	0.938	0.625	1/2	0.595	0.307
3/4	1.125	0.750	5/8	0.620	0.370
7/8	1.312	0.875	3/4	0.698	0.432
1	1.500	1.000	3/4	0.790	0.495
1 1/8	1.688	1.125	7/8	....	0.557
1 1/4	1.875	1.250	7/8	....	0.620
1 3/8	2.062	1.365	1	....	0.682
1 1/2	2.250	1.500	1	....	0.745

†Minimum.

where D_S is, of course, in millimeters.

See Tables 23.24 and 23.25 for basic dimensions of shoulder screws. These are made of the same material and of the same hardness as specified for cap screws.

23.3.5 Set Screws

Socket set screws (Fig. 23.7) are available in both inch and metric sizes with either hex or spline sockets for the inch series and hex sockets for the metric series. The cone point in Fig. 23.7*b* comes in seven different variations.

Square-head set screws (not shown) have a width across flats equal to the nominal size of the screw. The head height is three-quarters of the nominal size. These have a reduced-diameter neck just below the head.

23.3.6 Slotted-Head Cap Screws

The three standard head styles of the inch-series slotted-head cap screws are shown in Fig. 23.8, and the basic head dimensions are given in Table 23.26. The slot width is

TABLE 23.19 Basic Dimensions of Socket-Head Cap Screws (Metric Series)†

Nominal size *D*	Max. head diameter *A*	Max. head height *H*	Hex size *W*	Spline size *M*	Socket depth‡ *T*
M1.6	3.00	1.60	1.5	1.829	0.80
M2	3.80	2.00	1.5	1.829	1.00
M2.5	4.50	2.50	2.0	2.438	1.25
M3	5.50	3.00	2.5	2.819	1.50
M4	7.00	4.00	3.0	3.378	2.00
M5	8.50	5.00	4.0	4.648	2.50
M6	10.00	6.00	5.0	5.486	3.00
M8	13.00	8.00	6.0	7.391	4.00
M10	16.00	10.00	8.0	....	5.00
M12	18.00	12.00	10.0	....	6.00
M16	24.00	16.00	14.0	....	8.00
M20	30.00	20.00	17.0	....	10.00
M24	36.00	24.00	19.0	....	12.00
M30	45.00	30.00	22.0	....	15.00
M36	54.00	36.00	27.0	....	18.00

†All dimensions in millimeters.
‡Minimum.

TABLE 23.20 Basic Dimensions of Socket Flat-Head Cap Screws (Inch Series)

Nominal size *D*	Max. head diameter *A*	Max. head height *H*	Hex size *W*	Spline size *M*	Socket depth† *T*
0	0.138	0.044	0.035	0.048	0.025
1	0.168	0.054	0.050	0.060	0.031
2	0.197	0.064	0.050	0.060	0.038
3	0.226	0.073	1/16	0.072	0.044
4	0.255	0.083	1/16	0.072	0.055
5	0.281	0.090	5/64	0.096	0.061
6	0.307	0.097	5/64	0.096	0.066
8	0.359	0.112	3/32	0.111	0.076
10	0.411	0.127	1/8	0.145	0.087
1/4	0.531	0.161	5/32	0.183	0.111
5/16	0.656	0.198	3/16	0.216	0.135
3/8	0.781	0.234	7/32	0.251	0.159
7/16	0.844	0.234	1/4	0.291	0.159
1/2	0.938	0.251	5/16	0.372	0.172
5/8	1.188	0.324	3/8	0.454	0.220
3/4	1.438	0.396	1/2	0.454	0.220
7/8	1.688	0.468	9/16	....	0.248
1	1.938	0.540	5/8	....	0.297
1 1/8	2.188	0.611	3/4	....	0.325
1 1/4	2.438	0.683	7/8	....	0.358
1 3/8	2.688	0.755	7/8	....	0.402
1 1/2	2.938	0.827	1	....	0.435

†Minimum.

TABLE 23.21 Basic Dimensions of Socket Flat-Head Cap Screws (Metric Series)†

Nominal size *D*	Max. head diameter *A*	Max. head height *H*	Hex size *W*	Socket depth‡ *T*
M3	6.72	1.85	2	18
M4	8.96	2.69	2.5	20
M5	11.20	3.18	3	22
M6	13.44	3.58	4	24
M8	17.92	4.42	5	28
M10	22.40	6.01	6	32
M12	26.88	6.85	8	36
M16	33.60	8.10	10	44
M20	40.32	8.70	12	52
M24	40.42	16.05	14	60

†All dimensions in millimeters.
‡Minimum.
SOURCE: Unbrako, Division of SPS, Jenkintown, Pa. 19046

TABLE 23.22 Basic Dimensions of Socket Button-Head Cap Screws (Inch Series)

Nominal size *D*	Max. head diameter *A*	Max. head height *H*	Hex size *W*	Spline size *M*	Socket depth† *T*
0	0.114	0.032	0.035	0.048	0.020
1	0.139	0.039	0.050	0.060	0.028
2	0.164	0.046	0.050	0.060	0.028
3	0.188	0.052	1/16	0.072	0.035
4	0.213	0.059	1/16	0.072	0.035
5	0.238	0.066	5/64	0.096	0.044
6	0.262	0.073	5/64	0.096	0.044
8	0.312	0.087	3/32	0.111	0.052
10	0.361	0.101	1/8	0.145	0.070
1/4	0.437	0.132	5/32	0.183	0.087
5/16	0.547	0.166	3/16	0.216	0.105
3/8	0.656	0.199	7/32	0.251	0.122
1/2	0.875	0.265	5/16	0.372	0.175
5/8	1.000	0.331	3/8	0.454	0.210

†Minimum.

TABLE 23.23 Basic Dimensions of Socket Button-Head Cap Screws (Metric Series)†

Nominal size *D*	Max. head diameter *A*	Max. head height *H*	Hex size *W*	Socket depth‡ *T*
M3	5.70	1.65	2	1.04
M4	7.60	2.20	2.5	1.30
M5	9.50	2.75	3	1.56
M6	10.50	3.30	4	2.08
M8	14.00	4.40	5	2.60
M10	17.50	5.50	6	3.12
M12	21.00	6.60	8	4.16
M16	28.00	8.80	10	5.20

†All dimensions in millimeters.
‡Minimum.

TABLE 23.24 Basic Dimensions of Socket Shoulder Screws (Inch Series)

Shoulder diameter D_S	Max. head diameter A	Max. head height H	Hex size W	Socket depth† T	Thread size D	Thread length L_T
$\frac{1}{4}$	0.375	0.188	$\frac{1}{8}$	0.094	10	0.375
$\frac{5}{16}$	0.438	0.219	$\frac{5}{32}$	0.117	$\frac{1}{4}$	0.438
$\frac{3}{8}$	0.562	0.250	$\frac{3}{16}$	0.141	$\frac{5}{16}$	0.500
$\frac{1}{2}$	0.750	0.312	$\frac{1}{4}$	0.188	$\frac{3}{8}$	0.625
$\frac{5}{8}$	0.875	0.375	$\frac{5}{16}$	0.234	$\frac{1}{2}$	0.750
$\frac{3}{4}$	1.000	0.500	$\frac{3}{8}$	0.281	$\frac{5}{8}$	0.875
1	1.312	0.625	$\frac{1}{2}$	0.375	$\frac{3}{4}$	1.000
$1\frac{1}{4}$	1.750	0.750	$\frac{5}{8}$	0.469	$\frac{7}{8}$	1.125
$1\frac{1}{2}$	2.125	1.000	$\frac{7}{8}$	0.656	$1\frac{1}{8}$	1.500
$1\frac{3}{4}$	2.375	1.125	1	0.750	$1\frac{1}{4}$	1.750
2	2.750	1.250	$1\frac{1}{4}$	0.937	$1\frac{1}{2}$	2.000

†Minimum.

TABLE 23.25 Basic Dimensions of Socket-Head Shoulder Screws (Metric Series)†

Shoulder diameter D_S	Max. head diameter A	Max. head height H	Hex size W	Socket depth‡ T	Thread size D	Thread length L_T
6.5	10.00	4.50	3	2.4	M5	9.75
8.0	13.00	5.50	4	3.3	M6	11.25
10.0	16.00	7.00	5	4.2	M8	13.25
13.0	18.00	9.00	6	4.9	M10	16.40
16.0	24.00	11.00	8	6.6	M12	18.40
20.0	30.00	14.00	10	8.8	M16	22.40
25.0	36.00	16.00	12	10.0	M20	27.40

†All dimensions in millimeters.
‡Minimum.

$$J = \begin{cases} 0.160D + 0.024 & D \le 1 \\ 0.160D & 1 < D \le 1\frac{1}{2} \end{cases} \tag{23.6}$$

The slot depth varies, depending on the head type and the nominal size.

Slotted-head cap screws are normally made from carbon steel conforming to ASTM A307 properties (see Table 23.7). However, they can also be obtained in grade ASTM A449 material and properties.

23.3.7 Machine Screws

We can keep track of the many types of machine screws by classifying them as follows:

1. Flat countersunk head (80 degrees)
   - ***a.*** Regular or undercut
   - ***b.*** Slotted or cross-recessed

THREADED FASTENERS

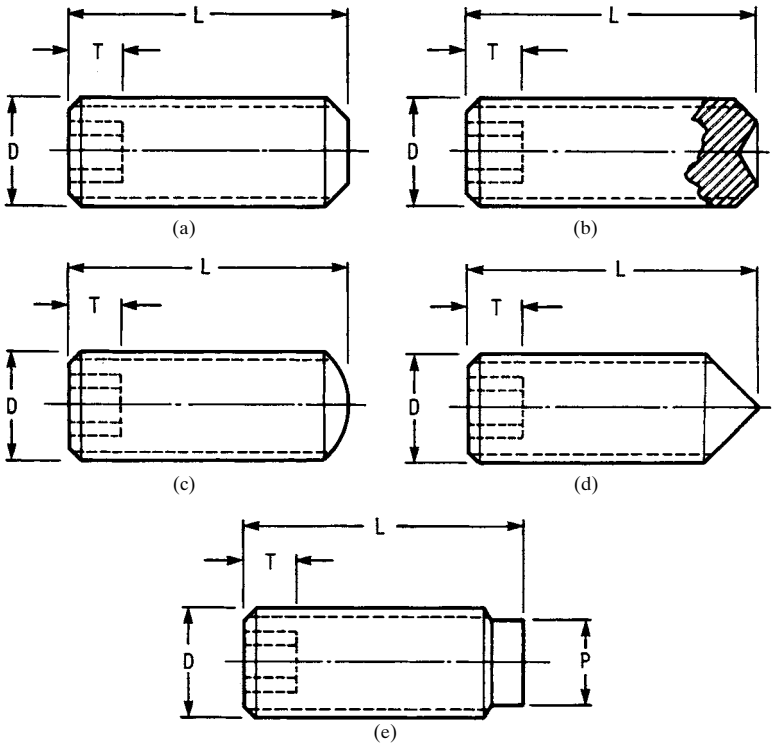

FIGURE 23.7 Socket set screws. (*a*) Flat point; (*b*) cup point; (*c*) oval point; (*d*) cone point; (*e*) half-dog point.

2. 100-degree flat countersunk head
  a. Regular or close tolerance
  b. Slotted or cross-recessed
3. Oval countersunk head
  a. Regular or undercut
  b. Slotted or cross-recessed
4. Flat countersunk trim head
  a. Regular or short
  b. Cross-recessed
5. Oval countersunk trim head
  a. Regular or short
  b. Cross-recessed
6. Pan head
  a. Slotted or cross-recessed
7. Fillister head
  a. Slotted and cross-drilled
  b. Slotted or cross-recessed
8. Truss head
  a. Slotted or cross-recessed

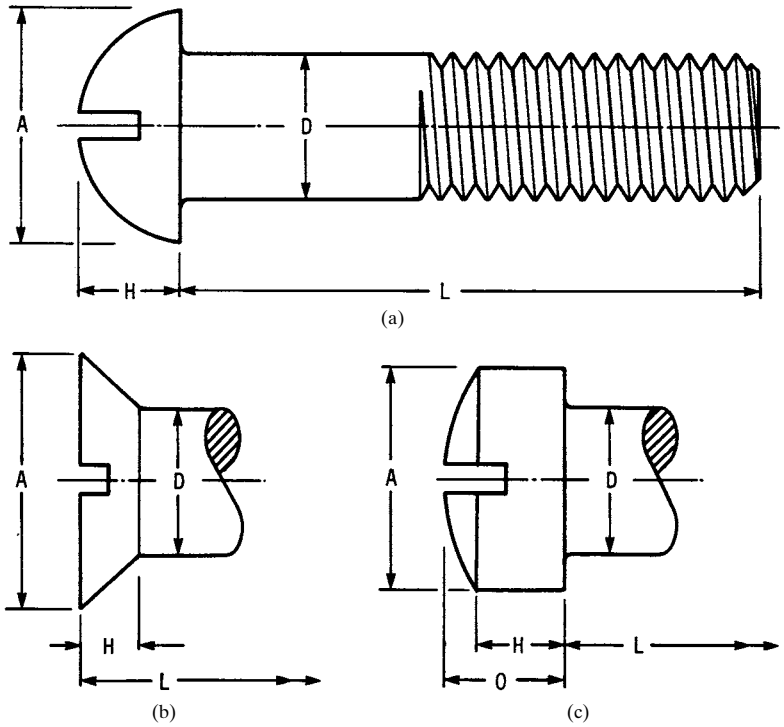

FIGURE 23.8 Slotted-head cap screws. (*a*) Round head; (*b*) flat countersunk head; (*c*) fillister head.

TABLE 23.26 Basic Head Dimensions of Slotted-Head Cap Screws (Inch Series)

Nominal size	Flat head†		Round head†		Fillister head†		
	A	*H*	*A*	*H*	*A*	*H*	*O*
1/4	0.500	0.140	0.437	0.191	0.375	0.172	0.216
5/16	0.625	0.177	0.562	0.245	0.437	0.203	0.253
3/8	0.750	0.210	0.625	0.273	0.562	0.250	0.314
7/16	0.812	0.210	0.750	0.328	0.625	0.297	0.368
1/2	0.875	0.210	0.812	0.354	0.750	0.328	0.413
9/16	1.000	0.244	0.937	0.409	0.812	0.375	0.467
5/8	1.125	0.281	1.000	0.437	0.875	0.422	0.521
3/4	1.375	0.352	1.250	0.546	1.000	0.500	0.612
7/8	1.625	0.423	....	....	1.125	0.594	0.720
1	1.875	0.494	....	....	1.312	0.656	0.803
1 1/8	2.062	0.529					
1 1/4	2.312	0.600					
1 3/8	2.562	0.665					
1 1/2	2.812	0.742					

†Maximum.

THREADED FASTENERS

9. Binding head
  a. Slotted or cross-recessed
10. Hex head
  a. Indented
  b. Slotted
  c. Indented and slotted
11. Hex washer head
  a. Indented
  b. Indented and slotted

The *round-head* machine screw is obsolete. Use the *pan-head* screw, instead; it has more driving power. Most of the head types outlined here are illustrated in Figs. 23.9 to 23.11, some slotted and some with cross-recesses.

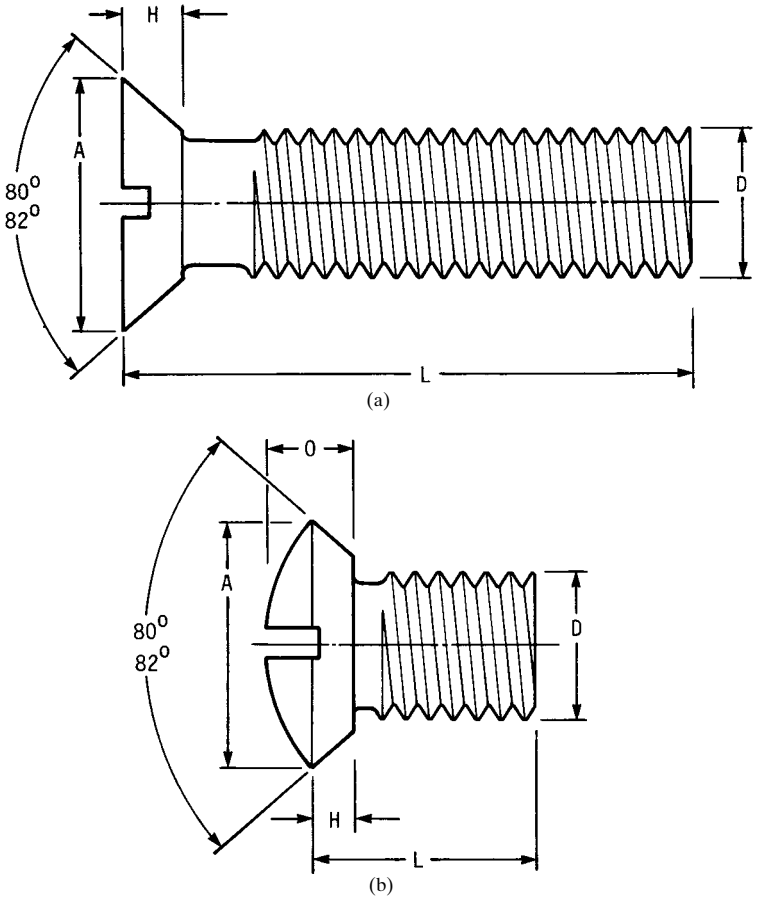

FIGURE 23.9 (*a*) Slotted flat countersunk-head machine screw; also available with 100-degree head; (*b*) short or undercut slotted oval countersunk-head machine screw. Note the difference between the body of a machine screw and that of a cap screw. Compare this figure with Fig. 23.8*a*.

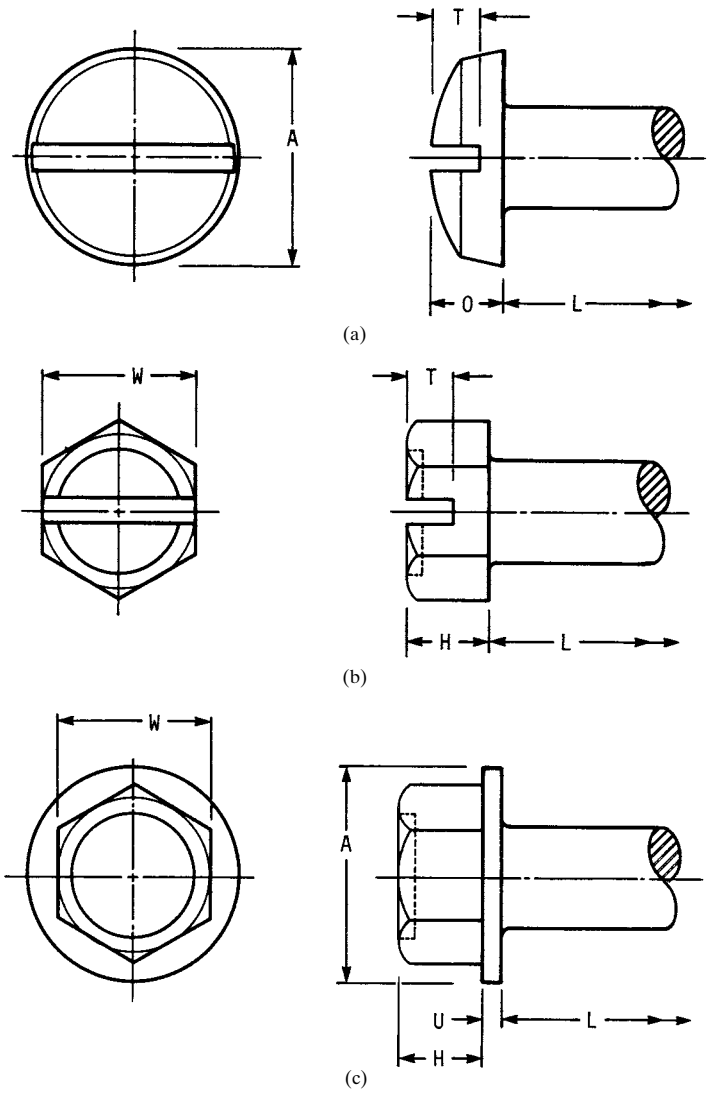

FIGURE 23.10 (*a*) Slotted binding-head machine screw; the edge angle is 5 degrees; (*b*) slotted and indented hex-head machine screw; (*c*) hex washer-head machine screw. Both hex screws in this figure may be obtained with or without slots and/or indentations.

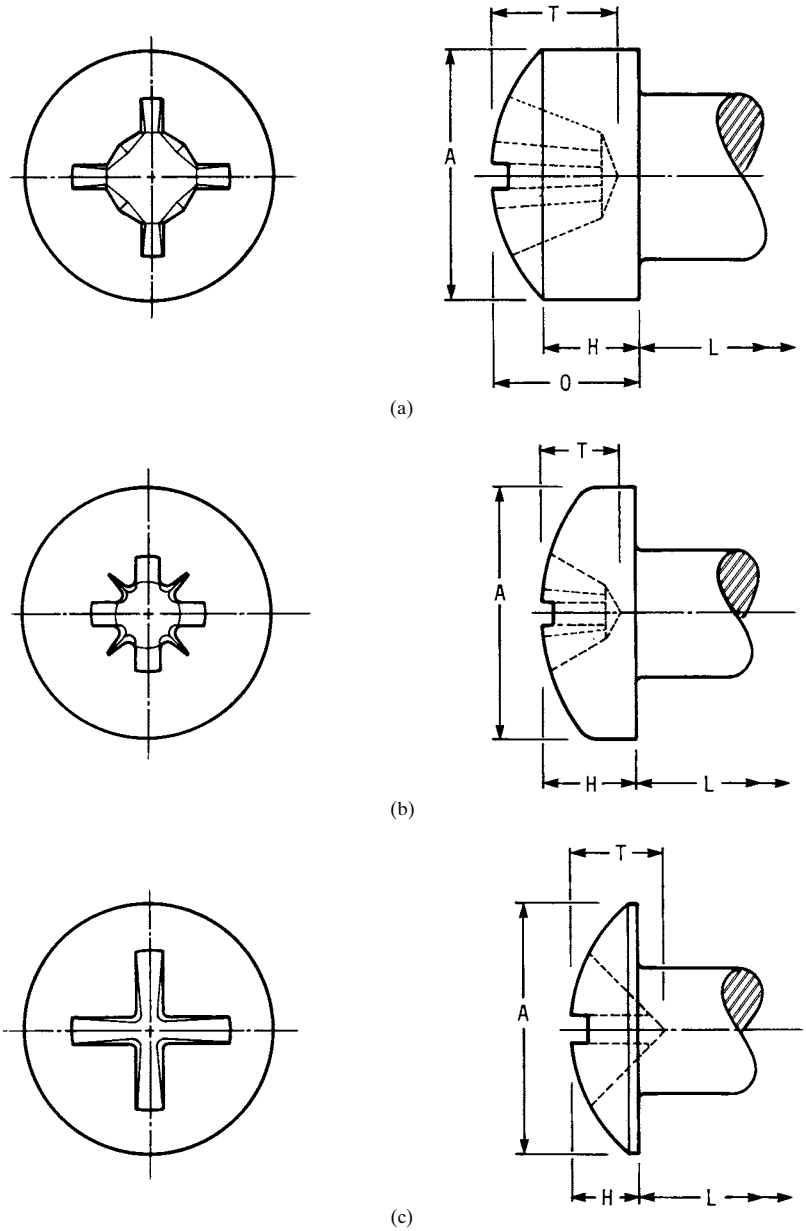

FIGURE 23.11 The three standard recesses. (*a*) Fillister-head machine screw with Type 1 cross-recess. This recess has a large center opening, tapered wings, and a blunt bottom. (*b*) Pan-head machine screw with Type 1A cross-recess. This recess has a large center opening, wide straight wings, and a blunt bottom. (*c*) Truss-head machine screw with Type 2 cross-recess. This recess has two intersecting slots with parallel sides. The sides converge to a slightly truncated apex at the bottom.

Figure 23.9 illustrates the difference between a regular and an undercut machine screw. Note also the reduced body diameter in this figure and compare it with that of cap screws. See Table 23.32 for undercut lengths.

Figure 23.11 is intended to illustrate the three standard cross-recesses, but it also illustrates three additional head styles. Use Table 23.32 to find the driver sizes for cross-recessed heads. Three more head styles are illustrated in Fig. 23.10.

Trim-head screws are not illustrated; the head diameters are smaller, and the screws are driven only with cross-recessed drivers. Long trim-head screws have a short shoulder and then a reduced body diameter. Short ones have a neck instead of the shoulder.

Tables 23.27 to 23.33 inclusive give the basic dimensions for all machine-screw head styles except the close-tolerance 100-degree flat countersunk-head screw.

Normal thread lengths are 1 in for screw sizes No. 5 and smaller and 1½ in for larger sizes. Steel machine screws are usually made from carbon steel having a minimum tensile strength of 60 kpsi.

23.4 NUTS

Flat nuts, such as the *square* or *flat hex* in Fig. 23.12, have only a chamfered top. All other hex nuts, except the castle, have chamfered tops and bottoms that are cham-

TABLE 23.27 Basic Head Dimensions of Flat Countersunk-Head Machine Screws†

Nominal size D	Head diameter‡ A	Head thickness‡ H		
		Regular, 80 degrees		
		Long	Undercut	100-degree head
0	0.119	0.035	0.025	0.026
1	0.146	0.043	0.031	0.031
2	0.172	0.051	0.036	0.037
3	0.199	0.059	0.042	0.043
4	0.225	0.067	0.047	0.049
5	0.252	0.075	0.053	
6	0.279	0.083	0.059	0.060
8	0.332	0.100	0.070	0.072
10	0.385	0.116	0.081	0.083
12	0.438	0.132	0.092	
¼	0.507	0.153	0.107	0.110
5/16	0.635	0.191	0.134	0.138
3/8	0.762	0.230	0.161	0.165
7/16	0.812	0.223	0.156	
½	0.875	0.223	0.156	
9/16	1.000	0.260		
5/8	1.125	0.298		
¾	1.375	0.372		

†All dimensions in inches.
‡Maximum.

TABLE 23.28 Total Head Heights *O* for Oval Countersunk-Head Machine Screws†

Nominal size *D*	Total head height ‡ *O*		Nominal size *D*	Total head height‡ *O*	
	Long	Undercut		Long	Undercut
0	0.056	0.046	12	0.200	0.161
1	0.068	0.056	1/4	0.232	0.186
2	0.080	0.065	5/16	0.290	0.232
3	0.092	0.075	3/8	0.347	0.278
4	0.104	0.084	7/16	0.345	0.279
5	0.116	0.094	1/2	0.354	0.288
6	0.128	0.104	9/16	0.410	
8	0.152	0.123	5/8	0.467	
10	0.176	0.142	3/4	0.578	

†Head dimensions *A* and *H* are the same as for regular 80-degree flat-head machine screws (Table 23.27). All dimensions are in inches.
‡Maximum.

TABLE 23.29 Basic Head Dimensions of Flat and Oval Countersunk Trim-Head Machine Screws (Available Only with Cross-Recessed Heads)†

Nominal size *D*	Shoulder diameter‡§	Head diameter‡ *A*	Flat head height *H*	Oval head height¶ *O*
4	0.112	0.199	0.052	0.086
5	0.125	0.225	0.060	0.099
6	0.138	0.225	0.052	0.091
6	0.138	0.252	0.068	0.112
8	0.164	0.252	0.052	0.096
8	0.164	0.279	0.069	0.117
10	0.190	0.332	0.085	0.141
12	0.216	0.332	0.069	0.125
12	0.216	0.385	0.101	0.166
1/4	0.250	0.385	0.080	0.146
1/4	0.250	0.438	0.112	0.187
5/16	0.312	0.438	0.075	0.150
5/16	0.312	0.507	0.116	0.202
3/8	0.375	0.635	0.155	0.265

†All dimensions are in inches.
‡Maximum.
§Screws having nominal lengths over 1 1/8 in for sizes No. 5 and smaller and over 2 in for sizes No. 6 and larger have a shoulder of this diameter and about 1 1/16 in long beneath the head.
¶This is the total height. The side height *H* is the same as for flat-head trim screws.

TABLE 23.30 Basic Head Dimensions of Pan- and Truss-Head Machine Screws†

	Pan head		Truss head	
Nominal size *D*	Diameter *A*	Height *H*	Diameter *A*	Height *H*
0	0.116	0.044	0.131	0.037
1	0.142	0.053	0.164	0.045
2	0.167	0.062	0.194	0.053
3	0.193	0.071	0.226	0.061
4	0.219	0.080	0.257	0.069
5	0.245	0.089	0.289	0.078
6	0.270	0.097	0.321	0.086
8	0.322	0.115	0.384	0.102
10	0.373	0.133	0.448	0.118
12	0.425	0.151	0.511	0.134
1/4	0.492	0.175	0.573	0.150
5/16	0.615	0.218	0.698	0.183
3/8	0.740	0.261	0.823	0.215
7/16	0.863	0.305	0.948	0.248
1/2	0.987	0.348	1.073	0.280
9/16	1.041	0.391	1.198	0.312
5/8	1.172	0.434	1.323	0.345
3/4	1.435	0.521	1.573	0.410

†All values are maximum; all dimensions are in inches.

TABLE 23.31 Basic Head Dimensions of Binding- and Fillister-Head Machine Screws†

	Fillister head			Binding head	
Nominal size *D*	Diameter *A*	Height *H*	Height *O*	Diameter *A*	Height *O*
0	0.096	0.043	0.055	0.126	0.032
1	0.118	0.053	0.066	0.153	0.041
2	0.140	0.062	0.083	0.181	0.050
3	0.161	0.070	0.095	0.208	0.059
4	0.183	0.079	0.107	0.235	0.068
5	0.205	0.088	0.120	0.263	0.078
6	0.226	0.096	0.132	0.290	0.087
8	0.270	0.113	0.156	0.344	0.105
10	0.313	0.130	0.180	0.399	0.123
12	0.357	0.148	0.205	0.454	0.141
1/4	0.414	0.170	0.237	0.525	0.165
5/16	0.518	0.211	0.295	0.656	0.209
3/8	0.622	0.253	0.355	0.788	0.253
7/16	0.625	0.265	0.368		
1/2	0.750	0.297	0.412		
9/16	0.812	0.336	0.466		
5/8	0.875	0.375	0.521		
3/4	1.000	0.441	0.612		

†All values are maximum; all dimensions are in inches.

TABLE 23.32 Undercut Lengths for Flat and Oval Countersunk-Head Machine Screws and Driver Sizes for Type I and IA Cross-Recesses†

Nominal size	Undercut lengths (or less)	Driver size	Nominal size	Undercut lengths (or less)	Driver size
0	1/8	0	10	5/16	2
1	1/8	0	12	3/8	3
2	1/8	1	1/4	7/16	3
3	1/8	1	5/16	1/2	4
4	3/16	1	3/8	9/16	4
5	3/16	2	7/16	5/8	4
6	3/16	2	1/2	3/4	4
8	1/4	2	9/16	....	4

†Type II drivers have the same point size for all screw sizes.

TABLE 23.33 Basic Head Dimensions for Regular-Hex- and Washer-Hex-Head Machine Screws†

Nominal size *D*	Head height *H*	Width across faults *W*		Washer face	
		Regular hex	Washer hex	Diameter *A*	Thickness *U*
1	0.044	0.120			
2	0.050	0.120	0.125	0.166	0.016
3	0.055	0.181	0.125	0.177	0.016
4	0.060	0.181	0.188	0.243	0.019
5	0.070	0.181	0.188	0.260	0.025
6	0.093	0.244	0.250	0.328	0.025
8	0.110	0.244	0.250	0.348	0.031
10	0.120	0.305	0.312	0.414	0.031
12	0.155	0.305	0.312	0.432	0.039
1/4	0.190	0.367	0.375	0.520	0.050
5/16	0.230	0.489	0.500	0.676	0.055
3/8	0.295	0.551	0.562	0.780	0.063

†All values are maximum; all dimensions are in inches.

fered or washer-faced, as in Fig. 23.12*c* and *d*. *Castle nuts* (Fig. 23.12*f*) are made in both styles, washer-faced or with chamfered bottoms.

Most styles can also be classified as regular, thick, or heavy. A thick nut has the same width *W* across flats as a regular nut, but the height *H* is greater. A *jam nut* is a thin hex nut. A *heavy nut* is larger in both dimensions, *W* and *H,* than the regular style.

It is convenient to outline these varieties of head styles with their accepted names and indicate in which table the dimensions are to be found:

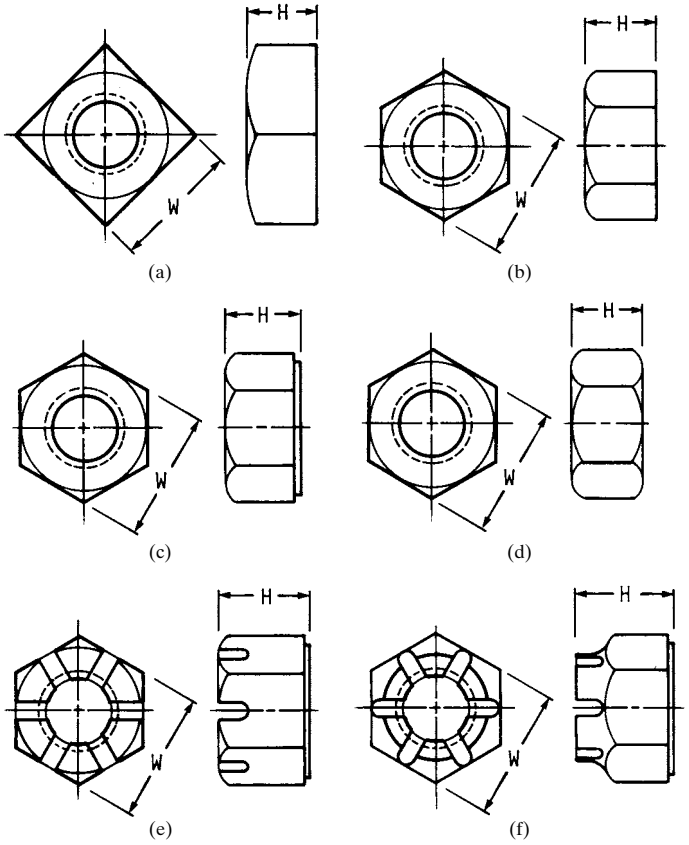

FIGURE 23.12 Types of nuts. (*a*) Square; (*b*) hex flat; (*c*) hex with washer face; (*d*) double-chamfered hex; (*e*) slotted hex; (*f*) hex castle.

1. Flat nuts
   - ***a.*** Square (Table 23.34)
   - ***b.*** Heavy square (Table 23.34)
   - ***c.*** Hex (Table 23.35)
   - ***d.*** Hex jam (Table 23.35)
   - ***e.*** Heavy hex (Table 23.39)
   - ***f.*** Heavy hex jam (Table 23.39)
2. Nuts with washer-faced or chamfered bottoms
   - ***a.*** Hex (Table 23.35)
     - (1) Metric style 1 (Table 23.36)
   - ***b.*** Hex jam (Table 23.35)
     - (1) Metric (Table 23.36)
   - ***c.*** Hex slotted (Table 23.35)
     - (1) Metric (Table 23.36)

TABLE 23.34 Basic Dimensions of Square Nuts (Inch Series)

Nominal size	Regular		Heavy	
	W	*H*	*W*	*H*
1/4	7/16	7/32	1/2	1/4
5/16	9/16	17/64	9/16	5/16
3/8	5/8	21/64	11/16	3/8
7/16	3/4	3/8	3/4	7/16
1/2	13/16	7/16	7/8	1/2
5/8	1	35/64	1 1/16	5/8
3/4	1 1/8	21/32	1 1/4	3/4
7/8	1 5/16	49/64	1 7/16	7/8
1	1 1/2	7/8	1 5/8	1
1 1/8	1 11/16	1	1 13/16	1 1/8
1 1/4	1 7/8	1 3/32	2	1 1/4
1 3/8	2 1/16	1 13/64	2 3/16	1 3/8
1 1/2	2 1/4	1 5/16	2 3/8	1 1/2

TABLE 23.35 Basic Dimensions of Hex, Hex Jam, Hex Flat, Hex Flat Jam, Hex Slotted, Hex Thick, and Hex Thick Slotted Nuts (Inch Series)

Nominal size *D*	Width *W*	Height *H*				
		Hex and hex slotted	Hex jam	Hex flat	Hex flat jam	Hex thick and thick slotted
1/4	7/16	7/32	5/32	...	...	9/32
5/16	1/2	17/64	3/16	...	...	21/64
3/8	9/16	21/64	7/32	...	...	13/32
7/16	11/16	3/8	1/4	...	...	29/64
1/2	3/4	7/16	5/16	...	...	9/16
9/16	7/8	21/64	5/16	...	...	29/64
5/8	15/16	35/64	3/8	...	...	23/32
3/4	1 1/8	41/64	27/64	...	...	13/16
7/8	1 5/16	3/4	31/64	...	...	29/32
1	1 1/2	55/64	35/64	...	...	1
1 1/8	1 11/16	31/32	39/64	1	5/8	1 5/32
1 1/4	1 7/8	1 1/16	23/32	1 3/32	3/4	1 1/4
1 3/8	2 1/16	1 11/64	25/32	1 13/64	13/16	1 3/8
1 1/2	2 1/4	1 9/32	27/32	1 5/16	7/8	1 1/2

TABLE 23.36 Basic Dimensions of Metric Hex Nuts†

Nominal size *D*	Width across flats‡ *W*	Height H‡		
		Style 1	Style 2 or slotted	Jam
M1.6	3.2	1.3		
M2	4	1.6		
M2.5	5	2.0		
M3	5.5	2.4	2.9§	
M3.5	6	2.8	3.3§	
M4	7	3.2	3.8§	
M5	8	4.7	5.1	2.7
M6	10	5.2	5.7	3.2
M8	13	6.8	7.5	4.0
M10	16	8.4	9.3	5.0
M12	18	10.8	12.0	6.0
M14	21	12.8	14.1	7.0
M16	24	14.8	16.4	8.0
M20	30	18.0	20.3	10.0
M24	36	21.5	23.9	12.0
M30	46	25.6	28.6	15.0
M36	55	31.0	34.7	18.0

†All dimensions are in millimeters.
‡Maximum.
§Not standard in slotted style.

TABLE 23.37 Basic Dimensions of Metric Heavy Hex Nuts†

Nominal size *D*	Width across flats‡ *W*	Height‡ *H*	Nominal size *D*	Width across flats‡ *W*	Height‡ *H*
M12	21	12,3	M24	41	24.2
M14	24	14.3	M27	46	27.6
M16	27	17.1	M30	50	30.7
M20	34	20.7	M36	60	36.6
M22	36	23.6	M42	70	42.0

†All dimensions are in millimeters.
‡Maximum.

d. Hex thick (Table 23.35)
  (1) Metric style 2 (Table 23.36)
e. Hex thick slotted (Table 23.35)
f. Heavy hex (Table 23.38)
  (1) Metric (Table 23.37)
g. Heavy hex jam (Table 23.38)
h. Hex castle (Table 23.38)

3. Machine screw nuts
a. Hex (Table 23.40)
b. Square (Table 23.40)

TABLE 23.38 Basic Dimensions of Heavy Hex, Heavy Hex Jam, Heavy Hex Slotted, and Heavy Hex Castle Nuts (Inch Series)

	Heavy hex			Hex castle	
		Height H			
Nominal size D	Width W	Plain or slotted	Jam	Width W	Height H
$\frac{1}{4}$	$\frac{1}{2}$	$\frac{15}{64}$	$\frac{11}{64}$	$\frac{7}{16}$	$\frac{9}{32}$
$\frac{5}{16}$	$\frac{9}{16}$	$\frac{19}{64}$	$\frac{13}{64}$	$\frac{1}{2}$	$\frac{21}{64}$
$\frac{3}{8}$	$\frac{11}{16}$	$\frac{23}{64}$	$\frac{15}{64}$	$\frac{9}{16}$	$\frac{13}{32}$
$\frac{7}{16}$	$\frac{3}{4}$	$\frac{27}{64}$	$\frac{17}{64}$	$\frac{11}{16}$	$\frac{29}{64}$
$\frac{1}{2}$	$\frac{7}{8}$	$\frac{31}{64}$	$\frac{19}{64}$	$\frac{3}{4}$	$\frac{9}{16}$
$\frac{9}{16}$	$\frac{15}{16}$	$\frac{35}{64}$	$\frac{21}{64}$	$\frac{7}{8}$	$\frac{39}{64}$
$\frac{5}{8}$	$1\frac{1}{16}$	$\frac{39}{64}$	$\frac{23}{64}$	$\frac{15}{16}$	$\frac{23}{32}$
$\frac{3}{4}$	$1\frac{1}{4}$	$\frac{47}{64}$	$\frac{27}{64}$	$1\frac{1}{8}$	$\frac{13}{16}$
$\frac{7}{8}$	$1\frac{7}{16}$	$\frac{55}{64}$	$\frac{31}{64}$	$1\frac{5}{16}$	$\frac{29}{32}$
1	$1\frac{5}{8}$	$\frac{63}{64}$	$\frac{35}{64}$	$1\frac{1}{2}$	1
$1\frac{1}{8}$	$1\frac{13}{16}$	$1\frac{7}{64}$	$\frac{39}{64}$	$1\frac{11}{16}$	$1\frac{5}{32}$
$1\frac{1}{4}$	2	$1\frac{7}{32}$	$\frac{23}{32}$	$1\frac{7}{8}$	$1\frac{1}{4}$
$1\frac{3}{8}$	$2\frac{3}{16}$	$1\frac{11}{32}$	$\frac{25}{32}$	$2\frac{1}{16}$	$1\frac{3}{8}$
$1\frac{1}{2}$	$2\frac{3}{8}$	$1\frac{15}{32}$	$\frac{27}{32}$	$2\frac{1}{4}$	$1\frac{1}{2}$

TABLE 23.39 Basic Dimensions of Heavy Hex Flat and Heavy Hex Flat Jam Nuts (Inch Series)

		Height H	
Nominal size D	Width across flats W	Regular	Jam
$1\frac{1}{8}$	$1\frac{13}{16}$	$1\frac{1}{8}$	$\frac{5}{8}$
$1\frac{1}{4}$	2	$1\frac{1}{4}$	$\frac{3}{4}$
$1\frac{3}{8}$	$2\frac{13}{16}$	$1\frac{3}{8}$	$\frac{13}{16}$
$1\frac{1}{2}$	$2\frac{3}{8}$	$1\frac{1}{2}$	$\frac{7}{8}$
$1\frac{3}{4}$	$2\frac{3}{4}$	$1\frac{3}{4}$	1
2	$3\frac{1}{8}$	2	$1\frac{1}{8}$

Carbon steel nuts usually are made to conform to ASTM A563 Grade A specifications or to SAE Grade 2.

23.5 TAPPING SCREWS

Self-tapping screws are available in all head styles and in sizes up to and including ⅜ in. They are hardened sufficiently to form their own mating threads when driven. In

TABLE 23.40 Basic Dimensions of Machine-Screw Nuts†

Nominal size D	Width W	Height‡ H	Nominal size D	Width W	Height‡ H
0	$\frac{5}{32}$	0.050	8	$\frac{11}{32}$	0.130
1	$\frac{5}{32}$	0.050	10	$\frac{3}{8}$	0.130
2	$\frac{3}{16}$	0.066	12	$\frac{7}{16}$	0.161
3	$\frac{3}{16}$	0.066	$\frac{1}{4}$	$\frac{7}{16}$	0.193
4	$\frac{1}{4}$	0.098	$\frac{5}{16}$	$\frac{9}{16}$	0.225
5	$\frac{5}{16}$	0.114	$\frac{3}{8}$	$\frac{5}{8}$	0.257
6	$\frac{5}{16}$	0.114			

†All dimensions are in inches; dimensions apply to both hex and square nuts.
‡Maximum.

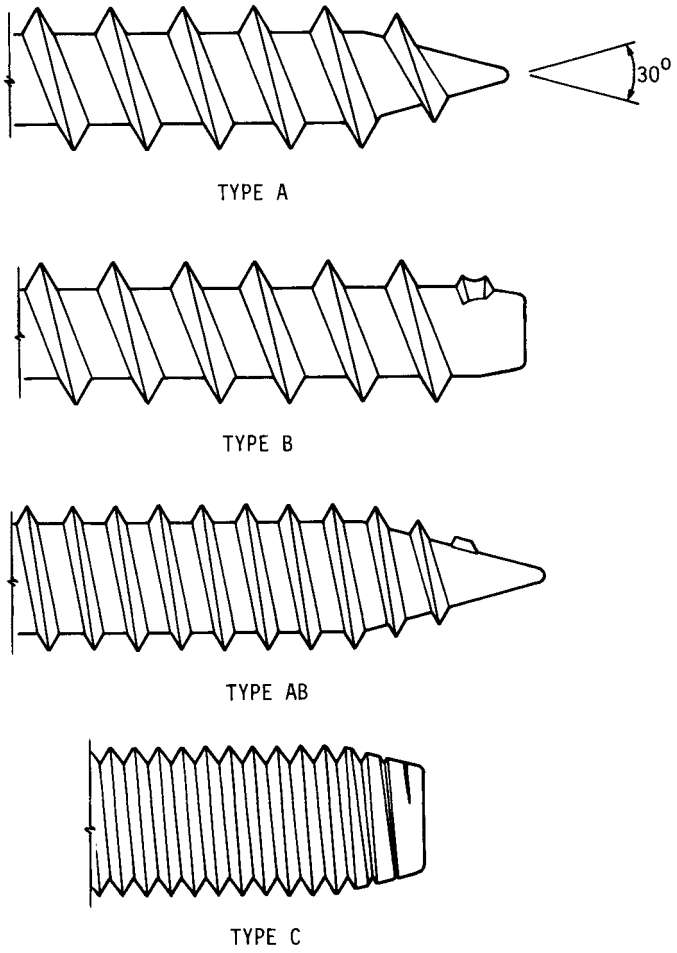

FIGURE 23.13 Thread-forming screws.

fact, at least one manufacturer has developed a screw which both drills and taps in a single operation.

Thread-forming screws are used when sufficient joint stresses can be developed to guard against loosening. The Type A screw (Fig. 23.13) has a gimlet point and is used to join sheet metal. It is sometimes used instead of a wood screw.

The Type B screw has a blunt point and, sometimes, a finer pitch than the Type A. With the finer pitch, it has a greater range of applications and is used in heavier sheet metal and nonferrous castings.

The Type AB screw is similar to Type A but has a finer pitch, which permits it to be used in more brittle materials, such as plastics or zinc die castings. It is also used as a wood screw.

The Type C screw has machine-screw threads, a blunt point, and tapered threads at the start, as shown in Fig. 23.13. This screw is useful for thick sections but may require large driving torques.

Thread-cutting screws (shown in Fig. 23.14) are used instead of thread-forming screws to lessen the driving torque and the internal stresses. Types D, G, F, and T all have machine-screw threads and an end taper with a blunt point. They are used for various die castings, cast iron, brass, plastics, and sheet steel.

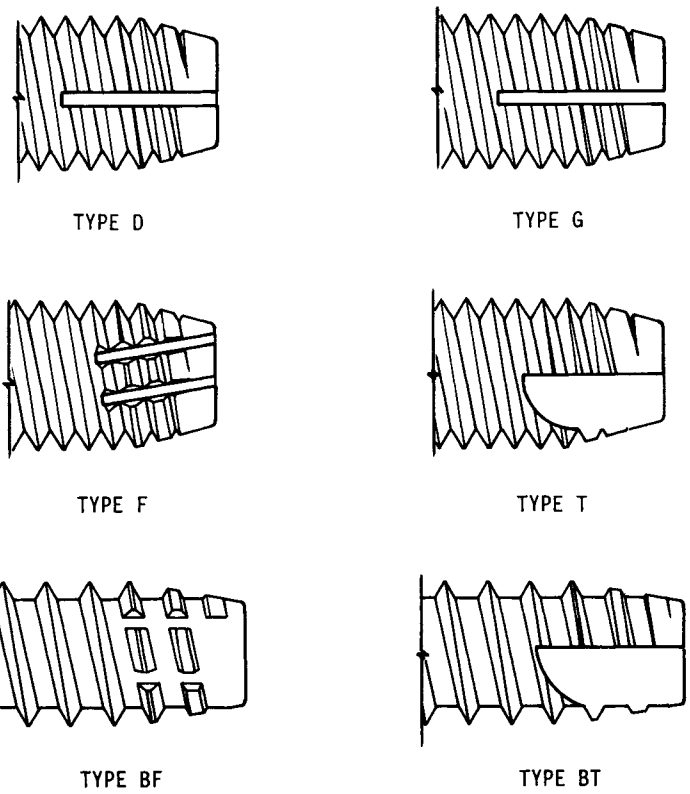

FIGURE 23.14 Thread-cutting screws.

Types BF and BT screws (shown in Fig. 23.14) have additional cutting edges and a greater chip-storage capacity. They are useful for various plastics and compositions.

Thread-rolling screws (not shown) have a unique point and body shape to make starting easier and to lessen the driving torque. The thread rolling cold-works the material, thus contributing to the strength of the joint.

REFERENCE

23.1 "Codes and Standards; Fasteners," in *ASME Publications Catalog,* American Society of Mechanical Engineers, New York, 1985.

CHAPTER 24
UNTHREADED FASTENERS

Joseph E. Shigley
Professor Emeritus
The University of Michigan
Ann Arbor, Michigan

24.1 RIVETS

A *rivet* is a fastener that has a head and a shank and is made of a deformable material. It is used to join several parts by placing the shank into holes through the several parts and creating another head by upsetting or deforming the projecting shank.

During World War II, Rosie the Riveter was a popular cartoon character in the United States. No better image can illustrate the advantages of riveted joints. These are

1. Low cost
2. Fast automatic or repetitive assembly
3. Permanent joints
4. Usable for joints of unlike materials such as metals and plastics
5. Wide range of rivet shapes and materials
6. Large selection of riveting methods, tools, and machines

Riveted joints, however, are not as strong under tension loading as are bolted joints (see Chap. 22), and the joints may loosen under the action of vibratory tensile or shear forces acting on the members of the joint. Unlike with welded joints, special sealing methods must be used when riveted joints are to resist the leakage of gas or fluids.

24.1.1 Head Shapes

A group of typical rivet-head styles is shown in Figs. 24.1 and 24.2. Note that the button head, the oval head, and the truss head are similar. Of the three, the oval head has an intermediate thickness.

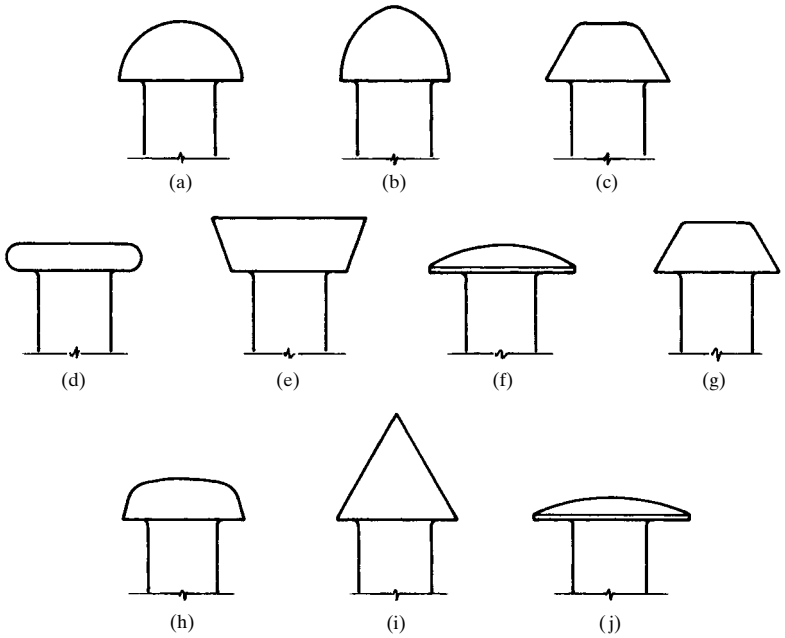

FIGURE 24.1 Standard rivet heads with flat bearing surfaces. (*a*) Button or round head; (*b*) high button or acorn head; (*c*) cone head; (*d*) flat head; (*e*) machine head; (*f*) oval head; (*g*) large pan head; (*h*) small pan head; (*i*) steeple head; (*j*) truss head, thinner than oval head.

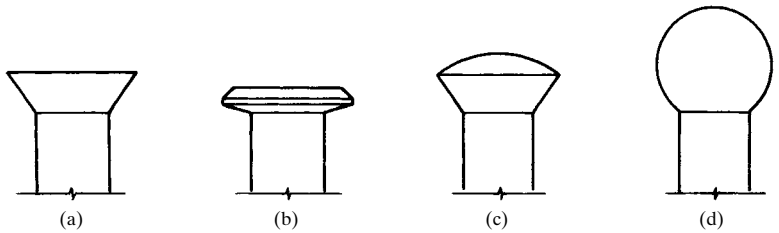

FIGURE 24.2 Various rivet heads. (*a*) Countersunk head; (*b*) countersunk head with chamfered top; (*c*) countersunk head with round top; (*d*) globe head.

A large rivet is one that has a shank diameter of ½ in or more; such rivets are mostly hot-driven. Head styles for these are button, high button, cone, countersunk, and pan. Smaller rivets are usually cold-driven. The countersunk head with chamfered flat top and the countersunk head with round top are normally used only on large rivets.

24.1.2 Rivet Types

The standard structural or machine rivet has a cylindrical shank and is either hot- or cold-driven.

A *boiler rivet* is simply a large rivet with a cone head.

A *cooper's rivet,* used for barrel-hoop joints, is a solid rivet with a head like that in Fig. 24.2*b* which has a shank end that is chamfered.

A *shoulder rivet* has a shoulder under the head.

A *tank rivet,* used for sheet-metal work, is a solid rivet with a button, countersunk, flat, or truss head.

A *tinner's rivet,* used for sheet-metal work, is a small solid rivet with a large flat head (Fig. 24.1*d*).

A *belt rivet,* shown in Fig. 24.3*a,* has a *riveting burr* and is used for leather or fabric joints.

A *compression* or *cutlery rivet,* shown in Fig. 24.3*b,* consists of a tubular rivet and a solid rivet. The hole and shank are sized to produce a drive fit when the joint is assembled.

A *split* or *bifurcated rivet,* shown in Fig. 24.3*c,* is a small rivet with an oval or countersunk head. The prongs cut their own holes when driven through softer metals or fibrous materials such as wood.

A *swell-neck rivet,* shown in Fig. 24.3*d,* is a large rivet which is used when a tight fit with the hole is desired.

A *tubular rivet,* shown in Fig. 24.3*e,* is a small rivet with a hole in the shank end. The rivet is cold-driven with a punchlike tool that expands or curls the shank end. *Semitubular rivets* are classified as those having hole depths less than 112 percent of the shank diameter.

A *blind rivet* is intended for use where only one side of the joint is within reach. The blind side is the side that is not accessible. However, blind rivets are also used where both sides of the joint can be accessed because of the simplicity of the assembly, the appearance of the completed joint, and the portability of the riveting tools. The rivets shown in Figs. 24.4 to 24.8 are typical of the varieties available.

24.1.3 Sizes and Materials

Large rivets are standardized in sizes from ½ to 1¾ in in ⅛-in increments. The nominal head dimensions may be calculated using the formulas in Table 24.1. The tolerances are found in Ref. [24.2]. The materials available are specified according to the following ASTM Specifications:

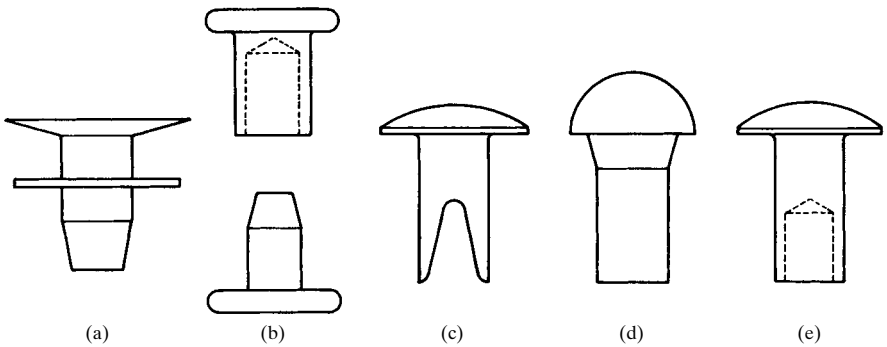

FIGURE 24.3 (*a*) Belt rivet; (*b*) compression rivet; (*c*) split rivet; (*d*) swell-neck rivet; (*e*) tubular rivet.

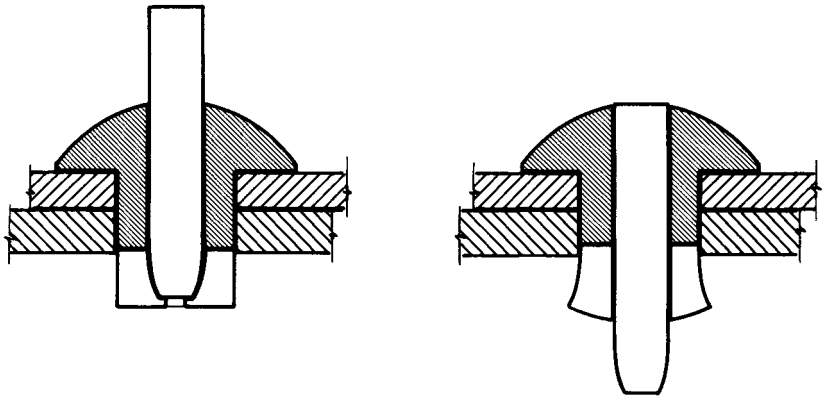

(a) (b)

FIGURE 24.4 Drive-pin type of blind rivet. (*a*) Rivet assembled into parts; (*b*) ears at end of rivet expand outward when pin is driven.

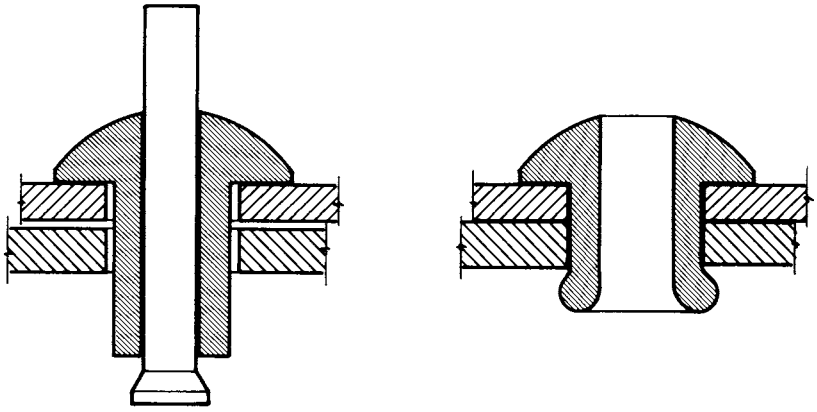

(a) (b)

FIGURE 24.5 Pull-through-type blind riveting. (*a*) Before riveting; (*b*) after riveting.

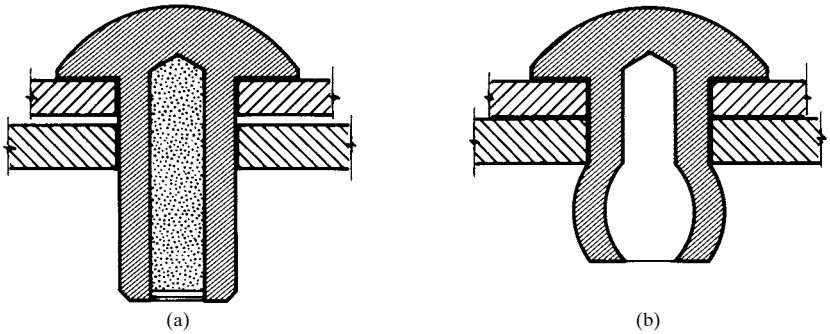

(a) (b)

FIGURE 24.6 Explosive blind rivet. (*a*) Before explosion; (*b*) after; notice that the explosion clamps the joint.

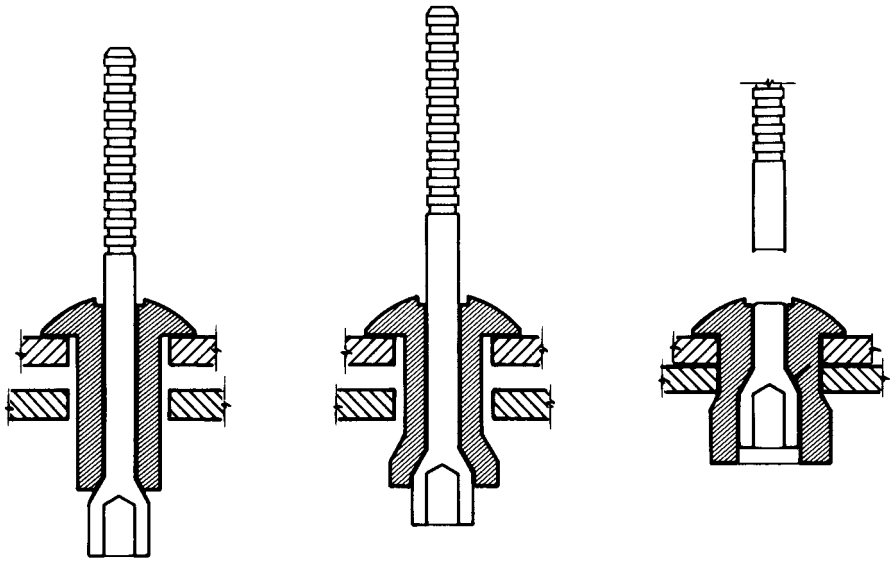

FIGURE 24.7 Self-plugging blind rivet. (*a*) Rivet inserted into prepared hole with power tool; (*b*) axial pull with power tool fills holes completely and clamps work pieces together; (*c*) stem separates flush with head and remaining section is locked in place. *(Avdel Corporation.)*

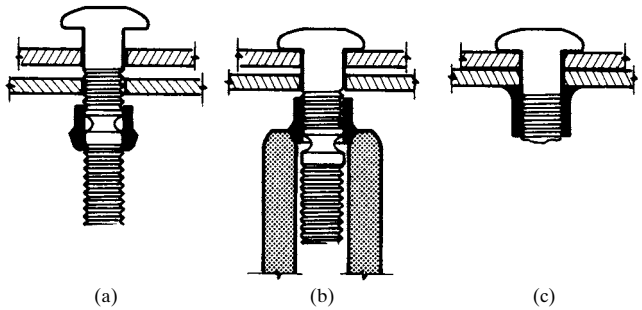

FIGURE 24.8 Lock-bolt or collar-type blind rivet. (*a*) Pin inserted through holes and collar placed over the pin tail; (*b*) nose tool pulls on the pin and reacts against the collar, clamping the work tightly; (*c*) installation finished by swaging the collar into the annular locking grooves and separating the pin at the breaker groove. *(Avdel Corporation.)*

A31 Boiler rivet steel.

A131 Rivet steel for ships.

A152 Wrought-iron rivets.

A502 Grade 1 carbon structural steel for general purposes. Grade 2 carbon-manganese steel for use with high-strength carbon and low-alloy steels.

TABLE 24.1 Head Dimensions for Large Rivets

Type of head	Diameter,† in		Height, in	Radius, in
	Major	Minor		
Button	1.750*D*	.....	0.750*D*	0.885*D*
High button‡	1.500*D* + 0.031	.....	0.750*D* + 0.125	0.750*D* + 0.281
Cone	1.750*D*	0.938*D*	0.875*D*	
Flat countersunk	1.810*D*	.....	0.483*D*§	
Oval countersunk¶	1.810*D*	.....	0.483*D*§	2.250*D*
Pan	1.600*D*	1.000*D*	0.700*D*	

†The nominal rivet diameter is *D*.
‡Side radius is 0.750*D* − 0.281.
§Varies, depending on shank and head diameters and the included angle.
¶Crown radius is 0.190*D*.
SOURCE: From Ref. [24.2].

Small solid rivets are standardized in sizes from 1/16 to 7/16 in in increments of 1/32 in. Note that some of these are not included in the table of preferred sizes (Table A.4). Table 24.2 is a tabulation of standard head styles available and formulas for head dimensions. ASTM standard A31 Grade A or the SAE standard J430 Grade 0 are used for small steel rivets. But other materials, such as stainless steel, brass, or aluminum may also be specified.

Tinner's and cooper's rivets are sized according to the weight of 1000 rivets. A 5-lb rivet has a shank diameter of about 3/16 in. See Ref. [24.1] for sizes and head dimensions.

Belt rivets are standardized in gauge sizes from No. 14 to No. 4 using the Stubs iron-wire gauge (Table A.17).

Tubular rivets are standardized in decimals of an inch; sizes corresponding to various head styles are listed in Tables 24.3 and 24.4. These are used with rivet caps, which are available in several styles and diameters for each rivet size. These rivets are manufactured from ductile wire using a cold-heading process. Thus any ductile material, such as steel, brass, copper, aluminum, etc., can be used. For standard tolerances, see Ref. [24.3].

Split rivet sizes are shown in Table 24.5. Split rivets are available in the same materials as tubular rivets and may be used with rivet caps too.

Some types of *blind rivets* are available in sizes from 3/32 to 3/8 in in diameter. The usual materials are carbon steel, stainless steel, brass, and aluminum. A variety of

TABLE 24.2 Head Dimensions for Small Solid Rivets

Head type	Diameter,† in	Height, in	Radius, in
Flat	2.000*D*	0.330*D*	
Flat countersunk	1.850*D*	0.425*D*	
Button	1.750*D*	0.750*D*	0.885*D*
Pan	1.720*D*	0.570*D*	3.430*D*‡
Truss	2.300*D*	0.330*D*	2.512*D*

TABLE 24.3 Sizes of Standard Semitubular Rivets†

Nominal size	Oval head		Truss head		Flat countersunk‡		Hole diameter§	Length increment
	Diameter	Thickness	Diameter	Thickness	Diameter	Thickness		
0.061	0.114	0.019	0.130	0.019	. . . .	. . . .	0.046	0.016
0.089	0.152	0.026	0.192	0.026	0.223	0.039	0.068	0.016
0.099	0.192	0.032	. . . .	. . . .	. . . .	. . . .	0.076	0.016
0.123	0.223	0.038	0.286	0.038	0.271	0.043	0.095	0.016
0.146	0.239	0.045	0.318	0.045	0.337	0.056	0.112	0.031
0.188	0.318	0.065	0.381	0.065	0.404	0.063	0.145	0.031
0.217	0.444	0.075	. . . .	. . . .	0.472	0.075	0.166	0.062
0.252	0.507	0.085	. . . .	. . . .	0.540	0.084	0.191	0.062
0.310	0.570	0.100	. . . .	. . . .	. . . .	. . . .	0.235	0.062

†Dimensions in inches; all values are maximums.
‡120-degree included angle; also available in 150-degree angle with chamfered top for friction materials.
§For Type T tapered hole; diameter is at end of rivet; also available as Type S straight hole.

SOURCE: From Ref. [24.3].

TABLE 24.4 Sizes of Standard Full Tubular Rivets†

Head shape	Nominal size	Head		Hole diameter
		Diameter	Thickness	
Oval	0.146	0.239	0.045	0.107
Truss	0.146	0.318	0.045	0.107
	0.188	0.381	0.065	0.141
Flat countersunk	0.146	0.317	0.050	0.107
	0.188	0.364	0.060	0.141

†Dimensions in inches; all values are maximum; maximum hole depth is to head.
‡Chamfered.
SOURCE: From Ref. [24.3].

TABLE 24.5 Sizes of Standard Split Rivets†

Nominal size	Oval head		Flat countersunk head	
	Diameter	Thickness	Diameter	Thickness
0.092	0.152	0.026		
0.125	0.223	0.035	0.223	0.036
0.152	0.318	0.045	0.317	0.053
0.152	....	....	0.380‡	0.062‡
0.190	0.349	0.055	0.443	0.061

†Dimensions in inches; all values are maximum.
‡Designates a *large flat countersunk head rivet.*
SOURCE: From Ref. [24.3].

head styles are available, but many of these are modifications of the countersunk head, the truss head, and the pan head. Head dimensions, lengths, and grips may be found in the manufacturer's catalogs.

24.2 PINS

When a joint is to be assembled in which the principal loading is shear, then the use of a pin should be considered because it may be the most cost-effective method. While a special pin can be designed and manufactured for any situation, the use of a standard pin will be cheaper.

Taper pins (Fig. 24.9*a*) are sized according to the diameter at the large end, as shown in Table 24.6. The diameter at the small end can be calculated from the equation

$$d = D - 0.208L$$

UNTHREADED FASTENERS

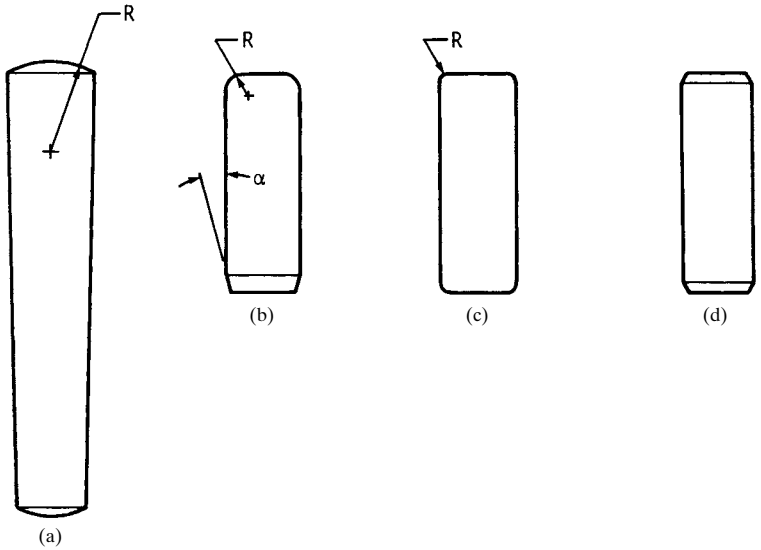

FIGURE 24.9 (*a*) Taper pin has crowned ends and a taper of 0.250 in/ft based on the diameter. (*b*) Hardened and ground machine dowel pin; the range of α is 4 to 16 degrees. (*c*) Hardened and ground production pin; corner radius is in the range 0.01 to 0.02 in. (*d*) Ground unhardened dowel pin or straight pin, both ends chamfered. Straight pins are also made with the corners broken.

where d = diameter at small end, in
D = diameter at large end, in
L = length, in

The constant in this equation is based on the taper. Taper pins can be assembled into drilled and taper-reamed holes or into holes which have been drilled by section. For the latter method, the first drill would be the smallest and would be drilled through. The next several drills would be successively larger and be drilled only part way (see Ref. [24.5]).

Dowel pins (Fig. 24.9*b, c,* and *d*) are listed in Tables 24.7 to 24.9 by dimensions and shear loads. They are case-hardened to a minimum case depth of 0.01 in and should have a single shear strength of 102 kpsi minimum. After hardening, the ductility should be such that they can be press-fitted into holes 0.0005 in smaller without cracking. See Chap. 27 for press fits.

Drive pins and studs are illustrated in Fig. 24.10 and tabulated in Tables 24.10 and 24.11. There are a large number of variations of these grooved drive pins. See Ref. [24.5] and manufacturers' catalogs. The standard grooved drive pin, as in Fig. 24.10*a* and *b,* has three equally spaced grooves. These pins are made from cold-drawn carbon-steel wire or rod, and the grooves are pressed or rolled into the stock. This expands the pin diameter and creates a force fit when assembled.

Spring pins are available in two forms. Figure 24.11*a* shows the slotted type of tubular spring pin. Another type, not shown, is a tubular pin made as a spiral by wrapping about 2¼ turns of sheet steel on a mandrel. This is called a *coiled spring pin.* Sizes and loads are listed in Tables 24.12 to 24.14.

TABLE 24.6 Dimensions of Standard Taper Pins (Inch Series)

	Diameter at large end				
	Commercial		Precision		
Size no.	Max.	Min.	Max.	Min.	Lengths†
7/0	0.0638	0.0618	0.0635	0.0625	$\frac{1}{4}$–1
6/0	0.0793	0.0773	0.0790	0.0780	$\frac{1}{4}$–$1\frac{1}{2}$
5/0	0.0953	0.0933	0.0950	0.0940	$\frac{1}{4}$–$1\frac{1}{2}$
4/0	0.1103	0.1083	0.1100	0.1090	$\frac{1}{4}$–2
3/0	0.1263	0.1243	0.1260	0.1250	$\frac{1}{4}$–2
2/0	0.1423	0.1403	0.1420	0.1410	$\frac{1}{2}$–$2\frac{1}{2}$
0	0.1573	0.1553	0.1570	0.1560	$\frac{1}{2}$–3
1	0.1733	0.1713	0.1730	0.1720	$\frac{3}{4}$–3
2	0.1943	0.1923	0.1940	0.1930	$\frac{3}{4}$–3
3	0.2203	0.2183	0.2200	0.2190	$\frac{3}{4}$–4
4	0.2513	0.2493	0.2510	0.2500	$\frac{3}{4}$–4
5	0.2903	0.2883	0.2900	0.2890	1–6
6	0.3423	0.3403	0.3420	0.3410	$1\frac{1}{4}$–6
7	0.4103	0.4083	0.4100	0.4090	$1\frac{1}{4}$–8
8	0.4933	0.4913	0.4930	0.4920	$1\frac{1}{4}$–8
9	0.5923	0.5903	0.5920	0.5910	$1\frac{1}{4}$–8
10	0.7073	0.7053	0.7070	0.7060	$1\frac{1}{2}$–8
11	0.8613	0.8593	.....	.....	2–8
12	1.0333	1.0313	.....	.....	2–9
13	1.2423	1.2403	.....	.....	3–11
14	1.5223	1.5203	.....	.....	3–13

†In preferred sizes but not in $\frac{1}{16}$-in increments; see Table A.4 for list of preferred sizes in fractions of inches.

SOURCE: From Ref. [24.5].

Slotted tubular pins can be used inside one another to form a double pin, thus increasing the strength and fatigue resistance. When this is done, be sure the slots are not on the same radial line when assembled.

Clevis pins, shown in Fig. 24.11*b,* have standard sizes listed in Table 24.15. They are made of low-carbon steel and are available soft or case-hardened.

Cotter pins are listed in Table 24.16. These are available in the square-cut type, as in Fig. 24.11*c,* or as a hammer-lock type, in which the extended end is bent over the short end.

24.3 EYELETS AND GROMMETS

For some applications, eyelets are a trouble-free and economical fastener. They can be assembled very rapidly using special eyeleting and grommeting machines, which punch the holes, if necessary, and then set the eyelets. The eyelets are fed automatically from a hopper to the work point.

TABLE 24.7 Dimensions of Hardened Ground Machine Dowel Pins (Inch Series) (Fig. 24.9*b*)

Nominal size	Diameter				Shear load,† kip	Length‡
	Standard series		Oversize series			
	Max.	Min.	Max.	Min.		
1/16	0.0628	0.0626	0.0636	0.0634	0.80	1/16–3/4
3/32	0.0941	0.0939	0.0949	0.0947	1.80	5/16–1
1/8	0.1253	0.1251	0.1261	0.1259	3.20	3/8–2
3/16	0.1878	0.1876	0.1886	0.1884	7.20	1/2–2
1/4	0.2503	0.2501	0.2511	0.2509	12.8	1/2–2 1/2
5/16	0.3128	0.3126	0.3136	0.3134	20.0	1/2–2 1/2
3/8	0.3753	0.3751	0.3761	0.3759	28.7	1/2–3
7/16	0.4378	0.4376	0.4386	0.4384	39.1	7/8–3
1/2	0.5003	0.5001	0.5011	0.5009	51.0	3/4–4
5/8	0.6253	0.6251	0.6261	0.6259	79.8	1 1/4–5
3/4	0.7503	0.7501	0.7511	0.7509	114.0	1 1/2–6
7/8	0.8753	0.8751	0.8761	0.8759	156.0	2–6
1	1.0003	1.0001	1.0011	1.0009	204.0	2–6

†Minimum double shear load for carbon or alloy steel, manufacturer's responsibility to achieve.
‡Use Table A.4 for preferred sizes in range given.
SOURCE: From Ref. [24.5].

TABLE 24.8 Dimensions of Hardened Ground Production Dowel Pins (Inch Series) (Fig. 24.9*c*)

Nominal size	Diameter		Load,† kip	Length‡
	Max.	Min.		
1/16	0.0628	0.0626	0.79	3/16–1
3/32	0.0940	0.0938	1.40	3/16–2
7/64	0.1096	0.1094	1.90	3/16–2
1/8	0.1253	0.1251	2.60	3/16–2
5/32	0.1565	0.1563	4.10	3/16–2
3/16	0.1878	0.1876	5.90	3/16–2
7/32	0.2190	0.2188	7.60	1/4–2
1/4	0.2503	0.2501	10.0	1/4–2 1/2
5/16	0.3128	0.3126	16.0	5/16–2 1/2
3/8	0.3753	0.3751	23.0	3/8–3

†Minimum double shear load for carbon steel, manufacturer's responsibility to achieve.
‡See Table A.4 for preferred sizes in range given.
SOURCE: From Ref. [24.5].

TABLE 24.9 Dimensions of Unhardened Dowel Pins and Straight Pins (Inch Series) (Fig. 24.9*d*)

	Unhardened dowel pins					Straight pins	
	Diameter		Load,† kip			Diameter	
Nominal size	Max.	Min.	Steel	Brass	Length‡	Max.	Min.
1/16	0.0600	0.0595	0.35	0.22	1/4–1	0.0625	0.0605
3/32	0.0912	0.0907	0.82	0.51	1/4–1 1/2	0.0937	0.0917
1/8	0.1223	0.1218	1.49	0.93	1/4–2	0.1250	0.1230
5/32	0.1535	0.1530	2.35	1.47	1/4–2	0.1562	0.1542
3/16	0.1847	0.1842	3.41	2.13	1/4–2	0.1875	0.1855
7/32	0.2159	0.2154	4.66	2.91	1/4–2	0.2187	0.2167
1/4	0.2470	0.2465	6.12	3.81	1/4–2 1/2	0.2500	0.2480
5/16	0.3094	0.3089	9.59	5.99	5/16–2 1/2	0.3125	0.3105
3/8	0.3717	0.3712	13.85	8.65	3/8–2 1/2	0.3750	0.3730
7/16	0.4341	0.4336	18.90	11.81	7/16–2 1/2	0.4375	0.4355
1/2	0.4964	0.4959	24.72	15.45	1/2–3	0.5000	0.4980
5/8	0.6211	0.6206	38.71	24.19	5/8–4	0.6250	0.6230
3/4	0.7548	0.7453	55.84	34.90	3/4–4	0.7500	0.7480
7/8	0.8705	0.8700	76.09	47.55	7/8–4	0.8750	0.8730
1	0.9952	0.9947	99.46	62.16	1–4	1.0000	0.9980

†Minimum double shear load, manufacturer's responsibility to achieve.
‡See Table A.4 for preferred sizes in range given.
SOURCE: From Ref. [24.5].

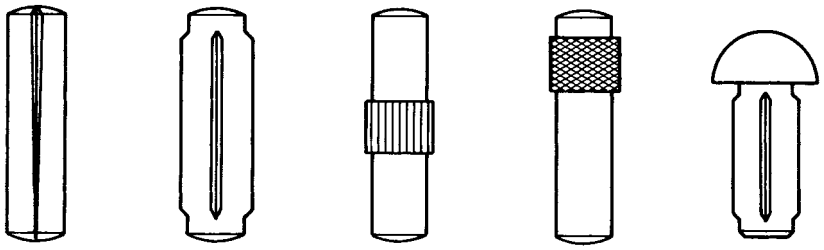

FIGURE 24.10 An assortment of drive pins. (*a*) Standard drive pin has three equally spaced grooves; (*b*) standard grooved drive pin with relief at each end; (*c*) (*d*) annular grooved and knurled drive pins; these may be obtained in a variety of configurations (*DRIV-LOK, Inc.*); (*e*) standard round head grooved stud.

TABLE 24.10 Dimensions of Grooved Drive Pins (Inch Series) (Fig. 24.10*a, b*)†

Basic size	Diameter		Expanded diameter‡	Length§
	Max.	Min.		
1/32	0.0312	0.0302	0.035	1/8–1/2
3/64	0.0469	0.0459	0.051	1/8–5/8
1/16	0.0625	0.0615	0.067	1/8–1
5/64	0.0781	0.0771	0.083	1/4–1
3/32	0.0938	0.0928	0.100	1/4–1 1/4
7/64	0.1094	0.1074	0.115	1/4–1 1/2
1/8	0.1250	0.1230	0.132	1/4–1 1/2
5/32	0.1563	0.1543	0.163	3/8–2
3/16	0.1875	0.1855	0.196	3/8–2 1/4
7/32	0.2188	0.2168	0.227	1/2–2 3/4
1/4	0.2500	0.2480	0.260	1/2–3
5/16	0.3125	0.3105	0.326	5/8–3 1/4
3/8	0.3750	0.3730	0.390	3/4–4 1/4
7/16	0.4375	0.4355	0.454	7/8–4 1/2
1/2	0.5000	0.4980	0.520	1–4 1/2

†Reference [24.5] lists a total of seven different types of grooved drive pins.
‡Minimum; varies a few thousandths with length; ±0.002 in; not for Monel or stainless steel pins.
§In 1/8-in increments only to 1 in.
SOURCE: From Ref [24.5].

TABLE 24.11 Dimensions of Round-Head Grooved Drive Studs (Inch Series) (Fig. 24.10*e*)

Size no.	Basic diameter	Head diameter max.	Head thickness max.	Expanded diameter†	Length
0	0.067	0.130	0.050	0.074	1/8–1/4
2	0.086	0.162	0.070	0.095	1/8–1/4
4	0.104	0.211	0.086	0.113	3/16–5/16
6	0.120	0.260	0.103	0.130	1/4–3/8
7	0.136	0.309	0.119	0.144	5/16–1/2
8	0.144	0.309	0.119	0.153	3/8–5/8
10	0.161	0.359	0.136	0.171	3/8–5/8
12	0.196	0.408	0.152	0.204	1/2–3/4
14	0.221	0.457	0.169	0.232	1/2–3/4
16	0.250	0.472	0.174	0.263	1/2 only

†Minimum; ±0.002 in.
SOURCE: From Ref. [24.5].

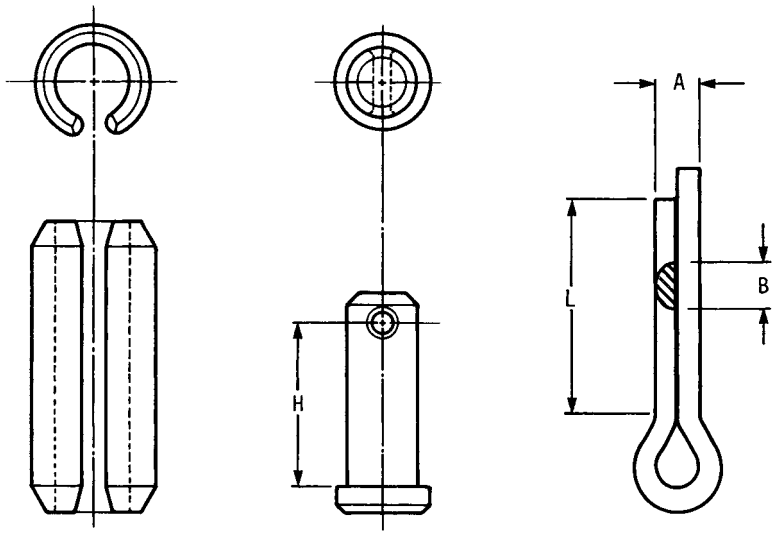

FIGURE 24.11 (*a*) Slotted spring pin; (*b*) clevis pin; (*c*) cotter pin.

TABLE 24.12 Dimensions and Safe Loads for Slotted Spring Pins (Inch Series) (Fig. 24.11*a*)

Size	Diameter		Hole size		Shear load,† kip		
	Max.	Min.	Max.	Min.	AISI 1070, AISI 1095, AISI 420	AISI 302	Beryllium copper
1/16	0.069	0.066	0.065	0.062	0.425	0.350	0.270
5/64	0.086	0.083	0.081	0.078	0.650	0.550	0.400
3/32	0.103	0.099	0.097	0.094	1.000	0.800	0.660
1/8	0.135	0.131	0.129	0.125	2.100	1.500	1.200
9/64	0.149	0.145	0.144	0.140	2.200	1.600	1.400
5/32	0.167	0.162	0.160	0.156	3.000	2.000	1.800
3/16	0.199	0.194	0.192	0.187	4.400	2.800	2.600
7/32	0.232	0.226	0.224	0.219	5.700	3.550	3.700
1/4	0.264	0.258	0.256	0.250	7.700	4.600	4.500
5/16	0.328	0.321	0.318	0.312	11.500	7.095	6.800
3/8	0.392	0.385	0.382	0.375	17.600	10.000	10.100
7/16	0.456	0.448	0.445	0.437	20.000	12.000	12.200
1/2	0.521	0.513	0.510	0.500	25.800	15.500	16.800
5/8	0.650	0.640	0.636	0.625	46.000‡	18.800	
3/4	0.780	0.769	0.764	0.750	66.000‡	23.200	

†Minimum double shear load, manufacturer's responsibility to achieve.
‡Sizes 3/8 in and larger are produced only in AISI 6150H.
SOURCE: From Ref. [24.5].

TABLE 24.13 Dimensions and Safe Loads for Coiled Spring Pins (Inch Series)

	Light duty				Standard duty				Heavy duty				Hole size	
	Diameter		Safe load,† kip		Diameter		Safe load,† kip		Diameter		Safe load,† kip			
Size	Max.	Min.	Mat. A‡	Mat. B§	Max.	Min.	Mat. A‡	Mat. B§	Max.	Min.	Mat. A‡	Mat. B§	Max.	Min.
1/32	....	....	....	....	0.035	0.033	0.075	0.060	....	....	....	....	0.032	0.031
3/64	....	....	....	....	0.052	0.049	0.170	0.140	....	....	....	....	0.048	0.046
1/16	0.073	0.067	....	0.135	0.072	0.067	0.300	0.250	0.070	0.066	0.450	0.350	0.065	0.061
5/64	0.089	0.083	....	0.225	0.088	0.083	0.475	0.400	0.086	0.082	0.700	0.550	0.081	0.077
3/32	0.106	0.099	0.375	0.300	0.105	0.099	0.700	0.550	0.103	0.099	1.000	0.800	0.097	0.093
7/64	0.121	0.114	0.525	0.425	0.120	0.114	0.950	0.750	0.118	0.113	1.400	1.250	0.112	0.108
1/8	0.139	0.131	0.675	0.550	0.138	0.131	1.250	1.000	0.136	0.130	2.100	1.700	0.129	0.124
5/32	0.172	0.163	1.100	0.875	0.171	0.163	1.925	1.550	0.168	0.161	3.000	2.400	0.160	0.155
3/16	0.207	0.196	1.500	1.200	0.205	0.196	2.800	2.250	0.202	0.194	4.400	3.500	0.192	0.185
7/32	0.240	0.228	2.100	1.700	0.238	0.228	3.800	3.000	0.235	0.226	5.700	4.600	0.224	0.217
1/4	0.273	0.260	2.700	2.200	0.271	0.260	5.000	4.000	0.268	0.258	7.700	6.200	0.256	0.247
5/16	0.339	0.324	4.440	3.500	0.337	0.324	7.700	6.200	0.334	0.322	11.500	9.200	0.319	0.308
3/8	0.405	0.388	6.000	5.000	0.403	0.388	11.200	9.000	0.400	0.386	17.600	14.000	0.383	0.370
7/16	0.471	0.452	8.400	6.700	0.469	0.452	15.200	13.000	0.466	0.450	22.500	18.000	0.446	0.431
1/2	0.537	0.516	11.000	8.800	0.535	0.516	20.000	16.000	0.532	0.514	30.000	24.000	0.510	0.493
5/8	....	....	....	....	0.661	0.642	31.000	25.000	0.658	0.640	46.000	37.000	0.635	0.618
3/4	....	....	....	....	0.787	0.768	45.000	36.000	0.784	0.766	66.000	53.000	0.760	0.743

†Minimum double shear load, manufacturer's responsibility to achieve.

‡Material A is AISI 1070, AISI 1095, or AISI 420; sizes 1/32 in and 3/64 in are available only in AISI 420; sizes 5/8 in and larger are available only in AISI 6150 steel.

§Material B is AISI 302.

SOURCE: From Ref. [24.5].

TABLE 24.14 Standard Lengths of Coiled and Slotted Spring Pins (Inch Series)†

Size	Length	Size	Length	Size	Length
1/32	1/8–5/8	1/8	5/16–2	5/16	3/4–4
3/64	1/8–5/8	9/64	3/8–2	3/8	3/4–4
1/16	3/16–1	5/32	7/16–2 1/2	7/16	1–4
5/64	3/16–1 1/2	3/16	1/2–2 1/2	1/2	1 1/4–4
3/32	3/16–1 1/2	7/32	1/2–3	5/8	2–6
7/64	1/4–1 3/4	1/4	1/2–3 1/2		

†See Table A.4 for list of preferred lengths.
SOURCE: From Ref. [24.5].

TABLE 24.15 Dimensions of Clevis Pins (Inch Series)

	Diameter		Maximum head			Distance *H*†			
Size	Max.	Min.	Diameter	Thickness	Hole Minimum	Max.	Min.	Length	Cotter pin size
3/16	0.186	0.181	0.32	0.07	0.073	0.504	0.484	0.58	1/16
1/4	0.248	0.243	0.38	0.10	0.073	0.692	0.672	0.77	1/16
5/16	0.311	0.306	0.44	0.10	0.104	0.832	0.812	0.94	3/32
3/8	0.373	0.368	0.51	0.13	0.104	0.958	0.938	1.06	3/32
7/16	0.436	0.431	0.57	0.16	0.104	1.082	1.062	1.19	3/32
1/2	0.496	0.491	0.63	0.16	0.136	1.223	1.203	1.36	1/8
5/8	0.621	0.616	0.82	0.21	0.136	1.473	1.453	1.61	1/8
3/4	0.746	0.741	0.94	0.26	0.167	1.739	1.719	1.91	5/32
7/8	0.871	0.866	1.04	0.32	0.167	1.989	1.969	2.16	5/32
1	0.996	0.991	1.19	0.35	0.167	2.239	2.219	2.41	5/32

†To hole center; see Fig. 24.11*b*.
SOURCE: From Ref. [24.4].

Figure 24.12 illustrates some of the more common eyelets and grommets. These are available in many other styles and in thousands of sizes. The usual materials are brass, copper, zinc, aluminum, steel, and nickel silver. Various finishing operations such as plating, anodizing, or lacquering can also be employed.

24.4 RETAINING RINGS

Shoulders are used on shafts and on the interior of bored parts to accurately position or retain assembled parts to prevent axial motion or play. It is often advantageous to use retaining rings as a substitute for these machined shoulders. Such rings can be used to axially position parts on shafts and in housing bores and often save a great deal in machining costs.

TABLE 24.16 Dimensions of Cotter Pins (Inch Series) (Fig. 24.11*c*)

Size	Shank diameter *A*		Wire width *B*		Hole size
	Max.	Min.	Max.	Min.	
1/32	0.032	0.028	0.032	0.022	0.047
3/64	0.048	0.044	0.048	0.035	0.062
1/16	0.060	0.056	0.060	0.044	0.078
5/64	0.076	0.072	0.076	0.057	0.094
3/32	0.090	0.086	0.090	0.069	0.109
7/64	0.104	0.100	0.104	0.080	0.125
1/8	0.120	0.116	0.120	0.093	0.141
9/64	0.134	0.130	0.134	0.104	0.156
5/32	0.150	0.146	0.150	0.116	0.172
3/16	0.176	0.172	0.176	0.137	0.203
7/32	0.207	0.202	0.207	0.161	0.234
1/4	0.225	0.220	0.225	0.176	0.266
5/16	0.280	0.275	0.280	0.220	0.312
3/8	0.335	0.329	0.335	0.263	0.375
7/16	0.406	0.400	0.406	0.320	0.438
1/2	0.473	0.467	0.473	0.373	0.500
5/8	0.598	0.590	0.598	0.472	0.625
3/4	0.723	0.715	0.723	0.572	0.750

SOURCE: From Ref. [24.4].

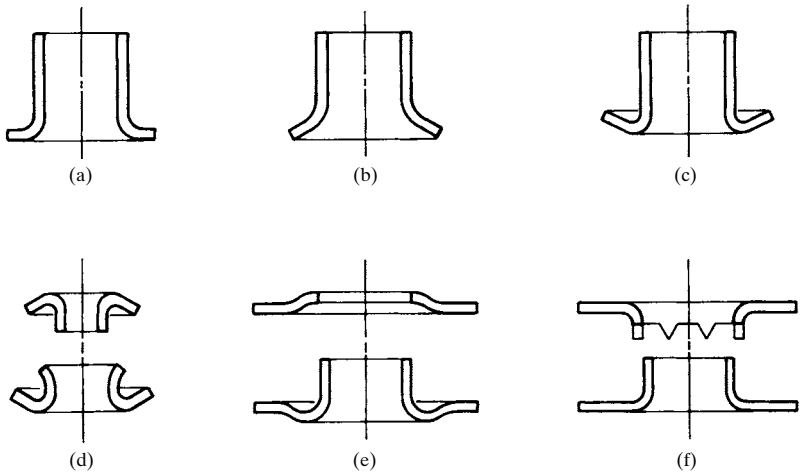

FIGURE 24.12 (*a*) Flat-flange eyelet; (*b*) funnel-flange eyelet; (*c*) rolled-flange eyelet; (*d*) telescoping eyelet with neck washer; (*e*) plain grommet; (*f*) toothed grommet.

Retaining rings may be as simple as a hardened spring wire bent into a C or U shape and fitted into a groove on a shaft or a housing. *Spiral-wound* and *stamped retaining rings* have been standardized (Refs. [24.7], [24.8], and [24.9]), and they are available in many shapes and sizes from various manufacturers.

24.4.1 Stamped Retaining Rings

Figure 24.13 shows a large variety of retaining rings. These are designated using the catalog numbers of a manufacturer, but can be changed to military standard numbers using Table 24.17.

The E rings shown in Fig. 24.13*a, b,* and *c* are intended to provide wide shoulders on small-diameter shafts. They are assembled by snapping them on in a radial direction. They are very satisfactory substitutes for cotter pins or the more expensive shaft shoulders or collars secured by set screws. Figure 24.14 shows typical mounting details for the rings in Fig. 24.13*a* and *b.* The ring in Fig. 24.13*c* is similar but is reinforced with tapered web sections for greater resistance to vibration and shock loads.

The C ring in Fig. 24.13*d* is also assembled radially, as will be shown in Fig. 24.17*a.* This ring is useful when axial access to the groove is difficult and for applications in which only a small shoulder is desired.

The internal rings in Fig. 24.13*e* and *f* are shown assembled in Fig. 24.15*a* and *b.* These are applied axially into grooved housings using specially designed pliers.

The external rings shown in Fig. 24.13*g* and *h* are shown assembled in Fig. 24.16. They are also assembled axially using pliers. Note how the bowed or dished ring in Fig. 24.16*b* can be used to take up end play or allow for temperature-induced dimensional changes.

The self-locking rings in Fig. 24.13*k* and *l* do not require grooves. They provide shoulders in soft materials, such as low-carbon steels or plastics, merely by pushing them axially into position. When a reverse force is applied, the prongs embed themselves into the mating material and resist removal.

The external self-locking ring in Figs. 24.13*m* and 24.17*b* may be used with or without a groove. This ring resists moderate thrust and provides an adjustable shoulder.

Materials for retaining rings are the spring steels, stainless steel, and beryllium copper. For dimensions and loads, see Refs. [24.7], [24.8], and [24.9] and the manufacturers' catalogs. They are available in both inch and metric sizes.

24.4.2 Spiral Wound Rings

Standard spiral-wound rings (Ref. [24.7]) have approximately two turns, although three-turn retaining rings are available. The rings are edge-wound from pretempered flat spring wire. The crimp or offset of the wire (see Fig. 24.18) produces a better seat, but rings are available without offset. Figure 24.18 also illustrates the machine methods of seating a ring into a housing or onto a shaft. Although difficult, manual seating is also possible.

Spiral-wound rings are sized by the inside diameter when they are to be used on a shaft and by the outside diameter when they are to be used in a housing. For sizes and thrust loads, see the manufacturers' catalogs. Usual materials are the plain carbon spring steels, stainless steel, nickel alloys, and beryllium copper.

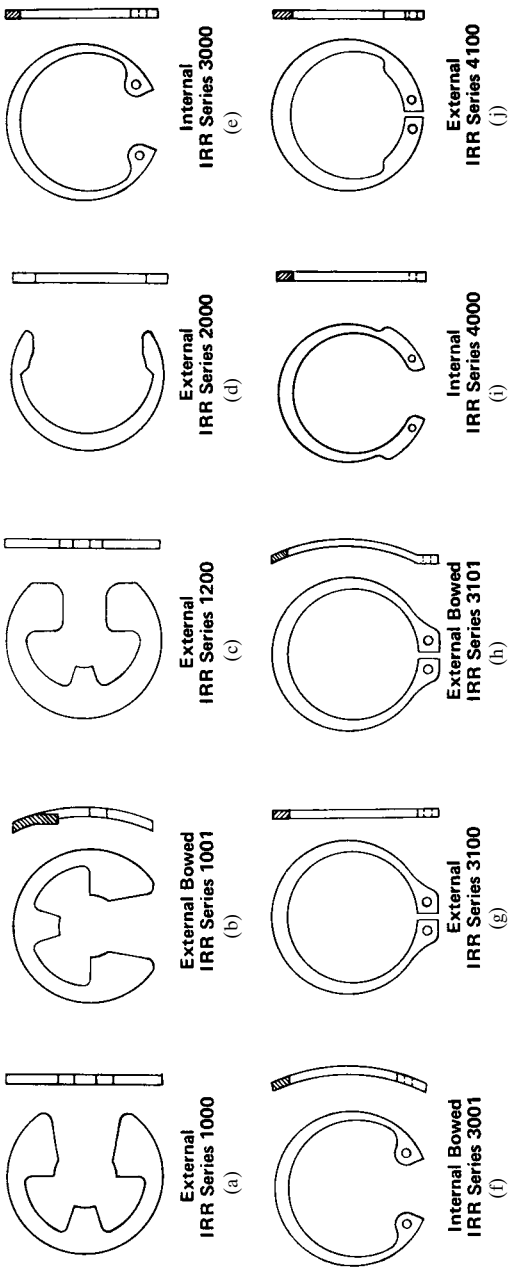

FIGURE 24.13 Retaining rings. The IRR numbers are catalog numbers. See Table 24.17 for conversion to military standard numbers. *(Industrial Retaining Ring Company.)*

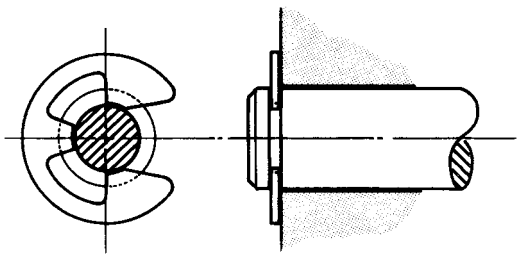

(a)

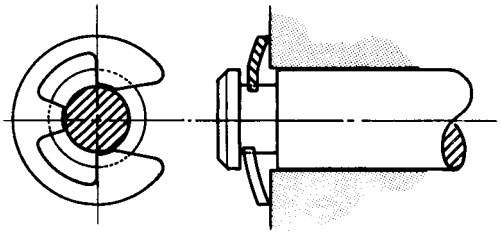

(b)

FIGURE 24.14 Open-type E rings. (*a*) Flat; (*b*) bowed. *(Industrial Retaining Ring Company.)*

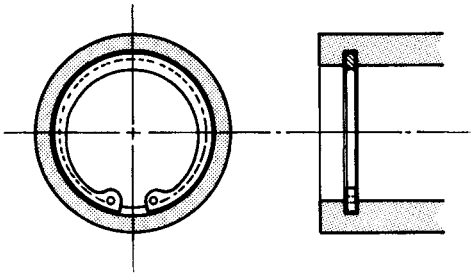

(a)

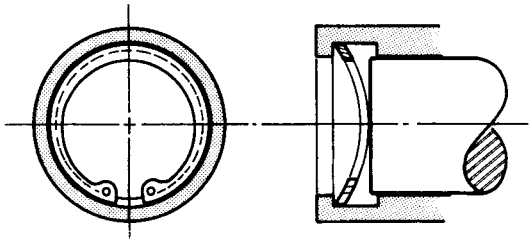

(b)

FIGURE 24.15 Internal rings. (*a*) Flat type (see Fig. 24.13*e* for shape before assembly); (*b*) bowed type (see Fig. 24.13*f* for shape before assembly).

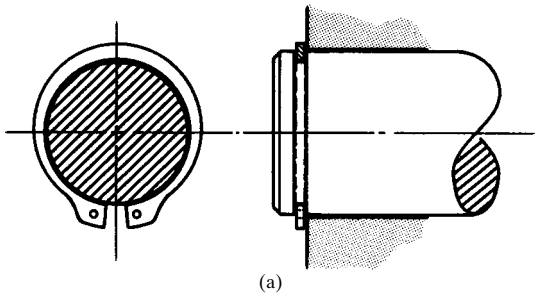

(a)

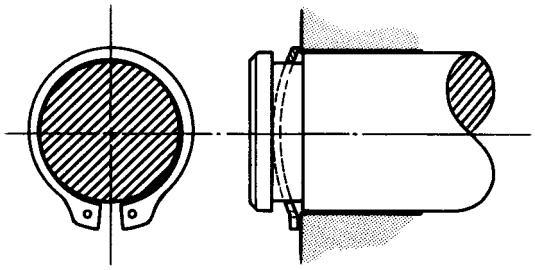

(b)

FIGURE 24.16 External rings. (*a*) Flat; (*b*) bowed. *(Industrial Retaining Ring Company.)*

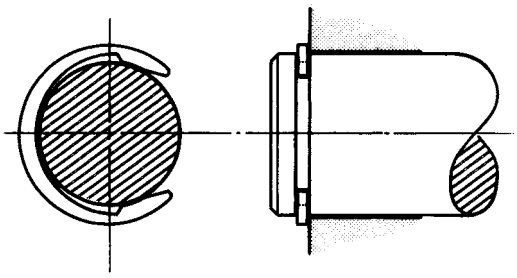

(a)

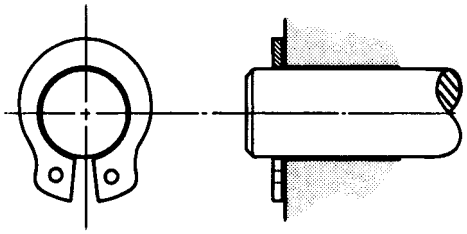

(b)

FIGURE 24.17 (*a*) External C-ring; (*b*) self-locking external ring. *(Industrial Retaining Ring Company.)*

TABLE 24.17 Conversion of IRR Catalog Numbers to Corresponding Military Standard Numbers of Retaining Rings

Government standard MS no.	IRR series no.	Government standard MS no.	IRR series no.
3215	1200	16628	3101
3217	7200	16629	3001
16624	3100	16632	2000
16625	3000	16633	1000
16626	4100	16634	1001
16627	4000	90707	7100

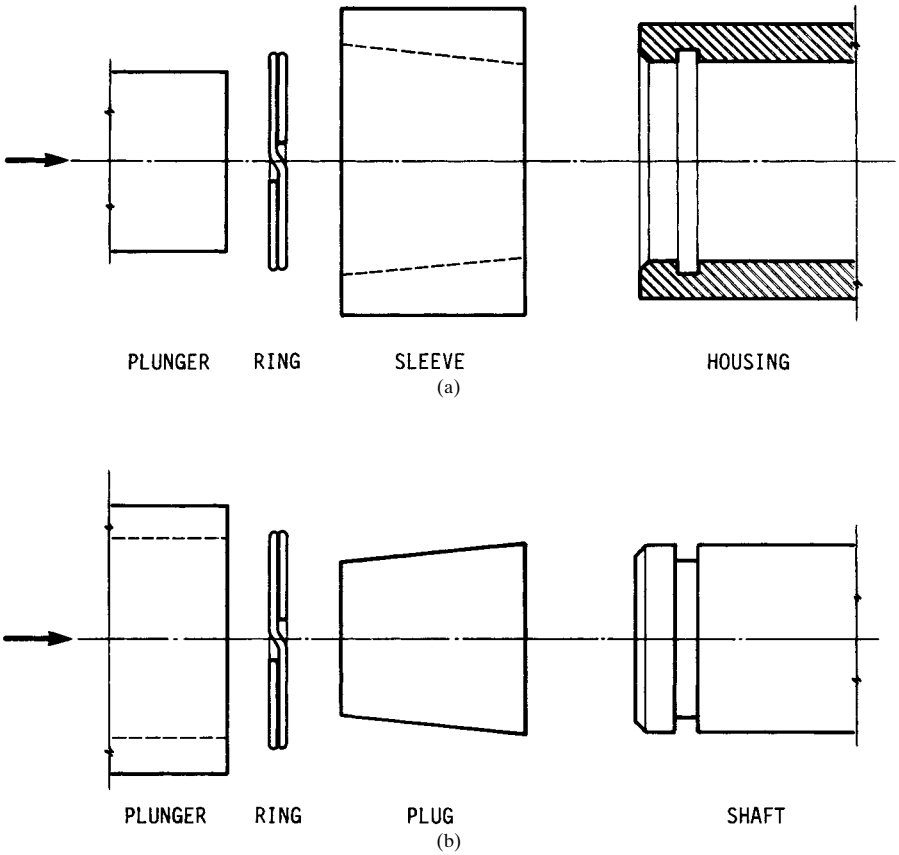

FIGURE 24.18 Spiral retaining rings. (*a*) Installation of ring into housing; (*b*) installation of ring onto shaft. *(Smalley Steel Ring Company.)*

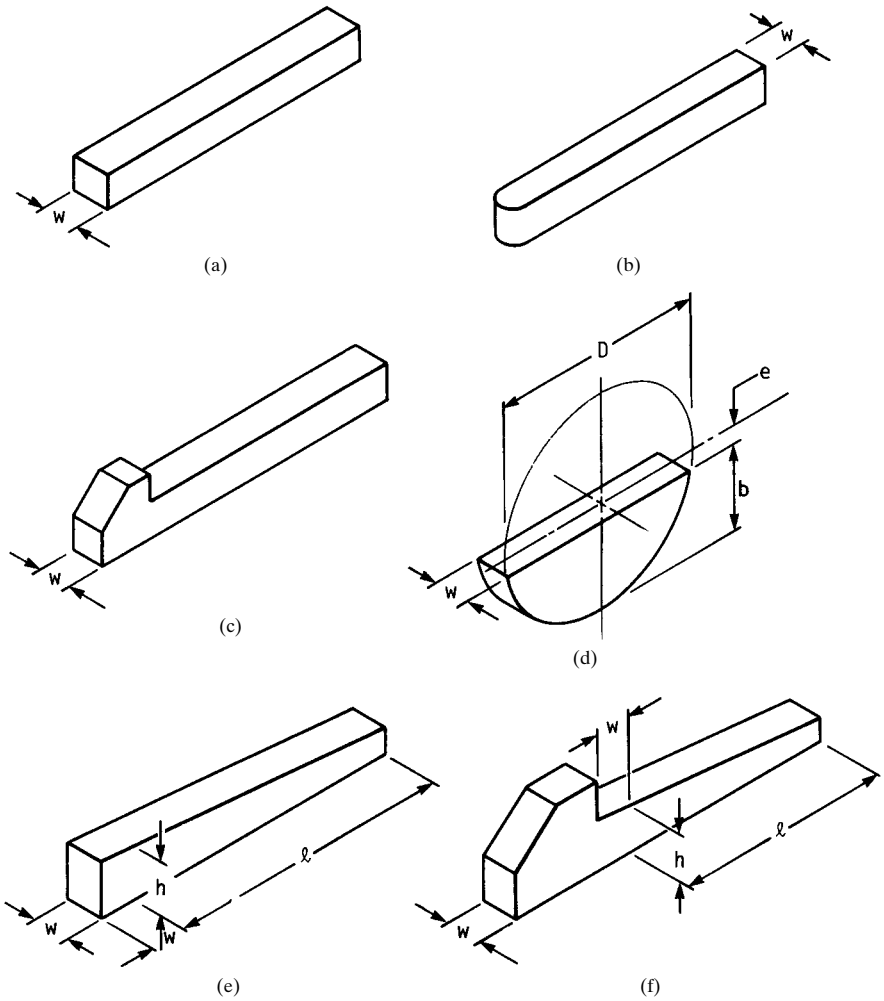

FIGURE 24.19 (*a*) Square or rectangular key. (*b*) Square or rectangular key with one end rounded; also available with both ends rounded. (*c*) Square or rectangular key with gib head. (*d*) Woodruff key; also available with flattened bottom. (*e*) Tapered rectangular key; ℓ = hub length, h = height; taper is ⅛ in for 12 in or 1 for 100 for metric sizes. (*f*) Tapered gib-head key; dimensions and taper same as in (*e*).

TABLE 24.18 Dimensions for Standard Square- and Rectangular-Key Applications†

Shaft diameter		Key size, $w \times h$	Keyway depth
Over	To (incl.)		
$\frac{5}{16}$	$\frac{7}{16}$	$\frac{3}{32} \times \frac{3}{32}$	$\frac{3}{64}$
$\frac{7}{16}$	$\frac{9}{16}$	$\frac{1}{8} \times \frac{3}{32}$	$\frac{3}{64}$
		$\frac{1}{8} \times \frac{1}{8}$	$\frac{1}{16}$
$\frac{9}{16}$	$\frac{7}{8}$	$\frac{3}{16} \times \frac{1}{8}$	$\frac{1}{16}$
		$\frac{3}{16} \times \frac{3}{16}$	$\frac{3}{32}$
$\frac{7}{8}$	$1\frac{1}{4}$	$\frac{1}{4} \times \frac{3}{16}$	$\frac{3}{32}$
		$\frac{1}{4} \times \frac{1}{4}$	$\frac{1}{8}$
$1\frac{1}{4}$	$1\frac{3}{8}$	$\frac{5}{16} \times \frac{1}{4}$	$\frac{1}{8}$
		$\frac{5}{16} \times \frac{5}{16}$	$\frac{5}{32}$
$1\frac{3}{8}$	$1\frac{3}{4}$	$\frac{3}{8} \times \frac{1}{4}$	$\frac{1}{8}$
		$\frac{3}{8} \times \frac{3}{8}$	$\frac{3}{16}$
$1\frac{3}{4}$	$2\frac{1}{4}$	$\frac{1}{2} \times \frac{3}{8}$	$\frac{3}{16}$
		$\frac{1}{2} \times \frac{1}{2}$	$\frac{1}{4}$
$2\frac{1}{4}$	$2\frac{3}{4}$	$\frac{5}{8} \times \frac{7}{16}$	$\frac{7}{32}$
		$\frac{5}{8} \times \frac{5}{8}$	$\frac{5}{16}$
$2\frac{3}{4}$	$3\frac{1}{4}$	$\frac{3}{4} \times \frac{1}{2}$	$\frac{1}{4}$
		$\frac{3}{4} \times \frac{3}{4}$	$\frac{3}{8}$
$3\frac{1}{4}$	$3\frac{3}{4}$	$\frac{7}{8} \times \frac{5}{8}$	$\frac{5}{16}$
		$\frac{7}{8} \times \frac{7}{8}$	$\frac{7}{16}$
$3\frac{3}{4}$	$4\frac{1}{2}$	$1 \times \frac{3}{4}$	$\frac{3}{8}$
		1×1	$\frac{1}{2}$
$4\frac{1}{2}$	$5\frac{1}{2}$	$1\frac{1}{4} \times \frac{7}{8}$	$\frac{7}{16}$
		$1\frac{1}{4} \times 1\frac{1}{4}$	$\frac{5}{8}$
$5\frac{1}{2}$	$6\frac{1}{2}$	$1\frac{1}{2} \times 1$	$\frac{1}{2}$
		$1\frac{1}{2} \times 1\frac{1}{2}$	$\frac{3}{4}$

†Dimensions in inches

SOURCE: From Ref. [24.10].

TABLE 24.19 Dimensions for Standard Square- and Rectangular-Key Applications†

Shaft diameter		Key size, $w \times h$	Keyway depth
Over	To (incl.)		
6	8	2 × 2	1.2
8	10	3 × 3	1.8
10	12	4 × 4	2.5
12	17	5 × 5	3
17	22	6 × 6	3.5
22	30	8 × 7	4
30	38	10 × 8	5
38	44	12 × 8	5
44	50	14 × 9	5.5
50	58	16 × 10	6
58	65	18 × 11	7
65	75	20 × 12	7.5
75	85	22 × 14	9
85	95	25 × 14	9
95	110	28 × 16	10
110	130	32 × 18	11
130	150	36 × 20	12
150	170	40 × 22	13
170	200	45 × 25	15
200	230	50 × 28	17

†Dimensions in millimeters.

A *wave spring* is a one-turn edge-wound spring washer also made from flat spring wire. A thrust load tends to flatten the spring, and hence such springs can be used to take up end play or to allow for expansion. Several of these can be used together, either crest-to-crest or nested, depending on the requirements for thrust loads or axial motion.

24.5 KEYS

All standard plain, tapered, and Woodruff keys are illustrated in Fig. 24.19. These are usually made with edges broken, but they may be chamfered if fillets are used in the

TABLE 24.20 Dimensions for Woodruff-Key Applications (Fig. 24.19*d*)†

Key size, $w \times D$	Height‡ b	Offset e	Keyseat depth	
			Shaft	Hub
1/16 × 1/4	0.109	1/64	0.0728	0.0372
× 5/16	0.140	1/64	0.1038	0.0372
× 3/8	0.172	1/64	0.1358	0.0372
3/32 × 5/16	0.140	1/64	0.0882	0.0529
× 3/8	0.172	1/64	0.1202	0.0529
× 1/2	0.203	3/64	0.1511	0.0529
× 5/8	0.250	1/16	0.1981	0.0529
1/8 × 3/8	0.172	1/64	0.1045	0.0685
× 1/2	0.203	3/64	0.1355	0.0685
× 5/8	0.250	1/16	0.1825	0.0685
× 3/4	0.313	1/16	0.2455	0.0685
5/32 × 5/8	0.250	1/16	0.1669	0.0841
× 3/4	0.313	1/16	0.2299	0.0841
× 7/8	0.375	1/16	0.2919	0.0841
3/16 × 5/8	0.250	1/16	0.1513	0.0997
× 3/4	0.313	1/16	0.2143	0.0997
× 7/8	0.375	1/16	0.2763	0.0997
× 1	0.438	1/16	0.3393	0.0997
× 1 1/8	0.484	5/64	0.3853	0.0997
× 1 1/4	0.547	5/64	0.4483	0.0997
× 2 1/8	0.406	21/32	0.3073	0.0997
7/32 × 7/8	0.375	1/16	0.2607	0.1153
× 1	0.438	1/16	0.3237	0.1153
× 1 1/8	0.484	5/64	0.3697	0.1153
× 1 1/4	0.547	5/64	0.4327	0.1153
1/4 × 3/4	0.313	1/16	0.1830	0.1310
× 7/8	0.375	1/16	0.2450	0.1310
× 1	0.438	1/16	0.3080	0.1310
× 1 1/8	0.484	5/64	0.3540	0.1310
× 1 1/4	0.547	5/64	0.4170	0.1310
× 1 3/8	0.594	3/32	0.4640	0.1310
× 1 1/2	0.641	7/64	0.5110	0.1310
× 2 1/8	0.531	17/32	0.4010	0.1310
× 2 3/4	0.750	5/8	0.4640	0.1310
5/16 × 1	0.438	1/16	0.2768	0.1622
× 1 1/8	0.484	5/64	0.3228	0.1622
× 1 1/4	0.547	5/64	0.3858	0.1622
× 1 3/8	0.594	3/32	0.4328	0.1622
× 1 1/2	0.641	7/64	0.4798	0.1622
× 2 1/8	0.531	17/32	0.3698	0.1622
× 2 3/4	0.750	5/8	0.5888	0.1622
3/8 × 1	0.438	1/16	0.2455	0.1935
× 1 1/4	0.547	5/64	0.3545	0.1935
× 1 3/8	0.594	3/32	0.4015	0.1935
3/8 × 1 1/2	0.641	7/64	0.4485	0.1935

TABLE 24.20 Dimensions for Woodruff-Key Applications (Fig. 24.19*d*)† *(Continued)*

Key size, $w \times D$	Height‡ b	Offset e	Keyseat depth	
			Shaft	Hub
$\times 2\frac{1}{8}$	0.531	$\frac{17}{32}$	0.3385	0.1935
$\times 2\frac{3}{4}$	0.750	$\frac{5}{8}$	0.5575	0.1935
$\times 3\frac{1}{2}$	0.938	$\frac{13}{16}$	0.7455	0.1935
$\frac{7}{16}\times 2\frac{3}{4}$	0.750	$\frac{5}{8}$	0.5263	0.2247
$\times 3\frac{1}{2}$	0.938	$\frac{13}{16}$	0.7143	0.2247
$\frac{1}{2} \times 2\frac{3}{4}$	0.750	$\frac{5}{8}$	0.4950	0.2560
$\times 3\frac{1}{2}$	0.938	$\frac{13}{16}$	0.6830	0.2560
$\frac{9}{16}\times 3\frac{1}{2}$	0.938	$\frac{13}{16}$	0.6518	0.2872
$\frac{5}{8} \times 3\frac{1}{2}$	0.938	$\frac{13}{16}$	0.6205	0.3185
$\frac{11}{16}\times 3\frac{1}{2}$	0.938	$\frac{13}{16}$	0.5893	0.3497
$\frac{3}{4} \times 3\frac{1}{2}$	0.938	$\frac{13}{16}$	0.5580	0.3810

†All dimensions in inches. If catalog or key numbers are given, the last two digits correspond to the nominal diameter D in eighths of an inch. The preceding digits give the nominal width w in thirty-seconds of an inch. Thus key no. 1208 is a size $\frac{3}{8}\times 1$.

‡This is the maximum height for a full-radius key; this dimension will be slightly less for a flat-bottom key.

SOURCE: From Ref. [24.11].

keyseats. Standard sizes and keyseat dimensions needed for design are given in Tables 24.18 to 24.20.

24.6 WASHERS

Plain washers, shown in Fig. 24.20*a,* are flat and circular and are used on bolts and screws. They are applied under the nut, under the head, or both. Plain washers can also be made square or triangular and are sometimes beveled for use on an inclined surface.

Cylindrically curved or bent washers, shown in Fig. 24.20*b,* are useful in certain applications as a means of obtaining additional bolt tension in the joint.

Conical or Belleville washers, shown in Fig. 24.20*c* and *d,* are springs and are useful for heavy loads with small deflections and where a nonlinear force-deflection relation is desired. See Chap. 6 for more details.

Spring washers, shown in Fig. 24.20*e* and *f,* are hardened circular washers that are split and then bent out of a flat plane. They are sometimes called *lock washers,* although their principal purpose is to take up for relaxing bolt tension or looseness in the joint.

Wood-grip washers, shown in Fig. 24.21*a,* are useful on soft materials, such as wood. When the joint is tightened, the bent-over end penetrates and grips the mating material.

Horseshoe or C-washers are useful where it is desirable to remove the washer without unbolting the connection (see Fig. 24.21*b*).

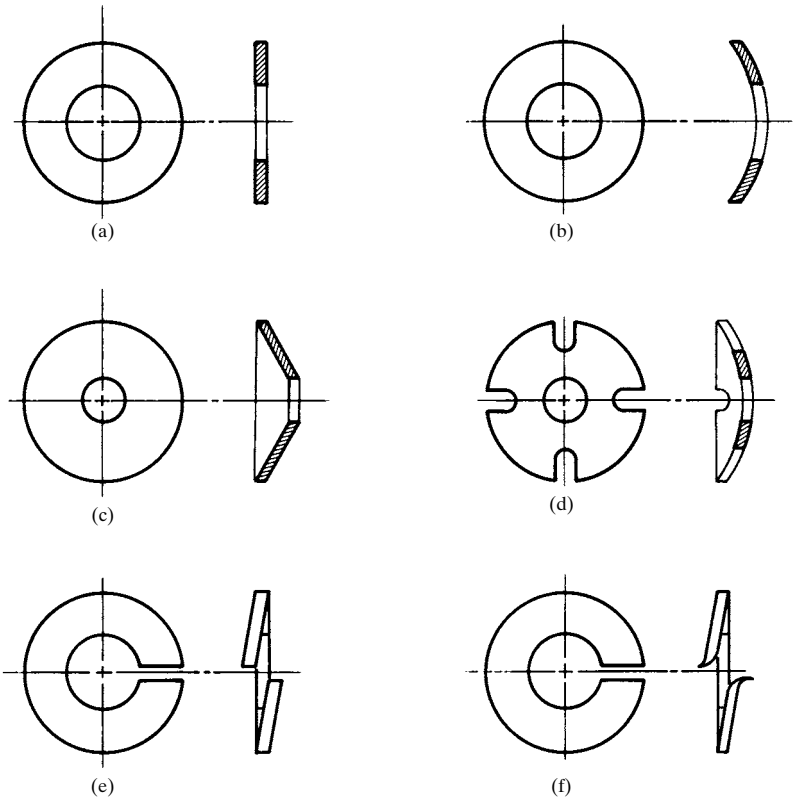

FIGURE 24.20 Washers. (*a*) Plain; (*b*) cylindrically curved; (*c*) conical or Belleville; (*d*) slotted; (*e*) spring; (*f*) spring-locking.

Lockplate or eared washers, shown in Fig. 24.21*c,* are used for locking purposes by bending some of the ears *up* against the flats of the nut or bolt head and others *down* over the edges of the joint members so as to prevent rotation of the nut or bolt head.

Cup washers, shown in Fig. 24.21*d,* are also available with a flange. When the depth of the cup is shallow, they are also called *back-up washers.*

Toothed lock washers, shown in Fig. 24.21*e,* have the teeth or prongs twisted so as to bite or penetrate the nut face as well as the adjoining part. These are hardened and made either with internal teeth or as internal-external toothed washers.

Countersunk washers, shown in Fig. 24.21*f,* serve the same purpose as plain washers when used with oval-head or countersunk-head screws.

Finish washers, shown in Fig. 24.22, are used under oval-head and flat-head screws to provide a more finished appearance and to increase the bearing surface between the fastener and the joint material.

Tables of washer sizes are not included here because of the large amount of space that would be required. Some manufacturers have as many as 60 000 stock dies, and so almost any size needed can be obtained. Washer materials include almost all the metals and many nonmetals as well.

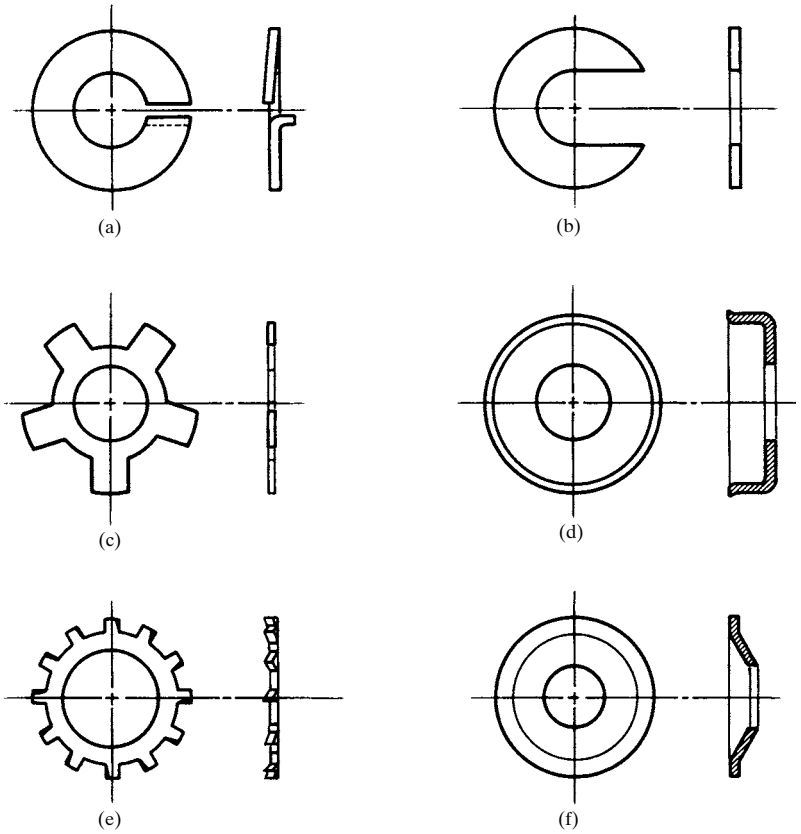

FIGURE 24.21 Washers. (*a*) Wood-grip; (*b*) C or horseshoe; (*c*) lockplate; (*d*) cup; (*e*) external-tooth locking; (*f*) countersunk.

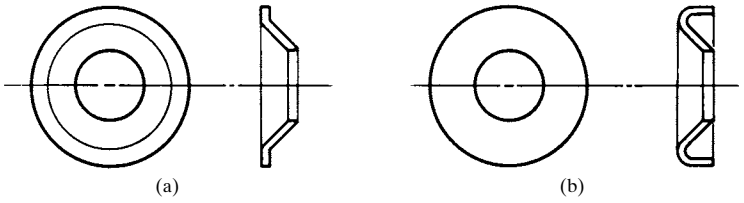

FIGURE 24.22 Finish washers. (*a*) Flush; (*b*) raised.

REFERENCES[†]

24.1 ANSI B18.1.1-1972 (R2001), "Small Solid Rivets."

24.2 ANSI B18.1.2-1972 (R2001), "Large Rivets."

24.3 ANSI B18.7-1972 (R2001), "General Purpose Semi-Tubular Rivets, Full Tubular Rivets, Split Rivets, and Rivet Caps."

24.4 ANSI B18.8.1-1994, "Clevis Pins and Cotter Pins."

24.5 ANSI B18.8.2-2000, "Taper Pins, Dowel Pins, Straight Pins, Grooved Pins, and Spring Pins (Inch Series)."

24.6 ASA B18.12-2001 (R2002), "Glossary of Terms for Mechanical Fasteners."

24.7 ANSI B27.6-1972 (R1977), "General Purpose Uniform Cross Section Spiral Retaining Rings."

24.8 ANSI B27.7-1977, "General Purpose Tapered and Reduced Cross Section Retaining Rings (Metric)."

24.9 ANSI B27.8M-1978, "General Purpose Metric Tapered and Reduced Cross Section Retaining Rings."

24.10 ANSI B17.1-1967 (R2003), "Keys and Keyseats."

24.11 ANSI B17.2-1967 (R2003), "Woodruff Keys and Keyseats."

[†] References [24.1] to [24.5] and [24.7] to [24.11] are published by American Society of Mechanical Engineers; Ref. [24.6] is published by American Standards Association.

CHAPTER 25
GASKETS

Daniel E. Czernik
Director of Product Engineering
Fel-Pro Inc.
Skokie, Illinois

In the field of gaskets and seals, the former are generally associated with sealing mating flanges while the latter are generally associated with sealing reciprocating shafts or moving parts. Some designers refer to gaskets as static seals and consider seals to be dynamic sealing components. This chapter covers gaskets, and Chap. 21 discusses seals.

25.1 DEFINITION

A *gasket* is a material or combination of materials clamped between two separable members of a mechanical joint. Its function is to effect a seal between the members (flanges) and maintain the seal for a prolonged period. The gasket must be capable of sealing mating surfaces, must be impervious and resistant to the medium being sealed, and must be able to withstand the application temperature. Figure 25.1 depicts the nomenclature associated with a gasketed joint.

25.2 STANDARD CLASSIFICATION SYSTEM FOR NONMETALLIC GASKET MATERIALS[†]

This classification system provides a means for specifying or describing pertinent properties of commercial nonmetallic gasket materials. Materials composed of

[†] Ref. [25.1] (ANSI/ASTM F104).

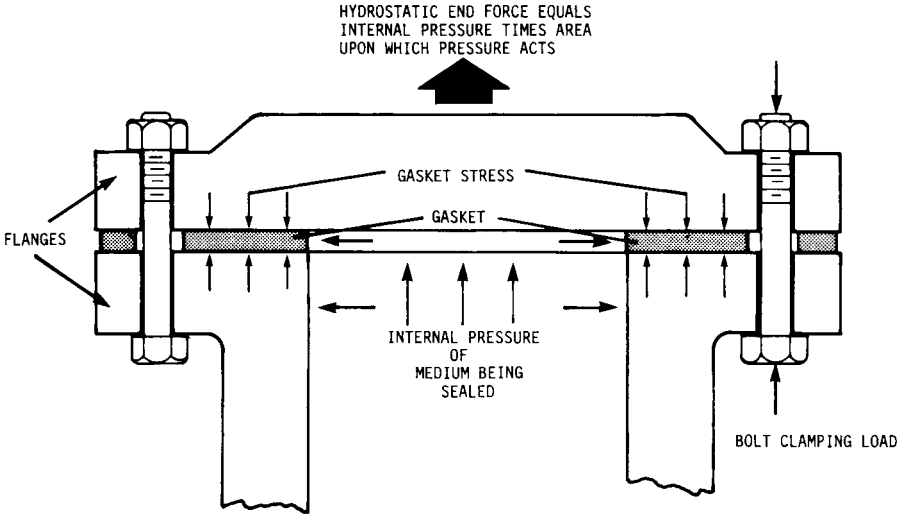

FIGURE 25.1 Nomenclature of a gasketed joint.

asbestos, cork, cellulose, and other organic or inorganic materials in combination with various binders or impregnants are included. Materials normally classified as rubber compounds are not included, since they are covered in ASTM Method D 2000 (SAE J200). Gasket coatings are not covered, since details are intended to be given on engineering drawings or in separate specifications.

This classification is based on the principle that nonmetallic gasket materials can be described in terms of specific physical and mechanical characteristics. Thus, users of gasket materials can, by selecting different combinations of statements, specify different combinations of properties desired in various parts. Suppliers, likewise, can report properties available in their products.

In specifying or describing gasket materials, each *line call-out* shall include the number of this system (minus the date symbol) followed by the letter F and six numerals, for example, ASTM F104 (F125400). Since each numeral of the call-out represents a characteristic (as shown in Table 25.1), six numerals are always required. The numeral 0 is used when the description of any characteristic is not desired. The numeral 9 is used when the description of any characteristic (or related test) is specified by some supplement to this classification system, such as notes on engineering drawings.

25.3 GASKET PROPERTIES, TEST METHODS, AND THEIR SIGNIFICANCE IN GASKETED JOINTS

Table 25.2 lists some of the most significant gasket properties which are associated with creating and maintaining a seal. This table also shows the test method and the significance of each property in a gasket application.

25.4 PERMEABILITY PROPERTIES

For a material to be impervious to a fluid, a sufficient density to eliminate voids which might allow capillary flow of the fluid through the construction must be achieved. This requirement may be met in two ways: by compressing the material to fill the voids and/or by partially or completely filling them during fabrication by means of binders and fillers. Also, for the material to maintain its impermeability for a prolonged time, its constituents must be able to resist degradation and disintegration resulting from chemical attack and temperature of the application [25.2].

Most gasket materials are composed of a fibrous or granular base material, forming a basic matrix or foundation, which is held together or strengthened with a binder. The choice of combinations of binder and base material depends on the compatibility of the components, the conditions of the sealing environment, and the load-bearing properties required for the application.

Some of the major constituents and the properties which are related to impermeability are listed here.

25.4.1 Base Materials—Nonmetallic

Cork and Cork-Rubber. High compressibility allows easy density increase of the material, thus enabling an effective seal at low flange pressures. The temperature limit is approximately 250°F (121°C) for cork and 300°F (149°C) for cork-rubber compositions. Chemical resistance to water, oil, and solvents is good, but resistance to inorganic acids, alkalies, and oxidizing environments is poor. These materials conform well to distorted flanges.

Cellulose Fiber. Cellulose has good chemical resistance to most fluids except strong acids and bases. The temperature limitation is approximately 300°F (149°C). Changes in humidity may result in dimensional changes and/or hardening.

Asbestos Fiber. This material has good heat resistance to 800°F (427°C) and is noncombustible. It is almost chemically inert (crocidolite fibers, commonly known as blue asbestos, resist even inorganic acids) and has very low compressibility. The binder dictates the resistance to temperature and the medium to be sealed.

Nonasbestos Fibers. A number of nonasbestos fibers are being used in gaskets. Some of these are glass, carbon, aramid, and ceramic. These fibers are expensive and are normally used only in small amounts. Temperature limits from 750 to 2400°F (399 to 1316°C) are obtainable. Use of these fillers is an emerging field today, and suppliers should be contacted before these fibers are specified for use.

25.4.2 Binders and Fillers

Rubber. Rubber binders provide varying temperature and chemical resistance depending on the type of rubber used. These rubber and rubberlike materials are used as binders and, in some cases, gaskets:

1. *Natural* This rubber has good mechanical properties and is impervious to water and air. It has uncontrolled swell in petroleum oil and fuel and chlorinated solvents. The temperature limit is 250°F (121°C).

TABLE 25.1 Basic Physical and Mechanical Characteristics

Basic six-digit number	Basic characteristic
First numeral	Type of material (the principal fibrous or particulate reinforcement material from which the gasket is made) shall conform to the first numeral of the basic six-digit number as follows: 0 = not specified 1 = asbestos or other inorganic fibers (type 1) 2 = cork (type 2) 3 = cellulose or other organic fibers (type 3) 4 = fluorocarbon polymer 9 = as specified†
Second numeral	Class of material (method of manufacture or common trade designation) shall conform to the second numeral of the basic six-digit number as follows: When first numeral is 1, for second numeral 0 = not specified 1 = compressed asbestos (class 1) 2 = beater addition asbestos (class 2) 3 = asbestos paper and millboard (class 3) 9 = as specified† When first numeral is 2, for second numeral 0 = not specified 1 = cork composition (class 1) 2 = cork and elastomeric (class 2) 3 = cork and cellular rubber (class 3) 9 = as specified† When first numeral is 3, for second numeral 0 = not specified 1 = untreated fiber—tag, chipboard, vulcanized fiber, etc. (class 1) 2 = protein treated (class 2) 3 = elastomeric treated (class 3) 4 = thermosetting resin treated (class 4) 9 = as specified† When first numeral is 4, for second numeral 0 = not specified 1 = sheet PTFE 2 = PTFE of expanded structure 3 = PTFE filaments, braided or woven 4 = PTFE felts 5 = filled PTFE 9 = as specified†
Third numeral	Compressibility characteristics, determined in accordance with 8.2, shall conform to the percentage indicated by the third numeral of the basic six-digit number (example: 4 = 15 to 25%): 0 = not specified 1 = 0 to 10% 2 = 5 to 15%‡ 3 = 10 to 20% 4 = 15 to 25% 5 = 20 to 30% 6 = 25 to 40% 7 = 30 to 50% 8 = 40 to 60% 9 = as specified†

TABLE 25.1 Basic Physical and Mechanical Characteristics (*Continued*)

Fourth numeral	Thickness increase when immersed in ASTM no. 3 oil, determined in accordance with 8.3, shall conform to the percentage indicated by the fourth numeral of the basic six-digit number (example: 4 = 15 to 30%): 0 = not specified 1 = 0 to 15% 2 = 5 to 20% 3 = 10 to 25% 4 = 15 to 30% 5 = 20 to 40% 6 = 30 to 50 % 7 = 40 to 60% 8 = 50 to 70% 9 = a specified†
Fifth numeral	Weight increase when immersed in ASTM no. 3 oil, determined in accordance with 8.3, shall conform to the percentage indicated by the fifth numeral of the basic six-digit number (example: 4 = 30% maximum): 0 = not specified 1 = 10% max. 2 = 15% max. 3 = 20% max. 4 = 30% max. 5 = 40% max. 6 = 60% max. 7 = 80% max. 8 = 100% max. 9 = as specified†
Sixth numeral	Weight increase when immersed in water, determined in accordance with 8.3, shall conform to the percentage indicated by the sixth numeral of the basic six-digit number (example: 4 = 30% maximum): 0 = not specified 1 = 10% max. 2 = 15% max. 3 = 20% max. 4 = 30% max. 5 = 40% max. 6 = 60% max. 7 = 80% max. 8 = 100% max. 9 = as specified†

†On engineering drawings or other supplement to this classification system. Suppliers of gasket materials should be contacted to find out what line call-out materials are available. Refer to ANSI/ASTM F104 for further details (Ref. [25.1]).

‡From 7 to 17% for type 1, class 1 compressed asbestos sheet.

2. *Styrene/butadiene* This rubber is similar to natural rubber but has slightly improved properties. The temperature limit also is 250°F (121°C).
3. *Butyl* This rubber has excellent resistance to air and water, fair resistance to dilute acids, and poor resistance to oils and solvents. It has a temperature limit of 300°F (149°C).
4. *Nitrile* This rubber has excellent resistance to oils and dilute acids. It has good compression set characteristics and has a temperature limit of 300°F (149°C).
5. *Neoprene* This rubber has good resistance to water, alkalies, nonaromatic oils, and solvents. Its temperature limit is 250°F (121°C).
6. *Ethylene propylene rubber* This rubber has excellent resistance to hot air, water, coolants, and most dilute acids and bases. It swells in petroleum fuels and oils without severe degradation. The temperature limit is 300°F (149°C).
7. *Acrylic* This rubber has excellent resistance to oxidation, heat, and oils. It has poor resistance to low temperature, alkalies, and water. The temperature limit is 450°F (232°C).

TABLE 25.2 Identification, Test Method, and Significance of Various Properties Associated with Gasket Materials

Property	Test method	Significance in gasket applications
Sealability	Fixtures per ASTM F37-62T	Resistance to fluid passage
Heat resistance	Exposure testing at elevated temperatures	Resistance to thermal degradation
Oil and water immersion characteristics	ASTM D-1170	Resistance to fluid attack
Antistick characteristics	Fixture testing at elevated termperatures	Ability to release from flanges after use
Stress vs. compression and spring rates	Various compression test machines	Sealing pressure at various compressions
Compressibility and recovery	ASTM F36-61T	Ability to follow deformation and deflection; indentation characteristics
Creep relaxation and compression set	ASTM F38-62T and D-395-59	Related to torque loss and subsequent loss of sealing pressure
Crush and extrusion characteristics	Compression test machines	Resistance to high loadings and extrusion characteristics at room and elevated temperatures

8. *Silicone* This rubber has good heat stability and low-temperature flexibility. It is not suitable for high mechanical pressure. Its temperature limit is 600°F (316°C).
9. *Viton* This rubber has good resistance to oils, fuel, and chlorinated solvents. It also has excellent low-temperature properties. Its temperature limit is 600°F (316°C).
10. *Fluorocarbon* This rubber has excellent resistance to most fluids, except synthetic lubricants. The temperature limit is 500°F (260°C).

Resins. These usually possess better chemical resistance than rubber. Temperature limitations depend on whether the resin is thermosetting or thermoplastic.

Tanned Glue and Glycerine. This combination produces a continuous gel structure throughout the material, allowing sealing at low flange loading. It has good chemical resistance to most oils, fuels, and solvents. It swells in water but is not soluble. The temperature limit is 200°F (93°C). It is used as a saturant in cellulose paper.

Fillers. In some cases, inert fillers are added to the material composition to aid in filling voids. Some examples are barytes, asbestine, and cork dust.

25.4.3 Reinforcements

Some of the properties of nonmetallic gasket materials can be improved if the gaskets are reinforced with metal or fabric cores. Major improvements in torque retention and blowout resistance are normally seen. Traditionally, perforated or upset metal cores have been used to support gasket facings. A number of designs have been utilized for production. Size of the perforations and their frequency in a given area are the usual specified parameters.

Adhesives have been developed that permit the use of an unbroken metal core to render support to a gasket facing. Laminated composites of this type have certain characteristics that are desired in particular gaskets [25.3].

25.4.4 Metallic Materials

Aluminum. This metal has good conformability and thermal conductivity. Depending on the alloy, aluminum suffers tensile strength loss as a function of temperature. Normally it is recommended up to 800°F (427°C). It is attacked by strong acids and alkalies.

Copper. This metal has good corrosion resistance and heat conductivity. It has ductility and excellent flange conformability. Normally 900°F (482°C) is considered the upper service temperature limit.

Steel. A wide variety of steels—from mild steel to stainless steel—have been used in gasketing. A high clamping load is required. Temperature limits range from 1000 to 2100°F (538 to 1149°C), depending on the alloy.

25.5 LOAD-BEARING PROPERTIES

25.5.1 Conformability and Pressure

Since sealing conditions vary widely depending on the application, it is necessary to vary the load-bearing properties of the gasket elements in accordance with these conditions. Figure 25.2 illustrates stress-compression curves for several gasket components and indicates the difference in the stress-compression properties used for different sealing locations.

Gasket thickness and compressibility must be matched to the rigidity, roughness, and unevenness of the mating flanges. An entire seal can be achieved only if the stress level imposed on the gasket at clampup is adequate for the specific material. Minimum seating stresses for various gasket materials are listed later in this chapter. In addition, the load remaining on the gasket during operation must be high enough to prevent blowout of the gasket. During operation, the hydrostatic end force, which is associated with the internal pressure, tends to unload the gasket. Figure 25.3 is a graphical representation of a gasketed joint depicting the effect of the hydrostatic end force [25.4].

The bolt should be capable of handling the maximum load imposed on it without yielding. The gasket should be capable of sealing at the minimum load resulting on it and should resist blowout at this load level.

Gaskets fabricated from compressible materials should be as thin as possible [25.5]. The gasket should be no thicker than is necessary if it is to conform to the unevenness of the mating flanges. The unevenness is associated with surface finish, flange flatness, and flange warpage during use. It is important to use the gasket's unload curve in considering its ability to conform. Figure 25.4 depicts typical load-compression and unload curves for nonmetallic gaskets.

The unload curve determines the recovery characteristics of the gasket which are required for conformance. Metallic gaskets will show no change in their load and unload curves unless yielding occurs. Load-compression curves are available from gasket suppliers.

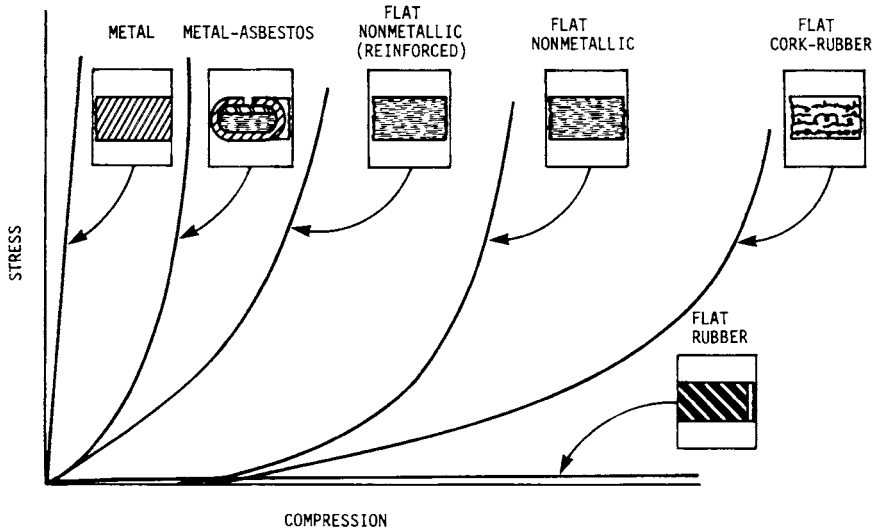

FIGURE 25.2 Stress versus compression for various gasket materials.

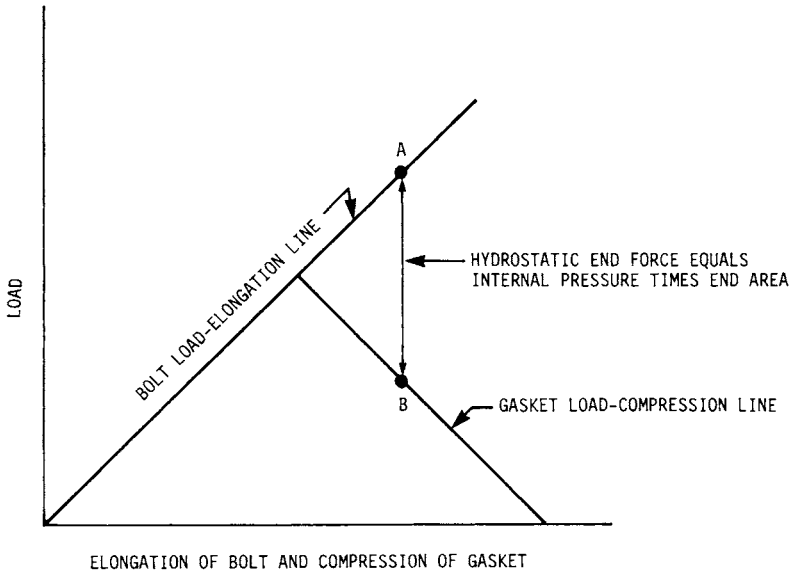

FIGURE 25.3 Graphical representation of a gasketed joint and effect of hydrostatic end force. *A,* Maximum load on gasket; *B,* minimum load on gasket.

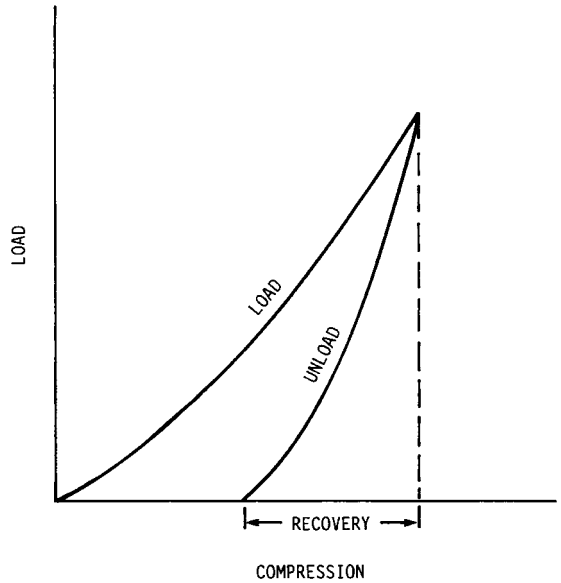

FIGURE 25.4 Load-compression and unload curves for a typical nonmetallic gasket material.

Some advantages of thin gaskets over thick gaskets are

1. Reduced creep relaxation and subsequent torque loss
2. Less distortion of mating flanges
3. Higher resistance to blowout
4. Fewer voids through which sealing media can enter, and so less permeability
5. Lower thickness tolerances
6. Better heat transfer

A common statement in the gasket industry is, "Make the gasket as thin as possible and as thick as necessary."

The following paragraphs describe some of the gasket's design specifications which need to be considered for various applications. A large array of gasket designs and sealing applications are used, and more are coming into use daily. Gaskets are constantly being improved for higher and higher performance.

In high-pressure, clamp load, and temperature applications, a high-spring-rate (stress per unit compression) material is necessary in order to achieve high loading at low compression, thereby sealing the high pressures developed. These applications generally rely on sealing resulting from localized yielding under the unit loading. In addition to the high spring rate, high heat resistance is mandatory. To economically satisfy these conditions, metal is the most commonly used material.

In applications where close tolerances in machining (surface finish and parallelism) are obtainable, a solid steel construction may be used. In those situations where close machining and assembly are not economical, it is necessary to sacrifice some gasket rigidity to allow for conformability. In such cases, conformability

exceeding that resulting from localized yielding must be inherent in the design. The metal can be corrugated, or a composite design consisting of asbestos could be used to gain the conformability required.

In very-high-pressure applications, flat gaskets may not have adequate recovery to seal as the hydrostatic end force unseats the gaskets [25.6]. In these cases, various types of self-energized metal seals are available. These seals utilize the internal pressure to achieve high-pressure sealing. They require careful machining of the flanges and have some fatigue restrictions.

In applications where increased surface conformity is necessary and lower temperatures are encountered, asbestos and/or other nonmetallic materials can be used under the limitations noted earlier.

Elastomeric inserts are used in some fluid passages where conformity with sealing surfaces and permeability are major problems and high fluid pressures are encountered. Since the inserts have low spring rates, they must be designed to have appropriate contact areas and restraint in order to effect high unit sealing stresses for withstanding the internal pressures. The inserts also have high degrees of recovery, which allow them to follow high thermal distortions normally associated in the mating flanges. Compression set and heat-aging characteristics must also be considered when elastomeric inserts are used.

25.5.2 Creep and Relaxation

After the initial sealing stress is applied to a gasket, it is necessary to maintain a sufficient sealing stress for the designed life of the unit or equipment. All materials exhibit, in varying degrees, a decrease in applied stress as a function of time, commonly referred to as *stress relaxation.* The reduction of stress on a gasket is actually a combination of two major factors: stress relaxation and creep (compression drift). By definition,

Stress relaxation is a reduction in stress on a specimen under constant strain ($d\sigma/dt;\ e = \text{constant}$).

Creep (compression drift) is a change in strain of a specimen under constant stress ($de/dt;\ \sigma = \text{constant}$).

In a gasketed joint, stress is applied by tension in a bolt or stud and transmitted as a compressive force to the gasket. After loading, stress relaxation and creep occur in the gasket, causing corresponding lower strain and tension in the bolt. This process continues indefinitely as a function of time. The change in tension of a bolt is related to the often quoted "torque loss" associated with a gasket application. Since the change in stress is due to two primary factors, a more accurate description of the phenomenon would be *creep relaxation,* from now on called *relaxation.*

Bolt elongation, or stretch, is linearly proportional to bolt length. The longer the bolt, the higher the elongation. The higher the elongation, the lower the percentage loss for a given relaxation. Therefore, the bolts should be made as long as possible for best torque retention.

Relaxation in a gasket material may be measured by applying a load on a specimen by means of a strain-gauged bolt-nut-platen arrangement as standardized by ASTM F38-62T. Selection of materials with good relaxation properties will result in the highest retained torque for the application. This results in the highest remaining stress on the gasket, which is desirable for long-term sealing.

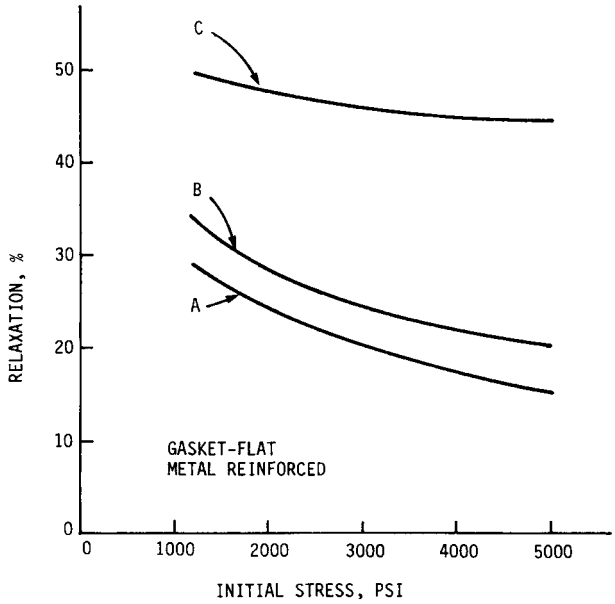

FIGURE 25.5 Relaxation versus stress on a gasket: *A,* 0.030 in–0.035 in thick; *B,* 0.042 in–0.047 in thick; *C,* 0.062 in–0.065 in thick.

The amount of relaxation increases as thickness is increased for a given gasket material. This is another reason why the thinnest gasket that will work should be selected. Figure 25.5 depicts the relaxation characteristics as a function of thickness for a particular gasket design.

Note that as clamping stress is increased, relaxation is decreased. This is the result of more voids being eliminated as the stress level is increased.

25.5.3 Effect of Geometry

The gasket's shape factor has an important effect on its relaxation characteristics. This is particularly true in the case of soft packing materials.

Much of the relaxation of a material may be attributed to the releasing of forces through lateral expansion. Therefore, the greater the area available for lateral expansion, the greater the relaxation. The *shape factor* of a gasket is the ratio of the area of one load face to the area free to bulge. For circular or annular samples, this may be expressed as

$$\text{Shape factor} = \frac{1}{4t}(\text{OD} - \text{ID}) \tag{25.1}$$

where t = thickness of gasket
OD = outside diameter
ID = inside diameter

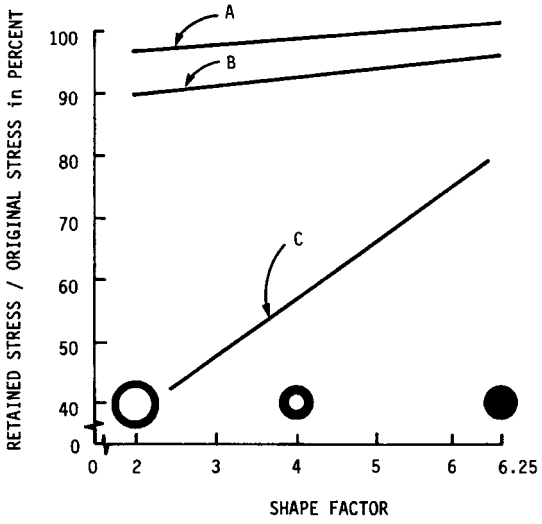

FIGURE 25.6 Retained stress for various gasket materials versus shape factor of the gasket. *A,* Asbestos fiber sheet; *B,* cellulose fiber sheet; *C,* cork-rubber.

As the area free to bulge increases, the shape factor decreases, and the relaxation will increase as the retained stress decreases. Figure 25.6 depicts the effect of shape factor on the gasket's ability to retain stress.

Note that the shape factor decreases with increasing thickness. Therefore, the gasket should be as thin as possible to reduce relaxation. It must be thick enough, however, to permit adequate conformity. The clamp area should be as large as possible, consistent with seating stress requirements. Often designers reduce gasket width, thereby increasing gasket clamping stress to obtain better sealing. Remember, however, that this reduction might decrease the gasket's shape factor, resulting in higher relaxation over time.

25.6 ENVIRONMENTAL CONDITIONS

Many environmental conditions and factors influence the sealing performance of gaskets. Flange design details, in particular, are most important. Design details such as number, size, length, and spacing of clamping bolts; flange thickness and modulus; and surface finish, waviness, and flatness are important factors. Application specifics such as the medium being sealed, as well as the temperatures and pressures involved, also affect the gasket's sealing ability. The material must withstand corrosive attack of the confined medium. In particular, flange bowing is a most common type of problem associated with the sealing of a gasketed joint. The amount of bowing can be reduced by reducing the bolt spacing. For example, if the bolt spacing were cut in half, the bowing would be reduced to one-eighth of its original value [25.7]. Doubling the flange thickness could also reduce bowing to one-eighth of its original value. A method of calculating the minimum stiffness required in a flange is available [25.8].

Different gasket materials and types require different surface finishes for optimum sealing. Soft gaskets such as rubber sheets can seal surface finishes in the vicinity of 500 microinches (μin), whereas some metallic gaskets may require finishes in the range of 32 μin for best sealing. Most gaskets, however, will seal adequately in the surface finish range of 63 to 125 μin, with 90 to 110 μin being preferred. There are two main reasons for the surface finish differences: (1) The gasket must be able to conform to the roughness for surface sealing. (2) It must have adequate bite into the mating flange to create frictional forces to resist radial motion due to the internal pressure, thereby preventing blowout. In addition, elimination of the radial micromotion will result in maintaining the initial clampup sealing condition. Micromotion can result in localized fretting, and a leakage path may be created [25.9].

Because of the complexity that results from the wide variety of environmental conditions, some gaskets for specific applications will have to be designed by trial and error. Understanding Sec. 25.7 will enable a designer to minimize the chance for leaks. Since the factors are so complex, however, adherence to the procedure will not ensure adequate performance in all cases. When inadequate gasket performance occurs, gasket manufacturers should be contacted for assistance.

25.7 GASKET DESIGN AND SELECTION PROCEDURE

25.7.1 Introduction

The first step in the selection of a gasket for sealing in a specific application is to choose a material that is both chemically compatible with the medium being sealed and thermally stable at the operating temperature of the application. The remainder of the selection procedure is associated with the minimum seating stress of the gasket and the internal pressure involved. In these regards, two methods are proposed: the American Society of Mechanical Engineers (ASME) Code method and the simplified method proposed by Whalen.

25.7.2 ASME Code Procedure

The ASME Code for Pressure Vessels, Sec. VIII, Div. 1, App. 2, is the most commonly used design guide for gasketed joints. An important part of this code focuses on two factors: an m factor, called the *gasket material factor,* which is associated with the hydrostatic end force, and a y factor, which is the minimum seating stress associated with particular gasket material. The m factor is essentially a safety factor to increase the clamping load to such an amount that the hydrostatic end force does not unseat the gasket to the point of leakage. The factors were originally determined in 1937, and even though there have been objections to their specific values, these factors have remained essentially unchanged to date. The values are only suggestions and are not mandatory.

This method uses two basic equations for calculating required bolt load, and the larger of the two calculations is used for design. The first equation is associated with W_{m2} and is the required bolt load to initially seat the gasket:

$$W_{m2} = \pi b G y \tag{25.2}$$

The second equation states that the required bolt operating load must be sufficient to contain the hydrostatic end force and simultaneously maintain adequate compression on the gasket to ensure sealing:

$$W_{m1} = \frac{\pi}{4} G^2 P + 2b\pi GmP \tag{25.3}$$

where W_{m1} = required bolt load for maximum operating or working conditions, lb
W_{m2} = required initial bolt load at atmospheric temperature conditions without internal pressure, lb
G = diameter at location of gasket load reaction, generally defined as follows: When $b_0 \le \frac{1}{4}$ in, G = mean diameter of gasket contact face, in; when $b_0 > \frac{1}{4}$ in, G = outside diameter of gasket contact face less $2b$, in
P = maximum allowable working pressure, psi
b = effective gasket or joint-contact-surface seating width, in
$2b$ = effective gasket or joint-contact-surface pressure width, in
b_0 = basic gasket seating width per Table 25.4 (the table defines b_0 in terms of flange finish and type of gasket, usually from one-half to one-fourth gasket contact width)
m = gasket factor per Table 25.3 (the table shows m for different types and thicknesses of gaskets ranging from 0.5 to 6.5)
y = gasket or joint-contact-surface unit seating load, psi (per Table 25.3, which shows values from 0 to 26 000 psi)

Tables 25.3 and 25.4 are reprints of Tables 2-5-1 and 2-5-2 of the 1980 ASME Code [25.10].

To determine bolt diameter based on required load and a specified torque for the grade of bolt, the following is used:

$$W_b = 0.17DT \quad \text{(for lubricated bolts)} \tag{25.4}$$

or

$$W_b = 0.2DT \quad \text{(for unlubricated bolts)} \tag{25.5}$$

where W_b = load per bolt, lb
D = bolt diameter, in
T = torque for grade of bolt selected, lb · in

Note that W_b is the load per bolt and must be multiplied by the number of bolts to obtain total bolt load.

To determine the bolt diameter based on the required load and the allowable bolt stress for a given grade of bolt, use

$$W_b = \sigma_b A_b \tag{25.6}$$

where W_b = load per bolt, lb
σ_b = allowable bolt stress for grade of bolt selected, psi
A_b = minimum cross-sectional area of bolt, in^2

25.7.3 Simplified Procedure

A simpler method of calculation has been suggested by Whalen [25.11]. This method is also based on the seating stress σ_g on the gasket, as shown in Table 25.5, and on the

hydrostatic end force involved in the application. Basically, Whalen's equations accomplish the same thing as the Code, but they are simplified since they use the full gasket contact width, regardless of the flange width and the surface finish of the sealing faces.

This method is based on the total bolt load F_b being sufficient to

1. Seat the gasket material into the flange surface
2. Prevent the hydrostatic end force from unseating the gasket to the point of leakage

In the first case, Table 25.5 lists a range of seating-stress values. The ranges shown were found in a search of the literature on gasket seating stresses. Gasket suppliers can be contacted to confirm these values.

Table 25.6 depicts various gasket types and comments on them. As a starting point in the design procedure, the mean value of σ_g could be used. Then, depending on the severity of the application and/or the safety factor desired, the upper and lower figures could be utilized.

Two equations are associated with this procedure. The first is

$$F_b = \sigma_g A_g \tag{25.7}$$

where F_b = total bolt load, lb
σ_g = gasket seating stress, psi (from Table 25.5)
A_g = gasket contact area, in^2

This equation states that the total bolt load must be sufficient to seat the gasket when the hydrostatic end force is not a major factor. The second equation associated with the hydrostatic end force is

$$F_b = KP_tA_m \tag{25.8}$$

where P_t = test pressure or internal pressure if no test pressure is used
A_m = hydrostatic area on which internal pressure acts (normally based on gasket's middiameter)
K = safety factor (from Table 25.7)

The safety factors K from Table 25.7 are based on the joint conditions and operating conditions but not on the gasket type or flange surface finish. They are similar to the m factors in the ASME Code. Equation (25.8) states that the total bolt load must be more than enough to overcome the hydrostatic end force. The middiameter is used in A_m since testing has shown that just prior to leakage, the internal pressure acts up to the middiameter of the gasket.

After the desired gasket has been selected, the minimum seating stress, as given in Table 25.5, is used to calculate the total bolt load required by Eq. (25.7). Then the bolt load required to ensure that the hydrostatic end force does not unseat the gasket is calculated from Eq. (25.8). The total bolt load F_b calculated by Eq. (25.7) must be greater than the bolt load calculated in Eq. (25.8). If it is not, then the gasket design must be changed, the gasket's area must be reduced, or the total bolt load must be increased.

Both the ASME procedure and the simplified procedure are associated with gasketed joints which have rigid, usually cast-iron flanges, have high clamp loads, and generally contain high pressures. A great many gasketed joints have stamped-metal covers and splash or very low fluid pressure. In these cases, the procedures do not

TABLE 25.3 Gasket Materials and Contact Facings†
Gasket Factors m *for Operating Conditions and Minimum Design Seating Stress* y

Gasket material	Gasket factor m	Minimum design seating stress *y*, psi	Sketches	Facing sketch and column to be used from Table 25-4
Self-energizing types (O-rings, metallic, elastomer, other gasket types considered as self-sealing)	0	0		
Elastomers without fabric or high percentage of asbestos fiber: Below 75A Shore Durometer 75A or higher Shore Durometer	 0.50 1.00	 0 200		(1a), (1b), (1c), (1d), (4), (5); column II
Asbestos with suitable binder for operating conditions: $\frac{1}{8}$ in thick $\frac{1}{16}$ in thick $\frac{1}{32}$ in thick	 2.00 2.75 3.50	 1 600 3 700 6 500		(1a), (1b), (1c), (1d), (4), (5); column II
Elastomers with cotton fabric insertion	1.25	400		(1a), (1b), (1c), (1d), (4), (5); column II
Elastomers with asbestos fabric insertion (with or without wire reinforcement): 3-ply 2-ply 1-ply	 2.25 2.50 2.75	 2 200 2 900 3 700	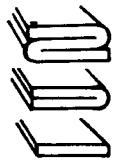	(1a), (1b), (1c), (1d), (4), (5); column II
Vegetable fiber	1.75	1 100	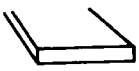	(1a), (1b), (1c), (1d), (4), (5); column II
Spiral wound metal, asbestos-filled: Carbon Stainless or Monel	 2.50 3.00	 10 000 10 000		(1a), (1b); column II
Corrugated metal, asbestos inserted or corrugated metal, jacketed asbestos-filled: Soft aluminum Soft copper or brass Iron or soft steel Monel or 4–6% chrome Stainless steels	 2.50 2.75 3.00 3.25 3.50	 2 900 3 700 4 500 5 500 6 500		(1a), (1b); column II

TABLE 25.3 Gasket Materials and Contact Facings†
Gasket Factors m *for Operating Conditions and Minimum Design Seating Stress* y (*Continued*)

Gasket material	Gasket factor m	Minimum design seating stress *y*, psi	Sketches	Facing sketch and column to be used from Table 25-4
Corrugated Metal:				
Soft aluminum	2.75	3 700		(1a), (1b), (1c), (1d); column II
Soft copper or brass	3.00	4 500		
Iron or soft steel	3.25	5 500		
Monel or 4–6% chrome	3.50	6 500		
Stainless steels	3.75	7 600		
Flat metal, jacketed asbestos-filled:			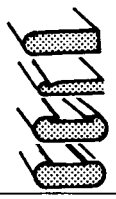	
Soft aluminum	3.25	5 500		(1a), (1b), (1c),‡ (1d),‡ (2)‡; column II
Soft copper or brass	3.50	6 500		
Iron or soft steel	3.75	7 600		
Monel or 4–6% chrome	3.50	8 000		
	3.75	9 000		
Stainless steels	3.75	9 000		
Grooved metal:				
Soft aluminum	3.25	5 500		(1a), (1b), (1c), (1d), (2), (3); column II
Soft copper or brass	3.50	6 500		
Iron or soft steel	3.75	7 600		
Monel or 4–6% chrome	3.75	9 000		
Stainless steels	4.25	10 100		
Solid flat metal:				
Soft aluminum	4.00	8 800		(1a), (1b), (1c), (1d), (2), (3), (4), (5); column I
Soft copper or brass	4.75	13 000		
Iron or soft steel	5.50	18 000		
Monel or 4–6% chrome	6.00	21 800		
Stainless steels	6.50	26 000		
Ring joint:				
Iron or soft steel	5.50	18 000		(6); column I
Monel or 4–6% chrome	6.00	21 800		
Stainless steels	6.50	26 000		

†This table gives a list of many commonly used gasket materials and contact facings with suggested design values of m and y that have generally proved satisfactory in actual service when using effective gasket seating width b given in Table 25.4. The design values and other details given in this table are only suggested and are not mandatory.

‡The surface of a gasket having a lap should not be against the nubbin.

TABLE 25.4 Effective Gasket Width†

Facing sketch (exaggerated)		Basic gasket seating width b_o	
		Column I	Column II
(1a) 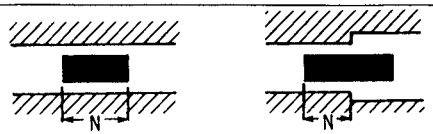		$\frac{N}{2}$	$\frac{N}{2}$
(1b)‡ 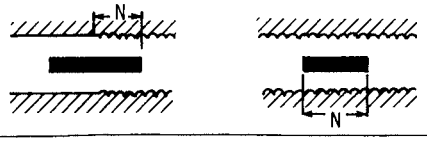			
(1c) 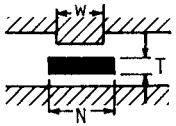	$w \leq N$	$\frac{w+T}{2}\left(\frac{w+N}{4}\text{ max.}\right)$	$\frac{w+T}{2}\left(\frac{w+N}{4}\text{ max.}\right)$
(1d)‡ 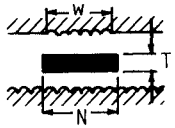	$w \leq N$		
(2) 1/64″ Nubbin 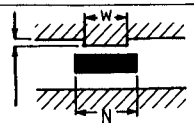	$w \leq \frac{N}{2}$	$\frac{w+N}{4}$	$\frac{w+3N}{8}$

(3) ⅛″ Nubbin 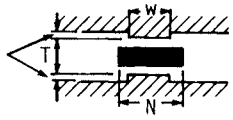	$w \le \frac{N}{2}$	$\frac{N}{4}$	$\frac{3N}{8}$
(4)‡ 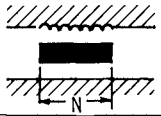		$\frac{3N}{8}$	$\frac{7N}{16}$
(5)‡ 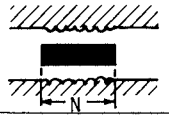		$\frac{N}{4}$	$\frac{3N}{4}$
(6) 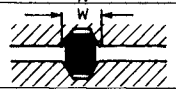		$\frac{w}{8}$	

S81 Effective gasket seating width b:

$b = b_o$ when $b_o \le \frac{1}{4}$ in $\quad b = 0.5\sqrt{b_o}$ when $b_o > \frac{1}{4}$ in

Location of gasket load reaction:

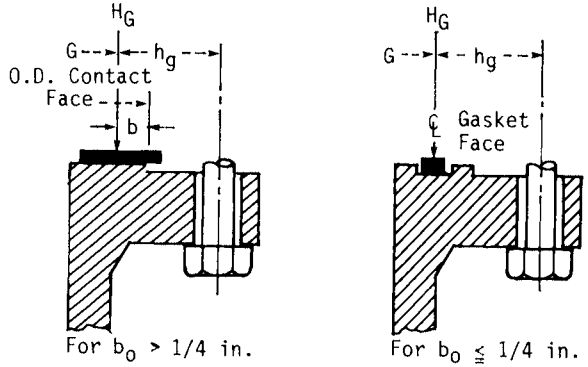

†The gasket factors listed apply only to flanged joints in which the gasket is contained entirely within the inner edges of the bolt holes.
‡Where separations do not exceed $\frac{1}{64}$-in-depth and $\frac{1}{32}$-in-width spacing, sketches (1b) and (1d) shall be used.

TABLE 25.5 Minimum Recommended Seating Stresses for Various Gasket Materials

	Material	Gasket type	Minimum seating stress range (S_g), psi†
Nonmetallic	Asbestos fiber sheet	Flat	
	$\frac{1}{8}$ in thick		1400 to 1600
	$\frac{1}{16}$ in thich		3500 to 3700
	$\frac{1}{32}$ in thick		6000 to 6500
	Asbestos fiber sheet $\frac{1}{32}$ in thick	Flat with rubber beads	1000 to 1500 lb/in on beads
	Asbestos fiber sheet $\frac{1}{32}$ in thick	Flat with metal grommet	3000 to 4000 lb/in on grommet
	Asbestos fiber sheet $\frac{1}{32}$ in thick	Flat with metal grommet and metal wire	2000 to 3000 lb/in on wire
	Cellulose fiber sheet	Flat	750 to 1100
	Cork composition	Flat	400 to 500
	Cork-rubber	Flat	200 to 300
	Fluorocarbon (TFE)	Flat	
	$\frac{1}{8}$ in thick		1500 to 1700
	$\frac{1}{16}$ in thick		3500 to 3800
	$\frac{1}{32}$ in thick		6200 to 6500
	Nonasbestos fiber sheets (glass, carbon, aramid, and ceramics)	Flat	1500 to 3000 depending on composition
	Rubber	Flat	100 to 200
	Rubber with fabric or metal reinforcement	Flat with reinforcement	300 to 500
Metallic	Aluminum	Flat	10 000 to 20 000
	Copper	Flat	15 000 to 45 000 depending on hardness
	Carbon steel	Flat	30 000 to 70 000 depending on alloy and hardness
	Stainless steel	Flat	35 000 to 95 000 depending on alloy and hardness
	Aluminum (soft)	Corrugated	1000 to 3700
	Copper (soft)	Corrugated	2500 to 4500
	Carbon steel (soft)	Corrugated	3500 to 5500
	Stainless steel	Corrugated	6000 to 8000
	Aluminum	Profile	25 000
	Copper	Profile	35 000
	Carbon steel	Profile	55 000
	Stainless steel	Profile	75 000
Jacketed metal-asbestos	Aluminum	Plain	2 500
	Copper	Plain	4 000
	Carbon steel	Plain	6 000
	Stainless steel	Plain	10 000
	Aluminum	Corrugated	2000
	Copper	Corrugated	2500
	Carbon steel	Corrugated	3000
	Stainless steel	Corrugated	4000
	Stainless steel	Spiral-wound	3000 to 30 000

†Stresses in pounds per square inch except where otherwise noted.

TABLE 25.6 Typical Gasket Designs and Descriptions

Type	Cross section	Comments
Flat	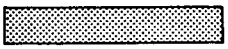	Basic form. Available in wide variety of materials. Easily fabricated into different shapes.
Reinforced		Fabric- or metal-reinforced. Improves torque retention and blowout resistance of flat types. Reinforced type can be corrugated.
Flat with rubber beads		Rubber beads located on flat or reinforced material afford high unit sealing pressure and high degree of conformability.
Flat with metal grommet		Metal grommet affords protection to base material from medium and provides high unit sealing stress. Soft metal wires can be put under grommet for higher unit sealing stress.
Plain metal jacket	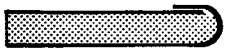	Basic sandwich type. Filler is compressible. Metal affords protection to filler on one edge and across surfaces.
Corrugated or embossed	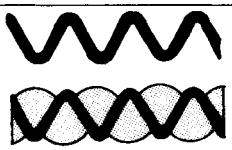	Corrugations provide for increased sealing pressure and higher conformability. Primarily circular. Corrugations can be filled with soft filler.
Profile		Multiple sealing surfaces. Seating stress decreases with increase in pitch. Wide varieties of designs are available.
Spiral-wound		Interleaving pattern of metal and filler. Ratio of metal to filler can be varied to meet demands of different applications.

TABLE 25.7 Safety Factors for Gasketed Joints

K factor	When to apply
1.2 to 1.4	For minimum-weight applications where all installation factors (bolt lubrication, tension, parallel seating, etc.) are carefully controlled; ambient to 250°F (121°C) temperature applications; where adequate proof pressure is applied.
1.5 to 2.5	For most normal designs where weight is not a major factor, vibration is moderate and temperatures do not exceed 750°F (399°C). Use high end of range where bolts are not lubricated.
2.6 to 4.0	For cases of extreme fluctuations in pressure, temperature, or vibration; where no test pressure is applied; or where uniform bolt tension is difficult to ensure.

apply, and the compression and stress distribution discussed next should be considered by the designer.

25.8 GASKET COMPRESSION AND STRESS-DISTRIBUTION TESTING

After a gasket has been selected and designed for a particular application, two simple tests can be performed to determine the gasket's compressed thickness and stress distribution. Inadequate compression or nonuniform stress distribution could result in a leaking joint. The tests can be performed to check for these possibilities and permit correction to ensure leaktight joints.

1. *Lead pellet test* In this test, lead pellets are used to accurately indicate the compressed thicknesses of a gasketed joint. The pellets, commonly called *lead shot,* are available from local gun supply stores. A size approximately twice the thickness of the gasket should be used. Lead solid-core solder can also be used if desired; the size requirements are the same. Pellets or solder are particularly well suited for doing this test, as they exhibit no recovery after compression, whereas the actual gasket material will almost always exhibit some recovery. The degree of nonuniform loading, flange bowing, or distortion will be indicated by the variations in the gasket's compressed thickness.

To begin, the original thickness of the gasket is measured and recorded at uniformly selected points across the gasket. At or near these points, holes are punched or drilled through the gasket. Care should be taken to remove any burrs. The punched holes should be approximately 1½ times the pellet diameter.

Then the gasket is mounted on the flange. A small amount of grease can be put in the punched holes to hold the lead pellets, if required. The pellets are mounted in the grease, and the mating flange is located and torqued to specifications.

Upon careful disassembly of the flange and removal of the pellets, their thicknesses are measured, recorded, and analyzed. Comparison of the pellets' compressed thicknesses to the gasket's stress-compression characteristics permits the desired stress-distribution analysis.

2. *NCR paper test* This test utilizes no-carbon-required (NCR) paper for visual determination of the stress distribution on a gasket. NCR paper is a pressure-sensitive, color-reactive paper. The intensity of color is proportional to the stress imposed on the paper, which is the same as the stress on the gasket.

NCR paper is available from the NCR Corp., the 3M Company, and other paper companies. Various grades are available, but the medium grade is usually chosen. Some papers are only one sheet, whereas others are composed of two sheets. Either type can be used.

To begin, the bolt holes are pierced in a piece of the impression paper. The pierced holes in the paper are made slightly larger than the bolts. The paper is placed on the flange, and the mating flange is assembled per torque specifications.

When you are using the two-piece carbonless paper, make sure to keep the two papers oriented to each other as they were purchased; otherwise, no impression may result. Upon torquing, the impression is made on the paper. The flange is removed, and the impression is inspected for stress distribution. A judgment of the gasket's sealing ability can now be made. Further analysis can be done by calibrating the load versus the color intensity of the paper. Various known stresses can be applied to the paper and the resulting color impressions identified. The impressions can be compared to the test sample, and then the stress on the sample can be determined.

In both the lead pellet and NCR paper tests, gasket manufacturers can be contacted for further interpretation of the results and more detailed analysis.

25.9 INSTALLATION SPECIFICATIONS

An installation is only as good as its gasket; likewise, a gasket is only as good as its installation [25.1]. The following are some recommendations associated with gasket installation:

1. Be sure that mating surfaces are clean and in specification with regard to finish, flatness, and waviness.
2. Check gasket for damage before installing it.
3. Make certain the gasket fits the application.
4. Specify lubricated bolts. Bolt threads and the underside of the bolt head should be lubricated.
5. Specify the torque level.
6. Specify the torquing sequence. In addition to the sequence, two or three stages of torque before reaching the specified level are recommended.

REFERENCES

25.1 ANSI/ASTM F104-03, *Standard Classification System for Nonmetallic Gasket Materials,* American Society for Testing and Materials.

25.2 D. E. Czernik, J. C. Moerk, Jr., and F. A. Robbins, "The Relationship of a Gasket's Physical Properties to the Sealing Phenomena," SAE paper 650431, May 1965.

25.3 D. E. Czernik, "Recent Developments and New Approaches in Mechanical and Chemical Gasketing," SAE paper 810367, February 1981.

25.4 V. M. Faires, *Design of Machine Elements,* Macmillan, New York, 1955.

25.5 D. J. McDowell, "Choose the Right Gasket Material," *Assembly Engineering,* October 1978.

25.6 H. A. Rothbart, *Mechanical Design and Systems Handbook,* 2d ed., McGraw-Hill, New York, 1985, Sec. 27.4.

25.7 *Armstrong Gasket Design Manual,* Armstrong Cork Co., Lancaster, Pa., 1978.

25.8 J. W. Oren, "Creating Gasket Seals with Rigid Flanges," SAE paper 810362, February 1981.

25.9 D. E. Czernik, "Gasketing the Internal Combustion Engine," SAE paper 800073, February 1980.

25.10 The American Society of Mechanical Engineers, Code for Pressure Vessels, Sec. VIII, Div. 1, App. 2, 1980 (see 2004 edition).

25.11 J. J. Whalen, "How to Select the Right Gasket Material," *Product Engineering,* October 1960.

25.12 D. E. Czernik, "Sealing Today's Engines," *Fleet Maintenance and Specifying,* Irving-Cloud, July 1977.

CHAPTER 26
WELDED CONNECTIONS

Richard S. Sabo
Manager, Educational Services
The Lincoln Electric Company
Cleveland, Ohio

Omer W. Blodgett
Design Consultant
The Lincoln Electric Company
Cleveland, Ohio

26.1 DEFINITIONS AND TERMINOLOGY

Arc welding is one of several fusion processes for joining metals. By the application of intense heat, metal at the joint between two parts is melted and caused to intermix—directly or, more commonly, with an intermediate molten filler metal. Upon cooling and solidification, a metallurgical bond results. Since the joining is by intermixture of the substance of one part with the substance of the other part, with or without an intermediate of like substance, the final weldment has the potential for exhibiting at the joint the same strength properties as the metal of the parts. This is in sharp contrast to nonfusion processes of joining—such as soldering, brazing, or adhesive bonding—in which the mechanical and physical properties of the base materials cannot be duplicated at the joint.

In arc welding, the intense heat needed to melt metal is produced by an electric arc. The arc is formed between the work to be welded and an electrode that is manually or mechanically moved along the joint (or the work may be moved under a stationary electrode). The electrode may be a carbon or tungsten rod, the sole purpose of which is to carry the current and sustain the electric arc between its tip and the workpiece. Or it may be a specially prepared rod or wire that not only conducts the

current and sustains the arc, but also melts and supplies filler metal to the joint. If the electrode is a carbon or tungsten rod and the joint requires added metal for fill, that metal is supplied by a separately applied filler-metal rod or wire. Most welding in the manufacture of steel products where filler metal is required, however, is accomplished with the second type of electrode—the type that supplies filler metal as well as providing the conductor for carrying electric current.

26.2 BASIC WELDING CIRCUIT

The basic arc-welding circuit is illustrated in Fig. 26.1. An ac or dc power source fitted with whatever controls may be needed is connected by a ground-work cable to the workpiece and by a "hot" cable to an electrode holder of some type, which makes electrical contact with the welding electrode. When the circuit is energized and the electrode tip is touched to the grounded workpiece and then withdrawn and held close to the spot of contact, an arc is created across the gap. The arc produces a temperature of about 6500°F at the tip of the electrode, a temperature more than adequate for melting most metals. The heat produced melts the base metal in the vicinity of the arc and any filler metal supplied by the electrode or by a separately introduced rod or wire. A common pool of molten metal is produced, called a *crater.* This crater solidifies behind the electrode as it is moved along the joint being welded. The result is a fusion bond and the metallurgical unification of the workpieces.

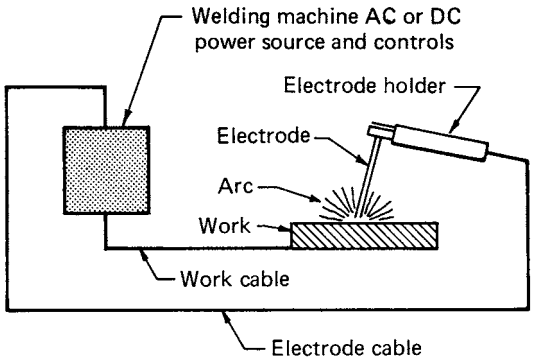

FIGURE 26.1 The basic arc-welding circuit. *(The Lincoln Electric Company.)*

26.3 ARC SHIELDING

Using the heat of an electric arc to join metals, however, requires more than the moving of the electrode with respect to the weld joint. Metals at high temperatures are chemically reactive with the main constituents of air—oxygen and nitrogen. Should the metal in the molten pool come in contact with air, oxides and nitrides would be formed, which upon solidification of the molten pool would destroy the strength properties of the weld joint. For this reason, the various arc-welding processes provide some means for covering the arc and the molten pool with a protective shield of

gas, vapor, or slag. This is referred to as *arc shielding,* and such shielding may be accomplished by various techniques, such as the use of a vapor-generating covering on filler-metal-type electrodes, the covering of the arc and molten pool with a separately applied inert gas or a granular flux, or the use of materials within the cores of tubular electrodes that generate shielding vapors.

Whatever the shielding method, the intent is to provide a blanket of gas, vapor, or slag that prevents or minimizes contact of the molten metal with air. The shielding method also affects the stability and other characteristics of the arc. When the shielding is produced by an electrode covering, by electrode core substances, or by separately applied granular flux, a fluxing or metal-improving function is usually also provided. Thus the core materials in a flux-core electrode may perform a deoxidizing function as well as a shielding function, and in submerged-arc welding, the granular flux applied to the joint ahead of the arc may add alloying elements to the molten pool as well as shielding it and the arc.

Figure 26.2 illustrates the shielding of the welding arc and molten pool with a covered "stick" electrode—the type of electrode used in most manual arc welding. The extruded covering on the filler metal rod, under the heat of the arc, generates a gaseous shield that prevents air from coming in contact with the molten metal. It also supplies ingredients that react with deleterious substances on the metals, such as oxides and salts, and ties these substances up chemically in a slag that, being lighter than the weld metal, rises to the top of the pool and crusts over the newly solidified metal. This slag, even after soldification, has a protective function: It minimizes contact of the very hot solidified metal with air until the temperature lowers to a point where reaction of the metal with air is lessened.

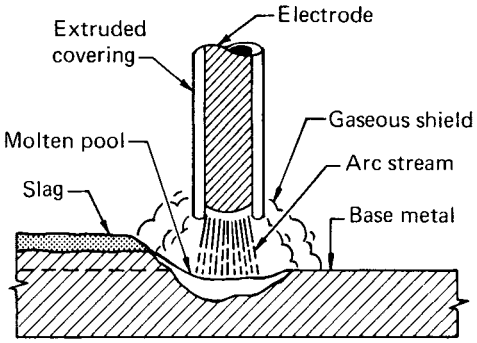

FIGURE 26.2 How the arc and molten pool are shielded by a gaseous blanket developed by the vaporization and chemical breakdown of the extruded covering on the electrode in stick-electrode welding. Fluxing material in the electrode covering reacts with unwanted substances in the molten pool, tying them up chemically and forming a slag that crusts over the hot solidified metal. The slag, in turn, protects the hot metal from reaction with the air while it is cooling. *(The Lincoln Electric Company.)*

While the main function of the arc is to supply heat, it has other functions that are important to the success of arc-welding processes. It can be adjusted or controlled to transfer molten metal from the electrode to the work, to remove surface films, and to bring about complex gas-slag-metal reactions and various metallurgical changes.

26.4 NATURE OF THE ARC

An arc is an electric current flowing between two electrodes through an ionized column of gas called a *plasma.* The space between the two electrodes—or, in arc welding, the space between the electrode and the work—can be divided into three areas of heat generation: the *cathode,* the *anode,* and the arc *plasma.*

The welding arc is characterized as a high-current, low-voltage arc that requires a high concentration of electrons to carry the current. Negative electrons are emitted from the cathode and flow—along with the negative ions of the plasma—to the positive anode, as shown in Fig. 26.3. Positive ions flow in the reverse direction. A *negative ion* is an atom that has picked up one or more electrons beyond the number needed to balance the positive charge on its nucleus—thus the negative charge. A *positive ion* is an atom that has lost one or more electrons—thus the positive charge. However, just as in a solid conductor, the principal flow of current in the arc is by electron travel.

Heat is generated in the cathode area mostly by the positive ions striking the surface of the cathode. Heat at the anode is generated mostly by electrons. These have been accelerated as they pass through the plasma by the arc voltage, and they give up their energy as heat when striking the anode.

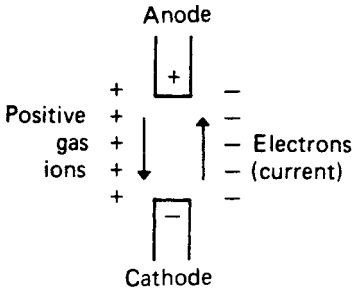

FIGURE 26.3 Characteristics of the arc. *(The Lincoln Electric Company.)*

The plasma, or arc column, is a mixture of neutral and excited gas atoms. In the central column of the plasma, electrons, atoms, and ions are in accelerated motion and are constantly colliding. The hottest part of the plasma is the central column, where the motion is most intense. The outer portion or the arc flame is somewhat cooler and consists of recombining gas molecules that were disassociated in the central column.

The distribution of heat or voltage drop in the three heat zones can be changed. Changing the arc length has the greatest effect on the arc plasma. Changing the shielding gas can change the heat balance between the anode and cathode. The addition of potassium salts to the plasma reduces the arc voltage because of increased ionization.

In welding, not only does the arc provide the heat needed to melt the electrode and the base metal, but under certain conditions it must also supply the means to transport the molten metal from the tip of the electrode to the work. Several mechanisms for metal transfer exist. In one, the molten drop of metal touches the molten metal in the crater, and transfer is by surface tension. In another, the drop is ejected from the molten metal at the electrode tip by an electric pinch. It is ejected at high speed and retains this speed unless slowed by gravitational forces. It may be accelerated by the plasma, as in the case of a pinched-plasma arc. These forces are the ones that transfer the molten metal in overhead welding. In flat welding, gravity is also a significant force in metal transfer.

If the electrode is consumable, the tip melts under the heat of the arc, and molten droplets are detached and transported to the work through the arc column. Any arc-welding system in which the electrode is melted off to become part of the weld is described as *metal arc.* If the electrode is refractory—carbon or tungsten—there are no molten droplets to be forced across the gap and onto the work. Filler metal is melted into the joint from a separate rod or wire.

More of the heat developed by the arc ends up in the weld pool with consumable electrodes than with nonconsumable electrodes, with the result that higher thermal efficiencies and narrower heat-affected zones are obtained. Typical thermal efficiencies for metal-arc welding are in the 75 to 80 percent range; for welding with nonconsumable electrodes, efficiencies are 50 to 60 percent.

Since there must be an ionized path to conduct electricity across a gap, the mere switching on of the welding current with a cold electrode poised over the work will not start the arc. The arc must first be *ignited.* This is accomplished either by supplying an initial voltage high enough to cause a discharge or by touching the electrode to the work and then withdrawing it as the contact area becomes heated. High-frequency spark discharges are frequently used for igniting gas-shielded arcs, but the most common method of striking an arc is the touch-and-withdraw method.

Arc welding may be done with either alternating or direct current and with the electrode either positive or negative. The choice of current and polarity depends on the process, the type of electrode, the arc atmosphere, and the metal being welded. Whatever the current, it must be controlled to satisfy the variables—amperage and voltage—which are specified by the welding procedures.

26.5 OVERCOMING CURRENT LIMITATIONS

The objective in commercial welding is to get the job done as fast as possible so as to lessen the time costs of skilled workers. One way to speed the welding process is to raise the current—use a higher amperage—since the faster electrical energy can be induced in the weld joint, the faster will be the welding rate.

With manual stick-electrode welding, however, there is a practical limit to the current. The covered electrodes are from 9 to 18 in long, and if the current is raised too high, electrical resistance heating within the unused length of electrode will become so great that the covering overheats and "breaks down"—the covering ingredients react with each other or oxidize and do not function properly at the arc. Also, the hot core wire increases the melt-off rate and the arc characteristics change. The mechanics of stick-electrode welding are such that electric contact with the electrode cannot be made immediately above the arc—a technique that would circumvent much of the resistance heating.

Not until semiautomatic guns and automatic welding heads (which are fed by continuous electrode wires) were developed was there a way of solving the resistance-heating problem and thus making feasible the use of high currents to speed the welding process. In such guns and heads, electric contact with the electrode is made close to the arc. The length between the tip of the electrode and the point of electric contact is then inadequate for enough resistance heating to take place to overheat the electrode in advance of the arc, even with currents two or three times those usable with stick-electrode welding.

This solving of the point-of-contact problem and circumventing of the effects of resistance heating in the electrode constituted a breakthrough that substantially lowered welding costs and increased the use of arc welding in industrial metals joining. In fact, through the ingenuity of welding equipment manufacturers, the resistance-heating effect has been put to work constructively in a technique known as long-stickout welding. Here, the length of electrode between the point of electric contact in the welding gun or head and the arc is adjusted so that resistance heating almost—but not quite—overheats the protruding electrode. Thus when a point on the electrode reaches the arc, the metal at that point is about

ready to melt and less arc heat is required to melt it. Because of this, still higher welding speeds are possible.

26.6 COMMERCIAL ARC-WELDING PROCESSES

26.6.1 Shielded Metal-Arc Welding

The *shielded metal-arc process*—commonly called *stick-electrode welding* or *manual welding*—is the most widely used of the various arc-welding processes. It is characterized by application versatility and flexibility and relative simplicity in equipment. It is the process used by the small welding shop, by the home mechanic, and by the farmer for repair of equipment; it is also a process having extensive application in industrial fabrication, structural steel erection, weldment manufacture, and other commercial metals joining. Arc welding, to persons only casually acquainted with welding, usually means shielded metal-arc welding.

With this process, an electric arc is struck between the electrically grounded work and a 9- to 18-in length of covered metal rod—the electrode. The electrode is clamped in an electrode holder, which is joined by a cable to the power source. The welder grips the insulated handle of the electrode holder and maneuvers the tip of the electrode with respect to the weld joint. When the welder touches the tip of the electrode against the work and then withdraws it to establish the arc, the welding circuit is completed. The heat of the arc melts base metal in the immediate area, the electrode's metal core, and any metal particles that may be in the electrode's covering. It also melts, vaporizes, or breaks down chemically nonmetallic substances incorporated in the covering for arc-shielding, metal-protection, or metal-conditioning purposes. The mixing of molten base metal and filler metal from the electrode provides the coalescence required to effect joining (see Fig. 26.2).

As welding progresses, the covered rod becomes shorter and shorter. Finally, the welding must be stopped to remove the stub and replace it with a new electrode. This periodic changing of electrodes is one of the major disadvantages of the process in production welding. It decreases the *operating factor,* or the percent of the welder's time spent in the actual laying of weld beads.

Another disadvantage of shielded metal-arc welding is the limitation placed on the current that can be used. High amperages, such as those used with semiautomatic guns or automatic welding heads, are impractical because of the long (and varying) length of electrode between the arc and the point of electric contact in the jaws of the electrode holder. The welding current is limited by the resistance heating of the electrode. The electrode temperature must not exceed the *breakdown temperature* of the covering. If the temperature is too high, the covering chemicals react with each other or with air and therefore do not function properly at the arc.

The versatility of the process—plus the simplicity of equipment—is viewed by many users whose work would permit some degree of mechanized welding as overriding its inherent disadvantages. This point of view was formerly well taken, but now that semiautomatic self-shielded flux-cored arc welding has been developed to a similar (or even superior) degree of versatility and flexibility, there is less justification for adhering to stick-electrode welding in steel fabrication and erection wherever substantial amounts of weld metals must be placed.

26.6.2 Self-Shielded Flux-Cored Welding

The self-shielded flux-cored arc-welding process is an outgrowth of shielded metal-arc welding. The versatility and maneuverability of stick electrodes in manual welding stimulated efforts to mechanize the shielded metal-arc process. The thought was that if some way could be found to put an electrode with self-shielding characteristics in coil form and to feed it mechanically to the arc, welding time lost in changing electrodes and the material lost as electrode stubs would be eliminated. The result of these efforts was the development of the semiautomatic and full-automatic processes for welding with continuous flux-cored tubular electrode "wires." Such fabricated wires (Fig. 26.4) contain in their cores the ingredients for fluxing and deoxidizing molten metal and for generating shielding gases and vapors and slag coverings.

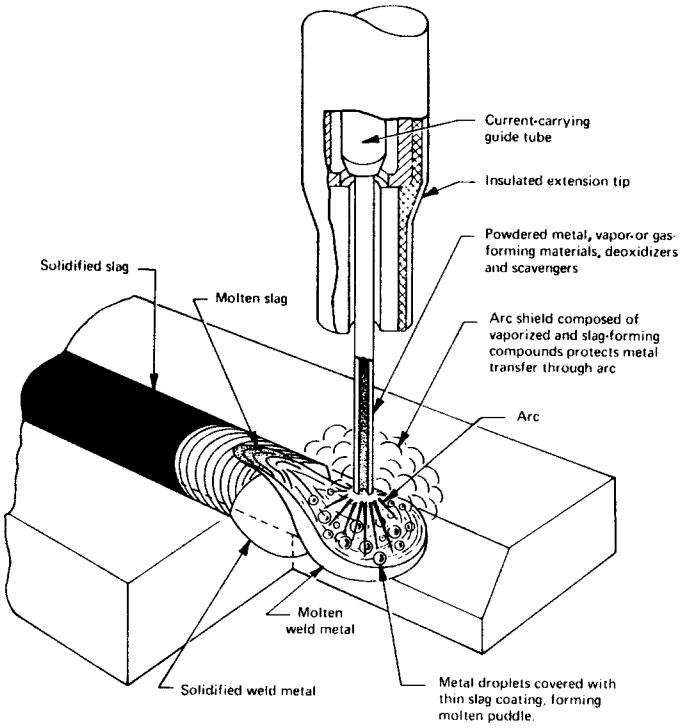

FIGURE 26.4 Principles of the self-shielded flux-cored arc-welding process. The electrode may be viewed as an *inside-out* construction of the stick electrode used in shielded metal-arc welding. Putting the shield-generating materials inside the electrode allows the coiling of long, continuous lengths of electrode and gives an outside conductive sheath for carrying the welding current from a point close to the arc. *(The Lincoln Electric Company.)*

In essence, semiautomatic welding with flux-cored electrodes is manual shielded metal-arc welding with an electrode many feet long instead of just a few inches long.

By pressing the trigger that completes the welding circuit, the operator activates the mechanism that feeds the electrode to the arc. The operator uses a gun instead of an electrode holder, but it is similarly light in weight and easy to maneuver. The only other major difference is that the weld metal of the electrode surrounds the shielding and fluxing chemicals rather than being surrounded by them.

Full-automatic welding with self-shielded flux-cored electrodes goes one step further in mechanization—the removal of direct manual manipulation in the utilization of the open-arc process.

One of the advantages of the self-shielded flux-cored arc-welding process is the high deposition rates that are made possible with the hand-held semiautomatic gun. Higher deposition rates, plus automatic electrode feed and elimination of lost time for changing electrodes, have resulted in substantial production economies wherever the semiautomatic process has been used to replace stick-electrode welding. Decreases in welding costs as great as 50 percent have been common, and in some production welding, deposition rates have been increased as much as 400 percent.

Another advantage of the process is its tolerance of poor fitup, which in shops often reduces rework and repair without affecting final product quality. The tolerance of the semiautomatic process for poor fitup has expanded the use of tubular steel members in structures by making possible sound connections where perfect fitup would be too difficult or costly to achieve.

26.6.3 Gas Metal-Arc Welding

Gas metal-arc welding, popularly known as *MIG welding,* uses a continuous electrode for filler metal and an externally supplied gas or gas mixture for shielding. The shielding gas—helium, argon, carbon dioxide, or mixtures thereof—protects the molten metal from reacting with constituents of the atmosphere. Although the gas shield is effective in shielding the molten metal from the air, deoxidizers are usually added as alloys in the electrode. Sometimes light coatings are applied to the electrode for arc stabilizing or other purposes. Lubricating films may also be applied to increase the electrode feeding efficiency in semiautomatic welding equipment. Reactive gases may be included in the gas mixture for arc-conditioning functions. Figure 26.5 illustrates the method by which shielding gas and continuous electrode are supplied to the welding arc.

MIG welding may be used with all the major commercial metals, including carbon, alloy, and stainless steels and aluminum, magnesium, copper, iron, titanium, and zirconium. It is a preferred process for the welding of aluminum, magnesium, copper, and many of the alloys of these reactive metals. Most of the irons and steels can be satisfactorily joined by MIG welding, including the carbon-free irons, the low-carbon and low-alloy steels, the high-strength quenched and tempered steels, the chromium irons and steels, the high-nickel steels, and some of the so-called superalloy steels. With these various materials, the welding techniques and procedures may vary widely. Thus carbon dioxide or argon-oxygen mixtures are suitable for arc shielding when welding the low-carbon and low-alloy steels, whereas pure inert gas may be essential when welding highly alloyed steels. Copper and many of its alloys and the stainless steels are successfully welded by this process.

Welding is either semiautomatic, using a hand-held gun to which electrode is fed automatically, or done with fully automatic equipment. The welding guns or heads are similar to those used with gas-shielded flux-cored welding.

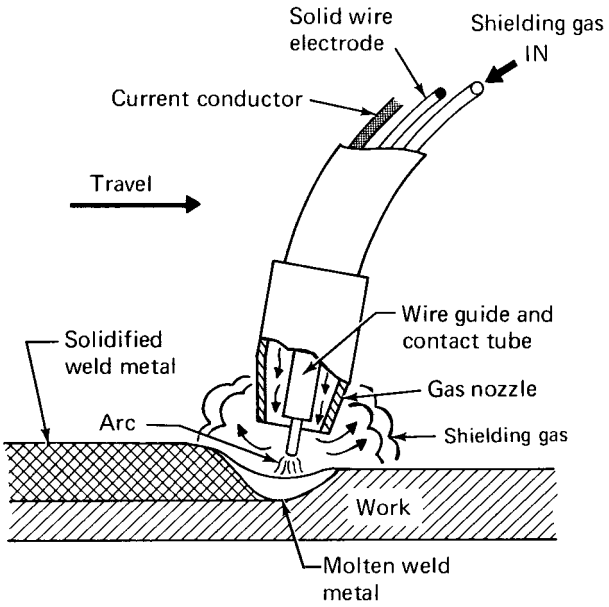

FIGURE 26.5 Principle of the gas metal-arc process. Continuous solid-wire electrode is fed to the gas-shielded arc. *(The Lincoln Electric Company.)*

26.6.4 The Gas-Shielded Flux-Cored Process

The *gas-shielded flux-cored process* may be looked on as a hybrid between self-shielded flux-cored arc welding and gas metal-arc welding. Tubular electrode wire is used (Fig. 26.6), as in the self-shielded process, but the ingredients in its core are for fluxing, deoxidizing, scavenging, and sometimes alloying additions rather than for these functions plus the generation of protective vapors. In this respect, the process has similarities to the self-shielded flux-cored electrode process, and the tubular electrodes used are classified by the American Welding Society (AWS) along with electrodes used in the self-shielded process. However, the process is similar to gas metal-arc welding in that a gas is separately applied to act as arc shield.

The gas-shielded flux-cored process is used for welding mild and low-alloy steels. It gives high deposition rates, high deposition efficiencies, and high operating factors. Radiographic-quality welds are easily produced, and the weld metal with mild and low-alloy steels has good ductility and toughness. The process is adaptable to a wide variety of joints and has the capability for all-position welding.

26.6.5 Gas Tungsten-Arc Welding

The AWS definition of *gas tungsten-arc* (TIG) welding is "an arc-welding process wherein coalescence is produced by heating with an arc between a tungsten electrode and the work." A filler metal may or may not be used. Shielding is obtained with a gas or a gas mixture.

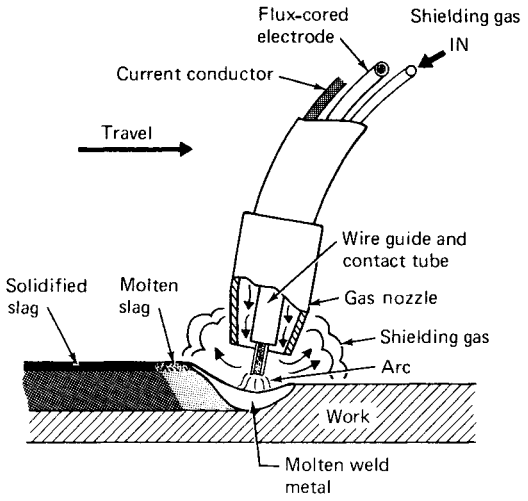

FIGURE 26.6 Principles of the gas-shielded flux-cored process. Gas from an external source is used for the shielding; the core ingredients are for fluxing and metal-conditioning purposes. *(The Lincoln Electric Company.)*

Essentially, the nonconsumable tungsten electrode is a *torch*—a heating device. Under the protective gas shield, metals to be joined may be heated above their melting points so that material from one part coalesces with material from the other part. Upon solidification of the molten area, unification occurs. Pressure may be used when the edges to be joined are approaching the molten state to assist coalescence. Welding in this manner requires no filler metal.

If the work is too heavy for the mere fusing of abutting edges, and if groove joints or reinforcements such as fillets are required, filler metal must be added. This is supplied by a filler rod that is manually or mechanically fed into the weld puddle. Both the tip of the nonconsumable tungsten electrode and the tip of the filler rod are kept under the protective gas shield as welding progresses.

Figure 26.7 illustrates the TIG torch. In automatic welding, filler wire is fed mechanically through a guide into the weld puddle. When running heavy joints manually, a variation in the mode of feeding is to lay or press the filler rod in or along the joint and melt it along with the joint edges. All the standard types of joints can be welded with the TIG process and filler metal.

Materials weldable by the TIG process are most grades of carbon, alloy, and stainless steels; aluminum and most of its alloys; magnesium and most of its alloys; copper and various brasses and bronzes; high-temperature alloys of various types; numerous hard-surfacing alloys; and such metals as titanium, zirconium, gold, and silver. The process is especially adapted for welding thin materials where the requirements for quality and finish are exacting. It is one of the few processes that is satisfactory for welding such tiny and thin-walled objects as transistor cases, instrument diaphragms, and delicate expansion bellows.

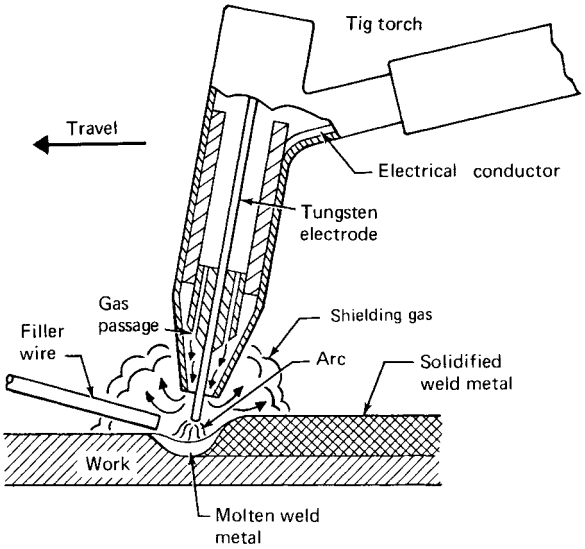

FIGURE 26.7 Principles of the gas tungsten-arc process. If filler metal is required, it is fed into the pool from a separate filler rod. *(The Lincoln Electric Company.)*

26.6.6 Submerged-Arc Welding

Submerged-arc welding differs from other arc-welding processes in that a blanket of fusible granular material—commonly called *flux*—is used for shielding the arc and the molten metal. The arc is struck between the workpiece and a bare wire electrode, the tip of which is submerged in the flux. Since the arc is completely covered by the flux, it is not visible, and the weld is run without the flash, spatter, and sparks that characterize the open-arc process. The nature of the flux is such that very little smoke or visible fumes are developed.

The process is either semiautomatic or fully automatic, and the electrode is fed mechanically to the welding gun, head, or heads. In semiautomatic welding, the welder moves the gun, usually equipped with a flux-feeding device, along the joint. Flux feed may be by gravity flow through a nozzle concentric with the electrode from a small hopper atop the gun, or it may be through a concentric nozzle tube connected to an air-pressurized flux tank. Flux may also be applied in advance of the welding operation or ahead of the arc from a hopper run along the joint. In fully automatic submerged-arc welding, flux is fed continuously to the joint ahead of or concentric with the arc, and fully automatic installations are commonly equipped with vacuum systems to pick up the unfused flux left by the welding head or heads for cleaning and reuse.

During welding, the heat of the arc melts some of the flux along with the tip of the electrode, as illustrated in Fig. 26.8. The tip of the electrode and the welding zone are always surrounded and shielded by molten flux, surmounted by a layer of unfused flux. The electrode is held a short distance above the workpiece. As the electrode progresses along the joint, the lighter molten flux rises above the molten metal in the form of a slag. The weld metal, having a higher melting (freezing) point, solidifies

while the slag above it is still molten. The slag then freezes over the newly solidified weld metal, continuing to protect the metal from contamination while it is very hot and reactive with atmospheric oxygen and nitrogen. Upon cooling and removal of any unmelted flux for reuse, the slag is readily peeled from the weld.

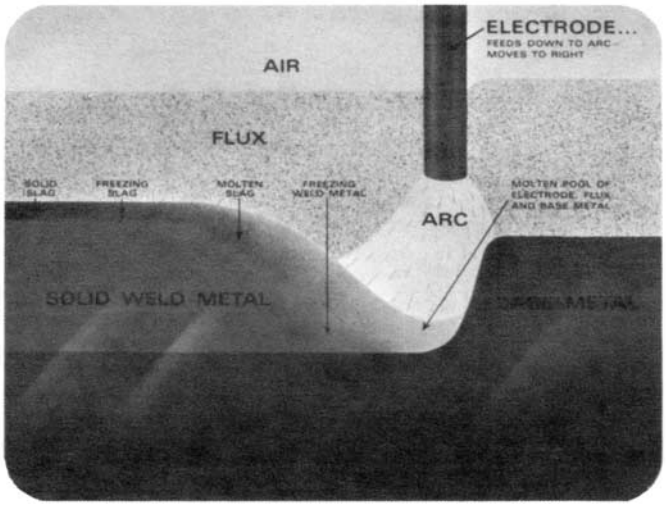

FIGURE 26.8 The mechanics of the submerged-arc process. The arc and the molten weld metal are buried in the layer of flux, which protects the weld metal from contamination and concentrates the heat into the joint. The molten flux arises through the pool, deoxidizing and cleansing the molten metal, and forms a protective slag over the newly deposited weld. *(The Lincoln Electric Company.)*

There are two general types of submerged-arc fluxes: bonded and fused. In *bonded* fluxes, the finely ground chemicals are mixed, treated with a bonding agent, and manufactured into a granular aggregate. The deoxidizers are incorporated in the flux. *Fused* fluxes are a form of glass resulting from fusing the various chemicals and then grinding the glass to a granular form. Fluxes are available that add alloying elements to the weld metal, enabling alloy weld metal to be made with mild-steel electrodes.

High currents can be used in submerged-arc welding, and extremely high heat can be developed. Because the current is applied to the electrode a short distance above its tip, relatively high amperages can be used on small-diameter electrodes. This results in extremely high current densities on relatively small cross sections of electrode. Currents as high as 600 A can be carried on electrodes as small as $\frac{5}{64}$ in, giving a density of the order of 100 000 A/in^2—6 to 10 times that carried on stick electrodes.

Because of the high current density, the melt-off rate is much higher for a given electrode diameter than with stick-electrode welding. The melt-off rate is affected by the electrode material, the flux, the type of current, the polarity, and the length of wire beyond the point of electric contact in the gun or head.

The insulating blanket of flux above the arc prevents rapid escape of heat and concentrates it in the welding zone. Not only are the electrode and base metal melted rapidly, but the fusion is deep into the base metal. The deep penetration allows the use of small welding grooves, thus minimizing the amount of filler metal

per foot of joint and permitting fast welding speeds. Fast welding, in turn, minimizes the total heat input into the assembly and thus tends to prevent problems of heat distortion. Even relatively thick joints can be welded in one pass by the submerged-arc process.

Welds made under the protective layer of flux have good ductility and impact resistance and uniformity in bead appearance. Mechanical properties at least equal to those of the base metal are consistently obtained. In single-pass welds, the amount of fused base material is large compared to the amount of filler metal used. Thus in such welds the base metal may greatly influence the chemical and mechanical properties of the weld. For this reason, it is sometimes unnecessary to use electrodes of the same composition as the base metal for welding many of the low-alloy steels.

With proper selection of equipment, submerged-arc welding is widely applicable to the welding requirements of industry. It can be used with all types of joints and permits welding a full range of carbon and low-alloy steels, from 16-gauge (1.5-mm) sheet to the thickest plate. It is also applicable to some high-alloy, heat-treated, and stainless steels and is a favored process for rebuilding and hard surfacing. Any degree of mechanization can be used—from the hand-held semiautomatic gun to boom- or track-carried and fixture-held multiple welding heads.

The high quality of submerged-arc welds, the high deposition rates, the deep penetration, the adaptability of the process to full mechanization, and the comfort characteristics (no glare, sparks, spatter, smoke, or excessive heat radiation) make it a preferred process in steel fabrication. It is used extensively in ship and barge building, in railroad car building, in pipe manufacture, and in fabricating structural beams, girders, and columns where long welds are required. Automatic submerged-arc installations are also key features of the welding areas of plants turning out mass-produced assemblies joined with repetitive short welds.

The high deposition rates attained with submerged-arc welding are chiefly responsible for the economies achieved with the process. The cost reductions from changing from the manual shielded metal-arc process to the submerged-arc process are frequently dramatic. Thus a hand-held submerged-arc gun with mechanized travel may reduce welding costs more than 50 percent; with fully automatic multiarc equipment, it is not unusual for the costs to be but 10 percent of those attained with stick-electrode welding.

26.6.7 Other "Arc-Welding" Processes

Various adaptations of the arc-welding processes described have been made to meet specialized joining needs. In addition, there are processes using electrical energy to join metals that do not fall under the category of arc welding—including electrical resistance welding and ultrasonic, electron beam, and electrodeposition welding.

Electroslag welding is an adaptation of the submerged-arc process for joining thick materials in a vertical position. Figure 26.9 is a diagrammatic sketch of the electroslag process. It will be noted that whereas some of the principles of submerged-arc welding apply, in other respects the process resembles a casting operation.

In Fig. 26.9, a square butt joint in heavy plate is illustrated, but the electroslag process—with modifications in equipment and technique—is also applicable to T joints, corner joints, girth seams in heavy-wall cylinders, and other joints. The process is suited best for materials at least 1 in in thickness and can be used with multiple electrodes on materials up to 10 in thick without excessive difficulties.

As illustrated by the open square butt joint, the assembly is positioned for the vertical deposition of weld metal. A starting pad at the bottom of the joint prevents

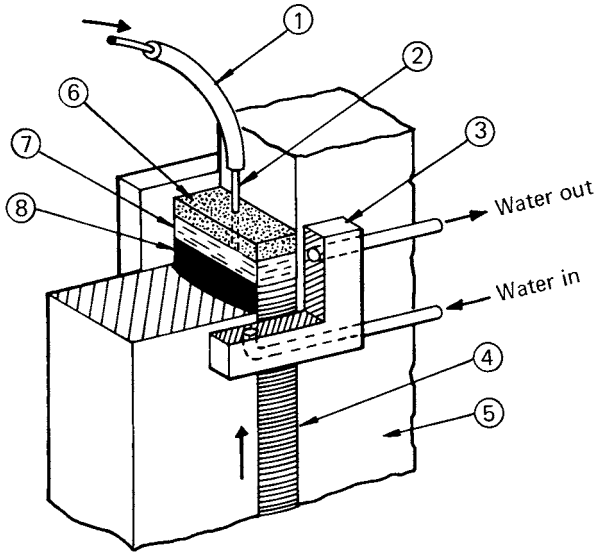

FIGURE 26.9 Schematic sketch of electroslag welding: (1) electrode guide tube, (2) electrode, (3) water-cooled copper shoes, (4) finished weld, (5) base metal, (6) molten slag, (7) molten weld metal, and (8) solidified weld metal. *(The Lincoln Electric Company.)*

the fall-out of the initially deposited weld metal and, since it is penetrated, ensures a full weld at this point. Welding is started at the bottom and progresses upward. Water-cooled dams, which may be looked on as molds, are placed on each side of the joint. These dams are moved upward as the weld-metal deposition progresses. The joint is filled in one *pass*—a single upward progression—of one or more consumable electrodes. The electrode or electrodes may be oscillated across the joint if the width of the joint makes this desirable.

At the start of the operation, a layer of flux is placed in the bottom of the joint and an arc is struck between the electrode (or electrodes) and the work. The arc melts the slag, forming a molten layer, which subsequently acts as an electrolytic heating medium. The arc is then quenched or shorted-out by this molten conductive layer. Heat for melting the electrode and the base metal subsequently results from the electrical resistance heating of the electrode section extending from the contact tube and from the resistance heating within the molten slag layer. As the electrode (or electrodes) is consumed, the welding head (or heads) and the cooling dams move upward.

In conventional practice, the weld deposit usually contains about one-third melted base metal and two-thirds electrode metal—which means that the base metal substantially contributes to the chemical composition of the weld metal. Flux consumption is low, since the molten flux and the unmelted flux above it "ride" above the progressing weld.

The flux used has a degree of electrical conductivity and low viscosity in the molten condition and a high vaporization temperature. The consumable electrodes may be either solid wire or tubular wire filled with metal powders. Alloying elements may be incorporated into the weld by each of these electrodes.

Weld quality with the electroslag process is generally excellent, because of the protective action of the heavy slag layer. Sometimes, however, the copper dams are provided with orifices just above the slag layer through which a protective gas—argon or carbon dioxide—is introduced to flush out the air above the weld and thus give additional assurance against oxidation. Such provisions are sometimes considered worthwhile when welding highly alloyed steels or steels that contain easily oxidized elements.

Electrogas welding is very similar to electroslag welding in that the equipment is similar and the joint is in the vertical position. As the name implies, the shielding is by carbon dioxide or an inert gas. A thin layer of slag, supplied by the flux-cored electrode, covers the molten metal, and the heat is supplied by an arc rather than by resistance heating, as in the electroslag process.

A disadvantage of the process is that it requires an external source of shielding gas. However, one advantage is that if the welding is stopped, the electrogas process can be started again with less difficulty than the electroslag process.

Stud arc welding is a variation of the shielded metal-arc process that is widely used for attaching studs, screws, pins, and similar fasteners to a large workpiece. The *stud* (or small part) itself—often plus a ceramic ferrule at its tip—is the arc-welding electrode during the brief period of time required for studding.

In operation, the stud is held in a portable pistol-shaped tool called a *stud gun* and positioned by the operator over the spot where it is to be weld-attached. At a press of the trigger, current flows through the stud, which is lifted slightly, creating an arc. After a very short arcing period, the stud is then plunged down into the molten pool created on the base plate, the gun is withdrawn from it, and the ceramic ferrule—if one has been used—is removed. The timing is controlled automatically, and the stud is welded onto the workpiece in less than a second. The fundamentals of the process are illustrated in Fig. 26.10.

Studs are of many shapes. All may be weld-attached with portable equipment. The stud may be used with a ceramic arc-shielding ferrule, as shown in Fig. 26.10, which prevents air infiltration and also acts as a dam to retain the molten metal, or it may have a granular flux, flux coating, or solid flux affixed to the welding end, as illustrated in Fig. 26.11. The flux may include any of the agents found in a regular electrode covering; most important to stud welding is a deoxidizer to guard against porosity.

Plasma-arc (*or plasma-torch*) *welding* is one of the newer welding processes which is used industrially, frequently as a substitute for the gas tungsten-arc process. In some applications, it offers greater welding speeds, better weld quality, and less sensitivity to process variables than the conventional processes it replaces. With the plasma torch, temperatures as high as 60 000°F are developed, and theoretically, temperatures as high as 200 000°F are possible.

The heat in plasma-arc welding originates in an arc, but this arc is not diffused as is an ordinary welding arc. Instead, it is constricted by being forced through a relatively small orifice. The *orifice,* or plasma gas, may be supplemented by an auxiliary source of shielding gas.

Orifice gas refers to the gas that is directed into the torch to surround the electrode. It becomes ionized in the arc to form the plasma and emerges from the orifice in the torch nozzle as a plasma jet. If a shielding gas is used, it is directed onto the workpiece from an outer shielding ring.

The workpiece may or may not be part of the electric circuit. In the *transferred-arc system,* the workpiece is a part of the circuit, as in other arc-welding processes. The arc *transfers* from the electrode through the orifice to the work. In the *nontransferred system,* the constricting nozzle surrounding the electrode acts as an elec-

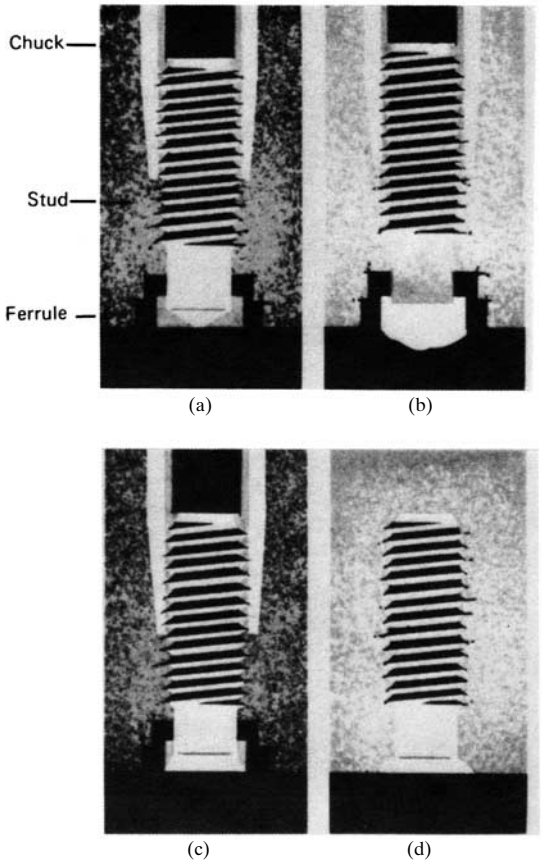

FIGURE 26.10 Principles of stud welding, using a ceramic ferrule to shield the pool. (*a*) The stud with ceramic ferrule is grasped by the chuck of the gun and positioned for welding. (*b*) The trigger is pressed, the stud is lifted, and the arc is created. (*c*) With the brief arcing period completed, the stud is plunged into the molten pool on the base plate. (*d*) The gun is withdrawn from the welded stud and the ferrule is removed. *(The Lincoln Electric Company.)*

tric terminal, and the arc is struck between it and the electrode tip; the plasma gas then carries the heat to the workpiece. Figure 26.12 illustrates transferred and nontransferred arcs.

The advantages gained by using a constricted-arc process rather than the gas tungsten-arc process include greater energy concentration, improved arc stability, higher welding speeds, and lower width-to-depth ratio for a given penetration. *Keyhole welding*—or penetrating completely through the workpiece—is possible.

The *atomic-hydrogen process of arc welding* may be regarded as a forerunner of gas-shielded and plasma-torch arc welding. Although largely displaced by other pro-

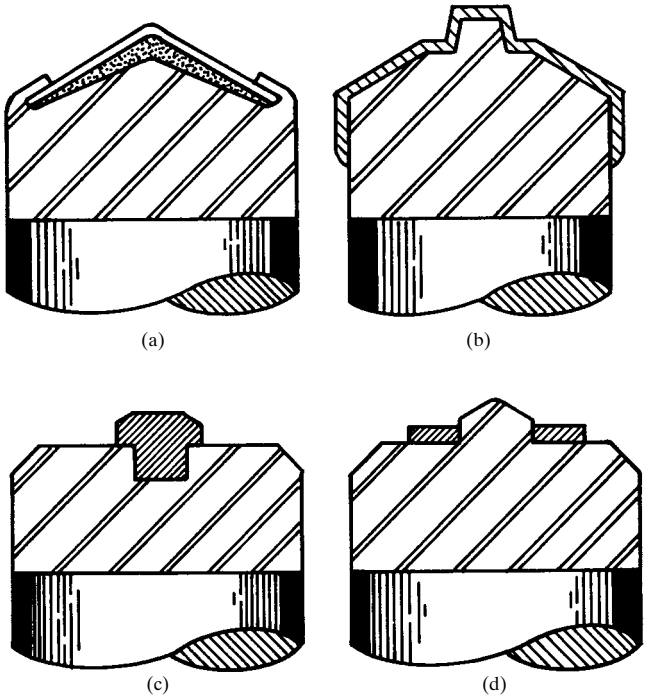

FIGURE 26.11 Three methods of containing flux on the end of a welding stud: (*a*) granular flux; (*b*) flux coating; (*c*) and (*d*) solid flux. *(The Lincoln Electric Company.)*

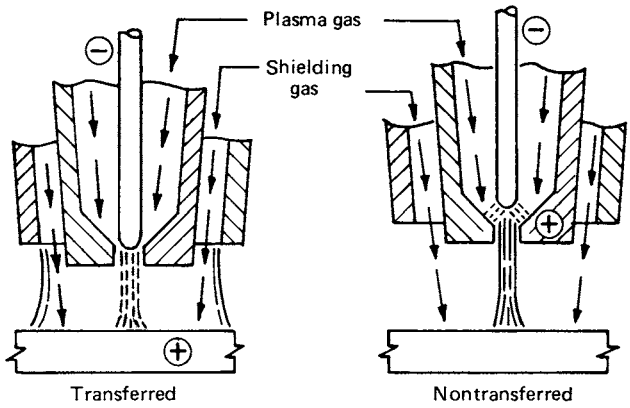

FIGURE 26.12 Transferred and nontransferred arcs. *(The Lincoln Electric Company.)*

cesses that require less skill and are less costly, it is still preferred in some manual operations where close control of heat input is required.

In the atomic-hydrogen process, an arc is established between two tungsten electrodes in a stream of hydrogen gas using alternating current. As the gas passes through the arc, molecular hydrogen is dissociated into atomic hydrogen under the intense heat. When the stream of hydrogen atoms strikes the workpiece, the environmental temperature is then at a level where recombining into molecules is possible. As a result of the recombining, the heat of dissociation absorbed in the arc is liberated, supplying the heat needed for fusing the base metal and any filler metal that may be introduced.

The atomic-hydrogen process depends on an arc, but is really a heating torch. The arc supplies the heat through the intermediate of the molecular-dissociation, atom-recombination mechanism. The hydrogen gas, however, does more than provide the mechanism for heat transfer. Before entering the arc, it acts as a shield and a coolant to keep the tungsten electrodes from overheating. At the weld puddle, the gas acts as a shield. Since hydrogen is a powerful reducing agent, any rust in the weld area is reduced to iron, and no oxide can form or exist in the hydrogen atmosphere. Weld metal, however, can absorb hydrogen, with unfavorable metallurgical effects. For this reason, the process gives difficulties with steels containing sulfur or selenium, since hydrogen reacts with these elements to form hydrogen sulfide or hydrogen selenide gases. These are almost insoluble in molten metal and either bubble out of the weld pool vigorously or become entrapped in the solidifying metal, resulting in porosity.

26.7 ARC-WELDING CONSUMABLES

Arc-welding consumables are the materials used up during welding, such as electrodes, filler rods, fluxes, and externally applied shielding gases. With the exception of the gases, all the commonly used consumables are covered by AWS specifications.

Twenty specifications in the AWS A5.x series prescribed the requirements for welding electrodes, rods, and fluxes.

26.7.1 Electrodes, Rods, and Fluxes

The first specification for mild-steel-covered electrodes, A5.1, was written in 1940. As the welding industry expanded and the number of types of electrodes for welding steel increased, it became necessary to devise a system of electrode classification to avoid confusion. The system used applies to both the mild-steel A5.1 and the low-alloy steel A5.5 specifications.

Classifications of *mild and low-alloy steel electrodes* are based on an *E* prefix and a four- or five-digit number. The first two digits (or three, in a five-digit number) indicate the minimum required tensile strength in thousands of pounds per square inch. For example, 60 = 60 kpsi, 70 = 70 kpsi, and 100 = 100 kpsi. The next to the last digit indicates the welding position in which the electrode is capable of making satisfactory welds: 1 = all positions—flat, horizontal, vertical, and overhead; 2 = flat and horizontal fillet welding (see Table 26.1). The last digit indicates the type of current to be used and the type of covering on the electrode (see Table 26.2).

Originally a color identification system was developed by the National Electrical Manufacturers Association (NEMA) in conjunction with the AWS to identify the electrode's classification. This was a system of color markings applied in a specific relationship on the electrode, as in Fig. 26.13*a*. The colors and their significance are

TABLE 26.1 AWS A5.1-69 and A5.5-69 Designations for Manual Electrodes

a. The prefix *E* designates arc-welding electrode.

b. The first two digits of four-digit numbers and the first three digits of five-digit numbers indicate minimum tensile strength:

E 60XX	60 000 psi minimum tensile strength
E 70XX	70 000 psi minimum tensile strength
E110XX	110 000 psi minimum tensile strength

c. The next-to-last digit indicates position:

EXX1X	All positions
EXX2X	Flat position and horizontal fillets

d. The suffix (for example, EXXXX-*A1*) indicates the approximate alloy in the weld deposit:

-A1	0.5% Mo
-B1	0.5% Cr, 0.5% Mo
-B2	1.25% Cr, 0.5% Mo
-B3	2.25% Cr, 1% Mo
-B4	2% Cr, 0.5% Mo
-B5	0.5% Cr, 1% Mo
-C1	2.5% Ni
-C2	3.25% Ni
-C3	1% Ni, 0.35% Mo, 0.15% Cr
-D1 and D2	0.25 to 0.45% Mo, 1.75% Mn
-G	0.5% min Ni, 0.3% min Cr, 0.2% min Mo, 0.1% min V, 1% min Mn (only one element required)

listed in Tables 26.3 and 26.4. The NEMA specification also included the choice of imprinting the classification number on the electrode, as in Fig. 26.13*b*.

Starting in 1964, new and revised AWS specifications for covered electrodes required that the classification number be imprinted on the covering, as in Fig. 26.13*b*. However, some electrodes can be manufactured faster than the imprinting equipment can mark them, and some sizes are too small to be legibly marked with an imprint. Although AWS specifies an imprint, the color code is accepted on electrodes if imprinting is not practical.

Bare mild-steel electrodes (electrode wires) for submerged-arc welding are classified on the basis of chemical composition, as shown in Table 26.5. In this classifying system, the letter *E* indicates an electrode as in the other classifying systems, but

TABLE 26.2 AWS A5.1-69 Electrode Designations for Covered Arc-Welding Electrodes

Designation	Current	Covering type
EXX10	dc+ only	Organic
EXX11	ac or dc+	Organic
EXX12	ac or dc−	Rutile
EXX13	ac or dc±	Rutile
EXX14	ac or dc±	Rutile, iron-powder (approx. 30%)
EXX15	dc+ only	Low-hydrogen
EXX16	ac or dc+	Low-hydrogen
EXX18	ac or dc+	Low-hydrogen, iron-powder (approx. 25%)
EXX20	ac or dc±	High iron-oxide
EXX24	ac or dc±	Rutile, iron-powder (approx. 50%)
EXX27	ac or dc±	Mineral, iron-powder (approx. 50%)
EXX28	ac or dc+	Low-hydrogen, iron-powder (approx. 50%)

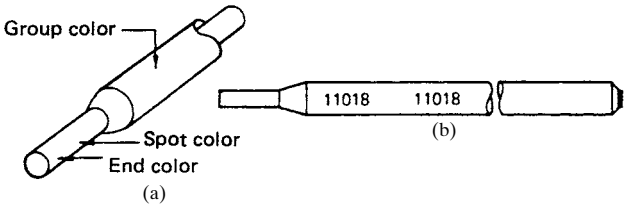

FIGURE 26.13 (*a*) National Electrical Manufacturers Association color-code method to identify an electrode's classification. (*b*) American Welding Society imprint method. *(The Lincoln Electric Company.)*

here the similarity stops. The next letter, *L, M,* or *H,* indicates low, medium, or high manganese, respectively. The following number or numbers indicate the approximate carbon content in hundredths of a percent. If there is a suffix *K,* this indicates a silicon-killed steel.

Fluxes for submerged-arc welding are classified on the basis of the mechanical properties of the weld deposit made with a particular electrode. The classification designation given to a flux consists of a prefix *F* (indicating a flux) followed by a two-digit number representative of the tensile-strength and impact requirements for test welds made in accordance with the specification. This is then followed by a

TABLE 26.3 Color Identification for Covered Mild-Steel and Low-Alloy Steel Electrodes

Spot color	End color			
	No color	Blue	Black	Orange
Group color—No color				
XX10, XX11, XX14, XX24, XX27, XX28, and all 60 XX				
No color	E6010	E7010G	....	EST
White	E6012	E7010-Ai	....	EC1
Brown	E6013	....	E7014	
Green	E6020			
Blue	E6011	E7011G		
Yellow	....	E7011-A1	E7024	
Black	....	....	E7028	
Silver	E6027			
Group color—Silver				
All XX13 and XX20 except E6013 and E6020				
Brown				
White				
Green	....	E7020G		
Yellow	....	E7020-A1		

TABLE 26.4 Color Identification for Covered Low-Hydrogen Low-Alloy Electrodes

Spot color	End color											
	No color	Blue	Black	White	Gray	Brown	Violet	Green	Red	Orange		
Group color—Green												
XX15, XX16, and XX18, except E6015 and E6016												
Red	E7015G	E7015	....	....	E8015G	E9015G	....	E10015G	....	E12015G		
White	....	E7015-A1	E90150-B3L	....	....	E9015-D1						
Brown												
Green	....	....	E8015-B2L	....	....	E9015-B3						
Bronze	....	....	E8015-B4L	....	....	E8015-B4						
Orange	E7016G	E7016	E7018	E8016-C3	....	E9016G	....	E10016G	....	E12016G		
Yellow	....	E7016-A1	E7018-A1	E8016G	....	E9016-D1	....	E10015-D2	E11016G			
Black	....	....	E8018-C3	E8016-B1	E8018-B1	....	E9018-B3					
Blue	E7018G	....	E8018G	E8016-C1	E8018-C1	E9016-B3	E9018G	E10018G	E11018G	E12018G		
Violet	....	....	....	E8016-C2	E8018-C2	E8016-B4	E9018-D1	E10018-D2				
Gray	....	....	E8018-B4	E8016-B2	E8018-B2	....		E10016-D2				
Silver	....	....	Mil-12018									

TABLE 26.5 AWS A5.17-69 Chemical-Composition Requirements for Submerged-Arc Electrodes

AWS classification	Chemical composition, percent						
	Carbon	Manganese	Silicon	Sulfur	Phosphorus	Copper†	Total other elements
Low manganese classes:							
EL8	0.10	0.30–0.55	0.05	0.035	0.03	0.15	0.50
EL8K	0.10	0.30–0.55	0.10–0.20	0.035	0.03	0.15	0.50
EL12	0.07–0.15	0.35–0.60	0.05	0.035	0.03	0.15	0.50
Medium manganese classes:							
EM5K‡	0.06	0.90–1.40	0.40–0.70	0.035	0.03	0.15	0.50
EM12	0.07–0.15	0.85–1.25	0.05	0.035	0.03	0.15	0.50
EM12K	0.07–0.15	0.85–1.25	0.15–0.35	0.035	0.03	0.15	0.50
EM13K	0.07–0.19	0.90–1.40	0.45–0.70	0.035	0.03	0.15	0.50
EM15K	0.12–0.20	0.85–1.25	0.15–0.35	0.035	0.03	0.15	0.50
High manganese class:							
EH14	0.10–0.18	1.75–2.25	0.05	0.035	0.03	0.15	0.50

†The copper limit is independent of any copper or other suitable coating which may be applied to the electrode.

‡This electrode contains 0.05 to 0.15 percent titanium, 0.02 to 0.12 percent zirconium, and 0.05 to 0.15 percent aluminum, which is exclusive of the "Total other elements" requirement.

Note: Analysis shall be made for the elements for which specific values are shown in this table. If, however, the presence of other elements is indicated in the course of routine analysis, further analysis shall be made to determine that the total of these other elements is not present in excess of the limits specified for "Total other elements" in the last column of the table. Single values shown are maximum percentages.

set of letters and numbers corresponding to the classification of the electrode used with the flux.

Gas-shielded flux-cored electrodes are available for welding the low-alloy high-tensile steels. *Self-shielded flux-cored electrodes* are available for all-position welding, as in building construction. Fabricators using or anticipating using the flux-cored arc-welding processes should keep in touch with the electrode manufacturers for new or improved electrodes not included in present specifications.

Mild-steel electrodes for gas metal-arc welding of mild and low-alloy steels are classified on the basis of their chemical compositions and the as-welded mechanical properties of the weld metal. Tables 26.6 and 26.7 are illustrative.

AWS specifications for electrodes also cover those used for welding the stainless steels, aluminum and aluminum alloys, and copper and copper alloys, as well as for weld surfacing.

Shielding gases are consumables used with the MIG and TIG welding processes. The AWS does not write specifications for gases. There are federal specifications, but the welding industry usually relies on *welding grade* to describe the required purity.

The primary purpose of a shielding gas is to protect the molten weld metal from contamination by the oxygen and nitrogen in air. The factors, in addition to cost, that affect the suitability of a gas include the influence of the gas on the arcing and metal-transfer characteristics during welding, weld penetration, width of fusion and surface shape, welding speed, and the tendency to undercut. Among the inert gases—helium, argon, neon, krypton, and xenon—the only ones plentiful enough for practical use in welding are helium and argon. These gases provide satisfactory shielding for the more reactive metals, such as aluminum, magnesium, beryllium, columbium, tantalum, titanium, and zirconium.

Although *pure* inert gases protect metal at any temperature from reaction with constituents of the air, they are not suitable for all welding applications. Controlled quantities of reactive gases mixed with inert gases improve the arc action and metal-transfer characteristics when welding steels, but such mixtures are not used for reactive metals.

Oxygen, nitrogen, and carbon dioxide are reactive gases. With the exception of carbon dioxide, these gases are not generally used alone for arc shielding. Carbon dioxide can be used alone or mixed with an inert gas for welding many carbon and low-alloy steels. Oxygen is used in small quantities with one of the inert gases—usually argon. Nitrogen is occasionally used alone, but it is usually mixed with argon as a shielding gas to weld copper. The most extensive use of nitrogen is in Europe, where helium is relatively unavailable.

26.8 DESIGN OF WELDED JOINTS

While designers need some basic knowledge of welding processes, equipment, materials, and techniques, their main interest is in how to transfer forces through welded joints most effectively and efficiently. Proper joint design is the key to good weld design.

The loads in a welded-steel design are transferred from one member to another through welds placed in weld joints. Both the type of joint and the type of weld are specified by the designer.

Figure 26.14 shows the joint and weld types. Specifying a joint does not by itself describe the type of weld to be used. Thus 10 types of welds are shown for making a

TABLE 26.6 AWS A5.18-69 Mechanical Property Requirements for Gas Metal-Arc Welding Weld Metal†

Electrode group	AWS classification	Shielding gas[a]	Current and polarity[b]	Tensile strength[d] min., kpsi	Yield strength[e] min., kpsi	Elongation in 2 in[d] min., %
A. Mild steel	E70S-1	AO	dc, reverse	72	60	22
	E70S-2 E70S-3	AO and CO_2[c]				
	E70S-4 E70S-5 E70S-6	CO_2				
	E70s-g	Not specified				
B. Low-alloy steel	E70S-1b	CO_2	dc, reverse	72	60	17
	E70S-GB	Not specified	Not specified	72	60	22
C. Emissive	E70U-1	AO and A[c]	dc, straight	72	60	22

†As-welded mechanical properties determined from an all-weld-metal tension-test specimen.

[a]Shielding gases are AO, argon plus 1 to 5 percent oxygen; CO_2, carbon dioxide; A, argon.

[b]*Reverse polarity* means electrode is positive; *straight polarity* means electrode is negative.

[c]Where two gases are listed as interchangeable (that is, AO and CO_2 and AO and A) for classification of a specific electrode, the classification may be conducted using either gas.

[d]For each increase of one percentage point in elongation over the minimum, the yield strength or tensile strength, or both, may decrease 1 kpsi to a minimum of 70 kpsi for the tensile strength and 58 kpsi for the yield strength, except for group C electrodes.

[e]0.2 percent offset value.

TABLE 26.7 AWS A5.18-69 Chemical-Composition Requirements for Gas Metal-Arc Welding Electrode

AWS classification	Chemical composition, percent											
	Carbon	Manganese	Silicon	Phosphorus	Sulfur	Nickel†	Chromium†	Molybdenum†	Vanadium†	Titanium	Zirconium	Aluminum
Group A: Mild-steel electrodes												
E70S-1	0.07–0.19	0.90–1.40	0.30–0.50	0.025	0.035							
E70S-2	0.06	0.90–1.40	0.40–0.70	0.025	0.035					0.05–0.15	0.02–0.12	0.05–0.15
E70S-3	0.06–0.15	0.90–1.40	0.45–0.70	0.025	0.035							
E70S-4	0.07–0.15	0.90–1.40	0.65–0.85	0.025	0.035							
E70S-5	0.07–0.19	0.90–1.40	0.30–0.60	0.025	0.035							0.50–0.90
E70S-6	0.07–0.15	1.40–1.85	0.80–1.15	0.025	0.035							
E70S-G	No chemical requirements‡											
Group B: Low-alloy steel electrodes												
E70S-1B	0.07–0.12	1.60–2.10	0.50–0.80	0.025	0.035	0.15		0.40–0.60				
E70S-GB	No chemical requirements											
Group C: Emissive electrode												
E70U-1	0.07–0.15	0.80–1.40	0.15–0.35	0.025	0.035							

†For groups A and C these elements may be present but are not intentionally added.
‡For this classification there are no chemical requirements for the elements listed with the exception that there shall be no intentional addition of Ni, Cr, Mo, or V.
Note: Single values shown are maximums.

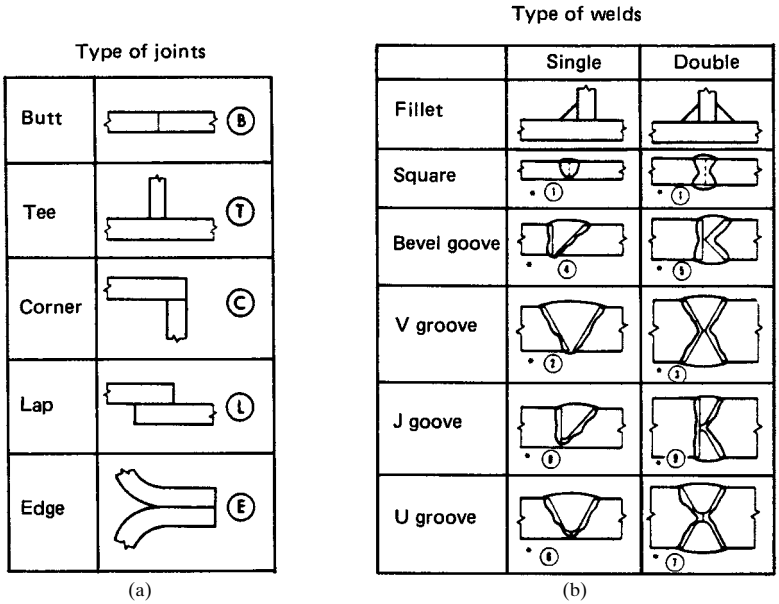

FIGURE 26.14 (*a*) Joint design; (*b*) weld grooves. *(The Lincoln Electric Company.)*

butt joint. Although all but two welds are illustrated with butt joints here, some may be used with other types of joints. Thus a single-bevel weld may also be used in a T or corner joint (Fig. 26.15), and a single-V weld may be used in a corner, T, or butt joint.

26.8.1 Fillet-Welded Joints

The fillet weld, requiring no groove preparation, is one of the most commonly used welds. Corner welds are also widely used in machine design. Various corner arrangements are illustrated in Fig. 26.16. The corner-to-corner joint, as in Fig. 26.16*a,* is difficult to assemble because neither plate can be supported by the other. A small electrode with low welding current must be used so that the first welding pass does not burn through. The joint requires a large amount of metal. The corner joint shown in Fig. 26.16*b* is easy to assemble, does not easily burn through, and requires just half

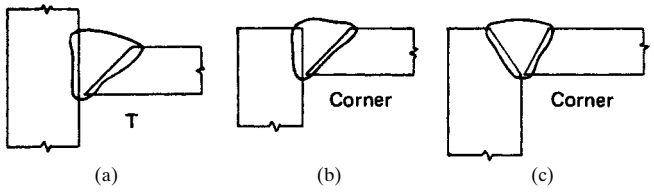

FIGURE 26.15 (*a*) Single-bevel weld used in T joint and (*b*) corner joint; (*c*) single-V weld in corner joint. *(The Lincoln Electric Company.)*

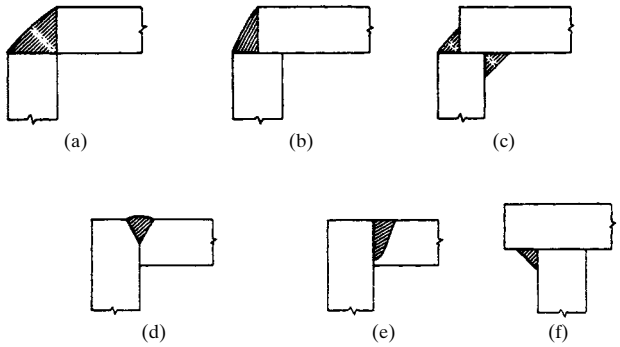

FIGURE 26.16 Various corner joints. *(The Lincoln Electric Company.)*

the amount of the weld metal as the joint in Fig. 26.16*a.* However, by using half the weld size but placing two welds, one outside and the other inside, as in Fig. 26.16*c,* it is possible to obtain the same total throat as with the first weld, but only half the weld metal need be used.

With thick plates, a partial-penetration groove joint, as in Fig. 26.16*d,* is often used. This requires beveling. For a deeper joint, a J preparation, as in Fig. 26.16*e,* may be used in preference to a bevel. The fillet weld in Fig. 26.16*f* is out of sight and makes a neat and economical corner.

The size of the weld should always be designed with reference to the size of the thinner member. The joint cannot be made any stronger by using the thicker member for the weld size, and much more weld metal will be required, as illustrated in Fig. 26.17.

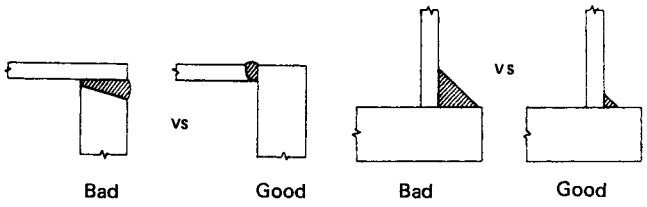

FIGURE 26.17 Size of weld should be determined with reference to thinner member. *(The Lincoln Electric Company.)*

In the United States, a fillet weld is measured by the leg size of the largest right triangle that may be inscribed within the cross-sectional area (Fig. 26.18). The throat, a better index to strength, is the shortest distance between the root of the joint and the face of the diagrammatical weld. As Fig. 26.18 shows, the leg size used may be shorter than the actual leg of the weld. With convex fillets, the actual throat may be longer than the throat of the inscribed triangle.

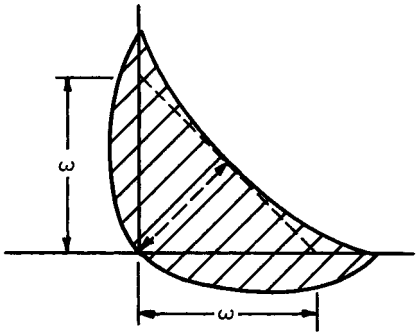

FIGURE 26.18 Leg size ω of a fillet weld. *(The Lincoln Electric Company.)*

26.8.2 Groove and Fillet Combinations

A combination of a partial-penetration groove weld and a fillet weld (Fig. 26.19) is used for many joints. The AWS prequalified single-bevel groove T joint is reinforced with a fillet weld.

The designer is frequently faced with the question of whether to use fillet or groove welds (Fig. 26.20). Here cost becomes a major consideration. The fillet welds in Fig. 26.20*a* are easy to apply and require no special plate preparation. They can be made using large-diameter electrodes with high welding currents, and as a consequence, the deposition rate is high. The cost of the welds increases as the square of the leg size.

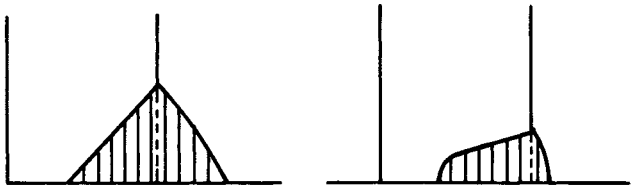

FIGURE 26.19 Combined groove- and fillet-welded joints. *(The Lincoln Electric Company.)*

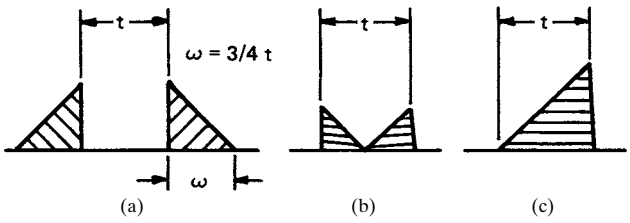

FIGURE 26.20 Comparison of fillet welds and groove welds. *(The Lincoln Electric Company.)*

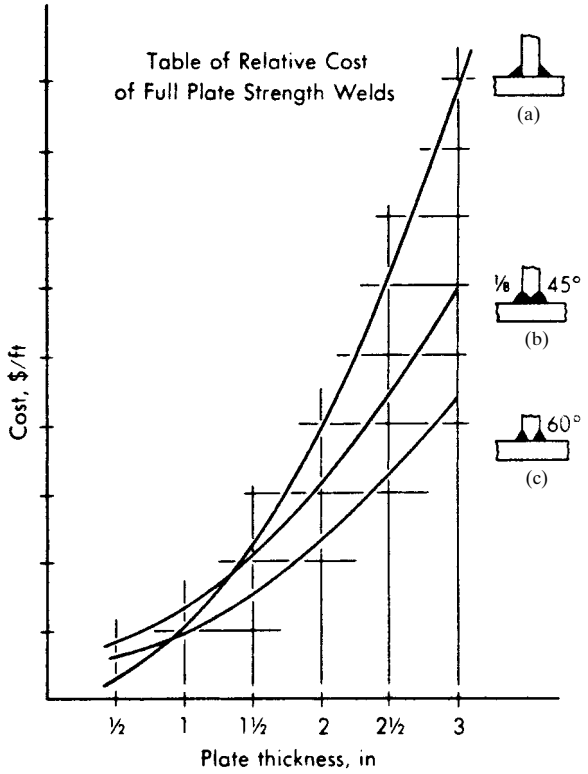

FIGURE 26.21 Relative cost of welds having the full strength of the plate. *(The Lincoln Electric Company.)*

In comparison, the double-bevel groove weld in Fig. 26.20*b* has about one-half the weld area of the fillet welds. However, it requires extra preparation and the use of smaller-diameter electrodes with lower welding currents to place the initial pass without burning through. As plate thickness increases, this initial low-deposition region becomes a less important factor and the higher cost factor decreases in significance. The construction of a curve based on the best possible determination of the actual cost of welding, cutting, and assembling, such as that illustrated in Fig. 26.21, is a possible technique for deciding at what point in plate thickness the double-bevel groove weld becomes less costly. The point of intersection of the fillet-weld curve with the groove-weld curve is the point of interest. The accuracy of this device is dependent on the accuracy of the cost data used in constructing the curves.

Referring to Fig. 26.20*c,* it will be noted that the single-bevel groove weld requires about the same amount of weld metal as the fillet welds deposited in Fig. 26.20*a.* Thus there is no apparent economic advantage. There are some disadvantages, though. The single-bevel joint requires bevel preparation and initially a lower deposition rate at the root of the joint. From a design standpoint, however, it offers a direct transfer of force through the joint, which means that it is probably better under fatigue loading. Although the illustrated full-strength fillet weld, having leg

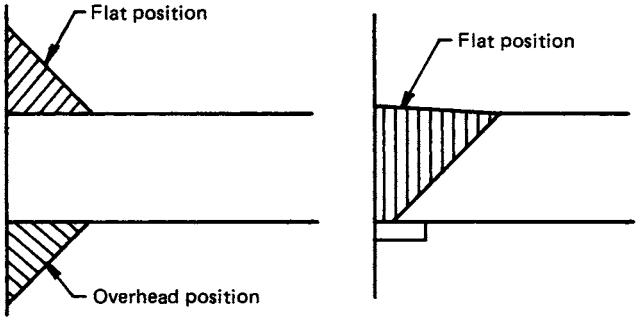

FIGURE 26.22 In the flat position, a single-bevel groove joint is less expensive than fillet welds in making a T joint. *(The Lincoln Electric Company.)*

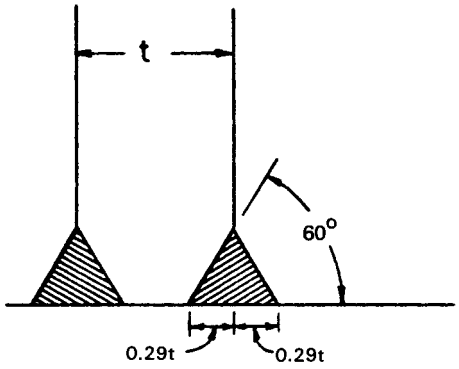

FIGURE 26.23 Partial-penetration double-bevel groove joint. *(The Lincoln Electric Company.)*

sizes equal to three-quarters the plate thickness, would be sufficient, some codes have lower allowable limits for welds, and many require a leg size equal to the plate thickness. In this case, the cost of the fillet-welded joint may exceed the cost of the single-bevel groove-welded joint in thicker plates. Also, if the joint is so positioned that the weld can be made in the flat position, a single-bevel groove weld would be less expensive than fillet welds. As can be seen in Fig. 26.22, one of the fillets would have to be made in the overhead position—a costly operation.

The partial-penetration double-bevel groove joint shown in Fig. 26.23 has been suggested as a full-strength weld. The plate is beveled to 60 degrees on both sides to give a penetration of at least 29 percent of the thickness of the plate ($0.29t$). After the groove is filled, it is reinforced with a fillet weld of equal cross-sectional area and shape. This partial-penetration double-bevel groove joint uses 57.8 percent of the weld metal used by the full-strength fillet weld. It requires joint preparation, but the 60-degree angle allows the use of large electrodes and high welding current.

Full-strength welds are not always required in the design, and economies can often be achieved by using partial-strength welds where these are applicable and

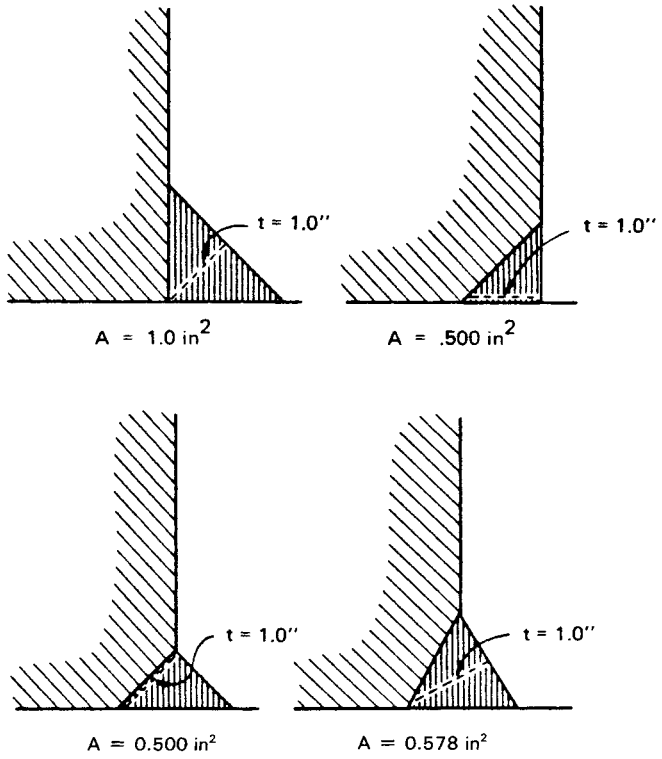

FIGURE 26.24 Comparison of weld joints having equal throats. *(The Lincoln Electric Company.)*

permissible. Referring to Fig. 26.24, it can be seen that on the basis of an unreinforced 1-in throat, a 45-degree partial-penetration single-bevel groove weld requires just one-half the weld area needed for a fillet weld. Such a weld may not be as economical as the same-strength fillet weld, however, because of the cost of edge preparation and the need to use a smaller electrode and lower current on the initial pass.

If the single-bevel groove joint were reinforced with an equal-leg fillet weld, the cross-sectional area for the same throat size would still be one-half the area of the

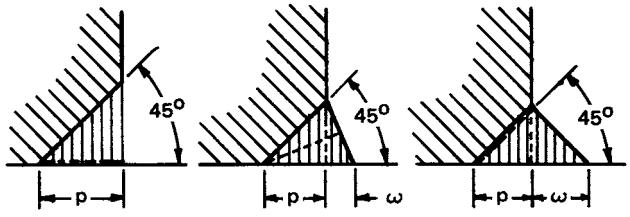

FIGURE 26.25 Comparison of weld joints with and without reinforcing fillet welds. *(The Lincoln Electric Company.)*

fillet, and less beveling would be required. The single-bevel 60-degree groove joint with an equal fillet-weld reinforcement for the same throat size would have an area 57.8 percent of that of the simple fillet weld. This joint has the benefit of smaller cross-sectional area—yet the 60-degree included angle allows the use of higher welding current and larger electrodes. The only disadvantage is the extra cost of preparation.

From this discussion it is apparent that the simple fillet-welded joint is the easiest to make, but it may require excessive weld metal for larger sizes. The single-bevel 45-degree included-angle joint is a good choice for larger weld sizes. However, one would miss opportunities by selecting the two extreme conditions of these two joints. The joints between these two should be considered. Referring to Fig. 26.25, one may start with the single-bevel 45-degree joint without the reinforcing fillet weld, gradually add a reinforcement, and finally increase the lower leg of the fillet reinforcement until a full 45-degree fillet weld is reached. In this figure, p = depth of preparation and ω = leg of reinforcing fillet.

When a partial-penetration groove weld is reinforced with a fillet weld, the minimum throat is used for design purposes, just as the minimum throat of a fillet or partial-penetration groove weld is used. However, as Fig. 26.26 shows, the allowable load for this combination weld is not the sum of the allowable limits for each portion of the combination weld. This would result in a total throat much larger than the actual throat.

Figure 26.27*a* shows the effect of using the incorrect throat in determining the allowable unit force on a combination weld. The allowable[†] for each weld was added separately. In Fig. 26.27*b*, weld size is correctly figured on the minimum throat.

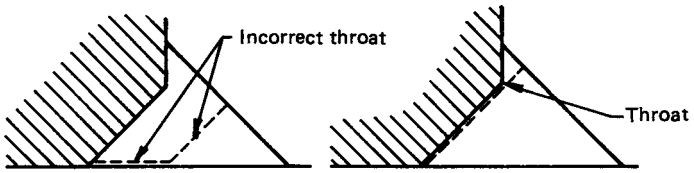

FIGURE 26.26 Determining minimum throat. (*a*) Incorrect result; (*b*) correct result. *(The Lincoln Electric Company.)*

26.8.3 Sizing of Fillets

Table 26.8 gives the sizing of fillet welds for rigidity at various strengths and plate thicknesses, where the strength of the weld metal matches the plate.

In machine design work, where the primary design requirement is rigidity, members are often made with extra-heavy sections, so that movement under load will be within very close tolerances. Because of the heavy construction, stresses are very low. Often the allowable stress in tension for mild steel is given as 20 kpsi, yet the welded machine base or frame may have a working stress of only 2 to 4 kpsi. The question arises as to how to determine the weld sizes for these types of rigidity designs.

[†] The term *allowable* is often used in the welding industry to indicate allowable load, allowable stress, or unit allowable load—EDS.

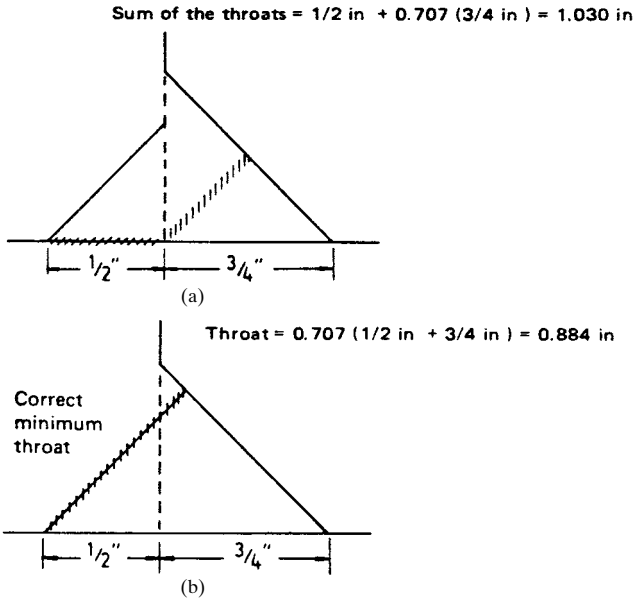

FIGURE 26.27 Examples showing the effect of correct and incorrect throat dimension in determining the allowable load on a combination weld. (*a*) The weld allowable load would be incorrectly figured by adding each weld throat separately; (*b*) weld allowable load is correctly figured using the minimum throat. *(The Lincoln Electric Company.)*

It is not very practical to first calculate the stresses resulting in a weldment when the unit is loaded within a predetermined dimensional tolerance and then use these stresses to determine the forces that must be transferred through the connecting welds. A very practical method, however, is to design the weld for the thinner plate, making it sufficient to carry one-third to one-half the carrying capacity of the plate. This means that if the plate were stressed to one-third to one-half its usual value, the weld would be sufficient. Most rigidity designs are stressed much below these values; however, any reduction in weld size below one-third the full-strength value would give a weld too small an appearance for general acceptance.

26.8.4 Groove Joints

Figure 26.28*a* indicates that the *root opening R* is the separation between the members to be joined. A root opening is used for electrode accessibility to the base or root of the joint. The smaller the angle of the bevel, the larger the root opening must be to get good fusion at the root. If the root opening is too small, root fusion is more difficult to obtain, and smaller electrodes must be used, thus slowing down the welding process. If the root opening is too large, weld quality does not suffer, but more weld metal is required; this increases welding cost and will tend to increase distortion.

TABLE 26.8 Rule-of-Thumb Fillet-Weld Sizes for Use in Cases Where the Strength of the Weld Metal Matches the Strength of the Plate

Plate thickness t, in	Strength design, full-strength weld, $\omega = 0.75t$	Rigidity design	
		50% of full-strength weld, $\omega = 0.375t$	33% of full-strength weld, $\omega = 0.25t$
< 1/4	1/8	1/8†	1/8†
1/4	3/16	3/16†	3/16†
5/16	1/4	3/16†	3/16†
3/8	5/16	3/16†	3/16†
7/16	3/8	3/16	3/16†
1/2	3/8	3/16	3/16†
9/16	7/16	1/4	1/4†
5/8	1/2	1/4	1/4†
3/4	9/16	5/16	1/4†
7/8	5/8	3/8	5/16†
1	3/4	3/8	5/16†
1 1/8	7/8	7/16	5/16
1 1/4	1	1/2	5/16
1 3/8	1	1/2	3/8
1 1/2	1 1/8	9/16	3/8
1 5/8	1 1/4	5/8	7/16
1 3/4	1 3/8	3/4	7/16
2	1 1/2	3/4	1/2
2 1/8	1 5/8	7/8	9/16
2 1/4	1 3/4	7/8	9/16
2 3/8	1 3/4	1	5/8
2 1/2	1 7/8	1	5/8
2 5/8	2	1	3/4
2 3/4	2	1	3/4
3	2 1/4	1 1/8	3/4

†These values have been adjusted to comply with AWS recommended minimums.
SOURCE: The Lincoln Electric Company, Cleveland, Ohio.

Figure 26.28*b* indicates how the root opening must be increased as the included angle of the bevel is decreased. Backup strips are used on larger root openings. All three preparations are acceptable; all are conducive to good welding procedure and good weld quality. Selection, therefore, is usually based on cost.

Root openings and joint preparation will directly affect weld cost (mass of weld metal required), and the choice should be made with this in mind. Joint preparation involves the work required on plate edges prior to welding and includes beveling and providing a root face.

Using a double-groove joint in preference to a single-groove joint (Fig. 26.29) cuts in half the amount of welding. This reduces distortion and makes possible alternating the weld passes on each side of the joint, again reducing distortion.

In Fig. 26.30*a,* if the bevel or gap is too small, the weld will bridge the gap, leaving slag at the root. Excessive back-gouging is then required. Figure 26.30*b* shows how

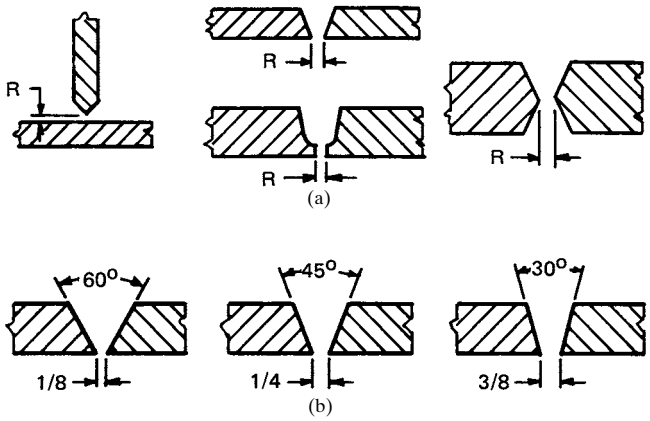

FIGURE 26.28 (*a*) Root opening is designated as *R;* (*b*) size of root opening depends on bevel angle. *(The Lincoln Electric Company.)*

proper joint preparation and procedure will produce good root fusion and will minimize back-gouging. In Fig. 26.30*c,* a large root opening will result in burnthrough. Spacer strip may be used, in which case the joint must be back-gouged.

Backup strips are commonly used when all welding must be done from one side or when the root opening is excessive. Backup strips, shown in Fig. 26.31*a* through *c,* are generally left in place and become an integral part of the joint. Spacer strips may be used, especially in the case of double-V joints, to prevent burnthrough. The spacer in Fig. 26.31*d* used to prevent burnthrough will be gouged out before welding the second side.

26.8.5 Backup Strips

Backup strip material should conform to the base metal. Feather edges of the plate are recommended when using a backup strip.

Short, intermittent tack welds should be used to hold the backup strip in place, and these should preferably be staggered to reduce any initial restraint on the joint. They should not be directly opposite one another (Fig. 26.32).

The backup strip should be in intimate contact with both plate edges to avoid trapped slag at the root, as shown in Fig. 26.33. On a butt joint, a nominal weld reinforcement (approximately 1/16 in above flush) is all that is necessary, as shown in Fig.

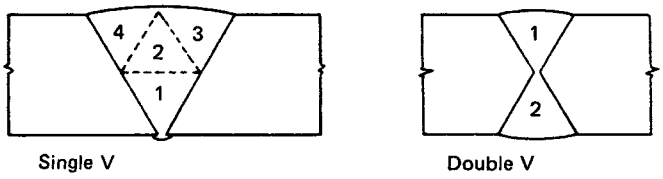

FIGURE 26.29 Using a double-groove joint in place of a single-groove joint reduces the amount of welding. *(The Lincoln Electric Company.)*

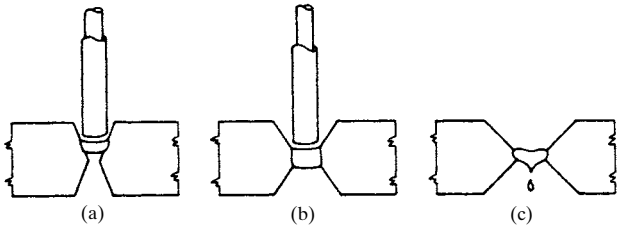

FIGURE 26.30 (*a*) If the gap is too small, the weld will bridge the gap, leaving slag at the root; (*b*) a proper joint preparation; (*c*) a root opening that is too large will result in burnthrough. *(The Lincoln Electric Company.)*

26.34*a.* Additional buildup, as shown in Fig. 26.34*b,* serves no useful purpose and will increase the weld cost. Care should be taken to keep both the width and the height of the reinforcement to a minimum.

26.8.6 Edge Preparation

The main purpose of a root face (Fig. 26.35*a*) is to provide an additional thickness of metal, as opposed to a feather edge, in order to minimize any burnthrough tendency. A feather-edge preparation is more prone to burnthrough than a joint with a root face, especially if the gap gets a little too large (Fig. 26.35*b*).

A root face is not as easily obtained as a feather edge. A feather edge is generally a matter of one cut with a torch, whereas a root face will usually require two cuts or possibly a torch cut plus machining.

A root face usually requires back-gouging if a 100 percent weld is required. A root face is not recommended when welding into a backup strip, since a gas pocket would be formed.

Plate edges are beveled to permit accessibility to all parts of the joint and to ensure good fusion throughout the entire weld cross section. Accessibility can be gained by compromising between maximum bevel and minimum root opening (Fig. 26.36).

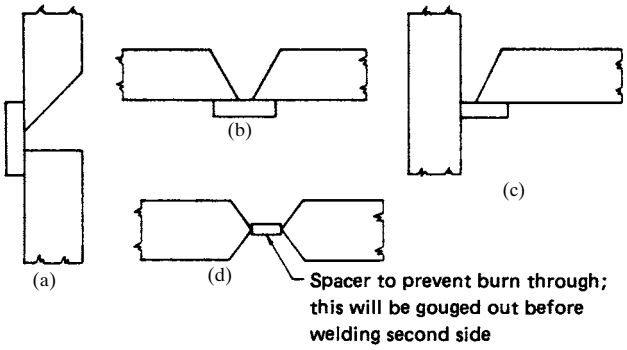

FIGURE 26.31 The backup strips shown in (*a*), (*b*), and (*c*) are used when all welding is done from one side or when the root opening is excessive; a spacer to prevent burnthrough as shown in (*d*) will be gouged out before welding the second side. *(The Lincoln Electric Company.)*

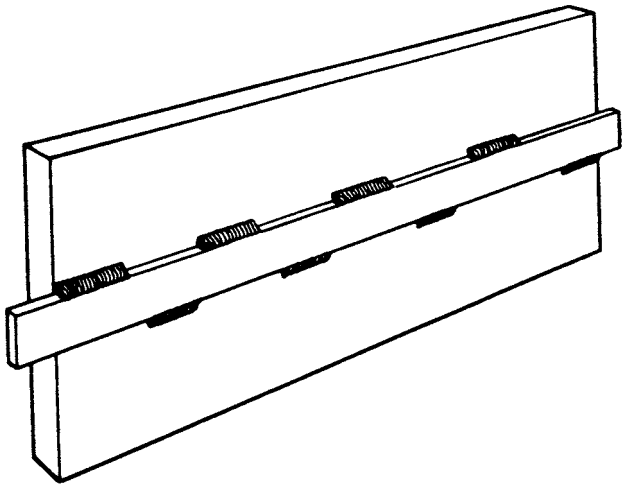

FIGURE 26.32 Short, intermittent tack welds should be used to hold the backup strip in place. *(The Lincoln Electric Company.)*

Degree of bevel may be dictated by the importance of maintaining proper electrode angle in confined quarters (Fig. 26.37). For the joint illustrated, the minimum recommended bevel is 45 degrees.

J and U preparations are excellent to work with, but economically they may have little to offer because preparation requires machining as opposed to simple torch cutting. Also, a J or U groove requires a root face (Fig. 26.38) and thus back-gouging.

To consistently obtain complete fusion when welding a plate, back-gouging is required on virtually all joints except bevel joints with a feather edge. This may be done by any convenient means: grinding, chipping, or gouging. The latter method is generally the most economical and leaves an ideal contour for subsequent beads.

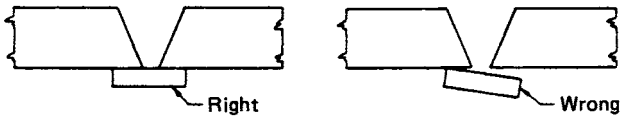

FIGURE 26.33 The backup strip should be in intimate contact with both edges of the plate. *(The Lincoln Electric Company.)*

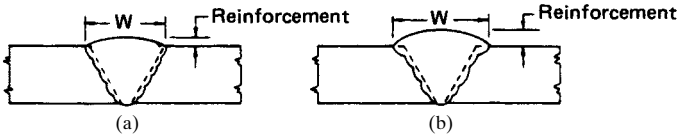

FIGURE 26.34 (*a*) A minimum reinforcement on a butt joint is preferred; (*b*) too much reinforcement. *(The Lincoln Electric Company.)*

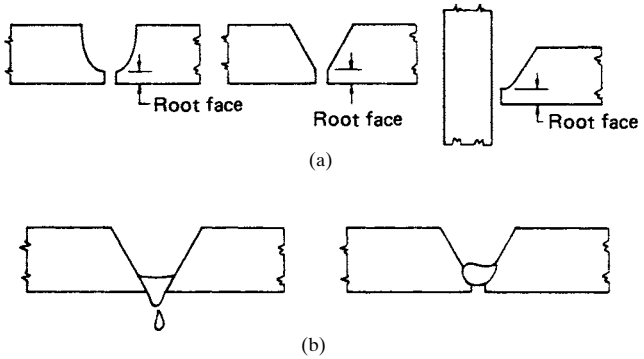

FIGURE 26.35 (*a*) A root face minimizes the tendency to burnthrough; (*b*) a feather edge is more prone to burnthrough than a joint with a root face. *(The Lincoln Electric Company.)*

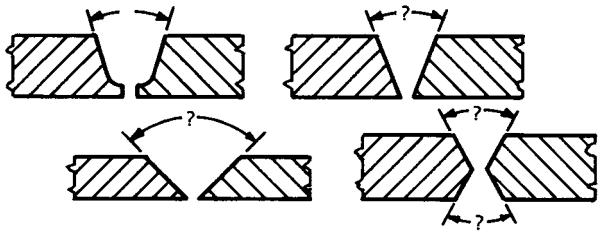

FIGURE 26.36 Accessibility is gained by compromising between bevel and root opening. *(The Lincoln Electric Company.)*

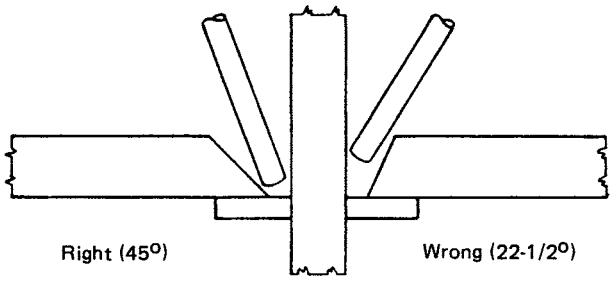

FIGURE 26.37 Degree of bevel may be dictated by the need for maintaining proper electrode angle. *(The Lincoln Electric Company.)*

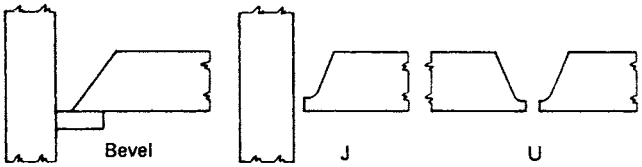

FIGURE 26.38 A bevel preparation with a backup strip may be more economical than a J or U groove. *(The Lincoln Electric Company.)*

Without back-gouging, penetration is incomplete (Fig. 26.39*a*). Proper back-chipping should be deep enough to expose sound weld metal, and the contour should permit the electrode complete accessibility (Fig. 26.39*b*).

26.9 CODES AND SPECIFICATIONS FOR WELDS

Welds are designed and executed in accordance with codes, standards, and specifications intended to enhance the integrity of the product and its safe performance in use. Codes and specifications are generally written by industrial groups, trade or professional organizations, or government bureaus, and each code or specification deals with applications pertaining specifically to the interest of the authoring body. Large manufacturing organizations may prepare their own specifications to meet their specific needs.

Among the major national organizations that write codes that involve arc welding are the American Welding Society (AWS), the American Institute of Steel Construction (AISC), the American Society for Testing Materials (ASTM), the American Society of Mechanical Engineers (ASME), and the American Petroleum Institute (API).

Among government agencies, the Interstate Commerce Commission (ICC) has rules for the fabrication of over-the-road vehicles and for containers used in interstate commerce. The various branches of the military services also prepare specifi-

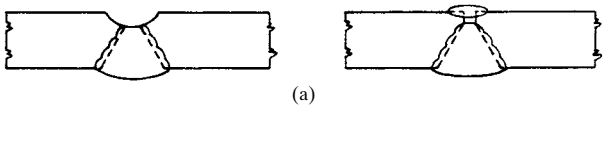

FIGURE 26.39 (*a*) Without back-gouging, penetration is incomplete; (*b*) proper back-gouging should be deep enough to expose sound weld metal. *(The Lincoln Electric Company.)*

cations. Some specifications—for example, those of the Society of Automotive Engineers (SAE)—actually are not standards, but are merely guides to recommended practices. Other specifications rigidly call out the design and fabrication procedures to be followed and are legally binding. In any event, neither the design nor the fabrication of a welded structure should be undertaken without full knowledge of all codes and requirements that must be met.

Meeting the requirements of a code does not protect anyone against liability concerning the performance of the welds or structure. Nor, in general, does any code-writing body approve, endorse, guarantee, or in any way attest to the correctness of the procedures, designs, or materials selected for code application.

The strength values permitted by governing codes are called *allowables.* Thus there are specified allowables for shear stress and unit force on various sizes of fillet welds, and there are fatigue allowables for various welds in reference to the geometry of the joint. Most weldments used in machinery are made in accordance with AWS and AISC specifications, with ASME and API rules applicable where pressure vessels and piping are involved.

26.9.1 Allowable Shear and Unit Forces

The basic formula for allowable shear stress τ for weld metal in a fillet or partial-penetration bevel-groove weld has been established by the AWS and AISC as

$$\tau = 0.30S_t \tag{26.1}$$

where S_t = minimum tensile strength. Table 26.9 shows the values for various weld-metal strength levels obtained by this formula and the more common fillet-weld sizes. These values are for equal-leg fillet welds where the effective throat $t_e = 0.707\omega$, where ω is the leg size. With Table 26.9 one can calculate the allowable unit force f per linear inch for a weld size made with a particular electrode type. For example, calculating the allowable unit force f per inch for a ½-in fillet weld made with an E70 electrode gives

$$\begin{aligned} f = 0.707\omega\tau &= 0.707\omega\tau(0.30S_t) \\ &= 0.707(\tfrac{1}{2})(0.30)(70)(10)^3 \\ &= 7420 \text{ lb per linear inch} \end{aligned}$$

An AISC provision gives limited credit for penetration beyond the root of a fillet weld made with the submerged-arc process. Since penetration increases the effective throat thickness of the weld, as shown in Fig. 26.40, the provision permits an increase in this value when calculating weld strength. For fillet welds ⅜ in and smaller, the effective throat t_e is now equal to the leg size of the weld ω. Thus,

$$t_e = \omega \qquad \omega \le \tfrac{3}{8} \text{ in} \tag{26.2}$$

For submerged-arc fillet welds larger than ⅜ in, the effective throat of the weld is obtained by adding 0.11 to 0.707ω. Thus,

$$t_e = 0.707\omega + 0.11 \qquad \omega > \tfrac{3}{8} \text{ in} \tag{26.3}$$

TABLE 26.9 Allowable Unit Load for Various Sizes of Fillet Welds

Tensile strength of weld metal, kpsi						
S_t =	60	70	80	90	100	110
Allowable shear stress on throat of fillet weld or partial-penetration groove weld, kpsi						
τ =	18.0	21.0	24.0	27.0	30.0	33.0
Allowable unit force on fillet weld kip/linear in						
f =	12.73	14.85	16.97	19.09	21.21	23.33
Leg size ω, in	Allowable unit force for various sizes of fillet welds, kip/linear in					
1	12.73	14.85	16.97	19.09	21.21	23.33
$\frac{7}{8}$	11.14	12.99	14.85	16.70	18.57	20.41
$\frac{3}{4}$	9.55	11.14	12.73	14.32	15.92	17.50
$\frac{5}{8}$	7.96	9.28	10.61	11.93	13.27	14.58
$\frac{1}{2}$	6.37	7.42	8.48	9.54	10.61	11.67
$\frac{7}{16}$	5.57	6.50	7.42	8.35	9.28	10.21
$\frac{3}{8}$	4.77	5.57	6.36	7.16	7.95	8.75
$\frac{5}{16}$	3.98	4.64	5.30	5.97	6.63	7.29
$\frac{1}{4}$	3.18	3.71	4.24	4.77	5.30	5.83
$\frac{3}{16}$	2.39	2.78	3.18	3.58	3.98	4.38
$\frac{1}{8}$	1.59	1.86	2.12	2.39	2.65	2.92
$\frac{1}{16}$	0.795	0.930	1.06	1.19	1.33	1.46

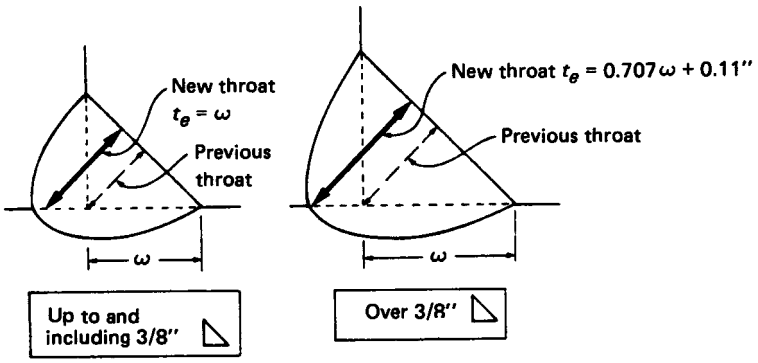

FIGURE 26.40 The AISC gives credit for penetration beyond the root of fillets made with the submerged-arc process. *(The Lincoln Electric Company.)*

where t_e is in inches. Note that allowance for penetration applies only to fillet welds made by the submerged-arc welding process. Electrode polarity will provide this penetration.

26.9.2 Minimum Fillet-Weld Size

The minimum sizes of fillet welds for specific material thicknesses are shown in Table 26.10. In the AISC Specifications and the AWS Structural Welding Code, this table has been expanded to include material less than ¼ in thick and ⅛-in fillets. Where materials of different thicknesses are being joined, the minimum fillet weld size is governed by the thicker material, but this size does not have to exceed the thickness of the thinner material unless required by the calculated stress.

TABLE 26.10 Minimum Fillet-Weld Size ω in Inches

Material thickness of thicker part joined	Minimum fillet size
To $\frac{1}{4}$ inclusive	$\frac{1}{8}$
Over $\frac{1}{4}$ to $\frac{1}{2}$	$\frac{3}{16}$
Over $\frac{1}{2}$ to $\frac{3}{4}$	$\frac{1}{4}$
Over $\frac{3}{4}$ to $1\frac{1}{2}$	$\frac{5}{16}$
Over $1\frac{1}{2}$ to $2\frac{1}{4}$	$\frac{3}{8}$
Over $2\frac{1}{4}$ to 6	$\frac{1}{2}$
Over 6	$\frac{5}{8}$

SOURCE: AISC Specifications, Sec. 1.17.5.

26.9.3 Allowables for Weld Metal—A Handy Reference

Table 26.11 summarizes the AWS Structural Welding Code and AISC allowables for weld metal. It is intended to provide a ready reference for picking the proper strength levels for the various types of steels. Once this selection has been made, the allowables can be quickly found for the various types of welds that may be required for the specific assembly.

26.9.4 AISC Fatigue Allowables

The AISC Specifications include fatigue allowables, which also are accepted by the AWS Building Code, Sec. 8. Therefore, designers have something other than the AWS Building Code, Sec. 10, Bridges, with its automatic 10 percent lower allowable design stress, on which to base fatigue considerations.

Although developed for structures, these allowables are adaptable to the fatigue problems of machine-tool makers, equipment manufacturers, and others who fabricate with welded steel. They cover a wide range of welded joints and members and not only provide values for various types of welds, but also take into consideration the strength of members attached by welds.

The conventional method of handling fatigue is based on a maximum fatigue stress. The AISC-suggested method is based on the range of stress. Either may be used in design; they will give comparable values. The AISC method is generally quicker.

Under the new approach, the allowables for members are designed *M* and for welds *W.* A tensile load is *T,* a compressive load *C,* a reversal *R,* and shear *S.* In the chart used for determining values for allowable range of stress (Fig. 26.41), there are four groups representing life. These are

1. 20 000 to 100 000 cycles
2. Over 100 000 to 500 000 cycles
3. Over 500 000 to 2 000 000 cycles
4. Over 2 000 000 cycles

And there are eight different categories representing type of joint and detail of member. The chart provides the allowable range in stress σ_{sr} or τ_{sr}, which value may be used in the conventional fatigue formulas. These formulas are

$$\sigma_{\max} = \frac{\sigma_{sr}}{1 - K} \qquad \text{or} \qquad \sigma_{\max} = \frac{\tau_{sr}}{1 - K} \tag{26.4}$$

where

$$K = \frac{\text{min. stress}}{\text{max. stress}} = \frac{\text{min. force}}{\text{max. force}}$$

$$= \frac{\text{min. moment}}{\text{max. moment}} = \frac{\text{min. shear}}{\text{max. shear}} \tag{26.5}$$

Of course, the maximum allowable fatigue value used should not exceed the allowable for steady loading.

An alternative use of the allowable range of stress—taken from the table—is to divide it into the range of applied load. This will provide the required property of the section—area or section modulus. The section, as determined, must additionally be large enough to support the total load (dead and live load) at steady allowable stresses.

Reference to the chart of joint types and conditions and the table of allowable range of stress for the different categories (Fig. 26.41) will help make clear their use. Such reference also points up some of the new ideas introduced.

One new concept is that the fatigue allowable of a member, for example, a welded plate girder as shown by (2) in the chart (Fig. 26.41), is now determined by the allowable of the plate when connected by the fillet welds parallel to the direction of the applied stress. M and W are equal, and the applicable category is B, rather than the allowable of plate without welds, category A.

If stiffeners are used on the girder, as in (4), the fatigue allowable of the web or flange is determined by the allowable in the member at the termination of the weld or adjacent to the weld, category C or D, depending on the shear value in the web.

The fatigue allowable of a flange plate at the termination of a cover plate, either square or tapered end, is represented by (5). The applicable category is E. The same category also applies to a plate or cover plate adjacent to the termination of an intermittent fillet weld, as in (6) and (39).

Groove welds in butt joints of plate loaded transversely to the weld are shown in (8) to (14). In (15), the groove weld is parallel to the load. In (10), (13), (14), (15), and

TABLE 26.11 Permissible Stress of Weld[†]

Type of Weld Stress	Permissible Stress	Required Strength Level (1)(2)
COMPLETE PENETRATION GROOVE WELDS		
Tension normal to the effective throat.	Same as base metal.	Matching weld metal must be used. See Table below.
Compression normal to the effective throat.	Same as base metal.	Weld metal with a strength level equal to or one classification (10 ksi) less than matching weld metal may be used.
Tension or compression parallel to the axis of the weld.	Same as base metal.	Weld metal with a strength level equal to or less than matching weld metal may be used.
Shear on the effective throat.	.30 x Nominal Tensile strength of weld metal (ksi) except stress on base metal shall not exceed .40 x yield stress of base metal.	
PARTIAL PENETRATION GROOVE WELDS		
Compression normal to effective throat.	Designed not to bear — .50 x Nominal Tensile strength of weld metal (ksi) except stress on base metal shall not exceed .60 x yield stress of base metal. Designed to bear. Same as base metal.	Weld metal with a strength level equal to or less than matching weld metal may be used.
Tension or compression parallel to axis of the weld. (3)	Same as base metal.	
Shear parallel to axis of weld.	.30 x Nominal Tensile strength of weld metal (ksi) except stress on base metal shall not exceed .40 x yield stress of base metal.	
Tension normal to effective throat. (4)	.30 x Nominal Tensile strength of weld metal (ksi) except stress on base metal shall not exceed .60 x yield stress of base metal.	

FILLET WELDS (3)		
Stress on effective throat, regarless of direction of application of load.	.30 x Nominal Tensile strength of weld metal (ksi) except stress on base metal shall not exceed .40 x yield stress of base metal.	Weld metal with a strength level equal to or less than matching weld metal may be used.
Tension or compression parallel to axis of weld.	Same as base metal.	
PLUG AND SLOT WELDS		
Shear parallel to faying surfaces.	.30 x Nominal Tensile strength of weld metal (ksi) except stress on base metal shall not exceed .40 x yield stress of base metal.	Weld metal with a strength level equal to or less than matching weld metal may be used.

(1) For matching weld metal, see AISC Table 1.17.2 or AWS Table 4.1.1 or table below.
(2) Weld metal, one strength level (10 KSI) stronger than matching weld metal may be used when using alloy weld metal on A242 or A588 steel to match corrosion resistance or coloring characteristics (Note 3 of Table 4.1.4 or AWS D1.1).
(3) Fillet welds and partial penetration groove welds joining the component elements of built up members (ex. flange to web welds) may be designed without regard to the axial tensile or compressive stress applied to them.
(4) Cannot be used in tension normal to their axis under fatigue loading (AWS 2.5). AWS Bridge prohibits their use on any butt joint (9.12.1.1), or any splice in a tension or compression member (9.17), or splice in beams or girders (9.21), however, are allowed on corner joints parallel to axial force of components of built up members (9.12.1.2 (2). Cannot be used in girder splices (AISC 1.10.8).

MATCHING WELD METAL AND BASE METAL

Weld Metal	60 or 70	70	80	100	110
Type of Steel	A36; A53, Gr. B; A106, Gr. B; A131, Gr. A, B, C, CS, D, E; A139, Gr. B; A381, Gr. Y35; A500, Gr. A, B; A501; A516, Gr. 55, 60; A524, Gr. I, II; A529; A570, Gr. D, E; A573, Gr. 65; A709, Gr. 36; API 5L, Gr. B; API 5LX, Gr. 42; ABS, Gr. A, B, D, CS, DS, E	A131, Gr. AH32, DH32, EH32, AH36, DH36, EH36; A242; A441; A516, Gr. 65; 70; A537, Class 17; A572, Gr. 42, 45, 50, 55; A588 (4 in and under); A595, Gr. A, B, C; A606; A607, Gr. 45, 50, 55; A618; A633, Gr. A, B, C, D (2-1/2 in and under); A709, Gr. 50, 50W; API 2H; ABS Gr. AH32, DH32, EH32, AH36, DH36, EH36.	A572, Gr. 60, 65; A537, Class 2; A63, Gr. E	A514 [over 2-1/2 in (63 mm)]; A709, Gr. 100, 100W [2-1/2 to 4 in (63 to 102 mm)]	A514 [2-1/2 in (63 mm) and under]; A517; A709, Gr. 100, 100W [2-1/2 in (63 mm) and under]

†This table summarizes the AISC Specifications and the AWS Structural Welding Code ("Specification for the Design, Fabrication and Erection of Structural Steel for Buildings," American Institute of Steel Construction; AWS D.1-82, American Welding Society).

SOURCE: The James F. Lincoln Arc Welding Foundation, Cleveland, Ohio.

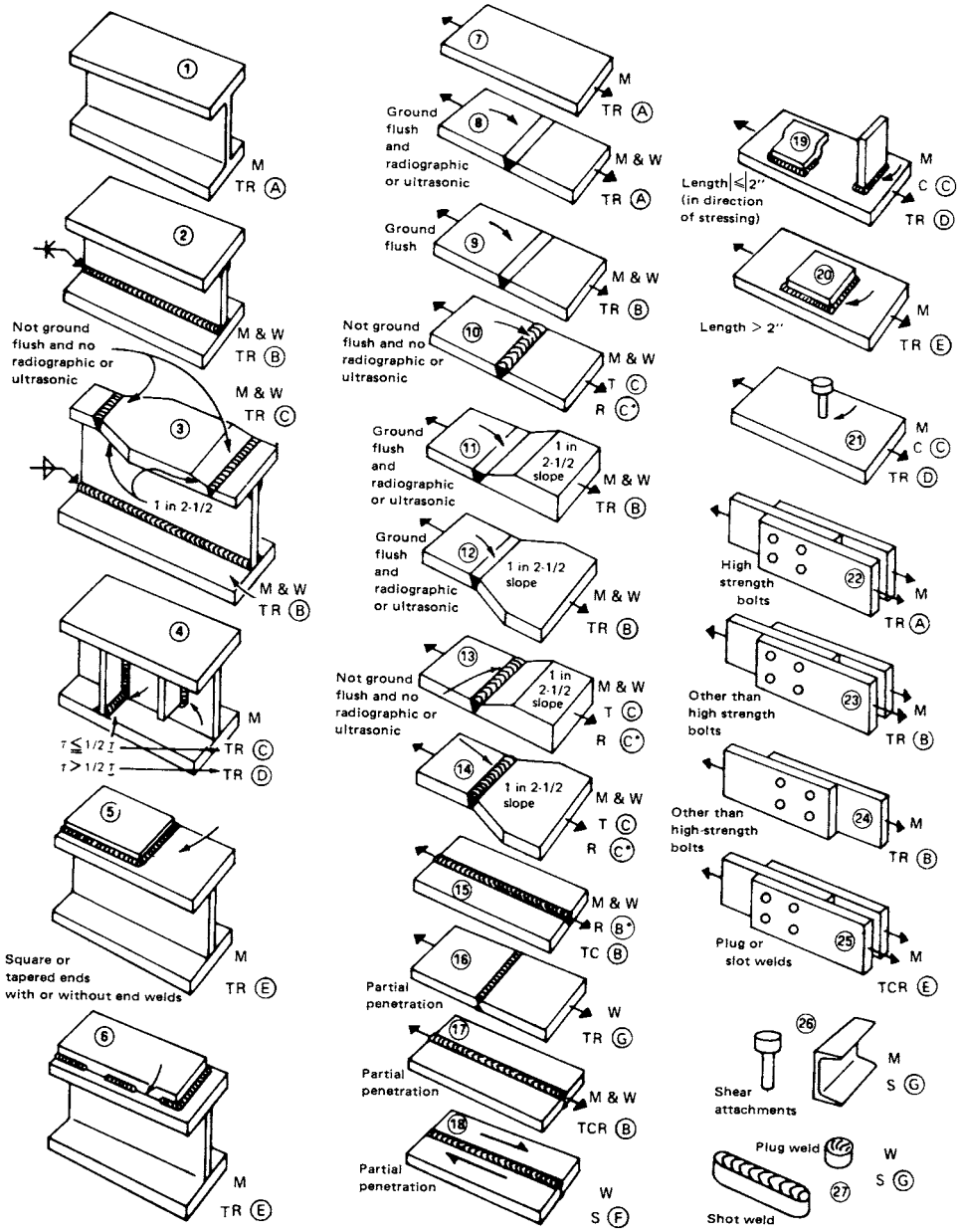

FIGURE 26.41 The AISC allowable range of stress σ_{sr} or τ_{sr}. *(The Lincoln Electric Company.)*

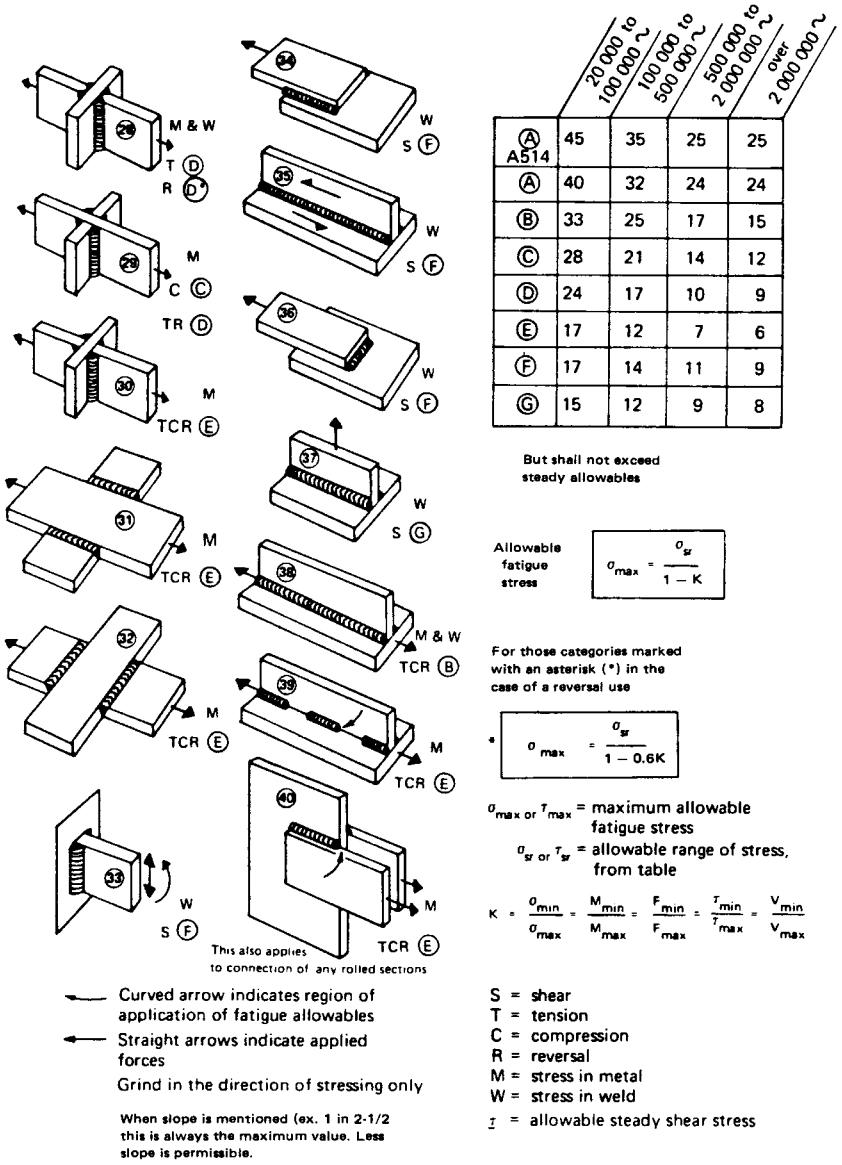

	20 000 to 100 000 ~	100 000 to 500 000 ~	500 000 to 2 000 000 ~	over 2 000 000 ~
Ⓐ A514	45	35	25	25
Ⓐ	40	32	24	24
Ⓑ	33	25	17	15
Ⓒ	28	21	14	12
Ⓓ	24	17	10	9
Ⓔ	17	12	7	6
Ⓕ	17	14	11	9
Ⓖ	15	12	9	8

But shall not exceed steady allowables

Allowable fatigue stress $\sigma_{max} = \dfrac{\sigma_{sr}}{1 - K}$

For those categories marked with an asterisk (*) in the case of a reversal use

* $\sigma_{max} = \dfrac{\sigma_{sr}}{1 - 0.6K}$

σ_{max} or τ_{max} = maximum allowable fatigue stress

σ_{sr} or τ_{sr} = allowable range of stress, from table

$K = \dfrac{\sigma_{min}}{\sigma_{max}} = \dfrac{M_{min}}{M_{max}} = \dfrac{F_{min}}{F_{max}} = \dfrac{\tau_{min}}{\tau_{max}} = \dfrac{V_{min}}{V_{max}}$

S = shear
T = tension
C = compression
R = reversal
M = stress in metal
W = stress in weld
τ = allowable steady shear stress

FIGURE 26.41 (*Continued*) The AISC allowable range of stress σ_{sr} or τ_{sr}. *(The Lincoln Electric Company.)*

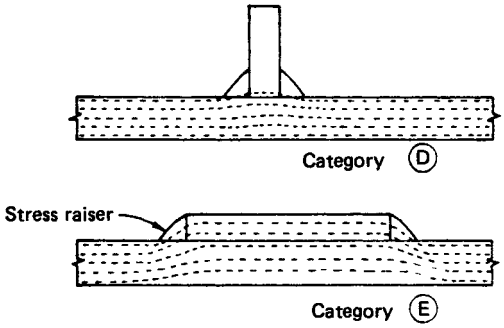

FIGURE 26.42 Note the decreased fatigue strength of the lower joint because of the stress raiser. *(The Lincoln Electric Company.)*

(28), an asterisk appears beside the category for reversal R of load. This means that a modified formula should be used for determining maximum fatigue stress:

$$\sigma_{\max} = \frac{\sigma_{sr}}{1 - 0.6K} \tag{26.6}$$

Using $0.6K$ provides a slight increase in fatigue allowable in the region of a complete reversal by changing the slope of the fatigue curve. The same butt joints used in a girder (3) do not show this increase in strength, and thus no asterisk appears beside R.

This approach gives, for the first time, fatigue allowables for partial-penetration groove welds, (16) to (18). Note by (19) and (20) that the fatigue allowable for a member with a transverse attachment is higher when the attachment is less than 2 in long, measured parallel to the axis of the load. Although there may be a similar geometric notch effect or abrupt change in section in both, it is the stress raiser that is

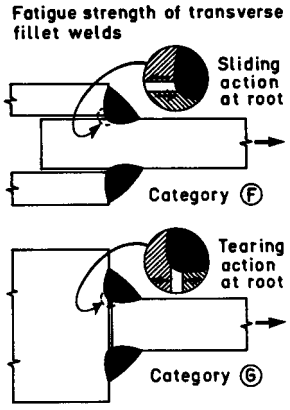

FIGURE 26.43 There is a greater tearing action at the root in category G, warranting a lower fatigue allowable. *(The Lincoln Electric Company.)*

WELDED CONNECTIONS

important. The transverse bar in (19) is so short as far as the axis of the member and load are concerned that very little of the force is able to swing up and into the bar and then back down again. Consequently, the stress raiser is not severe. The longer bar attachment in (20), however, is sufficiently long to provide a path for the force through it and the connecting welds. Because of this force transfer through the welds, there will be a higher stress raiser and, as a result, a reduction of the fatigue strength of the member. The difference is illustrated in Fig. 26.42.

Item (30) of the chart, which falls into category E, should not be confused with (37), category G. Both depict transverse fillet welds, but (30) provides a fatigue allowable for the member adjacent to the fillet weld, whereas (37) provides a fatigue shear allowable for the throat of the fillet weld.

Knowing that the steady strength of a transverse fillet is about a third stronger than that of a parallel fillet, one might question why the fatigue allowable for a parallel fillet, (34) and (35), category F, is the same as that for a transverse fillet (36) and higher than that for a transverse fillet (37), category G. The fatigue strength of the transverse fillet (36) is actually higher than that of a parallel fillet (34), but they both fall into the range covered by category F. However, there is a difference in the two transverse fillet welds in (36) and (37). In (36) there may be a slight stress raiser because of the pinching together of forces as they pass through the weld. But in (37) there is a greater tearing action at the root of the weld, thus producing a lower fatigue strength and warranting a lower fatigue allowable. This is illustrated by Fig. 26.43.

CHAPTER 27
FITS AND TOLERANCES

Joseph E. Shigley
Professor Emeritus
The University of Michigan
Ann Arbor, Michigan

Charles R. Mischke, Ph.D., P.E.
Professor Emeritus of Mechanical Engineering
Iowa State University
Ames, Iowa

NOMENCLATURE

a	Radius
B	Smallest bore diameter
b	Radius
c	Radius radial clearance
D	Diameter, mean of size range, largest journal diameter
E	Young's modulus
e	Bilateral tolerance expressing error
L	Upper or lower limit
p	Probability
p_f	Probability of failure
t	Bilateral tolerance of dimension
w	Left-tending vector representing gap
x	Right-tending dimensional vector magnitude
y	Left-tending dimensional vector magnitude
δ	Radial interference
υ	Poisson's ratio
σ	Normal stress
$\boldsymbol{\sigma}$	Standard deviation

27.1 INTRODUCTION

Standards of limits and fits for mating parts have been approved for general use in the United States for use with U.S. customary units [27.1] and for use with SI units [27.2]. The tables included in these standards are so lengthy that formulas are presented here instead of the tables to save space. As a result of rounding and other variations, the formulas are only close approximations. The nomenclature and symbols used in the two standards differ from each other, and so it is necessary to present the details of each standard separately.

27.2 METRIC STANDARDS

27.2.1 Definitions

Terms used are illustrated in Fig. 27.1 and are defined as follows:

1. *Basic size* is the size to which limits or deviations are assigned and is the same for both members of a fit. It is measured in millimeters.
2. *Deviation* is the algebraic difference between a size and the corresponding basic size.
3. *Upper deviation* is the algebraic difference between the maximum limit and the corresponding basic size.
4. *Lower deviation* is the algebraic difference between the minimum limit and the corresponding basic size.
5. *Fundamental deviation* is either the upper or the lower deviation, depending on which is closest to the basic size.
6. *Tolerance* is the difference between the maximum and minimum size limits of a part.
7. *International tolerance grade* (IT) is a group of tolerances which have the same relative level of accuracy but which vary depending on the basic size.
8. *Hole basis* represents a system of fits corresponding to a basic hole size.
9. *Shaft basis* represents a system of fits corresponding to a basic shaft size.

27.2.2 International Tolerance Grades

The *variation in part size,* also called the *magnitude of the tolerance zone,* is expressed in grade or IT numbers. Seven grade numbers are used for high-precision parts; these are

$$\text{IT01, IT0, IT1, IT2, IT3, IT4, IT5}$$

The most commonly used grade numbers are IT6 through IT16, and these are based on the Renard R5 geometric series of numbers. For these, the basic equation is

$$i = \frac{1}{1000}(0.45D^{1/3} + 0.001D) \tag{27.1}$$

FITS AND TOLERANCES

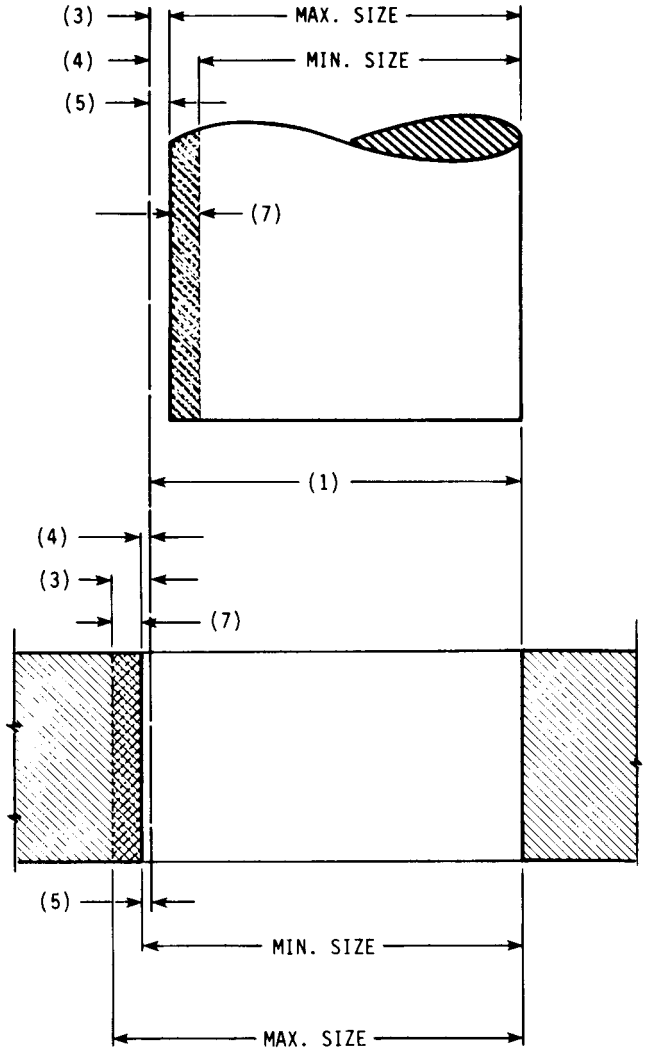

FIGURE 27.1 Definitions applied to a cylindrical fit. The numbers in parentheses are the definitions in Sec. 27.2.1.

where D is the geometric mean of the size range under consideration and is obtained from the formula

$$D = \sqrt{D_{\max} D_{\min}} \tag{27.2}$$

The ranges of basic sizes up to 1000 mm for use in this equation are shown in Table 27.1. For the first range, use $D_{\min} = 1$ mm in Eq. (27.2).

With D determined, tolerance grades IT5 through IT16 are found using Eq. (27.1) and Table 27.2. The grades IT01 to IT4 are computed using Table 27.3.

TABLE 27.1 Basic Size Ranges†

0–3	18–30	120–180	400–500
3–6	30–50	180–250	500–630
6–10	50–80	250–315	630–800
10–18	80–120	315–400	800–1000

†Sizes are for *over* the lower limit and *including* the upper limit (in millimeters).

TABLE 27.2 Formulas for Finding Tolerance Grades

Grade	Formula	Grade	Formula
IT5	$7i$	IT11	$100i$
IT6	$10i$	IT12	$160i$
IT7	$16i$	IT13	$250i$
IT8	$25i$	IT14	$400i$
IT9	$40i$	IT15	$640i$
IT10	$64i$	IT16	$1000i$

TABLE 27.3 Formulas for Higher-Precision Tolerance Grades

Grade	Formula
IT01	$(0.008D + 0.3)/1000$
IT0	$(0.012D + 0.5)/1000$
IT1	$(0.02D + 0.8)/1000$
IT2	$(IT1)[7i/(IT1)]^{1/4}$
IT3	$(IT2)^2$
IT4	$(IT2)^3$

27.2.3 Deviations

Fundamental deviations are expressed by *tolerance position letters* using capital letters for internal dimensions (holes) and lowercase letters for external dimensions (shafts). As shown by item 5 in Fig. 27.1, the fundamental deviation is used to position the tolerance zone relative to the basic size (item 1).

Figure 27.2 shows how the letters are combined with the tolerance grades to establish a fit. If the basic size for Fig. 27.2 is 25 mm, then the hole dimensions are defined by the ISO symbol

25D9

where the letter D establishes the fundamental deviation for the holes, and the number 9 defines the tolerance grade for the hole.

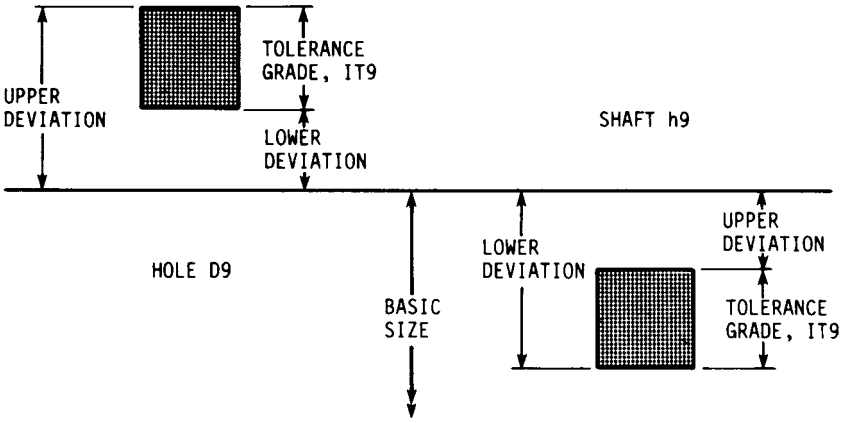

FIGURE 27.2 Illustration of a shaft-basis free-running fit. In this example the upper deviation for the shaft is actually zero, but it is shown as nonzero for illustrative purposes.

Similarly, the shaft dimensions are defined by the symbol

25h9

The formula for the fundamental deviation for shafts is

$$\text{Fundamental deviation} = \alpha + \frac{\beta D^{\gamma}}{1000} \tag{27.3}$$

where D is defined by Eq. (27.2), and the three coefficients are obtained from Table 27.4.

Shaft Deviations. For shafts designated a through h, the upper deviation is equal to the fundamental deviation. Subtract the IT grade from the fundamental deviation to get the lower deviation. Remember, the deviations are defined as algebraic, so be careful with signs.

Shafts designated j through zc have the lower deviation equal to the fundamental deviation. For these, the upper deviation is the sum of the IT grade and the fundamental deviation.

Hole Deviations. Holes designated A through H have a lower deviation equal to the negative of the upper deviation for shafts. Holes designated as J through ZC have an upper deviation equal to the negative of the lower deviation for shafts.

An exception to the rule occurs for a hole designated as N having an IT grade from 9 to 16 inclusive and a size over 3 mm. For these, the fundamental deviation is zero.

A second exception occurs for holes J, K, M, and N up to grade IT8 inclusive and holes P through ZC up to grade 7 inclusive for sizes over 3 mm. For these, the upper deviation of the hole is equal to the negative of the lower deviation of the shaft plus the change in tolerance of that grade and the next finer grade. In equation form, this can be written

Upper deviation (hole)

$$= -\text{lower deviation (shaft)} + \text{IT (shaft)} - \text{IT (next finer shaft)} \tag{27.4}$$

TABLE 27.4 Coefficients for Use in Eq. (27.3) to Compute the Fundamental Deviations for Shafts†

Fundamental deviation	α	β	γ	Notes
a	−0.265	−1.3	1	$D \leq 120$
	0	−3.5	1	$D > 120$
b	−0.140	−0.85	1	$D \leq 160$
	0	−1.8	1	$D > 160$
c	0	−5.2	0.2	$D \leq 40$
	−0.095	−0.8	1	$D > 40$
cd				$cd = (c \cdot d)^{1/2}$
d	0	−16	0.44	
e	0	−11	0.41	
ef				$ef = (e \cdot f)^{1/2}$
f	0	−5.5	0.41	
fg				$fg = (f \cdot g)^{1/2}$
g	0	−2.5	0.34	
h	0	0	0	
j				No formula
js				js = IT/2
k	0	0.6	0.33	IT4 to IT7, $D \leq 500$
	0	0	0	IT8 to IT16, $D > 500$
m	IT7/1000	−IT6	0	$D \leq 500$
	0.013	0.024	1	$D > 500$
n	0	5	0.34	$D \leq 500$
	0.021	0.04	1	$D > 500$
p	IT7	2	0	$D \leq 500$
	0.038	0.072	D	$D > 500$
r				$r = (p \cdot s)^{1/2}$
s	IT8	2	0	$D \leq 50$
	IT7	0.4	1	$D > 50$
t	IT7	0.63	1	
u	IT7	1	1	
v	IT7	1.25	1	
x	IT7	1.6	1	
y	IT7	2	1	
z	IT7	2.5	1	
za	IT8	3.15	1	
zb	IT9	4	1	
zc	IT10	5	1	

†These coefficients will give results that may not conform exactly to the fundamental deviations tabulated in the standards. Use the standards if exact conformance is required.

SOURCE: From Ref. [27.2].

TABLE 27.5 Preferred Fits

Type	Hole basis	Shaft basis†	Name and application
Clearance	H11/c11	C11/h11	*Loose-running fit* for wide commercial tolerances or allowances on external members
	H9/d9	D9/h9	*Free-running fit* not for use where accuracy is essential, but good for large temperature variations, high running speeds, or heavy journal pressures
	H8/f7	F8/h7	*Close-running fit* for running on accurate machines and for accurate location at moderate speeds and journal pressures
	H7/g6	G7/h6	*Sliding fit* not intended to run freely, but to move and turn freely and locate accurately
	H7/h6	H7/h6	*Locational-clearance fit* provides snug fit for locating stationary parts, but can be freely assembled and disassembled
Transition	H7/k6	K7/h6	*Locational-transition fit* for accurate location, a compromise between clearance and interference
	H7/n6	N7/h6	*Locational-transition fit* for more accurate location where greater interference is permissible
Interference	H7/p6	P7/h6	*Locational-interference fit* for parts requiring rigidity and alignment with prime accuracy of location but without special bore pressure requirements
	H7/s6	S7/h6	*Medium-drive fit* for ordinary steel parts or shrink fits on light sections, the tightest fit usable with cast iron
	H7/u6	U7/h6	*Force fit* suitable for parts which can be highly stressed or for shrink fits where the heavy pressing forces required are impracticable

†The transition and interference shaft-basis fits shown do not convert to exactly the same hole-basis fit conditions for basic sizes from 0 to 3 mm. Interference fit P7/h6 converts to a transition fit H7/p6 in the size range 0 to 3 mm.

SOURCE: From Ref. [27.2].

27.2.4 Preferred Fits

Table 27.5 lists the preferred fits for most common applications. Either first or second choices from Table 27.3 should be used for the basic sizes.

Example 1. Using the shaft-basis system, find the limits for both members using a basic size of 25 mm and a free-running fit.

Solution. From Table 27.5, we find the fit symbol as D9/h9, the same as Fig. 27.2. Table 27.1 gives $D_{\min} = 18$ and $D_{\max} = 30$ for a basic size of 25. Using Eq. (27.2), we find

$$D = \sqrt{D_{\max} D_{\min}} = \sqrt{30(18)} = 23.2 \text{ mm}$$

Then, from Eq. (27.1) and Table 27.2,

$$40i = \frac{40}{1000}(0.45D^{1/3} + 0.001D)$$

$$= \frac{40}{1000}[0.45(23.2)^{1/3} + 0.001(23.2)] = 0.052 \text{ mm}$$

This is the IT9 tolerance grade for the size range 18 to 30 mm.

We proceed next to find the limits on the 25D9 hole. From Table 27.4, for a d shaft, we find $\alpha = 0$, $\beta = -16$, and $\gamma = 0.44$. Therefore, using Eq. (19.3), we find the fundamental deviation for a d shaft to be

$$\text{Fundamental deviation} = \alpha + \frac{\beta D^{\gamma}}{1000} = 0 + \frac{-16(23.2)^{0.44}}{1000}$$

$$= -0.064 \text{ mm}$$

But this is also the upper deviation for a d shaft. Therefore, for a D hole, we have

$$\text{Lower deviation (hole)} = -\text{upper deviation (shaft)}$$

$$= -(-0.064) = 0.064 \text{ mm}$$

The upper deviation for the hole is the sum of the lower deviation and the IT grade. Thus

$$\text{Upper deviation (hole)} = 0.064 + 0.052 = 0.116 \text{ mm}$$

The two limits of the hole dimensions are therefore

$$\text{Upper limit} = 25 + 0.116 = 25.116 \text{ mm}$$

$$\text{Lower limit} = 25 + 0.064 = 25.064 \text{ mm}$$

For the h shaft, we find from Table 19.4 that $\alpha = \beta = \gamma = 0$. Therefore, the fundamental deviation, which is the same as the upper deviation, is zero. The lower deviation equals the upper deviation minus the tolerance grade, or

$$\text{Lower deviation (shaft)} = 0 - 0.052 = -0.052 \text{ mm}$$

Therefore, the shaft limits are

$$\text{Upper limit} = 25 + 0 = 25.000 \text{ mm}$$

$$\text{Lower limit} = 25 - 0.052 = 24.948 \text{ mm}$$

27.3 U.S. STANDARD—INCH UNITS

The fits described in this section are all on a *unilateral hole basis.* The kind of fit obtained for any one class will be similar throughout the range of sizes. Table 27.6 describes the various fit designations. Three classes, RC9, LC10, and LC11, are described in the standards [27.1] but are not included here. These standards include recommendations for fits up to a basic size of 200 in. However, the tables included here are valid only for sizes up to 19.69 in; this is in accordance with the American-British-Canadian (ABC) recommendations.

The coefficients listed in Table 27.7 are to be used in the equation

$$L = CD^{1/3} \tag{27.5}$$

where L is the limit in thousandths of an inch corresponding to the coefficient C and the basic size D in inches. The resulting four values of L are then summed algebraically to the basic hole size to obtain the four limiting dimensions.

It is emphasized again that the limits obtained by the use of these equations and tables are only close approximations to the standards.

27.4 INTERFERENCE-FIT STRESSES

The assembly of two cylindrical parts by press-fitting or shrinking one member onto another creates a contact pressure between the two members. The stresses resulting from the interference fit can be computed when the contact pressure is known. This pressure may be obtained from Eq. (2.67) of Ref. [27.3]. The result is

$$p = \frac{\delta}{bA} \tag{27.6}$$

where δ = radial interference and A is given by

$$A = \frac{1}{E_i}\left(\frac{b^2 + a^2}{b^2 - a^2} - \nu_i\right) + \frac{1}{E_o}\left(\frac{c^2 + b^2}{c^2 - b^2} + \nu_o\right) \tag{27.7}$$

The dimensions a, b, and c are the radii of the members, as shown in Fig. 27.3. The terms E_i and E_o are the elastic moduli for the inner and outer cylinders, respectively. If the inner cylinder is solid, then $a = 0$ and Eq. (27.7) becomes

$$A = \frac{1}{E_i}(1 - \nu_i) + \frac{1}{E_o}\left(\frac{c^2 + b^2}{c^2 - b^2} + \nu_o\right) \tag{27.8}$$

Sometimes the mating parts have identical moduli. In this case, Eq. (27.6) becomes

$$p = \frac{E\delta}{b}\left[\frac{(c^2 - b^2)(b^2 - a^2)}{2b^2(c^2 - a^2)}\right] \tag{27.9}$$

This equation simplifies still more if the inner cylinder is solid. We then have

$$p = \frac{E\delta}{2bc^2}(c^2 - b^2) \tag{27.10}$$

TABLE 27.6 Standard Fits

Designation	Name and application
RC1	*Close sliding fits* are intended for the accurate location of parts which must be assembled without perceptible play.
RC2	*Sliding fits* are intended for accurate location, but with greater maximum clearance than an RC1 fit.
RC3	*Precision running fits* are about the loosest fits which can be expected to run freely and are intended for precision work at slow speeds and light journal pressures but are not suitable where appreciable temperature differences are likely.
RC4	*Close-running fits* are intended chiefly for running fits on accurate machinery with moderate surface speeds and journal pressure, where accurate location and minimum play are desired.
RC5	*Medium-running fits* are intended for higher running speeds or heavy journal pressures, or both.
RC6	*Medium-running fits* are intended for applications where more play than RC5 is required.
RC7	*Free-running fits* are intended for use where accuracy is not essential or where large temperature variations are likely, or both.
RC8	*Loose-running fits* are intended for use where wide commercial tolerances may be necessary, together with an allowance, on the hole.
LC1 to LC9	*Locational-clearance fits* are intended for parts which are normally stationary, but which can be freely assembled or disassembled. Snug fits are for parts requiring accuracy of location. Medium fits are for parts such as ball, race, and housings. The looser fastener fits are needed where freedom of assembly is of first importance.
LT1 to LT6	*Locational-transitional fits* are a compromise between clearance and interference fits for application where accuracy of location is important but either a small amount of clearance or interference is permissible.
LN1 to LN3	*Locational-interference fits* are used where accuracy of location is of prime importance and for parts requiring rigidity and alignment with no special requirements for bore pressure. These fits are not intended for parts that must transmit frictional loads to one another.
FN1	*Light-drive fits* are those requiring light assembly pressures and produce more or less permanent assemblies. They are suitable for thin sections or long fits or in cast-iron external members.
FN2	*Medium-drive fits* are suitable for ordinary steel parts or for shrink fits on light sections. They are about the tightest fits that can be used with high-grade cast-iron external members.
FN3	*Heavy-drive fits* are suitable for heavier steel parts or for shrink fits in medium sections.
FN4 and FN5	*Force fits* are suitable for parts which can be highly stressed or for shrink fits where the heavy pressing forces required are impractical.

The maximum stresses occur at the contact surface. Here the stresses are biaxial, if the longitudinal direction is neglected, and for the outer member are given in Ref. [27.3] as

$$\sigma_{ot} = p\,\frac{c^2 + b^2}{c^2 - b^2} \qquad \sigma_{or} = -p \tag{27.11}$$

TABLE 27.7 Coefficients C for Use in Eq. (27.5)

	Hole limits		Shaft limits	
Class of fit	Lower	Upper	Lower	Upper
RC1	0	+0.392	−0.588	−0.308
RC2	0	+0.571	−0.700	−0.308
RC3	0	+0.907	−1.542	−0.971
RC4	0	+1.413	−1.879	−0.971
RC5	0	+1.413	−2.840	−1.932
RC6	0	+2.278	−3.345	−1.932
RC7	0	+2.278	−4.631	−3.218
RC8	0	+3.570	−7.531	−5.253
LC1	0	+0.571	−0.392	0
LC2	0	+0.907	−0.571	0
LC3	0	+1.413	−0.907	0
LC4	0	+3.570	−2.278	0
LC5	0	+0.907	−0.879	−0.308
LC6	0	+2.278	−2.384	−0.971
LC7	0	+3.570	−4.211	−1.933
LC8	0	+3.570	−5.496	−3.218
LC9	0	+5.697	−8.823	−5.253
LT1	0	+0.907	−0.281	+0.290
LT2	0	+1.413	−0.442	+0.465
LT3†	0	+0.907	+0.083	+0.654
LT4†	0	+1.413	+0.083	+0.990
LT5	0	+0.907	+0.656	+1.227
LT6	0	+0.907	+0.656	+1.563
LN1	0	+0.571	+0.656	+1.048
LN2	0	+0.907	+0.994	+1.565
LN3	0	+0.907	+1.582	+2.153
FN1	0	+0.571	+1.660	+2.052
FN2	0	+0.907	+2.717	+3.288
FN3‡	0	+0.907	+3.739	+4.310
FN4	0	+0.907	+5.440	+6.011
FN5	0	+1.413	+7.701	+8.608

†Not for sizes under 0.24 in.
‡Not for sizes under 0.95 in.

where t and r designate the tangential and radial directions, respectively.

For the inner member, the stresses at the contact surface are

$$\sigma_{it} = -p\,\frac{b^2 + a^2}{b^2 - a^2} \qquad \sigma_{ir} = -p \tag{27.12}$$

A stress-concentration factor may be needed for certain situations. A hub press-fitted to a shaft, for example, would be likely to have an increased pressure at the ends. So if either a brittle fracture or a fatigue failure is a possibility, then for such cases a stress-concentration factor in the range from 1.5 to 2 should be used.

Example 2. A 1½-in solid-steel shaft is fitted to a steel forging having an outside diameter of 2½ in using a class FN3 fit. Determine the worst-condition stresses for each member.

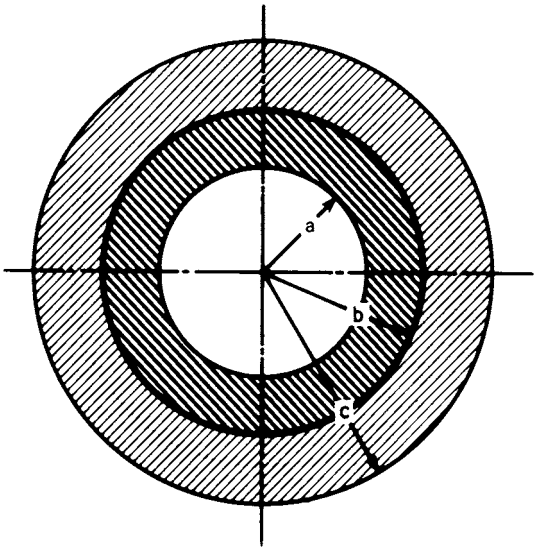

FIGURE 27.3 A press-fitted assembly. Inner member has hole of radius *a*. Contact surface has radius *b*. Outer member has outside radius *c*.

Solution. The worst condition would occur when the hole is minimum and the shaft is maximum. From Table 27.7, we find $C = 0$ and $C = +4.310$ for the lower limit of the hole and upper limit of the shaft, respectively. Using Eq. (27.5), we find

$$L = CD^{1/3} = \frac{+4.310(1.5)^{1/3}}{1000} = 0.0049 \text{ in}$$

Therefore, the maximum shaft has a diameter $d_i = 1.5 + 0.0049 = 1.5049$ in. Similarly, the minimum hole is $d_o = 1.5000$ in. The radial interference is $\delta = 0.5(0.0049) = 0.00245$ in. For use in Eq. (27.10), we observe that $b = 0.75$ in and $c = 1.25$ in based on the nominal dimensions. Using $E = 30$ Mpsi, we find the contact pressure to be

$$p = \frac{E\delta}{bc^2}(c^2 - b^2)$$

$$= \frac{30(10)^6(0.00245)}{0.75(1.25)^2}[(1.25)^2 - (0.75)^2]$$

$$= 62.7 \text{ kpsi}$$

Using Eq. (27.11) to get the stresses in the outer member gives

$$\sigma_{ot} = p\frac{c^2 + b^2}{c^2 - b^2} = 62.7\left[\frac{(1.25)^2 + (0.75)^2}{(1.25)^2 - (0.75)^2}\right] = 133.2 \text{ kpsi}$$

$$\sigma_{or} = -p = -62.7 \text{ kpsi}$$

For the inner member, the worst stress is given by

$$\sigma_{it} = \frac{-pb^2}{b^2 - a^2} = -p = -62.7 \text{ kpsi}$$

and the result is

$$\sigma_{ir} = \sigma_{it} = -62.7 \text{ kpsi}$$

27.5 ABSOLUTE TOLERANCES†

When an aggregate of several parts is assembled, the gap, grip, or interference is related to dimensions and tolerances of the individual parts. Consider an array of parallel vectors as depicted in Fig. 27.4, the x's directed to the right and the y's directed to the left. They may be treated as scalars and represented algebraically. Let t_i be the bilateral tolerance on $\bar{x}_i$ and t_j be the bilateral tolerance on $\bar{y}_j$, all being positive numbers. The gap remaining short of closure is called w and may be viewed as the slack variable permitting summation to zero. Thus,

$$(x_1 + x_3 + \cdots) - (y_2 + y_4 + \cdots) - w = 0$$

or

$$w = \Sigma x_i - \Sigma y_j \tag{27.13}$$

The largest gap w exists when the right-tending vectors are the largest possible and the left-tending vectors are the smallest possible. Expressing Eq. (19.13) in terms of the greatest deviations from the means gives

$$w_{\max} = \Sigma(\bar{x}_i + t_i) - \Sigma(\bar{y}_j - t_j) = \Sigma\bar{x}_i - \Sigma\bar{y}_j + \sum_{\text{all}} t \tag{27.14}$$

† See Ref. [27.4].

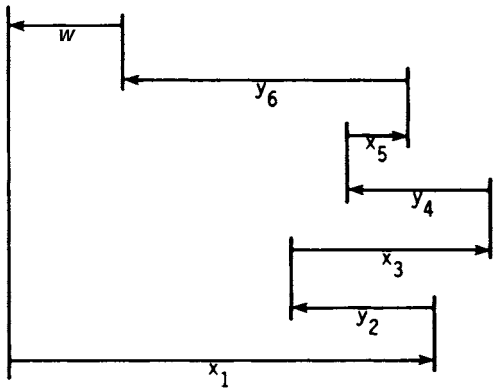

FIGURE 27.4 An array of parallel vectors.

Similarly, for the smallest gap,

$$w_{\min} = \Sigma(\bar{x}_i - t_i) - \Sigma(\bar{y}_j + t_j) = \Sigma\bar{x}_i - \Sigma\bar{y}_j - \sum_{\text{all}} t \tag{27.15}$$

The mean of w is

$$\bar{w} = \frac{1}{2}(z_{\max} + z_{\min}) = \frac{1}{2}[(\Sigma\bar{x}_i - \Sigma\bar{y}_j + \Sigma t) + (\Sigma\bar{x}_i - \Sigma\bar{y}_j - \Sigma t)] \tag{27.16}$$

$$\bar{w} = \Sigma\bar{x}_i - \Sigma\bar{y}_j$$

The bilateral tolerance of w is

$$t_w = \frac{1}{2}(w_{\max} - w_{\min}) = \frac{1}{2}[(\Sigma\bar{x}_i - \Sigma\bar{y}_j + \Sigma t) - (\Sigma\bar{x}_i - \Sigma\bar{y}_j - \Sigma t)] \tag{27.17}$$

$$t_w = \sum_{\text{all}} t$$

Equation (27.15) gives rise to expressions such as "the stacking of tolerances" in describing the conditions at the gap. All the bilateral tolerances of the constituent x's and y's add to the tolerance of the gap. If the gap is an interference, then w is a right-tending vector (negative). For all instances to be interference fits, both $w_{\max}$ and $w_{\min}$ have to be negative.

Example 3. In the pin-washer-sleeve–snap-ring assembly depicted in Fig. 27.5, identify the mean gap $\bar{w}$, gap tolerance t_w, maximum gap $w_{\max}$, and minimum gap $w_{\min}$ if $x_1 = 1.385 \pm 0.005$, $y_2 = 0.125 \pm 0.001$, $y_3 = 1.000 \pm 0.002$, and $y_4 = 0.250 \pm 0.001$ in.

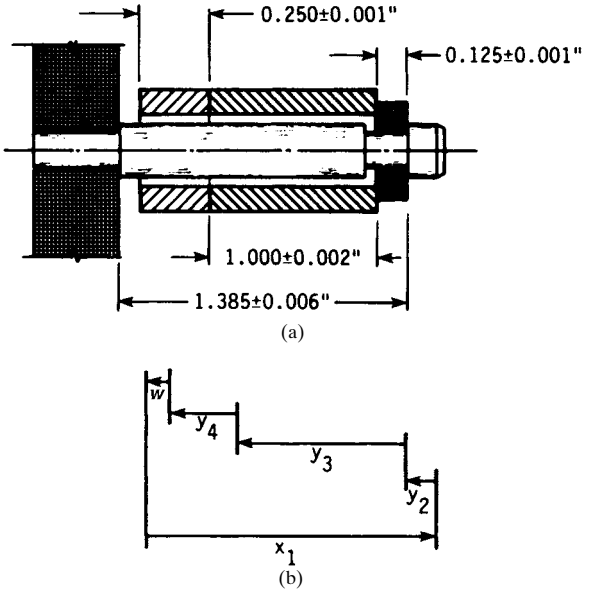

FIGURE 27.5 (*a*) A pin-washer–snap-ring assembly and associated gap; (*b*) parallel vectors describing gap.

Solution. From Eq. (27.16),

$$\overline{w} = \Sigma x_i - \Sigma y_j = 1.385 - 0.125 - 1.000 - 0.250 = 0.010 \text{ in}$$

From Eq. (27.17), $t_w = \sum_{\text{all}} t = 0.005 + 0.001 + 0.002 + 0.001 = 0.009$ in

From Eq. (27.14), $w_{\max} = \overline{w} + t_w = 0.010 + 0.009 = 0.019$ in

From Eq. (27.15), $w_{\min} = \overline{w} - t_w = 0.010 - 0.009 = 0.001$ in

All instances of the gap w are positive, and therefore noninterfering.

Example 4. In Example 3, the washer, sleeve, and snap ring are vendor-supplied parts, and the pin is machined in-house. To assure a noninterfering assembly, what should the pin tolerance t_1 be?

Solution. From Eq. (27.16),

$$\overline{w} = \Sigma x_i - \Sigma y_j = 1.385 - 0.125 - 1.000 - 0.250 = 0.010 \text{ in}$$

From Eq. (27.17), $t_w = \sum_{\text{all}} t = t_1 + 0.001 + 0.002 + 0.001 = t_1 + 0.004$

$$t_1 = t_w - 0.004$$

As long as $t_w \le \overline{w}$—that is, $t_w \le 0.010$ in—there will be a gap.

$$t_w = t_1 + 0.004 \le 0.010$$

$$t_1 \le 0.006 \text{ in}$$

If t_1 cannot be economically maintained at 0.006 or less, but may be 0.007 in or more, then there will be instances of interference, unless

1. Vendors can reduce the tolerance on the washer, spacer, and snap ring.
2. Inspection and selective assembly are acceptable.
3. Some interference, when detected, is solved by selective assembly for some parts, or scrapping.

Important to alternatives 2 and 3 is a prediction of the chance of encountering an interference fit.

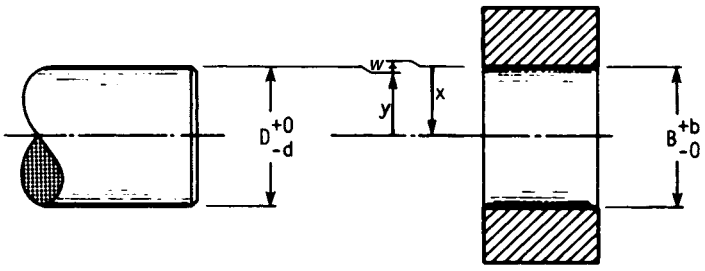

FIGURE 27.6 A journal-bushing assembly with unilateral tolerances.

TABLE 27.8 Absolute Tolerance Worksheet

i	t	x_i	y_i
1	0.006	1.385	
2	0.001		0.125
3	0.002		1.000
4	0.001		0.250
	$\Sigma = 0.010$	1.385	1.375
		−1.375	
		$\bar{w} = 0.010$	

Example 5. Figure 27.6 shows a journal-bushing assembly with unilateral tolerances. What is the description of the radial clearances resulting from these specifications?

Solution. From Eq. (27.14),

$$\bar{w} = \bar{c} = \Sigma x_i - \Sigma y_j = \left(\frac{B}{2} + \frac{b}{4}\right) - \left(\frac{D}{2} + \frac{d}{4}\right)$$

$$= \frac{B - D}{2} + \frac{b + d}{4} \tag{27.18}$$

From Eq. (27.17), $$t_w = \sum_{\text{all}} t = \frac{b}{4} + \frac{d}{4} \tag{27.19}$$

From Eq. (27.14), $$w_{\max} = c_{\max} = \bar{w} + t_w = \left(\frac{B - D}{2} + \frac{b + d}{4}\right)$$

$$+ \frac{b + d}{4} = \frac{B - D}{2} + \frac{b + d}{2} \tag{27.20}$$

From Eq. (27.15), $$w_{\min} = c_{\min} = \bar{w} - t_w = \left(\frac{B - D}{2} + \frac{b + d}{4}\right)$$

$$- \frac{b + d}{4} = \frac{B - D}{2} \tag{27.21}$$

Table 27.8 is an absolute tolerance worksheet, a convenient nonalgebraic form suitable to the manufacturing floor.

REFERENCES

27.1 "Preferred Limits and Fits for Cylindrical Parts," ANSI B4.1-1967 (R1999).†

27.2 "Preferred Metric Limits and Fits," ANSI B4.2-1978 (R1999).

† The symbol R indicates that the standard has been reaffirmed as up-to-date.

27.3 Joseph E. Shigley and Charles R. Mischke, *Mechanical Engineering Design,* 5th ed., McGraw-Hill, New York, 1989.

27.4 M. F. Spotts, *Dimensioning and Tolerancing for Quality Production,* Prentice-Hall, Englewood Cliffs, N.J., 1983. (Excellent bibliography on standards and handbooks, dimensioning and tolerancing, quality control, gauging and shop practice, probability and statistics.)

P · A · R · T · 7

LOAD CAPABILITY CONSIDERATIONS

CHAPTER 28
STRENGTH UNDER STATIC CIRCUMSTANCES

Charles R. Mischke, Ph.D., P.E.
Professor Emeritus of Mechanical Engineering
Iowa State University
Ames, Iowa

Joseph E. Shigley
Professor Emeritus
The University of Michigan
Ann Arbor, Michigan

GLOSSARY OF SYMBOLS

a	Crack semilength
A	Area
D, d	Diameter
F	Force or load
I	Second moment of area
J	Second polar moment of area
K	Stress-intensity factor
K'	Stress-concentration factor for static loading
K_c	Critical-stress-intensity factor
K_t	Normal-stress-concentration factor
K_{ts}	Shear-stress-concentration factor
M	Moment
n	Design factor
q_s	Sensitivity index

r	Radius or ratio
S_{sy}	Yield strength in shear
S_{uc}	Ultimate compressive strength
S_{ut}	Ultimate tensile strength
S_y	Yield strength
η	Factor of safety
σ	Normal stress
σ'	von Mises stress
τ	Shear stress
τ_o	Octahedral shear stress or nominal shear stress

28.1 PERMISSIBLE STRESSES AND STRAINS

The discovery of the relationship between stress and strain during elastic and plastic deformation allows interpretation either as a stress problem or as a strain problem. Imposed conditions on machine elements are more often loads than deformations, and so the usual focus is on stress rather than strain. Consequently, when durability under static conditions is addressed, attention to permissible stress is more common than attention to permissible strain.

Permissible stress levels are established by

- Experience with successful machine elements
- Laboratory simulations of field conditions
- Corporate experience manifested as a design-manual edict
- Codes, standards, and state of the art

During the design process, permissible stress levels are established by dividing the significant strength by a *design factor n.* The design factor represents the original intent or goal. As decisions involving discrete sizes are made, the stress levels depart from those intended. The quotient, obtained by dividing the significant strength by the load-induced stress at the critical location, is the *factor of safety* η, which is unique to the completed design. The design factor represents the goal and the factor of safety represents attainment. The adequacy assessment of a design includes examination of the factor of safety. Finding a permissible stress level which will provide satisfactory service is not difficult. Competition forces a search for the highest stress level which still permits satisfactory service. This is more difficult.

Permissible stress level is a function of material strength, which is assessible only by test. Testing is costly. Where there is neither time nor money available or testing the part is impossible, investigators have proposed theories of failure for guidance of designers. Use of a theory of failure involves (1) identifying the significant stress at the critical location and (2) comparing that stress condition with the strength of the part at that location in the condition and geometry of use. Standardized tests, such as the simple tension test, Jominy test, and others, provide some of the necessary information. For example, initiation of general yielding in a ductile part is predicted on the basis of yield strength exhibited in the simple tension test and modified by the manufacturing process. Rupture of brittle parts is predicted on the basis of ultimate strength (see Chap. 33).

STRENGTH UNDER STATIC CIRCUMSTANCES

Estimates of permissible stress level for long and satisfactory performance of function as listed above are based on design factors reflecting these experiences and are modified by the following:

1. Uncertainty as to material properties within a part, within a bar of steel stock, and within a heat of steel or whatever material is being considered for the design. Properties used by a designer may come not from an actual test, but from historical experience, since parts are sometimes designed before the material from which they will be made has even been produced.

2. Uncertainty owing to the discrepancy between the designed part and the necessarily small size of the test specimen. The influence of size on strength is such that smaller parts *tend* to exhibit larger strengths.

3. Uncertainty concerning the actual effects of the manufacturing process on the local material properties at the critical locations in the part. Processes such as upsetting, cold or hot forming, heat treatment, and surface treatment change strengths and other properties.

4. Uncertainties as to the true effect of peripheral assembly operations on strengths and other properties. Nearby weldments, mechanical fasteners, shrink fits, etc., all have influences that are difficult to predict with any precision.

5. Uncertainty as to the effect of elapsed time on properties. Aging in steels, aluminums, and other alloys occurs, and some strengthening mechanisms are time-dependent. Corrosion is another time-dependent enemy of integrity.

6. Uncertainty as to the actual operating environment.

7. Uncertainty as to the validity and precision of the mathematical models employed in reaching decisions on the geometric specifications of a part.

8. Uncertainty as to the intensity and dispersion of loads that may or will be imposed on a machine member and as to the understanding of the effect of impact.

9. Uncertainty as to the stress concentrations actually present in a manufactured part picked at random for assembly and use. Changes in tool radius due to wear, regrinding, or replacement can have a significant influence on the stress levels actually attained in parts in service.

10. Company design policies or the dictates of codes.

11. Uncertainty as to the completeness of a list of uncertainties.

Although specific recommendations that suggest design factors qualified by usage are to be found in many places, such factors depend on the stochastic nature of properties, loading, geometry, the form of functional relationships between them, and the reliability goal.

28.2 THEORY OF STATIC FAILURE

For ductile materials, the best estimation method for predicting the onset of yielding, for materials exhibiting equal strengths in tension and compression, is the octahedral shear theory (distortion energy or Hencky-von Mises). The *octahedral shear stress* is

$$\tau_o = \tfrac{1}{3}[(\sigma_1 - \sigma_2)^2 + (\sigma_2 - \sigma_3)^2 + (\sigma_3 - \sigma_1)^2]^{1/2}$$

where σ_1, σ_2, and σ_3 are ordered principal stresses (see Chap. 36). In terms of orthogonal stress components in any other directions, the octahedral shear stress is

$$\tau_o = \tfrac{1}{3}\left[(\sigma_x - \sigma_y)^2 + (\sigma_y - \sigma_z)^2 + (\sigma_z - \sigma_x)^2 + 6(\tau_{xy}^2 + \tau_{yz}^2 + \tau_{zx}^2)\right]^{1/2}$$

The limiting value of the octahedral shear stress is that which occurs during uniaxial tension at the onset of yield. This limiting value is

$$\tau_o = \frac{\sqrt{2}S_y}{3}$$

By expressing this in terms of the principal stresses and a design factor, we have

$$\frac{S_y}{n} = \frac{3}{\sqrt{2}}\,[\tau_o]_{\text{lim}} = \frac{1}{\sqrt{2}}\left[(\sigma_1 - \sigma_2)^2 + (\sigma_2 - \sigma_3)^2 + (\sigma_3 - \sigma_1)^2\right]^{1/2} = \sigma' \qquad (28.1)$$

The term σ' is called the *von Mises stress.* It is the uniaxial tensile stress that induces the same octahedral shear (or distortion energy) in the uniaxial tension test specimen as does the triaxial stress state in the actual part.

For plane stress, one principal stress is zero. If the larger nonzero principal stress is σ_A and the smaller σ_B, then

$$\sigma' = (\sigma_A^2 + \sigma_B^2 - \sigma_A\sigma_B)^{1/2} = \frac{S_y}{n} \qquad (28.2)$$

By substituting the relation

$$\sigma_{A,B} = \frac{\sigma_x - \sigma_y}{2} \pm \sqrt{\left(\frac{\sigma_x - \sigma_y}{2}\right)^2 + \tau_{xy}^2}$$

we get a more convenient form:

$$\sigma' = (\sigma_x^2 + \sigma_y^2 - \sigma_x\sigma_y + 3\tau_{xy}^2)^{1/2} = \frac{S_y}{n} \qquad (28.3)$$

Example 1. A thin-walled pressure cylinder has a tangential stress of σ and a longitudinal stress of $\sigma/2$. What is the permissible tangential stress for a design factor of n?

Solution

$$\sigma' = (\sigma_A^2 + \sigma_B^2 - \sigma_A\sigma_B)^{1/2}$$

$$= \left[\sigma^2 + \left(\frac{\sigma}{2}\right)^2 - \sigma\left(\frac{\sigma}{2}\right)\right]^{1/2} = \frac{S_y}{n}$$

From which

$$\sigma = \frac{2}{\sqrt{3}}\,\frac{S_y}{n}$$

Note especially that this result is larger than the uniaxial yield strength divided by the design factor.

Example 2. Estimate the shearing yield strength from the tensile yield strength.

Solution. Set $\sigma_A = \tau, \sigma_B = -\tau$, and at yield, $\tau = S_{sy}$, so

$$\sigma' = (\sigma_A^2 + \sigma_B{}^2 - \sigma_A\sigma_B)^{1/2}$$

$$= [S_{sy}^2 + (-S_{sy})^2 - S_{sy}(-S_{sy})]^{1/2} = S_y$$

Solving gives

$$S_{sy} = \frac{S_y}{\sqrt{3}} = 0.577 S_y$$

28.2.1 Brittle Materials

To define the criterion of failure for brittle materials as *rupture,* we require that the fractional reduction in area be less than 0.05; this corresponds to a true strain at fracture of about 0.05. Brittle materials commonly exhibit an ultimate compressive strength significantly larger than their ultimate tensile strength. And unlike with ductile materials, the ultimate torsional strength is approximately equal to the ultimate tensile strength. If σ_A and σ_B are ordered-plane principal stresses, then there are five points on the rupture locus in the $\sigma_A\sigma_B$ plane that can be immediately identified (Fig. 28.1). These are

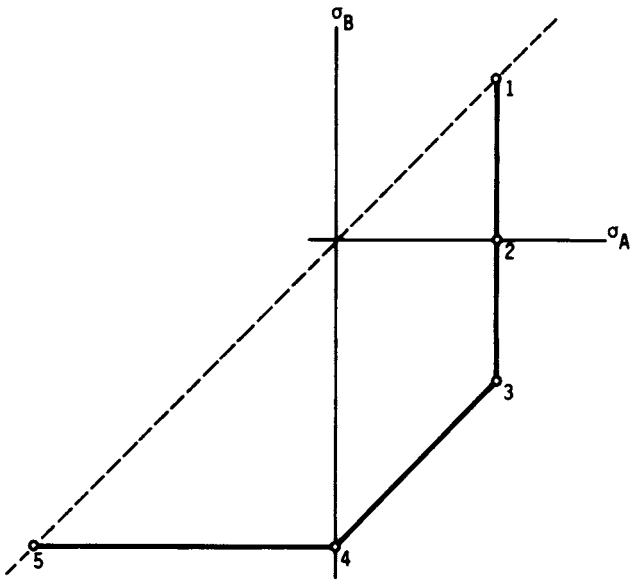

FIGURE 28.1 $\sigma_A\sigma_B$ plane with straight-line Coulomb-Mohr strength locus.

Locus 1–2: $\sigma_A = S_{ut}, \sigma_A > \sigma_B > 0$
Point 3: $\sigma_A = S_{ut} = S_{su}, \sigma_B = -S_{ut} = -S_{su}$
Point 4: $\sigma_A = 0, \sigma_B = S_{uc}$
Locus 4–5: $\sigma_B = S_{uc}, \sigma_A < 0$

Connecting points 2, 3, and 4 with straight-line segments defines the *modified Mohr theory of failure*. This theory evolved from the *maximum normal stress theory* and the *Coulomb-Mohr internal friction theory*. We can state this in algebraic terms by defining $r = \sigma_B/\sigma_A$. The result is

$$\sigma_A = \frac{S_{ut}}{n} \qquad \text{when } \sigma_A > 0, \sigma_B > -\sigma_A$$

$$\sigma_A = \frac{S_{uc}S_{ut}/n}{(1+r)S_{ut} + S_{uc}} \qquad \text{when } \sigma_A > 0, \sigma_B < 0, r < -1 \tag{28.4}$$

$$\sigma_B = \frac{S_{uc}}{n} \qquad \text{when } \sigma_A < 0$$

Figure 28.2 shows some experimental points from tests on gray cast iron.

Example 3. A ¼-in-diameter ASTM No. 40 cast iron pin with S_{ut} = 40 kpsi and S_{uc} = –125 kpsi is subjected to an axial compressive load of 800 lb and a torsional moment of 100 lb · in. Estimate the factor of safety.

Solution. The axial stress is

$$\sigma_x = \frac{F}{A} = \frac{-800}{\pi(0.25)^2/4} = -16.3 \text{ kpsi}$$

The surface shear stress is

$$\tau_{xy} = \frac{16T}{\pi d^3} = \frac{16(100)}{\pi(0.25)^3} = 32.6 \text{ kpsi}$$

The principal stresses are

$$\sigma_{A,B} = \frac{\sigma_x + \sigma_y}{2} \pm \sqrt{\left(\frac{\sigma_x - \sigma_y}{2}\right)^2 + \tau_{xy}^2}$$

$$= \frac{-16.3}{2} \pm \sqrt{\left(\frac{-16.3}{2}\right)^2 + (32.6)^2} = 25.45, -41.25 \text{ kpsi}$$

$$r = \frac{\sigma_B}{\sigma_A} = \frac{-41.25}{25.45} = -1.64$$

The rupture line is the 3–4 locus, and the factor of safety is

$$\eta = \frac{S_{uc}S_{ut}}{(1+r)S_{ut} + S_{uc}} \frac{1}{\sigma_A}$$

STRENGTH UNDER STATIC CIRCUMSTANCES

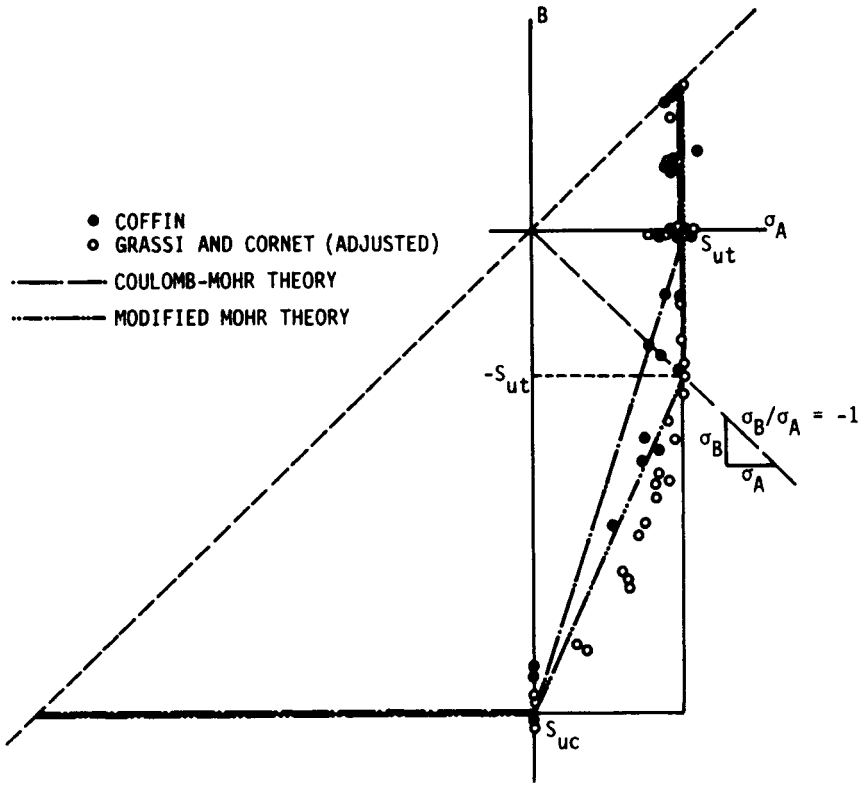

FIGURE 28.2 Experimental data from tests of gray cast iron subjected to biaxial stresses. The data were adjusted to correspond to $S_{ut} = 32$ kpsi and $S_{uc} = 105$ kpsi. Superposed on the plot are graphs of the maximum-normal-stress theory, the Coulomb-Mohr theory, and the modified Mohr theory. (*Adapted from J. E. Shigley and L. D. Mitchell,* Mechanical Engineering Design, *4th ed., McGraw-Hill, 1983, with permission.*)

$$= \frac{(-125)(40)}{[(1 - 1.64)(40) - 125](25.45)} = 1.30$$

28.3 STRESS CONCENTRATION

Geometric discontinuities increase the stress level beyond the nominal stresses, and the elementary stress equations are inadequate estimators. The geometric discontinuity is sometimes called a *stress raiser,* and the domains of departure from the elementary equation are called the *regions of stress concentration.* The multiplier applied to the nominal stress to estimate the peak stress is called the *stress-concentration factor,* denoted by K_t or K_{ts}, and is defined as

$$K_t = \frac{\sigma_{\max}}{\sigma_o} \qquad K_{ts} = \frac{\tau_{\max}}{\tau_o} \tag{28.5}$$

respectively. These factors depend solely on part geometry and manner of loading and are independent of the material. Methods for determining stress-concentration factors include theory of elasticity, photoelasticity, numerical methods including finite elements, gridding, brittle lacquers, brittle models, and strain-gauging techniques.

Peterson [28.1] has been responsible for many useful charts. Some charts representing common geometries and loadings are included as Figs. 28.3 through 28.17. The user of any such charts is cautioned to use the nominal stress equation upon which the chart is based.

When the region of stress concentration is small compared to the section resisting the static loading, localized yielding in ductile materials limits the peak stress to the approximate level of the yield strength. The load is carried without gross plastic distortion. The stress concentration does no damage (strain strengthening occurs), and it can be ignored. No stress-concentration factor is applied to the stress. For low-ductility materials, such as the heat-treated and case-hardened steels, the full geometric stress-concentration factor is applied unless notch-sensitivity information to the contrary is available. This notch-sensitivity equation is

$$K' = 1 + q_s(K_t - 1) \tag{28.6}$$

where K' = the actual stress-concentration factor for static loading and q_s = an index of sensitivity of the material in static loading determined by test. The value of q_s for hardened steels is approximately 0.15 (if untempered, 0.25). For cast irons, which have internal discontinuities as severe as the notch, q_s approaches zero and the full value of K_t is rarely applied.

Kurajian and West [28.3] have derived stress-concentration factors for hollow stepped shafts. They develop an equivalent solid stepped shaft and then use the usual charts (Figs. 28.10 and 28.11) to find K_t. The formulas are

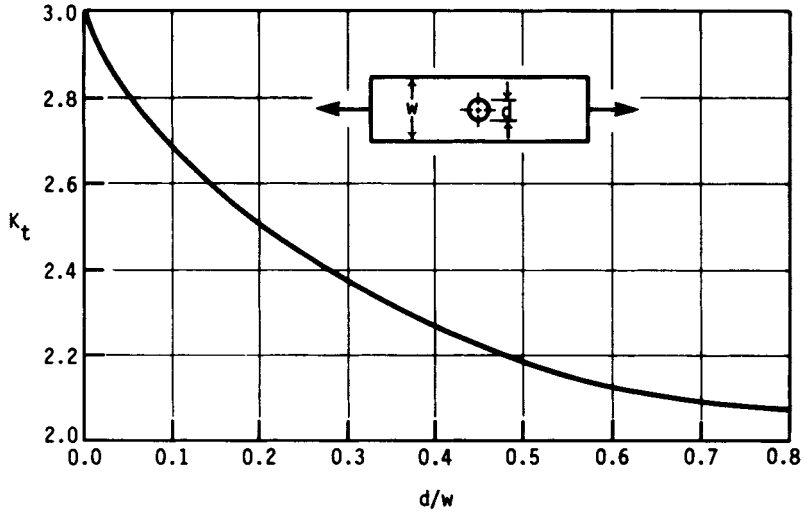

FIGURE 28.3 Bar in tension or simple compression with a transverse hole. $\sigma_o = F/A$, where $A = (w - d)t$, and t = thickness. *(From Peterson [28.2].)*

STRENGTH UNDER STATIC CIRCUMSTANCES

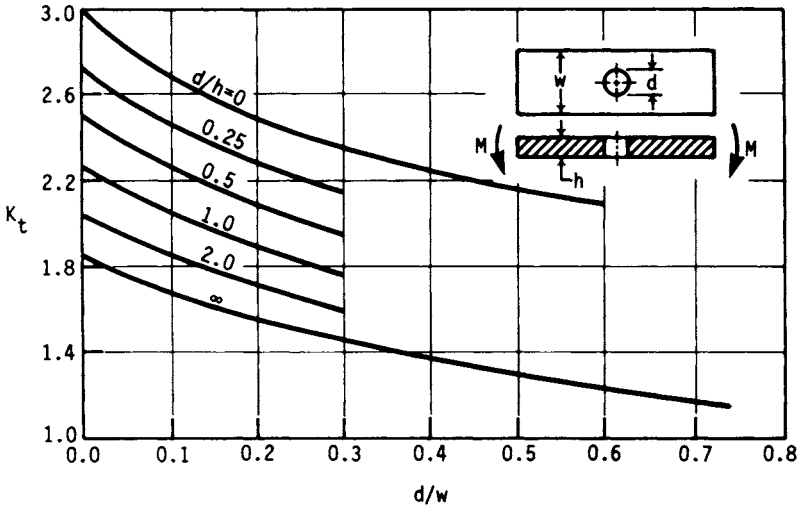

FIGURE 28.4 Rectangular bar with a transverse hole in bending. $\sigma_o = Mc/I$, where $I = (w - d)h^3/12$. *(From Peterson [28.2].)*

$$D = \left(\frac{D_o^4 - d_i^4}{D_o}\right)^{1/3} \quad d = \left(\frac{d_o^4 - d_i^4}{d_o}\right)^{1/3} \tag{28.7}$$

where D, d = diameters of solid stepped shaft (Fig. 28.10)
D_o, d_o = diameters of hollow stepped shaft
d_i = hole diameter

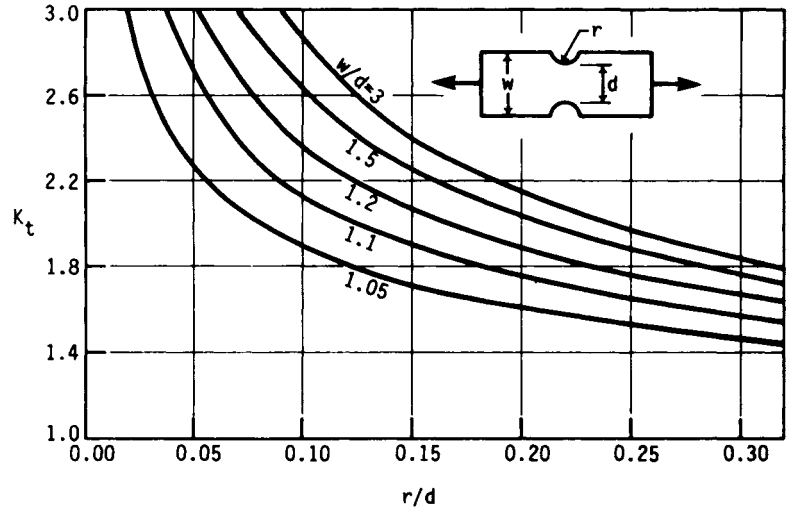

FIGURE 28.5 Notched rectangular bar in tension or simple compression. $\sigma_o = F/A$, where $A = td$ and t = thickness. *(From Peterson [28.2].)*

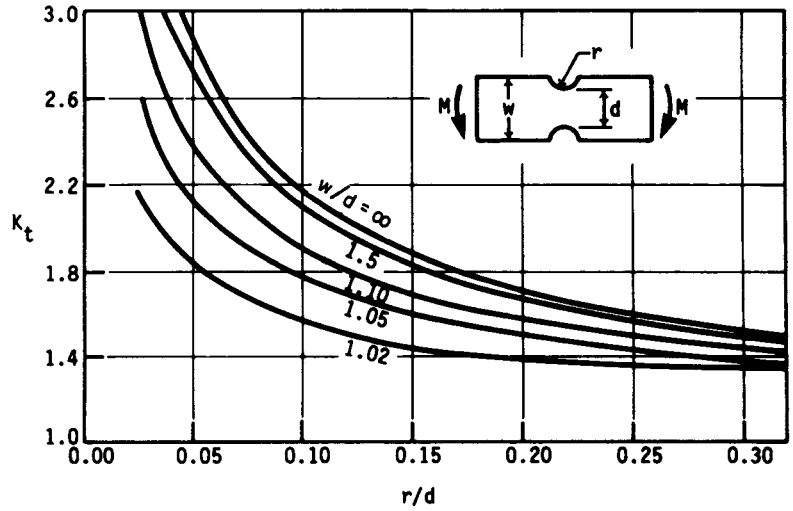

FIGURE 28.6 Notched rectangular bar in bending. $\sigma_o = Mc/I$, where $c = d/2$, $I = td^3/12$, and t = thickness. *(From Peterson [28.2].)*

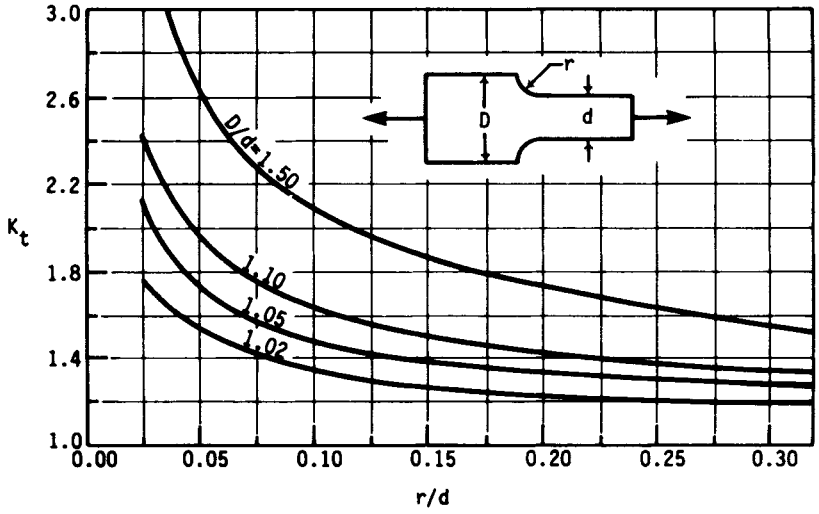

FIGURE 28.7 Rectangular filleted bar in tension or simple compression. $\sigma_o = F/A$, where $A = td$ and t = thickness. *(From Peterson [28.2].)*

STRENGTH UNDER STATIC CIRCUMSTANCES

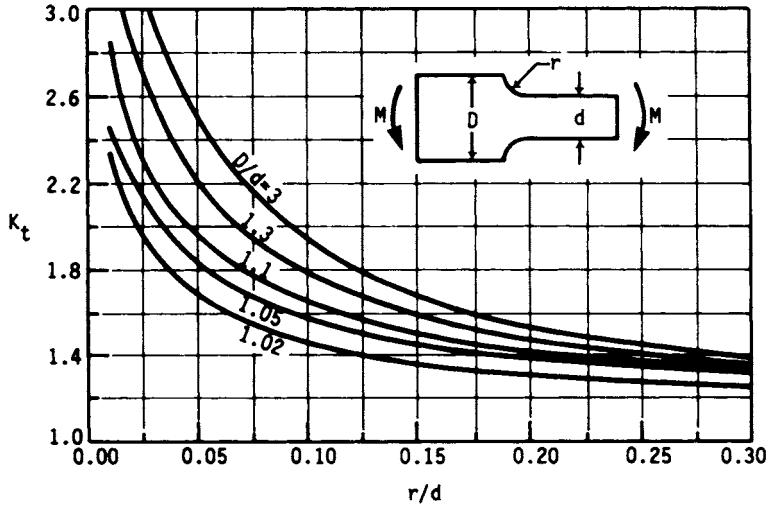

FIGURE 28.8 Rectangular filleted bar in bending. $\sigma_o = Mc/I$, where $c = d/2$, $I = td^3/12$, and t = thickness. *(From Peterson [28.2].)*

The fillet radius is unchanged. No change is necessary for axial loading because of the uniform stress distribution.

28.4 FRACTURE MECHANICS

Stress-concentration factors are really of little use when brittle materials are used or when a very small crack or flaw exists in the material. Ductile materials also may fail

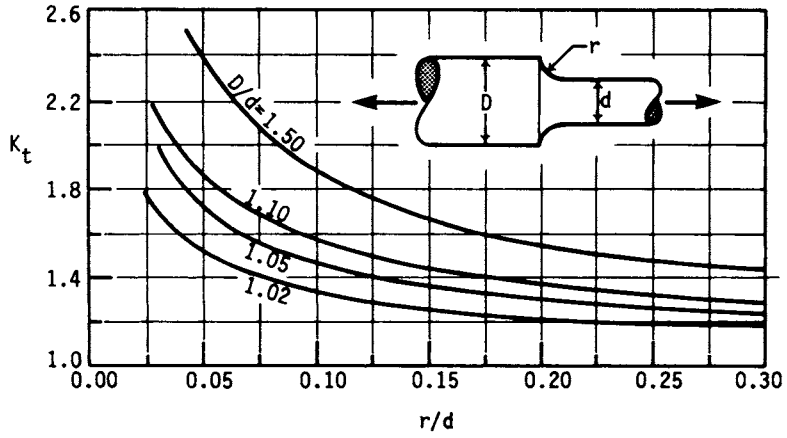

FIGURE 28.9 Round shaft with shoulder fillet in tension. $\sigma_o = F/A$, where $A = \pi d^2/4$. *(From Peterson [28.2].)*

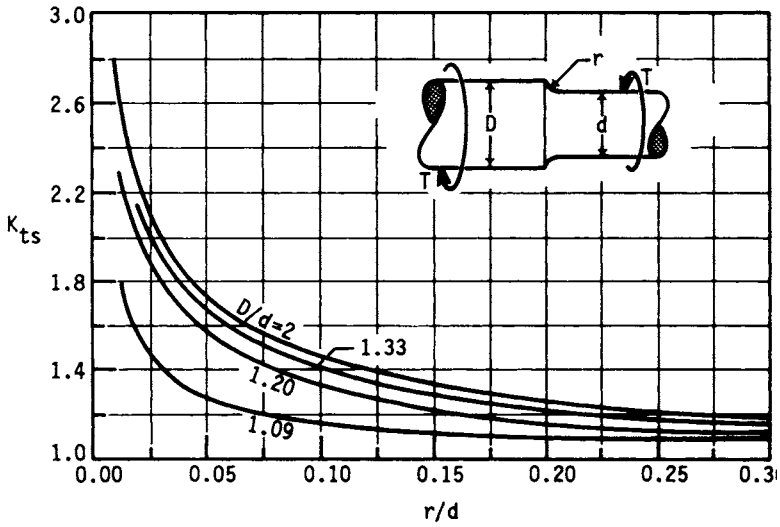

FIGURE 28.10 Round shaft with shoulder fillet in torsion. $\tau_o = Tc/J$, where $c = d/2$ and $J = \pi d^4/32$. *(From Peterson [28.2].)*

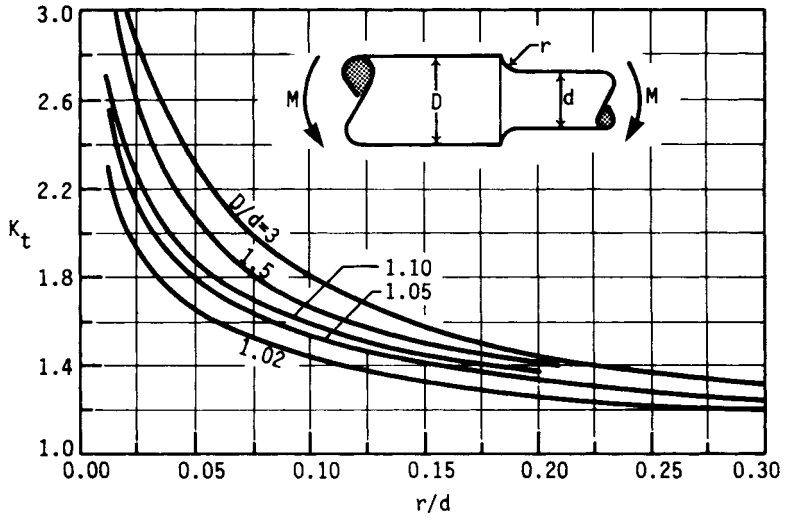

FIGURE 28.11 Round shaft with shoulder fillet in bending. $\sigma_o = Mc/I$, where $c = d/2$ and $I = \pi d^4/64$. *(From Peterson [28.2].)*

STRENGTH UNDER STATIC CIRCUMSTANCES

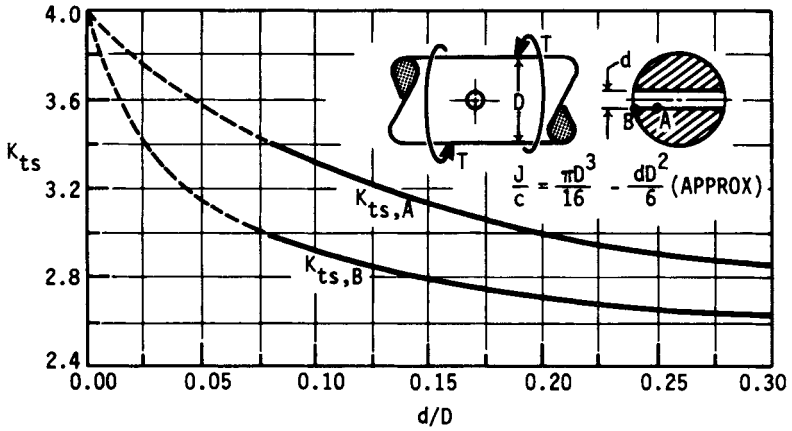

FIGURE 28.12 Round shaft in torsion with transverse hole. *(From Peterson [28.2].)*

in a brittle manner, possibly because of low temperature or other causes. So another method of analysis is necessary for all materials that cannot yield and relieve the stress concentration at a notch, defect, or crack.

Fracture mechanics can be used to determine the average stress in a part that will cause a crack to grow; energy methods of analysis are used (see Ref. [28.4]).

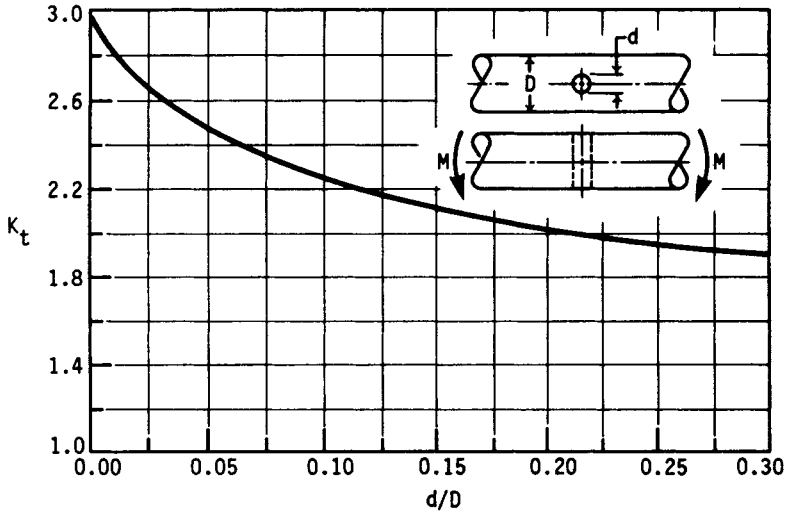

FIGURE 28.13 Round shaft in bending with a transverse hole. $\sigma_o = M/[(\pi D^3/32) - (dD^2/6)]$, approximately. *(From Peterson [28.2].)*

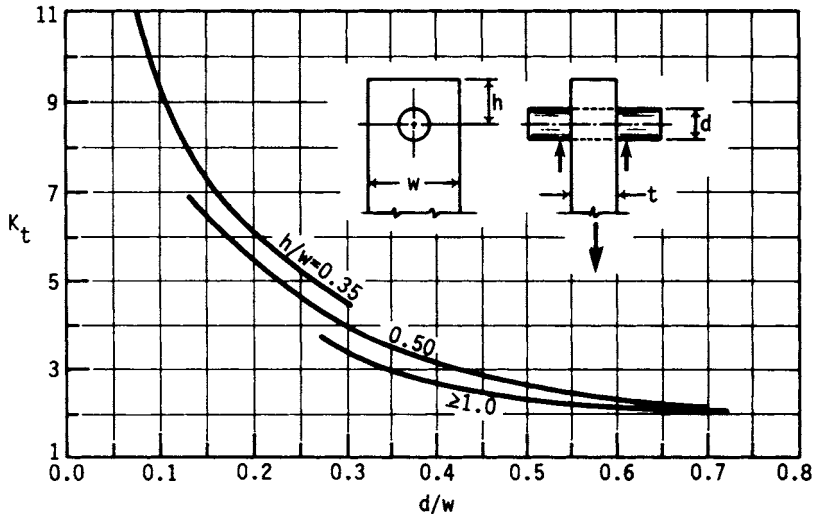

FIGURE 28.14 Plate loaded in tension by a pin through a hole. $\sigma_o = F/A$, where $A = (w - d)t$. When clearance exists, increase K_t by 35 to 50 percent. (*From M. M. Frocht and H. N. Hill, "Stress Concentration Factors around a Central Circular Hole in a Plate Loaded through a Pin in Hole,"* Journal of Applied Mechanics, *vol. 7, no. 1, March 1940, p. A-5, with permission.*)

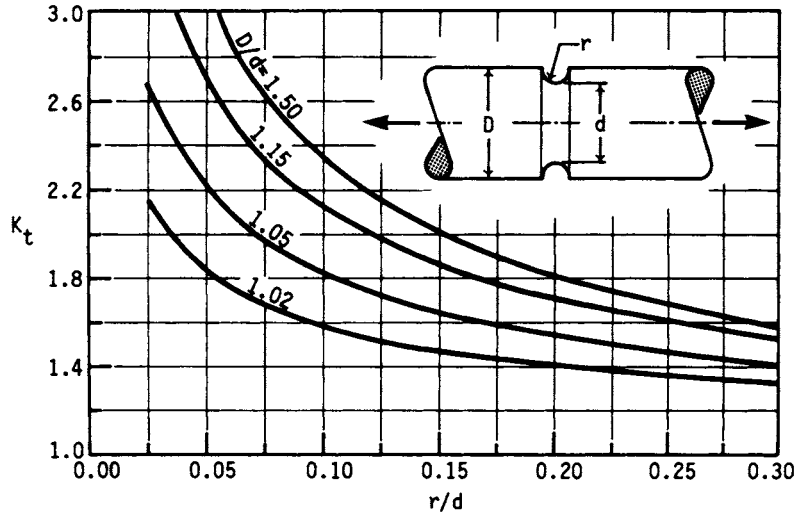

FIGURE 28.15 Grooved round bar in tension. $\sigma_o = F/A$, where $A = \pi d^2/4$. *(From Peterson [28.2].)*

STRENGTH UNDER STATIC CIRCUMSTANCES

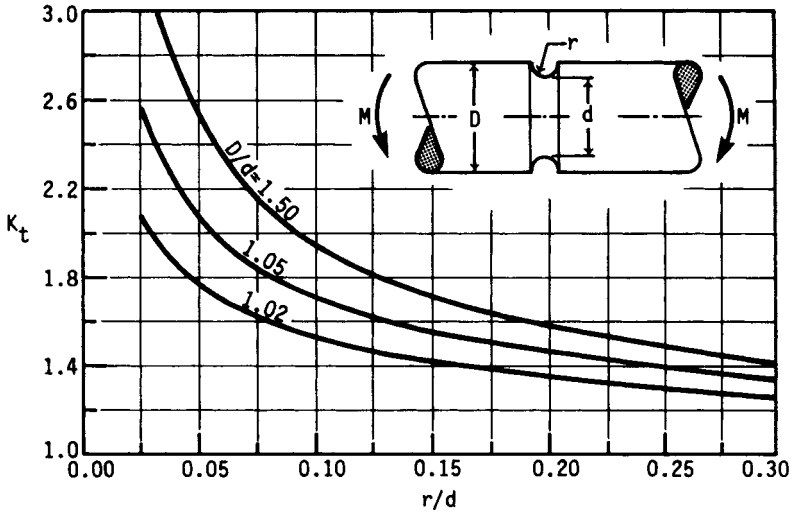

FIGURE 28.16 Grooved round bar in bending. $\sigma_o = Mc/I$, where $c = d/2$ and $I = \pi d^4/64$. *(From Peterson [28.2].)*

28.4.1 Stress Intensities

In Fig. 28.18*a*, suppose the length of the tensile specimen is large compared to the width 2*b*. Also, let the crack, of length 2*a*, be centrally located. Then a stress-intensity factor K can be defined by the relation

$$K_0 = \sigma(\pi a)^{1/2} \tag{28.8}$$

where σ = average tensile stress. The units of K_0 are kpsi · $in^{1/2}$ or, in SI, MPa · $m^{1/2}$.

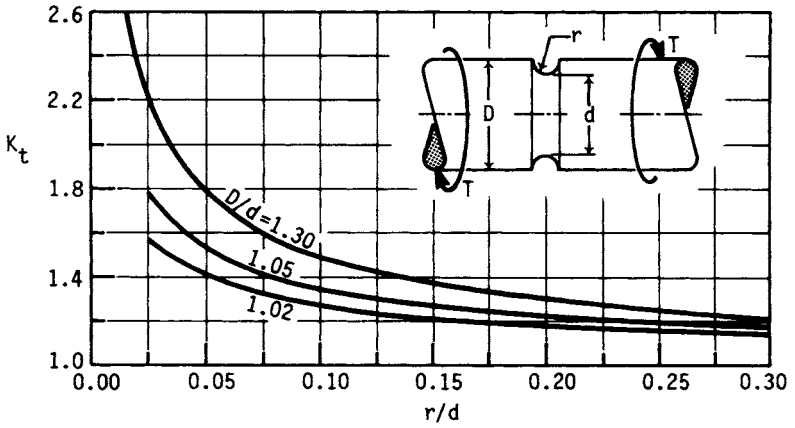

FIGURE 28.17 Grooved round bar in torsion. $\tau_o = Tc/J$, where $c = d/2$ and $J = \pi d^4/32$. *(From Peterson [28.2].)*

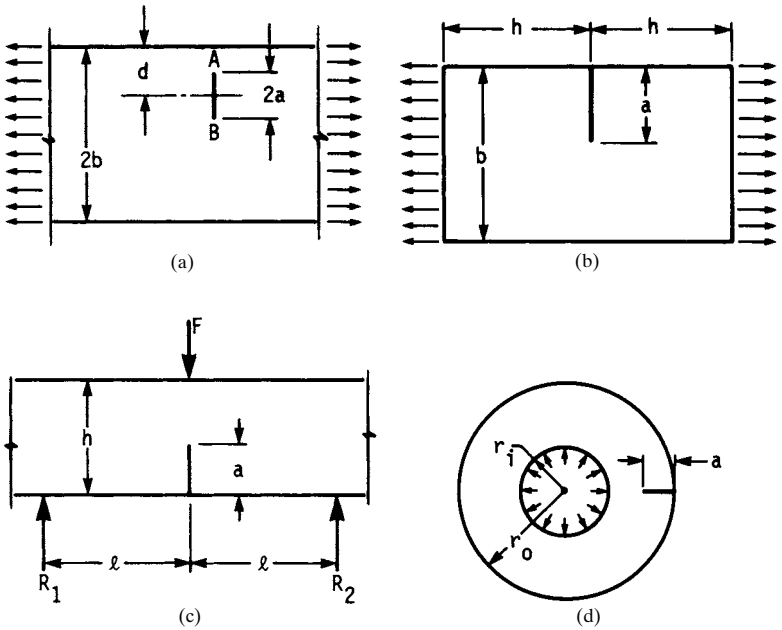

FIGURE 28.18 Typical crack occurrences. (*a*) Bar in tension with interior crack; (*b*) bar in tension with edge crack; (*c*) flexural member of rectangular cross section with edge crack; (*d*) pressurized cylinder with radial edge crack parallel to cylinder axis.

Since the actual value of K for other geometries depends on the loading too, it is convenient to write Eq. (28.8) in the form

$$K_{\mathrm{I}} = C\sigma(\pi a)^{1/2} \tag{28.9}$$

where

$$C = \frac{K_{\mathrm{I}}}{K_0} \tag{28.10}$$

Values of this ratio for some typical geometries and loadings are given in Figs. 28.19 and 28.20. Note that Fig. 28.18 must be used to identify the curves on these charts. Additional data on stress-intensity factors can be found in Refs. [28.5], [28.6], and [28.7].

The Roman numeral I used as a subscript in Eq. (28.9) refers to the deformation mode. Two other modes of fracture not shown in Fig. 28.18 are in-plane and out-of-plane shear modes, and these are designated by the Roman numerals II and III. These are not considered here (see Ref. [28.4], p. 262).

28.4.2 Fracture Toughness

When the stress σ of Eq. (28.9) reaches a certain critical value, crack growth begins, and the equation then gives the *critical-stress-intensity factor* K_{Ic}. This is also called the

STRENGTH UNDER STATIC CIRCUMSTANCES

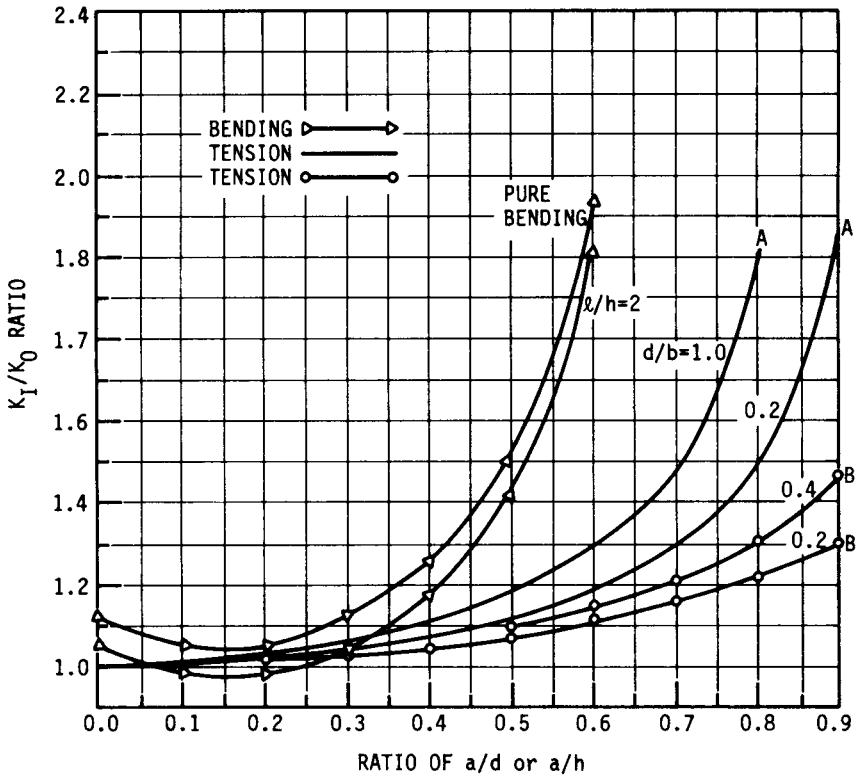

FIGURE 28.19 Stress-intensity charts for cracks shown in Fig. 28.18*a* and *c*. Letters *A* and *B* identify the ends of the crack shown in Fig. 28.18*a*. Values of $\ell/h > 2$ will produce curves closer to the curve for pure bending.

fracture toughness. Since it is analogous to strength, we can define the design factor as

$$n = \frac{K_c}{K} \tag{28.11}$$

Some typical values of K_c are given in Table 28.1. For other materials, see Ref. [28.8].

28.5 NONFERROUS METALS

Designing for static loads with aluminum alloys is not much different from designing for the steels. Aluminum alloys, both cast and wrought, have strengths in tension and compression that are about equal. The yield strengths in shear vary from about 55 to 65 percent of the tensile yield strengths, and so the octahedral shear theory of failure is valid.

The corrosion resistance (see Chap. 35), workability, and weldability obtainable from some of the alloys make this a very versatile material for design. And the extrusion capability means that a very large number of wrought shapes are available.

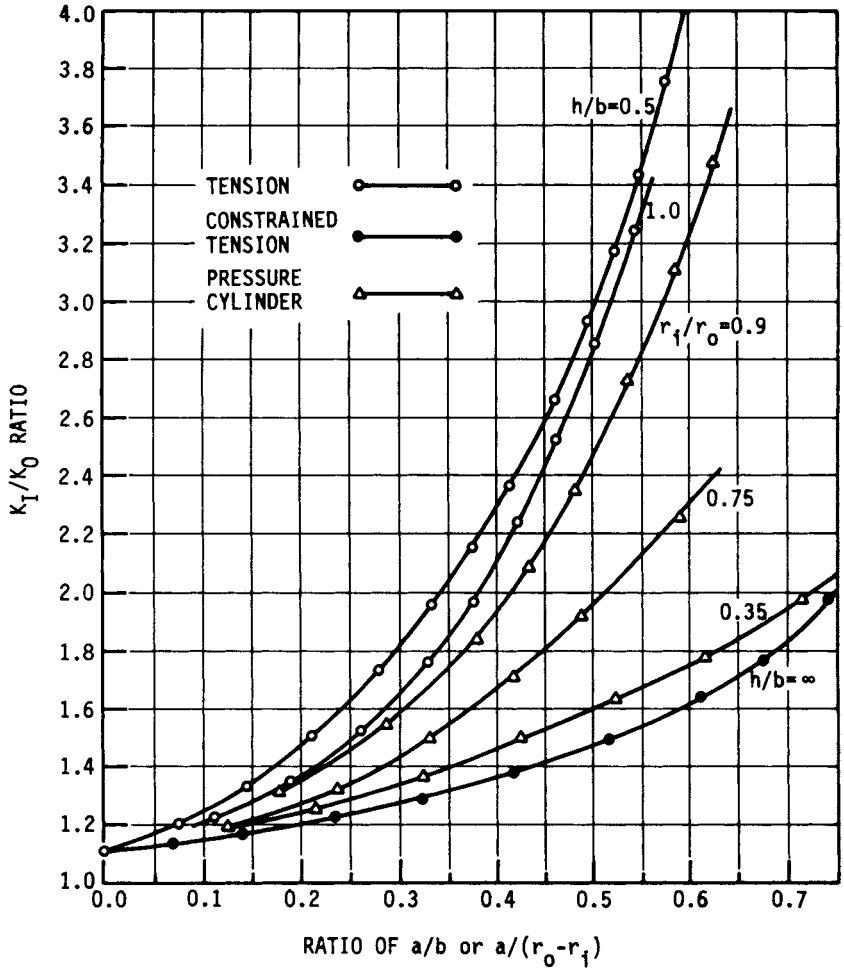

FIGURE 28.20 Stress-intensity chart for cracks shown in Figs. 28.18*b* and *d*. The curve $h/b = \infty$ has bending constraints acting on the member.

However, these alloys do have a temperature problem, as shown by the curves of strength versus temperature in Fig. 28.21. Other aluminum alloys will exhibit a similar characteristic.

Alloying elements used with copper as the base element include zinc, lead, tin, aluminum, silicon, manganese, phosphorus, and beryllium. Hundreds of variations in the percentages used are possible, and consequently, the various copper alloys may have widely differing properties. The primary consideration in selecting a copper alloy may be the machinability, ductility, hardness, temperature properties, or corrosion resistance. Strength is seldom the primary consideration. Because of these variations in properties, it is probably a good idea to consult the manufacturer concerning new applications until a backlog of experience can be obtained.

STRENGTH UNDER STATIC CIRCUMSTANCES

TABLE 28.1 Values of the Fracture Toughness K_{Ic} for a Few Engineering Materials

Material	Designation	UNS no.	Yield strength		Fracture toughness	
			MPa	kpsi	$MPa \cdot m^{1/2}$	$kpsi \cdot in^{1/2}$
Aluminum	2024-T851	A92094-T851	455	66	26	24
	7075-T651	A97075-T651	495	72	24	22
Titanium	Ti-6AL-4V	R56401	910	132	115	105
	Ti-6AL-4V	R56401	1035	150	55	50
Steel	AISI 4340	G43400	860	125	99	90
	AISI 4340	G43400	1515	220	60	55
	AISI 52100	G52986	2070	300	14	13

SOURCE: Professor David K. Felbeck, The University of Michigan, by personal communication.

Magnesium alloys have a weight about two-thirds that of aluminum and one-fourth that of steel. Magnesium alloys are not very strong and are characterized by having a compressive strength that is somewhat less than the tensile strength. They are also so sensitive to temperature that they are weakened even by contact with boiling water.

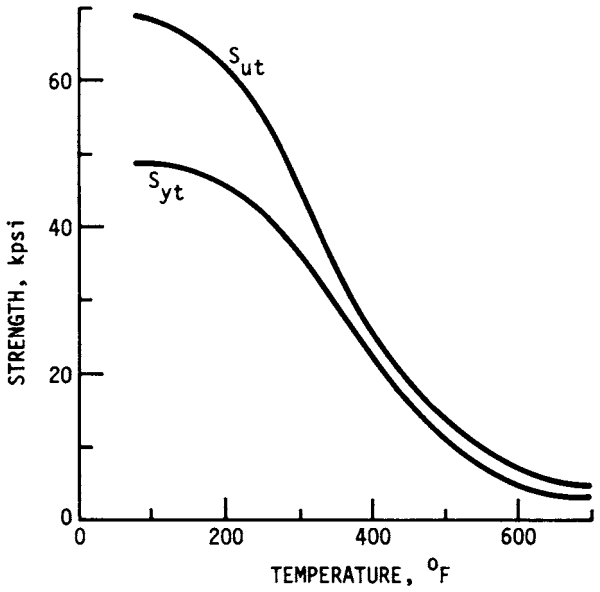

FIGURE 28.21 Effect of temperature on the yield strength and tensile strength of aluminum alloy A92024-T4. *(ALCOA.)*

REFERENCES

28.1 R. E. Peterson, *Stress Concentration Factors,* John Wiley & Sons, New York, 1974.

28.2 R. E. Peterson, "Design Factors for Stress Concentration," *Machine Design,* vol. 23, no. 2, p. 161; no. 5, p. 159; no. 6, p. 173; no. 7, p. 155; 1951.

28.3 G. M. Kurajian and D. J. West, "Stress Concentration Factor Determination in Stepped Hollow Shafts," *Failure Prevention and Reliability,* American Society of Mechanical Engineers, New York, 1977.

28.4 R. W. Hertzberg, *Deformation and Fracture Mechanics of Engineering Materials,* John Wiley & Sons, New York, 1976.

28.5 H. Tada, P. C. Paris, and G. R. Irwin, *The Stress Analysis of Cracks Handbook,* Del Research, Hellertown, Pa., 1973.

28.6 G. C. M. Sih, *Handbook of Stress Intensity Factors,* Lehigh University, Bethlehem, Pa., 1973.

28.7 D. P. Rooke and D. J. Cartwright, *Compendium of Stress Intensity Factors,* Hillingdon Press, Uxbridge, England, 1976.

28.8 *Damage Tolerant Handbook,* Metals and Ceramics Information Center, Battelle, Columbus, Ohio, 1975.

CHAPTER 29
STRENGTH UNDER DYNAMIC CONDITIONS

Charles R. Mischke, Ph.D., P.E.
Professor Emeritus of Mechanical Engineering
Iowa State University
Ames, Iowa

NOMENCLATURE

a	Distance, exponent, constant
A	Area, addition factor, ΣiN_i
b	Distance, width, exponent
B	$\Sigma i^2 N_i$
bhn	Brinell hardness, roller or pinion
BHN	Brinell hardness, cam or gear
c	Exponent
C	Coefficient of variation
C_p	Materials constant in rolling contact
d	Difference in stress level, diameter
d_e	Equivalent diameter
D	Damage per cycle or block of cycles
D_I	Ideal critical diameter
E	Young's modulus
f	Fraction of mean ultimate tensile strength
f_i	Fraction of life measure

F	Force
$\mathscr{F}$	Significant force in contact fatigue
h	Depth
H_B	Brinell hardness
I	Second area moment
k_a	Marin surface condition modification factor
k_b	Marin size modification factor
k_c	Marin load modification factor
k_d	Marin temperature modification factor
k_e	Marin miscellaneous-effects modification factor
K	Load-life constant
K_f	Fatigue stress concentration factor
K_t	Geometric (theoretical) stress concentration factor
ℓ	Length
log	Base 10 logarithm
ln	Natural logarithm
L	Life measure
LN	Lognormal
m	Strain-strengthening exponent, revolutions ratio
M	Bending moment
$\mathbf{n}, n$	Design factor
N	Cycles
N_f	Cycles to failure
$N(\mu, \sigma)$	Normal distribution with mean μ and standard deviation σ
p	Pressure
P	Axial load
q	Notch sensitivity
r	Notch radius, slope of load line
r_i	Average peak-to-valley distance
R	Reliability
R_a	Average deviation from the mean
R_{rms}	Root-mean-squared deviation from the mean
RA	Fraction reduction in area
R_Q	As-quenched hardness, Rockwell C scale
R_T	Tempered hardness, Rockwell C scale
S	Strength
S'_{ax}	Axial endurance limit
S'_e	Rotating-beam endurance limit
S_f	Fatigue strength

STRENGTH UNDER DYNAMIC CONDITIONS

S'_{se}	Torsional endurance limit
S_u, S_{ut}	Ultimate tensile strength
S_y	Yield strength
t_f	Temperature, °F
T	Torque
w	Width
x	Variable, coordinate
y	Variable, coordinate
z	Variable, coordinate, variable of $N(0, z)$
α	Prot loading rate, psi/cycle
β	Rectangular beam width
Δ	Approach of center of roller
ε	True strain
ε_f	True strain at fracture
η	Factor of safety
θ	Angle, misalignment angle
λ	Lognormally distributed
μ	Mean
ν	Poisson's ratio
ξ	Normally distributed
σ	Normal stress
σ_a	Normal stress amplitude component
σ'_f	Fatigue strength coefficient
σ_m	Steady normal stress component
$\sigma_{\max}$	Largest normal stress
$\sigma_{\min}$	Smallest normal stress
σ_0	Nominal normal stress
$\overline{\sigma}_0$	Strain-strengthening coefficient
σ	Standard deviation
τ	Shear stress
ϕ	Pressure angle

29.1 TESTING METHODS AND PRESENTATION OF RESULTS

The designer has need of knowledge concerning endurance limit (if one exists) and endurance strengths for materials specified or contemplated. These can be estimated from the following:

- Tabulated material properties (experience of others)
- Personal or corporate R. R. Moore endurance testing
- Uniaxial tension testing and various correlations
- For plain carbon steels, if heat treating is involved, Jominy test and estimation of tempering effects by the method of Crafts and Lamont
- For low-alloy steels, if heat treating is involved, prediction of the Jominy curve by the method of Grossmann and Fields and estimation of tempering effects by the method of Crafts and Lamont
- If less than infinite life is required, estimation from correlations
- If cold work or plastic strain is an integral part of the manufacturing process, using the method of Datsko

The representation of data gathered in support of fatigue-strength estimation is best made probabilistically, since inferences are being made from the testing of necessarily small samples. There is a long history of presentation of these quantities as deterministic, which necessitated generous design factors. The plotting of cycles to failure as abscissa and corresponding stress level as ordinate is the common SN curve. When the presentation is made on logarithmic scales, some piecewise rectification may be present, which forms the basis of useful curve fits. Some ferrous materials exhibit a pronounced knee in the curve and then very little dependency of strength with life. Deterministic researchers declared the existence of a zero-slope portion of the curve and coined the name *endurance limit* for this apparent asymptote.

Based on many tests over the years, the general form of a steel SN curve is taken to be approximately linear on log-log coordinates in the range 10^3 to 10^6 cycles and nearly invariant beyond 10^7 cycles. With these useful *approximations* and knowledge that cycles-to-failure distributions at constant stress level are lognormal and that stress-to-failure distributions at constant life are likewise lognormal, specialized methods can be used to find some needed attribute of the SN picture. The cost and time penalties associated with developing the complete picture motivate the experimentor to seek only what is needed.

29.1.1 Sparse Survey

On the order of a dozen specimens are run to failure in an R. R. Moore apparatus at stress levels giving lives of about 10^3 to 10^7 cycles. The points are plotted on log-log paper, and in the interval $10^3 < N < 10^7$ cycles, a "best" straight line is drawn. Those specimens which have not failed by 10^8 or 5×10^8 cycles are used as evidence of the existence of an endurance limit. All that this method produces is estimates of two median lines, one of the form

$$S'_f = CN^b \qquad 10^3 < N < 10^6 \tag{29.1}$$

and the other of the form

$$S'_f = S'_e \qquad N > 10^6 \tag{29.2}$$

This procedure "roughs in" the SN curve as a gross estimate. No standard deviation information is generated, and so no reliability contours may be created.

STRENGTH UNDER DYNAMIC CONDITIONS

29.1.2 Constant-Stress-Level Testing

If high-cycle fatigue strength in the range of 10^3 to 10^6 cycles is required and reliability (probability of survival) contours are required, then constant-stress-level testing is useful. A dozen or more specimens are tested at each of several stress levels. These results are plotted on lognormal probability paper to "confirm" by inspection the lognormal distribution, or a statistical goodness-of-fit test (Smirnov-Kolomogorov, chi-squared) is conducted to see if lognormal distribution can be rejected. If not, then reliability contours are established using lognormal statistics. Nothing is learned about endurance limit. Sixty to 100 specimens usually have been expended.

29.1.3 Probit Method

If statistical information (mean, standard deviation, distribution) concerning the endurance limit is needed, the probit method is useful. Given a priori knowledge that a "knee" exists, stress levels are selected that at the highest level produce one or two runouts and at the lowest level produce one or two failures. This places the testing at the "knee" of the curve and within a couple of standard deviations on either side of the endurance limit. The method requires exploratory testing to estimate the stress levels that will accomplish this. The results of the testing are interpreted as a lognormal distribution of stress either by plotting on probability paper or by using a goodness-of-fit statistical reduction to "confirm" the distribution. If it is confirmed, the mean endurance limit, its variance, and reliability contours can be expressed. The existence of an endurance limit has been assumed, not proven. With specimens declared runouts if they survive to 10^7 cycles, one can be fooled by the "knee" of a nonferrous material which exhibits no endurance limit.

29.1.4 Coaxing

It is intuitively appealing to think that more information is given by a failed specimen than by a censored specimen. In the preceding methods, many of the specimens were unfailed (commonly called *runouts*). Postulating the existence of an endurance limit and no damage occurring for cycles endured at stress levels less than the endurance limit, a method exists that raises the stress level of unfailed (by, say, 10^7 cycles) specimens to the next higher stress level and tests to failure starting the cycle count again. Since every specimen fails, the specimen set is smaller. The results are interpreted as a normal stress distribution. The method's assumption that a runout specimen is neither damaged nor strengthened complicates the results, since there is evidence that the endurance limit can be enhanced by such coaxing [29.1].

29.1.5 Prot Method[†]

This method involves steadily increasing the stress level with every cycle. Its advantage is reduction in number of specimens; its disadvantage is the introduction of (1) coaxing, (2) an empirical equation, that is,

$$S_\alpha = S'_e + K\alpha^n \tag{29.3}$$

[†] See Ref. [29.2].

where S_α = Prot failure stress at loading rate, α psi/cycle
S'_e = material endurance limit
K, n = material constants
α = loading rate, psi/cycle

and (3) an extrapolation procedure. More detail is available in Collins [29.3].

29.1.6 Up-Down Method†

The up-down method of testing is a common scheme for reducing R. R. Moore data to an estimate of the endurance limit. It is adaptable to seeking endurance strength at any arbitrary number of cycles. Figure 29.1 shows the data from 54 specimens

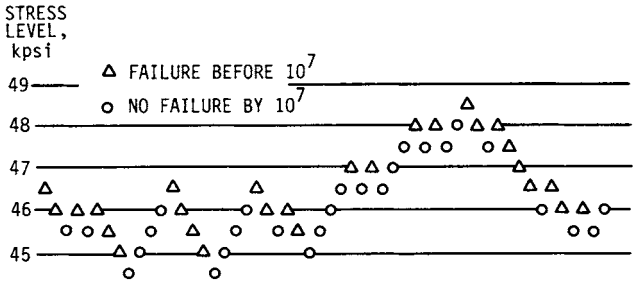

FIGURE 29.1 An up-down fatigue test conducted on 54 specimens. *(From Ransom [29.5], with permission.)*

gathered for determining the endurance strength at 10^7 cycles. The step size was 0.5 kpsi. The first specimen at a stress level of 46.5 kpsi failed before reaching 10^7 cycles, and so the next lower stress level of 46.0 kpsi was used on the subsequent specimen. It also failed before 10^7 cycles. The third specimen, at 45.5 kpsi, survived 10^7 cycles, and so the stress level was increased. The data-reduction procedure eliminates specimens until the first runout-fail pair is encountered. We eliminate the first specimen and add as an observation the next (no. 55) specimen, $\sigma = 46.5$ kpsi. The second step is to identify the least frequent event—failures or runouts. Since there are 27 failures and 27 runouts, we arbitrarily choose failures and tabulate N_i, iN_i, and i^2N_i as shown in Table 29.1. We define $A = \Sigma iN_i$ and $B = \Sigma i^2N_i$. The estimate of the mean of the 10^7-cycle strength is

$$\hat{\mu} = S_0 + d\left(\frac{A}{\Sigma N_i} \pm \frac{1}{2}\right) \tag{29.4}$$

where S_0 = the lowest stress level on which the less frequent event occurs, d = the stress-level increment or step, and N_i = the number of less frequent events at stress level σ_i. Use +½ if the less frequent event is runout and –½ if it is failure. The estimate of the mean 10^7-cycle strength is

† See Refs. [29.4] and [29.5].

STRENGTH UNDER DYNAMIC CONDITIONS

TABLE 29.1 Extension of Up-Down Fatigue Data

Stress level, kpsi	Coded level	Class failures		
		N_i	iN_i	i^2N_i
48.5	7	1	7	49
48.0	6	4	24	144
47.5	5	1	5	25
47.0	4	3	12	48
46.5	3	5	15	45
46.0	2	8	16	32
45.5	1	3	3	3
45.0	0	2	0	0
		Σ 27	82	346

$$\hat{\mu} = 45.0 + 0.5\left(\frac{82}{27} - \frac{1}{2}\right) = 46.27 \text{ kpsi}$$

The standard deviation is

$$\hat{\sigma} = 1.620d\left[\frac{B\Sigma N_i - A^2}{(\Sigma N_i)^2} + 0.029\right] \tag{29.5}$$

as long as $(B\Sigma N_i - A^2)/(\Sigma N_i)^2 \geq 0.3$. Substituting test data into Eq. (29.5) gives

$$\hat{\sigma} = 1.620(0.5)\left[\frac{342(27) - 82^2}{27^2} + 0.029\right] = 2.93 \text{ kpsi}$$

The result of the up-down test can be expressed as $(S_f')_{10^7}(\hat{\mu}, \hat{\sigma})$ or $(S_f')_{10^7}(46.27, 2.93)$. Consult Refs. [29.3] and [29.4] for modification of the usual t-statistic method of placing a confidence interval on μ and Ref. [29.4] for placing a confidence interval on σ. A point estimate of the coefficient of variation is $\sigma/\mu = 2.93/46.27$, or 0.063. Coefficients of variation larger than 0.1 have been observed in steels. One must examine the sources of tables that display a single value for an endurance strength to discover whether the mean or the smallest value in a sample is being reported. This can also reveal the coefficient of variation.

29.2 SN DIAGRAM FOR SINUSOIDAL AND RANDOM LOADING

The usual presentation of R. R. Moore testing results is on a plot of S_f' (or S_f'/S_u) versus N, commonly on log-log coordinates because segments of the locus appear to be rectified. Figure 29.2 is a common example. Because of the dispersion in results, sometimes a $\pm 3\sigma$ band is placed about the median locus or (preferably) the data points are shown as in Fig. 29.3. In any presentation of this sort, the only things that might be true are the observations. All lines or loci are curve fits of convenience, there being no theory to suggest a rational form. What will endure are the data and

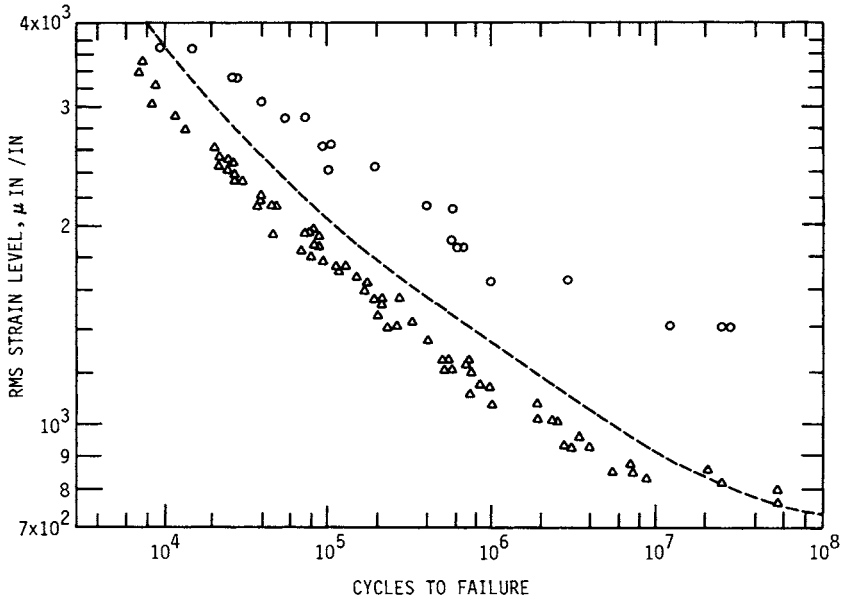

FIGURE 29.2 Fatigue data on 2024-T3 aluminum alloy for narrow-band random loading, △, and for constant-amplitude loading, ○. *(Adapted with permission from Haugen [29.14], p. 339.)*

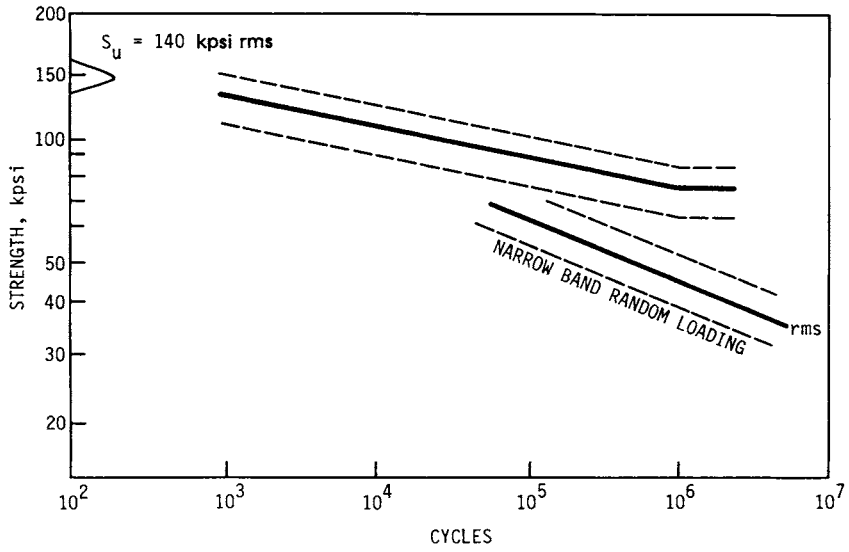

FIGURE 29.3 Statistical SN diagram for constant-amplitude and narrow-band random loading for a low-alloy steel. Note the absence of a "knee" in the random loading.

STRENGTH UNDER DYNAMIC CONDITIONS

not the loci. Unfortunately, too much reported work is presented without data; hence early effort is largely lost as we learn more.

The R. R. Moore test is a sinusoidal completely reversed flexural loading, which is typical of much rotating machinery, but not of other forms of fatigue. Narrow-band random loading (zero mean) exhibits a lower strength than constant-amplitude sine-wave loading. Figure 29.3 is an example of a distributional presentation, and Fig. 29.2 shows the difference between sinusoidal and random-loading strength.

29.3 FATIGUE-STRENGTH MODIFICATION FACTORS

The results of endurance testing are often made available to the designer in a concise form by metals suppliers and company materials sections. Plotting coordinates are chosen so that it is just as easy to enter the plot with maximum-stress, minimum-stress information as steady and alternating stresses. The failure contours are indexed from about 10^3 cycles up to about 10^9 cycles. Figures 29.4, 29.5, and 29.6 are

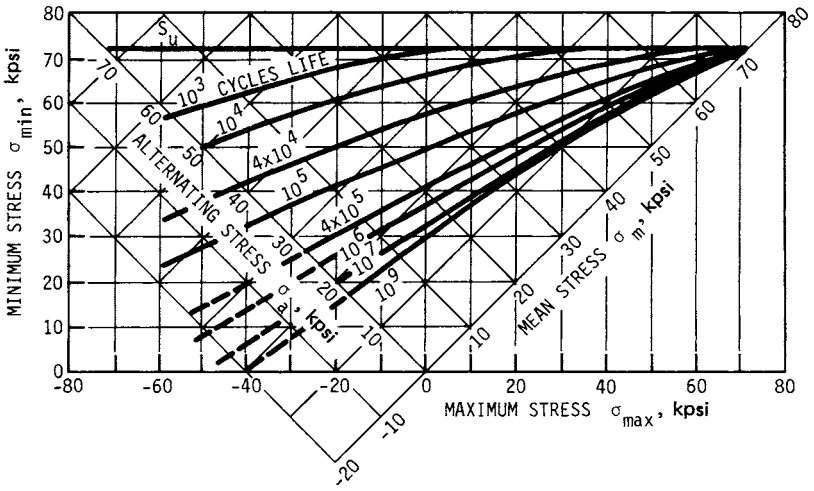

FIGURE 29.4 Fatigue-strength diagram for 2024-T3, 2024-T4, and 2014-T6 aluminum alloys, axial loading. Average of test data for polished specimens (unclad) from rolled and drawn sheet and bar. Static properties for 2024: $S_u = 72$ kpsi, $S_y = 52$ kpsi; for 2014: $S_u = 72$ kpsi, $S_y = 63$ kpsi. *(Grumman Aerospace Corp.)*

examples. The usual testing basis is bending fatigue, zero mean, constant amplitude. Figure 29.6 represents axial fatigue. The problem for the designer is how to adjust this information to account for all the discrepancies between the R. R. Moore specimen and the contemplated machine part. The Marin approach [29.6] is to introduce multiplicative modification factors to adjust the endurance limit, in the deterministic form

$$S_e = k_a k_b k_c k_d k_e S'_e \tag{29.6}$$

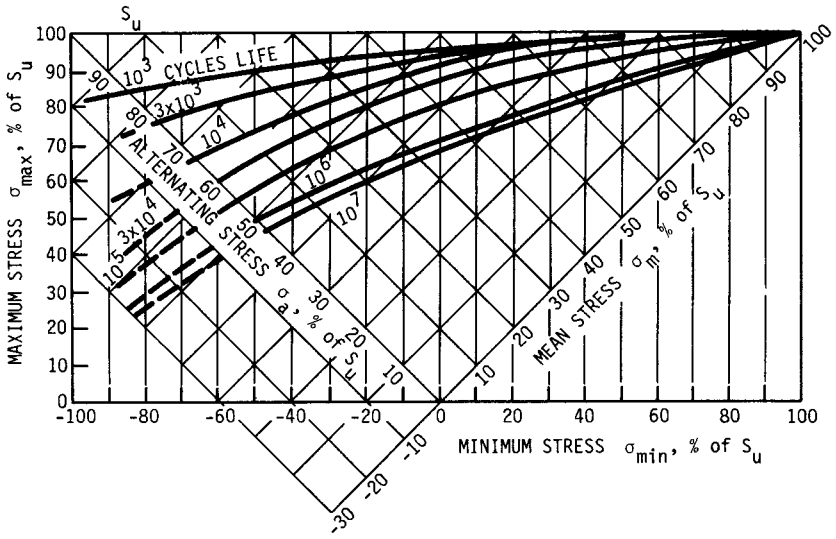

FIGURE 29.5 Fatigue-strength diagram for alloy steel, $S_u = 125$ to 180 kpsi, axial loading. Average of test data for polished specimens of AISI 4340 steel (also applicable to other alloy steels, such as AISI 2330, 4130, 8630). *(Grumman Aerospace Corp.)*

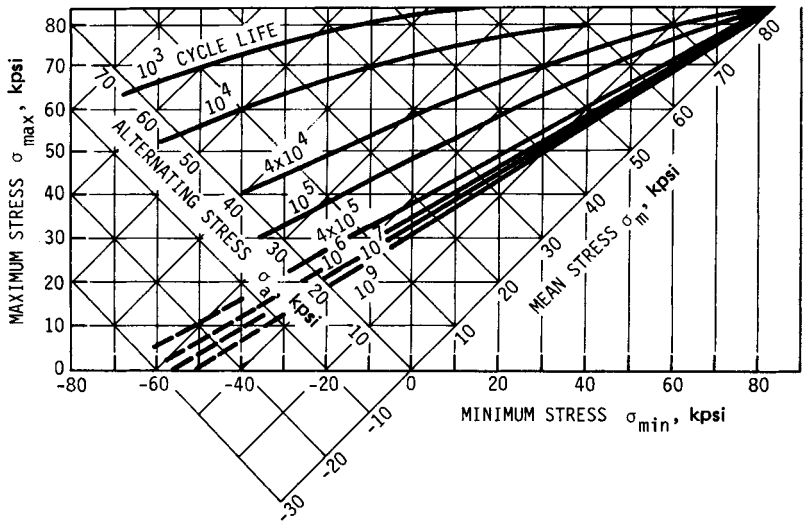

FIGURE 29.6 Fatigue-strength diagram for 7075-T6 aluminum alloy, axial loading. Average of test data for polished specimens (unclad) from rolled and drawn sheet and bar. Static properties: $S_u = 82$ kpsi, $S_y = 75$ kpsi. *(Grumman Aerospace Corp.)*

STRENGTH UNDER DYNAMIC CONDITIONS

where k_a = surface condition modification factor
k_b = size modification factor
k_c = loading modification factor
k_d = temperature modification factor
k_e = miscellaneous-effects modification factor
S'_e = endurance limit of rotating-beam specimen
S_e = endurance limit at critical location of part in the geometry and condition of use

29.3.1 Marin Surface Factor k_a

The Marin surface condition modification factor for steels may be expressed in the form

$$k_a = aS_{ut}^b \tag{29.7}$$

Table 29.2 gives values of *a, b* for various surface conditions. See also Fig. 29.7.

TABLE 29.2 Parameters of Marin Surface Condition Factor

	a		
Surface finish	kpsi	MPa	*b*
Ground	1.34	1.58	–0.086
Machined, cold-rolled	2.67	4.45	–0.265
Hot-rolled	14.5	58.1	–0.719
As-forged	39.8	271	–0.995

Source: Data from C. G. Noll and C. Lipson, "Allowable Working Stresses," *Society of Experimental Stress Analysis,* vol. 3, no. 2, 1946, p. 49, reduced from their graphed data points.

Example 1. A steel has a mean ultimate tensile strength of 520 MPa and a machined surface. Estimate k_a.

Solution: From Table 29.2,

$$k_a = 4.45(520)^{-0.265} = 0.848$$

29.3.2 Marin Size Factor k_b

In bending and torsion, where a stress gradient exists, Kuguel observed that the volume of material stressed to 0.95 or more of the maximum stress controls the risk of encountering a crack nucleation, or growth of an existing flaw becoming critical. The equivalent diameter d_e of the R. R. Moore specimen with the same failure risk is

$$d_e = \sqrt{\frac{A_{0.95}}{0.076\,576}} \tag{29.8}$$

where $A_{0.95}$ is the cross-sectional area exposed to 95 percent or more of the maximum stress. For a round in rotating bending or torsion, $A_{0.95} = 0.075\,575d^2$. For a round in nonrotating bending, $A_{0.95} = 0.010\,462d^2$. For a rectangular section $b \times h$ in

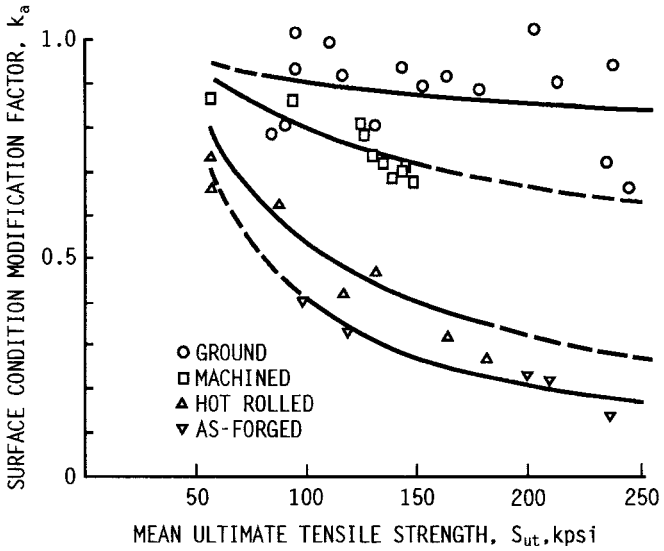

FIGURE 29.7 Marin endurance limit fatigue modification factor k_a for various surface conditions of steels. See also Table 29.2.

bending, $A_{0.95} = 0.05bh$. See [29.6], p. 284 for channels and I-beams in bending. Table 29.3 gives useful relations. In bending and torsion,

$$k_b = \begin{cases} (d_e/0.30)^{-0.107} = 0.879d_e^{-0.107} & d_e \text{ in inches} \quad (29.9) \\ (d_e/7.62)^{-0.107} = 1.24d_e^{-0.107} & d_e \text{ in mm} \quad (29.10) \end{cases}$$

For axial loading, $k_b = 1$. Table 29.4 gives various expressions for k_b. The Marin size factor is scalar (deterministic). At less than standard specimen diameter (0.30 in), many engineers set $k_b = 1$.

29.3.3 Marin Loading Factor k_c

The Marin loading factor k_c can be expressed as

$$k_c = \alpha S_{ut}^{\beta} \quad (29.11)$$

TABLE 29.3 Equivalent Diameters for Marin Size Factor

Section	Equivalent diameter d_e
Round, rotary bending, torsion	d
Round, nonrotating bending	$0.37d$
Rectangle, nonrotating bending	$0.808bh$

TABLE 29.4 Quantitative Expression for Size Factor

Expression	Range	Proposer
$k_b = \dfrac{0.947}{1 - 0.016/d}$	$0.125 \le d \le 1.875$ in	Moore
$k_b = 0.931\left(1 + \dfrac{0.014}{0.1 + d^2}\right)$	$d \ge 2$ in	Heywood
$k_b = \begin{cases} 0.869d^{-0.097} \\ 1 \\ 1.189d^{-0.97} \end{cases}$	$0.3 < d < 10$ in $d \le 0.3$ in or $d \le 8$ mm $8 < d \le 250$ mm	Shigley and Mitchell
$k_b = \begin{cases} 1 \\ 0.9 \\ 0.8 \\ 0.7 \end{cases}$	$d < 0.4$ in or 10 mm (0.4 in or 10 mm) $< d <$ (2 in or 50 mm) (2 in or 50 mm) $< d <$ (4 in or 100 mm) (4 in or 100 mm) $< d <$ (5 in or 150 mm)	Juvinall
$k_b = 1 - \dfrac{d - 0.3}{15}$	$2 \le d \le 9$ in	Roark

Table 29.5 gives values for α, β. For axial loading of steel based on Table 29.5, Table 29.6 was prepared. Juvinall [29.12] reports that for steel, $0.75 < \bar{k}_c < 1.0$, and suggests using $k_c = 0.90$ for accurate control of loading eccentricity and $0.60 < k_c < 0.85$ otherwise. The problem of load eccentricity plagues testing as well as the designer. Axial loading in fatigue requires caution. See Fig. 29.8.

For torsion, Table 29.7 summarizes experimental experience. In metals described by distortion-energy failure theory, the average value of k_c would be 0.577.

29.3.4 Marin Temperature Factor k_d

Steels exhibit an increase in endurance limit when temperatures depart from ambient. For temperatures up to about 600°F, such an increase is often seen, but above 600°F, rapid deterioration occurs. See Fig. 29.9. If specific material endurance limit–temperature testing is not available, then an ensemble of 21 carbon and alloy

TABLE 29.5 Parameters of Marin Loading Factor

	α		
Mode of loading	kpsi	MPa	β
Bending	1	1	0
Axial	1.23	1.43	–0.078
Torsion	0.328	0.258	0.125

TABLE 29.6 Marin Loading Factor for Axial Loading

S_{ut}, kpsi	$\bar{k}_c$†
50	0.907
100	0.859
150	0.822
200	0.814

† Average entry is 0.853.

TABLE 29.7 Torsional Loading, k_c

Material	Range k_c	$(k_c)_{avg}$
Wrought steels	0.52–0.69	0.60
Wrought Al	0.43–0.74	0.55
Wrought Cu and alloys	0.41–0.67	0.56
Wrought Mg and alloys	0.49–0.61	0.54
Titaniums	0.37–0.57	0.48
Cast irons	0.79–1.01	0.90
Cast Al, Mg, and alloys	0.71–0.91	0.85

steels gives, for t_f in °F,

$$k_d = [0.975 + (0.432 \times 10^{-3})t_f - (0.115 \times 10^{-5})t_f^2 + (0.104 \times 10^{-8})t_f^3 - (0.595 \times 10^{-12})t_f^4]$$
$$70 < t_f < 600°\text{F} \tag{29.12}$$

which equation may be useful. The distribution of k_d is lognormal. See Fig. 29.9 for some specific materials.

29.3.5 Stress Concentration and Notch Sensitivity

The modified Neuber equation (after Heywood) is

$$K_f = \frac{K_t}{1 + \dfrac{2}{\sqrt{r}}\dfrac{K_t - 1}{K_t}\sqrt{a}} \tag{29.13}$$

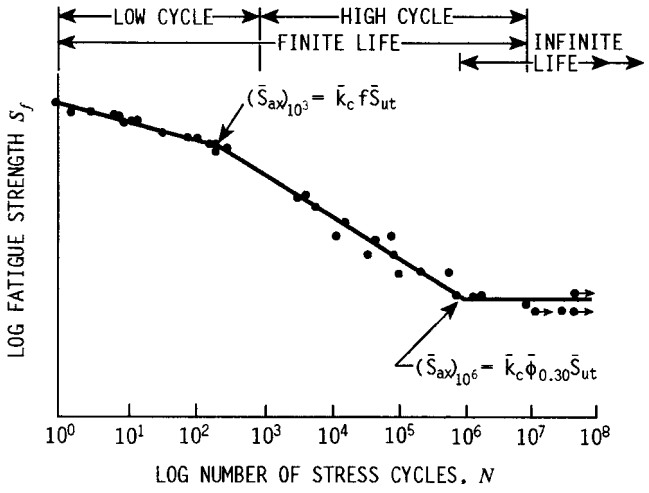

FIGURE 29.8 An SN diagram plotted from the results of completely reversed axial fatigue tests on a normalized 4130 steel, $S_{ut} = 116$ kpsi (data from NACA *Tech. Note* 3866, Dec. 1966).

STRENGTH UNDER DYNAMIC CONDITIONS

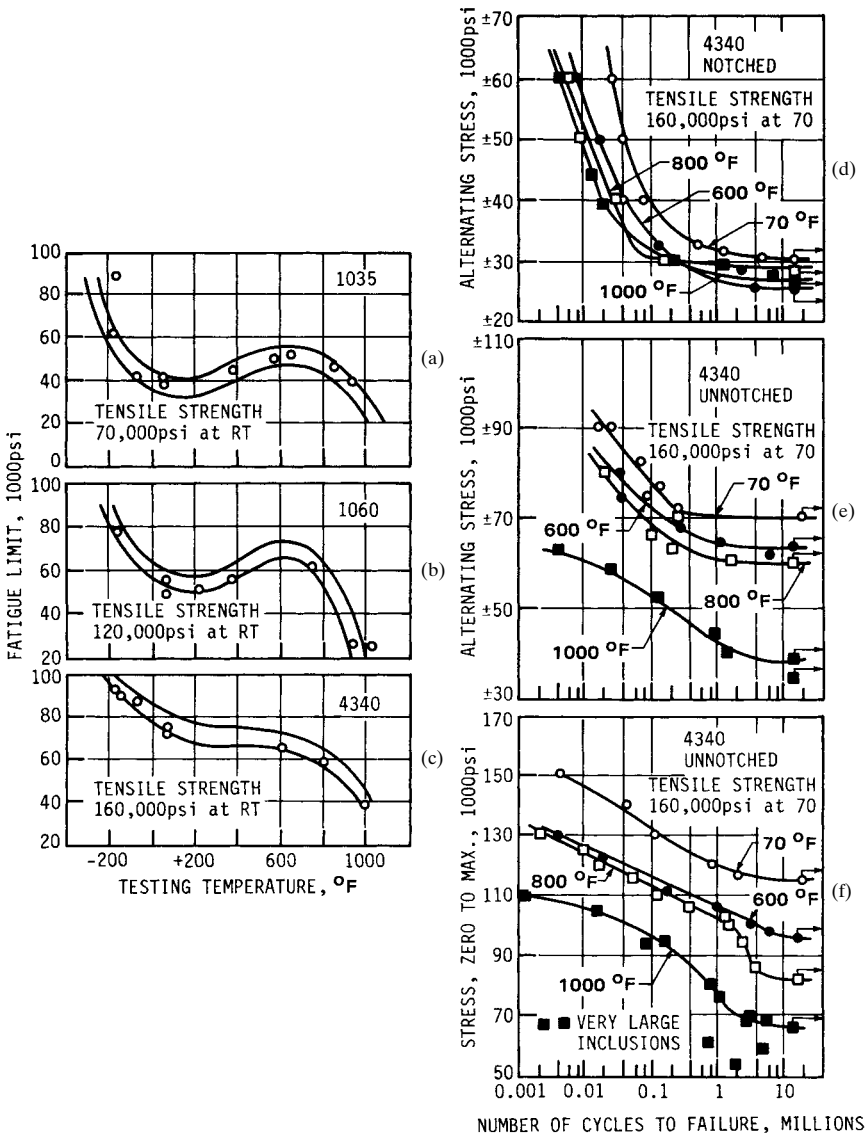

FIGURE 29.9 Effect of temperature on the fatigue limits of three steels: (*a*) 1035; (*b*) 1060; (*c*) 4340; (*d*) 4340, completely reversed loading $K = 3$ to 3.5; (*e*) 4340, completely reversed loading, unnotched; (*f*) 4340, repeatedly applied tension. *(American Society for Metals.)*

Table 29.8 gives values of $\sqrt{a}$. The stress-concentration factor K_f may be applied to the nominal stress σ_0 as $K_f\sigma_0$ as an augmentation of stress (preferred) or as a strength reduction factor $k_e = 1/K_f$ (sometimes convenient).

The finite life stress-concentration factor for steel for N cycles is obtained from the notch sensitivities $(q)_{10^3}$ and $(q)_{10^6}$. For 10^3 cycles,

TABLE 29.8 Heywood's Parameters, Eq. (29.13), Stress Concentration

	$\sqrt{a}$			
Feature	Using $\bar{S}_{ut}$, kpsi	Using $\bar{S}'_e$, kpsi	Using $\bar{S}_{ut}$, MPa	Using $\bar{S}'_e$, MPa
Transverse hole	$5/S_{ut}$	$2.5/S'_e$	$174/S_{ut}$	$87/S'_e$
Shoulder	$4/S_{ut}$	$2/S'_e$	$139/S_{ut}$	$69.5/S'_e$
Groove	$3/S_{ut}$	$1.5/S'_e$	$104/S_{ut}$	$52/S'_e$

$$(q)_{10^3} = \frac{(K_f)_{10^3} - 1}{K_t - 1}$$

$$= -0.18 + (0.43 \times 10^{-2})\bar{S}_{ut} - (0.45 \times 10^{-5})\bar{S}^2_{ut} \tag{29.14}$$

where $\bar{S}_{ut} < 330$ kpsi. For 10^6 cycles,

$$(q)_{10^6} = \frac{(K_f)_{10^6} - 1}{K_t - 1} \tag{29.15}$$

and for N cycles,

$$(K_f)_N = (K_f)_{10^3}\left[\frac{(K_f)_{10^6}}{(K_f)_{10^3}}\right]^{(1/3 \log N - 1)} \tag{29.16}$$

There is some evidence that $\bar{K}_f$ does not exceed 4 for Q&T steels and 3 for annealed steels [29.11]. Figure 29.10 shows scatter bands, and Fig. 29.11 relates notch radius to notch sensitivity.

29.3.6 Miscellaneous-Effects Modification Factor k_e

There are other effects in addition to surface texture, size loading, and temperature that influence fatigue strength. These other effects are grouped together because their influences are not always present, and are not well understood quantitatively in any comprehensive way. They are largely detrimental ($\bar{k}_e < 1$), and consequently cannot be ignored. For each effect present, the designer must make an estimate of the magnitude and probable uncertainty of k_e. Such effects include

- Introduction of complete stress fields due to press or shrink fits, hydraulic pressure, and the like
- Unintentional residual stresses that result from grinding or heat treatment and intentional residual stresses that result from shot peening or rolling of fillets
- Unintended coatings, usually corrosion products, and intentional coatings, such as plating, paint, and chemical sheaths
- Case hardening for wear resistance by processes such as carburization, nitriding, tuftriding, and flame and induction hardening
- Decarburizing of surface material during processing

STRENGTH UNDER DYNAMIC CONDITIONS

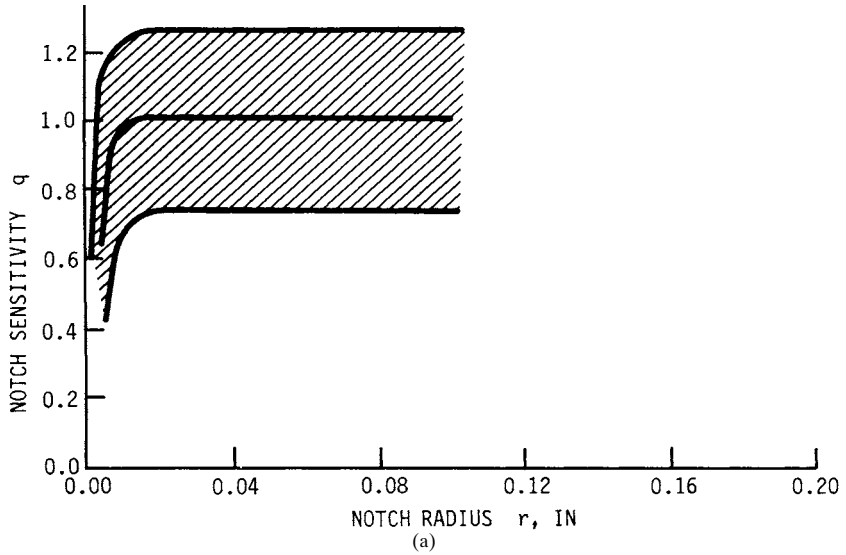

(a)

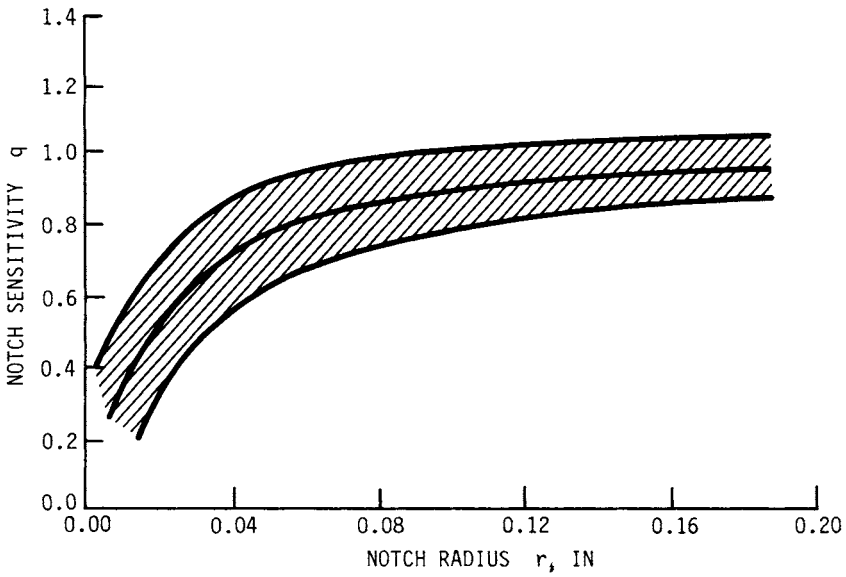

(b)

FIGURE 29.10 Scatter bands of notch sensitivity q as a function of notch radius and heat treatment for undifferentiated steels. (*a*) Quenched and tempered; (*b*) normalized or annealed. *(Adapted from Sines and Waisman [29.16], with permission of McGraw-Hill, Inc.)*

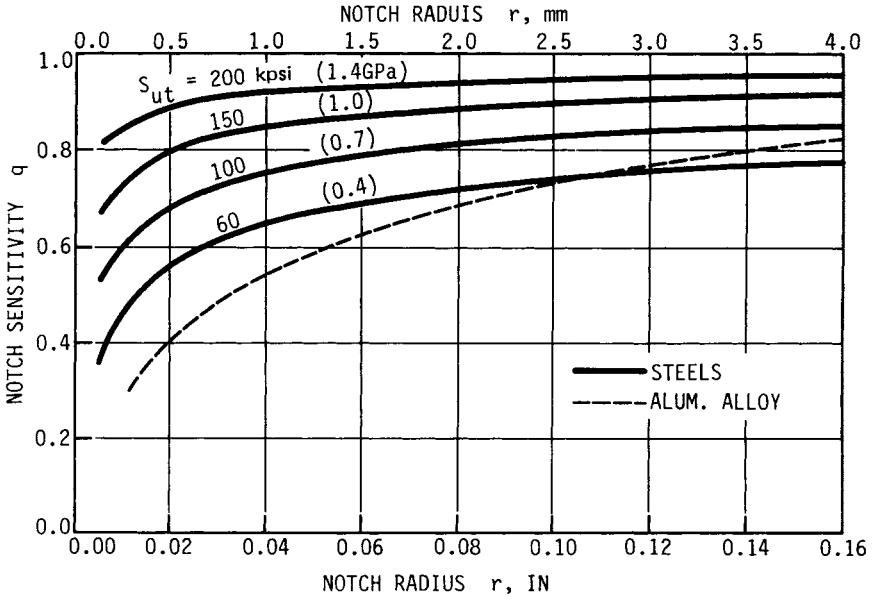

FIGURE 29.11 Notch-sensitivity chart for steels and UNS A92024T wrought aluminum alloys subjected to reversed bending or reversed axial loads. For larger notch radii, use values of q corresponding to $r = 0.16$ in (4 mm). *(From Sines and Waisman [29.16], with permission of McGraw-Hill, Inc.)*

When these effects are present, tests are needed in order to assess the extent of such influences and to form a rational basis for assignment of a fatigue modification factor k_e.

29.4 FLUCTUATING STRESS

Variable loading is often characterized by an amplitude component σ_a as ordinate and a steady component σ_m as abscissa. Defined in terms of maximum stress $\sigma_{\max}$ and minimum stress $\sigma_{\min}$ the coordinates are as follows:

$$\sigma_a = \frac{1}{2}|\sigma_{\max} - \sigma_{\min}| \qquad \sigma_m = \frac{1}{2}(\sigma_{\max} + \sigma_{\min}) \tag{29.17}$$

The designer's fatigue diagram is depicted in Fig. 29.12.

If one plots combinations σ_a and σ_m that partition part survival from part failure, a failure locus is defined. Properties such as ultimate tensile strength $\bar{S}_{ut}$, yield strength in tension $\bar{S}_y$, yield strength in compression $\bar{S}_{yc}$, endurance strength $\bar{S}_e$, or fatigue strength $\bar{S}_f$ appear as axis intercepts. In the range in which σ_m is negative and fatigue fracture is a threat, the failure locus is taken as a horizontal line unless specific experimental data allow another locus. In the range in which σ_m is positive, the preferred locus is Gerber or ASME-Elliptic. The Goodman and Soderberg loci have

STRENGTH UNDER DYNAMIC CONDITIONS

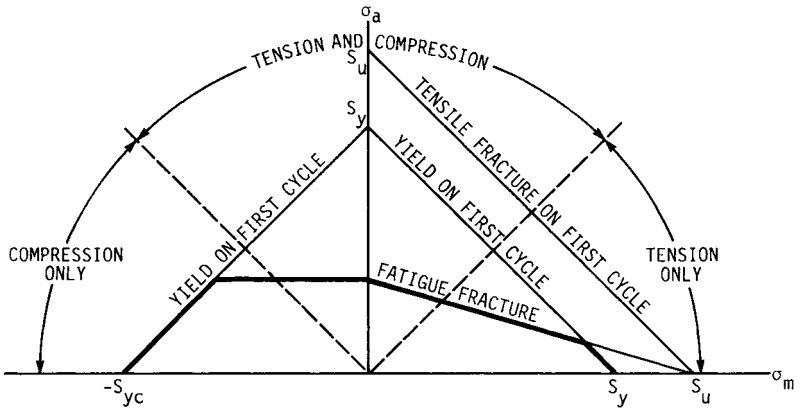

FIGURE 29.12 Designer's fatigue diagram using a Goodman failure locus for push-pull (axial) fatigue.

historical importance and algebraic simplicity, but these loci do not fall centrally among the data, and they are not dependably conservative.

For the Gerber locus,

$$\frac{\sigma_a}{\bar{S}_e} + \left(\frac{\sigma_m}{\bar{S}_{ut}}\right)^2 = 1 \tag{29.18}$$

For the ASME-elliptic fatigue locus,

$$\left(\frac{\sigma_a}{\bar{S}_e}\right)^2 + \left(\frac{\sigma_m}{\bar{S}_y}\right)^2 = 1 \tag{29.19}$$

Brittle materials subject to fluctuating stresses which follow the Smith-Dolan fatigue locus in the first quadrant of the designer's fatigue diagram have

$$\frac{\sigma_a}{\bar{S}_e} = \frac{1 - \sigma_m/\bar{S}_{ut}}{1 + \sigma_m/\bar{S}_{ut}} \tag{29.20}$$

When endurance strengths of steels are plotted against cycles to failure, a logarithmic transformation of each coordinate results in a linear data string in the interval $10^3 \le N \le 10^6$ cycles (see Fig. 29.8). At 10^6 cycles, $\bar{S}_f = \bar{S}_e = \bar{\phi}_{0.30}\bar{S}_{ut}$. At 10^3 cycles, $(\bar{S}_f)_{10^3} = f\bar{S}_{ut}$, where f is a fraction. Arguments in [29.6], p. 279, give

$$f = \frac{S_e}{S_{ut}}\left(\frac{\sigma'_f}{S_e}\right)^{1/2.1} = \frac{S_e}{S_{ut}}\left(\frac{\bar{\sigma}_0\varepsilon_f^m}{S_e}\right)^{1/2.1} \tag{29.21}$$

The fraction of ultimate tensile strength realized at 10^3 cycles is a function of the fatigue ratio $\phi_{0.30}$ and the ultimate tensile strength. The fraction f is in the range $0.8 < f < 1$ for steels. One can estimate f from Eq. (29.21). The constants a and b of $S_f = aN^b$ can then be found from

$$a = \frac{f^2 \bar{S}_{ut}^2}{\bar{S}_e} \tag{29.22}$$

$$b = -\frac{1}{3} \log \frac{f \bar{S}_{ut}}{\bar{S}_e} \tag{29.23}$$

For axial fatigue, the $(\bar{S}_{ax})_{10^3}$ ordinate in Fig. 29.8 is $\bar{k}_c f \bar{S}_{ut}$ and the $(\bar{S}_{ax})_{10^6}$ ordinate is $\bar{k}_c \bar{\phi}_{0.30} \bar{S}_{ut}$, where $\bar{k}_c$ is determined by interpolation in Table 29.6. For torsional fatigue, the $(\bar{S}_{sf})_{10^3}$ ordinate is $\bar{k}_c f \bar{S}_{ut}$ and the $(\bar{S}_{sf})_{10^6}$ ordinate is $\bar{k}_c \bar{\phi}_{0.30} \bar{S}_{ut}$, where $\bar{k}_c$ is taken from Table 29.7 or, for materials following the distortion-energy theory of failure closely, $\bar{k}_c = 0.577$.

29.5 COMPLICATED STRESS-VARIATION PATTERNS

Many loading patterns depart from the sinusoidal character of smoothly rotating machinery and the convenient equation pair displayed as Eq. (29.17). In complicated patterns, characterization in the form of maximum force F_{max} (or maximum stress σ_{max}) and minimum force F_{min} (or minimum stress σ_{min}) is more useful. In fact, max-min (max/min/same max or min/max/same min) will avoid losing a damaging cycle.

Consider a full cycle with stresses varying 60, 80, 40, 60 kpsi and another cycle with stresses –40, –60, –20, –40 kpsi, as depicted in Fig. 29.13*a*. These two cycles cannot be imposed on a part by themselves, but in order for this to be a repetitive block, it is necessary to acknowledge the loading shown by the dashed lines. This adds a hidden cycle that is often ignored. To ensure not losing the hidden cycle, begin the analysis block with the largest (or smallest) stress, adding any preceding history to the right end of the analysis block as shown in Fig. 29.13*b*. One now searches for cycles using max-min characterizations. Taking the "hidden" cycle first so that it is not lost, one moves along the trace as shown by the dashed line in Fig. 29.13*b,* identifying a cycle with a maximum of 80 kpsi and a minimum of –60 kpsi. Looking at the

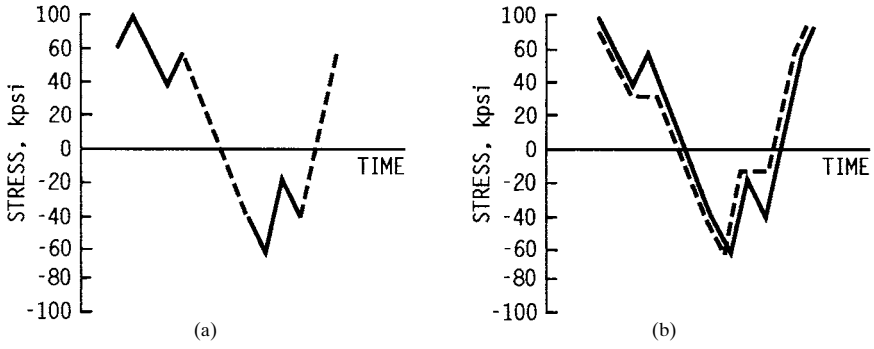

FIGURE 29.13

remaining cycles, one notes a cycle with a maximum of 60 and a minimum of 40 kpsi. There is another with a maximum of –20 and a minimum of –40 kpsi. Since failure theories are expressed in terms of σ_a and σ_m components, one uses Eqs. (29.17) and constructs the table below.

Cycle	σ_{max}	σ_{min}	σ_a	σ_m
1	80	–60	70	10
2	60	40	10	50
3	–20	–40	10	–30

Note that the most damaging cycle, cycle 1, has been identified because care was taken not to lose it. The method used is a variation of the *rainflow counting* technique. One is now ready to apply Miner's rule. Note that if the original cycles were doubled in the block, there would be five cycles, with the additional two duplicating cycles 2 and 3 above.

Example 2. The loading of Fig. 29.13*a* is imposed on a part made of 1045 HR steel. Properties at the critical location are $S_{ut} = 92.5$ kpsi, $S'_e = 46$ kpsi, strain-strengthening coefficient $\bar{\sigma}_0 = 140$ kpsi, true strain at fracture $\varepsilon_f = 0.58$, and strain-strengthening exponent $m = 0.14$. Estimate how many repetitions of the loading block may be applied if a Gerber fatigue locus is used.

Solution. From Eq. (29.21),

$$f = \frac{S_e}{S_{ut}}\left(\frac{\sigma'_f}{S_e}\right)^{1/2.1} = \frac{S_e}{S_{ut}}\left(\frac{\bar{\sigma}_0 \varepsilon_f^m}{S_e}\right)^{1/2.1}$$

$$= \frac{46}{92.5}\left(\frac{140(0.58)^{0.14}}{46}\right)^{1/2.1} = 0.815$$

From Eq. (29.22), $a = \dfrac{0.815^2 92.5^2}{46} = 123.5$ kpsi

From Eq. (29.23),

$$b = -\frac{1}{3}\log\frac{0.815(92.5)}{46} = -0.0715$$

$$(S_f)_{10^3} = fS_{ut} = 0.815(92.5) = 75.39 \text{ kpsi}$$

For cycle 1, which has $\sigma_a = 70$ kpsi and $\sigma_m = 10$ kpsi, using Eq. (29.18),

$$S_f = \frac{\sigma_a}{1 - (\sigma_m/S_{ut})^2} = \frac{70}{1 - (10/92.5)^2} = 70.83 \text{ kpsi}$$

Since required endurance strength 70.83 kpsi is less than $(S_f)_{10^3}$, the number of cycles exceeds 10^3.

$$N_1 = \left(\frac{S_f}{a}\right)^{1/b} = \left(\frac{70.83}{123.5}\right)^{-1/0.0715} = 2383 \text{ cycles}$$

For cycle 2, $S_f = 14.1$ kpsi and $N_2 = 1.5(10^{13}) \doteq \infty$. For cycle 3, $S_f = \sigma_a = 10$ kpsi and $N_3 = 1.8(10^{15}) \doteq \infty$. Extend the previous table:

Cycle	S_f	N
1	70.8	2383
2	14.1	∞
3	10.0	∞

The damage per block application according to Miner's rule is

$$D = \Sigma\,(1/N_i) = 1/2383 + 1/\infty + 1/\infty = 1/2383$$

The number of repetitions of the block is $1/D = 1/(1/2383) = 2383$. For the original two cycles, the damage per block application is $1/\infty + 1/\infty = 0$ and the number of repetitions is infinite. Note the risk of an analysis conclusion associated with not drawing how the cycles connect.

29.6 STRENGTH AT CRITICAL LOCATIONS

The critical locations of strength-limited designs can be identified as regions in which load-induced stresses peak as a result of distribution of bending moment and/or changes in geometry. Since the strength at the critical location in the geometry and at condition of use is required, it is often necessary to reflect the manufacturing process in this estimation. For heat-treatable steels under static loading, an estimate of yield or proof strength is required, and under fatigue loading, an estimate of the ultimate strength of the endurance limit is needed for an adequacy assessment. For the design process, strength as a function of intensity of treatment is required. In Chap. 33, the quantitative estimation methods of Crafts and Lamont and of Grossmann and Field for heat-treatable steels are useful. For cold work and cold heading, the methods of Datsko and Borden give useful estimates.

Consider an eyebolt of cold-formed 1045 steel hot-rolled quarter-inch-diameter rod in the geometry of Fig. 29.14. The properties of the hot-rolled bar are

$$S_y = 60 \text{ kpsi} \qquad m = 0.14 \qquad \bar{\sigma}_o = 140 \text{ kpsi}$$

$$S_u = 92.5 \text{ kpsi} \qquad \varepsilon_f = 0.58$$

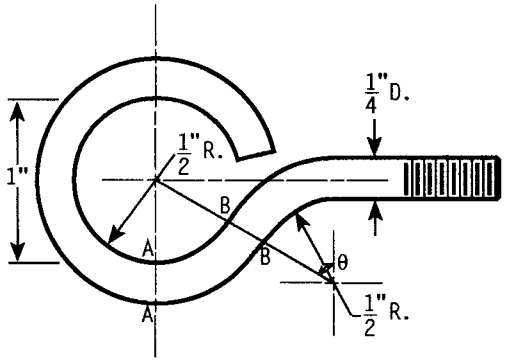

FIGURE 29.14 Geometry of a cold-formed eyebolt.

STRENGTH UNDER DYNAMIC CONDITIONS

At section AA on the inside surface, the true strain is estimated as

$$\varepsilon_i = \left| -\frac{1}{2} \ln \left(1 + \frac{2d}{D} \right) \right| = \left| -\frac{1}{2} \ln \left[1 + \frac{2(0.25)}{1} \right] \right|$$

$$= |-0.203| = 0.203$$

The yield strength of the surface material at this location is estimated as, from Table 33.1,

$$\varepsilon_{quo} = \frac{0.203}{1+1} = 0.1015 \qquad \varepsilon_{qyo} = \frac{0.1015}{1 + 2(0.1015)} = 0.0844$$

$$(S_y)_{tLc} = \bar{\sigma}_o \, (\varepsilon_{qyo})^m = 140(0.0844)^{0.14} = 99 \text{ kpsi}$$

The ultimate strength at this location is estimated as, from Table 33.1,

$$(S_u)_{tLc} = (S_u)_o \exp (\varepsilon_{quo}) = 92.5 \exp (0.1015) = 102.4 \text{ kpsi}$$

Both the yield strength and the ultimate strength have increased. They are nominally equal because the true strain of 0.203 exceeds the true strain of 0.14 which occurs at ultimate load. The yield strength has increased by 65 percent and the ultimate strength has increased by 11 percent at this location. The strength at the inside and outside surface at section BB has not changed appreciably. The changes at the sections above BB are improvements in accord with the local geometry. For dynamic strength, the endurance limits have changed in proportion to the changes in ultimate strength. At section AA the R. R. Moore endurance limit is estimated to be

$$S'_e = \frac{S_u}{2} = \frac{102.4}{2} = 51.2 \text{ kpsi}$$

an improvement of 11 percent. Since the strengths vary with position and stresses vary with position also, a check is in order to see if section AA or section BB is critical in a tensile loading of the eyebolt.

The increase in yield strength and endurance limit due to cold work, while present, may not be helpful. Consider the strip spring formed from bar stock to the geometry of Fig. 29.15. Just to the right of the radius the original properties prevail, and the bending moment is only slightly less than to the left of section AA. In this case, the increased strength at the critical location is not really exploitable.

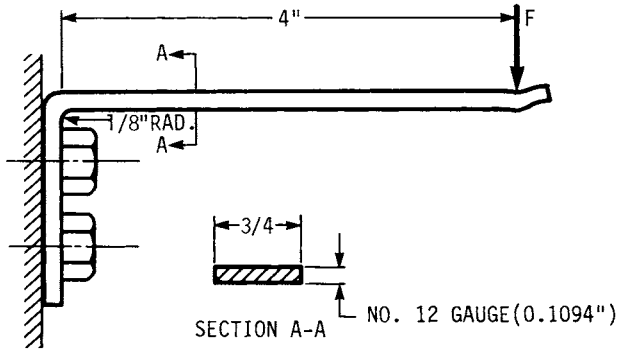

FIGURE 29.15 A latching spring cold formed from ¾-in-wide No. 12 gauge strip.

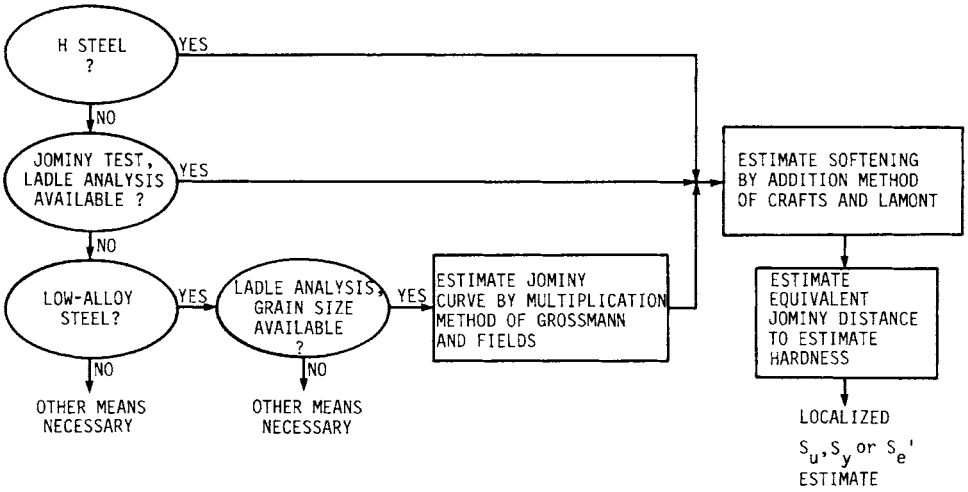

FIGURE 29.16 Logic flowchart for estimation of localized ultimate strength or endurance limit for heat-treated steels.

For parts that are heat-treated by quenching and tempering, the methods and procedures are given in Fig. 29.16 (see Chap. 33). If a shaft has been designed, an adequacy assessment is required. An estimate of the strength at a location where the shaft steps in Fig. 29.17 from 1 to 1.125 in is necessary. The specifications include the material to be 4140 steel quenched in still oil with mild part agitation and tempered for 2 hours at 1000°F. The material earmarked for manufacture has a ladle analysis of

	C	Mn	P	S	Si	Ni	Cr	Mo
Percent	0.40	0.83	0.012	0.009	0.26	0.11	0.94	0.21
Multiplier	0.207	3.87	—	—	1.18	1.04	3.04	1.65

The experience is that a grain size of 7½ can be maintained with this material and heat treatment. The multipliers are determined by the methods of Chap. 33. The ideal critical diameter is estimated as

$$D_I = 0.207(3.87)(1.18)(1.04)(3.04)(1.65) = 4.93 \text{ in}$$

The factors are $D = 5.3$, $B = 10$, and $f = 0.34$. The addition factors are

$$A_{Mn} = 2.1$$

$$A_{Si} = 1.1$$

$$A_{Ni} = 0.03$$

$$A_{Cr} = 4.9$$

$$A_{Mo} = 3.78$$

$$\Sigma A = 11.91$$

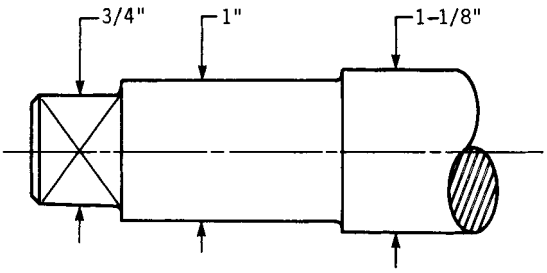

FIGURE 29.17 A portion of a 4140 steel shaft quenched in still oil ($H = 0.35$) and tempered for 2 hours at 1000°F, grain size 7.5.

The tempered hardness equation becomes

$$R_T = (R_Q - 5.3 - 10)0.34 + 10 + 11.91 = 0.34R_Q + 16.71$$

The Jominy curve is predicted by noting that the Rockwell C-scale hardness at Jominy station 1 is

$$(R_Q)_1 = 32 + 60(\%\text{C}) = 32 + 60(0.40) = 56.0$$

and a table is prepared as depicted in Table 29.9 for 1000°F tempering temperature. The variation of surface strength with size of round is prepared using equivalent Jominy distances as depicted in Table 29.10. Table 29.11 shows an ultimate-strength traverse of a 1⅛-in round. There is only a mild strength profile in the traverse. The significant strength for bending and torsion is at the surface. For the 1⅛-in round, the surface ultimate strength is estimated by interpolation to be 164.3 kpsi. The R. R. Moore endurance limit at this location is estimated to be 164.3/2, or 82 kpsi. Steels in large sections or with less alloying ingredients (smaller ideal critical diameters) exhibit larger transverse strength changes. For sections in tension, significant strength is at the center. When testing, machined specimens from the center of a round say little about the strength at the surface. Heat treating a specimen proves little about strengths in the actual part. Some variations in strength attributed to size result from differences in cooling rates.

When the number of cycles is less than 10^7, the endurance strength must be estimated. Reference [29.8] gives a useful curve fit for steels:

$$S'_f = \begin{cases} S_u m^{-m} \exp(m) \varepsilon_f^m N_f^{cm} \exp(-\varepsilon_f N_f^c) & \varepsilon_f N_f^c \le m \\ S_u & \varepsilon_f N_f^c > m \end{cases} \tag{29.24}$$

TABLE 29.9 Surface Ultimate Strength as a Function of Jominy Distance for 4140 Steel Oil Quenched ($H = 0.35$) and Tempered 2 Hours at 1000°F, Grain Size 7½

Jominy distance, $\frac{1}{16}$ in	IH/DH	Predicted Jominy R_Q, Rockwell C	Tempered hardness R_T, Rockwell C	Surface ultimate strength S_u, kpsi
1	1	56.0	44.1	206.6
4	1	56.0	44.1	206.6
8	1.09	51.4	42.0	196.0
12	1.18	47.5	40.3	187.5

TABLE 29.10 Variation of Surface Strength with Diameter of 4140 Steel Round Quenched in Still Oil ($H = 0.35$) and Tempered for 2 Hours at 1000°F, Grain Size 7½

Diameter, in	Equivalent Jominy distance, $\frac{1}{16}$ in	Surface ultimate strength, kpsi
0.1	1.0	167
0.5	2.7	167
1	5.1	165
2	8.2	159.1
3	10.0	156.1
4	11.4	153.2

where m = strain-strengthening exponent
ε_f = true strain at fracture
c = an exponent commonly in the neighborhood of –½
N_f = the number of cycles to failure
S_u = ultimate tensile strength

Example 3. Estimate the finite-life engineering fatigue strength of an annealed 4340 steel with the following properties:

$$S_u = 103 \text{ kpsi} \qquad S_y = 65.6 \text{ kpsi at 0.2 percent offset}$$

$$RA = 0.56$$

Solution. The endurance limit is estimated as $S_u/2 = 103/2 = 51.5$ kpsi at 10^7 cycles. Because no strain-hardening information is supplied, it is necessary to estimate m from

$$\frac{S_u}{S_y} = \left[\frac{m}{(\text{offset}) \exp 1}\right]^m$$

or

$$\frac{103}{65.6} - \left[\frac{m}{0.002(2.718)}\right]^m = 0$$

from which $m = 0.14$. The true strain at fracture can be assessed from the reduction in area:

$$\varepsilon_f = \ln \frac{1}{1 - RA} = \ln \frac{1}{1 - 0.56} = 0.821$$

TABLE 29.11 Variation of Local Strength in a 1.125-in Round of 4140 Steel Quenched in Still Oil ($H = 0.35$) and Tempered for 2 Hours at 1000°F, Grain Size 7½

Radial position	Equivalent Jominy distance, $\frac{1}{16}$ in	Local ultimate strength, kpsi
(0)r	7.33	161.0
0.5r	6.35	162.8
0.8r	5.95	163.5
r	5.55	164.2

The true stress coefficient of the strain-strengthening equation $\bar{\sigma} = \bar{\sigma}_o \varepsilon^m$ is

$$\bar{\sigma}_o = S_u m^{-m} \exp m = 103(0.14)^{-0.14} \exp 0.14$$
$$= 156.0 \text{ kpsi}$$

The constructive strain ε_1 is a root of the equation

$$\frac{\bar{\sigma}_o}{S'_e} \varepsilon_1^m \exp(-\varepsilon_1) - 1 = 0$$

or alternatively,

$$\frac{S_u}{S'_e} m^{-m} \exp(m) \varepsilon_1^m \exp(-\varepsilon_1) - 1 = 0$$

When ε_1 is small, the term $\exp -\varepsilon_1$ approaches 1, and ε_1 can be found explicitly from

$$\varepsilon_1 = \left(\frac{S'_e}{\bar{\sigma}_o}\right)^{1/m} \quad \text{or} \quad \varepsilon_1 = \frac{m}{2.718}\left(\frac{S'_e}{S_u}\right)^{1/m}$$

From the first,

$$\varepsilon_1 = \left(\frac{51.5}{156}\right)^{1/0.14} = 0.000365$$

This value of the constructive strain allows estimation of the exponent c from $\varepsilon_1 = \varepsilon_f N_f^c$:

$$c = \frac{\log \varepsilon_1/\varepsilon_f}{\log N_e} = \frac{\log(0.000\,365/0.821)}{\log 10^7} = -0.4788$$

Now Eq. (29.24) can be written as

$$S'_f = 103(0.14)^{-0.14} \exp(0.14) 0.821^{0.14} N_f^{-0.4778(0.14)} \exp(0.821 N_f^{-0.4788})$$

which simplifies to

$$S'_f = 151.8 N_f^{-0.067} \exp(0.821 N_f^{-0.4788})$$

Table 29.12 can be constructed. See Ref. [29.8] for notch-sensitivity corrections for low cycle strengths.

29.7 COMBINED LOADING

Simple loading is regarded as an influence that results in tension, compression, shear, bending, or torsion, and the stress fields that result are regarded as simple. *Combined loading* is the application of two or more of these simple loading schemes. The stresses that result from both simple and combined loading are three-dimensional. Applying the adjective *combined* to stresses is inappropriate. The nature of both yielding and fatigue for ductile materials is best explained by distortion-energy (octahedral shear, Henckey-von Mises) theory. For variable loading, the stress state is plotted on a modified Goodman diagram that has tensile mean stresses as abscissa and

TABLE 29.12 Fatigue Strength Ratio S_f'/S_u as a Function of Cycles to Failure for Annealed 4340 Steel†

Number of cycles-to-failure N_f	Constructive true strain ε_1	Endurance strength S_f', kpsi	Ratio S_f'/S_u
10^0	0.821	103‡	1‡
10^1	0.273	103‡	1‡
10^2	0.091	101.8	0.99
10^3	0.030	92.7	0.90
10^4	0.010	81.0	0.79
10^5	0.0033	69.9	0.68
10^6	0.0011	60.1	0.58
10^7	0.000 37	51.5	0.50

†S_u = 103 kpsi, S_y = 65.6 kpsi (0.002 offset), reduction in area 56 percent.
‡Since $\varepsilon_1 > m$, $S_f' = S_u$ and $S_f'/S_u = 1$.

tensile stress amplitude as ordinate. The stress amplitude is that present in a uniform tension that induces the same distortion-energy amplitude (octahedral shear amplitude) as is present in the critical location of the machine part. The steady stress is that stress present in a uniform tension that induces the same steady distortion energy (steady octahedral shear) as is present in the critical location of the machine part. The plotting process involves conversion of the actual stress state to the equivalent uniform tension circumstances.

The von Mises axial tensile stress that has the same distortion energy as a general three-dimensional stress field is, in terms of the ordered principal stresses σ_1, σ_2, and σ_3,

$$\sigma_v = \left[\frac{(\sigma_1 - \sigma_2)^2 + (\sigma_2 - \sigma_3)^2 + (\sigma_3 - \sigma_1)^2}{2}\right]^{1/2} \tag{29.25}$$

If one of the principal stresses is zero and the other two are σ_A and σ_B, then

$$\sigma_v = (\sigma_A^2 + \sigma_B^2 - \sigma_A\sigma_B)^{1/2} \tag{29.26}$$

If the axes xy are not principal, then

$$\sigma_v = (\sigma_x^2 + \sigma_y^2 - \sigma_x\sigma_y + 3\tau_{xy}^2)^{1/2} \tag{29.27}$$

If the concern is yielding, then yielding begins when the von Mises stress equals the tensile value of S_y. If the concern is fatigue, then failure occurs when the von Mises steady stress and amplitude equal the simple steady tension and amplitude that result in failure. If Eq. (29.26) is equated to a critical value σ_{cr}, then

$$\sigma_A^2 + \sigma_B^2 - \sigma_A\sigma_B = \sigma_{cr}^2$$

Treating the preceding equation as a quadratic in σ_A, we have

$$\sigma_A = \frac{1}{2}\sigma_B \pm \frac{1}{2}\sqrt{(2\sigma_{cr})^2 - 3\sigma_B^2} \tag{29.28}$$

On a plot in the $\sigma_A\sigma_B$ plane, the critical-stress magnitude can be observed at six places, three tensile and three compressive. The locus is an ellipse with the major axis

STRENGTH UNDER DYNAMIC CONDITIONS

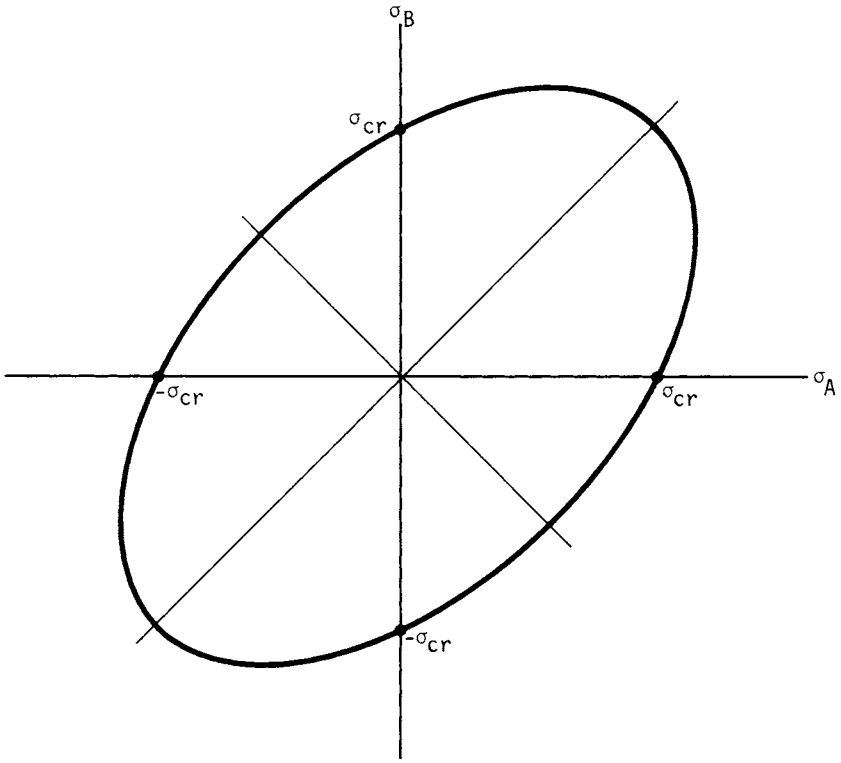

FIGURE 29.18 The distortion-energy critical-stress ellipse. For any point σ_A, σ_B on the ellipse, the uniaxial tension with the same distortion energy is the positive abscissa intercept σ_{cr}, 0.

having a unity slope, as depicted in Fig. 29.18. The octahedral stress (von Mises stress) tensile equivalent is the σ_A-axis intercept of the ellipse. For the Goodman diagram, the transformation is to move the point representing the stress condition σ_A, σ_B to the abscissa, while staying on the ellipse. This is done by Eq. (29.26). For three-dimensional stress, the surface is an ellipsoid in the $\sigma_1\sigma_2\sigma_3$ space, and the transformation is accomplished by Eq. (29.25). Figure 29.19 shows the conversions of the steady-stress condition and the stress-amplitude condition to the respective simple-tension equivalents for the purposes of plotting a point representing the equivalent stress state on the modified Goodman diagram. In Fig. 29.20 an element on a shaft sees a steady torque and fully reversed bending stresses. For the steady-stress element,

$$\tau_{xym} = \frac{16T}{\pi d^3} \qquad \sigma_{Am} = \frac{16T}{\pi d^3} \qquad \sigma_{Bm} = -\frac{16T}{\pi d^3}$$

and the corresponding von Mises stress is

$$\sigma_{vm} = (\sigma_{Am}^2 + \sigma_{Bm}^2 - \sigma_{Am}\sigma_{Bm})^{1/2} = \frac{\sqrt{3}\,16T}{\pi d^3}$$

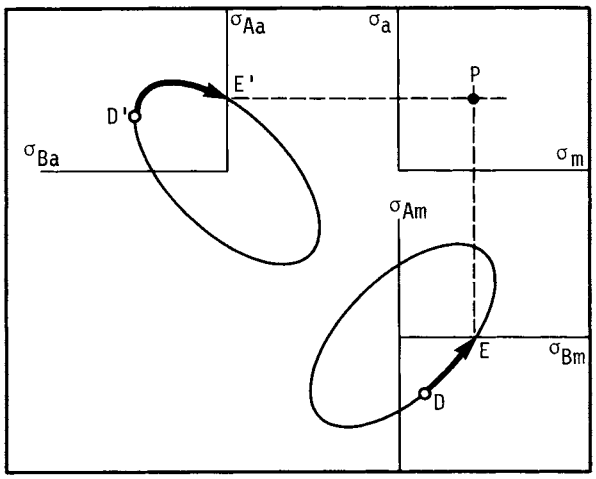

FIGURE 29.19 The principal stresses due to the steady stresses σ_{Am} and σ_{Bm} appear on the distortion-energy ellipse as point *D*. The transform to equivalent distortion energy in tension is point *E*, which becomes the abscissa of point *P*. The principal stresses due to stress amplitude σ_{Aa} and σ_{Ba} appear as point *D′*; the transform is *E′*, which becomes the ordinate of point *P*.

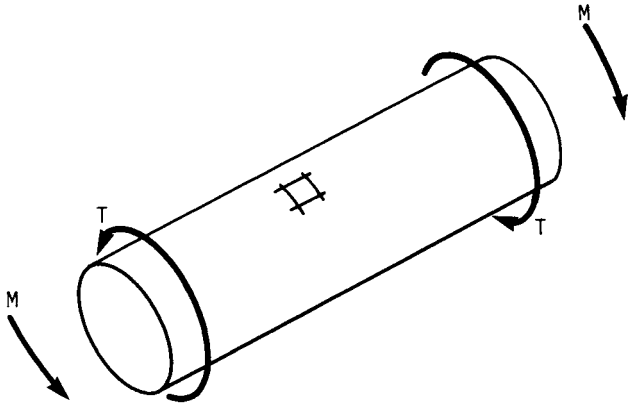

(a)

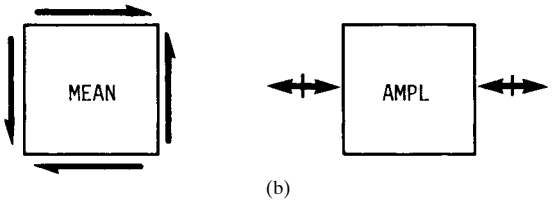

(b)

FIGURE 29.20 (*a*) A shaft subjected to a steady torque *T* and completely reversed flexure due to bending moment *M;* (*b*) the mean-stress element and the stress-amplitude element.

STRENGTH UNDER DYNAMIC CONDITIONS

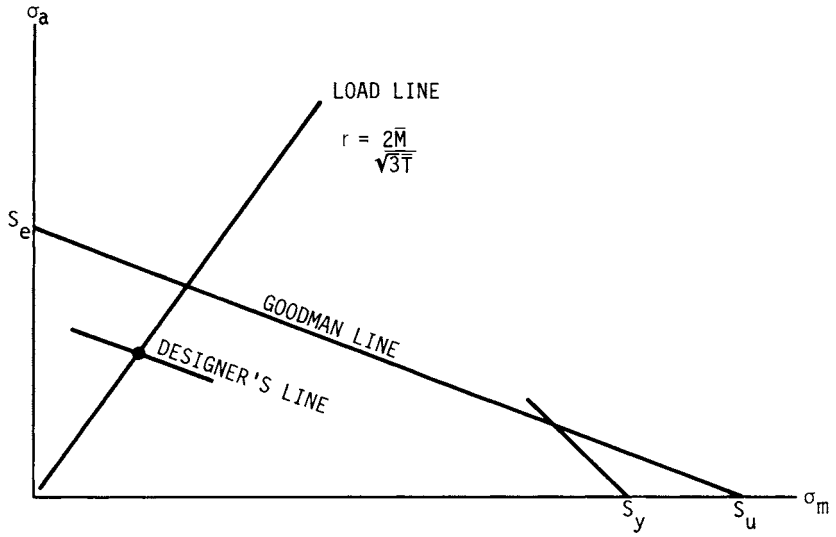

FIGURE 29.21 Designer's fatigue diagram for geared shaft showing load line of slope $r = 2M/(\sqrt{3}T)$, the operating point P, using the Goodman failure locus, and the designer's line reflecting a design factor of n.

For the amplitude-stress element,

$$\sigma_{x,\max} = \frac{32M}{\pi d^3} \qquad \sigma_{x,\min} = -\frac{32M}{\pi d^3}$$

$$\sigma_{Aa} = \frac{32M}{\pi d^3} \qquad \sigma_{Ba} = 0$$

and the corresponding von Mises stress is

$$\sigma_{va} = (\sigma_{Aa}^2 + \sigma_{Ba}^2 - \sigma_{Aa}\sigma_{Ba})^{1/2} = \frac{32M}{\pi d^3}$$

If this is an element of a geared shaft, then M and T are proportional and the locus of possible points is a radial line from the origin with a slope of

$$r = \frac{\sigma_{va}}{\sigma_{vm}} = \frac{32M}{\pi d^3}\,\frac{\pi d^3}{\sqrt{3}\,16T} = \frac{2M}{\sqrt{3}T} \tag{29.29}$$

This is called the *load line.* If data on failures have been collected and converted to von Mises components and a Goodman line is an adequate representation of the failure locus, then for the designer's line in Fig. 29.21,

$$\frac{\sigma_{va}}{S_e} + \frac{\sigma_{vm}}{S_u} = \frac{1}{n} \tag{29.30}$$

where n = design factor. Substituting for σ_{va} and σ_{vm} and solving for d, we obtain

$$d = \left[\frac{32n}{\pi}\left(\frac{M}{S_e} + \frac{\sqrt{3}T}{2S_u}\right)\right]^{1/3} \tag{29.31}$$

Data points representing failure are plotted embracing a significant stress commitment, and the plotted load line represents the same belief. It is appropriate that equations such as Eq. (29.31) be labeled with two adjectives: (1) *significant stress* and (2) *failure locus.* For example, Eq. (29.31) could be called a distortion-energy Goodman equation.

For the case where moments, torques, and thrusts contribute both steady and alternating components of stress, then the distortion-energy Goodman equation for the critical location is

$$\frac{16}{\pi d^3 S_e}\left[\left(2M_a + \frac{P_a d}{4}\right)^2 + 3T_a^2\right]^{1/2} + \frac{16}{\pi d^3 S_u}\left[\left(2M_m + \frac{P_m d}{4}\right)^2 + 3T_m^2\right]^{1/2} - \frac{1}{n} = 0 \quad (29.32)$$

where n = design factor
M_a = component of bending moment causing flexural stress amplitude
M_m = component of bending moment causing flexural stress, steady
T_a = component of torque causing shear-stress amplitude
T_m = component of torque causing shear stress, steady
P_a = component of axial thrust causing tensile-stress amplitude
P_m = component of axial thrust causing tensile stress, steady
S_e = local fatigue strength of shaft material
S_u = ultimate local tensile strength
d = local shaft diameter

Since the equation cannot be solved for d explicitly, numerical methods are used.

29.8 SURFACE FATIGUE

When cylinders are in line contact, sustained by a force F, a flattened rectangular zone exists in which the pressure distribution is elliptical. The half width of the contact zone b is

$$b = \sqrt{\frac{2F}{\pi\ell}\frac{[1-\nu_1^2]/E_1 + [1-\nu_2^2]/E_2}{(1/d_1) + (1/d_2)}} \quad (29.33)$$

The largest stress in magnitude is compressive and exists on the z axis. As a pressure, its magnitude is

$$p_{\max} = \frac{2F}{\pi b \ell} \quad (29.34)$$

Along the z axis, the orthogonal stresses are [29.6]

$$\sigma_x = -2p_{\max}\left[\sqrt{1 + \left(\frac{z}{b}\right)^2} - \frac{z}{b}\right] \quad (29.35)$$

$$\sigma_y = -p_{\max}\left\{\left[2 - \frac{1}{1 + (z/b)^2}\right]\sqrt{1 + \left(\frac{z}{b}\right)^2} - 2\frac{z}{b}\right\} \quad (29.36)$$

$$\sigma_z = \frac{-p_{\max}}{\sqrt{1 + (z/b)^2}} \quad (29.37)$$

These equations can be useful with rolling contact, such as occurs in cams, roller bearings, and gear teeth. The approach of the center of the rollers is

$$\Delta = \frac{2F}{\pi \ell}\left(\frac{1-\nu_1^2}{E_1}+\frac{1-\nu_2^2}{E_2}\right)\left(\ln\frac{d_1}{b}+\ln\frac{d_2}{b}+\frac{2}{3}\right) \tag{29.38}$$

The largest principal stress is compressive and located at the center of the rectangular flat and is $-p_{\max}$ in magnitude. The largest shear stress is approximately $0.30p_{\max}$ and is located at about $0.78b$ below the surface. The maximum compressive stress is repeatedly applied in rolling cylinders. At a position of $z = 0.4b$, $y = 0.915b$ the shear stress has a magnitude of $0.242p_{\max}$ but is completely reversed in rolling cylinders.

The loss of surface integrity due to repeated application of hertzian contact stresses is called *surface fatigue.* The phenomenon is marked by the loss of material from the surface, leaving pits or voids. The onset of fatigue is often defined as the appearance of craters larger than a specified breadth. If Eq. (29.33) is substituted into Eq. (29.34) and the magnitude of $p_{\max}$ associated with the first tangible evidence of fatigue at a specified number of cycles is called the *surface endurance strength* S_{fe}, then

$$\frac{F}{\ell}\left(\frac{2}{d_1}+\frac{2}{d_2}\right)=\pi S_{fe}^2\left(\frac{1-\nu_1^2}{E_1}+\frac{1-\nu_2^2}{E_2}\right)=K \tag{29.39}$$

The left-hand side of the equation consists of parameters under the designer's control. The right-hand side consists of materials properties. The factor K is called *Buckingham's load-stress factor* and is associated with a number of cycles. In gear studies a similar K factor is used and is related to K through

$$K_g = \frac{K}{4}\sin\phi \tag{29.40}$$

where ϕ = gear-tooth pressure angle. Note that $p_{\max}$ is proportional to other stresses present, and it is conventional to describe surface fatigue in terms of the strength S_{fe}. Reference [29.1] gives K_g information for pressure angles of $\phi = 14\frac{1}{2}$ degrees and $\phi = 20$ degrees, as well as S_{fe} for various materials and numbers of cycles. The implication in the literature that above various cycles K_g does not change is unsupported. Log-log plots of K or K_g versus cycles to failure produce "parallel" lines with some consistency in slope for classes of material. AGMA standard 218.01 (Dec. 1982) suggests allowable contact-stress numbers for steel as high as

$$(\sigma)_{10^7} = 0.364H_B + 27 \text{ kpsi} \tag{29.41}$$

for 10^7 cycles, and for the curve fit for other than 10^7 cycles,

$$\sigma_N = C_L\sigma_{10^7} = 2.46N^{-0.056}(0.364H_B + 27) \text{ kpsi} \tag{29.42}$$

For applications where little or no pitting is permissible, the slope of –0.056 persists to 10^{10} (end of presentation). Another curve fit to S_{fe} data for steel at 10^8 cycles is

$$(S_{fe})_{10^8} = 0.4H_B - 10 \text{ kpsi} \tag{29.43}$$

When a gear and pinion are in mesh, the number of cycles to which a point on the tooth surface is exposed is different. Consequently, the material strengths can be tuned to have both pinion and gear show tangible signs of wear simultaneously. For steel gears, using Eq. (29.43), the appropriate gear hardness BHN for a stipulated pinion hardness bhn is

$$\text{BHN} = m_G^{b/2}(\text{bhn} - 25) + 25 \tag{29.44}$$

where m_G = gear ratio, i.e., teeth on the gear per tooth on the pinion. This matching can be done by controlling surface hardness. Strength matching for bending resistance is accomplished by control of core properties.

When needle bearings are specified, the needle assembly is a vendor's product, but the roller track is supplied by the user and is a design concern. The equivalent load F_{eq} accumulating the same damage as a variable radial load F is

$$F_{eq} = \left(\frac{1}{2\pi} \int_0^{2\pi} F^a \, d\theta \right)^{1/a}$$

If the entire assembly is vendor-supplied as a needle-bearing cam follower, then the average load is dictated by the cam-follower force F_{23}. The follower makes m turns per cam revolution. The follower's first turn has an average load to the a power of

$$(F_{23})_1^a = \frac{1}{2\pi/m} \int_0^{2\pi/m} F_{23}^a \, d\theta$$

where $d\theta$ = cam angular displacement. The subsequent averages are

$$(F_{23})_2^a = \frac{1}{2\pi/m} \int_{2\pi/m}^{4\pi/m} F_{23}^a \, d\theta$$

$$\vdots$$

The global average to the a power is

$$F_{\text{global}}^a = \frac{1}{m} \sum_{i=1}^{m} (F_{23})_i^a = \frac{1}{2\pi} \int_0^{2\pi} F_{23}^a \, d\theta$$

Consequently, the roller average radial load is identical to the cam's, but the follower makes m times as many turns.

The follower contact surface between the cam and follower has an endurance strength cycles-to-failure relation of the form of $S^{-1/b}N = K$, and so the average hertzian stress can be written

$$\begin{aligned} \overline{\sigma}_H &= \left(\frac{1}{2\pi} \int_0^{2\pi} \sigma_H^{-1/b} \, d\theta \right)^{-b} \\ &= \frac{C_p}{\sqrt{w}} \left\{ \frac{1}{2\pi} \int_0^{2\pi} [F_{23}(K_c + K_r)]^{-1/2b} \, d\theta \right\}^{-b} \end{aligned} \tag{29.45}$$

where θ = cam rotation angle, b = slope of the rectified SN locus, w = width of the roller or cam (whichever is less), C_p = a joint materials constant

$$C_p = \sqrt{\frac{1}{\pi \left(\dfrac{1 - \nu_1^2}{E_1} + \dfrac{1 - \nu_2^2}{E_2} \right)}} \tag{29.46}$$

and the parameters K_c and K_r = the curvatures of the cam and roller surfaces, respectively.

One surface location on the cam sees the most intense hertzian stress every revolution. That spot has a hertzian stress of

$$\sigma_H = \frac{C_p}{\sqrt{w}} [F_{23}(K_c + K_r)]_{\max}^{1/2} \tag{29.47}$$

Relative strengths can be assessed by noting that the cam requires a strength of $(S_{fe})_{mN}$ at the critical location in order to survive N cycles. The roller sees the average stress everywhere on its periphery mN times, and its strength requirement is $(S_{fe})_{mN}$. The strength ratio is

$$\frac{[(S_{fe})_N]_{\text{cam}}}{[(S_{fe})_{mN}]_{\text{roller}}} = \frac{[F_{23}(K_c + K_r)]_{\max}^{1/2}}{\left\{\frac{1}{2\pi}\int_0^{2\pi} [F_{23}(K_c + K_r)]^{-1/2b}\, d\theta\right\}^{-b}} = \frac{\sqrt{\mathscr{F}_{\max}}}{(\sqrt{\mathscr{F}})_{\text{avg}}}$$

If cam and roller are steel,

$$(S_{fe})_{mN} = m^b (S_{fe})_N$$

enabling us to place endurance strengths on the same life basis, namely, N, which is convenient when consulting tables of Buckingham load-strength data giving K or its equivalent. Thus,

$$\frac{[(S_{fe})_N]_{\text{cam}}}{[(S_{fe})_N]_{\text{roller}}} = \frac{m^b \sqrt{\mathscr{F}_{\max}}}{(\sqrt{\mathscr{F}})_{\text{avg}}}$$

For steel, a 10^8 cycle expression, that is, $(S_{fe}) = 0.4H_B - 10$ kpsi, can be used. Using bhn for roller Brinell hardness and BHN for cam Brinell hardness, we can write

$$\text{BHN} = \frac{m^b \sqrt{\mathscr{F}_{\max}}}{(\sqrt{\mathscr{F}})_{\text{avg}}} (\text{bhn} - 25) + 25 \tag{29.48}$$

This form is convenient because the roller follower is often a vendor-supplied item and the cam is manufactured elsewhere. Since $\sqrt{\mathscr{F}_{\max}}$ is larger than $(\sqrt{\mathscr{F}})_{\text{avg}}$, this alone tends to require that the cam be harder, but since the roller endures more turns, the roller should be harder, since $m > 1$ and $b < 0$. Matching (tuning) the respective hardnesses so that the cam and roller will wear out together is often a design goal.

Design factor can be introduced by reducing strength rather than increasing load (not equivalent when stress is not directly proportional to load). Since the loads are often more accurately known than strengths in these applications, design factors are applied to strength. The relative hardnesses are unaffected by design factor, but the necessary widths are

$$w = \left(\frac{C_p}{S_{fe}/n}\right)^2_{\text{cam}} \mathscr{F}_{\max} \qquad w = \left(\frac{C_p}{S_{fe}/n}\right)^2_{\text{roller}} (\sqrt{\mathscr{F}})_{\text{avg}} m^{-2b} \tag{29.49}$$

Either equation may be used. The width decision controls the median cycles to failure.

REFERENCES

29.1 R. C. Juvinall, *Stress Strain and Strength,* McGraw-Hill, New York, 1967, p. 218.

29.2 E. M. Prot, "Fatigue Testing under Progressive Loading: A New Technique for Testing Materials," E. J. Ward (trans.), Wright Air Development Center Tech. Rep., TR52-148, September 1952.

29.3 J. A. Collins, *Failure of Materials in Mechanical Design,* Wiley-Interscience, New York, 1981, chap. 10.

29.4 W. J. Dixon and F. J. Massey, Jr., *Introduction to Statistical Analysis,* 3d ed., McGraw-Hill, New York, 1969, p. 380.

29.5 J. T. Ransom, *Statistical Aspects of Fatigue,* Special Technical Publication No. 121, American Society for Testing Materials, Philadelphia, Pa., 1952, p. 61.

29.6 J. E. Shigley and C. R. Mischke, *Mechanical Engineering Design,* 5th ed., McGraw-Hill, New York, 1989.

29.7 C. R. Mischke, "A Probabilistic Model of Size Effect in Fatigue Strength of Rounds in Bending and Torsion," *Transactions of ASME, Journal of Machine Design,* vol. 102, no. 1, January 1980, pp. 32–37.

29.8 C. R. Mischke, "A Rationale for Mechanical Design to a Reliability Specification," *Proceedings of the Design Engineering Technical Conference of ASME,* American Society of Mechanical Engineers, New York, 1974, pp. 221–248.

29.9 L. Sors, *Fatigue Design of Machine Components,* Part 1, Pergamon Press, Oxford, 1971, pp. 9–13.

29.10 H. J. Grover, S. A. Gordon, and L. R. Jackson, *Fatigue of Metals and Structures,* Bureau of Naval Weapons Document NAVWEPS 00-25-534, Washington, D.C., 1960, pp. 282–314.

29.11 C. Lipson and R. C. Juvinall, *Handbook of Stress and Strength,* Macmillan, New York, 1963.

29.12 R. C. Juvinall, *Fundamentals of Machine Component Design,* John Wiley & Sons, New York, 1983.

29.13 A. D. Deutschman, W. J. Michels, and C. E. Wilson, *Machine Design,* MacMillan, New York, 1975.

29.14 E. B. Haugen, *Probabilistic Mechanical Design,* John Wiley & Sons, New York, 1980.

29.15 C. R. Mischke, *Mathematical Model Building,* 2d rev. ed., Iowa State University Press, Ames, 1980.

29.16 G. Sines and J. L. Waisman (eds.), *Metal Fatigue,* McGraw-Hill, New York, 1959.

29.17 H. O. Fuchs and R. I. Stephens, *Metal Fatigue in Engineering,* John Wiley & Sons, New York, 1980.

RECOMMENDED READING

Proceedings of the Society of Automotive Engineers Fatigue Conference, P109, Warrendale, Pa. April 1982.

CHAPTER 30
INSTABILITIES IN BEAMS AND COLUMNS

Harry Herman
Professor of Mechanical Engineering
New Jersey Institute of Technology
Newark, New Jersey

NOTATION

A	Area of cross section
$B(n)$	Arbitrary constants
$c(n)$	Coefficients in series
$c(y), c(z)$	Distance from y and z axis, respectively, to outermost compressive fiber
e	Eccentricity of axial load P
E	Modulus of elasticity of material
$E(t)$	Tangent modulus for buckling outside of elastic range
$F(x)$	A function of x
G	Shear modulus of material
h	Height of cross section
H	Horizontal (transverse) force on column
I	Moment of inertia of cross section
$I(y), I(z)$	Moment of inertia with respect to y and z axis, respectively
J	Torsion constant; polar moment of inertia
k^2	P/EI
K	Effective-length coefficient
$K(0)$	Spring constant for constraining spring at origin

$K(T, 0), K(T, L)$	Torsional spring constants at $x = 0, L,$ respectively
l	Developed length of cross section
L	Length of column or beam
L_{eff}	Effective length of column
M, M'	Bending moments
$M(0), M(L), M_{\text{mid}}$	Bending moments at $x = 0, L,$ and midpoint, respectively
$M(0)_{\text{cr}}$	Critical moment for buckling of beam
M_{tr}	Moment due to transverse load
$M(y), M(z)$	Moment about y and z axis, respectively
n	Integer; running index
P	Axial load on column
P_{cr}	Critical axial load for buckling of column
r	Radius of gyration
R	Radius of cross section
s	Running coordinate, measured from one end
t	Thickness of cross section
T	Torque about x axis
x	Axial coordinate of column or beam
y, z	Transverse coordinates and deflections
Y	Initial deflection (crookedness) of column
Y_{tr}	Deflection of beam-column due to transverse load
η	Factor of safety
σ	Stress
ϕ	Angle of twist

As the terms *beam* and *column* imply, this chapter deals with members whose cross-sectional dimensions are small in comparison with their lengths. Particularly, we are concerned with the stability of beams and columns whose axes in the undeformed state are substantially straight. Classically, instability is associated with a state in which the deformation of an idealized, perfectly straight member can become arbitrarily large. However, some of the criteria for stable design which we will develop will take into account the influences of imperfections such as the eccentricity of the axial load and the crookedness of the centroidal axis of the column. The magnitudes of these imperfections are generally not known, but they can be estimated from manufacturing tolerances. For axially loaded columns, the onset of instability is related to the moment of inertia of the column cross section about its minor principal axis. For beams, stability design requires, in addition to the moment of inertia, the consideration of the torsional stiffness.

30.1 EULER'S FORMULA

We will begin with the familiar Euler column-buckling problem. The column is idealized as shown in Fig. 30.1. The top and bottom ends are pinned; that is, the moments

INSTABILITIES IN BEAMS AND COLUMNS

at the ends are zero. The bottom pin is fixed against translation; the top pin is free to move in the vertical direction only; and the force P acts along the x axis, which coincides with the centroidal axis in the undeformed state. It is important to keep in mind that the analysis which follows applies only to columns with cross sections and loads that are symmetrical about the xy plane in Fig. 30.1 and satisfy the usual assumptions of linear beam theory. It is particularly important in this connection to keep in mind that this analysis is valid only when the deformation is such that the square of the slope of the tangent at any point on the deflection curve is negligibly small compared to unity (fortunately, this is generally true in design applications). In such a case, the familiar differential equation for the bending of a beam is applicable. Thus,

$$EI\frac{d^2y}{dx^2} = M \tag{30.1}$$

For the column in Fig. 30.1,

$$M = -Py \tag{30.2}$$

We take E and I as constant, and let

$$\frac{P}{EI} = k^2 \tag{30.3}$$

Then we get, from Eqs. (30.1), (30.2), and (30.3),

$$\frac{d^2y}{dx^2} + k^2y = 0 \tag{30.4}$$

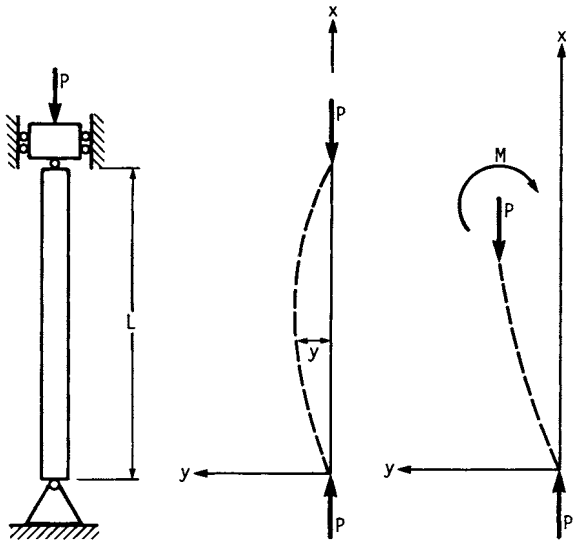

FIGURE 30.1 Deflection of a simply supported column. (*a*) Ideal simply supported column; (*b*) column-deflection curve; (*c*) free-body diagram of deflected segment.

The boundary conditions at $x = 0$ and $x = L$ are

$$y(0) = y(L) = 0 \tag{30.5}$$

In order that Eqs. (30.4) and (30.5) should have a solution $y(x)$ that need not be equal to zero for all values of x, k must take one of the values in Eq. (30.6):

$$k(n) = \frac{n\pi}{L} \qquad n = 1, 2, 3, \ldots \tag{30.6}$$

which means that the axial load P must take one of the values in Eq. (30.7):

$$P(n) = \frac{n^2\pi^2 EI}{L^2} \qquad n = 1, 2, 3, \ldots \tag{30.7}$$

For each value of n, the corresponding nonzero solution for y is

$$y(n) = B(n) \sin\left(\frac{n\pi x}{L}\right) \qquad n = 1, 2, 3, \ldots \tag{30.8}$$

where $B(n)$ is an arbitrary constant.

In words, the preceding results state the following: Suppose that we have a perfectly straight prismatic column with constant properties over its entire length. If the column is subjected to a perfectly axial load, there is a set of load values, together with a set of sine-shaped deformation curves for the column axis, such that the applied moment due to the axial load and the resisting internal moment are in equilibrium everywhere along the column, no matter what the amplitude of the sine curve may be. From Eq. (30.7), the smallest load at which such deformation occurs, called the *critical load,* is

$$P_{cr} = \frac{\pi^2 EI}{L^2} \tag{30.9}$$

This is the familiar Euler formula.

30.2 EFFECTIVE LENGTH

Note that the sinusoidal shape of the solution function is determined by the differential equation and does not depend on the boundary conditions. If we can find a segment of a sinusoidal curve that satisfies our chosen boundary conditions and, in turn, we can find some segment of that curve which matches the curve in Fig. 30.1, we can establish a correlation between the two cases. This notion is the basis for the "effective-length" concept. Recall that Eq. (30.9) was obtained for a column with both ends simply supported (that is, the moment is zero at the ends). Figure 30.2 illustrates columns of length L with various idealized end conditions. In each case, there is a multiple of L, KL, which is called the *effective length of the column* L_{eff}, that has a shape which is similar to and behaves like a simply supported column of that length. To determine the critical loads for columns whose end supports may be idealized as shown in Fig. 30.2, we can make use of Eq. (30.9) if we replace L by KL, with the appropriate value of K taken from Fig. 30.2. Particular care has to be taken

INSTABILITIES IN BEAMS AND COLUMNS

to distinguish between the case in Fig. 30.2*c,* where both ends of the column are secured against rotation and transverse translation, and the case in Fig. 30.2*e,* where the ends do not rotate, but relative transverse movement of one end of the column with respect to the other end is possible. The effective length in the first case is half that in the second case, so that the critical load in the first case is four times that in the second case. A major difficulty with using the results in Fig. 30.2 is that in real problems a column end is seldom perfectly fixed or perfectly free (even approximately) with regard to translation or rotation. In addition, we must remember that the critical load is inversely proportional to the square of the effective length. Thus a change of 10 percent in L_{eff} will result in a change of about 20 percent in the critical load, so that a fair approximation of the effective length produces an unsatisfactory approximation of the critical load. We will now develop more general results that will allow us to take into account the elasticity of the structure surrounding the column.

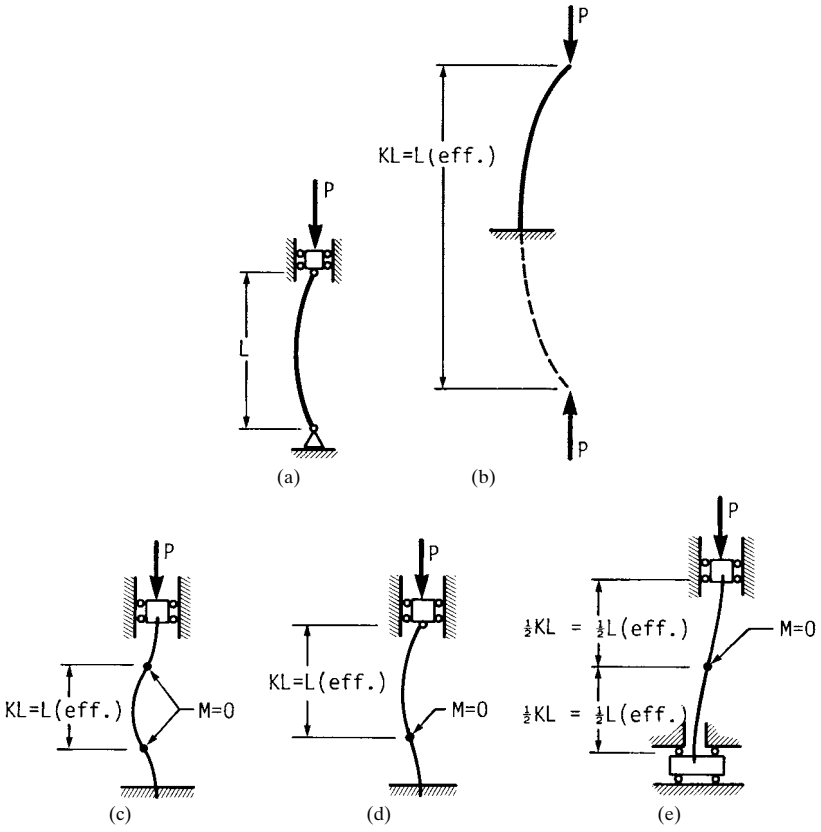

FIGURE 30.2 Effective column lengths for different types of support. (*a*) Simply supported, $K = 1$; (*b*) fixed-free, $K = 2$; (*c*) fixed-fixed, $K = ½$; (*d*) fixed-pinned, $K = 0.707$; (*e*) ends nonrotating, but have transverse translation.

30.3 GENERALIZATION OF THE PROBLEM

We will begin with a generalization of the case in Fig. 30.2*e.* In Fig. 30.3, the lower end is no longer free to translate, but instead is elastically constrained. The differential equation is

$$EI\frac{d^2y}{dx^2} = M = M(0) + P[y(0) - y] + Hx \tag{30.10}$$

Here H, the horizontal force at the origin, may be expressed in terms of the deflection at the origin $y(0)$ and the constant of the constraining spring $K(0)$:

$$H = -K(0)y(0) \tag{30.11}$$

$M(0)$ is the moment which prevents rotation of the beam at the origin. The moment which prevents rotation of the beam at the end $x = L$ is $M(L)$. The boundary conditions are

$$y(L) = 0 \qquad \frac{dy(L)}{dx} = 0 \qquad \frac{dy(0)}{dx} = 0 \tag{30.12}$$

The rest of the symbols are the same as before. We define k as in Eq. (30.3). As in the case of the simply supported column, Eqs. (30.10), (30.11), and (30.12) have solutions in which $y(x)$ need not be zero for all values of x, but again these solutions occur only for certain values of kL. Here these values of kL must satisfy Eq. (30.13):

$$[2(1 - \cos kL) - kL \sin kL]L^3K(0) + EI(kL)^3 \sin kL = 0 \tag{30.13}$$

The physical interpretation is the same as in the simply supported case. If we denote the lowest value of kL that satisfies Eq. (30.13) by $(kL)_{cr}$, then the column buckling load is given by

$$P_{cr} = \frac{EI(kL)_{cr}^2}{L^2} \tag{30.14}$$

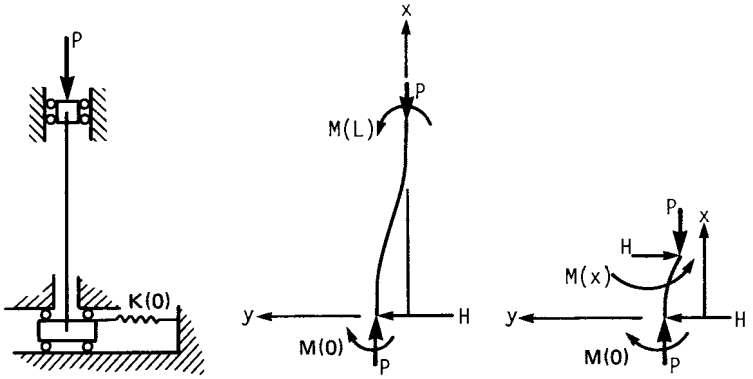

FIGURE 30.3 Column with ends fixed against rotation and an elastic end constraint against transverse deflection. (*a*) Undeflected column; (*b*) deflection curve; (*c*) free-body diagram of deflected segment.

Since the column under consideration here has greater resistance to buckling than the case in Fig. 30.2*e,* the $(kL)_{cr}$ here will be greater than π. We can therefore evaluate Eq. (30.13) beginning with $kL = \pi$ and increasing it slowly until the value of the left side of Eq. (30.13) changes sign. Since $(kL)_{cr}$ lies between the values of kL for which the left side of Eq. (30.13) has opposite signs, we now have bounds on $(kL)_{cr}$. To obtain improved bounds, we take the average of the two bounding values, which we will designate by $(kL)_{av}$. If the value of the left side of Eq. (30.13) obtained by using $(kL)_{av}$ is positive (negative), then $(kL)_{cr}$ lies between $(kL)_{av}$ and that value of kL for which the left side of Eq. (30.13) is negative (positive). This process is continued, using the successive values of $(kL)_{av}$ to obtain improved bounds on $(kL)_{cr}$, until the desired accuracy is obtained.

The last two equations in Eq. (30.12) imply perfect rigidity of the surrounding structure with respect to rotation. A more general result may be obtained by taking into account the elasticity of the surrounding structure in this respect. Suppose that the equivalent torsional spring constants for the surrounding structure are $K(T, 0)$ and $K(T, L)$ at $x = 0$ and $x = L$, respectively. Then Eq. (30.12) is replaced by

$$\begin{aligned} y(L) &= 0 \\ M(0) &= K(T, 0)\,\frac{dy(0)}{dx} \\ M(L) &= -K(T, L)\,\frac{dy(L)}{dx} \end{aligned} \tag{30.15}$$

Proceeding as before, with Eq. (30.15) replacing Eq. (30.12), we obtain the following equation for kL:

$$\begin{aligned} &\left\{\left[\frac{L^3}{EI(kL)^3}\right][K(T, 0) + K(T, L)]K(0) - \left[\frac{L^4K(0)K(T, 0)K(T, L)}{(EI)^2(kL)^3}\right]\right. \\ &\quad \left. + \left[\frac{K(0)L^2}{(kL)}\right] + \left[\frac{LK(T, 0)K(T, L)}{EI(kL)}\right] - \left[\frac{EI(kL)}{L}\right]\right\} \sin kL \\ &\quad + \left\{K(T, 0) + K(T, L) - \left[\frac{L^3}{EI(kL)^2}\right][K(T, 0) + K(T, L)]K(0)\right\} \cos kL \\ &\qquad + 2\left[\frac{L^4K(0)K(T, 0) + K(T, L)}{(EI)^2(kL)^4}\right](1 - \cos kL) = 0 \end{aligned} \tag{30.16}$$

The lowest value of kL satisfying Eq. (30.16) is the $(kL)_{cr}$ to be substituted in Eq. (30.14) in order to obtain the critical load. Here there is no apparent good guess with which to begin computations. Considering the current accessibility of computers, a convenient approach would be to obtain a plot of the left side of Eq. (30.16) for $0 \le kL < \pi$, and if there is no change in sign, extend the plot up to $kL = 2\pi$, which is the solution for the column with a perfectly rigid surrounding structure (Fig. 30.2*c*).

30.4 MODIFIED BUCKLING FORMULAS

The critical-load formulas developed above provide satisfactory values of the allowable load for very slender columns for which buckling, as manifested by unaccept-

ably large deformation, will occur within the elastic range of the material. For more massive columns, the deformation enters the plastic region (where strain increases more rapidly with stress) prior to the onset of buckling. To take into account this change in the stress-strain relationship, we modify the Euler formula. We define the *tangent modulus* $E(t)$ as the slope of the tangent to the stress-strain curve at a given strain. Then the modified formulas for the critical load are obtained by substituting $E(t)$ for E in Eq. (30.9) and Eq. (30.13) plus Eq. (30.14) or Eq. (30.16) plus Eq. (30.14). This will produce a more accurate prediction of the buckling load. However, this may not be the most desirable design approach. In general, a design which will produce plastic deformation under the operating load is undesirable. Hence, for a column which will undergo plastic deformation prior to buckling, the preferred design-limiting criterion is the onset of plastic deformation, not the buckling.

30.5 STRESS-LIMITING CRITERION

We will now develop a design criterion which will enable us to use the yield strength as the upper bound for acceptable design regardless of whether the stress at the onset of yielding precedes or follows buckling. Here we follow Ref. [30.1]. This approach has the advantage of providing a single bounding criterion that holds irrespective of the mode of failure. We begin by noting that, in general, real columns will have some imperfection, such as crookedness of the centroidal axis or eccentricity of the axial load. Figure 30.4 shows the difference between the behavior of an ideal, perfectly straight column subjected to an axial load, in which case we obtain a distinct critical point, and the behavior of a column with some imperfection.

It is clear from Fig. 30.4 that the load-deflection curve for an imperfect column has no distinct critical point. Instead, it has two distinct regions. For small axial loads, the deflection increases slowly with load. When the load is approaching the critical value obtained for a perfect column, a small increment in load produces a large change in deflection. These two regions are joined by a "knee." Thus the advent of buckling in a real column corresponds to the entry of the column into the second, above-the-knee, load-deflection region. A massive column will reach the stress at the yield point prior to buckling, so that the yield strength will be the limiting criterion for the maximum allowable load. A slender column will enter the above-the-

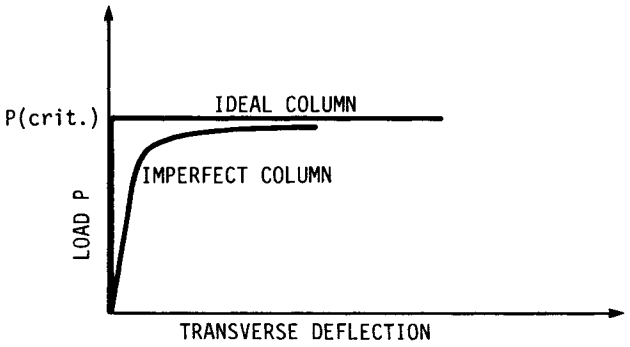

FIGURE 30.4 Typical load-deflection curves for ideal and real columns.

knee region prior to reaching the stress at the yield point, but once in the above-the-knee region, it requires only a small increment in load to produce a sufficiently large increase in deflection to reach the yield point. Thus the corresponding yield load may be used as an adequate approximation of the buckling load for a slender column as well. Hence the yield strength provides an adequate design bound for both massive and slender columns. It is also important to note that, in general, columns found in applications are sufficiently massive that the linear theory developed here is valid within the range of deflection that is of interest.

Application of Eq. (30.1) to a simply supported imperfect column with constant properties over its length yields a modification of Eq. (30.4). Thus,

$$\frac{d^2y}{dx^2} + k^2y = k^2(e - Y) \tag{30.17}$$

where e = eccentricity of the axial load P (taken as positive in the positive y direction) and Y = initial deflection (crookedness) of the unloaded column. The x axis is taken through the end points of the centroidal axis, so that Eq. (30.5) still holds and Y is zero at the end points. Note that the functions in the right side of Eq. (30.8) form a basis for a trigonometric (Fourier) series, so that any function of interest may be expressed in terms of such a series. Thus we can write

$$Y = \sum_{n=1}^{\infty} c(n) \sin \frac{n\pi x}{L} \tag{30.18}$$

where

$$c(n) = \frac{2}{L} \int_0^L Y(x) \sin \frac{n\pi x}{L}\, dx \tag{30.19}$$

The solution for the deflection y in Eq. (15.17) is given by

$$y = P \sum_{n=1}^{\infty} \left[c(n) - \frac{4e}{n\pi} \right] \frac{\sin (n\pi x/L)}{[EI(n\pi/L)^2 - P]} \tag{30.20}$$

The maximum deflection y_{max} of a simply supported column will usually (except for cases with a pronounced and asymmetrical initial deformation or antisymmetrical load eccentricity) occur at the column midpoint. A good approximation (probably within 10 percent) of y_{max} in the above-the-knee region that may be used in deflection-limited column design is given by the coefficient of the first term in Eq. (30.20):

$$y_{max} = \frac{P[c(1) - (4e/\pi)]}{EI(\pi/L)^2 - P} \tag{30.21}$$

The maximum bending moment will also usually occur at the column midpoint and at incipient yielding is closely approximated by

$$M_{max} = P\left\{ e - Y_{mid} + \left[\frac{4e}{\pi} - c(1) \right] \frac{P}{[EI(\pi/L)^2 - P]} \right\} \tag{30.22}$$

The immediately preceding analysis deals with the bending moment about the z axis (normal to the paper). Clearly, a similar analysis can be made with regard to bending about the y axis (Fig. 30.1). Unlike the analysis of the perfect column, where it is merely a matter of finding the buckling load about the weaker axis, in the

present approach the effects about the two axes interact in a manner familiar from analysis of an eccentrically loaded short strut. We now use the familiar expression for combining direct axial stresses and bending stresses about two perpendicular axes. Since there is no ambiguity, we will suppress the negative sign associated with compressive stress:

$$\sigma = \frac{P}{A} + \frac{M(z)c(y)}{I(z)} + \frac{M(y)c(z)}{I(y)} \tag{30.23}$$

where $c(y)$ and $c(z)$ = perpendicular distances from the z axis and y axis, respectively (these axes meet the x axis at the cross-section centroid at the origin), to the outermost fiber in compression; A = cross-sectional area of the column; and σ = total compressive stress in the fiber which is farthest removed from both the y and z axes. For an elastic design limited by yield strength, σ is replaced by the yield strength; $M(z)$ in the right side of Eq. (30.23) is the magnitude of the right side of Eq. (30.22); and $M(y)$ is an expression similar to Eq. (30.22) in which the roles of the y and z axes interchange.

Usually, in elastic design, the yield strength is divided by a chosen factor of safety η to get a permissible or allowable stress. In problems in which the stress increases linearly with the load, dividing the yield stress by the factor of safety is equivalent to multiplying the load by the factor of safety. However, in the problem at hand, it is clear from the preceding development that the stress is not a linear function of the axial load and that we are interested in the behavior of the column as it enters the above-the-knee region in Fig. 30.4. Here it is necessary to multiply the applied axial load by the desired factor of safety. The same procedure applies in introducing a factor of safety in the critical-load formulas previously derived.

Example 1. We will examine the design of a nominally straight column supporting a nominally concentric load. In such a case, a circular column cross section is the most reasonable choice, since there is no preferred direction. For this case, Eq. (30.23) reduces to

$$\sigma = \frac{P}{A} + \frac{Mc}{I} \tag{1}$$

For simplicity, we will suppose that the principal imperfection is due to the eccentric location of the load and that the column crookedness effect need not be taken into account, so that Eq. (30.22) reduces to

$$M_{\max} = P\left\{e + \left(\frac{4e}{\pi}\right)\frac{P}{[EI(\pi/L)^2 - P]}\right\} \tag{2}$$

Note that for a circular cross section of radius R, the area and moment of inertia are, respectively,

$$A = \pi R^2 \qquad \text{and} \qquad I = \frac{\pi R^4}{4} = \frac{A^2}{4\pi} \tag{3}$$

We will express the eccentricity of the load as a fraction of the cross-section radius. Thus,

$$e = \varepsilon R \tag{4}$$

INSTABILITIES IN BEAMS AND COLUMNS

Then we have, from Eqs. (1) through (4),

$$\sigma_{\text{allow}} = \frac{P}{A} + \frac{4P\varepsilon}{A}\left\{1 + \left(\frac{4}{\pi}\right)\frac{P}{[(EA^2)/(4\pi)](\pi/L)^2 - P}\right\} \tag{5}$$

Usually P and L are given, σ and E are the properties of chosen material, and ε is determined from the clearances, tolerances, and kinematics involved, so that Eq. (5) is reduced to a cubic in A.

At the moment, however, we are interested in comparing the allowable nominal column stress P/A with the allowable stress of the material σ_{allow} for columns of different lengths. Keeping in mind that the radius of gyration r of a circular cross section of geometric radius R is $R/2$, we will define

$$\frac{R}{2} = r$$

$$\frac{\sigma_{\text{allow}}}{P/A} = p \tag{6}$$

$$\frac{E}{\sigma_{\text{allow}}} = q$$

Then Eq. (5) may be written as

$$p = 1 + 4\varepsilon + \frac{16\varepsilon}{\pi[\pi^2 pq(r/L)^2 - 1]} \tag{7}$$

The first term on the right side of Eq. (7) is due to direct compressive stress; the second term is due to the bending moment produced by the load eccentricity; the third term is due to the bending moment arising from the column deflection. When ε is small, p will be close to unity unless the denominator in the third term on the right side of Eq. (7) becomes small—that is, the moment due to the column deflection becomes large. The ratio L/r, whose reciprocal appears in the denominator of the third term, is called the *slenderness ratio.* Equation (7) may be rewritten as a quadratic in p. Thus,

$$\pi^2 q\left(\frac{r}{L}\right)^2 p^2 - \left[(1 + 4\varepsilon)\pi^2 q\left(\frac{r}{L}\right)^2 + 1\right]p + (1 + 4\varepsilon) - \frac{16\varepsilon}{\pi} = 0 \tag{8}$$

We will take for q the representative value of 1000 and tabulate $1/p$ for a number of values of L/r and ε. To compare the value of $1/p$ obtained from Eq. (8) with the corresponding result from Euler's formula, we will designate the corresponding result obtained by Euler's formula as $1/p_{\text{cr}}$ and recast Eq. (30.9) as

$$\frac{1}{p_{\text{cr}}} = \pi^2 q\left(\frac{r}{L}\right)^2 \tag{9}$$

To interpret the results in Table 30.1, note that the quantities in the second and third columns of the table are proportional to the allowable loads calculated from the respective equations. As expected, the Euler formula is completely inapplicable when L/r is 50. Also, as expected, the allowable load decreases as the eccentricity increases. However, the effect of eccentricity on the allowable load decreases as the slenderness ratio L/r increases. Hence when L/r is 250, the Euler buckling load, which is the limiting case for which the eccentricity is zero, is only about 2 percent higher than when the eccentricity is 2 percent.

TABLE 30.1 Influence of Eccentricity and Slenderness Ratio on Allowable Load

ε	L/r	p^{-1}	p_{cr}^{-1}
0.02	50	0.901	3.95
	150	0.408	0.439
	250	0.155	0.158
0.05	50	0.791	3.95
	150	0.374	0.439
	250	0.151	0.158
0.10	50	0.665	3.95
	150	0.333	0.439
	250	0.145	0.158

30.6 BEAM-COLUMN ANALYSIS

A member that is subjected to both a transverse load and an axial load is frequently called a *beam-column.* To apply the immediately preceding stress-limiting criterion to a beam-column, we first determine the moment distribution, say, M_{tr}, and the corresponding deflection, say, Y_{tr}, resulting from the transverse load acting alone. Suppose that the transverse load is symmetrical about the column midpoint, and let $Y_{tr,mid}$ and $M_{tr,mid}$ be the values of Y_{tr} and M_{tr} at the column midpoint. Then the only modifications necessary in the preceding development are to replace Y by $Y + Y_{tr}$ in Eqs. (30.17) and (30.20), and to replace Y_{mid} by $Y_{mid} + Y_{tr,mid}$ and add $M_{tr,mid}$ on the right side of Eq. (30.23). If the transverse load is not symmetrical, then it is necessary to determine the maximum moment by using an approach which will now be developed.

Note that, at any point, x, the moment about the z axis is

$$M(z) = P(e - y - Y) + M(z)_{tr} \tag{30.24}$$

where Y includes the deflection due to $M(z)_{tr}$. $M(y)$ has the same form as Eq. (30.24), but with the roles of y and z interchanged. The maximum stress for any given value of x is given by Eq. (30.23). We seek to apply this equation at that value of x which yields the maximum value of σ. A method that is reasonably efficient in locating a minimum or maximum to any desired accuracy is the golden-section search. However, this method is limited to finding the minimum (maximum) of a unimodal function, that is, a function which has only one minimum (maximum) in the interval in which the search is conducted. We therefore have to conduct some exploratory calculation to find the stress at, say, a dozen points on the beam-column in order to locate the unimodal interval of interest within which to apply the golden-section search. The actual number of exploratory calculations will depend on the individual case. For example, in a simply supported case with a unimodal transverse moment, there is clearly only one maximum. But, in general, we must check enough points to be sure that a potential maximum is not overlooked.

The golden-section search procedure is as follows: Suppose that we seek the minimum value of $F(x)$ in Fig. 30.5 within the interval D (note that if we sought a maximum in Fig. 30.5, we would have to conduct two searches). We locate two points $x(1)$ and $x(2)$. The first is $0.382D$ from the left end of the interval; the second is $0.382D$

INSTABILITIES IN BEAMS AND COLUMNS

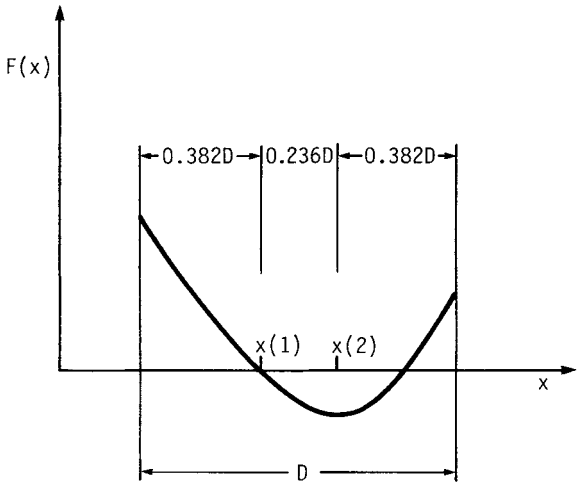

FIGURE 30.5 Finding min $F(x)$ in the interval D.

from the right end. We evaluate $F(x)$ at the chosen points. If the value of $F(x)$ at $x(1)$ is algebraically smaller than at $x(2)$, then we eliminate the subinterval between $x(2)$ and the right end of the search interval. In the oppositive event, we eliminate the subinterval between $x(1)$ and the left end. The distance of $0.236D$ between $x(1)$ and $x(2)$ equals 0.382 of the new search interval, which is $0.618D$ overall. Thus we have already located one point at 0.382 of the new search interval, and we have determined the value of $F(x)$ at that point. We need only locate a point that is 0.382 from the opposite end of the new search interval, evaluate $F(x)$ at that point, and go through the elimination procedure, as before, to further reduce the search interval. The process is repeated until the entire remaining interval is small and the value of $F(x)$ at the two points at which it is evaluated is the same within the desired accuracy. The preceding method may run into difficulty if the function $F(x)$ is flat, that is, if $F(x)$ does not vary over a substantial part of the search interval or if $F(x)$ happens to have the same value at the two points that are compared with each other. The first case is not likely to occur in the types of problems under consideration here. In the second case, we calculate $F(x)$ at another point, near one of the two points of comparison, and use the newly chosen point in place of the nearby original point. Reference [30.2] derives the golden-section search strategy and provides equations (p. 289) for predicting the number of function evaluations required to attain a specified fractional reduction of search interval or an absolute final search interval size.

30.7 APPROXIMATE METHOD

The reason why we devoted so much attention to uniform prismatic column problems is that their solution is analytically simple, so that we could obtain the results directly. In most other cases, we have to be satisfied with approximate formulations for computer (or programmable calculator) calculation of the solution. The finite-element method is the approximation method most widely used in engineering at

the present time to reduce problems dealing with continuous systems, such as beams and columns, to sets of algebraic equations that can be solved on a digital computer. When there is a single independent variable involved (as in our case), the interval of interest of the independent variable is divided into a set of subintervals called *finite elements.* Within each subinterval, the solution is represented by an arc that is defined by a simple function, usually a polynomial of low degree. The curve resulting from the connected arc segments should have a certain degree of smoothness (for the problems under discussion, the deflection curve and its first derivative should be continuous) and should approximate the solution. An effective method of obtaining a good approximation to the solution is based on the mechanical energy involved in the deformation process.

30.8 INSTABILITY OF BEAMS

Beams that have rectangular cross sections with the thickness much smaller than the depth are prone to instability involving rotation of the beam cross section about the beam axis. This tendency to instability arises because such beams have low resistance to torsion about their axes. In preparation for the analysis of this problem, recall that for a circular cylindrical member of length L and radius R, subjected to an axial torque T, the angle of twist ϕ is given by

$$\phi = \frac{TL}{JG} \tag{30.25}$$

where G = shear modulus and J = polar moment of inertia of the cross section. For noncircular cross sections, the form of the right side of Eq. (30.25) does not change; the only change is in the expression for J, the torsion constant of the cross section. If the thickness of the cross section, to be denoted by t, is small and does not vary much, then J is given by

$$3J = \int_0^l t^3 \, ds \tag{30.26}$$

where s = running coordinate measured from one end of the cross section and l = total developed length of the cross section. Thus, for a rectangular cross section of depth h,

$$J = \frac{ht^3}{3} \tag{30.27}$$

Clearly, J decreases rapidly as t decreases. To study the effect of this circumstance on beam stability, we will examine the deformation of a beam with rectangular cross section subjected to end moments $M(0)$, taking into account rotation of the cross section about the beam axis. The angle of rotation ϕ is assumed to be small, so that $\sin \phi$ may be replaced by ϕ and $\cos \phi$ by unity.

The equations of static equilibrium may be written from Fig. 30.6, where the moments are shown as vectors, using the right-hand rule:

$$\begin{aligned} -M'(z) + M(0) &= 0 \\ M'(y) + M(0)\phi &= 0 \\ \frac{dT}{dx} + \frac{dM'(z)}{dx} &= 0 \end{aligned} \tag{30.28}$$

INSTABILITIES IN BEAMS AND COLUMNS

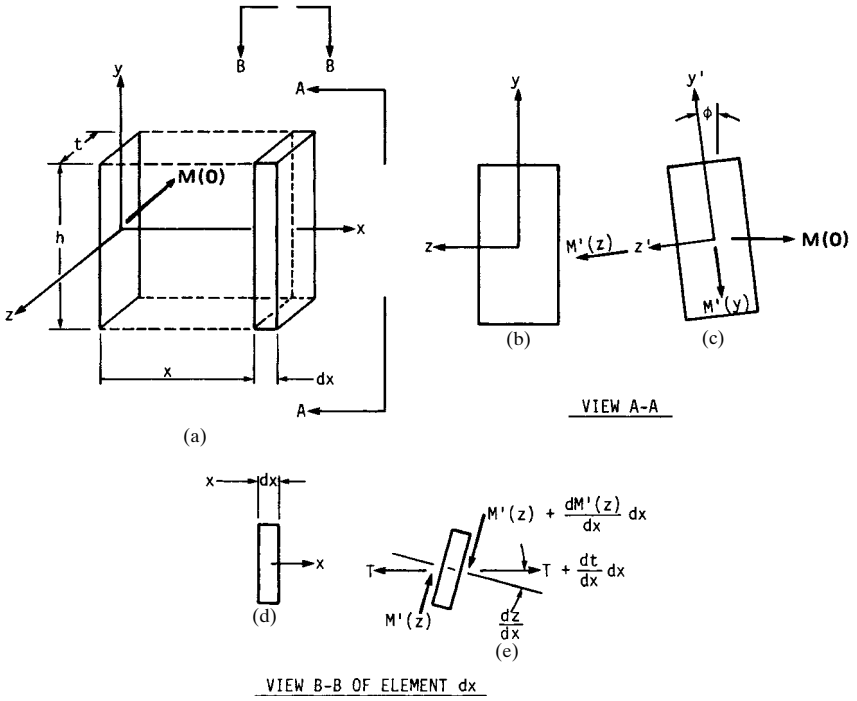

FIGURE 30.6 Instability of beams. (*a*) Segment of a beam with applied moment $M(0)$ at the ends; (*b*) cross section of undeformed beam; (*c*) cross section after onset of beam instability; (*d*) top view of undeformed differential beam element; (*e*) the element after onset of instability.

These, combined with Eq. (30.25) and the standard moment-curvature relation as given by Eq. (30.1), lead to the defining differential equation (30.29) for the angle ϕ:

$$GJ\frac{d^2\phi}{dx^2} + M^2(0)\phi\left[\frac{1}{EI(y)} - \frac{1}{EI(z)}\right] = 0 \tag{30.29}$$

Suppose that the end faces of the beam are fixed against rotation about the x axis. Then the boundary conditions are

$$\phi(0) = \phi(L) = 0 \tag{30.30}$$

Noting the similarity between Eq. (30.4) with its boundary conditions Eq. (30.5) and Eq. (30.29) with its boundary conditions Eq. (30.30), the similarity of the solutions is clear. Thus we obtain the expression for $M(0)_{cr}$:

$$[M(0)_{cr}]^2 = \frac{\pi^2 E}{L^2} GJ\left[\frac{I(z)I(y)}{I(z) - I(y)}\right] \tag{30.31}$$

It may be seen from Eq. (30.31) that if the torsion constant J is small, the critical moment is small. In addition, it may be seen from the bracketed term in Eq. (30.31) that as the cross section approaches a square shape, the denominator becomes small, so that the critical moment becomes very large. The disadvantage of a square cross

section is, of course, well known. To demonstrate it explicitly, we rewrite the expression for stress in a beam with rectangular cross section t by h:

$$\sigma = \frac{M(h/2)}{th^3/12} \tag{30.32}$$

in the form

$$th = \frac{6M}{\sigma h} \tag{30.33}$$

Thus, for given values of M and σ, the cross-sectional area required decreases as we increase h. Hence the role of Eq. (30.31) is to define the constraint on the maximum allowable depth-to-thickness ratio. The situation is similar for flanged beams. Here we have obtained the results for a simple problem to illustrate the disadvantage involved and the caution necessary in designing beams with thin-walled open cross sections. Implicit in this is the advantage of using, when possible, closed cross sections, such as box beams, which have a high torsional stiffness.

As we have seen, when the applied moment is constant over the entire length of the beam, the problem of definition and its solution have the same form as for the column-buckling problem. We can also have similar types of boundary conditions. The boundary conditions used in Eq. (30.30) correspond to a simply supported column. If dy/dx and dz/dx are equal to zero at $x = 0$ for all y and z, then $d\phi/dx$ is equal to zero at $x = 0$. If this condition is combined with $\phi(0) = 0$, then we have the equivalent of a clamped column end. Hence we can use here the concept of equivalent beam length in the same manner as we used the equivalent column length before. In case a beam is subjected to transverse loads, so that the applied moment varies with x, the problem is more complex. For the proportioning of flanged beams, Ref. [30.3] should be used as a guide. This reference deals with structural applications, so that the size range of interest dealt with is different from the size range of interest in machine design. But the underlying principles of beam stability are the same, and the proportioning of the members should be similar.

Example 2. We will examine the design of a beam of length L and rectangular cross section t by h. The beam is subjected to an applied moment M (we will not use any modifying symbols here, since there is no ambiguity), which is constant over the length of the beam. As noted previously, the required cross-sectional area th will decrease as h is increased. We take the allowable stress in the material to be σ. The calculated stress in the beam is not to exceed this value. Thus,

$$\sigma \geq \frac{M(h/2)}{th^3/12} \qquad \sigma \geq \frac{6M}{th^2} \qquad th \geq \frac{6M}{h\sigma} \tag{1}$$

We want the cross-sectional area th as small as possible. Hence h should be as large as possible. We can, therefore, replace the inequality in Eq. (1) by the equality

$$th = \frac{6M}{h\sigma} \tag{2}$$

The maximum value of h that we can use is subject to a constraint based on Eq. (30.31). We will use a factor of safety η in this connection. Thus,

$$(\eta M)^2 \leq \frac{\pi^2 E}{L^2} GJ\left[\frac{I(z)I(y)}{I(z) - I(y)}\right] \tag{3}$$

INSTABILITIES IN BEAMS AND COLUMNS

Here

$$I(z) = \frac{th^3}{12} \qquad I(y) = \frac{ht^3}{12} \qquad J = \frac{ht^3}{3} \tag{4}$$

Using Eq. (4), we may write Eq. (3) as

$$(\eta M)^2 \le \frac{\pi^2 EG}{(6L)^2}\left(\frac{t}{h}\right)^2\left[\frac{1}{1-(t/h)^2}\right](th)^4 \tag{5}$$

or, from Eq. (2),

$$(\eta M)^2 \le \frac{\pi^2 EG}{(6L)^2}\left(\frac{6M}{h^3\sigma}\right)^2\left[\frac{1}{1-[(6M/(h^3\sigma)]^2}\right]\left(\frac{6M}{h\sigma}\right)^4 \tag{6}$$

Since we seek to minimize *th* and maximize *h,* it may be seen from Eqs. (5) and (6) that the inequality sign may be replaced by the equality sign in those two equations. In Eq. (6), *h* is the only unspecified quantity. Further, since the square of *t*/*h* may be expected to be small compared to unity, we can obtain substantially simpler approximations of reasonable accuracy. As a first step, we have

$$\frac{1}{1-(t/h)^2} = 1 + \left(\frac{t}{h}\right)^2 + \left(\frac{t}{h}\right)^4 + \cdots \tag{7}$$

If we retain only the first two terms in the right side of Eq. (7), we have

$$\eta M = \frac{\pi(EG)^{1/2}}{6L}\left[1 + \left(\frac{6M}{h^3\sigma}\right)^2\right]\left(\frac{6M}{h^3\sigma}\right)\left(\frac{6M}{h\sigma}\right)^2 \tag{8}$$

If we also neglect the square of *t*/*h* in comparison with unity, we obtain

$$h = \left[\frac{\pi(6M)^2(EG)^{1/2}}{\eta L\sigma^3}\right]^{1/5} \tag{9}$$

as a reasonable first approximation. Thus if we take the factor of safety η as 1.5, we have, for a steel member with $E = 30$ Mpsi, $G = 12$ Mpsi, and $\sigma = 30$ kpsi,

$$h = \left[\frac{\pi(36)[(30\times10^6)(12\times10^6)]^{1/2}}{(1.5)(30\,000)}\frac{M^2}{L}\right]^{1/5} = 8.62\left(\frac{M^2}{L}\right)^{1/5} \tag{10}$$

This is a reasonable approximation to the optimal height of the beam cross section. It may also be used as a starting point for an iterative solution to the exact expression, Eq. (6). For the purpose of iteration, we rewrite Eq. (6) as

$$h = \left\{\frac{\pi(6M)^2}{\eta L\sigma^3}\left[\frac{EG}{1-[(6M)/(h^3\sigma)]^2}\right]^{1/2}\right\}^{1/5} \tag{11}$$

The value of *h* obtained from Eq. (9) is substituted into the right side of Eq. (11). The resultant value of *h* thus obtained is then resubstituted into the right side of Eq. (11); the iterative process is continued until the computed value of *h* coincides with the value substituted into the right side to the desired degree of accuracy. Having determined *h,* we can determine *t* from Eq. (2).

REFERENCES

30.1 H. Herman, "On the Analysis of Uniform Prismatic Columns," *Transactions of the ASME, Journal of Mechanical Design,* vol. 103, 1981, pp. 274–276.

30.2 C. R. Mischke, *Mathematical Model Building,* 2d rev. ed., Iowa State University Press, Ames, 1980.

30.3 American Institute of Steel Construction, *LRFD Manual of Steel Construction,* 3d ed., AISC, Chicago, 2003.

CHAPTER 31
VIBRATION AND CONTROL OF VIBRATION

T. S. Sankar, Ph.D., Eng.
Professor and Chairman
Department of Mechanical Engineering
Concordia University
Montreal, Quebec, Canada

R. B. Bhat, Ph.D.
Associate Professor
Department of Mechanical Engineering
Concordia University
Montreal, Quebec, Canada

31.1 INTRODUCTION

Vibration analysis and control of vibrations are important and integral aspects of every machine design procedure. Establishing an appropriate mathematical model, its analysis, interpretation of the solutions, and incorporation of these results in the design, testing, evaluation, maintenance, and troubleshooting require a sound understanding of the principles of vibration. All the essential materials dealing with various aspects of machine vibrations are presented here in a form suitable for most design applications. Readers are encouraged to consult the references for more details.

31.2 SINGLE-DEGREE-OF-FREEDOM SYSTEMS

31.2.1 Free Vibration

A single-degree-of-freedom system is shown in Fig. 31.1. It consists of a mass m constrained by a spring of *stiffness k,* and a damper with *viscous damping coefficient c.* The stiffness coefficient k is defined as the spring force per unit deflection. The coef-

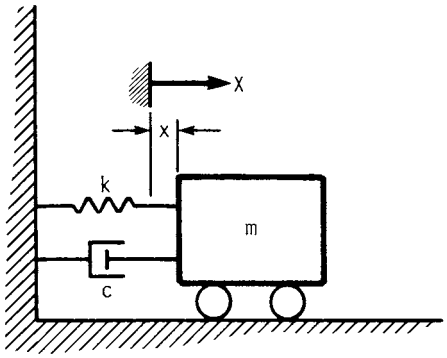

FIGURE 31.1 Representation of a single-degree-of-freedom system.

ficient of viscous damping c is the force provided by the damper opposing the motion per unit velocity.

If the mass is given an initial displacement, it will start vibrating about its equilibrium position. The equation of motion is given by

$$m\ddot{x} + c\dot{x} + kx = 0 \tag{31.1}$$

where x is measured from the equilibrium position and dots above variables represent differentiation with respect to time. By substituting a solution of the form $x = e^{st}$ into Eq. (31.1), the characteristic equation is obtained:

$$ms^2 + cs + k = 0 \tag{31.2}$$

The two roots of the characteristic equation are

$$s = \zeta\omega_n \pm i\omega_n(1 - \zeta^2)^{1/2} \tag{31.3}$$

where $\omega_n = (k/m)^{1/2}$ is undamped *natural frequency*
$\zeta = c/c_c$ is *damping ratio*
$c_c = 2m\omega_n$ is *critical damping coefficient*
$i = \sqrt{-1}$

Depending on the value of ζ, four cases arise.

Undamped System ($\zeta = 0$). In this case, the two roots of the characteristic equation are

$$s = \pm i\omega_n = \pm i(k/m)^{1/2} \tag{31.4}$$

and the corresponding solution is

$$x = A\cos\omega_n t + B\sin\omega_n t \tag{31.5}$$

where A and B are arbitrary constants depending on the initial conditions of the motion. If the initial displacement is x_0 and the initial velocity is v_0, by substituting these values in Eq. (31.5) it is possible to solve for constants A and B. Accordingly, the solution is

$$x = x_0 \cos \omega_n t + \frac{v_0}{\omega_n} \sin \omega_n t \tag{31.6}$$

Here, ω_n is the natural frequency of the system in radians per second (rad/s), which is the frequency at which the system executes free vibrations. The *natural frequency* is

$$f_n = \frac{\omega_n}{2\pi} \tag{31.7}$$

where f_n is in cycles per second, or hertz (Hz). The *period* for one oscillation is

$$\tau = \frac{1}{f_n} = \frac{2\pi}{\omega_n} \tag{31.8}$$

The solution given in Eq. (31.6) can also be expressed in the form

$$x = X \cos (\omega_n - \theta) \tag{31.9}$$

where

$$X = \left[x_0^2 + \left(\frac{v_0}{\omega_n} \right)^2 \right]^{1/2} \qquad \theta = \tan^{-1} \frac{v_0}{\omega_n x_0} \tag{31.10}$$

The motion is harmonic with a *phase angle* θ as given in Eq. (31.9) and is shown graphically in Fig. 31.4.

Underdamped System (0 < ζ < 1). When the system damping is less than the critical damping, the solution is

$$x = [\exp(-\zeta \omega_n t)] \, (A \cos \omega_d t + B \sin \omega_d t) \tag{31.11}$$

where

$$\omega_d = \omega_n (1 - \zeta^2)^{1/2} \tag{31.12}$$

is the *damped natural frequency* and A and B are arbitrary constants to be determined from the initial conditions. For an initial amplitude of x_0 and initial velocity v_0,

$$x = [\exp (-\zeta \omega_n t)] \left(x_0 \cos \omega_d t + \frac{\zeta \omega_n x_0 + v_0}{\omega_d} \sin \omega_d t \right) \tag{31.13}$$

which can be written in the form

$$\begin{aligned} x &= [\exp (-\zeta \omega_n t)] \, X \cos (\omega_d t - \theta) \\ X &= \left[x_0^2 + \left(\frac{\zeta \omega_n x_0 + v_0}{\omega_d} \right)^2 \right]^{1/2} \end{aligned} \tag{31.14}$$

and

$$\theta = \tan^{-1} \frac{\zeta \omega_n x_0 + v_0}{\omega_d}$$

An underdamped system will execute exponentially decaying oscillations, as shown graphically in Fig. 31.2.

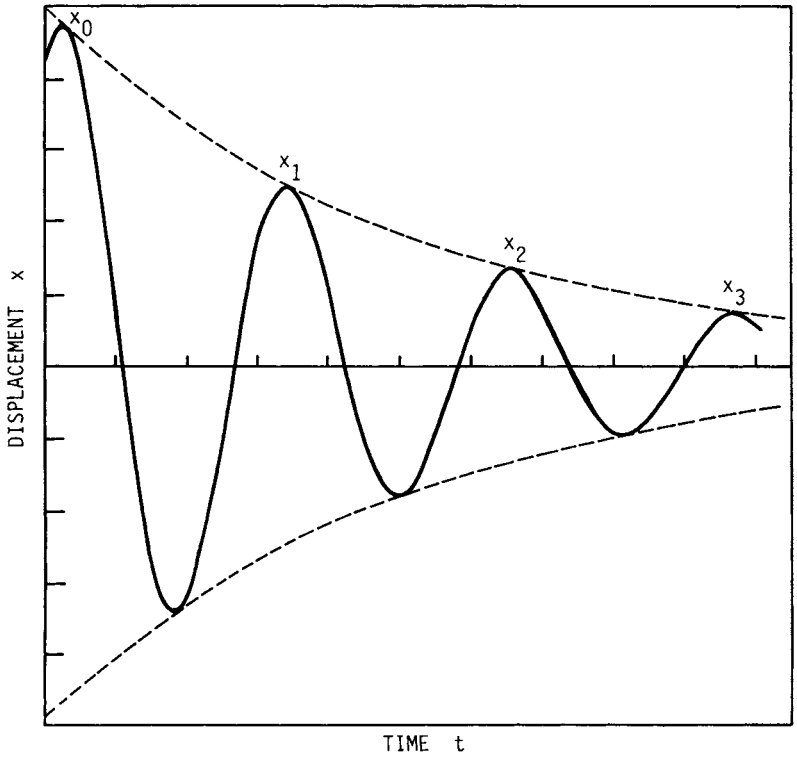

FIGURE 31.2 Free vibration of an underdamped single-degree-of-freedom system.

The successive maxima in Fig. 31.2 occur in a periodic fashion and are marked $X_0, X_1, X_2, \ldots$. The ratio of the maxima separated by n cycles of oscillation may be obtained from Eq. (31.13) as

$$\frac{X_n}{X_0} = \exp(-n\delta) \tag{31.15}$$

where

$$\delta = \frac{2\pi\zeta}{(1-\zeta^2)^{1/2}}$$

is called the *logarithmic decrement* and corresponds to the ratio of two successive maxima in Fig. 31.2. For small values of damping, that is, $\zeta << 1$, the logarithmic decrement can be approximated by

$$\delta = 2\pi\zeta \tag{31.16}$$

Using this in Eq. (31.14), we find

$$\frac{X_n}{X_0} = \exp(-2\pi n\zeta) \simeq 1 - 2\pi n\zeta \tag{31.17}$$

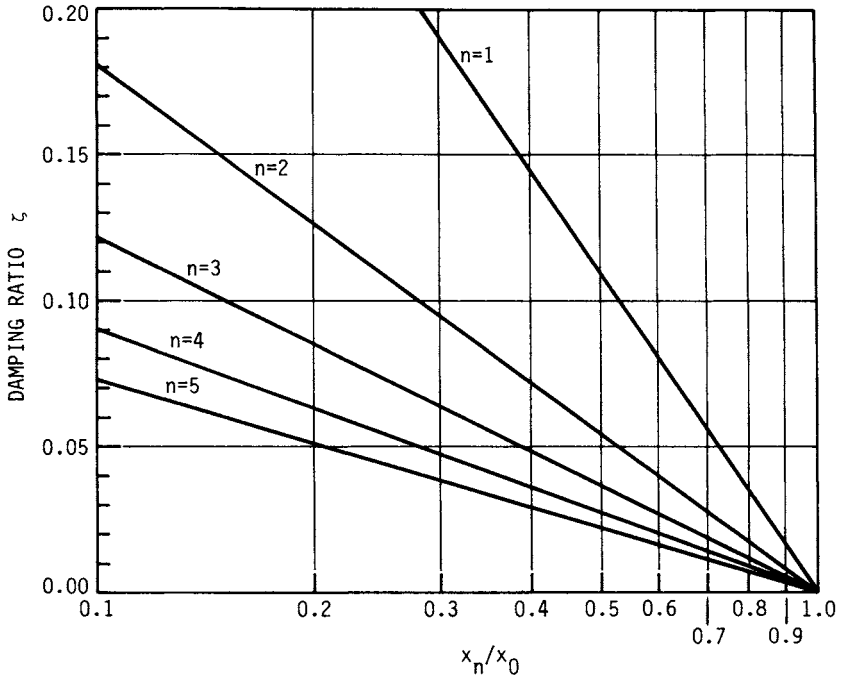

FIGURE 31.3 Variation of the ratio of displacement maxima with damping.

The equivalent viscous damping in a system is measured experimentally by using this principle. The system at rest is given an impact which provides initial velocity to the system and sets it into free vibration. The successive maxima of the ensuing vibration are measured, and by using Eq. (31.17) the damping ratio can be evaluated. The variation of the decaying amplitudes of free vibration with the damping ratio is plotted in Fig. 31.3 for different values of n.

Critically Damped System ($\zeta = 1$). When the system is critically damped, the roots of the characteristic equation given by Eq. (31.3) are equal and negative real quantities. Hence, the system does not execute oscillatory motion. The solution is of the form

$$x = (A + Bt) \exp(-\omega_n t) \tag{31.18}$$

and after substitution of initial conditions,

$$x = [x_0 + (v_0 + x_0\omega_n)t] \exp(-\omega_n t) \tag{31.19}$$

This motion is shown graphically in Fig. 31.4, which gives the shortest time to rest.

Overdamped System ($\zeta > 1$). When the damping ratio ζ is greater than unity, there are two distinct negative real roots for the characteristic equation given by Eq. (31.3). The motion in this case is described by

$$x = \exp(-\zeta\omega_n t)\left[A \exp \omega_n t\sqrt{\zeta^2 - 1} + B \exp(-\omega_n t\sqrt{\zeta^2 - 1})\right] \tag{31.20}$$

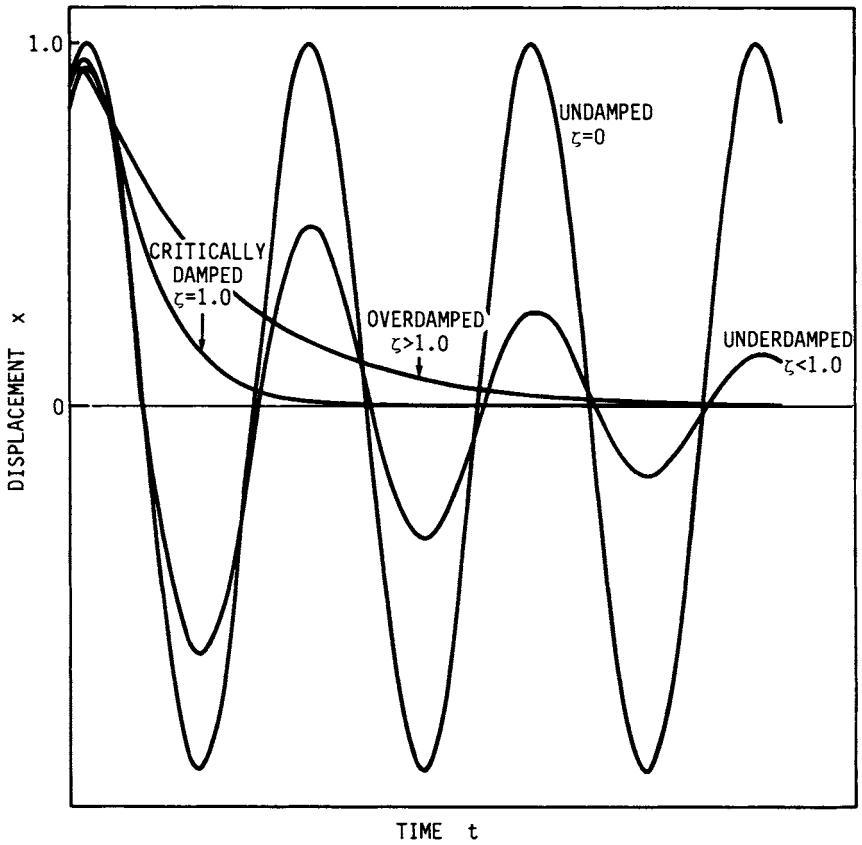

FIGURE 31.4 Free vibration of a single-degree-of-freedom system under different values of damping.

where

$$A = \frac{1}{2}\left(x_0 + \frac{v_0 + \zeta\omega_n x_0}{\omega_n}\right) \qquad B = \frac{1}{2}\left(\frac{x_0 + \zeta\omega_n x_0}{\omega_0}\right)$$

and

$$\omega_0 = \omega_n\sqrt{\zeta^2 - 1}$$

All four types of motion are shown in Fig. 31.4.

If the mass is suspended by a spring and damper as shown in Fig. 31.5, the spring will be stretched by an amount δ_{st}, the static deflection in the equilibrium position. In such a case, the equation of motion is

$$m\ddot{x} + c\dot{x} + k(x + \delta_{st}) = mg \tag{31.21}$$

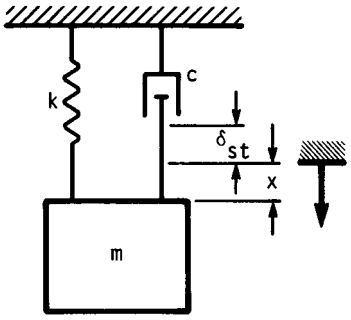

FIGURE 31.5 Model of a single-degree-of-freedom system showing the static deflection due to weight.

Since the force in the spring due to the static equilibrium is equal to the weight, or $k\delta_{st} = mg = W$, the equation of motion reduces to

$$m\ddot{x} + c\dot{x} + kx = 0 \tag{31.22}$$

which is identical to Eq. (31.1). Hence the solution is also similar to that of Eq. (31.1). In view of Eq. (31.21) and since $\omega_n = (k/m)^{1/2}$, the natural frequency can also be obtained by

$$\omega_n = \left(\frac{g}{\delta_{st}}\right)^{1/2} \tag{31.23}$$

An approximate value of the fundamental natural frequency of any complex mechanical system can be obtained by reducing it to a single-degree-of-freedom system. For example, a shaft supporting several disks (wheels) can be reduced to a single-degree-of-freedom system by lumping the masses of all the disks at the center and obtaining the equivalent stiffness of the shaft by using simple flexure theory.

31.2.2 Torsional Systems

Rotating shafts transmitting torque will experience torsional vibrations if the torque is nonuniform, as in the case of an automobile crankshaft.

In rotating shafts involving gears, the transmitted torque will fluctuate because of gear-mounting errors or tooth profile errors, which will result in torsional vibration of the geared shafts.

A single-degree-of-freedom torsional system is shown in Fig. 31.6. It has a massless shaft of torsional stiffness k, a damper with damping coefficient c, and a disk with polar mass moment of inertia J. The torsional stiffness is defined as the resisting torque of the shaft per unit of angular twist, and the damping coefficient is the resisting torque of the damper per unit of angular velocity. Either the damping can be externally applied, or it can be inherent structural damping. The equation of motion of the system in torsion is given

$$J\ddot{\theta} + c\dot{\theta} + k\theta = 0 \tag{31.24}$$

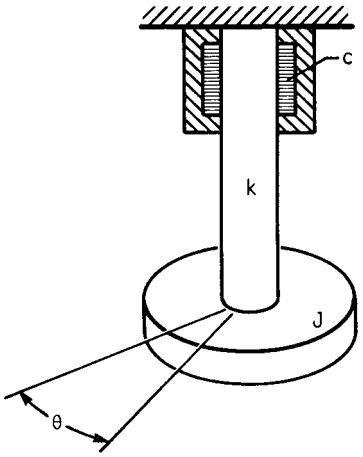

FIGURE 31.6 A representation of a single-degree-of-freedom torsional system.

Equation (31.24) is in the same form as Eq. (31.1), except that the former deals with moments whereas the latter deals with forces. The solution of Eq. (31.24) will be of the same form as that of Eq. (31.1), except that J replaces m and k and c refer to torsional stiffness and torsional damping coefficient.

31.2.3 Forced Vibration

System Excited at the Mass. A vibrating system with a sinusoidal force acting on the mass is shown in Fig. 31.7. The equation of motion is

$$m\ddot{x} + c\dot{x} + kx = F_0 \sin \omega t \tag{31.25}$$

Assuming that the steady-state response lags behind the force by an angle θ, we see that the solution can be written in the form

$$x_s = X \sin (\omega t - \theta) \tag{31.26}$$

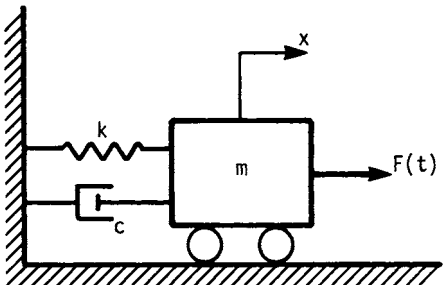

FIGURE 31.7 Oscillating force $F(t)$ applied to the mass.

Substituting in Eq. (31.26), we find that the steady-state solution can be obtained:

$$x_s = \frac{(F_0/k)\sin(\omega t - \theta)}{[(1 - \omega^2/\omega_n^2)^2 + (2\zeta\omega/\omega_n)^2]^{1/2}} \tag{31.27}$$

Using the complementary part of the solution from Eq. (31.19), we see that the complete solution is

$$x = x_s + \exp(-\zeta\omega_n t)\,[A \exp(\omega_n t\sqrt{\zeta^2 - 1}) + B \exp(-\omega_n t\sqrt{\zeta^2 - 1})] \tag{31.28}$$

If the system is undamped, the response is obtained by substituting $c = 0$ in Eq. (31.25) or $\zeta = 0$ in Eq. (31.28). When the system is undamped, if the exciting frequency coincides with the system natural frequency, say $\omega/\omega_n = 1.0$, the system response will be infinite. If the system is damped, the complementary part of the solution decays exponentially and will be nonexistent after a few cycles of oscillation; subsequently the system response is the steady-state response. At steady state, the nondimensional response amplitude is obtained from Eq. (31.27) as

$$\frac{X}{F_0/k} = \left[\left(\frac{1 - \omega^2}{\omega_n^2}\right)^2 + \left(\frac{2\zeta\omega}{\omega_n}\right)^2\right]^{-1/2} \tag{31.29}$$

and the phase between the response and the force is

$$\theta = \tan^{-1}\frac{2\zeta\omega/\omega_n}{1 - \omega^2/\omega_n^2} \tag{31.30}$$

When the forcing frequency ω coincides with the damped natural frequency ω_d, the response amplitude is given by

$$\frac{X_{\max}}{F_0/k} = \frac{1}{\zeta(4 - 3\zeta^2)^{1/2}} \tag{31.31}$$

The maximum response or resonance occurs when $\omega = \omega_n(1 - 2\zeta^2)^{1/2}$ and is

$$\frac{X_{\max}}{F_0/k} = \frac{1}{2\zeta(1 - \zeta^2)^{1/2}} \tag{31.32}$$

For structures with low damping, ω_d approximately equals ω_n, and the maximum response is

$$\frac{X_{\max}}{F_0/k} = \frac{1}{2\zeta} \tag{31.33}$$

The response amplitude in Eq. (31.29) is plotted against the forcing frequency in Fig. 31.8. The curves start at unity, reach a maximum in the neighborhood of the system natural frequency, and decay to zero at large values of the forcing frequency. The response is larger for a system with low damping, and vice versa, at any given frequency. The phase difference between the response and the excitation as given in Eq. (31.30) is plotted in Fig. 31.9. For smaller forcing frequencies, the response is nearly in phase with the force; and in the neighborhood of the system natural frequency, the response lags behind the force by approximately 90°. At large values of forcing frequencies, the phase is around 180°.

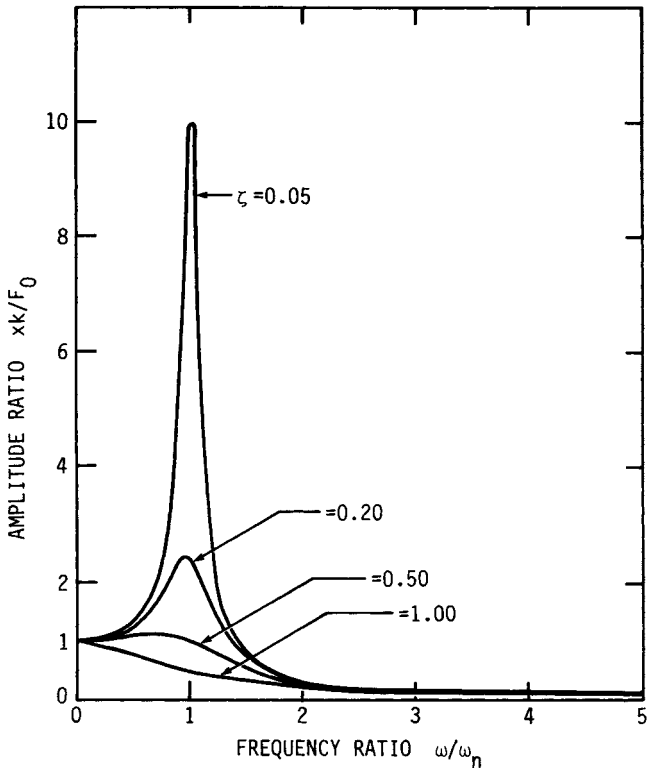

FIGURE 31.8 Displacement-amplitude frequency response due to oscillating force.

Steady-State Velocity and Acceleration Response. The steady-state velocity response is obtained by differentiating the displacement response, given by Eq. (31.27), with respect to time:

$$\frac{\dot{x}_s}{F_0\omega_n/k} = \frac{\omega/\omega_n}{[(1-\omega^2/\omega_n^2)^2 + (2\zeta\omega/\omega_n)^2]^{1/2}} \tag{31.34}$$

And the steady-state acceleration response is obtained by further differentiation and is

$$\frac{\ddot{x}_s}{F_0\omega_n^2/k} = \frac{(\omega/\omega_n)^2}{[(1-\omega^2/\omega_n^2)^2 + (2\zeta\omega/\omega_n)^2]^{1/2}} \tag{31.35}$$

These are shown in Figs. 31.10 and 31.11 and also can be obtained directly from Fig. 31.8 by multiplying the amplitude by ω/ω_n and $(\omega/\omega_n)^2$, respectively.

Force Transmissibility. The force F_T transmitted to the foundation by a system subjected to an external harmonic excitation is

$$F_T = c\dot{x} + kx \tag{31.36}$$

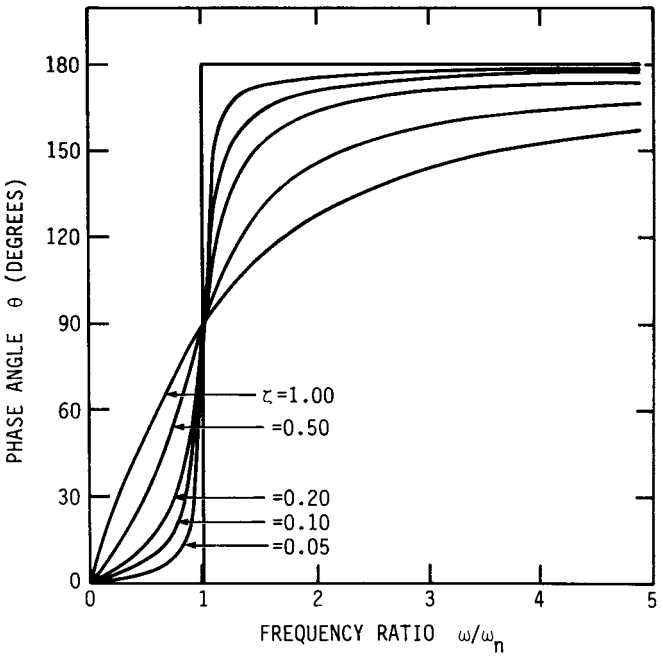

FIGURE 31.9 Phase-angle frequency response for forced motion.

Substituting the system response from Eq. (31.27) into Eq. (31.36) gives

$$\frac{F_T}{F_0} = T \sin(\omega t - \theta) \tag{31.37}$$

where the nondimensional magnitude of the transmitted force T is given by

$$T = \left[\frac{1 + (2\zeta\omega/\omega_n)^2}{(1 - \omega^2/\omega_n^2)^2 + (2\zeta\omega/\omega_n)^2}\right]^{1/2} \tag{31.38}$$

and the phase between F_T and F_0 is given by

$$\theta = \tan^{-1}\frac{2\zeta(\omega/\omega_n)^3}{1 - \omega^2/\omega_n^2 + 4\zeta^2\omega^2/\omega_n^2} \tag{31.39}$$

The *transmissibility* T is shown in Fig. 31.12 versus forcing frequency. At very low forcing frequencies, the transmissibility is close to unity, showing that the applied force is directly transmitted to the foundation. The transmissibility is very large in the vicinity of the system natural frequency, and for high forcing frequencies the transmitted force decreases considerably. The phase variation between the transmitted force and the applied force is shown in Fig. 31.13.

Rotating Imbalance. When machines with rotating imbalances are mounted on elastic supports, they constitute a vibrating system subjected to excitation from the

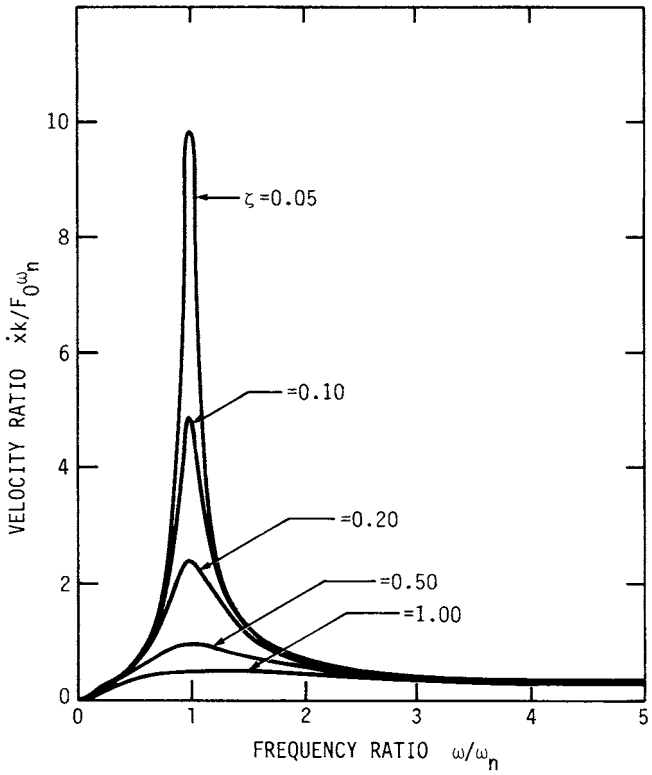

FIGURE 31.10 Velocity frequency response.

rotating imbalance. If the natural frequency of the system coincides with the frequency of rotation of the machine imbalance, it will result in severe vibrations of the machine and the support structure.

Consider a machine of mass M supported as shown in Fig. 31.14. Let the imbalance be a mass m with an eccentricity e and rotating with a frequency ω. Consider the motion x of the mass $M - m$, with x_m as the motion of the unbalanced mass m relative to the machine mass M. The equation of motion is

$$(M - m)\ddot{x} + m(\ddot{x} + \ddot{x}_m) + c\dot{x} + kx = 0 \tag{31.40}$$

The motion of the unbalanced mass relative to the machine is

$$x_m = e \sin \omega t \tag{31.41}$$

Substitution in Eq. (31.40) leads to

$$M\ddot{x} + c\dot{x} + kx = me\omega^2 \sin \omega t \tag{31.42}$$

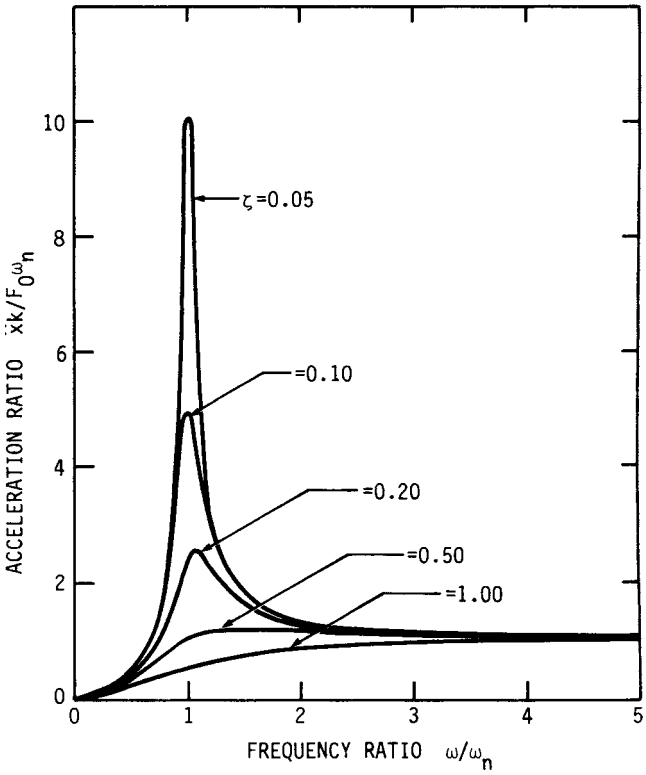

FIGURE 31.11 Acceleration frequency response.

This equation is similar to Eq. (31.25), where the force amplitude F_0 is replaced by $me\omega^2$. Hence, the steady-state solution of Eq. (31.42) is similar in form to Eq. (31.27) and is given nondimensionally as

$$\frac{x}{e}\frac{M}{m} = \frac{(\omega/\omega_n)^2 \sin(\omega t - \theta)}{[(1 - \omega^2/\omega_n^2)^2 + (2\zeta\omega/\omega_n)^2]^{1/2}} \tag{31.43}$$

where

$$\tan\theta = \frac{2\zeta\omega/\omega_n}{1 - \omega^2/\omega_n^2} \tag{31.44}$$

Note that since the excitation is proportional to ω^2, the response has an ω^2 term in the numerator and resembles the acceleration response of a system subjected to a force of constant magnitude, given by Eq. (31.35). The complete solution consists of the complementary part of the solution and is

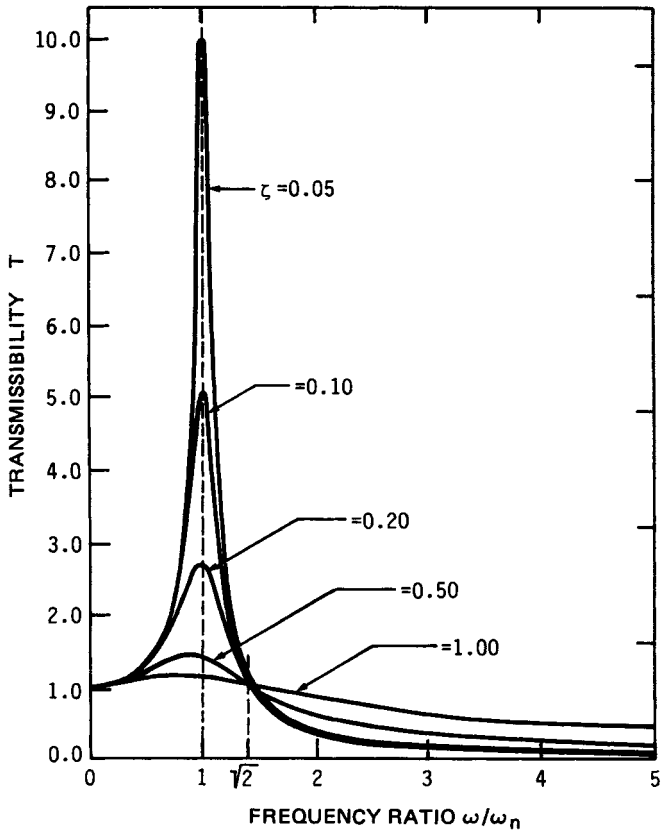

FIGURE 31.12 Transmissibility plot.

$$x = \exp -\zeta\omega_n t \{A \exp [(\zeta^2 - 1)^{1/2}\, \omega_n t] + B \exp [-(\zeta^2 - 1)^{1/2}\, \omega_n t]\} + \frac{me(\omega/\omega_n)^2 \sin(\omega t - \theta)}{M[(1 - \omega^2/\omega_n^2)^2 + (2\zeta\omega/\omega_n)^2]^{1/2}} \tag{31.45}$$

System Excited at the Foundation. When the system is excited at the foundation, as shown in Fig. 31.15, with a certain displacement $u(t) = U_0 \sin \omega t$, the equation of motion can be written as

$$m\ddot{x} + c(\dot{x} - \dot{u}) + k(x - u) = 0 \tag{31.46}$$

This equation can be written in the form

$$m\ddot{x} + c\dot{x} + k\dot{x} = cu_0\omega \cos \omega t + ku_0 \sin \omega t = F_0 \sin(\omega t + \phi) \tag{31.47}$$

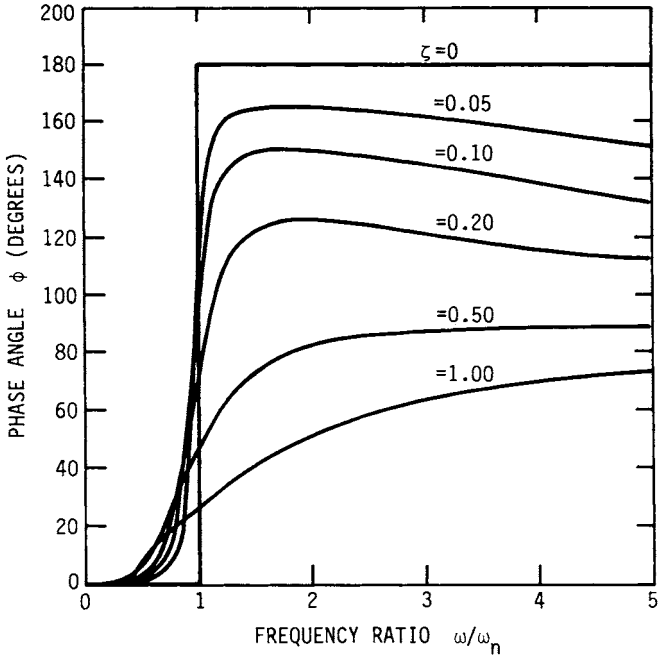

FIGURE 31.13 Phase angle between transmitted and applied forces.

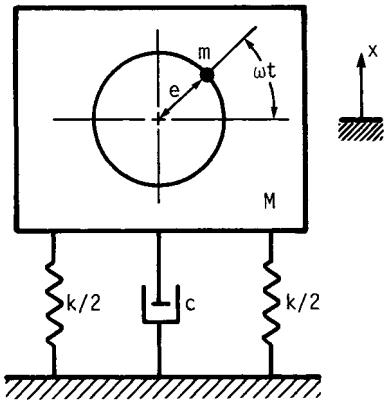

FIGURE 31.14 Dynamic system subject to unbalanced excitation.

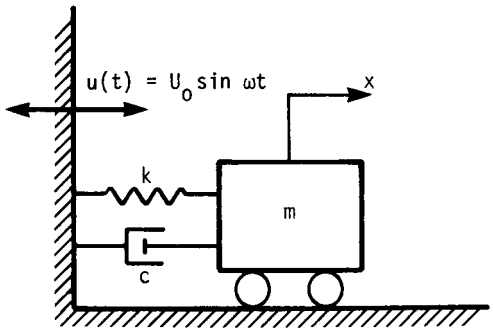

FIGURE 31.15 A base excited system.

where

$$F_0 = u_0 (k^2 + c^2\omega^2)^{1/2} \tag{31.48}$$

and

$$\phi = \tan^{-1} \frac{k}{c\omega} \tag{31.49}$$

Equation (31.47) is identical to Eq. (31.25) except for the phase ϕ. Hence the solution is similar to that of Eq. (31.25). If the ratio of the system response to the base displacement is defined as the motion transmissibility, it will have the same form as the force transmissibility given in Eq. (31.38).

Resonance, System Bandwidth, and* Q *Factor. A vibrating system is said to be in resonance when the response is maximum. The displacement and acceleration responses are maximum when

$$\omega = \omega_n(1 - 2\zeta^2)^{1/2} \tag{31.50}$$

whereas velocity response is maximum when

$$\omega = \omega_n \tag{31.51}$$

In the case of an undamped system, the response is maximum when $\omega = \omega_n$, where ω_n is the frequency of free vibration of the system. For a damped system, the frequency of free oscillations or the damped natural frequency is given by

$$\omega_d = \omega_n (1 - \zeta^2)^{1/2} \tag{31.52}$$

In many mechanical systems, the damping is small and the resonant frequency and the damped natural frequency are approximately the same.

When the system has negligible damping, the frequency response has a sharp peak at resonance; but when the damping is large, the frequency response near resonance will be broad, as shown in Fig. 31.8. A section of the plot for a specific damping value is given in Fig. 31.16.

The Q factor is defined as

$$Q = \frac{1}{2\zeta} = R_{\max} \tag{31.53}$$

VIBRATION AND CONTROL OF VIBRATION

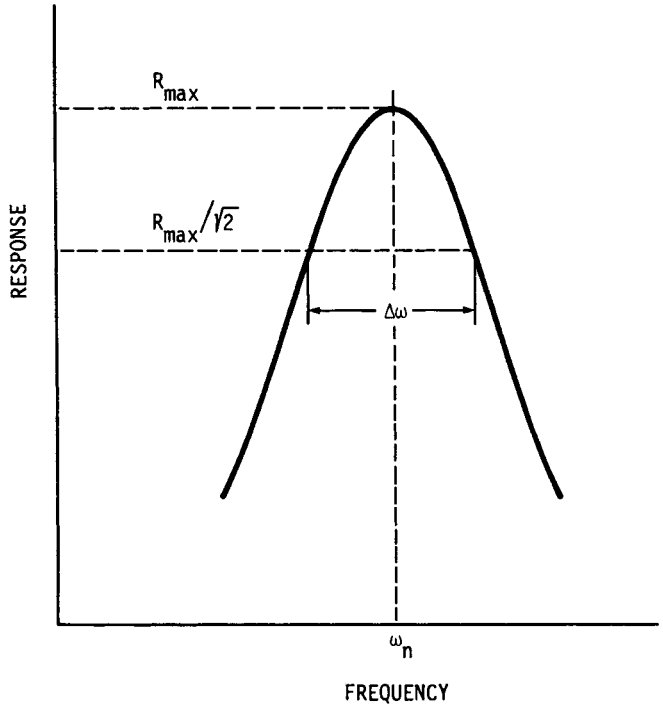

FIGURE 31.16 Resonance, bandwidth, and Q factor.

which is equal to the maximum response in physical systems with low damping. The bandwidth is defined as the width of the response curve measured at the "half-power" points, where the response is $R_{max}/\sqrt{2}$. For physical systems with $\zeta < 0.1$, the bandwidth can be approximated by

$$\Delta\omega = 2\zeta\omega_n = \frac{\omega_n}{Q} \tag{31.54}$$

Forced Vibration of Torsional Systems. In the torsional system of Fig. 31.3, if the disk is subjected to a sinusoidal external torque, the equation of motion can be written as

$$J\ddot{\theta} + c\dot{\theta} + k\theta = T_0 \sin \omega t \tag{31.55}$$

Equation (31.55) has the same form as Eq. (31.25). Hence the solution can be obtained by replacing m by J and F_0 by T_0 and by using torsional stiffness and torsional damping coefficients for k and c, respectively, in the solution of Eq. (31.25).

31.2.4 Numerical Integration of Differential Equations of Motion: Runge-Kutta Method

When the differential equation cannot be integrated in closed form, numerical methods can be employed. If the system is nonlinear or if the system excitation can-

not be expressed as a simple analytical function, then the numerical method is the only recourse to obtain the system response.

The differential equation of motion of a system can be expressed in the form

$$\ddot{x} = f(x,\dot{x},t)$$

or

$$\dot{x} = y = F_1(x,y,t)$$
$$y = f(x,\dot{x},t) = F_2(x,y,t) \tag{31.56}$$
$$x_0 = x(0) \qquad \dot{x}_0 = \dot{x}(0)$$

where x_0 and $\dot{x}_0$ are the initial displacement and velocity of the system, respectively. The form of the equation is the same whether the system is linear or nonlinear.

Choose a small time interval h such that

$$t_j = jh \qquad \text{for } j = 0, 1, 2, \ldots$$

Let w_{ij} denote an approximation to $x_i\,(t_j)$ for each $j = 0, 1, 2, \ldots$ and $i = 1, 2$. For the initial conditions, set $w_{1,0} = x_0$ and $w_{2,0} = \dot{x}_0$. Obtain the approximation w_{ij+1}, given all the values of the previous steps w_{ij}, as [31.1]

$$w_{i,j+1} = w_{i,j} + \frac{1}{6}\,(k_{1,i} + 2k_{2,i} + 2k_{3,i} + k_{4,i}) \qquad i = 1, 2 \tag{31.57}$$

where

$$k_{1,i} = hF_i(t_j + w_{1,j},\, w_{2,j})$$
$$k_{2,i} = hF_i\left(t_j + \frac{h}{2},\, w_{1,j} + \frac{1}{2}\,k_{1,1},\, w_{2i,j} + \frac{1}{2}\,k_{1,2}\right)$$
$$k_{3,i} = hF_i\left(t_j + \frac{h}{2},\, w_{1,j} + \frac{1}{2}\,k_{2,1},\, w_{2,j} + \frac{1}{2}\,k_{2,2}\right) \tag{31.58}$$
$$k_{4,i} = hF_i(t_j + h,\, w_{1,i} + k_{3,1},\, w_{2,i} + k_{3,2}) \qquad i = 1, 2$$

Note that $k_{1,1}$ and $k_{1,2}$ must be computed before we can obtain $k_{2,1}$.

Example 1. Obtain the response of a generator rotor to a short-circuit disturbance given in Fig. 31.17.

The generator shaft may be idealized as a single-degree-of-freedom system in torsion with the following values:

$$\omega_1 = 1737 \text{ cpm} = 28.95(2\pi) \text{ rad/s} = 182 \text{ rad/s}$$
$$J = 8.5428 \text{ lb} \cdot \text{in} \cdot \text{s}^2 \ (25 \text{ kg} \cdot \text{m}^2)$$
$$k = 7.329 \times 10^6 \text{ lb} \cdot \text{in/rad} \ (828\,100 \text{ N} \cdot \text{m/rad})$$

Solution $\quad J\ddot{\theta} + k\theta = f(t) \qquad \ddot{\theta} = \dfrac{k}{J}\,\theta + \dfrac{f(t)}{J}$

Hence,

$$\dot{\theta} = \phi \qquad \dot{\phi} = \frac{-k}{J}\,\theta + \frac{f(t)}{J} \tag{31.59}$$

where $f(t)$ is tabulated.

Since $\omega_1 = 182$ rad/s, the period $\tau = 2\pi/182 = 0.00345$ s and the time interval h must be chosen to be around 0.005 s. Hence, tabulated values of $f(t)$ must be available for t intervals of 0.005 s, or it has to be interpolated from Fig. 31.17.

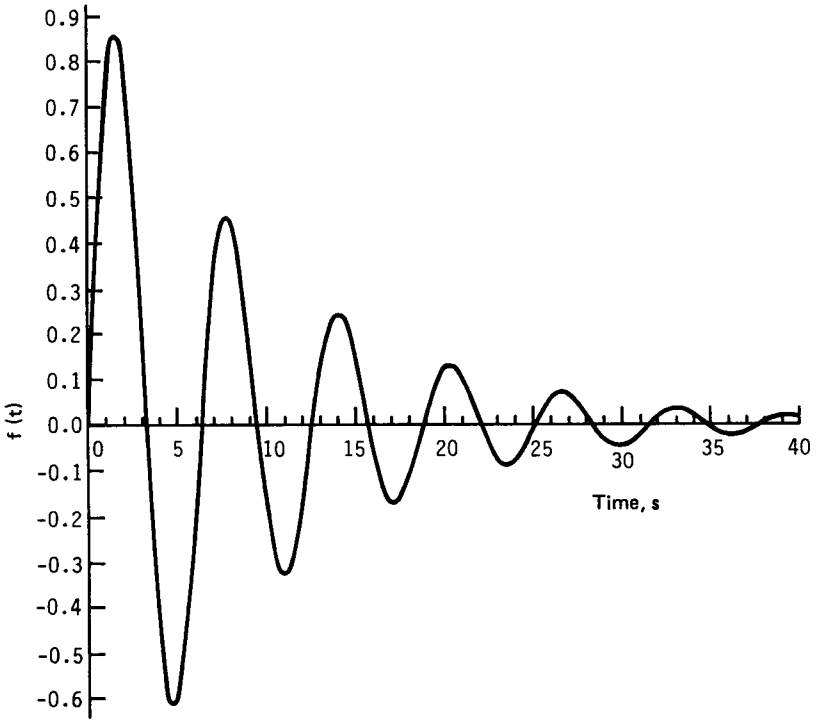

FIGURE 31.17 Short-circuit excitation form.

31.3 SYSTEMS WITH SEVERAL DEGREES OF FREEDOM

Quite often, a single-degree-of-freedom system model does not sufficiently describe the system vibrational behavior. When it is necessary to obtain information regarding the higher natural frequencies of the system, the system must be modeled as a multidegree-of-freedom system. Before discussing a system with several degrees of freedom, we present a system with two degrees of freedom, to give sufficient insight into the interaction between the degrees of freedom of the system. Such interaction can also be used to advantage in controlling the vibration.

31.3.1 System with Two Degrees of Freedom

Free Vibration. A system with two degrees of freedom is shown in Fig. 31.18. It consists of masses m_1 and m_2, stiffness coefficients k_1 and k_2, and damping coefficients c_1 and c_2. The equations of motion are

$$\begin{aligned} m_1\ddot{x}_1 + (c_1 + c_2)\dot{x}_1 + (k_1 + k_2)x_1 - c_2\dot{x}_2 - k_2x_2 = 0 \\ m_2\ddot{x}_2 + c_2\dot{x}_2 + k_2x_2 - c_2\dot{x}_1 - k_2x_1 = 0 \end{aligned} \tag{31.60}$$

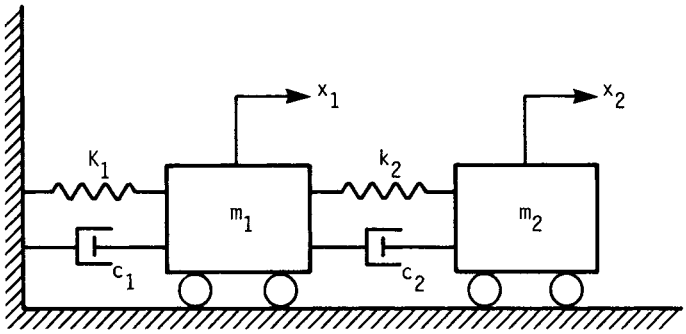

FIGURE 31.18 Two-degree-of-freedom system.

Assuming a solution of the type

$$x_1 = Ae^{st} \qquad x_2 = Be^{st} \tag{31.61}$$

and substituting into Eqs. (31.60) yield

$$\begin{aligned}[m_1 s^2 + (c_1 + c_2)s + k_1 + k_2]A - (c_2 s + k_2)B = 0 \\ -(k_2 + c_2 s)A + (m_2 s^2 + c_2 s + k_2)B = 0\end{aligned} \tag{31.62}$$

Combining Eqs. (31.62), we obtain the frequency equation

$$[m_1 s^2 + (c_1 + c_2)s + k_1 + k_2]\,(m_2 s^2 + c_2 s + k_2) - (c_2 s + k_2)^2 = 0 \tag{31.63}$$

This is a fourth-degree polynomial in s, and it has four roots; hence, the complete solution will consist of four constants which can be determined from the four initial conditions $x_1, x_2, \dot{x}_1$, and $\dot{x}_2$. If damping is less than critical, oscillatory motion occurs, and all four roots of Eq. (31.63) are complex with negative real parts, in the form

$$s_{1,2} = -n_1 \pm ip_1 \qquad s_{3,4} = -n_2 \pm ip_2 \tag{31.64}$$

So the complete solution is

$$\begin{aligned}x_1 &= \exp(-n_1 t)\,(A_1 \cos p_1 t + A_2 \sin p_1 t) \\ &\quad + \exp(-n_2 t)\,(B_1 \cos p_2 t + B_2 \sin p_2 t) \\ x_2 &= \exp(-n_1 t)\,(A_1' \cos p_1 t + A_2' \sin p_1 t) \\ &\quad + \exp(-n_2 t)\,(B_1' \cos p_2 t + B_2' \sin p_2 t)\end{aligned} \tag{31.65}$$

Since the amplitude ratio A/B is determined by Eq. (31.62), there are only four independent constants in Eq. (31.65) which are determined by the initial conditions of the system.

Forced Vibration. Quite often an auxiliary spring-mass-damper system is added to the main system to reduce the vibration of the main system. The secondary system is

called a *dynamic absorber.* Since in such cases the force acts on the main system only, consider a force $P \sin \omega t$ acting on the primary mass m. Referring to Fig. 31.18, we see that the equations of motion are

$$\begin{aligned} m_1\ddot{x}_1 + (c_1 + c_2)\dot{x}_1 + (k_1 + k_2)x_1 - c_2\dot{x}_2 - k_2 x_2 &= P \sin \omega t \\ m_2\ddot{x}_2 + c_2\dot{x}_2 + k_2 x_2 - c_2\dot{x}_1 - k_2 x_1 &= 0 \end{aligned} \tag{31.66}$$

Assuming a solution of the type

$$\begin{aligned} \frac{x_1}{P/k_1} &= A_1 \cos \omega t + A_2 \sin \omega t \\ \frac{x_2}{P/k_1} &= A_3 \cos \omega t + A_4 \sin \omega t \end{aligned} \tag{31.67}$$

and substituting into Eqs. (31.66), we find that the A_i are given as

$$\begin{aligned} A_1 &= \frac{\omega_1^2[2D_1\omega\zeta_2\omega_2 - D_2(\omega_2^2 - \omega^2)]}{D_1^2 + D_2^2} \\ A_2 &= \frac{\omega_1^2[D_1(\omega_2^2 - \omega^2) + 2D_2\omega\zeta_2\omega_2]}{D_1^2 + D_2^2} \\ A_3 &= \frac{\omega_1^2(2D_1\omega\zeta_2\omega_2 - D_2\omega_2^2)}{D_1^2 + D_2^2} \\ A_4 &= \frac{\omega_1^2(D_1\omega_2^2 + 2D_2\omega\zeta_2\omega_2)}{D_1^2 + D_2^2} \end{aligned} \tag{31.68}$$

where

$$\begin{aligned} D_1 &= (\omega^2 - \omega_2^2)\,(\omega^2 - \omega_1^2 - \mu\omega_2^2) - 4\omega^2\zeta_2\omega_2(\zeta_1\omega_1 + \mu\zeta_2\omega_2) - \mu(\omega_2^4 - 4\omega^2\zeta_2^2\omega_2^2) \\ D_2 &= 2\omega[(\omega_2^2 - \omega^2)\,(\zeta_1\omega_1 + \mu\zeta_2\omega_2) + \zeta_2\omega_2(\omega_1^2 - \omega^2 + \mu\omega_2^2) - 2\mu\zeta_2\omega_2^3] \end{aligned} \tag{31.69}$$

$$\omega_1^2 = \frac{k_1}{m_1} \qquad \omega_2^2 = \frac{k_2}{m_2}$$

$$\zeta_1 = \frac{c_1}{2m_1\omega_1} \qquad \zeta_2 = \frac{c_2}{2m_2\omega_2} \tag{31.70}$$

$$\mu = \frac{m_2}{m_1}$$

Responses may also be written in the form

$$x_1 = B_1 \sin(\omega t - \theta_1) \qquad x_2 = B_2 \sin(\omega t - \theta_2) \tag{31.71}$$

where

$$B_1 = (A_1^2 + A_2^2)^{1/2} \qquad B_2 = (A_3^2 + A_4^2)^{1/2}$$
$$\tan \theta_1 = -\frac{A_1}{A_2} \qquad \tan \theta_2 = -\frac{A_3}{A_4} \tag{31.72}$$

Here θ_1 and θ_2 are the phase angles by which the responses of masses m_1 and m_2, respectively, will lag behind the applied force. The response amplitudes B_1 and B_2 are plotted in Figs. 31.19 and 31.20, respectively. The amplitude B_1 has a minimum between ω_1 and ω_2.

The equations of motion for torsional systems with two degrees of freedom have the same form as Eqs. (31.60) and (31.66). The solution will also be similar and will exhibit the same characteristics as discussed earlier.

31.3.2 Multidegree-of-Freedom Systems

In many applications, it is necessary to know several higher modes of a vibrating system and evaluate the vibration response. Here, the elastic system has to be treated as one with distributed mass and elasticity. This is possible for simple elements such as beams, plates, or shells of regular geometry. However, when the structural system is complex, it may be modeled as a multidegree-of-freedom discrete

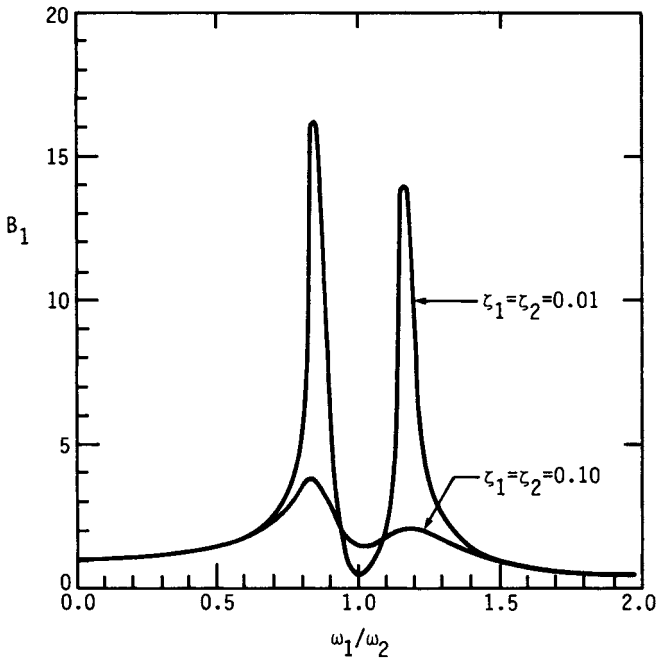

FIGURE 31.19 Amplitude frequency response of the mass of a two-degree-of-freedom system subject to forced excitation.

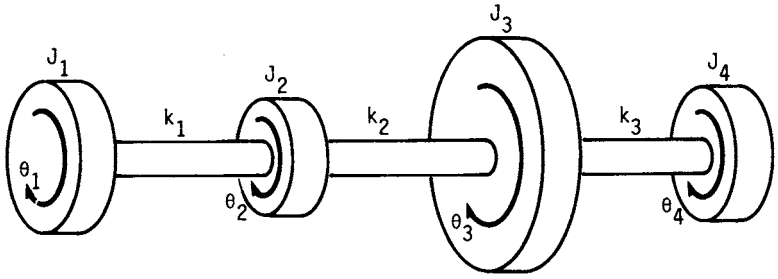

FIGURE 31.20 Torsional system with four freedoms.

system by concentrating its mass and stiffness properties at a number of locations on the structure.

The number of degrees of freedom of a structure is the number of independent coordinates needed to describe the configuration of the structure. In a lumped-mass model, if motion along only one direction is considered, the number of degrees of freedom is equal to the number of masses; and if motion in a plane is of interest, the number of degrees of freedom will equal twice the number of lumped masses.

Holzer Method. When an undamped torsional system consisting of several disks connected by shafts vibrates freely in one of its natural frequencies, it does not need any external torque to maintain the vibration. In Holzer's method, this fact is used to calculate the natural frequencies and natural modes of a vibrating system. Figure 31.20 shows a torsional system with several disks connected by shafts. In this procedure, an initial value is assumed for the natural frequency, and a unit amplitude is specified at one end. The resulting torques and angular displacements are progressively calculated from disk to disk and carried to the other end. If the resulting torque and displacement at the other end are compatible with boundary conditions, the initial assumed value for the natural frequency is a correct natural frequency; if not, the whole procedure is repeated with another value for the natural frequency until the boundary conditions are satisfied. For a frequency ω and $\theta_1 = 1$, the corresponding inertial torque of the first disk in Fig. 31.20 is

$$T_1 = -J_1\ddot{\theta}_1 = J_1\omega^2\theta_1 \tag{31.73}$$

This torque is transmitted to disk 2 through shaft 1; hence,

$$T_1 = J_1\omega^2\theta_1 = k_1\,(\theta_1 - \theta_2) \tag{31.74}$$

which relates θ_2 and θ_1. The inertial torque of the second disk is $J_2\omega^2\theta_2$, and the sum of the inertial torques of disk 1 and disk 2 is transmitted to disk 3 through shaft 2, which gives

$$J_1\omega^2\theta_1 + J_2\omega^2\theta_2 = k_2(\theta_2 - \theta_3) \tag{31.75}$$

Continuing this process, we see the torque at the far end is the combined inertial torques of all the disks and is given by

$$T = \sum_{i=1}^{n} J_i\omega^2\theta_i \tag{31.76}$$

where n is the total number of disks. If the disk is free at that end, the total torque T should vanish. Hence, the frequency ω which makes T zero at the far end is a natural frequency.

Example 2. Determine the natural frequencies and mode shapes of a torsional system consisting of three disks connected by two shafts.

$$J_1 = 1.7086 \times 10^4 \text{ lb} \cdot \text{in} \cdot \text{s}^2 \qquad (5 \text{ kg} \cdot \text{m}^2)$$

$$J_2 = 3.7588 \times 10^4 \text{ lb} \cdot \text{in} \cdot \text{s}^2 \qquad (11 \text{ kg} \cdot \text{m}^2)$$

$$J_3 = 3.4171 \times 10^4 \text{ lb} \cdot \text{in} \cdot \text{s}^2 \qquad (10 \text{ kg} \cdot \text{m}^2)$$

$$k_1 = 8.8504 \times 10^5 \text{ lb} \cdot \text{in/rad} \qquad (1 \times 10^5 \text{ rad})$$

$$k_2 = 1.7701 \times 10^6 \text{ lb} \cdot \text{in/rad} \qquad (2 \times 10^5 \text{ rad})$$

Solution. Holzer's procedure can be carried out in a tabulated form as shown in Table 31.1. Two trials are shown in Table 31.1. The calculation can be carried out for more values of ω, and the resulting T_3 can be plotted versus ω, as shown in Fig. 31.21. The frequencies at which $T_3 = 0$ are then the natural frequencies of the system. Better approximation can be obtained by employing the method of false position [31.1]; if $\omega(+)$ and $\omega(-)$ are the frequencies when the torque has corresponding values of $T_3(+)$ and $T_3(-)$, the natural frequency can be obtained by

$$\omega = \frac{\omega(-)T_3(+) - \omega(+)T_3(-)}{T_3(+) - T_3(-)}$$

TABLE 31.1 Holzer's Procedure

Frequency, rad/s	Station					
	1		2		3	
ω	θ	$T = J\omega^2\theta$	$\theta = 1 - \frac{T}{K}$	$T = T + J\omega^2\theta$	$\theta = \theta - \frac{T}{K}$	$T = T + J\omega^2\theta$
	1	1 1 1	2 1 1	2 1 2 2	3 2 2 2	3 2 3 3
10	1.0	4 425.2 (500.0)	0.995	1 412.0 (1 594.5)	0.987	22 847.0 (2 581.5)
20	1.0	17 701.0 (2 000.0)	0.980	55 864.0 (6 312.0)	0.948	89 442.0 (10 106.0)

The mode shape corresponding to a natural frequency can be obtained by recalculating the values of θ_1, θ_2, and θ_3 in the Holzer table. In the example, the first natural frequency is $\omega_1 = 141.4214$ rad/s, and the corresponding mode shape is

$$\{\theta_1, \theta_2, \theta_3\} = \{1.0, 0.0, -0.5\}$$

VIBRATION AND CONTROL OF VIBRATION

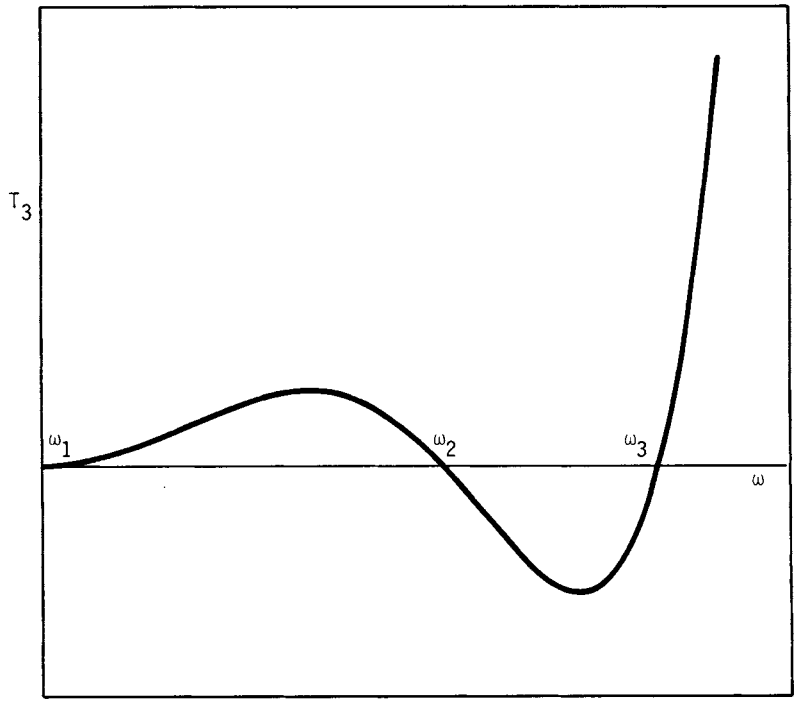

FIGURE 31.21 Variation of end torque with assumed natural frequency.

Geared Systems. When a shaft transmits torque to another through a gear drive of speed ratio n, it is necessary to reduce the geared torsional system to an equivalent single-shaft system to find its natural frequency. The moments of inertia and the stiffness of the equivalent system are obtained through a consideration of the kinetic and potential energies of the system.

Consider the geared torsional system in Fig. 31.22*a*. The speed of the second shaft is $\dot{\theta}_2 = n\dot{\theta}_1$. Assuming massless gears, we see that the kinetic energy of the system is

$$T = \frac{1}{2} J_1 \dot{\theta}_1^2 + \frac{1}{2} J_2 n^2 \dot{\theta}_1^2 \tag{31.77}$$

Thus the equivalent mass moment of inertia of disk 2 referred to shaft 1 is $n^2 J_2$. If disks 1 and 2 are clamped and a torque is applied to gear 1, rotating it through an angle θ_1, there will be deformations in both shafts 1 and 2. Gear 2 will rotate through an angle $\theta_2 = n\theta_1$. The potential energy stored in the two shafts is

$$U = \frac{1}{2} k_1 \theta_1^2 + \frac{1}{2} k_2 n^2 \theta_1^2 \tag{31.78}$$

Hence the equivalent stiffness of shaft 2 referred to shaft 1 is $n^2 k_2$. The equivalent torsional system is shown in Fig. 31.22*b*, where the stiffness and inertia of one side of the system are multiplied by the square of the speed ratio to obtain the corresponding equivalent values for Holzer calculations.

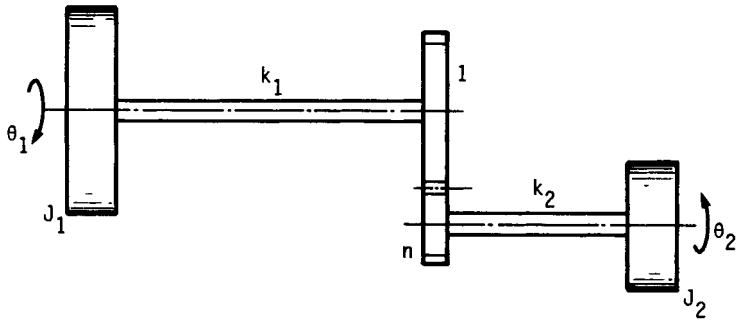

(a)

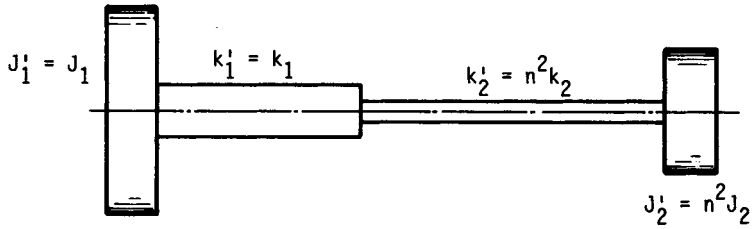

(b)

FIGURE 31.22 (*a*) Geared shaft disk system; (*b*) equivalent torsional system.

31.3.3 Continuous Systems

Engineering structures, in general, have distributed mass and elasticity. Such structures can be treated as multidegree-of-freedom systems by lumping their masses at certain locations and connecting them by representative spring elements. However, it is necessary to consider several such lumped masses and springs to get sufficiently accurate values for the natural frequencies. If only the fundamental natural frequency or the first few natural frequencies are of interest, it is convenient to use some approximate methods based on energy formulations discussed here.

Rayleigh Method. This method can give the natural frequency of a structure of any specific mode of vibration. A deflection shape satisfying the geometric boundary conditions has to be assumed initially. If the natural frequency of the fundamental mode of vibration is of interest, then a good approximation would be the static deflection shape. For a harmonic motion, the maximum kinetic energy of a structure can be written in the form

$$T_{\max} = \omega^2 C_1 \tag{31.79}$$

where C_1 depends on the assumed deflection shape. The maximum potential energy is of the form

$$U_{\max} = C_2 \tag{31.80}$$

Neglecting damping, we see that the maximum kinetic energy must be equal to the maximum potential energy. Hence, the natural frequency is

$$\omega^2 = \frac{C_2}{C_1} \tag{31.81}$$

This estimate will always be higher than the true natural frequency.

Example 3. Determine the fundamental natural frequency of a uniform cantilever beam of length L supporting a disk of mass M and diametral mass moment of inertia I_d, as shown in Fig. 31.23. The modulus of elasticity of the beam material is E, the mass moment of inertia of the cross section is I, and the mass per unit length of the beam is m.

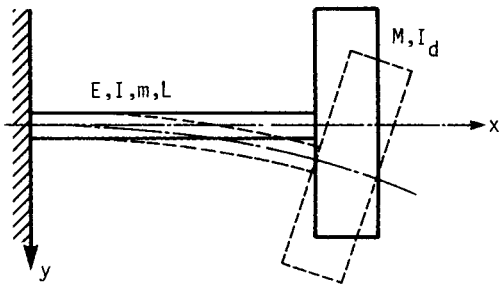

FIGURE 31.23 Cantilever with end mass.

Solution. The deflection shape may be assumed to be $y(x) = Cx^2$, which satisfies the geometric boundary conditions of zero deflection and zero slope at $x = 0$. The maximum kinetic energy of the structure for harmonic vibration is

$$T_{\max} = \frac{1}{2} m\omega^2 \int_0^L y^2(x)\, dx + \frac{1}{2} M\omega^2 y^2(L) + \frac{1}{2} I_d \omega^2 y'^2(L)$$

The strain energy is given by

$$U_{\max} = \frac{1}{2} EI \int_0^L y''^2(x)\, dx$$

Substituting $y(x) = Cx^2$ in the above expressions and equating $T_{\max} = U_{\max}$, we find the natural frequency

$$\omega^2 = \frac{20EI}{mL^4 + 5ML^3 + 20I_d L}$$

In the absence of the disk, $\omega = 4.47\ (EI/mL^4)^{1/2}$. By comparing this to the exact result $\omega = 3.52\ (EI/mL^4)^{1/2}$, the error in the approximation is error = $0.95\ (EI/mL^4)^{1/2}$, or 26.9 percent.

This error can be reduced by obtaining the strain energy by using a different method. The shear at any section is obtained by integrating the inertial loading from the free end as

$$V(\xi) = \left[\omega^2 \int_{\xi}^{L} m(\xi) y(\xi)\, d\xi\right] + M\omega^2 y(L)$$

$$= \frac{1}{3}\omega^2 mc(L^3 - \xi^3) + M\omega^2 cL^2$$

and the moment at any point x is

$$M(x) = \int_{x}^{L} V(\xi)\, d\xi + I_d y'(L) = \frac{1}{12}\omega^2 mc(3L^4 - 4L^3 x + x^4) + M\omega^2 cL^2(L - x) + 2I_d cL$$

The strain energy is then

$$U_{\max} = \frac{1}{2}\int_{0}^{L} \frac{M^2(x)}{EI}\, dx$$

When the disk is absent,

$$U_{\max} = \frac{\omega^4}{2EI}\,\frac{m^2c^2}{144}\,\frac{312}{135}\,L^9$$

With $T_{\max}$ and $U_{\max}$ equated, the natural frequency $\omega = 3.53\ (EI/ML^4)^{1/2}$ has an error of only 0.28 percent.

31.4 VIBRATION ISOLATION

Often machines and components which exhibit vibrations have to be mounted in locations where vibrations may not be desirable. Then the machine has to be isolated properly so that it does not transmit vibrations.

31.4.1 Transmissibility

Active Isolation and Transmissibility. From Eq. (31.38), the force transmissibility, which is the magnitude of the ratio of the force transmitted to the force applied, is given by

$$T = \left[\frac{1 + (2\zeta\omega/\omega_n)^2}{(1 - \omega^2/\omega_n^2)^2 + (2\zeta\omega/\omega_n)^2}\right]^{1/2} \tag{31.82}$$

Equation (31.82) is plotted in Fig. 31.12 for different values of ζ. All the curves cross at $\omega/\omega_n = \sqrt{2}$. For $\omega/\omega_n > \sqrt{2}$, transmissibility, although below unity, increases with

an increase in damping, contrary to normal expectations. At higher frequencies, transmissibility goes to zero.

Since the force amplitude $me\omega^2$ in the case of an unbalanced machine is dependent upon the operating speed of the machine, transmissibility can be defined as

$$T = \frac{F_T}{me\omega^2} = \left(\frac{\omega}{\omega_n}\right)^2 \left[\frac{1 + (2\zeta\omega/\omega_n)^2}{(1 - \omega^2/\omega_n^2)^2 + (2\zeta\omega/\omega_n)^2}\right]^{1/2} \tag{31.83}$$

where F_T is the amplitude of the transmitted force.

Equation (31.83) is plotted in Fig. 31.24. Transmissibility starts from zero at zero operating frequency, and curves for different damping ratios cross at $\omega/\omega_n = \sqrt{2}$. For higher values of operating speed, transmissibility increases indefinitely with frequency.

Passive Isolation. When a sensitive instrument is isolated from a vibrating foundation, it is called *passive isolation*. Consider the system shown in Fig. 31.15, where the base has a motion $u = U_0 \sin \omega t$. The equation of motion of the system is given in Eq. (31.46).

The ratio of the response and excitation amplitudes is

$$\frac{X}{X_f} = \frac{k + i\omega c}{k - m\omega^2 + i\omega c} \tag{31.84}$$

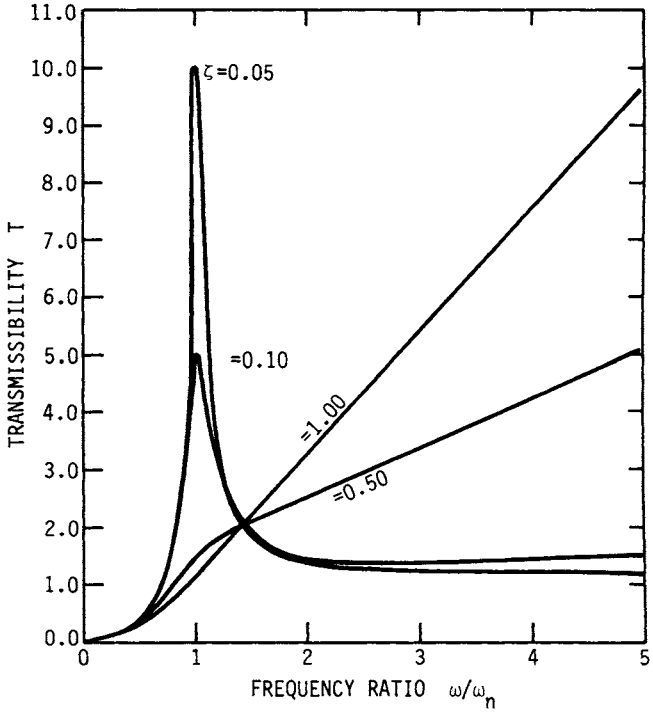

FIGURE 31.24 Transmissibility of a system under unbalanced excitation.

Since we are interested in the motion transmissibility in the case of passive isolation, Eq. (31.84) gives the transmissibility T, which can be put in terms of nondimensional parameters, as

$$T = \frac{X}{U_0}\left[\frac{1 + (2\zeta\omega/\omega_n)^2}{(1 - \omega^2/\omega_n^2)^2 + (2\zeta\omega/\omega_n)^2}\right]^{1/2} \tag{31.85}$$

Equation (31.85) is identical to the force transmissibility in the case of active isolation given in Eq. (31.82).

REFERENCES

31.1 R. L. Burden, J. D. Faires, and A. C. Reynolds, *Numerical Analysis,* 2d ed., Prindle, Weber and Schmidt, Boston, 1981.

31.2 R. B. Bhat, J. S. Rao, and T. S. Sankar, "Optimum Journal Bearing Parameters for Minimum Unbalance Response in Synchronous Whirl," ASME Design Engineering Conference, Paper No. 81-DET-55, 1981. (To be published in *ASME Transactions.*)

31.3 J. P. Den Hartog, *Mechanical Vibrations,* McGraw-Hill, New York, 1962.

31.4 W. T. Thomson, *Theory of Vibration with Applications,* Prentice-Hall, Englewood Cliffs, N.J., 1981.

31.5 T. S. Sankar and G. D. Xistris, "Failure Prediction through the Theory of Stochastic Excursions of Extreme Vibration Amplitudes," *J. Eng. Ind., Trans. ASME,* 1972.

31.6 *NASTRAN Computer Program,* McNeil Schwendler Corporation, Los Angeles.

31.7 *ANSYS Computer Program,* SWANSON Analysis Systems Incorporated, Houston, Pennsylvania.

31.8 *ADINA Computer Program,* ADINA Engineering AB VASTERAS, Sweden.

31.9 *SPAR Structural Analysis System,* Engineering Information Systems, Inc., San Jose, California.

31.10 *PROSSS—Programming Structural Synthesis System,* NASA Langley Research Center, Hampton, Virginia.

P · A · R · T · 8

PERFORMANCE OF ENGINEERING MATERIALS

CHAPTER 32
SOLID MATERIALS

Joseph Datsko
Professor Emeritus of Mechanical Engineering
The University of Michigan
Ann Arbor, Michigan

This chapter summarizes the structure of solids, including atomic bonding forces, atomic structures, crystal imperfections, slip, and mechanical strength. The section on mechanical properties and tests discusses all the hardness tests and includes a detailed explanation of the tensile test and tensile properties. The section on strength, stress, and strain relations includes many new relationships that have been developed during the past two decades and are not found in other handbooks. The mechanical property data presented in this section are in a new format that is well suited for use in computer-aided-engineering (CAE) applications.

32.1 STRUCTURE OF SOLIDS

A study of the mechanical properties of materials must begin with an understanding of the structure of solid materials. In this context, *structure* refers to the atomistic and crystalline patterns of which the solid material is composed. The definitions of the mechanical properties given in the following sections are on the basis of the crystalline structure of material. For example, *strength* (and *hardness*) is defined as the ability of the material to resist slip along its crystallographic planes. Thus, in order to increase the strength of a material, something must be done to it which will make

slip more difficult to initiate. The following sections will explain the manner in which the various thermal and mechanical processes affect the structure of a material, which in turn determines the mechanical properties. The next section presents a brief review of atomic structure.

32.2 ATOMIC BONDING FORCES

The smallest particles that must be considered in the preceding context are atoms. The manner in which atoms are arranged in a solid material determines the material's crystal structure. The crystal structure and the type of interatomic bonding forces determine the strength and ductility of the material.

The simple model of an atom is a dense *nucleus,* consisting of *protons* and *neutrons,* surrounded by discrete numbers of planetary *electrons* orbiting in shells at specific distances from the nucleus. Each proton has a positive electric charge of unity (1+). The number of protons in the nucleus determines the nuclear charge of the atom and is called the *atomic number.* The neutrons have no charge, but they do have mass. The *atomic weight* of an atom is the sum of the number of protons and neutrons. The electrons have negligible mass and a negative charge of unity (1–). The number of electrons in a given type of atom is also equal to the atomic number of that element. The maximum number of electrons in any shell is $2n^2$, where n is the *quantum number* of the shell. Thus the maximum number of electrons that can be present in the first (innermost) shell is 2, and 8 is the maximum in the second shell. However, no more than 8 electrons are ever present in the outermost shell of an atom. The *valence* of an element is either the number of electrons in its outermost shell or the number of electrons necessary to fill that shell, whichever number is lower.

The interatomic bonding forces are determined by the valence, or outer-shell, electrons. There are four types of atomic bonding forces that hold the atoms of a solid material in their relatively fixed positions. The three strongest (*ionic, covalent,* and *metallic*) types of bond are referred to as *primary;* the fourth (*molecular*) is referred to as a *secondary* type of bond.

32.2.1 Ionic Bonds

From the preceding brief description of atomic structure, it is evident that the uncombined atom is electrically neutral—the number of protons (+ charges) in the nucleus exactly equals the number of electrons (– charges). When atoms combine, only the valence electrons are involved and not the nuclei. When a metal combines with a nonmetal, each metal atom "loses" its valence electrons and thus acquires a positive charge that is equal to the number of electrons so lost. Likewise each nonmetallic atom "gains" a number of electrons equal to its valence and acquires an equal negative charge. While in this state, the positively charged metallic atom and the negatively charged nonmetallic atom are called *ions.*

Like-charged particles repel each other and oppositely charged particles attract each other with an electric force called the *Coulomb force.* When a material is maintained in the solid state by the mutual attraction of positively and negatively charged ions, the interatomic bonding force is called *ionic.*

The Coulomb forces attracting oppositely charged ions are very large. Therefore, ionic-bonded solids exhibit very high strength and relatively low melting tempera-

tures. However, they exhibit very low ductility under normal conditions because the interatomic bonds must be broken in order for the atoms to slide past each other. This is one of the most important distinctions between ionic (or covalent) bonding and metallic bonding and is discussed later.

32.2.2 Covalent Bonds

Covalent bonds are those in which the atoms reach a stable configuration (filled outer shell) by *sharing* valence electrons. Unlike ionic bonds, which are nondirectional, covalent bonds act between specific pairs of atoms and thus form molecules. Covalent bonds are most prevalent in gas molecules. Covalent bonding also results in the formation of very large molecules which are present as solids rather than as liquids and gases. Diamond, silicon, and silicon carbide are examples of such covalent-bonded solids. They are characterized by high strength and melting temperature and low ductility. The atoms in the diamond structure are arranged on two interpenetrating face-centered cubic lattices. The entire crystal is composed of only one molecule, and in order to fracture the crystal, the strong covalent interatomic bonds must be broken.

32.2.3 Metallic Bonds

Of the three primary bonding forces, the metallic bond is by far the most important for an understanding of the mechanical properties of the materials with which the practicing engineer is concerned. The *metallic bond* is a special type of covalent bond wherein the positively charged nuclei of the metal atoms are attracted by electrostatic forces to the valence electrons that surround them. Unlike the common covalent bond, which is directional, i.e., between a pair of atoms, the metallic bond is nondirectional, and each nucleus attracts as many valence electrons as possible. This leads to a dense packing of the atoms, and thus the most common crystal structures of the metals are the close-packed ones: face- and body-centered cubic and hexagonal close-packed structures.

The reason that metal atoms have their own unique type of bonding force is the looseness with which their valence electrons are held in the outer shell. This is evident from the fact that the ionization potential of metal atoms is one-half to two-thirds that of nonmetal atoms. The mean radius of the valence electrons in a free (isolated) metal atom is larger than the interatomic distance of that metal in the solid crystalline state. This means that the valence electrons are closer to a nucleus in the solid metal than they are in a free atom, and thus their potential energy is lower in the solid.

Since the valence electrons are not localized between a pair of positive ions, they are free to move through the solid. Thus the structure of the solid metal is a close-packed arrangement of positive ion "cores" (the nucleus plus the nonvalence electrons) that is permeated by an electron "gas" or "cloud." This ability of the valence electrons to move freely through the solid explains the high thermal and electrical conductivities of metals. Also, the fact that the valence electrons are nondirectional (not shared by only two atoms) explains the relatively low strength and high ductility of elemental metals, since the positive ions can move relative to one another without breaking any primary bonds. This mechanism is referred to as *slip* and is discussed in more detail in a following section on crystal structures.

32.2.4 Molecular or van der Waals Bonds

In addition to the three strong primary bonds discussed above, there are also several much weaker (and therefore called *secondary*) bonds which provide the interatomic attractive forces that hold some types of atoms together in a solid material. These forces are referred to as either *secondary* bonds, *molecular* bonds, or *van der Waals* bonds. These bonds are due to residual electrostatic fields between neutral molecules whose charge distribution is not uniform.

Covalently bonded atoms frequently form molecules that behave as electric or magnetic *dipoles*. Although the molecule itself is electrically neutral, there is an electrical imbalance within the molecule. That is, the center of the positive charge and the center of the negative charge do not coincide, and it is this dipole that creates molecular bonding.

32.3 ATOMIC STRUCTURES

Whereas the electrical properties of a material depend on the internal structure of the atoms, the mechanical properties depend on the types of structures that groups of atoms form. In this context, *atomic structures* refer to the structures that are built by particular arrangements of atoms, not to the internal structure of individual atoms. All solid materials can be classified on the basis of atomic structure into three groups: amorphous, molecular, or crystalline (in order of increasing importance to mechanical properties). Knowledge of the atomic structure of solids makes it possible to understand why a given material has its unique properties and thus to be able to specify the type of material and the condition it should be in to achieve optimum mechanical properties.

32.3.1 Amorphous Solids

Amorphous materials are those whose structure has no repetitive arrangement of the atoms of which it is comprised. In a sense, they have no "structure." Although gases and liquids are amorphous materials, the only important amorphous solids are the glasses, and they are frequently considered simply as supercooled liquids.

Glass behaves as a typical liquid at high temperatures. The atoms are very mobile and do not vibrate in a fixed location in space. A given mass of hot glass, like any liquid, takes the shape of the container in which it is placed.

As a hot glass cools, its atoms vibrate at lower amplitudes and come closer together, resulting in an overall thermal contraction or decrease in specific volume. This decrease in specific volume of a liquid as temperature decreases is approximately linear and occurs with all liquids, including liquid metals. This is illustrated in Fig. 32.1.

When any unalloyed liquid metal (a pure metallic element) or chemical compound is cooled to its freezing (or melting) temperature T_m, the atoms come much closer together and become relatively immobile with respect to one another. They form a crystalline structure with very efficient packing, and thus there is a very marked decrease in specific volume at this temperature, as shown in Fig. 32.1. When an alloyed liquid metal freezes to form a solid solution, the transition from liquid to solid takes place in the range of temperatures between the liquidus and the solidus. Further cooling of both solid metals results in a further decrease in specific volume, also linear but of lower slope than in the liquid state.

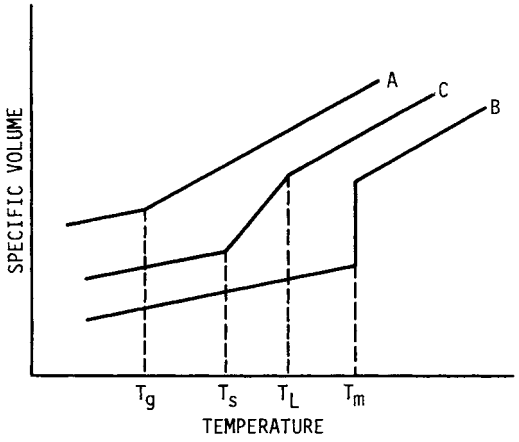

FIGURE 32.1 Specific volume versus temperature. (A) Glass with a transition temperature T_g; (B) a crystal that melts at a fixed temperature T_m, such as a pure element or a compound; (C) a crystal that melts over a range of temperature, such as a solid-solution alloy with T_L the liquidus temperature and T_s the solidus temperature.

When hot liquid glass is cooled to some temperature T_g, called the *glass transition temperature,* there is an abrupt change in the slope of the specific volume versus temperature curve. Unlike crystalline solids, the glass shows no marked decrease in specific volume at this temperature. Below T_g, glass behaves as a typical solid.

32.3.2 Molecular Solids

A *molecule* is a group of atoms that are held together by strong ionic or covalent bonds. A *molecular solid* is a structure made up of molecules that are attracted to each other by weak van der Waals forces. The two most common types of molecular solids are silicates and polymers. The silicates have ionic intramolecular bonds, and the polymers have covalent ones. Since it is the latter materials that are more important in terms of mechanical properties, they will be discussed in more detail.

Polymers are organic compounds of carbon, hydrogen, and oxygen to which other elements such as chlorine or fluorine may be added. They cover a wide range of structural arrangements, with resulting variations in properties. Large molecules are constructed from a repeating pattern of small structural units. The hydrocarbons have repeating structural units of carbon and hydrogen atoms.

Figure 32.2 shows some of the more common monomers or unsaturated molecules that are used in the building of macromolecules. The simplest monomer is ethylene (C_2H_4); it is shown in Fig. 32.2*a.* It is the base of the group of hydrocarbons called *olefins.* The olefins have the chemical formula C_nH_{2n}. The benzene molecule, shown in Fig. 32.2*d,* is another important building unit. Because of the shape of the molecule, it is described as a ring molecule or compound. The benzene group is also called the *aromatic* hydrocarbons.

Figure 32.3 illustrates the addition polymerization of the ethylene monomer. The double bonds of ethylene are broken in the presence of a catalyst such as boron tri-

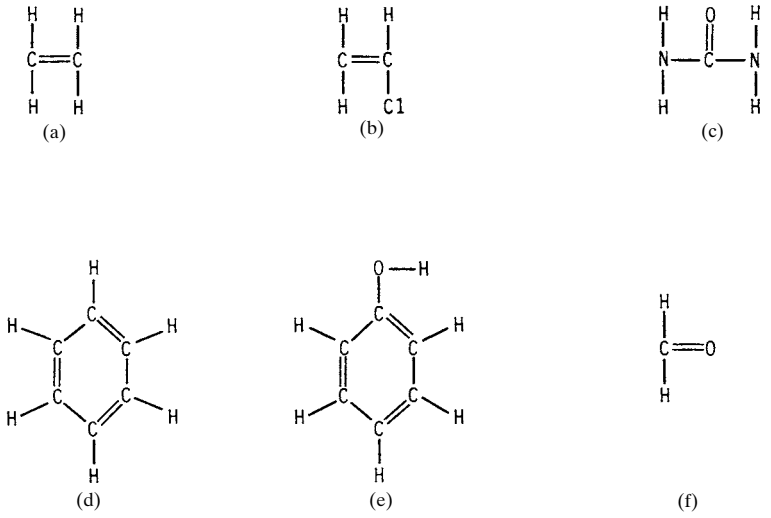

FIGURE 32.2 Monomers: Small unsaturated (double-bonded) molecules that are building units for large polymer molecules. (*a*) Ethylene; (*b*) vinyl chloride; (*c*) urea; (*d*) benzene; (*e*) phenol; (*f*) formaldehyde.

fluoride. The vinyl chloride monomer, as shown in Fig. 32.2*b,* is similar to ethylene except that one of the hydrogen atoms is replaced with a chlorine atom. The polymerization of this monomer results in polyvinyl chloride. These macromolecules resemble, more or less, smooth strings or chains, as can be seen from their structural arrangement.

Some macromolecules resemble rough chains—that is, chains with many short side arms branching from them. Polystyrene, which is a very important industrial polymer, is of this type. The styrene monomer is made from the benzene ring (C_6H_6) with one of the hydrogen atoms replaced with a $CH{=}CH_2$ molecule, as shown in Fig. 32.4*a.* Polymerization then occurs by breaking the double bond in the $CH{=}CH_2$ group with the help of a peroxide catalyst and joining two of them together, as shown in Fig. 32.4*b.*

The polymers just described are *thermoplastic;* they melt or soften when they are heated. This is due to the fact that the individual macromolecules are stable and the linkages to other macromolecules are loose (since they are attracted to each

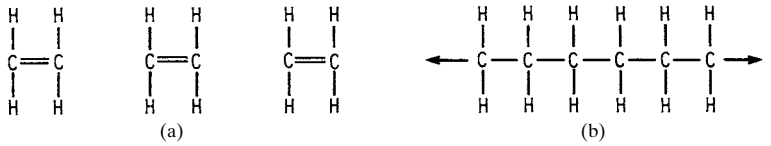

FIGURE 32.3 Addition polymerization. (*a*) Three individual monomers of ethylene; (*b*) a portion of a polyethylene molecule formed when each double bond of the monomers is broken by a catalyst to form two single bonds and join the individual molecules together.

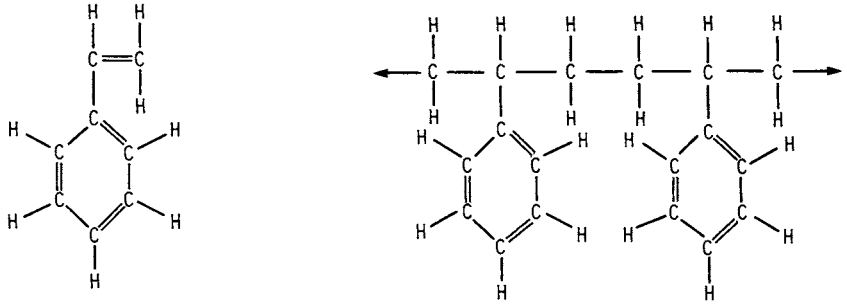

(a) (b)

FIGURE 32.4 (*a*) Styrene structure; (*b*) polystyrene structure. The polymerization takes place in the presence of a peroxide catalyst.

other by weak van der Waals forces). Some polymers are *thermosetting;* they do not soften when they are heated, but retain their "set" or shape until charred. This is due to the fact that the individual macromolecules unite with each other and form many cross-linkages. Bakelite (phenol formaldehyde) is such a polymer. Figure 32.5 shows how each formaldehyde monomer joins two phenol monomers together, under suitable heat and pressure, to form a macromolecule. This is a condensation type of polymerization because one water molecule is formed from the oxygen atom of each formaldehyde molecule and a hydrogen atom from each of the two phenol molecules.

32.3.3 Mechanical Properties of Molecular Structures

The mechanical properties of polymers are determined by the types of forces acting between the molecules. The polymers are amorphous with random chain orientations while in the liquid state. This structure can be retained when the polymer is cooled rapidly to the solid state. In this condition, the polymer is quite *isotropic.* However, with slow cooling or plastic deformation, such as stretching or extruding, the molecules can become aligned. That is, the long axes of the chains of all the molecules tend to be parallel. A material in this condition is said to be "oriented" or "crystalline," the degree of orientation being a measure of the crystallinity. When the molecular chains of a polymer have this type of directionality, the mechanical properties are also directional and the polymer is *anisotropic.* The strength of an aligned polymeric material is stronger along the axis of the chains and much lower in the perpendicular directions. This is due to the fact that only weak van der Waals forces hold the individual, aligned macromolecules together, whereas the atoms along the axes of the chains are held together by strong and covalent bonds. The intermolecular strength of linear polymers can be increased by the addition of polar (dipole) groups along the length of the chain. The most frequently used polar groups are chlorine, fluorine, hydroxyl, and carboxyl.

The thermosetting (cross-linked) types of polymers have all the macromolecules connected together in three directions with strong covalent bonds. Consequently, these polymers are stronger than thermoplastic ones, and they are also more isotropic.

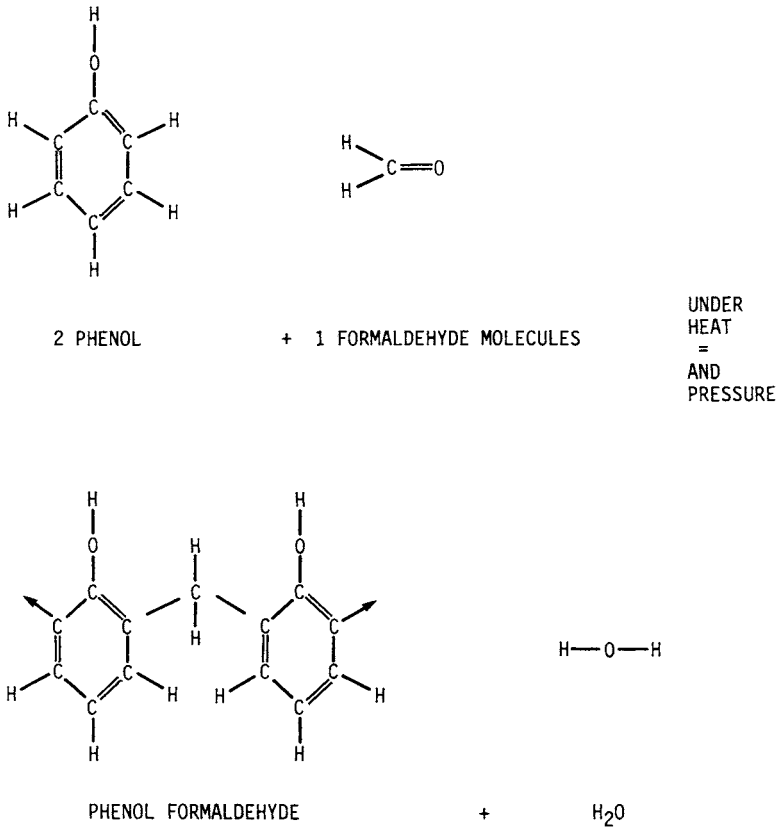

FIGURE 32.5 Condensation polymerization of phenol and formaldehyde into bakelite.

32.3.4 Crystalline Solids

Crystalline solids are by far the most frequently used ones on the basis of mechanical properties or load-carrying capacity. Moreover, of all the crystalline solids, metals are the most important. A *crystal* (or crystalline solid) is an orderly array of atoms having a repeating linear pattern in three dimensions. The atoms are represented as spheres of radius *r.* A *space lattice* is the three-dimensional network of straight lines that connects the centers of the atoms along three axes. The intersections of the lines are *lattice points,* and they designate the locations of the atoms. Although the atoms vibrate about their centers, they occupy the fixed positions of the lattice points. Figure 32.6 is a sketch of a space lattice, with the circles representing the centers of the atoms. A space lattice has two important characteristics: (1) The space-lattice network divides space into equal-sized prisms whose faces contact one another in such a way that no void spaces are present, and (2) every lattice point of a space lattice has identical surroundings.

The individual prisms that make up a space lattice are called *unit cells.* Thus a unit cell is the smallest group of atoms which, when repeated in all three directions, make up the space lattice, as illustrated by the dark-lined parallelepiped in Fig. 32.6.

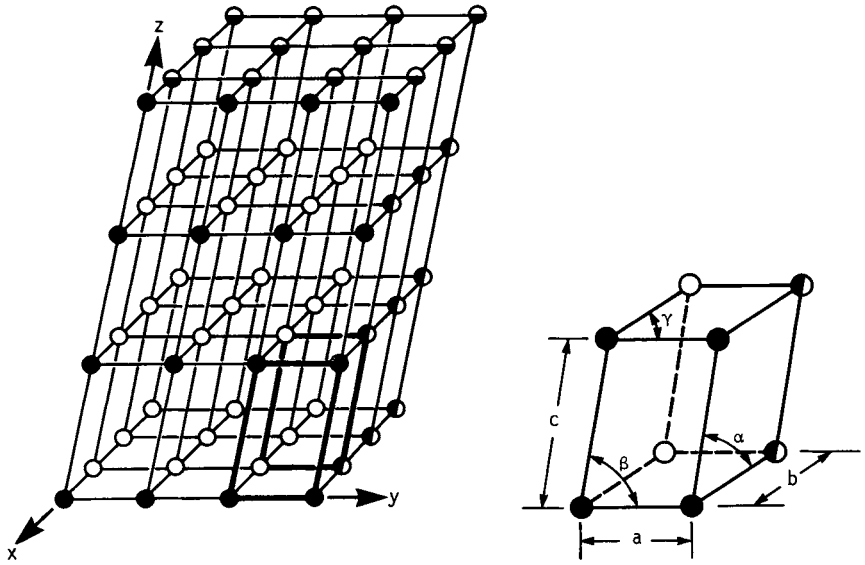

(a) (b)

FIGURE 32.6 A space lattice. (*a*) A unit cell is marked by the heavy lines. Black circles are on the front face; horizontal shading on the top face; vertical shading on the right side face; hidden circles are white. (*b*) An isolated unit cell showing dimensions *a, b,* and *c* and angles α, β, and γ.

Only 14 different space lattices and 7 different systems of axes are possible. Most of the metals belong to three of the space-lattice types: face-centered cubic, body-centered cubic, and hexagonal close-packed. They are listed in Table 32.1, along with four metals that have a rhombohedral and two that have orthorhombic structures.

TABLE 32.1 Lattice Structure of Metal Crystals

Face-centered cubic	Body-centered cubic	Hexagonal close-packed	Rhombohedral	Orthorhombic
Ag	Cb	Be	As	Ga
Al	α-Cr	Cd	Bi	U
Au	Cs	α-Co	Hg	
Ce	α-Fe	β-Cr	Sb	
β-Co	δ-Fe	Hf		
Cu	K	Mg		
γ-Fe	Li	Os		
Ir	Mo	Ru		
Ni	Na	Se		
Pb	Ta	Te		
Pd	V	Ti		
Pt	W	Tl		
Rh		Y		
Sc		Zn		
Th		Zr		
β-Tl				

The crystalline structure is not restricted to metallic bonding; ionic and covalent bonding are also common. Metallic-bonded crystals are very ductile because their valence electrons are not associated with specific pairs of ions.

32.3.5 Face-Centered Cubic

Most of the common metals (see Table 32.1) have face-centered cubic structures. Figure 32.7 shows the arrangement of the atoms, represented by spheres, in the face-centered cubic (FCC) structure as well as that fraction or portion of each atom associated with an individual unit cell. Each atom in the FCC structure has 12 contacting atoms. The number of contacting atoms (or nearest neighbors) is called the *coordination number.*

The FCC structure is referred to as a dense or closely packed structure. A quantitative measure of how efficiently the atoms are packed in a structure is the *atomic packing factor* (APF), which is the ratio of the volume of the atoms in a cell to the total volume of the unit cell. The APF for the FCC structure is 0.74. This means that 26 percent of the FCC unit cell is "void" space.

32.3.6 Body-Centered Cubic

Many of the stronger metals (Cr, Fe, Mo, W) have body-centered cubic (BCC) lattice structures, whereas the softer, more ductile metals (Ag, Al, Au, Cu, Ni) have the FCC structure (see Table 32.1). Figure 32.8 shows the arrangement of atoms in the BCC structure. There are two atoms per unit cell: one in the center (body center) and ⅛ in each of the eight corners. As can be seen in Fig. 32.8, each atom is contacted by eight other atoms, and so its coordination number is 8. The atomic packing factor for the BCC structure is 0.68, which is a little lower than that for the FCC structure.

The *Miller indices* are used to designate specific crystallographic planes with respect to the axes of the unit cell. They do not fix the position in terms of distance from the origin; thus, parallel planes have the same designation. The Miller indices are determined from the three intercepts that the plane makes with the three axes of the crystal. Actually it is the reciprocal of the distances between the intercepts with

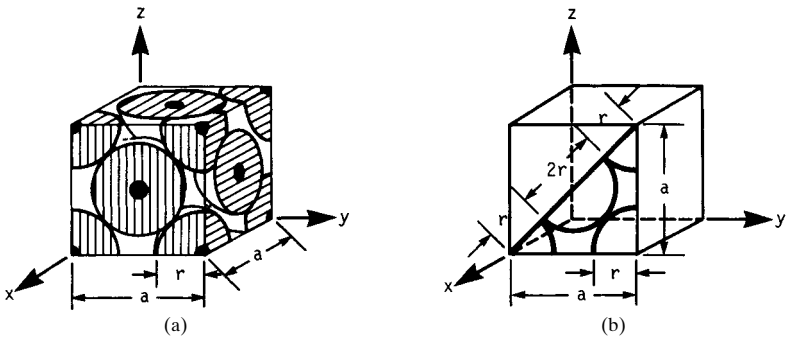

FIGURE 32.7 Unit cell of face-centered cubic structure. (*a*) The unit cell has 8 corners with ⅛ atom at each plus 6 faces with ½ atom, for a total of 4 atoms per unit cell; (*b*) one half of the front face showing the relationship between the lattice parameter *a* and the atomic radius *r.*

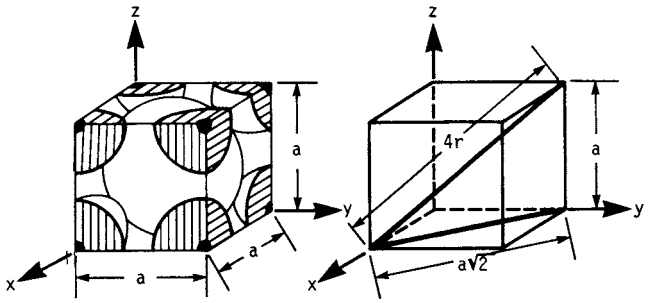

FIGURE 32.8 Unit cell of body-centered cubic structure. (*a*) The unit cell has ⅛ atom at each of 8 corners and 1 atom at the geometric center of the cell, for a total of 2 atoms; (*b*) the relationship of the lattice parameter *a* and atomic radius *r*.

the axis and the origin measured in terms of multiples or fractions of the unit cell lengths *a, b,* and *c* used in the determination. The final steps in specifying the Miller indices are to reduce the three reciprocals to the lowest integers having the same ratio and then to enclose them in parentheses. As is true with direction indices, the sequence of integers relates to the distances along the *x, y,* and *z* axes, respectively. The following examples should make this procedure clear.

Figure 32.9*a* identifies the front face of the crystal with the Miller indices (100). This notation is arrived at as follows: The front face intercepts the *x* axis at one *a* distance, and it does not intercept the *y* and *z* axes (or it intercepts at zero *b* and zero *c* units). If the side lengths are dropped, the intercepts are 1, 0, and 0. The reciprocals of these are also 1, 0, and 0. Since these are already the smallest integers, the Miller indices are specified by enclosing them in parentheses: (100). The commas are not included because they are simply part of the sentence structure.

Figure 32.9*b* shows the (110) plane that is parallel to the *z* axis and is a face diagonal on the top and bottom faces of the unit cell. This plane intercepts the *x* axis at one *a* distance, the *y* axis at one *b* distance, and the *z* axis at zero *c* distance. The intercepts are 1, 1, and 0, and so are the reciprocals. Since these are the smallest integers, the Miller indices are specified as (110).

Figure 32.9*d* shows the crystallographic plane that intercepts the *x* axis at ½*a,* the *y* axis at one *b,* and the *z* axis at one *c.* The reciprocals are therefore 2, 1, and 1, and so this plane is identified as the (211) plane.

Parentheses are used, as in the preceding examples, to specify a single plane or a family of parallel planes. Thus (100) represents all the planes that are parallel to the *yz* axes and intercept the lattice structure at one *a,* two *a,* three *a,* etc. distances. Wavy brackets, or braces, are used to designate all planes in a crystal that are equivalent. For example, the six face planes of a unit cell such as that in Fig. 32.9*a* are (100), (010), (001), $(\bar{1}00)$, $(0\bar{1}0)$, and $(00\bar{1})$. The notation {100} includes all these six planes.

32.4 CRYSTAL IMPERFECTIONS

The previous discussions on crystal structure assumed a perfect lattice; that is, an atom occupied each and every lattice point, and the distances between equivalent

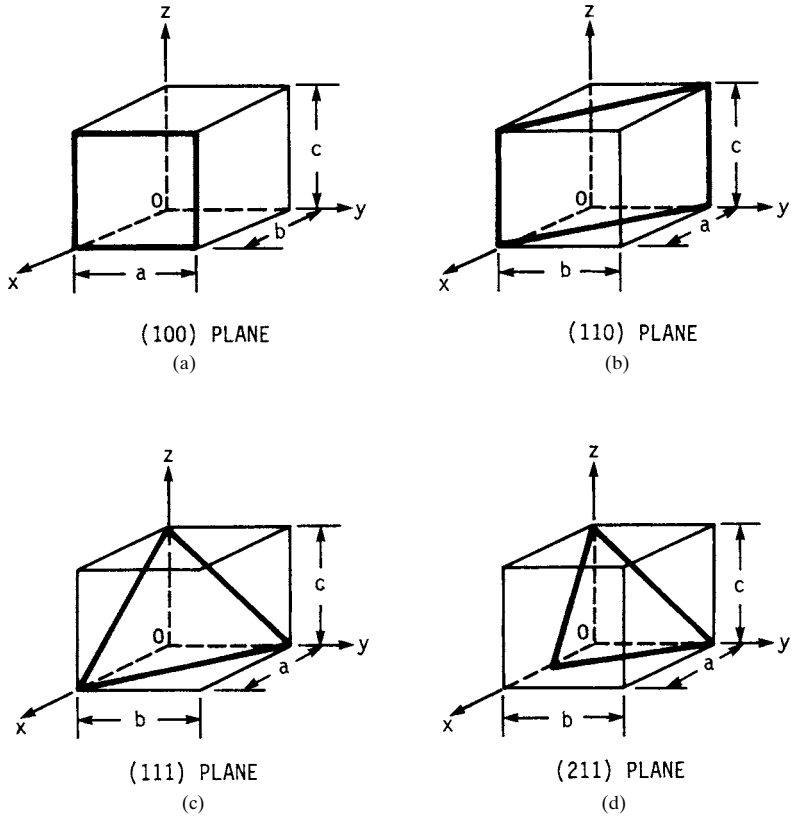

FIGURE 32.9 Miller indices for some crystallographic planes.

lattice points were all exactly the same. In the early 1900s it was found that real crystals did not have perfect properties. Notable among these properties was a mechanical strength much lower than crystals should have. As early as 1928 Prandtl suggested that slip (plastic deformation) in a crystal and the strength of a crystal are related to the presence of linear imperfections within the crystal. This type of imperfection is now called a *dislocation.* At the present time, the terms *imperfection* and *defect* refer to a deviation from a perfectly ordered lattice structure.

Lattice imperfections are classified into three types: *point defects,* where the imperfection is localized about a single lattice point and involves only a few atoms; *line defects,* where the imperfection lies along a line of finite length involving a row (line) or many atoms; and *planar defects* or *boundaries,* where the imperfections involve entire planes or atoms such as the interface between adjacent crystals.

32.4.1 Point Defects

Point defects are caused by (1) the absence of an atom from a lattice point, (2) the presence of an extra atom (usually a small foreign one) in the "void" spaces of the lattice,

SOLID MATERIALS

(3) the presence of a foreign atom at one of the lattice sites, or (4) atoms that are displaced from their normal positions in the array. Figure 32.10 illustrates these defects.

The first type of point defect, the absence of an atom from a lattice point, is called a *vacancy.* Figure 32.10*a* shows a vacancy on the (100) planes of an FCC lattice. The sketch was not made to be a true representation in order to make the defect more apparent. In reality, the atoms that are near neighbors to the vacant site would be displaced from their normal positions in the array toward centers closer to the vacancy. Thus the lattice lines joining the centers of the atoms are not straight in the vicinity of the vacancy. In three dimensions this means that the crystallographic planes are warped inward near a vacancy. Individual vacancies can cluster together to form larger voids. Vacancies have no effect on the metallurgical control of the mechanical properties discussed in later sections. However, they do affect properties such as conductivity and diffusivity.

The second type of point defect, the presence of an extra atom at the interstices of the lattice, is known as an *interstitial defect.* This type of defect in the lattice structure is the basis for the strengthening mechanism known as *interstitial alloying,* where the solute atom fits in the interstices of the solvent lattice, and it accounts for the high strength in fully hardened (heat-treated) steel. Commercially pure iron (ferrite with a BCC structure) has a yield strength of 70 to 140 MPa. However, with 0.8 percent carbon dissolved interstitially in the iron and stress relieved after heat treating, it has a yield strength of 2400 to 2800 MPa. No other metal has such high room-temperature strength, and no other strengthening mechanism has a greater effect than the interstitial alloying of carbon in iron. The details of these strengthening mechanisms are discussed later.

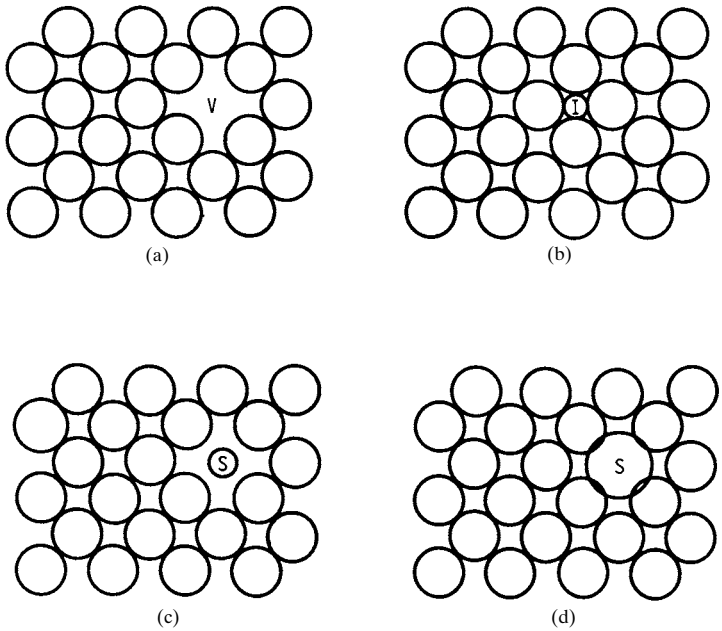

FIGURE 32.10 Some common point defects. (*a*) Vacancy; (*b*) interstitial atom I; (*c*) substitution of a smaller atom S; (*d*) substitution of a larger atom S.

Figure 32.10*b* shows an interstitial atom I in the solvent matrix. However, it does not lie in the plane of the solvent lattice but lies either above or below the sketched plane. Also, the foreign atom is always larger than the "void" space it occupies, and so it necessarily forces the surrounding solvent atoms out of their normal array. Therefore, the crystallographic planes are warped outward in the vicinity of an interstitial defect.

The third type of point defect, the presence of a foreign atom at one of the lattice points, is referred to as a *substitutional defect.* When an alloy is made by adding solute atoms that replace (substitute for) solvent atoms in the lattice structure, it is called a *substitutional alloy.* This type is the most common one in the metal system. Figure 32.10*c* and *d* shows the substitution of a smaller and a larger atom S at one of the lattice points. Unlike the interstitial atom, the substitutional one is in the plane of the solvent matrix. The crystallographic planes are also warped in the vicinity of the substitutional defect, inward for the smaller atom and outward for the larger atom. The distortion of the crystallographic planes is very important to an understanding of control of the strength of materials, which is presented later.

The fourth type of point defect, atoms that are displaced from their normal position, occurs in several forms. The atoms in the "contacting" planes of two adjoining crystals are not in their normal positions as a result of the crystals having solidified from the liquid without being in perfect registry with each other. This is considered to be a *grain boundary defect,* which has a significant effect on the strength of all polycrystalline materials.

Two additional types of atom displacement defects occur in ionic crystals that are not present in metallic-bonded crystals. A vacancy in an ionic crystal that is associated with a displaced pair, one cation and one anion, is called a *Schottky defect.* A *Frenkel defect* occurs when a small cation moves from a lattice point, leaving a vacancy, and occupies an interstitial site.

32.4.2 Line Defects or Dislocations

Examinations of crystals under the electron microscope have shown interruptions in the periodicity of the lattice structure in certain directions. In a two-dimensional representation these interruptions appear as lines; hence the name *line defects.* It is believed that a perfect crystal of a metal such as pure iron should have a strength of 1 or 2 million pounds force per square inch, whereas in reality such perfect crystals have a yield strength of only a few thousand. The reason given for the three orders of magnitude difference between the postulated and actual strength of metal crystals is the presence of these line defects.

The two most common line defects are edge dislocation and screw dislocation. An *edge dislocation* is the line defect that results from the presence of an extra plane of atoms in one portion of a crystal compared to the adjacent part. Actually, it is the edge of this extra plane of atoms and runs from one end of the crystal to the other. When looking at the crystalline plane that is perpendicular to the dislocation line, the imperfection appears as an extra row of atoms in a part of the crystal.

An edge dislocation is customarily represented by a symbol in which the vertical leg designates the extra plane of atoms. When the vertical leg is above the horizontal leg, the dislocation is considered positive. When the extra plane of atoms is in the bottom portion of the crystal, the vertical leg is placed below the horizontal one and the dislocation is said to be negative. The part of the crystal containing the extra plane of atoms is in compression, whereas that portion on the other side of the dislocation line is in tension. Since one dislocation line runs completely across a crystal, it deforms the lattice structure to a greater extent than does one point defect.

A *screw dislocation* is a crystal defect in which the lattice points lie on a spiral or helical surface that revolves around a center line that is called the *dislocation line.* A screw dislocation terminates at a crystal surface. Shear stresses are set up in the lattice surrounding a screw dislocation as a result of the distortion in atomic array that the defect causes.

The *Burgers vector* is the distance, measured in multiples of the lattice parameter, that is needed to close a straight-sided loop around a dislocation when going the same number of lattice distances in all four directions. It is the term used to define the size of a dislocation and is designated by the letter *b.* A characteristic of an edge dislocation is that it lies perpendicular to its Burgers vector, whereas a screw dislocation lies parallel to its Burgers vector.

32.4.3 Planar Defects

There are several types of planar (or surface) defects that occur from a change in the orientation of crystallographic planes across a surface boundary. The most important planar defect is the *grain boundary,* which is the imperfect plane surface that separates two crystals of different orientation in a polycrystalline solid. Grain boundaries originate when the last few remaining atoms of a liquid freeze onto the meeting faces of two adjacent crystals that have grown from the melt or, similarly, when two adjacent crystals that grow by recrystallization meet each other.

The material in the grain boundary is at a higher energy level than the material near the center of the grain because of the increased elastic strain energy of the atoms that are forced from their normal (lowest-energy) sites in a perfect lattice. This higher energy level and lattice distortion cause the grain boundary material to be stronger, have a higher diffusion rate, and serve as a more favorable site for the nucleation of second phases than the interior materials.

Another important planar defect is the *twin boundary,* which is the plane that separates two portions of a single crystal having slightly different orientations. The two twins are mirror images of each other. The distortion of the twinned lattice is low in comparison to that at a grain boundary. Twins which form in most FCC metal crystals, especially the copper- and nickel-base alloys, during freezing from the melt or recrystallization are called *annealing twins.* Twins which form in some metals during cold work (plastic deformation) are called *mechanical twins.*

A third planar defect is the *low-angle grain boundary* or *low-angle tilt boundary,* where the angular misalignment of the two grains is very small, on the order of a few degrees. In a sense it is a very undistorted grain boundary. The angular mismatch of the crystal planes is due to a row of dislocations piled above each other.

A *stacking fault* is a planar defect that occurs when one crystalline plane is stacked out of its normal sequence in the lattice array. The lattice on both sides of the defect is normal. For example, the normal FCC stacking of planes may be interrupted by one layer of a hexagonal close-packed (HCP) plane, since both are close-packed structures with atomic packing factors of 0.74. Such stacking faults can occur during the formation of a crystal or by plastic deformation.

32.5 SLIP IN CRYSTALLINE SOLIDS

Slip can be defined as the massive sliding movement of one large body of atoms with respect to the remaining body of atoms of the crystal along crystallographic planes. Slip can also be considered as an avalanche of dislocations along one plane that pile

up at grain boundaries or inclusions. The planes along which slip occurs are called *slip planes.* Slip occurs only with relatively high stresses, greater than the yield strength, and it causes plastic deformation.

When a crystalline solid or a single crystal is subjected to low loads, the atoms move slightly from their normal lattice sites and return to their proper positions when the load is removed. The displacements of the individual atoms are very small during elastic deformation. They are submicroscopic, a fraction of an atomic distance. Although there are some dislocation movements, they are few in number, involve very short distances, and are reversible.

Slip, however, is microscopic in size and causes plastic (permanent) deformation that is macroscopic. Figure 32.11 contains several two-dimensional lattice arrays which, in a simplified manner, illustrate the mechanism by means of which slip takes place. A typical perfect cubic lattice is shown in Fig. 32.11*a,* which is a small part of a single crystal. If sufficiently large shear stresses τ are placed on the crystal, all the atoms above the labeled slip plane move to the right simultaneously with respect to the atoms below the slip plane, as shown in Fig. 32.11*b.* The lattice is still a perfect cubic structure; only the outline or exterior shape of the single crystal has changed. It is believed, on the basis of the theories of elasticity, that the shear stress must be equal to the value of $G/2\pi$, where G is the shear modulus of elasticity. Young's modulus of elasticity E, Poisson's ratio ν, and G are related to one another by the equation

$$G = \frac{E}{2(1+\nu)} \tag{32.1}$$

For iron, E = 30 Mpsi and ν = 0.30, and so G = 11.5 Mpsi. Therefore, the so-called theoretical shear strength for slip to occur in iron is

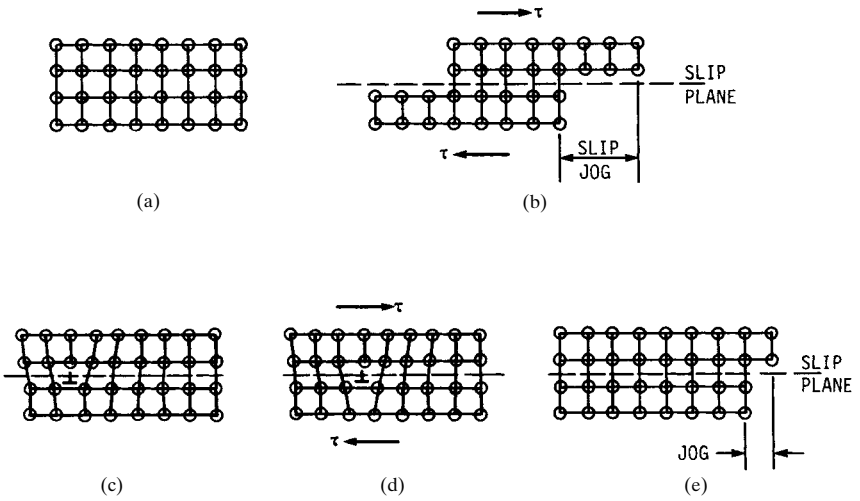

FIGURE 32.11 Two-dimensional sketch of the slip mechanism. (*a*) A perfect crystal; (*b*) idealized slip in a perfect crystal; (*c*) part of a crystal with one edge dislocation; (*d*) movement of dislocation subject to shear stress; (*e*) jog produced in the crystal face by dislocation motion.

$$\tau = \frac{G}{2\pi} = \frac{11.5}{2\pi} = 1.83 \text{ Mpsi}$$

However, slip occurs in iron crystals with shear stresses of only 4 to 5 kpsi, which is more than two orders of magnitude smaller. The "theoretical" shear strength of the other pure metals is also 400 to 500 times larger than the actual shear strength. The commonly accepted explanation of why the actual shear stress is so much lower than the theoretical value is that slip does not occur by the simultaneous movement of all the atoms along the slip plane; rather, it occurs by the movement of individual rows (the dislocation row or plane) of atoms. Thus it is the movement of dislocations along the slip plane to the grain boundary that causes the actual shear stress for plastic deformation to be so low. Figure 32.11*c, d,* and *e* illustrates the movement of a dislocation that results in slip.

In real crystals of metals, slip terminates at the grain boundaries or the free-surface faces and causes substantial jogs or steps, much larger than shown in Fig. 32.11. Experimental study of the spacings of the slip planes and the sizes of the jog have been made on some of the common metals. The spacing of the parallel planes along which slip occurs varies randomly, with an average distance between slip planes of about 2000 atom diameters. The length of the step or jog at the surface of the grain is approximately 200 to 700 atom diameters.

The atomic displacements associated with slip, unlike those of the initial movements of dislocations, are irreversible in that the slip jog remains when the shear stresses are removed. That is, slip causes a permanent change in shape, or *plastic deformation,* as it is called.

The evidence of slip is seen on metallurgically prepared samples as slip lines when examined under a microscope. The slip lines are the intersection of the crystallographic planes along which slip occurred with the etched surface of the specimen. Slip results in a narrow band on either side of the slip plane within which the lattice structure is severely distorted. These slip lines do not appear on the face of a specimen that is metallurgically polished after slip occurs; they appear only after etching with a suitable chemical reagent that dissolves the metal being studied. The slip lines become visible for the same reason that grain boundaries are visible after etching: The internal energy of the material within the distorted area is considerably higher than that of the material within the rest of the crystal. The metal in the higher energy level dissolves into the reagent much more rapidly than the rest of the crystal, leaving a narrow groove where the severely distorted band intersects the surface. Slip lines can also be seen on specimens that are polished prior to being plastically deformed and that have not been etched.

32.6 MECHANICAL STRENGTH

Although the specific mechanical properties of real materials are discussed in detail in the material that follows, it is very appropriate at this time to relate the concepts of the strengthening mechanisms to the previously described crystalline structures. Mechanical properties can best be studied on the basis of three precepts which encompass all the strengthening mechanisms. These three principles are stated here because they involve the distortion of the lattice structure that has just been discussed.

32.6.1 Principles of Mechanical Strength

Strength can be defined as a material's ability to resist slip. Thus it follows that the first principle of mechanical strength is this: *A material is strengthened when slip is made more difficult to initiate.* Therefore, to make a material stronger, it must be given a treatment that retards the avalanche of dislocations or, in other words, "pegs" the slip planes.

The second principle of mechanical strength is this: *Slip is retarded by inducing mechanical strains, or distortions, in the lattice structure of the material.* These distortions were discussed previously as lattice imperfections or defects. Thus it is a paradox that the source of strength in real polycrystalline materials is "crystal imperfections" or "crystal defects."

The third principle of mechanical strength is this: *There are four methods to induce mechanical strains or lattice distortions in a material, namely, decreasing the grain size, low-temperature plastic deformation (cold work), single-phase alloying, and multiple-phase alloying.*

32.6.2 Grain Size

Local distortion of the lattice structure at the grain boundaries induces substantial strain energy in those regions. This distortion impedes slip, or causes the dislocations to pile up, and consequently, the grain-boundary material is stronger than the material at the central portions of the crystal. This is true for most metals at room temperature. However, as additional energy is added to a polycrystalline material by raising the temperature, the grain-boundary material softens (and also melts) sooner or at a lower temperature than the bulk of the grain. At some temperature, called the *equicohesive temperature,* the strengths at these two regions are equal. Above the equicohesive temperature, the grain-boundary material is the weaker of the two. This explains why materials that are used at elevated temperatures have higher creep strengths when their grains are coarse rather than fine.

The surface-area-to-volume ratio of a sphere is inversely proportional to its diameter. Therefore, as the diameter of a sphere decreases, its ratio of surface area to volume increases. This means that for a given weight or volume of a polycrystalline solid, the total grain-boundary surface increases as the grain size decreases. Since the grain-boundary material is stronger than the interior material, the strength also varies inversely with the grain size. Also, since the surface area of a sphere is proportional to the square of its diameter, it can be assumed as a first approximation that the yield strength is proportional to the reciprocal of the square of the grain diameter.

Figure 32.12*a* shows how the 0.2 percent offset yield strength of 70Cu-30Zn brass varies with grain size. In this case, the yield strength increases by a factor of 4 with a grain diameter ratio of 24. The strengths of some materials, such as aluminum or steel, are not so greatly affected by grain size alone.

32.6.3 Cold Work

Cold work is a more significant strengthening mechanism than decreasing the grain size for most metals. When a crystalline material is plastically deformed, there is an avalanche of dislocations (called *slip*) that terminates at the grain boundaries. It is a mass movement of a body of atoms along a crystallographic plane. This movement in a polycrystalline material distorts both the grain boundaries and the crystalline planes in the grain so that slip occurs in the adjacent grains as well. Actually, a por-

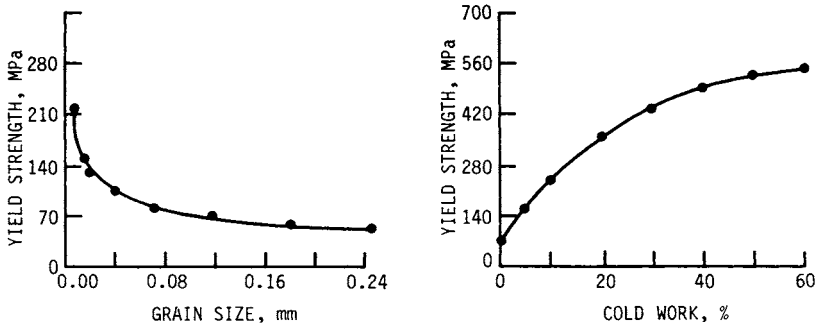

FIGURE 32.12 Yield strength versus grain size (*a*) and percent cold work (*b*) for 70Cu-30Zn brass.

tion of one grain intrudes into the space that was previously occupied by another grain, with a resulting distortion of the lattice in both grains.

Figure 32.12*b* illustrates the effect of cold work on the yield strength of 70Cu-30Zn brass. With only 10 percent cold work, the yield strength is raised by a factor of 3.5, and 60 percent cold work increases the strength nearly 8 times. In general, 10 percent cold work more than doubles the yield strength of most metals.

32.6.4 Single-Phase Alloying

Alloying (single- and multiple-phase) is the most important of the methods available to control or manipulate the mechanical properties of materials. The greatest increase in strength known today occurs when iron having a yield strength of 10 to 20 kpsi (70 to 140 MPa) is alloyed with less than 1.0 percent carbon to form a single phase (martensite) that has a yield strength of nearly 435 kpsi (3000 MPa).

The lattice is distorted and dislocation movement is impeded when foreign (solute) atoms are added to the lattice structure of a pure material. Figure 32.10*b* through *d* illustrates this condition, which was discussed previously under the heading "Point Defects." Vacancy defects, as shown in Fig. 32.10*a,* are not a practical strengthening method. The reason single-phase alloying has such a great effect on strength is that the entire lattice network is distorted, and uniformly, whereas in the other mechanism, there are regions in each crystal that are severely distorted and other regions that are hardly distorted at all.

Figure 32.13*a* shows the effect on the strength of the material of adding a foreign element B or C to the lattice structure of element A. From this figure it is clear that not all elements have the same strengthening effect. In general, the further the ratio of diameters of solute to solvent atoms is from unity, the greater will be the strengthening effect. However, the further this ratio is from unity, as previously explained, the less soluble the two atoms are in each other's lattice.

32.6.5 Multiple-Phase Alloying

This mechanism is sometimes referred to as *fine-particle strengthening.* In a sense, multiple-phase alloying is a combination of single-phase alloying and grain-boundary

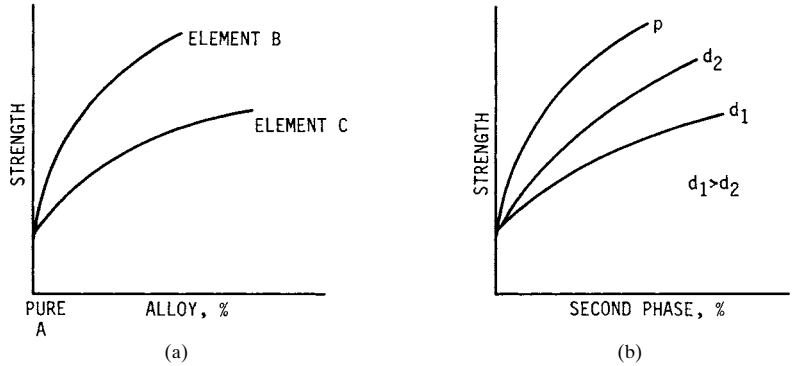

FIGURE 32.13 The effect of alloying on strength. (*a*) Single-phase alloying; atomic diameter ratio $B/A > C/A$; (*b*) multiple-phase alloying; *p* is a nonspherical-shaped particle, and *d* is the spherical particle diameter.

strengthening. That is, some of the added element goes into solution in the solvent lattice and thus has a strengthening effect; the remainder of the added element forms a second phase (either another solid solution or a compound) that is present as small grains or crystals.

Multiple-phase alloys can be made in three different ways. One method is by *annealing.* In this case, the alloy is heated to a one-phase region where the second element is completely soluble in the first. On slow cooling, the second phase precipitates as a massive network in the grain-boundary regions of the solvent matrix. This is the least beneficial form of alloying. The second method is similar except that the alloy is rapidly cooled from the high one-phase region so that a supersaturated solid phase occurs at room temperature. This material is then reheated to a relatively low temperature so that the second phase precipitates throughout the entire crystal as extremely fine particles rather than concentrating at the grain boundaries. This is the common *precipitation-hardening procedure.* The third method is to add a compound, in the form of small particles, that is insoluble in the parent material. Thus the two phases must be mixed in powder form and then sintered. This method is called *dispersion hardening.* At the present time there are only about a half dozen dispersion-hardenable alloys in commercial use. The most notable ones are Al_2O_3 particles in aluminum (called SAP, for sintered aluminum powder) and ThO in nickel.

32.7 MECHANICAL PROPERTIES AND TESTS

Most mechanical properties are structure-sensitive; that is, they are affected by changes in either the lattice structure or the microstructure. However, modulus of elasticity is one property that is structure-insensitive. For example, ductility and toughness of any material (regardless of whether it is a pure element such as copper, a simple alloy such as AISI 1080 steel, or a complex alloy such as a cobalt-base superalloy) vary with grain size, amount of cold work if any, or the microstructure if heat-treated. The modulus of elasticity of any material is the same regardless of grain size, amount of cold work, or microstructure.

Mechanical properties are discussed individually in the sections that follow. Several new quantitative relationships for the properties are presented here which make it possible to understand the mechanical properties to a depth that is not possible by means of the conventional tabular listings, where the properties of each material are listed separately.

32.8 HARDNESS

Hardness is used more frequently than any other of the mechanical properties by the design engineer to specify the final condition of a structural part. This is due in part to the fact that hardness tests are the least expensive in time and money to conduct. The test can be performed on a finished part without the need to machine a special test specimen. In other words, a hardness test may be a nondestructive test in that it can be performed on the actual part without affecting its service function.

Hardness is frequently defined as a measure of the ability of a material to resist plastic deformation or penetration by an indenter having a spherical or conical end. At the present time, hardness is more a technological property of a material than it is a scientific or engineering property. In a sense, hardness tests are practical shop tests rather than basic scientific tests. All the hardness scales in use today give relative values rather than absolute ones. Even though some hardness scales, such as the Brinell, have units of stress (kg/mm^2) associated with them, they are not absolute scales because a given piece of material (such as a 2-in cube of brass) will have significantly different Brinell hardness numbers depending on whether a 500-kg or a 3000-kg load is applied to the indenter.

32.8.1 Rockwell Hardness

The *Rockwell hardnesses* are hardness numbers obtained by an indentation type of test based on the depth of the indentation due to an increment of load. The Rockwell scales are by far the most frequently used hardness scales in industry even though they are completely relative. The reasons for their large acceptance are the simplicity of the testing apparatus, the short time necessary to obtain a reading, and the ease with which reproducible readings can be obtained, the last of these being due in part to the fact that the testing machine has a "direct-reading" dial; that is, a needle points directly to the actual hardness value without the need for referring to a conversion table or chart, as is true with the Brinell, Vickers, or Knoop hardnesses. Table 32.2 lists the most common Rockwell hardness scales.

TABLE 32.2 Rockwell Hardness Scales

	Scale								
	A	B	C	D	E	F	G	H	K
Indenter	1	2	1	1	3	2	2	3	3
Load, kg	60	100	150	100	100	60	150	60	150

Indenter 1 is a diamond cone having an included angle of 120° and a spherical end radius of 0.008 in. Indenters 2 and 3 are 1/16-in-diameter and 1/8-in-diameter balls, respectively. In addition to the preceding scales, there are several others for testing very soft bearing materials, such as babbit, that use 1/4-in-diameter and 1/2-in-diameter balls. Also, there are several "superficial" scales that use a special diamond cone with loads less than 50 kg to test the hardness of surface-hardened layers.

The particular materials that each scale is used on are as follows: the A scale on the extremely hard materials, such as carbides or thin case-hardened layers on steel; the B scale on soft steels, copper and aluminum alloys, and soft-case irons; the C scale on medium and hard steels, hard-case irons, and all hard nonferrous alloys; the E and F scales on soft copper and aluminum alloys. The remaining scales are used on even softer alloys.

Several precautions must be observed in the proper use of the Rockwell scales. The ball indenter should not be used on any material having a hardness greater than 50 R_C; otherwise the steel ball will be plastically deformed or flattened and thus give erroneous readings. Readings taken on the sides of cylinders or spheres should be corrected for the curvature of the surface. Readings on the C scale of less than 20 should not be recorded or specified because they are unreliable and subject to much variation.

The hardness numbers for all the Rockwell scales are an inverse measure of the depth of the indentation. Each division on the dial gauge of the Rockwell machine corresponds to an 80×10^6 in depth of penetration. The penetration with the C scale varies between 0.0005 in for hard steel and 0.0015 in for very soft steel when only the minor load is applied. The total depth of penetration with both the major and minor loads applied varies from 0.003 in for the hardest steel to 0.008 in for soft steel (20 R_C). Since these indentations are relatively shallow, the Rockwell C hardness test is considered a nondestructive test and it can be used on fairly thin parts.

Although negative hardness readings can be obtained on the Rockwell scales (akin to negative Fahrenheit temperature readings), they are usually not recorded as such, but rather a different scale is used that gives readings greater than zero. The only exception to this is when one wants to show a continuous trend in the change in hardness of a material due to some treatment. A good example of this is the case of the effect of cold work on the hardness of a fully annealed brass. Here the annealed hardness may be –20 R_B and increase to 95 R_B with severe cold work.

32.8.2 Brinell Hardness

The *Brinell hardness* H_B is the hardness number obtained by dividing the load that is applied to a spherical indenter by the surface area of the spherical indentation produced; it has units of kilograms per square millimeter. Most readings are taken with a 10-mm ball of either hardened steel or tungsten carbide. The loads that are applied vary from 500 kg for soft materials to 3000 kg for hard materials. The steel ball should not be used on materials having a hardness greater than about 525 H_B (52 R_C) because of the possibility of putting a flat spot on the ball and making it inaccurate for further use.

The Brinell hardness machine is as simple as, though more massive than, the Rockwell hardness machine, but the standard model is not direct-reading and takes a longer time to obtain a reading than the Rockwell machine. In addition, the indentation is much larger than that produced by the Rockwell machine, and the machine cannot be used on hard steel. The method of operation, however, is simple. The prescribed load is applied to the 10-mm-diameter ball for approximately 10 s. The part

is then withdrawn from the machine and the operator measures the diameter of the indentation by means of a millimeter scale etched on the eyepiece of a special Brinell microscope. The Brinell hardness number is then obtained from the equation

$$H_B = \frac{L}{(\pi D/2)[D - (D^2 - d^2)^{1/2}]} \tag{32.2}$$

where L = load, kg
D = diameter of indenter, mm
d = diameter of indentation, mm

The denominator in this equation is the spherical area of the indentation.

The Brinell hardness test has proved to be very successful, partly due to the fact that for some materials it can be directly correlated to the tensile strength. For example, the tensile strengths of all the steels, if stress-relieved, are very close to being 0.5 times the Brinell hardness number when expressed in kilopounds per square inch (kpsi). This is true for both annealed and heat-treated steel. Even though the Brinell hardness test is a technological one, it can be used with considerable success in engineering research on the mechanical properties of materials and is a much better test for this purpose than the Rockwell test.

The Brinell hardness number of a given material increases as the applied load is increased, the increase being somewhat proportional to the strain-hardening rate of the material. This is due to the fact that the material beneath the indentation is plastically deformed, and the greater the penetration, the greater is the amount of cold work, with a resulting high hardness. For example, the cobalt base alloy HS-25 has a hardness of 150 H_B with a 500-kg load and a hardness of 201 H_B with an applied load of 3000 kg.

32.8.3 Meyer Hardness

The *Meyer hardness* H_M is the hardness number obtained by dividing the load applied to a spherical indenter by the projected area of the indentation. The Meyer hardness test itself is identical to the Brinell test and is usually performed on a Brinell hardness-testing machine. The difference between these two hardness scales is simply the area that is divided into the applied load—the projected area being used for the Meyer hardness and the spherical surface area for the Brinell hardness. Both are based on the diameter of the indentation. The units of the Meyer hardness are also kilograms per square millimeter, and hardness is calculated from the equation

$$H_M = \frac{4L}{\pi d^2} \tag{32.3}$$

Because the Meyer hardness is determined from the projected area rather than the contact area, it is a more valid concept of stress and therefore is considered a more basic or scientific hardness scale. Although this is true, it has been used very little since it was first proposed in 1908, and then only in research studies. Its lack of acceptance is probably due to the fact that it does not directly relate to the tensile strength the way the Brinell hardness does.

Meyer is much better known for the original strain-hardening equation that bears his name than he is for the hardness scale that bears his name. The strain-hardening equation for a given diameter of ball is

$$L = Ad^p \tag{32.4}$$

where L = load on spherical indenter
d = diameter of indentation
p = Meyer strain-hardening exponent

The values of the strain-hardening exponent for a variety of materials are available in many handbooks. They vary from a minimum value of 2.0 for low-work-hardening materials, such as the PH stainless steels and all cold-rolled metals, to a maximum of about 2.6 for dead soft brass. The value of p is about 2.25 for both annealed pure aluminum and annealed 1020 steel.

Experimental data for some metals show that the exponent p in Eq. (32.4) is related to the strain-strengthening exponent m in the tensile stress-strain equation $\sigma = \sigma_0 \varepsilon^m$, which is to be presented later. The relation is

$$p - 2 = m \tag{32.5}$$

In the case of 70-30 brass, which had an experimentally determined value of $p = 2.53$, a separately run tensile test gave a value of $m = 0.53$. However, such good agreement does not always occur, partly because of the difficulty of accurately measuring the diameter d. Nevertheless, this approximate relationship between the strain-hardening and the strain-strengthening exponents can be very useful in the practical evaluation of the mechanical properties of a material.

32.8.4 Vickers or Diamond-Pyramid Hardness

The *diamond-pyramid hardness* H_p, or the *Vickers hardness* H_V, as it is frequently called, is the hardness number obtained by dividing the load applied to a square-based pyramid indenter by the surface area of the indentation. It is similar to the Brinell hardness test except for the indenter used. The indenter is made of industrial diamond, and the area of the two pairs of opposite faces is accurately ground to an included angle of 136°. The load applied varies from as low as 100 g for microhardness readings to as high as 120 kg for the standard macrohardness readings. The indentation at the surface of the workpiece is square-shaped. The diamond pyramid hardness number is determined by measuring the length of the two diagonals of the indentation and using the average value in the equation

$$H_p = \frac{2L \sin(\alpha/2)}{d^2} = \frac{1.8544L}{d^2} \tag{32.6}$$

where L = applied load, kg
d = diagonal of the indentation, mm
α = face angle of the pyramid, 136°

The main advantage of a cone or pyramid indenter is that it produces indentations that are geometrically similar regardless of depth. In order to be geometrically similar, the angle subtended by the indentation must be constant regardless of the depth of the indentation. This is not true of a ball indenter. It is believed that if geometrically similar deformations are produced, the material being tested is stressed to the same amount regardless of the depth of the penetration. On this basis, it would be expected that conical or pyramidal indenters would give the same hardness num-

ber regardless of the load applied. Experimental data show that the pyramid hardness number is independent of the load if loads greater than 3 kg are applied. However, for loads less than 3 kg, the hardness is affected by the load, depending on the strain-hardening exponent of the material being tested.

32.8.5 Knoop Hardness

The *Knoop hardness* H_K is the hardness number obtained by dividing the load applied to a special rhombic-based pyramid indenter by the projected area of the indentation. The indenter is made of industrial diamond, and the four pyramid faces are ground so that one of the angles between the intersections of the four faces is 172.5° and the other angle is 130°. A pyramid of this shape makes an indentation that has the projected shape of a parallelogram having a long diagonal that is 7 times as large as the short diagonal and 30 times as large as the maximum depth of the indentation.

The greatest application of Knoop hardness is in the microhardness area. As such, the indenter is mounted on an axis parallel to the barrel of a microscope having magnifications of 100× to 500×. A metallurgically polished flat specimen is used. The place at which the hardness is to be determined is located and positioned under the hairlines of the microscope eyepiece. The specimen is then positioned under the indenter and the load is applied for 10 to 20 s. The specimen is then located under the microscope again and the length of the long diagonal is measured. The Knoop hardness number is then determined by means of the equation

$$H_K = \frac{L}{0.070\,28d^2} \tag{32.7}$$

where L = applied load, kg
d = length of long diagonal, mm

The indenter constant 0.070 28 corresponds to the standard angles mentioned above.

32.8.6 Scleroscope Hardness

The *scleroscope hardness* is the hardness number obtained from the height to which a special indenter bounces. The indenter has a rounded end and falls freely a distance of 10 in in a glass tube. The rebound height is measured by visually observing the maximum height the indenter reaches. The measuring scale is divided into 140 equal divisions and numbered beginning with zero. The scale was selected so that the rebound height from a fully hardened high-carbon steel gives a maximum reading of 100.

All the previously described hardness scales are called *static hardnesses* because the load is slowly applied and maintained for several seconds. The scleroscope hardness, however, is a *dynamic hardness.* As such, it is greatly influenced by the elastic modulus of the material being tested.

32.9 THE TENSILE TEST

The tensile test is conducted on a machine that can apply uniaxial tensile or compressive loads to the test specimen, and the machine also has provisions for accu-

rately registering the value of the load and the amount of deformation that occurs to the specimen. The tensile specimen may be a round cylinder or a flat strip with a reduced cross section, called the *gauge section,* at its midlength to ensure that the fracture does not occur at the holding grips. The minimum length of the reduced section for a standard specimen is four times its diameter. The most commonly used specimen has a 0.505-in-diameter gauge section (0.2-in^2 cross-sectional area) that is 2¼ in long to accommodate a 2-in-long gauge section. The overall length of the specimen is 5½ in, with a 1-in length of size ¾-10NC screw threads on each end. The ASTM specifications list several other standard sizes, including flat specimens.

In addition to the tensile properties of strength, rigidity, and ductility, the tensile test also gives information regarding the stress-strain behavior of the material. It is very important to distinguish between *strength* and *stress* as they relate to material properties and mechanical design, but it is also somewhat awkward, since they have the same units and many books use the same symbol for both.

Strength is a property of a material—it is a measure of the ability of a material to withstand stress or it is the load-carrying capacity of a material. The numerical value of strength is determined by dividing the appropriate load (yield, maximum, fracture, shear, cyclic, creep, etc.) by the original cross-sectional area of the specimen and is designated as *S.* Thus

$$S = \frac{L}{A_0} \tag{32.8}$$

The subscripts *y, u, f,* and *s* are appended to *S* to denote yield, ultimate, fracture, and shear strength, respectively. Although the strength values obtained from a tensile test have the units of stress [psi (Pa) or equivalent], they are not really values of stress.

Stress is a condition of a material due to an applied load. If there are no loads on a part, then there are no stresses in it. (Residual stresses may be considered as being caused by unseen loads.) The numerical value of the stress is determined by dividing the actual load or force on the part by the actual cross section that is supporting the load. Normal stresses are almost universally designated by the symbol σ, and the stresses due to tensile loads are determined from the expression

$$\sigma = \frac{L}{A_i} \tag{32.9}$$

where A_i = instantaneous cross-sectional area corresponding to that particular load. The units of stress are pounds per square inch (pascals) or an equivalent.

During a tensile test, the stress varies from zero at the very beginning to a maximum value that is equal to the true fracture stress, with an infinite number of stresses in between. However, the tensile test gives only three values of strength: yield, ultimate, and fracture. An appreciation of the real differences between strength and stress will be achieved after reading the material that follows on the use of tensile-test data.

32.9.1 Engineering Stress-Strain

Traditionally, the tensile test has been used to determine the so-called engineering stress-strain data that are needed to plot the engineering stress-strain curve for a given material. However, since engineering stress is not really a stress but is a mea-

sure of the strength of a material, it is more appropriate to call such data either *strength–nominal strain* or *nominal stress–strain data.* Table 32.3 illustrates the data that are normally collected during a tensile test, and Fig. 32.14 shows the condition of a standard tensile specimen at the time the specific data in the table are recorded. The load-versus-gauge-length data, or an elastic stress-strain curve drawn by the machine, are needed to determine Young's modulus of elasticity of the material as well as the proportional limit. They are also needed to determine the yield strength if the offset method is used. All the definitions associated with engineering stress-strain, or, more appropriately, with the strength–nominal strain properties, are presented in the section which follows and are discussed in conjunction with the experimental data for commercially pure titanium listed in Table 32.3 and Fig. 32.14.

The elastic and elastic-plastic data listed in Table 32.3 are plotted in Fig. 32.15 with an expanded strain axis, which is necessary for the determination of the yield strength. The nominal (approximate) stress or the strength S which is calculated by means of Eq. (32.8) is plotted as the ordinate.

The abscissa of the engineering stress-strain plot is the *nominal strain,* which is defined as the unit elongation obtained when the change in length is divided by the original length and has the units of inch per inch and is designated as n. Thus, for tension,

$$n = \frac{\Delta \ell}{\ell} = \frac{\ell_f - \ell_0}{\ell_0} \tag{32.10}$$

where ℓ = gauge length and the subscripts 0 and f designate the original and final state, respectively. This equation is valid for deformation strains that do not exceed the strain at the maximum load of a tensile specimen.

It is customary to plot the data obtained from a tensile test as a stress-strain curve such as that illustrated in Fig. 32.16, but without including the word *nominal.* The reader then considers such a curve as an actual stress-strain curve, which it obviously is not. The curve plotted in Fig. 32.16 is in reality a load-deformation curve. If the ordinate axis were labeled load (lb) rather than stress (psi), the distinction between

TABLE 32.3 Tensile Test Data.

Material: A40 titanium; condition: annealed; specimen size: 0.505-in diameter by 2-in gauge length; $A_0 = 0.200$ in^2

Yield load	9 040 lb	Yield strength	45.2 kpsi
Maximum load	14 950 lb	Tensile strength	74.75 kpsi
Fracture load	11 500 lb	Fracture strength	57.5 kpsi
Final length	2.480 in	Elongation	24%
Final diameter	0.352 in	Reduction of area	51.15%

Load, lb	Gauge length, in	Load, lb	Gauge length, in
1 000	2.0006	6 000	2.0044
2 000	2.0012	7 000	2.0057
3 000	2.0018	8 000	2.0070
4 000	2.0024	9 000	2.0094
5 000	2.0035	10 000	2.0140

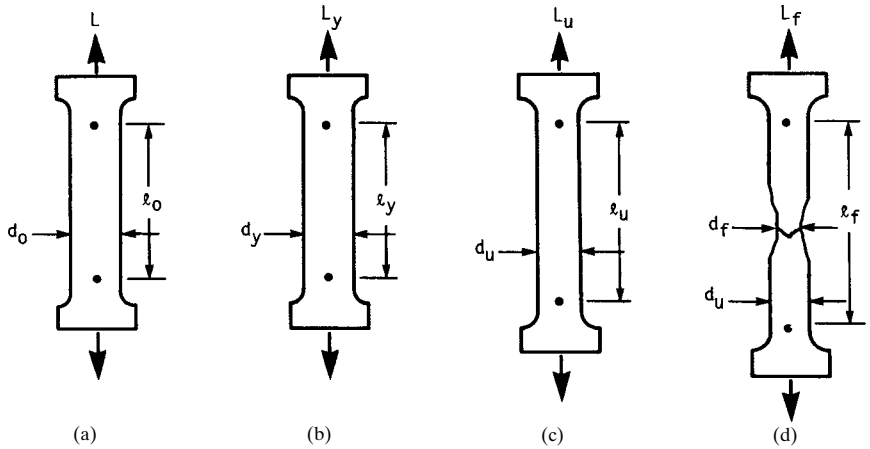

FIGURE 32.14 A standard tensile specimen of A40 titanium at various stages of loading. (*a*) Unloaded, $L = 0$ lb, $d_0 = 0.505$ in, $\ell_0 = 2.000$ in, $A_0 = 0.200$ in^2; (*b*) yield load $L_y = 9040$ lb, $d_y = 0.504$ in, $\ell_y = 2.009$ in, $A_y = 0.1995$ in^2; (*c*) maximum load $L_u = 14\,950$ lb, $d_u = 0.470$ in, $\ell_u = 2.310$ in, $A_u = 0.173$ in^2; (*d*) fracture load $L_f = 11\,500$ lb, $d_f = 0.352$ in, $\ell_f = 2.480$ in, $A_f = 0.097$ in^2, $d_u = 0.470$ in.

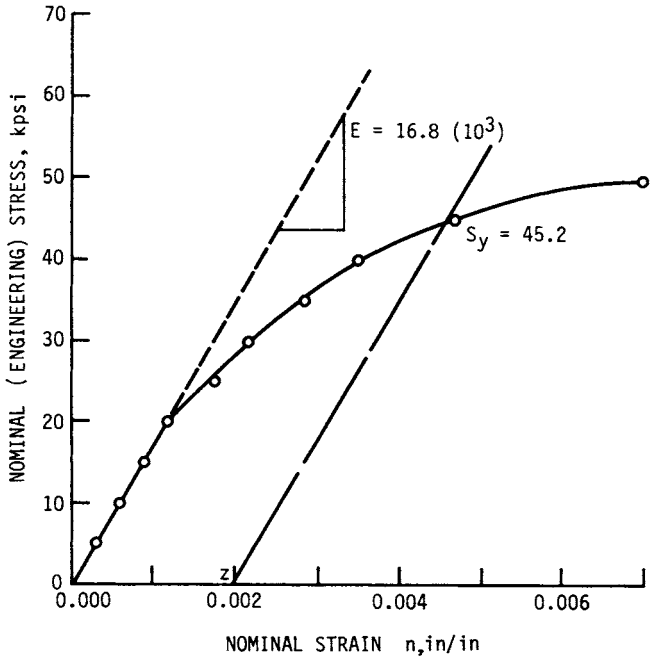

FIGURE 32.15 The elastic-plastic portion of the engineering stress-strain curve for annealed A40 titanium.

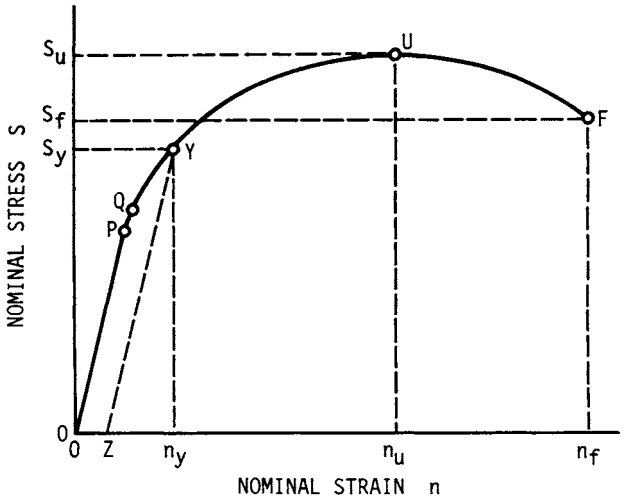

FIGURE 32.16 The engineering stress-strain curve. P = proportional limit, Q = elastic limit, Y = yield load, U = ultimate (maximum) load, and F = fracture load.

strength and stress would be easier to make. Although the fracture load is lower than the ultimate load, the stress in the material just prior to fracture is much greater than the stress at the time the ultimate load is on the specimen.

32.9.2 True Stress-Strain

The tensile test is also used to obtain true stress-strain or true stress–natural strain data to define the plastic stress-strain characteristics of a material. In this case it is necessary to record simultaneously the cross-sectional area of the specimen and the load on it. For round sections it is sufficient to measure the diameter for each load recorded. The load-deformation data in the plastic region of the tensile test of an annealed titanium are listed in Table 32.4. These data are a continuation of the tensile test in which the elastic data are given in Table 32.3.

The load-diameter data in Table 32.4 are recorded during the test and the remainder of the table is completed afterwards. The values of stress are calculated by means of Eq. (32.9). The strain in this case is the *natural strain* or *logarithmic strain,* which is the sum of all the infinitesimal nominal strains, that is,

$$\varepsilon = \frac{\Delta\ell_1}{\ell_0} + \frac{\Delta\ell_2}{\ell_0 + \Delta\ell_1} + \frac{\Delta\ell_3}{\ell_0 + \Delta\ell_1 + \Delta\ell_2} + \cdots$$

$$= \ln \frac{\ell_f}{\ell_0} \tag{32.11}$$

The volume of material remains constant during plastic deformation. That is,

$$V_0 = V_f \qquad \text{or} \qquad A_0\ell_0 = A_f\ell_f$$

TABLE 32.4 Tensile Test Data†

Load, lb	Diameter, in	Area, in^2	Area ratio	Stress, kpsi	Strain, in/in
12 000	0.501	0.197	1.015	60.9	0.0149
14 000	0.493	0.191	1.048	73.5	0.0473
14 500	0.486	0.186	1.075	78.0	0.0724
14 950	0.470	0.173	1.155	86.5	0.144
14 500	0.442	0.153	1.308	94.8	0.268
14 000	0.425	0.142	1.410	99.4	0.344
11 500	0.352	0.097	2.06	119.0	0.729

†This table is a continuation of Table 32.3.

Thus, for tensile deformation, Eq. (32.11) can be expressed as

$$\varepsilon = \ln \frac{A_0}{A_f} \tag{32.12}$$

Quite frequently, in calculating the strength or the ductility of a cold-worked material, it is necessary to determine the value of the strain ε that is equivalent to the amount of the cold work. The *amount of cold work* is defined as the percent reduction of cross-sectional area (or simply the percent reduction of area) that is given the material by a plastic-deformation process. It is designated by the symbol W and is determined from the expression

$$W = \frac{A_0 - A_f}{A_0} (100) \tag{32.13}$$

where the subscripts 0 and f refer to the original and the final area, respectively. By solving for the A_0/A_f ratio and substituting into Eq. (32.12), the appropriate relationship between strain and cold work is found to be

$$\varepsilon_W = \ln \frac{100}{100 - W} \tag{32.14}$$

The stress-strain data of Table 32.4 are plotted in Fig. 32.17 on cartesian coordinates. The most significant difference between the shape of this stress-strain curve and that of the load-deformation curve in Fig. 32.16 is the fact that the stress continues to rise until fracture occurs and does not reach a maximum value as the load-deformation curve does. As can be seen in Table 32.4 and Fig. 32.17, the stress at the time of the maximum load is 86 kpsi, and it increases to 119 kpsi at the instant that fracture occurs. A smooth curve can be drawn through the experimental data, but it is not a straight line, and consequently many experimental points are necessary to accurately determine the shape and position of the curve.

The stress-strain data obtained from the tensile test of the annealed A40 titanium listed in Tables 32.3 and 32.4 are plotted on logarithmic coordinates in Fig. 32.18. The elastic portion of the stress-strain curve is also a straight line on logarithmic coordinates as it is on cartesian coordinates. When plotted on cartesian coordinates, the slope of the elastic modulus is different for the different materials. However, when

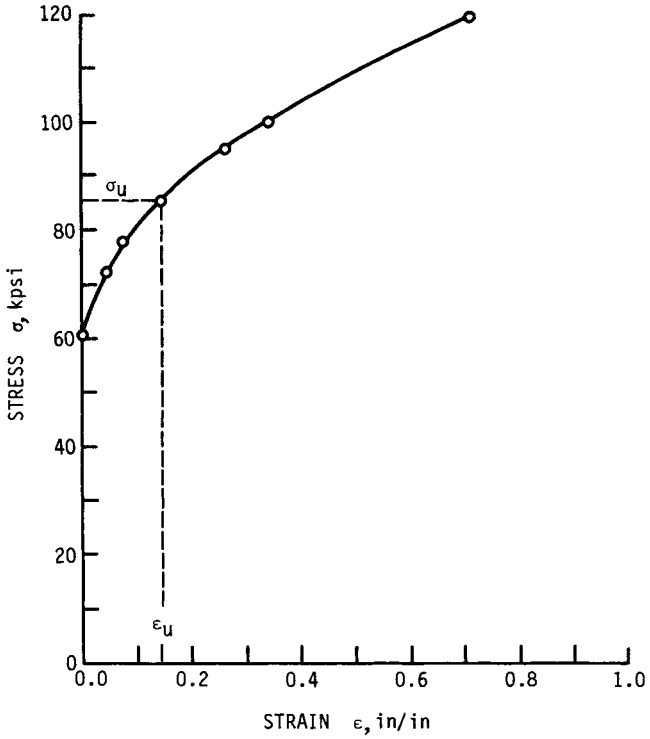

FIGURE 32.17 Stress-strain curve for annealed A40 titanium. The strain is the natural or logarithmic strain and the data of Tables 32.3 and 32.4 are plotted on cartesian coordinates.

plotted on logarithmic coordinates, the slope of the elastic modulus is 1 (unity) for all materials—it is only the height, or position, of the line that is different for different materials. In other words, the elastic moduli for all the materials are parallel lines making an angle of 45° with the ordinate axis.

The experimental points in Fig. 32.18 for strains greater than 0.01 (1 percent plastic deformation) also fall on a straight line having a slope of 0.14. The slope of the stress-strain curve in logarithmic coordinates is called the *strain-strengthening exponent* because it indicates the increase in strength that results from plastic strain. It is sometimes referred to as the *strain-hardening exponent,* which is somewhat misleading because the real strain-hardening exponent is the Meyer exponent *p,* discussed previously under the subject of strain hardening. The strain-strengthening exponent is represented by the symbol *m.*

The equation for the plastic stress-strain line is

$$\sigma = \sigma_0 \varepsilon^m \tag{32.15}$$

and is known as the *strain-strengthening equation* because it is directly related to the yield strength. The proportionality constant σ_0 is called the *strength coefficient.* The strength coefficient σ_0 is related to the plastic behavior of a material in exactly

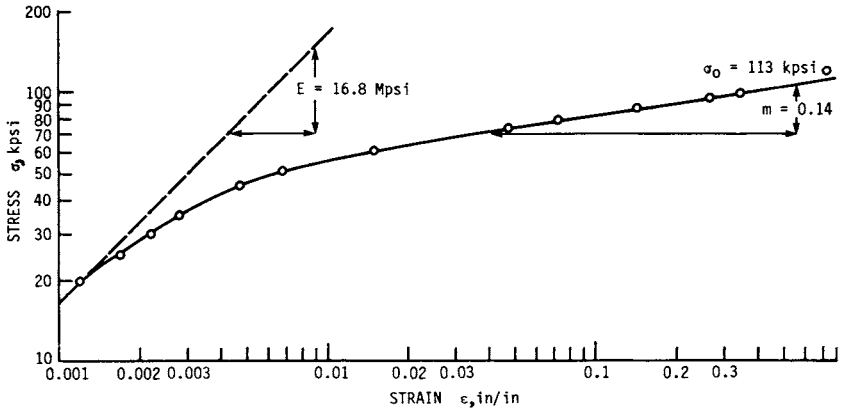

FIGURE 32.18 Stress-strain curve for annealed A40 titanium plotted on logarithmic coordinates. The data are the same as in Fig. 32.17.

the same manner in which Young's modulus E is related to elastic behavior. Young's modulus E is the value of stress associated with an elastic strain of unity; the strength coefficient σ_0 is the value of stress associated with a plastic strain of unity. The amount of cold work necessary to give a strain of unity is determined from Eq. (32.14) to be 63.3 percent.

For most materials there is an elastic-plastic region between the two straight lines of the fully elastic and fully plastic portions of the stress-strain curve. A material that has no elastic-plastic region may be considered an "ideal" material because the study and analysis of its tensile properties are simpler. Such a material has a complete stress-strain relationship that can be characterized by two intersecting straight lines, one for the elastic region and one for the plastic region. Such a material would have a stress-strain curve similar to the one labeled *I* in Fig. 32.19. A few real materials have a stress-strain curve that approximates the "ideal" curve. However, most engineering materials have a stress-strain curve that resembles curve *O* in Fig. 32.19. These materials appear to "overyield"; that is, they have a higher yield strength than the "ideal" value, followed by a region of low or no strain strengthening before the fully plastic region begins. Among the materials that have this type of curve are steel, stainless steel, copper, brass alloys, nickel alloys, and cobalt alloys.

Only a few materials have a stress-strain curve similar to that labeled *U* in Fig. 32.19. The characteristic feature of this type of material is that it appears to "underyield"; that is, it has a yield strength that is lower than the "ideal" value. Some of the fully annealed aluminum alloys have this type of curve.

32.10 TENSILE PROPERTIES

Tensile properties are those mechanical properties obtained from the tension test; they are used as the basis of mechanical design of structural components more frequently than any other of the mechanical properties. More tensile data are available for materials than any other type of material property data. Frequently the design engineer must base his or her calculations on the tensile properties even under

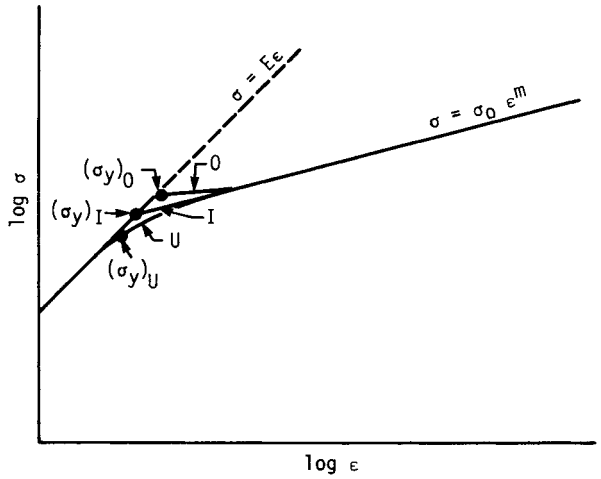

FIGURE 32.19 Schematic representation of three types of stress-strain curves. *I* is an "ideal" curve, and *O* and *U* are two types of real curve.

cyclic, shear, or impact loading simply because the more appropriate mechanical property data are not available for the material he or she may be considering for a specific part. All the tensile properties are defined in this section and are briefly discussed on the basis of the tensile test described in the preceding section.

32.10.1 Modulus of Elasticity

The *modulus of elasticity,* or *Young's modulus,* is the ratio of stress to the corresponding strain during elastic deformation. It is the slope of the straight-line (elastic) portion of the stress-strain curve when drawn on cartesian coordinates. It is also known, as indicated previously, as Young's modulus, or the proportionality constant in Hooke's law, and is commonly designated as E with units of pounds per square inch (pascals) or the equivalent. The modulus of elasticity of the titanium alloy whose tensile data are reported in Table 32.3 is shown in Fig. 32.15, where the first four experimental data points fall on a straight line having a slope of 16.8 Mpsi.

32.10.2 Proportional Limit

The *proportional limit* is the greatest stress which a material is capable of developing without any deviation from a linear proportionality of stress to strain. It is the point where a straight line drawn through the experimental data points in the elastic region first departs from the actual stress-strain curve. Point *P* in Fig. 32.16 is the proportional limit (20 kpsi) for this titanium alloy. The proportional limit is very seldom used in engineering specifications because it depends so much on the sensitivity and accuracy of the testing equipment and the person plotting the data.

32.10.3 Elastic Limit

The *elastic limit* is the greatest stress which a material is capable of withstanding without any permanent deformation after removal of the load. It is designated as point *Q* in Fig. 32.16. The elastic limit is also very seldom used in engineering specifications because of the complex testing procedure of many successive loadings and unloadings that is necessary for its determination.

32.10.4 Yield Strength

The *yield strength* is the nominal stress at which a material undergoes a specified permanent deformation. There are several methods to determine the yield strength, but the most reliable and consistent method is called the *offset method.* This approach requires that the nominal stress-strain diagram be first drawn on cartesian coordinates. A point *z* is placed along the strain axis at a specified distance from the origin, as shown in Figs. 32.15 and 32.16. A line parallel to the elastic modulus is drawn from *Z* until it intersects the nominal stress-strain curve. The value of stress corresponding to this intersection is called the *yield strength* by the offset method. The distance 0*Z* is called the *offset* and is expressed as percent. The most common offset is 0.2 percent, which corresponds to a nominal strain of 0.002 in/in. This is the value of offset used in Fig. 32.15 to determine the yield strength of the A40 titanium. An offset of 0.01 percent is sometimes used, and the corresponding nominal stress is called the *proof strength,* which is a value very close to the proportional limit. For some nonferrous materials an offset of 0.5 percent is used to determine the yield strength.

Inasmuch as all methods of determining the yield strength give somewhat different values for the same material, it is important to specify what method, or what offset, was used in conducting the test.

32.10.5 Tensile Strength

The *tensile strength* is the value of nominal stress obtained when the maximum (or ultimate) load that the tensile specimen supports is divided by the original cross-sectional area of the specimen. It is shown as S_u in Fig. 32.16 and is sometimes called the *ultimate strength.* The tensile strength is a commonly used property in engineering calculations even though the yield strength is a measure of when plastic deformation begins for a given material. The real significance of the tensile strength as a material property is that it indicates what maximum load a given part can carry in uniaxial tension without breaking. It determines the absolute maximum limit of load that a part can support.

32.10.6 Fracture Strength

The *fracture strength,* or *breaking strength,* is the value of nominal stress obtained when the load carried by a tensile specimen at the time of fracture is divided by its original cross-sectional area. The breaking strength is not used as a material property in mechanical design.

32.10.7 Reduction of Area

The *reduction of area* is the maximum change in area of a tensile specimen divided by the original area and is usually expressed as a percent. It is designated as A_r and is calculated as follows:

$$A_r = \frac{A_0 - A_f}{A_0} (100) \tag{32.16}$$

where the subscripts 0 and f refer to the original area and area after fracture, respectively. The percent reduction of area and the strain at ultimate load ε_u are the best measure of the ductility of a material.

32.10.8 Fracture Strain

The *fracture strain* is the true strain at fracture of the tensile specimen. It is represented by the symbol ε_f and is calculated from the definition of strain as given in Eq. (32.12). If the percent reduction of area A_r is known for a material, the fracture strain can be calculated from the expression

$$\varepsilon_f = \ln \frac{100}{100 - A_r} \tag{32.17}$$

32.10.9 Percentage Elongation

The *percentage elongation* is a crude measure of the ductility of a material and is obtained when the change in gauge length of a fractured tensile specimen is divided by the original gauge length and expressed as percent. Because of the ductility relationship, we express it here as

$$D_e = \frac{\ell_f - \ell_0}{\ell_0} (100) \tag{32.18}$$

Since most materials exhibit nonuniform deformation before fracture occurs on a tensile test, the percentage elongation is some kind of an average value and as such cannot be used in meaningful engineering calculations.

The percentage elongation is not really a material propety, but rather it is a combination of a material property and a test condition. A true material property is not significantly affected by the size of the specimen. Thus a ¼-in-diameter and a ½-in-diameter tensile specimen of the same material give the same values for yield strength, tensile strength, reduction of area or fracture strain, modulus of elasticity, strain-strengthening exponent, and strength coefficient, but a 1-in gauge-length specimen and a 2-in gauge-length specimen of the same material do not give the same percentage elongation. In fact, the percentage elongation for a 1-in gauge-length specimen may actually be 100 percent greater than that for the 2-in gauge-length specimen even when they are of the same diameter.

32.11 STRENGTH, STRESS, AND STRAIN RELATIONS

The following relationships between strength, stress, and strain are very helpful to a complete understanding of tensile properties and also to an understanding of their use in specifying the optimum material for a structural part. These relationships also help in solving manufacturing problems where difficulty is encountered in the fabrication of a given part because they enable one to have a better concept of what can be expected of a material during a manufacturing process. A further advantage of these relations is that they enable an engineer to more readily determine the mechanical properties of a fabricated part on the basis of the original properties of the material and the mechanisms involved with the particular process used.

32.11.1 Natural and Nominal Strain

The relationship between these two strains is determined from their definitions. The expression for the natural strain is $\varepsilon = \ln (\ell_f/\ell_0)$. The expression for the nominal strain can be rewritten as $\ell_f/\ell_0 = n + 1$. When the latter is substituted into the former, the relationship between the two strains can be expressed in the two forms

$$\varepsilon = \ln (n + 1) \qquad \exp (\varepsilon) = n + 1 \tag{32.19}$$

32.11.2 True and Nominal Stress

The definition of true stress is $\sigma = L/A_i$. From constancy of volume it is found that $A_i = A_0(\ell_0/\ell_i)$, so that

$$\sigma = \frac{L}{A_0}\left(\frac{\ell_i}{\ell_0}\right)$$

which is the same as

$$\sigma = \begin{cases} S(n + 1) \\ S \exp (\varepsilon) \end{cases} \tag{32.20}$$

32.11.3 Strain-Strengthening Exponent and Maximum-Load Strain

One of the more useful of the strength-stress-strain relationships is the one between the strain-strengthening exponent and the strain at maximum load. It is also the simplest, since the two are numerically equal; that is, $m = \varepsilon_u$. This relation is derived on the basis of the load-deformation curve shown in Fig. 32.20. The load at any point along this curve is equal to the product of the true stress on the specimen and the corresponding area. Thus

$$L = \sigma A$$

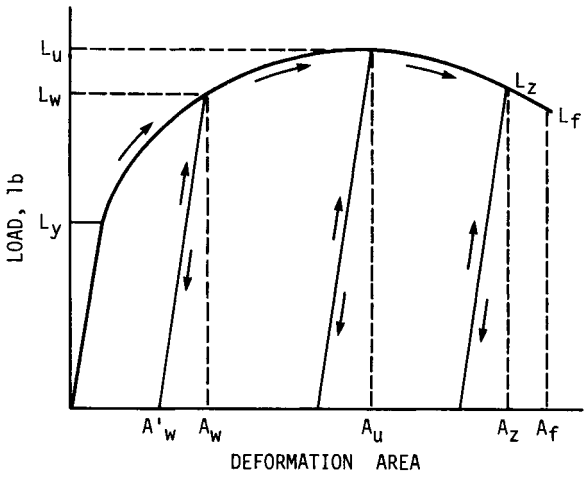

FIGURE 32.20 A typical load-deformation curve showing unloading and reloading cycles.

Now, since

$$\sigma = \sigma_0 \varepsilon^m$$

and

$$\varepsilon = \ln \frac{A_0}{A} \qquad \text{or} \qquad A = \frac{A_0}{\exp(\varepsilon)}$$

the load-strain relationship can be written as

$$L = \sigma_0 A_0 \varepsilon^m \exp(-\varepsilon)$$

The load-deformation curve shown in Fig. 32.20 has a maximum, or zero-slope, point on it. Differentiating the last equation and equating the result to zero gives the simple expression $\varepsilon = m$. Since this is the strain at the ultimate load, the expression can be written as

$$\varepsilon_u = m \tag{32.21}$$

32.11.4 Yield Strength and Percent Cold Work

The stress-strain characteristics of a material obtained from a tensile test are shown in Fig. 32.18. In the region of plastic deformation, the relationship between stress and strain for most materials can be approximated by the equation $\sigma = \sigma_0 \varepsilon^m$. When a load is applied to a tensile specimen that causes a given amount of cold work W (which is a plastic strain of ε_W), the stress on the specimen at the time is σ_W and is defined as

$$\sigma_W = \sigma_0(\varepsilon_W)^m \tag{32.22}$$

Of course, σ_W is also equal to the applied load L_W divided by the actual cross-sectional area of the specimen A_W.

If the preceding tensile specimen were immediately unloaded after reading L_W, the cross-sectional area would increase to A'_W from A_W because of the elastic recovery or springback that occurs when the load is removed. This elastic recovery is insignificant for engineering calculations with regard to the strength or stresses on a part.

If the tensile specimen that has been stretched to a cross-sectional area of A'_W is now reloaded, it will deform elastically until the load L_W is approached. As the load is increased above L_W, the specimen will again deform plastically. This unloading-reloading cycle is shown graphically in Fig. 32.20. The yield load for this previously cold-worked specimen before the reloading is A'_W. Therefore, the yield strength of the previously cold-worked (stretched) specimen is approximately

$$(S_y)_W = \frac{L_W}{A'_W}$$

But since $A'_W = A_W$, then

$$(S_y)_W = \frac{L_W}{A_W}$$

By comparing the preceding equations, it is apparent that

$$(S_y)_W \cong \sigma_W$$

And by substituting this last relationship into Eq. (32.22), we get

$$(S_y)_W = \sigma_0(\varepsilon_W)^m \tag{32.23}$$

Thus it is apparent that *the plastic portion of the* $\sigma - \varepsilon$ *curve is approximately the locus of yield strengths for a material as a function of the amount of cold work.* This relationship is valid only for the axial tensile yield strength after tensile deformation or for the axial compressive yield strength after axial deformation.

32.11.5 Tensile Strength and Cold Work

It is believed by materials and mechanical-design engineers that the only relationships between the tensile strength of a cold-worked material and the amount of cold work given it are the experimentally determined tables and graphs that are provided by the material manufacturers and that the results are different for each family of materials. However, on the basis of the concepts of the tensile test presented here, two relations are derived in Ref. [32.1] between tensile strength and percent cold work that are valid when the prior cold work is tensile. These relations are derived on the basis of the load-deformation characteristics of a material as represented in Fig. 32.20. This model is valid for all metals that do not strain age.

Here we designate the tensile strength of a cold-worked material as $(S_u)_W$, and we are interested in obtaining the relationship to the percent cold work W. For any

specimen that is given a tensile deformation such that A_W is equal to or less than A_u, we have, by definition, that

$$(S_u)_W = \frac{L_u}{A'_W}$$

And also, by definition,

$$L_u = A_0(S_u)_0$$

where $(S_u)_0$ = tensile strength of the original non-cold-worked specimen and A_0 = its original area.

The percent cold work associated with the deformation of the specimen from A_0 to A'_W is

$$W = \frac{A_0 - A'_W}{A_0}(100) \qquad \text{or} \qquad w = \frac{A_0 - A'_W}{A_0}$$

where $w = W/100$. Thus

$$A'_W = A_0(1 - w)$$

By substitution into the first equation,

$$(S_u)_W = \frac{A_0(S_u)_0}{A_0(1 - w)} = \frac{(S_u)_0}{1 - w} \tag{32.24}$$

Of course, this expression can also be expressed in the form

$$(S_u)_W = (S_u)_0 \exp(\varepsilon) \tag{32.25}$$

Thus *the tensile strength of a material that is prestrained in tension to a strain less than its ultimate load strain is equal to its original tensile strength divided by 1 minus the fraction of cold work.* This relationship is valid for deformations less than the deformation associated with the ultimate load, that is, for

$$A_W \le A_u \qquad \text{or} \qquad \varepsilon_W \le \varepsilon_u$$

Another relationship can be derived for the tensile strength of a material that has been previously cold-worked in tension by an amount greater than the deformation associated with the ultimate load. This analysis is again made on the basis of Fig. 32.20. Consider another standard tensile specimen of 1020 steel that is loaded beyond L_u (12 000 lb) to some load L_z, say, 10 000 lb. If dead weights were placed on the end of the specimen, it would break catastrophically when the 12 000-lb load was applied. But if the load had been applied by means of a mechanical screw or a hydraulic pump, then the load would drop off slowly as the specimen is stretched. For this particular example the load is considered to be removed instantly when it drops to L_z or 10 000 lb. The unloaded specimen is not broken, although it may have a "necked" region, and it has a minimum cross-sectional area $A_z = 0.100$ in^2 and a diameter of 0.358 in. Now when this same specimen is again loaded in tension, it

deforms elastically until the load reaches L_z (10 000 lb) and then it deforms plastically. But L_z is also the maximum value of load that this specimen reaches on reloading. It never again will support a load of L_u = 12 000 lb. On this basis, the yield strength of this specimen is

$$(S_y)_W = \frac{L_z}{A'_z} = \frac{10\,000}{0.101} = 99\,200 \text{ psi}$$

And the tensile strength of this previously deformed specimen is

$$(S_u)_W = \frac{L_z}{A_z} = \frac{10\,000}{0.101} = 99\,200 \text{ psi}$$

32.11.6 Ratio of Tensile Strength to Brinell Hardness

It is commonly known by mechanical-design engineers that the tensile strength of a steel can be estimated by multiplying its Brinell hardness number by 500. As stated earlier, this fact led to the wide acceptance of the Brinell hardness scale. However, this ratio is not 500 for all materials—it varies from as low as 450 to as high as 1000 for the commonly used metals. The ratio of the tensile strength of a material to its Brinell hardness number is identified by the symbol K_B, and it is a function of both the load used to determine the hardness and the strain-strengthening exponent of the material.

Since the Brinell hardness number of a given material is not a constant but varies in proportion to the applied load, it then follows that the proportionality coefficient K_B is not a constant for a given material, but it too varies in proportion to the load used in determining the hardness. For example, a 50 percent cobalt alloy (L605 or HS25) has a Brinell hardness number of 201 when tested with a 3000-kg load and a hardness of only 150 when tested with a 500-kg load. Since the tensile strength is about 145 000 psi for this annealed alloy, the value for K_B is about 970 for the low load and about 730 for the high load.

Since the material is subjected to considerable plastic deformation when both the tensile strength and the Brinell hardness are measured, these two values are influenced by the strain-strengthening exponent m for the material. Therefore, K_B must also be a function of m.

Figure 32.21 is a plot of experimental data obtained by this author over a number of years that shows the relationships between the ratio K_B and the two variables strain-strengthening exponent m and diameter of the indentation, which is a function of the applied load. From these curves it is apparent that K_B varies directly with m and inversely with the load or diameter of the indentation d. The following examples will illustrate the applicability of these curves.

A test was conducted on a heat of alpha brass to see how accurately the tensile strength of a material could be predicted from a hardness test when the strain-strengthening exponent of the material is not known. Loads varying from 200 to 2000 kg were applied to a 10-mm ball, with the following results:

Load, kg	200	500	1000	1500	2000
Diameter, mm	2.53	3.65	4.82	5.68	6.30

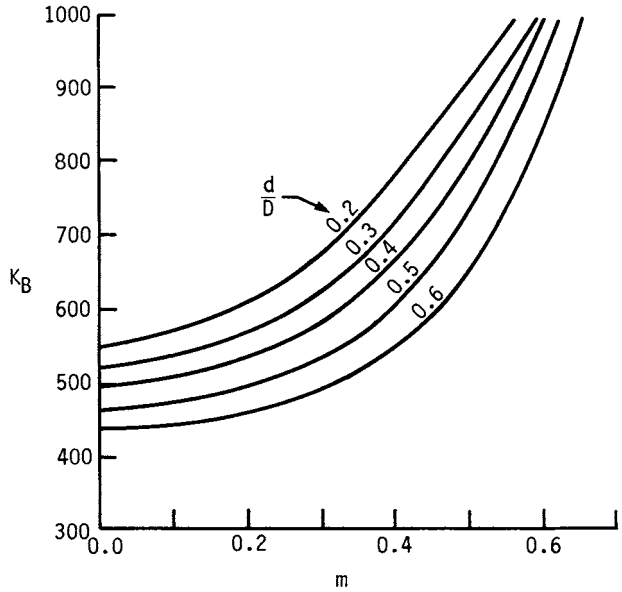

FIGURE 32.21 Relationships between the S_u/H_B ratio (K_B) and the strain-strengthening exponent m. D = diameter of the ball, and d = diameter of the indentation. Data are based on experimental results obtained by the author.

When plotted on log-log paper, these data fall on a straight line having a slope of 2.53, which is the Meyer strain-hardening exponent n. The equation for this straight line is

$$L = 18.8d^{2.53}$$

Since, for some metals, $m = n - 2$, the value of m is 0.53.

For ease in interpreting Fig. 32.21, the load corresponding to an indentation of 3 mm is calculated from Eq. (32.2) as 43. K_B can now be determined from Fig. 32.21 as 890. Thus the tensile strength is $S_u = K_B H_B = 890(43) = 38\,300$ psi. In a similar fashion, the load for a 5-mm diameter is 110 kg, and the corresponding Brinell hardness number is 53. From Fig. 32.21, the value of K_B is found to be 780, and the tensile strength is estimated as $S_u = K_B H_B = 780(53) = 41\,300$ psi. The average value of these two calculated tensile strengths is 39 800 psi. The experimentally determined value of the tensile strength for this brass was 40 500 psi, which is just 2 percent lower than the predicted value.

As another example, consider the estimation of tensile strength for a material when its typical strain-strengthening exponent is known. Annealed 3003 aluminum has an average m value of 0.28. What is the tensile strength of a heat that has a Brinell hardness number of 28 when measured with a 500-kg load? The diameter of the indentation for this hardness number is 4.65. Then from Fig. 32.21 the value of K_B is determined as 535. The tensile strength can then be calculated as $S_u = K_B H_B = 535(28) = 15\,000$ psi.

32.12 IMPACT STRENGTH

In some cases a structural part is subject to a single, large, suddenly applied load. A standard test has been devised to evaluate the ability of a material to absorb the impact energy through plastic deformation. The test can be described as a technological one, like the Rockwell hardness test, rather than as a scientific one. The values obtained by the impact test are relative rather than absolute. They serve as a basis of comparison and specification of the toughness of a material.

The *impact strength* is the energy, expressed in footpounds, required to fracture a standard specimen with a single-impact blow. The impact strength of a material is frequently referred to as being a measure of the toughness of the material, that is, its ability to absorb energy. The area under the tensile stress–strain curve is also a measure of the ability of a material to absorb energy (its toughness). Unfortunately, there is only a very general relationship between these two different measures of toughness; namely, if the material has a large area under its tensile stress–strain curve, it also has a relatively high impact strength.

Most impact-strength data are obtained with the two types of notched specimens shown in Fig. 32.22. Figure 32.22*a* illustrates the Charpy V-notch specimen as well as how the impact load is applied. Figure 32.22*b* does the same for the Izod V-notch specimen, and the details of the notch are shown in Fig. 32.22*c*. There are several modifications of the standard V-notch specimen. One is called the *keyhole notch* and another the *U-notch*. Both have a 1-mm radius at the bottom rather than the 0.25-mm radius of the V-notch. There is no correlation between the various types of notch-bar impact-strength values. However, the Charpy V-notch impact-strength value is considerably greater than the Izod V-notch value, particularly in the high toughness range.

The impact-testing machine consists of a special base mounted on the floor to support the specimen and a striking hammer that swings through an arc of about 32-in radius, much like a pendulum. When the hammer is "cocked" (raised to a locked elevation), it has a potential energy that varies between 25 and 250 ft · lb, depending on the mass of the hammer and the height to which it is raised. When the hammer is released and allowed to strike the specimen, a dial registers the energy that was absorbed by the specimen. The standards specify that the striking velocity must be in the range of 10 to 20 ft/s because velocities outside this range have an effect on the impact strength.

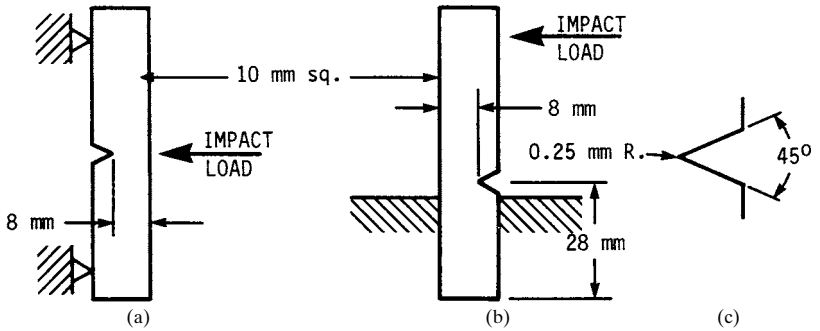

FIGURE 32.22 Impact tests and specimens. (*a*) Charpy $L = 55$ mm; (*b*) Izod $L = 75$ mm; (*c*) details of the notch.

The impact strengths of some materials, particularly steel, vary significantly with the testing temperature. Figure 32.23 shows this variation for a normalized AISI 1030 steel. At the low testing temperature the fracture is of the cleavage type, which has a bright, faceted appearance. At the higher temperatures the fractures are of the shear type, which has a fibrous appearance. The *transition temperature* is that temperature that results in 50 percent cleavage fracture and 50 percent shear fracture, or it may be defined as the temperature at which the impact strength shows a marked drop. The *nil-ductility temperature* is the highest temperature at which the impact strength starts to increase above its minimum value. These two temperatures are shown in Fig. 32.23.

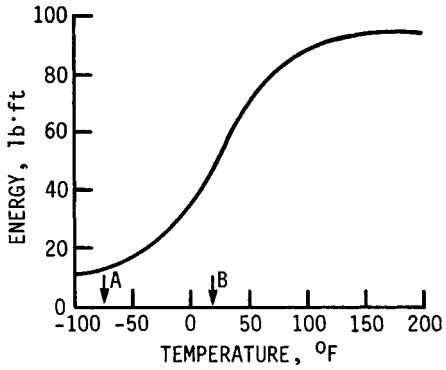

FIGURE 32.23 Charpy V-notch impact strength of 1030 steel versus temperature. A = nil-ductility temperature; B = transition temperature.

32.13 CREEP STRENGTH

A part may fail with a load that induced stresses in it that lie between the yield strength and the tensile strength of the material even if the load is steady and constant rather than alternating and repeating as in a fatigue failure. This type of constant loading causes the part to elongate or creep. The failure point may be when the part stretches to some specified length, or it may be when the part completely fractures.

The *creep strength* of a material is the value of nominal stress that will result in a specified amount of elongation at a specific temperature in a given length of time. It is also defined as the value of nominal stress that induces a specified creep rate at a specific temperature. The creep strength is sometimes called the *creep limit.* The *creep rate* is the slope of the strain-time creep curve in the steady-creep region, referred to as a *stage 2 creep.* It is illustrated in Fig. 32.24.

Most creep failures occur in parts that are exposed to high temperatures rather than room temperature. The stress necessary to cause creep at room temperature is considerably higher than the yield strength of a material. In fact, it is just slightly less than the tensile strength of a material. The stress necessary to induce creep at a temperature that is higher than the recrystallization temperature of a material, however, is very low.

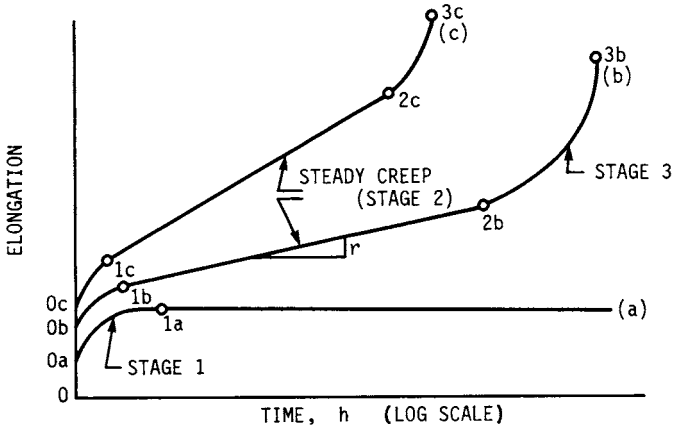

FIGURE 32.24 Creep data plotted on semilog coordinates. (*a*) Low stress (slightly above S_y) or low temperature (well below recrystallization); (*b*) moderate stress (midway between S_y and S_u) or moderate temperature (at recrystallization); (*c*) high stress (slightly below S_u) or high temperature (well above recrystallization). The elastic elongations are designated as 0*a,* 0*b,* and 0*c.*

The specimens used for creep testing are quite similar to round tensile specimens. During the creep test the specimen is loaded with a dead weight that induces the required nominal stress applied throughout the entire test. The specimen is enclosed in a small round tube-type furnace to maintain a constant temperature throughout the test, and the gauge length is measured after various time intervals. Thus the three variables that affect the creep rate of the specimen are (1) nominal stress, (2) temperature, and (3) time.

Figure 32.24 illustrates the most common method of presenting creep-test data. Three different curves are shown. Curve (*a*) is typical of a creep test conducted at a temperature well below the recrystallization temperature of the material (room temperature for steel) and at a fairly high stress level, slightly above the yield strength. Curve (*a*) is also typical of a creep test conducted at a temperature near the recrystallization temperature of a material but at a low stress level. Curve (*c*) is typical of either a high stress level, such as one slightly below S_u, at a low temperature, or else a low stress level at a temperature significantly higher than the recrystallization temperature of the material. Curve (*b*) illustrates the creep rate at some intermediate combination of stress and temperature.

A creep curve consists of four separate parts, as illustrated with curve (*b*) in Fig. 32.24. These are explained as follows:

1. An initial elastic extension from the origin 0 to point 0*b.*
2. A region of primary creep, frequently referred to as *stage 1 creep.* The extension occurs at a decreasing rate in this portion of the creep curve.
3. A region of secondary creep, frequently called *stage 2 creep.* The extension occurs at a constant rate in this region. Most creep design is based on this portion of the creep curve, since the creep rate is constant and the total extension for a given number of hours of service can be easily calculated.
4. A region of tertiary creep or *stage 3 creep.* The extension occurs at an increasing rate in this region until the material fractures.

Another practical way of presenting creep data is illustrated in Fig. 32.25, which is a log-log plot of nominal stress versus the second-stage creep rate expressed as percent per hour with the temperature as a parameter. Figure 32.26 illustrates still another type of plot that is used to present creep data where both the stress and temperature are drawn on cartesian coordinates.

The mechanism of creep is very complex inasmuch as it involves the movements of vacancies and dislocations, strain hardening, and recrystallization, as well as grain-boundary movements. At low temperatures, creep is restricted by the pile-up of dislocations at the grain boundaries and the resulting strain hardening. But at higher temperatures, the dislocations can climb out of the original slip plane and thus permit further creep. In addition, recrystallization, with its resulting lower strength, permits creep to occur readily at high temperatures.

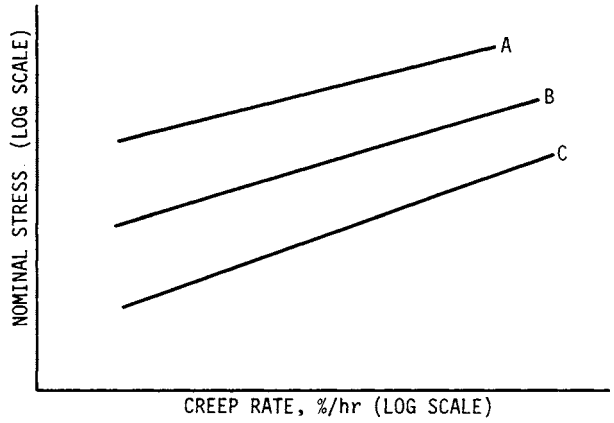

FIGURE 32.25 Second-stage creep rate versus nominal stress. *A, B,* and *C* are for low, medium, and high temperatures, respectively.

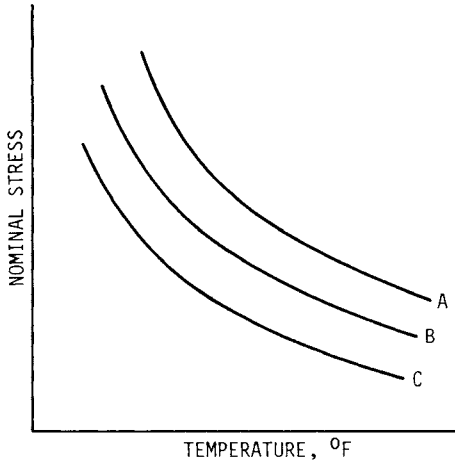

FIGURE 32.26 Second-stage creep rate versus temperature and nominal stress. *A,* 1%/h creep rate; *B,* 0.1%/h creep rate; *C,* 0.001%/h creep rate.

As explained in an earlier section, the grain-boundary material is stronger than the material at the interior portions at low temperatures, but the opposite is true at high temperatures. The temperature where these two portions of the grains are equal is called the *equicohesive temperature.* Consequently, parts that are exposed to high temperatures have lower creep rates if they are originally heat-treated to form coarse grains.

32.14 MECHANICAL-PROPERTY DATA

The number of different combinations of thermal and mechanical treatments for each family of materials plus the large number of individual material compositions within one family makes it impossible to compile a complete listing in one handbook. For more information on the typical values of the mechanical properties of a specific material, you should consult the engineering manuals published by the various material manufacturers as well as the references at the end of this chapter. The total number of pages of mechanical-property data listed in all the sources cited at the end of this chapter runs into the thousands, making it impossible to include it all in one handbook. The mechanical properties are simply listed as the experimentally obtained values for each of the many conditions of a given metal.

This section includes some select mechanical-property data in tabular form for a variety of materials in Table 32.5. Both the format of the data and the actual mechanical properties listed are different from the traditional handbook presentations. There are several advantages to presenting the data in this manner. One of the main advantages is that it requires much less space. For example, as shown in Table 32.5, only five numbers have to be recorded for each metal in its original non-cold-worked condition. These numbers refer to the five primary mechanical properties. From these original values it is very easy to calculate the new strengths of the metal after any specific amount of cold work or to construct tables or graphs of strength versus percent cold work. This is in sharp contrast to the large amount of space required to store the tables or graphs in any handbook or manual of properties.

A second advantage of presenting the data in this manner is that it is possible to make use of the rules and relationships included in Chap. 33 to calculate both the compressive and tensile properties in all directions in a cold-worked part. This is extremely important because for some materials (those having a high strain-strengthening exponent m) it is possible to have a compressive yield strength for a given amount of cold work that is one-half the tensile yield strength that may be tabulated in a materials handbook.

Table 32.6 includes some of the properties of very-high-strength steels. To illustrate the versatility of documenting mechanical properties in the format of Table 32.5, consider the annealed 303 stainless steel listed in the table. In the annealed condition it has the following listed properties: $S_y = 35$ kpsi, $S_u = 87.3$ kpsi, strength coefficient $\sigma_0 = 205$ kpsi, strain-strengthening exponent $m = 0.51$, and fracture strain $\varepsilon_f = 1.16$. In an upsetting operation, a 2-in-diameter bar is upset to a diameter of 2½ in for a length of 1½ in prior to having splines machined on the end. Since the splines are cantilevered beams subject to bending stresses in the circumferential or transverse direction, the strength of the material in this direction rather than in the axial or longitudinal direction is required. Also, the stresses are compressive on one side of the splines and tensile on the other. Therefore, the designer should know both the tensile and compressive strengths in the transverse direction. The following sample calculations will demonstrate how this can be done.

TABLE 32.5 Tensile Properties of Some Metals[a]

Material	Condition	Strength			Strain-strengthening exponent m	Fracture strain ϵ_f
		Yield S_y, kpsi	Ultimate S_u, kpsi	Coefficient σ_0, kpsi		
		Carbon and alloy steels				
1002	1500°F @ 1 h, A 0.032 in	22.0	39.5	76.0	0.29	1.25
1002[a]	1800°F @ 1 h, A	19.0	42.0	78.0	0.27	1.25
1008 DQ	As rec'd 0.024 in	25.0	39.0	70.0	0.24	1.20
1008 DQ	As above—trans	27.0	43.0	70.0	0.24	1.10
1008 DQ	1600°F @ 1 h A	26.5	40.0			
1010	0.024-in CD strip	33.2	47.5	84.0	0.23	1.20
1010	As above—trans	36.8	48.5	88.0	0.26	1.00
1010	1600°F @ 1 h A	28.6	44.2	82.0	0.23	1.20
1010	As above—trans	29.1	43.8	82.0	0.23	1.20
1018	A	32.0	49.5	90.0	0.25	1.05
1020	HR	42.0	66.2	115.0	0.22	0.90
1045	HR	60.0	92.5	140.0	0.14	0.58
1144	A	52.0	93.7	144.0	0.14	0.49
1144[b]	A	50.0	93.7	144.0	0.14	0.05
1212	HR	28.0	61.5	110.0	0.24	0.85
4340	HR	132.0	151.0	210.0	0.09	0.45
52100	Spher. A	80.0	101.0	165.0	0.18	0.58
52100	1500°F A	131.0	167.0	210.0	0.07	0.40
		Stainless steels				
18-8	1600°F @ 1 h A	37.0	89.5	210.0	0.51	1.08
18-8	1800°F @ 1 h A	37.5	96.5	230.0	0.53	1.38
302	1800°F @ 1 h A	34.0	92.4	210.0	0.48	1.20
303	A	35.0	87.3	205.0	0.51	1.16
304	A	40.0	82.4	185.0	0.45	1.67
202	1900°F @ 1 h A	55.0	105.0	195.0	0.30	1.00
17-4 PH	1100°F aged	240.0	246.0	260.0	0.01	0.65
17-4 PH	A	135.0	142.0	173.0	0.05	1.20
17-7 PH	1050°F aged	155.0	185.0	225.0	0.05	0.90
17-7 PH	900°F aged	245.0	255.0	300.0	0.04	0.50
440 C	Solution H T	63.5	107.0	153.0	0.11	0.36
440 C	A 1600°F–50°F/h	67.6	117.0	180.0	0.14	0.12
		Aluminum alloys				
1100	900°F @ 1 h A	4.5	12.1	22.0	0.25	2.30
3003	800°F @ 1 h A	6.0	15.0	29.0	0.30	1.50
2024[c]	T-351	52.0	68.8	115.0	0.20	0.37
2024	T-4	43.0	64.8	100.0	0.15	0.18
7075	800°F A	14.3	33.9	61.0	0.22	0.53
7075	T-6	78.6	86.0	128.0	0.13	0.18
2011	800°F @ 1 h A	7.0	25.2	41	0.18	0.35
2011	T-6	24.5	47.0	90	0.28	0.10

TABLE 32.5 Tensile Properties of Some Metals[a] (*Continued*)

Material	Condition	Strength			Strain-strengthening exponent m	Fracture strain ϵ_f
		Yield S_y, kpsi	Ultimate S_u, kpsi	Coefficient σ_0, kpsi		
Magnesium alloys						
HK31 XA	800°F @ 1 h A	19.0	25.5	49.5	0.22	0.33
HK31 XA	H-24	31.0	36.2	48.0	0.08	0.20
Copper alloys						
ETP Cu	100°F @ 1 h A	4.7	31.0	78.0	0.55	1.19
ETP Cu	1250°F @ 1 h A	4.6	30.6	72.0	0.50	1.21
ETP Cu	1500°F @ 1 h A	4.2	30.0	68.0	0.48	1.26
OFHC Cu	1250°F @ 1 h A	5.3	33.1	67.0	0.35	1.00
90-10 brass	As rec'd[c]	12.8	38.0	85.0	0.43	
90-10 brass	1200°F @ 1 h A	8.4	36.4	83.0	0.46	
90-10 brass	As above, 10% CW, 1200°F A	6.9	35.0	87.0	1.83	
80-20 brass	1200°F @ 1 h A	7.2	35.8	84.0	0.48	
80-20 brass	As above, 10% CW, 1200°F A	6.4	34.6	85.0	0.51	1.83
70-30 brass	1200°F @ 1 h A	12.1	44.8	112.0	0.59	
70-30 brass	As above, 10% CW, 1200°F A	10.7	43.4	107.0	0.59	1.62
70-30 brass[b]	1000°F @ 1 h A	11.5	45.4	110.0	0.56	1.50
70-30 brass[b]	1200°F @ 1 h A	10.5	44.0	105.0	0.52	1.55
70-30 brass[b]	1400°F @ 1 h A	8.8	42.3	105.0	0.60	1.60
70-30 leaded brass	1250°F @ 1 h A	11.0	45.0	105.0	0.50	1.10
Naval brass[d]	1350°F @ $\frac{1}{2}$ h A	17.0	54.5	125.0	0.48	1.00
Naval brass[d]	1350°F @ $\frac{1}{2}$ h WQ	27.0	66.2	135.0	0.37	0.50
Naval brass[d]	850°F @ $\frac{1}{2}$ h A	17.5	56.0	125.0	0.48	0.90
Naval brass[d]	850°F @ $\frac{1}{2}$ h WQ	31.5	64.5	135.0	0.37	0.80
Naval brass[d]	1500°F @ 3 h A	11.0	48.0			0.74
Nickel alloys						
Ni 200	1700°F @ $\frac{1}{4}$ h WQ	16.2	72.1	150.0	0.375	1.805
99.44% Ni	CD, A	20.5	73.7	160.0	0.40	1.47
Monel 400	1700°F @ $\frac{1}{4}$ h WQ	26.5	77.7	157.0	0.337	1.184
Monel K500	1700°F @ $\frac{1}{4}$ h WQ	34.4	92.6	182.0	0.32	1.305
Inconel 600	1700°F @ $\frac{1}{4}$ h WQ	46.6	102.5	201.0	0.315	1.14
Inconel 625	1700°F @ $\frac{1}{2}$ h WQ	77.1	139.7	297.0	0.395	0.75
Inconel 718	1750°F @ 20 min AC	43.6	99.4	205.0	0.363	1.337
Inconel X750	2050°F @ 45 min WQ	36.4	106.4	230.0	0.415	1.27
Incoloy 800	2050°F @ 2 h AC	22.2	77.1	169.0	0.420	1.262
Incoloy 825	1700°F @ 20 min WQ	66.7	138.0	283.0	0.353	0.715
Ni, 2% Be	1800°F sol. T WQ	41.0	104.0	222.0	0.39	1.00

TABLE 32.5 Tensile Properties of Some Metals[a] (*Continued*)

Material	Condition	Strength			Strain-strengthening exponent m	Fracture strain ε_f
		Yield S_y, kpsi	Ultimate S_u, kpsi	Coefficient σ_0, kpsi		
Nickel alloys (*Continued*)						
Ni, 2% Be	As above + 1070°F @ 2 h aged	140.0	195.0	300.0	0.15	0.18
Ni, 15.8% Cr, 7.2% Fe	A	36.0	90.0	203.0	0.45	0.92
Special alloys						
Cobalt alloy[f]	2250°F solution HT	65.0	129.0	300.0	0.50	0.51
Cobalt alloy[f]	As above—trans[c]	65.0	129.0	300.0	0.50	0.40
Cobalt alloy[e,g]	As rec'd, annealed	62.8	119.5	283.0	0.52	0.75
Cobalt alloy[e,g]	Machined, 2250°F sol. HT	48.0	112.5	283.0	0.62	0.70
Cobalt alloy[e,g]	2250°F sol. HT, 925°F aged	48.0	107.5	270.0	0.63	1.00
Molybdenum	Extr'd A	49.5	70.7	106.0	0.12	0.38
Vanadium	A	45.0	63.0	97.0	0.17	1.10

[a]All values are for longitudinal specimens except as noted. These are values obtained from only one or two heats. The values will vary from heat to heat because of the differences in composition and annealing temperatures. The fracture strain may vary as much as 100 percent.
[b]$\frac{3}{4}$-in-diameter bar.
[c]Tensile specimen machined from a 4-in-diameter bar transverse to rolling direction.
[d]Specimens cut from $\frac{1}{2}$-in hot-rolled plate.
[e]$\frac{1}{2}$-in-diameter bar.
[f]HS 25 or L 605 alloy; 50 Co, 20 Cr, 15 W, 10 Ni, 3 Fe.
[g]Eligiloy; 50 Co, 20 Cr, 15 Ni, 7 Mo, 15 Fe.

SOURCE: From Datsko [32.1].

The strain associated with upsetting a 2-in-diameter bar to a 2½-in-diameter can be calculated by means of Eq. (32.12). Thus

$$\varepsilon = -\ln\left(\frac{2}{2.5}\right)^2 = 0.45$$

The negative sign in front of the function is needed because Eq. (32.12) is for tensile deformation, whereas in this problem the deformation is axial compression. The equivalent amount of cold work can be calculated from Eq. (32.14) as 36.2 percent.

The axial compressive yield strength can be approximated by means of Eq. (32.23). Thus

$$(S_y)_c = \sigma_0(\varepsilon_W)^m = 205(0.45)^{0.51} = 136 \text{ kpsi}$$

If one were to interpolate in a table of yield strength versus cold work in a handbook, this value of 136 kpsi would be approximately the value that would be

TABLE 32.6 Properties of Some High-Strength Steels

AISI number	Processing[a]	Brinell hardness H_B	Modulus of elasticity E, Mpsi	Yield strength[b] S_y, kpsi	Ultimate strength S_u, kpsi	Reduction in area, %	True fracture strength σ_F, kpsi	True fracture ductility[c] ϵ_F	Strain-strengthening exponent m
1045	Q & T 80°F	705	29	265T[d] 300C[d]	300	2	310T 420C	0.02	0.186
1045	Q & T 360°F	595	30	270	325	41	430/ 395	0.52	0.071
1045	Q & T 500°F	500	30	245	265	51	370/ 330	0.71	0.047
1045	Q & T 600°F	450	30	220	230	55	345/ 305	0.81	0.041
1045	Q & T 720°F	390	30	185	195	59	315/ 270	0.89	0.044
4142	Q & T 80°F	670	29	235T 275C	355	6	375	0.06	0.136
4142	Q & T 400°F	560	30	245	325	27	405/ 385	0.31	0.091
4142	Q & T 600°F	475	30	250	280	35	340/ 315	0.43	0.048
4142	Q & T 700°F	450	30	230	255	42	320/ 290	0.54	0.043
4142	Q & T 840°F	380	30	200	205	48	295/ 265	0.66	0.051
4142[e]	Q & D 550°F	475	29	275T 225C	295	20	310/ 300	0.22	0.101T 0.060C
4142	Q & D 650°F	450	29	270T 205C	280	37	330/ 305	0.46	0.016T 0.070C
4142	Q & D 800°F	400	29	210T[f] 175C	225	47	305/ 275	0.63	0.032T 0.085C

[a]AISI 1045: Cold drawn to $\frac{9}{16}$-in rounds from hot-rolled rod. Austenized 1500°F (oxidizing atmosphere) 20 min, water quenched at 70°F. AISI 4142: Cold-drawn to $\frac{9}{16}$-in rounds from annealed rod. Austenized at 1500°F (neutral atmosphere), quenched in agitated oil at 180°F. AISI 4142 Def: Austenized at 1500°F, oil quenched. Reheated in molten lead, drawn 14 percent through die at reheating temperature to $\frac{5}{8}$-in rods.

[b]0.2 percent offset method.

[c]Bridgman's correction for necking.

[d]T, tension; C, compression.

[e]Deformed 14 percent.

[f]Proportional limit in tension.

SOURCE: Data from R. W. Landgraf, *Cyclic Deformation and Fatigue Behavior of Hardened Steels,* Report no. 320, Dept. of Theoretical and Applied Mechanics, University of Illinois, Urbana, 1968.

obtained for 36 percent cold work. And the handbook would not indicate whether it was a compressive or tensile yield strength, nor in what direction it was applied.

However, for this problem, the designer really needs both the tensile and compressive yield strengths in the transverse, i.e., circumferential, direction. These values can be closely approximated by means of Table 33.1. The tensile yield strength in the transverse direction is designated by the code $(S_y)_{tTt}$, which is in group 2 of Table 33.1. Since the bar was given only one cycle of deformation (a single upset), ε_{qus} is 0.45 and the tensile yield strength is calculated to be 123 kpsi. The compressive yield strength in the transverse direction is designated by the code $(S_y)_{cTt}$, which is in group 4 of Table 33.1. The compressive yield strength is then calculated to be $0.95(S_y)_{tTt} = 0.95(123) = 117$ kpsi; this is 14 percent lower than the 136 kpsi that would normally be listed in a materials handbook.

In some design situations, the actual value of the yield strength in a given part for a specific amount of cold work may be 50 percent less than the value that would be listed in the materials handbook. In order to have a reliable design, the designer must be able to determine the strength of the material in a part in the direction and sense of the induced stresses. The information in this chapter and in Chap. 33 makes it possible for the design engineer to make a reasonable prediction of the mechanical properties of a fabricated part. However, it must be recognized that the original non-cold-worked properties of a given metal vary from heat to heat, and that the calculations are valid only for a part having the original properties that are used in the calculations.

32.15 NUMBERING SYSTEMS†

32.15.1 AISI and SAE Designation of Steel

Carbon and alloy steels are specified by a code consisting of a four-digit (sometimes five) number, as illustrated below with the substitution of the letters X, Y, and Z for the numbers. A steel specification of XYZZ (or XYZZZ) has the following meaning:

X indicates the type of alloy or alloys present.

Y indicates the total percent of the alloys present.

ZZ (or ZZZ) indicates the "points" of carbon in the steel (points of carbon equals the percent carbon times 100). For example, if ZZ is 40, then the steel has 0.40 percent carbon (C). If ZZZ is 120, then the steel has 1.20 percent carbon.

Table 32.7 identifies the number X corresponding to the alloy or alloys present. In addition, the following two special classes are included. A resulfurized free-machining steel is identified as 11ZZ and 12ZZ. These steels have a high sulfur content, which combines with the manganese to form the compound manganese sulfide. It is the presence of this compound that makes the steel more machinable. The 13ZZ and 15ZZ groups are plain carbon steels that have high and moderate amounts of manganese, respectively.

† This section presents the numbering systems now in general use in order to correspond with those used in other sections of this handbook. See Ref. [32.2] for details of the unified numbering system (UNS).

TABLE 32.7 Alloy Designations for Steels

Number X	Alloying elements
1	None (plain carbon)
2	Nickel
3	Nickel-chromium
4	Molybdenum-nickel-chromium
5	Chromium
6	Chromium-vanadium
8	Nickel-chromium-molybdenum
9	Silicon-manganese

Some examples:

2130 is a steel with 1 percent nickel and 0.3 percent carbon.

4340 is a steel with a total of 3 percent Mo, Ni, and Cr and 0.4 percent C.

52100 is a steel with 2 percent Cr and 1 percent C.

32.15.2 Designation System for Aluminum Alloys

Wrought aluminum alloys are specified by a code consisting of four-digit numbers such as 1100, 2024, or 7075. To explain this code, the letters XYZZ are substituted for the four digits. The types of alloys present in the aluminum are identified by the letter X from Table 32.8.

The second digit in the code, Y, indicates alloy modifications. When Y is zero, it indicates the original alloy, or in the 1YZZ series it indicates that the alloy is made to the standard impurity limits. When Y is any digit from 1 to 9, it indicates that a modification has been made to the original alloy and then designates which of the sequential changes were made. For example, 7075 refers to the original zinc alloy, whereas 7175 and 7475 refer to the first and fourth modifications made to it.

The third and fourth digits (ZZ in the code) have no numerical significance but simply relate to the chemical composition of the alloys.

TABLE 32.8 Alloy Designations for Wrought Aluminum Alloys

Number X	Alloying elements
1	None (99.00% Al min.)
2	Copper
3	Manganese
4	Silicon
5	Magnesium
6	Magnesium-silicon
7	Zinc

SOLID MATERIALS

Temper Designation. The temper designation for aluminum alloys consists of a suffix which is a letter that may be followed by several digits. The suffix is separated from the alloy designation by a hyphen or dash. For example, 7075-T4 identifies both the alloy composition and its temper. The T in this suffix identifies the tempering treatment as a heat-treating process. Table 32.9 shows the letters used to identify the type of process used in the tempering treatment.

In addition to the T temper designations, other two- or three-digit numbers have been assigned to some specific treatments to certain special alloys or types of products.

32.15.3 Designation System for Copper Alloys

The designation system for copper alloys is not based on a coded system as those for steel and aluminum alloys are. It is simply a means of defining the chemical composition of the specific alloys. Table 32.10 identifies the principal alloying elements for the common classes of copper alloys.

Temper Designation. The temper designation for copper alloys refers to the amount of cold work given to the metal. Table 32.11 defines the amount of cold work associated with each temper designation.

TABLE 32.9 Tempering Processes and Designations for Aluminum Alloys

Designation	Process
F	As fabricated
O	Annealed
H	Strain hardened; the H is followed by two or more digits to indicate the amount of strain hardening
H1	Strain hardened only
H2	Strain hardened and partially annealed
H3	Strain hardened and stabilized
W	Solution heat treated
T	Heat treated; the T is always followed by one or more digits to specify the particular process used
T1	Cooled from a high-temperature forming process and naturally aged
T2	Cooled from a high-temperature forming process, cold worked, and naturally aged
T3	Solution heat treated, cold worked, and naturally aged
T4	Solution heat treated and naturally aged
T5	Cooled from a high-temperature forming process and artificially aged
T6	Solution heat treated and artificially aged
T7	Solution heat treated
T8	Solution heat treated, cold worked, and artificially aged
T9	Solution heat treated, artificially aged, and cold worked
T10	Cooled from a high-temperature forming process, cold worked, and artificially aged

TABLE 32.10 Designation of Copper Alloys

UNS Number	Alloy	Class or name
C10000-C13000	None	Commercially pure (ETP or OFHC)
C21000	Zn	Gilding brass (95% Cu)
C22000	Zn	Commercial bronze (90% Cu)
C23000	Zn	Red brass (85% Cu)
C24000	Zn	Low brass (80% Cu)
C26000	Zn	Cartridge brass (70% Cu)
C28000	Zn	Muntz metal (60% Cu)
C50000	Sn	Phosphor bronze
C60600-C64200	Al	Aluminum bronze
C64700-C66100	Li	Silicon bronze
C70000	Ni	Copper-nickel

TABLE 32.11 Temper Designation of Copper Alloys

Temper	Percent cold work	
	Rolled sheet	Drawn wire
¼ hard	10.9	20.7
½ hard	20.7	37.1
¾ hard	29.4	50.1
Hard	37.1	60.5
Extra hard	50.1	75.1
Spring	60.5	84.4
Extra spring	68.6	90.2
Special spring	75.1	93.8

32.15.4 Designation System for Magnesium Alloys

The designation system for magnesium alloys consists of four parts that include a combination of letters and digits. A typical example is AZ31B-H24.

The first part of the designation consists of two letters representing the two main alloying elements in order of decreasing amounts. The 10 principal alloying elements are given the following letters: A, aluminum; E, rare earth; H, thorium; K, zirconium; L, lithium; M, manganese; Q, silver; S, silicon; T, tin; and Z, zinc. Thus, in the preceding alloy, the main element is aluminum and the second one is zinc.

The second part consists of two digits corresponding to rounded-off percentages of the two main alloying elements. In the preceding example the alloy contains 3 percent aluminum and 1 percent zinc.

The third part of the designation consists of a letter that indicates the chronologic order of when that particular composition became a standard one. In the preceding example the letter B indicates that this particular alloy is the second one, having 3 percent aluminum and 1 percent zinc, that became an industry standard.

The fourth part consists of a letter preceded by a hyphen and followed by a number. It indicates the specific condition or temper that the alloy is in. Table 32.12 specifies the symbols that are used for each temper.

TABLE 32.12 Temper Designation of Magnesium Alloys

Designation	Process
F	As fabricated
O	Annealed
H10, H11	Slightly strain hardened
H23, H24, H26	Strain hardened and partially annealed
T4	Solution heat treated
T5	Solution heat treated and artificially aged
T8	Solution heated treated, cold worked, and artificially aged

REFERENCES

32.1 J. Datsko, *Materials in Design and Manufacture,* J. Datsko Consultants, Ann Arbor, Mich., 1978.

32.2 *Metals and Alloys in the Unified Numbering System,* 3d ed., Society of Automotive Engineers, Inc. (SAE), 1983.

32.3 *Metals Handbook Desk Edition,* American Society for Metals (ASM), Metals Park, Ohio, 1984.

32.4 R. M. Brick, A. W. Pense, and R. B. Gordon, *Structure and Properties of Engineering Materials,* 4th ed., McGraw-Hill, New York, 1977.

32.5 M. M. Schwartz, *Composite Materials Handbook,* McGraw-Hill, New York, 1984.

32.6 L. H. Van Vlack, *Elements of Materials Science,* 4th ed., Addison-Wesley, Reading, Mass., 1980.

SOLID MATERIALS

CHAPTER 33
THE STRENGTH OF COLD-WORKED AND HEAT-TREATED STEELS

Charles R. Mischke, Ph.D., P.E.
Professor Emeritus of Mechanical Engineering
Iowa State University
Ames, Iowa

GLOSSARY

AR	Fractional area reduction
A	Area
B	Critical hardness for carbon content and tempering temperature, Rockwell C scale
d	Diameter
D	Tempering decrement, Rockwell C scale; carbon ideal diameter, in
D_I	Ideal critical diameter, in
DH	Distant hardness, Rockwell C scale
EJD	Equivalent Jominy distance, sixteenths of inch
f	Tempering factor for carbon content and tempering temperature
F	Load, temperature, degrees Fahrenheit
H	Quench severity, in^{-1}
IH	Initial hardness, Rockwell C scale

m	Strain-strengthening exponent
n	Design factor
r	Radius
$R_{\max}$	Maximum hardness attainable, Rockwell C scale
R_Q	As-quenched Jominy test hardness, Rockwell C scale
R_T	Tempered hardness, Rockwell C scale
S'_e	Engineering endurance limit
S_u	Engineering ultimate strength in tension
S_y	Engineering yield strength, 0.2 percent offset
t	Time
ε	True strain
η	Factor of safety
$\overline{\sigma}_0$	Strain-strengthening coefficient
σ	Normal stress
ΣA	Sum of alloy increments, Rockwell C scale
τ_o	Octahedral shear stress
τ	Shearing stress

Subscripts

a	Axial
B	Long traverse
c	Compression
C	Circumferential
D	Short traverse
e	Endurance
f	Fracture
L	Longitudinal
R	Radial
s	Shear
t	Tension
u	Ultimate
y	Yield
0	No prior strain

33.1 INTRODUCTION

The mechanical designer needs to know the yield strength of a material so that a suitable margin against permanent distortion can be provided. The yield strength provided by a standardized tensile test is often not helpful because the manufactur-

ing process has altered this property. Hot or cold forming and heat treatment (quenching and tempering) change the yield strength. The designer needs to know the yield strength of the material at the critical location in the geometry and at condition of use.

The designer also needs knowledge of the ultimate strength, principally as an estimator of fatigue strength, so that a suitable margin against fracture or fatigue can be provided. Hot and cold forming and various thermomechanical treatments during manufacture have altered these properties too. These changes vary within the part and can be directional. Again, the designer needs strength information for the material at the critical location in the geometry and at condition of use.

This chapter addresses the effect of plastic strain or a sequence of plastic strains on changes in yield and ultimate strengths (and associated endurance limits) and gives quantitative methods for the estimation of these properties. It also examines the changes in ultimate strength in heat-treated plain carbon and low-alloy steels.

33.2 STRENGTH OF PLASTICALLY DEFORMED MATERIALS

Methods for strength estimation include the conventional uniaxial tension test, which routinely measures true and engineering yield and ultimate strengths, percentage elongation and reduction in area, true ultimate and fracture strains, strain-strengthening exponent, strain-strengthening coefficient, and Young's modulus. These results are for the material in specimen form. Machine parts are of different shape, size, texture, material treatment, and manufacturing history and resist loading differently. Hardness tests can be made on a prototype part, and from correlations of strength with hardness and indentor size ([33.1], p. 5–35) and surface, ultimate strength can be assessed. Such information can be found in corporate manuals and catalogs or scattered in the literature. Often these are not helpful.

In the case of a single plastic deformation in the manufacturing process, one can use the true stress-strain curve of the material in the condition prior to straining provided the plastic strain can be determined. The results are good. For a sequence of successive strains, an empirical method is available which approximates what happens but is sometimes at variance with test results.

Cold work or *strain strengthening* is a common result of a cold-forming process. The process changes the properties, and such changes must be incorporated into the application of a theory of failure. The important strength is that of the part in the critical location in the geometry and at condition of use.

33.2.1 Datsko's Notation

In any discussion of strength it is necessary to identify

1. The kind of strength: ultimate, *u;* yield, *y;* fracture, *f;* endurance, *e.*
2. The sense of the strength: tensile, *t;* compressive, *c;* shear, *s.*
3. The direction or orientation of the strength: longitudinal, *L;* long transverse, *B;* short transverse, *D;* axial, *a;* radial, *R;* circumferential, *C.*
4. The sense of the most recent prior strain in the axial direction of the envisioned test specimen: tension, *t;* compression, *c.* If there is no prior strain, the subscript 0 is used.

33.2.2 Datsko's Rules

Datsko [33.1] suggests a notation $(S_1)_{234}$, where the subscripts correspond to 1, 2, 3, and 4 above. In Fig. 33.1 an axially deformed round and a rolled plate are depicted. A strength $(S_u)_{tLc}$ would be read as the engineering ultimate strength S_u, in tension $(S_u)_t$, in the longitudinal direction $(S_u)_{tL}$, after a last prior strain in the specimen direction that was compressive $(S_u)_{tLc}$. Datsko [33.1] has articulated rules for strain strengthening that are in approximate agreement with data he has collected. Briefly,

Rule 1. Strain strengthening is a bulk mechanism, exhibiting changes in strength in directions free of strain.

Rule 2. The maximum strain that can be imposed lies between the true strain at ultimate load ε_u and the true fracture strain ε_f. In upsetting procedures devoid of flexure, the limit is ε_f, as determined in the tension test.

Rule 3. The significant strain in a deformation cycle is the largest absolute strain, denoted ε_w. In a round $\varepsilon_w = \max(|\varepsilon_r|, |\varepsilon_\theta|, |\varepsilon_x|)$. The largest absolute strain ε_w is used in calculating the equivalent plastic strain ε_q, which is defined for two categories of strength, ultimate and yield, and in four groups of strength in Table 33.1.

Rule 4. In the case of several strains applied sequentially (say, cold rolling then upsetting), in determining ε_{qu}, the significant strains in each cycle ε_{wl} are added in decreasing order of magnitude rather than in chronological order.

Rule 5. If the plastic strain is imposed below the material's recrystallization temperature, the ultimate tensile strength is given by

$$S_u = (S_u)_o \exp \varepsilon_{qu} \qquad \varepsilon_{qu} < m$$

$$= \overline{\sigma}_0(\varepsilon_{qu})^m \qquad \varepsilon_{qu} > m$$

Rule 6. The yield strength of a material whose recrystallization temperature was not exceeded is given by

$$S_y = \overline{\sigma}_0(\varepsilon_{qy})^m$$

Table 33.1 summarizes the strength relations for plastically deformed metals.

33.3 ESTIMATING ULTIMATE STRENGTH AFTER PLASTIC STRAINS

This topic is best illuminated by example, applying ideas expressed in Secs. 33.2.1 and 33.2.2.

Example 1. A 1045HR bar has the following properties from tension tests:

$$S_y = 60 \text{ kpsi} \qquad S_u = 92.5 \text{ kpsi}$$

$$\text{AR} = 0.44 \qquad m = 0.14$$

The material is to be used to form an integral pinion on a shaft by cold working from 2¼ in to 2 in diameter and then upsetting to 2½ in to form a pinion blank, as depicted in Fig. 33.2. Find, using Datsko's rules, an estimate of the ultimate strength in a direction resisting tooth bending at the root of the gear tooth to be cut in the blank.

THE STRENGTH OF COLD-WORKED AND HEAT-TREATED STEELS

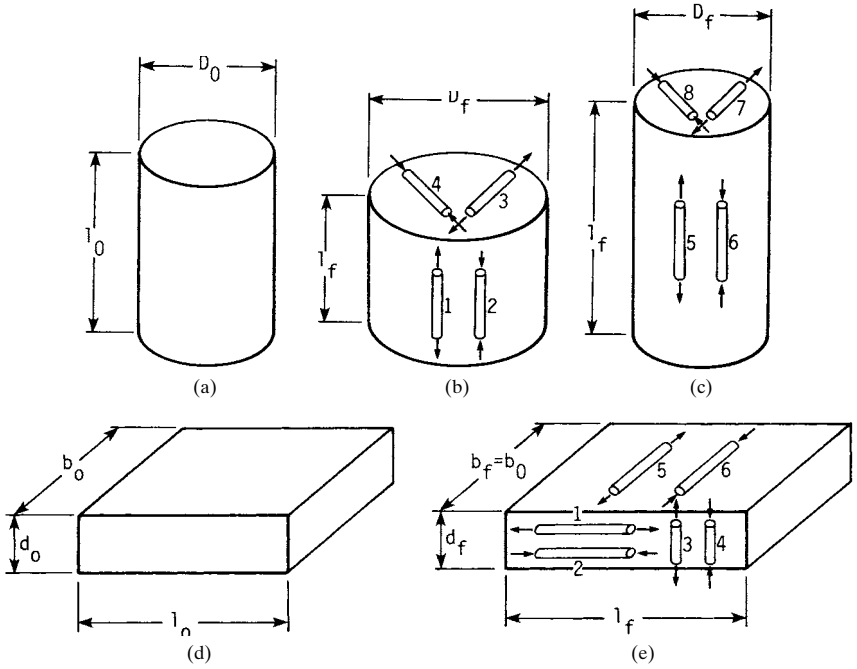

FIGURE 33.1 Sense of strengths in bar and plate. *(Adapted from [33.1], p. 7-7 with permission.)*

(*a*) Original bar before axial deformation.

	Specimen	Sense of strength	Direction in the bar	Prior strain	Designation
(*b*)	1	*t*	*L*	*c*	$(S)_{tLc}$
	2	*c*	*L*	*c*	$(S)_{cLc}$
	3	*t*	*T*	*t*	$(S)_{tTt}$
	4	*c*	*T*	*t*	$(S)_{cTt}$
(*c*)	5	*t*	*L*	*t*	$(S)_{tLt}$
	6	*c*	*L*	*t*	$(S)_{cLt}$
	7	*t*	*T*	*c*	$(S)_{tTc}$
	8	*c*	*T*	*c*	$(S)_{cTc}$

(*d*) Plate prior to rolling.

	Specimen	Sense of strength	Direction in the bar	Prior strain	Designation
(*e*)	1	*t*	*L*	*t*	$(S)_{tLt}$
	2	*c*	*L*	*t*	$(S)_{cLt}$
	3	*t*	*D*	*c*	$(S)_{tDc}$
	4	*c*	*D*	*c*	$(S)_{cDc}$
	5	*t*	*B*	0	$(S)_{tB0}$
	6	*c*	*B*	0	$(S)_{cB0}$

TABLE 33.1 Strength Relations for Plastically Deformed Metals†

$$(s_y)_w = \bar{\sigma}_0(\varepsilon_{qy})^m \qquad (S_u)_w = \begin{cases} (S_u)_0 \exp \varepsilon_{qu} & \varepsilon_{qu} < m \\ \bar{\sigma}_w & \varepsilon_{qu} > m \end{cases}$$

Group	Strength designation	ε_{qu}	ε_{qy}
1	$(S)_{cLc}$ $(S)_{tLt}$ $(S)_{tB0}$ $(S)_{cB0}$ $(S)_{cDc}$	$\varepsilon_{qus} = \sum_{i=1}^{n} \frac{\varepsilon_{wi}}{i}$	$\varepsilon_{qys} = \frac{\varepsilon_{qus}}{1 + 0.2\varepsilon_{qus}}$
2	$(S)_{tTt}$ $(S)_{cTc}$	$\varepsilon_{qus} = \sum_{i=1}^{n} \frac{\varepsilon_{wi}}{i}$	$\varepsilon_{qys} = \frac{\varepsilon_{qus}}{1 + 0.5\varepsilon_{qus}}$
3	$(S)_{cLt}$ $(S)_{tLc}$ $(S)_{tDc}$	$\varepsilon_{qu0} = \sum_{i=1}^{n} \frac{\varepsilon_{wi}}{i+1}$	$\varepsilon_{qy0} = \frac{\varepsilon_{qu0}}{1 + 2\varepsilon_{qu0}}$
4	$(S)_{tTc}$ $(S)_{cTt}$	$\varepsilon_{qu0} = \sum_{i=1}^{n} \frac{\varepsilon_{wi}}{i+1}$	‡

† Plastic deformation below material's recrystallization temperature.
‡ $(S_y)_{tTc} = (S_y)_{cTt} = 0.95(S_y)_{tTt}$ or $0.95(S_y)_{cTc}$
ε_{qus} = equivalent strain when prestrain sense is same as sense of strength
ε_{qu0} = equivalent strain when prestrain sense is opposite to sense of strength
SOURCE: From Datsko [33.1] and Hertzberg [33.2].

The strain-strengthening coefficient $\bar{\sigma}_0$ is, after [33.3],

$$\bar{\sigma}_0 = S_u \exp(m) m^{-m} = 92.5 \exp(0.14) 0.14^{-0.14} = 140.1 \text{ kpsi}$$

The fracture strain (true) of the hot-rolled material from the tension test is

$$\varepsilon_f = \ln \frac{1}{1 - \text{AR}} = \ln \frac{1}{1 - 0.44} = 0.58$$

which represents limiting strain in deformation free of bending (rule 2). In the first step (cold rolling), the largest strain is axial, and it has a magnitude of (rule 3)

$$\varepsilon_1 = \left| \ln \left(\frac{D_0}{D_1} \right)^2 \right| = \left| \ln \left(\frac{2.25}{2} \right)^2 \right| = 0.236$$

In the second step (upsetting), the largest strain is axial, and it has a magnitude (rule 3) of

$$\varepsilon_2 = \left| \ln \left(\frac{D_1}{D_2} \right)^2 \right| = \left| \ln \left(\frac{2}{2.5} \right)^2 \right| = |-0.446| = 0.446$$

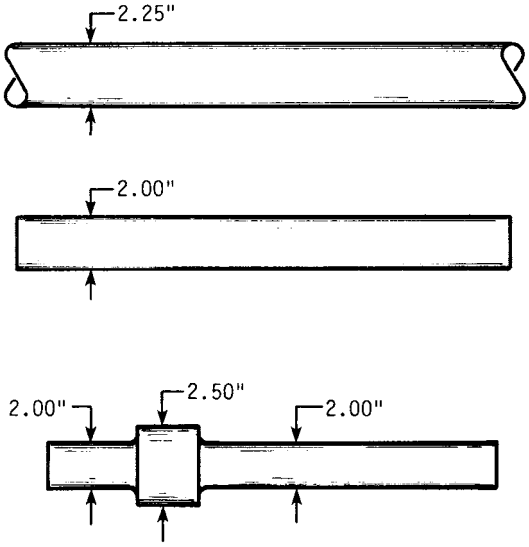

FIGURE 33.2 Cold working bar stock in two steps to form integral pinion blank on spindle.

The significant strains ε_{w1} and ε_{w2} are (rule 4) $\varepsilon_{w1} = 0.446$ and $\varepsilon_{w2} = 0.236$. Strengths will be carried with four computational digits until numerical work is done. For group 1 strengths,

$$\varepsilon_{qu} = \sum \frac{\varepsilon_{wi}}{i} = \frac{0.446}{1} + \frac{0.236}{2} = 0.564$$

$$S_u = \overline{\sigma}_0(\varepsilon_{qu})^m = 140.1(0.564)^{0.14} = 129.3 \text{ kpsi}$$

According to rule 5, $\varepsilon_{qu} > m$.

For group 2 strengths,

$$\varepsilon_{qu} = \sum \frac{\varepsilon_{wi}}{i} = \frac{0.446}{1} + \frac{0.236}{2} = 0.564$$

$$S_u = \overline{\sigma}_0(\varepsilon_{qu})^m = 140.1(0.564)^{0.14} = 129.3 \text{ kpsi}$$

For group 3 strengths,

$$\varepsilon_{qu} = \sum \frac{\varepsilon_{wi}}{1+i} = \frac{0.446}{2} + \frac{0.236}{3} = 0.302$$

$$S_u = \overline{\sigma}_0(\varepsilon_{qu})^m = 140.1(0.302)^{0.14} = 118.5 \text{ kpsi}$$

For group 4 strengths,

$$\varepsilon_{qu} = \sum \frac{\varepsilon_{wi}}{1+i} = \frac{0.446}{2} + \frac{0.236}{3} = 0.302$$

$$S_u = \overline{\sigma}_0(\varepsilon_{qu})^m = 140.1(0.302)^{0.14} = 118.5 \text{ kpsi}$$

The endurance limit and the ultimate strength resisting tensile bending stresses are $(S'_e)_{tTt}$ and $(S_u)_{tTt}$, namely, 129.3/2 = 64.7 kpsi and 129.3 kpsi, respectively (group 2 strengths). The endurance limit and the ultimate strength resisting compressive bending stresses are $(S'_e)_{cTt}$ and $(S_u)_{cTt}$, namely, 118.5/2 = 59.3 kpsi and 118.5 kpsi, respectively (group 4 strengths). In fatigue the strength resisting tensile stresses is the significant one, namely, 64.7 kpsi. A summary of this information concerning the four group ultimate strengths forms part of Table 33.2. Note that these two successive plastic strains have improved the ultimate tensile strength (which has become directional). The pertinent endurance limit has risen from 92.5/2 = 46.3 kpsi to 59.3 kpsi.

33.4 ESTIMATING YIELD STRENGTH AFTER PLASTIC STRAINS

This topic is best presented by extending the conditions of Example 1 to include the estimation of yield strengths.

Example 2. The same material as in Example 1 is doubly cold-worked as previously described. The strain-strengthening coefficient $\bar{\sigma}_0$ is still 140.1 kpsi, true fracture strain ε_f is 0.58, and $\varepsilon_1 = 0.236$, $\varepsilon_2 = 0.446$, $\varepsilon_{w1} = 0.446$, and $\varepsilon_{w2} = 0.236$ as before. For group 1 strengths,

$$\varepsilon_{qy} = \frac{\varepsilon_{qu}}{1 + 0.2\varepsilon_{qu}} = \frac{0.564}{1 + 0.2(0.564)} = 0.507$$

$$S_y = \bar{\sigma}_0(\varepsilon_{qy})^m = 140.1(0.507)^{0.14} = 127.4 \text{ kpsi} \qquad \text{(rule 6)}$$

For group 2 strengths,

$$\varepsilon_{qy} = \frac{\varepsilon_{qu}}{1 + 0.5\varepsilon_{qu}} = \frac{0.564}{1 + 0.5(0.564)} = 0.440$$

$$S_y = \bar{\sigma}_0(\varepsilon_{qy})^m = 140.1(0.440)^{0.14} = 124.9 \text{ kpsi}$$

For group 3 strengths,

$$\varepsilon_{qy} = \frac{\varepsilon_{qu}}{1 + 2\varepsilon_{qu}} = \frac{0.302}{1 + 2(0.302)} = 0.188$$

$$S_y = \bar{\sigma}_0(\varepsilon_{qy})^m = 140.1(0.188)^{0.14} = 110.9 \text{ kpsi}$$

TABLE 33.2 Summary of Ultimate and Yield Strengths for Groups 1 to 4 for Upset Pinion Blank

Group	ε_{qu}	S_u, kpsi	ε_{qy}	S_y, kpsi
1	0.564	129.3	0.507	127.4
2	0.564	129.3	0.440	124.9
3	0.302	118.5	0.188	110.9
4	0.302	118.5	. . .	118.7

THE STRENGTH OF COLD-WORKED AND HEAT-TREATED STEELS

Group 4 yield strengths are 0.95 of group 2:

$$S_y = 0.95(S_y)_2 = 0.95(124.9) = 118.7 \text{ kpsi}$$

Table 33.2 summarizes the four group strengths.

The yield strength resisting tensile bending stresses is $(S_y)_{tTt}$, a group 2 strength equaling 124.9 kpsi. The yield strength resisting compressive bending stresses is $(S_y)_{cTt}$, a group 4 strength equaling 118.7 kpsi. Yielding will commence at the weaker of the two strengths. If the bending stress level is 60 kpsi, the factor of safety against yielding is

$$\eta_y = \frac{(S_y)_{cTt}}{\sigma} = \frac{118.7}{60} = 1.98$$

If the estimate were to be based on the original material,

$$\eta_y = \frac{(S_y)_0}{\sigma} = \frac{60}{60} = 1$$

Datsko reports that predictions of properties after up to five plastic strains are reasonably accurate. For a longer sequence of different strains, Datsko's rules are approximate. They give the sense (improved or impaired) of the strength change and a prediction of variable accuracy. This is the only method of estimation we have, and if it is used cautiously, it has usefulness in preliminary design and should be checked by tests later in the design process.

33.5 ESTIMATING ULTIMATE STRENGTH OF HEAT-TREATED PLAIN CARBON STEELS

For a plain carbon steel the prediction of heat-treated properties requires that Jominy tests be carried out on the material. The addition method of Crafts and Lamont [33.4] can be used to estimate tempered-part strengths. Although the method was devised over 30 years ago, it is still the best approximation available, in either graphic or tabular form. The method uses the Jominy test, the ladle analysis, and the tempering time and temperature.

A 1040 steel has a ladle analysis as shown in Table 33.3 and a Jominy test as shown in Table 33.4. The symbol R_Q is the Jominy-test Rockwell C-scale hardness. The Jominy distance numbers are sixteenths of an inch from the end of the standard Jominy specimen. The tempered hardness after 2 hours (at 1000°F, for example) may be predicted from

$$R_T = (R_Q - D - B)f + B + \Sigma A \qquad R_T < R_Q - D \tag{33.1}$$

$$R_T = R_Q - D \qquad R_T > R_Q - D \tag{33.2}$$

TABLE 33.3 Ladle Analysis of a 1040 Steel

Element	C	Mn	P	S	Si
Percent	0.39	0.71	0.019	0.036	0.15

TABLE 33.4 Jominy Test of a 1040 Steel

Station	1	2	3	4	5	6	7	8	9	10	11	12	13	14	15	16	20	24	28	32
R_Q	55	49	29	25	25	24	23	22	21	20	19	18	17	17	16	16	14	12	11	9

where R_T = tempered hardness, Rockwell C scale
R_Q = as-quenched hardness, Rockwell C scale
D = tempering decrement, Rockwell C scale
B = critical hardness for carbon content and tempering temperature, Rockwell C scale
f = tempering factor of carbon content and tempering temperature
ΣA = sum of alloy increments, Rockwell C scale

From the appropriate figures for tempering for 2 hours at 1000°F, we have

$$D = 5.4 \quad \text{(Fig. 33.3)} \qquad A_{\text{Mn}} = 1.9 \quad \text{(Fig. 33.6)}$$

$$B = 10 \quad \text{(Fig. 33.4)} \qquad A_{\text{Si}} = 0.7 \quad \text{(Fig. 33.7)}$$

$$f = 0.34 \quad \text{(Fig. 33.5)} \qquad \overline{\Sigma A = 2.6}$$

The transition from Eq. (33.1) to Eq. (33.2) occurs at a Rockwell hardness determined by equating these two expressions:

$$(R_Q - 5.4 - 10)0.34 + 10 + 2.6 = R_Q - 5.4$$

from which R_Q = 19.3, Rockwell C scale. The softening at each station and corresponding ultimate tensile strength can be found using Eq. (33.1) or Eq. (33.2) as appropriate and converting R_T to Brinell hardness and then to tensile strength or converting directly from R_T to tensile strength. Table 33.5 displays the sequence of steps in estimating the softening due to tempering at each Jominy distance of interest.

A shaft made from this material, quenched in oil ($H = 0.35$)[†] and tempered for 2 hours at 1000°F would have surface properties that are a function of the shaft's diameter. Figures 33.8 through 33.11 express graphically and Tables 33.6 through 33.9 express numerically the equivalent Jominy distance for the surface and interior of rounds for various severities of quench. A 1-in-diameter round has a rate of cooling at the surface that is the same as at Jominy distance 5.1 (see Table 33.6). This means an as-quenched hardness of about 15.9 and a surface ultimate strength of about 105.7 kpsi. Similar determinations for other diameters in the range 0.1 to 4 in lead to the display that is Table 33.10. A table such as this is valuable to the designer and can be routinely produced by computer [33.5]. A plot of the surface ultimate strength versus diameter from this table provides the 1000°F contour shown in Fig. 33.12. An estimate of 0.2 percent yield strength at the surface can be made (after Ref. [33.4], p. 191):

$$S_y = [0.92 - 0.006(R_{\max} - R_Q)]S_u \tag{33.3}$$

[†] The quench severity H is the ratio of the film coefficient of convective heat transfer h [Btu/(h·in^2·°F)] to the thermal conductivity of the metal k [Btu/(h·in·°F)], making the units of H in $^{-1}$.

THE STRENGTH OF COLD-WORKED AND HEAT-TREATED STEELS

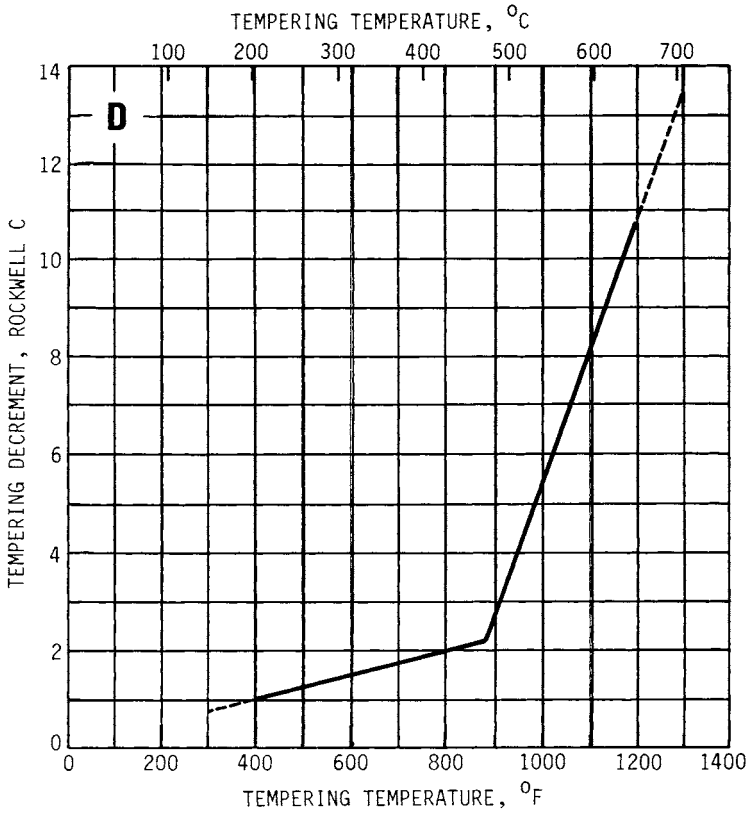

FIGURE 33.3 Hardness decrement D caused by tempering for "unhardened" steel. *(From [33.4] with permission of Pitman Publishing Ltd., London.)*

where R_{max} = maximum Rockwell C-scale hardness attainable for this steel, 32 + 60(%C), and R_Q = as-quenched hardness. An estimate of yield strength at the surface of a 1-in round of this material is as follows (equivalent Jominy distance is 5.1):

$$S_y = [0.92 - 0.006(55 - 25)]105.7 = 78.2 \text{ kpsi}$$

Different properties exist at different radii. For example, at the center of a 1-in round the properties are the same as at Jominy distance 6.6, namely, a predicted ultimate strength of 104.5 kpsi and a yield strength of 76.3 kpsi, which are not very different from surface conditions. This is not always the case.

33.6 ESTIMATING ULTIMATE STRENGTH OF HEAT-TREATED LOW-ALLOY STEELS

For heat-treated low-alloy steels, the addition method of Crafts and Lamont changes only in that additional constituents are present in the ΣA term if a Jominy test is

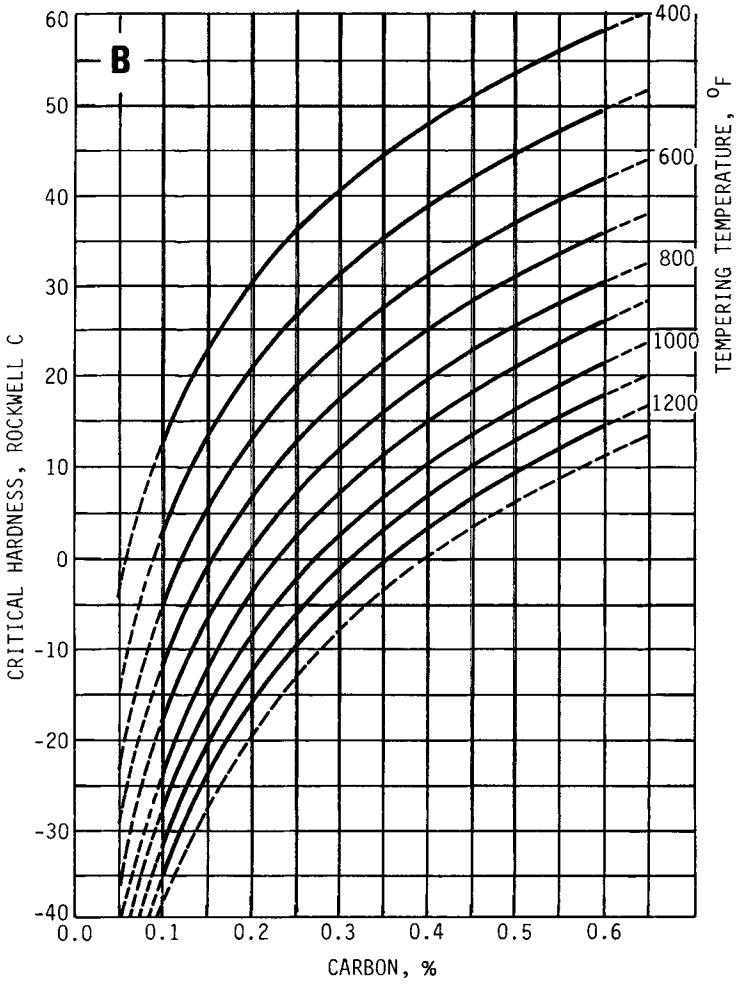

FIGURE 33.4 Critical hardness *B* for alloy-free steel as affected by carbon content and tempering temperature. *(From [33.4] with permission of Pitman Publishing Ltd., London.)*

available. However, for heat-treated low-alloy steels, the Jominy test may be replaced by an estimate based on the multiplication method of Grossmann and Fields coupled with knowledge of grain size and ladle analysis. Again, although the method was devised over 30 years ago, it is still the best approach available, in either graphic or tabular form. The multiplying factors for sulfur and phosphorus in this method are close to unity in the trace amounts of these two elements. The basic equation is

$$\begin{matrix}\text{Ideal}\\ \text{critical}\\ \text{diameter } D_I\end{matrix} = \begin{pmatrix}\text{carbon}\\ \text{ideal}\\ \text{diameter } D\end{pmatrix}\begin{pmatrix}\text{Mn}\\ \text{multiplying}\\ \text{factor}\end{pmatrix}\begin{pmatrix}\text{Cr}\\ \text{multiplying}\\ \text{factor}\end{pmatrix}\cdots$$

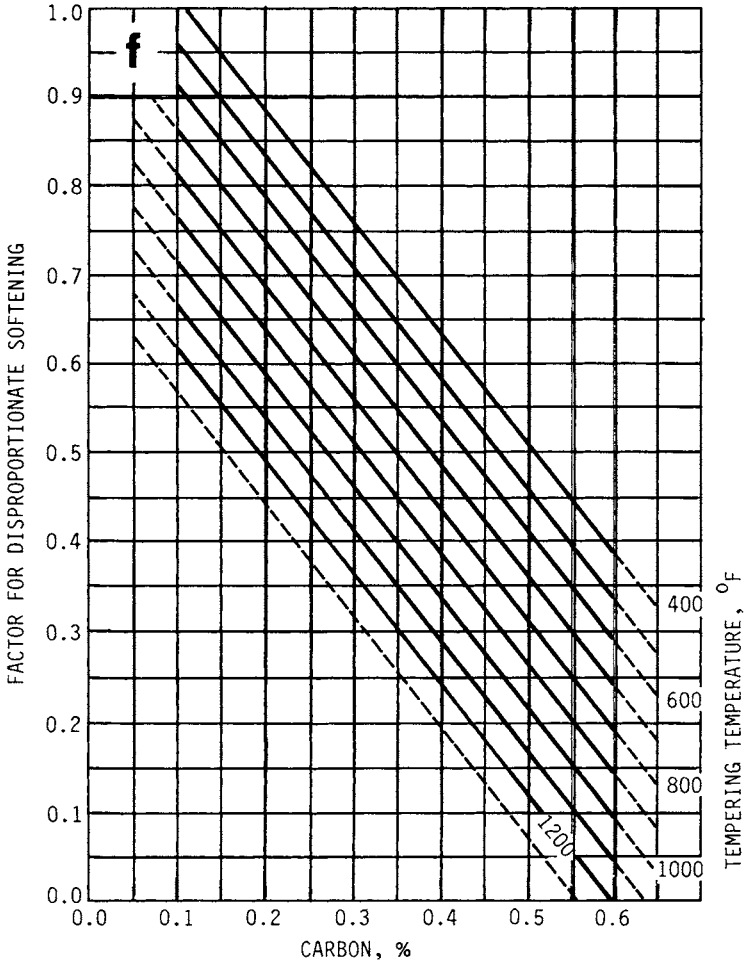

FIGURE 33.5 Factor *f* for disproportionate softening in "hardened" steel as affected by carbon content and tempering temperature. *(From [33.4] with permission of Pitman Publishing Ltd., London.)*

The multiplying factors for the elements Mn, Si, Cr, Ni, Mo, and Cu are presented in Fig. 33.13. The carbon ideal diameter D is available from Fig. 33.14 as a function of percent carbon and grain size of the steel.

Example 3. Determine the surface properties of an 8640 steel with average grain size 8 that was oil-quenched ($H = 0.35$) and tempered 2 hours at 1000°F. The ladle analysis and the multiplying factors are shown in Table 33.11. The multiplying factors are determined from Figs. 33.13 and 33.14. If boron were present, the multiplying factor would be

$$B = 17.23(\text{percent boron})^{-0.268}$$

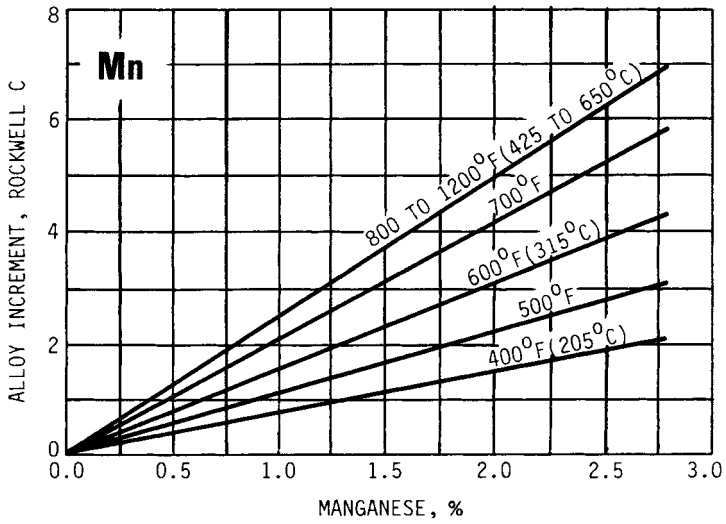

FIGURE 33.6 Effect of manganese on resistance to softening at various temperatures. *(From [33.4] with permission of Pitman Publishing Ltd., London.)*

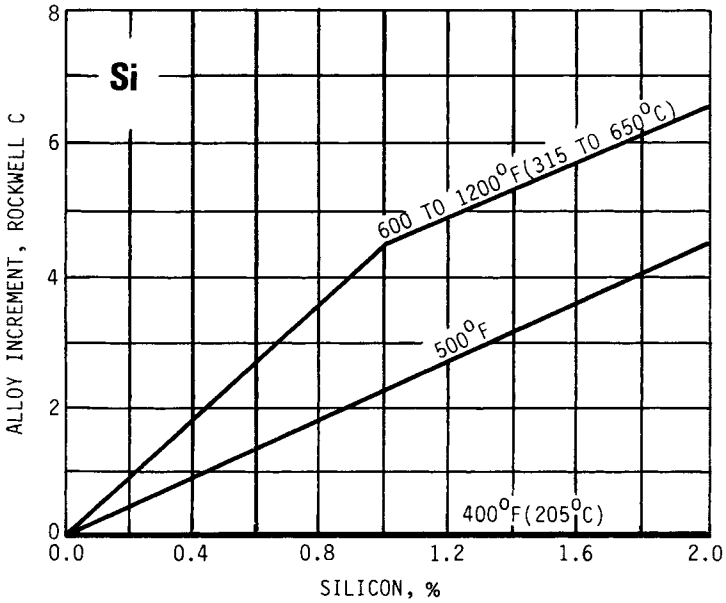

FIGURE 33.7 Effect of silicon on resistance to softening at various tempering temperatures. *(From [33.4] with permission of Pitman Publishing Ltd., London.)*

TABLE 33.5 Softening of 1040 Round Due to Tempering at 1000°F for 2 Hours

Jominy distance	R_Q	R_T	H_B	S_u, kpsi	
1	55	26.1	258.6	129.3	
2	49	24.0	247.0	123.5	
3	29	17.2	216.2	108.1	
4	25	15.9	211.6	105.8	
5	25	15.9	211.6	105.8	
6	24	15.3	209.8	104.9	
7	23	15.2	208.4	104.2	
8	22	14.8	206.6	103.3	
9	21	14.5	205.3	102.6	
10	20	14.2	203.9	102.0	←Transition
11	19	13.6	201.2	100.6	
12	18	12.6	196.7	98.4	

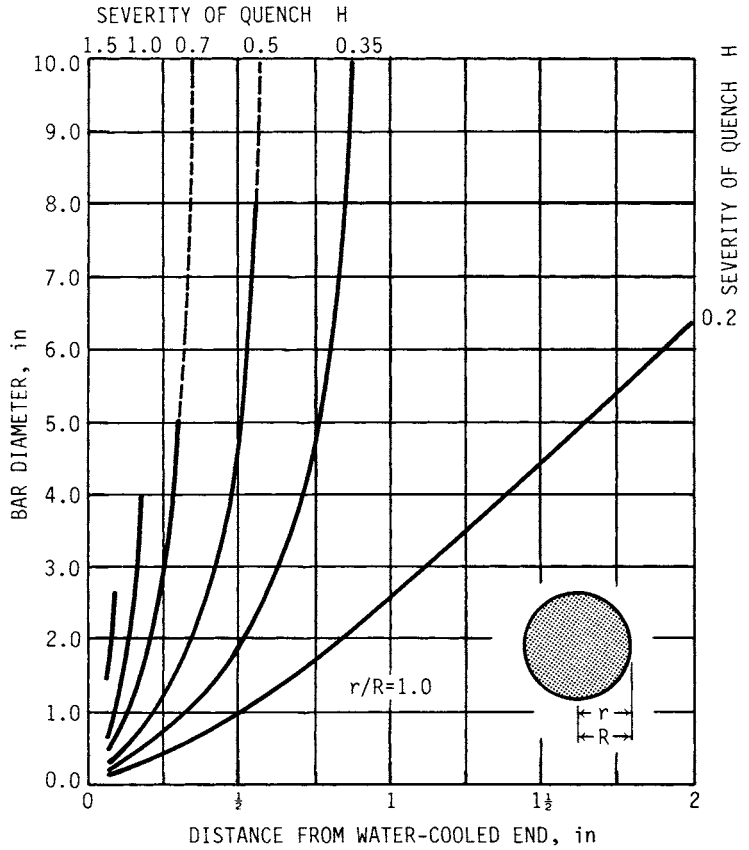

FIGURE 33.8 Location on end-quenched Jominy hardenability specimen corresponding to the surface of round bars. *(From [33.4] with permission of Pitman Publishing Ltd., London.)*

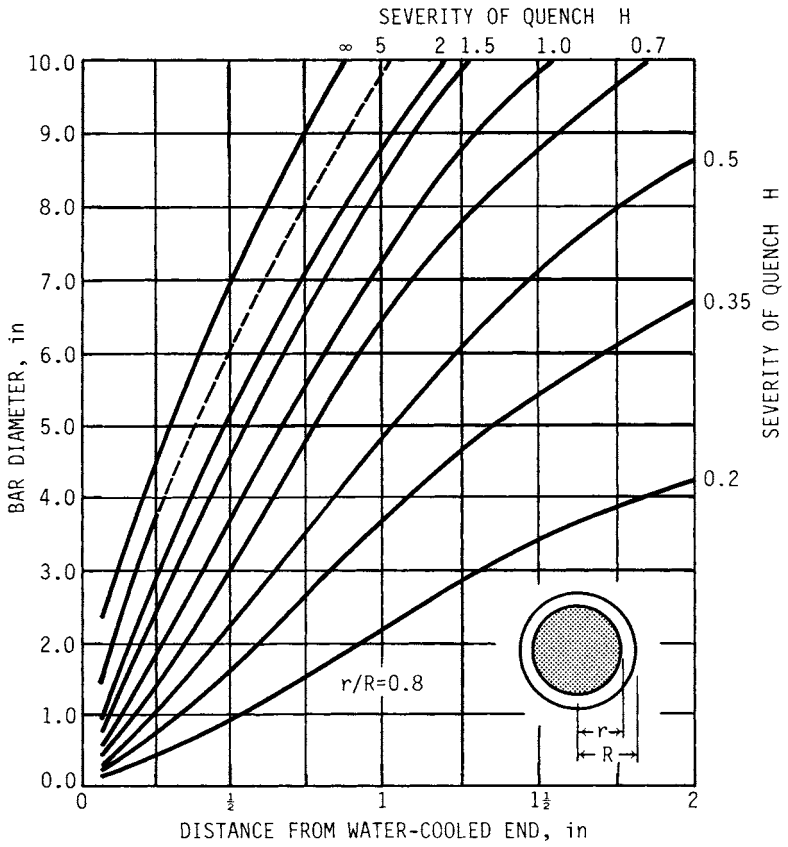

FIGURE 33.9 Location on end-quenched Jominy hardenability specimen corresponding to 80 percent from center of round. *(From [33.4] with permission of Pitman Publishing Ltd., London.)*

where percent boron is less than about 0.002. The calculation for ideal critical diameter D_I is

$$D_I = 0.197(3.98)(1.18)(2.08)(1.20)(1.60)(1.00) = 3.70 \text{ in}$$

The meaning of D_I is that it describes the largest diameter of a round that has at least 50 percent martensite structure everywhere in the cross section and exactly 50 percent at the center. The surface hardness of quenched steels is independent of alloy content and a function of carbon content alone. The Rockwell C-scale hardness is approximated by 32 + 60(%C), although it is not a strictly linear relationship ([33.4], p. 88. For the 8640 steel, the hardness at Jominy distance 1 is estimated to be 32 + 60(0.40) or 56 Rockwell C scale.

The ratio of initial hardness (distance 1), denoted IH, to distant hardness (at any other Jominy distance), denoted DH, is available as a function of the ideal critical

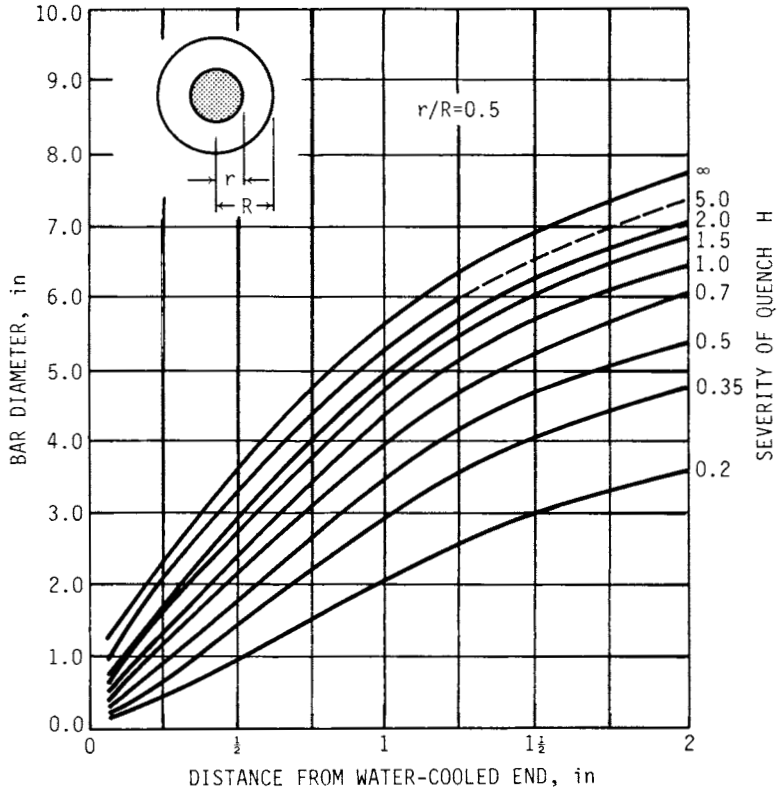

FIGURE 33.10 Location on end-quenched Jominy hardenability specimen corresponding to 50 percent from the center of round bars. *(From [33.4] with permission of Pitman Publishing Ltd., London.)*

diameter and the Jominy distance (Fig. 33.15). For the 8640 steel the Jominy hardnesses are estimated as displayed in Table 33.12. The Rockwell C-scale hardness is plotted against Jominy distance in Fig. 33.16, upper contour. The softening due to 2 hours of tempering at 1000°F can be estimated as before using the addition method of Crafts and Lamont. The ΣA term is evaluated as follows:

$D = 5.31$	(Fig. 33.3)	$A_{Mn} = 2.25$	(Fig. 33.6)
$B = 9.90$	(Fig. 33.4)	$A_{Si} = 1.13$	(Fig. 33.7)
$f = 0.34$	(Fig. 33.5)	$A_{Cr} = 2.59$	(Fig. 33.17)
		$A_{Ni} = 0.11$	(Fig. 33.18)
		$A_{Mo} = 3.60$	(Fig. 33.19)
		$\Sigma A = 9.67$	

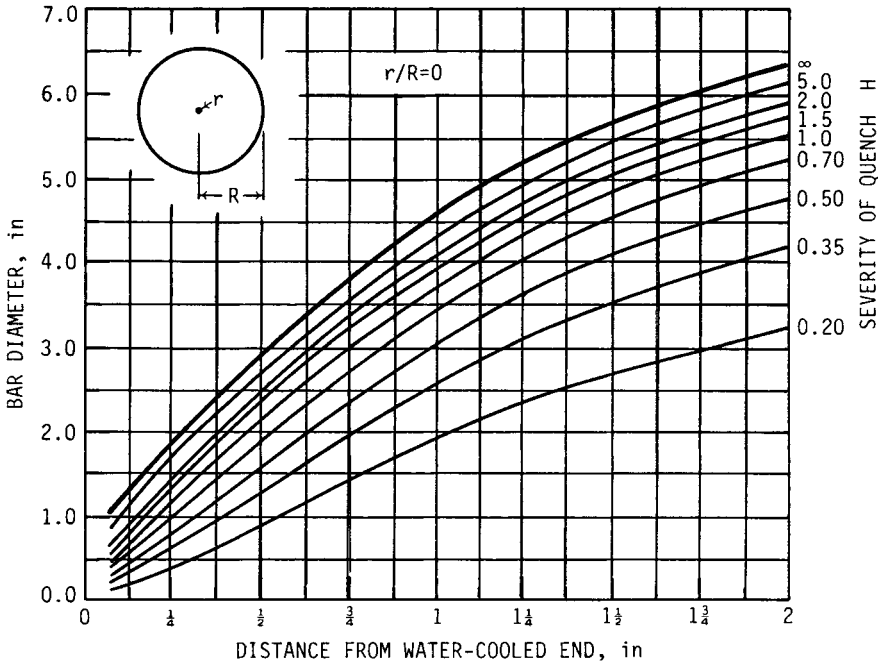

FIGURE 33.11 Location on end-quenched Jominy hardenability specimen corresponding to the center of round bars. *(From [33.4] with permission of Pitman Publishing Ltd., London.)*

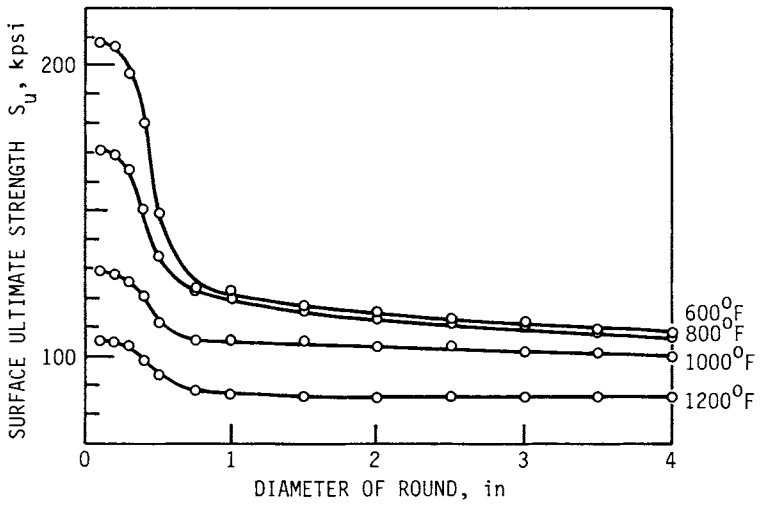

FIGURE 33.12 Variation of surface ultimate strength with diameter for a 1040 steel oil-quenched ($H = 0.35$) from 1575°F and tempered 2 hours at 1000°F.

TABLE 33.6 Equivalent Jominy Distances for Quenched Rounds at $r/R = 1$

	Severity of quench H, in^{-1}						
Diameter, in	0.20	0.30	0.35	0.40	0.50	0.60	0.70
0.1	1.0	1.0	1.0	1.0	1.0	1.0	1.0
0.2	1.8	1.3	1.1	1.0	1.0	1.0	1.0
0.3	2.7	1.9	1.6	1.4	1.2	1.0	1.0
0.4	3.6	2.5	2.2	1.9	1.5	1.2	1.0
0.5	4.5	3.2	2.7	2.3	1.9	1.5	1.2
0.75	6.7	4.8	4.0	3.5	2.9	2.2	1.7
1.0	8.3	6.0	5.1	4.4	3.5	2.7	2.2
1.5	10.7	8.0	6.9	6.0	4.6	3.5	2.8
2.0	13.2	9.6	8.2	7.1	5.4	4.2	3.3
2.5	15.4	11.0	9.2	7.8	6.1	4.6	3.7
3.0	17.6	12.1	10.0	8.4	6.6	5.0	4.0
3.5	19.8	13.1	10.7	8.9	7.0	5.4	4.3
4.0	22.1	14.2	11.4	9.4	7.6	5.7	4.5

The tempered hardness equations become either

$$R_T = (R_Q - 5.31 - 9.90)0.34 + 9.90 + 9.67$$
$$= 0.34R_Q + 14.4$$

or

$$R_T = R_Q - 5.31$$

TABLE 33.7 Equivalent Jominy Distances for Quenched Rounds at $r/R = 0.8$

	Severity of quench H, in^{-1}						
Diameter, in	0.20	0.30	0.35	0.40	0.50	0.60	0.70
0.1	1.0	1.0	1.0	1.0	1.0	1.0	1.0
0.2	1.8	1.3	1.1	1.0	1.0	1.0	1.0
0.3	2.7	1.9	1.7	1.5	1.3	1.1	1.0
0.4	3.6	2.6	2.2	2.0	1.7	1.4	1.2
0.5	4.5	3.2	2.8	2.5	2.1	1.8	1.5
0.75	6.7	4.9	4.2	3.7	3.2	2.6	2.2
1.0	8.3	6.2	5.4	4.8	4.0	3.4	3.0
1.5	11.5	8.7	7.6	6.7	5.6	4.8	4.4
2.0	14.6	10.9	9.6	8.5	7.3	6.3	5.7
2.5	17.7	13.1	11.4	10.2	8.9	7.7	7.0
3.0	21.0	15.4	13.4	11.9	10.4	9.0	8.1
3.5	24.9	18.0	15.5	13.7	12.0	10.3	9.3
4.0	29.4	21.1	18.0	15.9	13.4	11.5	10.3

TABLE 33.8 Equivalent Jominy Distances for Quenched Rounds at $r/R = 0.5$

	Severity of quench H, in^{-1}						
Diameter, in	0.20	0.30	0.35	0.40	0.50	0.60	0.70
0.1	1.0	1.0	1.0	1.0	1.0	1.0	1.0
0.2	1.8	1.3	1.2	1.1	1.0	1.0	1.0
0.3	2.7	2.0	1.8	1.6	1.4	1.2	1.0
0.4	3.6	2.7	2.4	2.1	1.8	1.6	1.4
0.5	4.5	3.4	3.0	2.6	2.3	2.0	1.1
0.75	6.7	5.0	4.4	4.0	3.4	2.9	2.6
1.0	8.3	6.4	5.7	5.2	4.5	4.0	3.5
1.5	11.9	9.2	8.3	7.5	6.7	5.9	5.4
2.0	15.4	12.0	10.8	9.8	8.9	8.0	7.3
2.5	19.3	15.0	13.4	12.2	11.1	10.1	9.3
3.0	24.2	18.4	16.3	14.8	13.6	12.3	11.5
3.5	30.3	22.4	19.6	17.7	16.2	14.7	13.8
4.0	32.0	25.9	23.5	21.6	19.1	17.3	16.4

The transition hardness obtained by equating the preceding pair of equations is $R_Q = 29.9$. The Jominy curve may be corrected for tempering. Table 33.13 shows the tempered hardness and ultimate strength corresponding to the Jominy distances. The column R_T is plotted against Jominy distance as the lower curve in Fig. 33.16. The surface ultimate strength can be estimated for diameters 0.5, 1, 2, 3, and 4 in. At a diameter of 2 in, the equivalent Jominy distance is 8.2 from Table 33.6. The surface ultimate strength as a function of diameter of round is displayed in Table 33.14. The ultimate tensile strength is found by interpolation in the prior display, entering with equivalent Jominy distance. The tensile ultimate strength at the surface versus diam-

TABLE 33.9 Equivalent Jominy Distances for Quenched Rounds at $r/R = 0$

	Severity of quench H, in^{-1}						
Diameter, in	0.20	0.30	0.35	0.40	0.50	0.60	0.70
0.1	1.0	1.0	1.0	1.0	1.0	1.0	1.0
0.2	1.8	1.5	1.4	1.2	1.0	1.0	1.0
0.3	2.7	2.2	2.0	1.9	1.5	1.3	1.2
0.4	3.6	3.0	2.7	2.5	2.0	1.8	1.6
0.5	4.5	3.7	3.4	3.1	2.6	2.2	2.0
0.75	6.7	5.6	5.1	4.6	3.8	3.3	3.0
1.0	8.3	7.1	6.6	6.1	5.1	4.5	4.1
1.5	12.4	10.3	9.5	8.7	7.7	6.9	6.4
2.0	16.7	13.5	12.3	11.4	10.2	9.2	8.6
2.5	21.8	17.2	15.5	14.2	12.9	11.7	11.0
3.0	28.1	21.6	19.3	17.5	15.8	14.4	13.6
3.5	32.0	26.2	23.9	21.9	19.2	17.3	16.5
4.0	32.0	30.9	29.7	27.9	23.0	20.6	19.9

TABLE 33.10 Surface Ultimate Strength of a 1040 Steel Heat-Treated Round as a Function of Diameter†

Diameter, in	Equivalent Jominy distance, $\frac{1}{16}$ in	Surface ultimate strength S_u, kpsi
0.1	1.0	129.3
0.2	1.1	128.7
0.3	1.6	125.8
0.4	2.2	120.4
0.5	2.7	112.7
1.0	5.1	105.7
1.5	6.9	104.3
2.0	8.2	103.2
3.0	10.0	102.0
4.0	11.4	99.7

† Round quenched from 1575°F in still oil ($H = 0.35$) tempered for 2 hours at 1000°F. Predictions by the addition method of Crafts and Lamont.

eter of round is plotted in Fig. 33.20. Note the greater hardening ability of the 8640 compared to the 1040 steel of the previous section. Local interior properties are available using Figs. 33.9, 33.10, and 33.11. An estimate of the variation of properties across the section of a round 4 in in diameter will be made. The equivalent Jominy distances are 11.2 at $r = 2$ in, 18.0 at $r = 1.6$ in, 23.5 at $r = 1$ in, and 29.7 at $r = 0$. Thus Table 33.15 may be formed. The values of S_u are obtained by interpolation; the values of S_y are estimated using Eq. (33.3). A plot is shown in Fig. 33.21.

A common source for properties of steels is *Modern Steels and Their Properties* [33.5]. It is well to note that hardness was taken in this reference at the surface of a

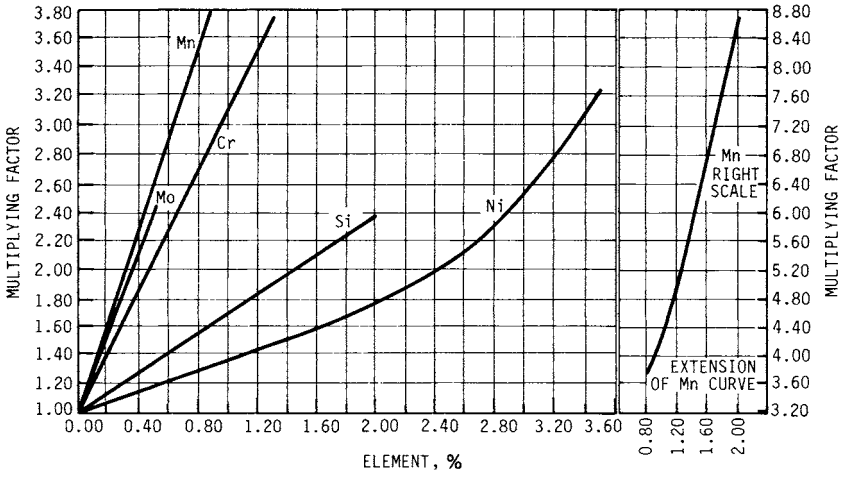

FIGURE 33.13 Multiplying factors for five common alloying elements (for trace copper, use nickel curve). *(From [33.4] with permission of Pitman Publishing Ltd., London).*

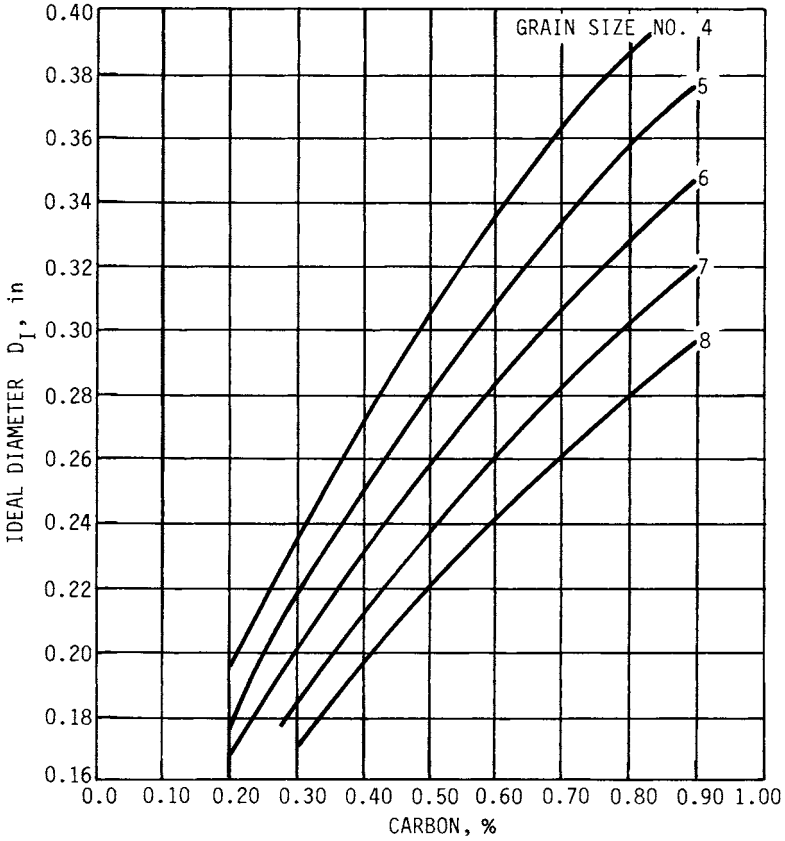

FIGURE 33.14 Relationship between ideal diameter D_I, carbon content, and grain size. *(From [33.4] with permission of Pitman Publishing Ltd., London.)*

TABLE 33.11 Ladle Analysis and Multiplying Factors for 8640 Steel, Grain Size 8

Element	C	Mn	Si	Cr	Ni	Mo	Cu
Percent	0.40	0.90	0.25	0.50	0.55	0.20	0.00
Factor	0.197	3.98	1.18	2.08	1.20	1.60	1.00

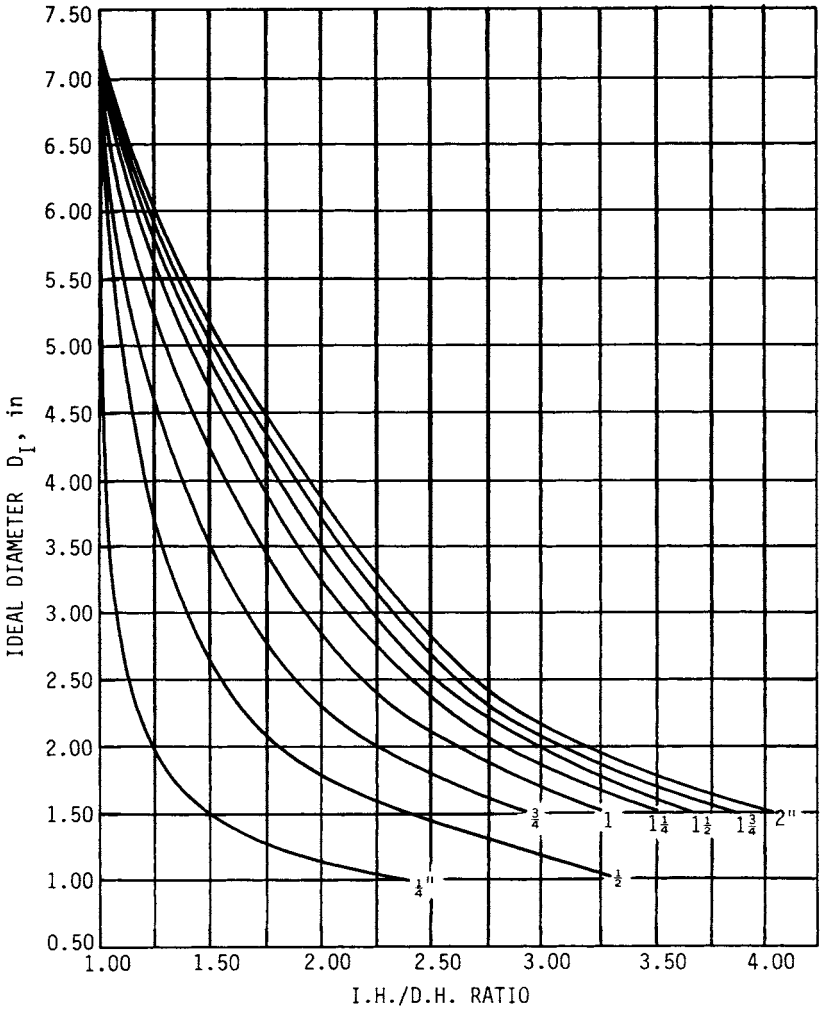

FIGURE 33.15 Relation between ideal critical diameter and the ratio of initial hardness IH to distant hardness DH. *(From [33.4] with permission of Pitman Publishing Ltd., London.)*

1-in-diameter quenched and tempered bar, and that the tensile specimen was taken from the center of that bar for plain carbon steels. Alloy-steel quenched and tempered bars were 0.532 in in diameter machined to a standard 0.505-in-diameter specimen. From the traverse of strengths in the previous array, it is clear that central and surface properties differ. In addition, the designer needs to know the properties of the critical location in the geometry and at condition of use. Methods of estimation such as the Crafts and Lamont addition method and the Grossmann and Fields multiplication method are useful prior to or in the absence of tests on the machine part.

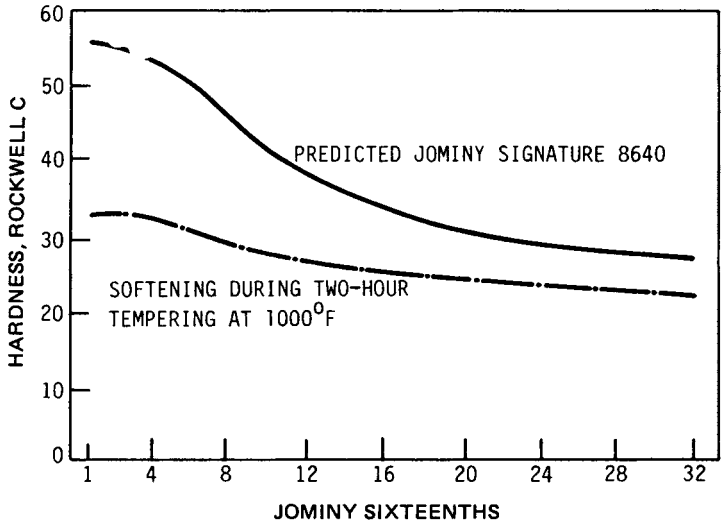

FIGURE 33.16 Predicted Jominy signature for a 8640 steel with softening produced by 2-hour tempering at 1000°F.

These methods have produced for a 4-in round of 8640, quenched in oil ($H = 0.35$) from 1575°F, and tempered for 2 hours at 1000°F, the property estimates displayed as Table 33.16. Reference [33.6] is a circular slide rule implementation of the multiplication method of Grossmann and Fields.

Current efforts are directed toward refining the information rather than displacing the ideas upon which Secs. 33.5 and 33.6 are based ([33.7], [33.8]). Probabilistic elements of the predicted Jominy curve are addressed in Ho [33.9].

TABLE 33.12 Prediction of Jominy Curve for 8640 Steel by Multiplication Method of Grossmann and Fields

Jominy distance	$\frac{IH}{DH}$	$R_Q = \frac{IH}{(IH/DH)}$
1	1.00	56.0
4	1.03	54.3
8	1.24	45.0
12	1.46	38.4
16	1.67	33.6
20	1.82	30.7
24	1.92	29.2
28	2.00	28.0
32	2.04	24.7

THE STRENGTH OF COLD-WORKED AND HEAT-TREATED STEELS

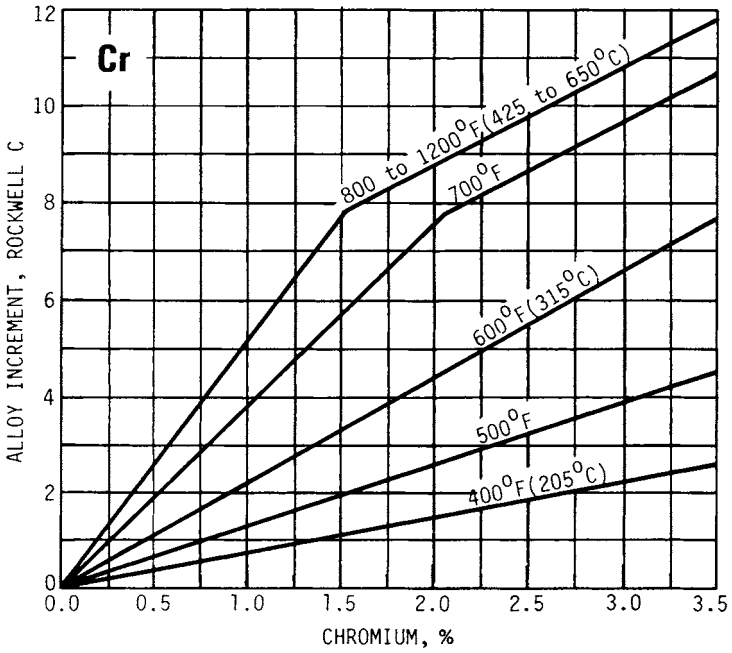

FIGURE 33.17 Effect of chromium on resistance to softening at various tempering temperatures. *(From [33.4] with permission of Pitman Publishing Ltd., London.)*

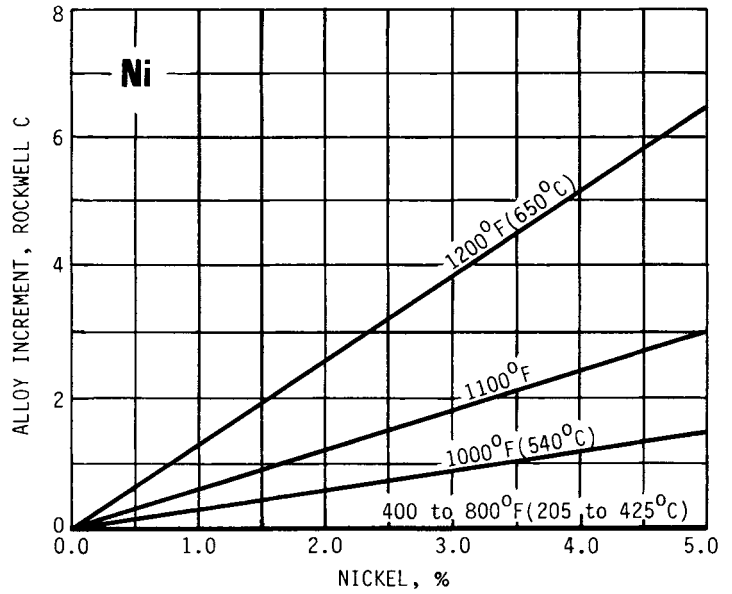

FIGURE 33.18 Effect of nickel on resistance to softening at various tempering temperatures. *(From [33.4] with permission of Pitman Publishing Ltd., London.)*

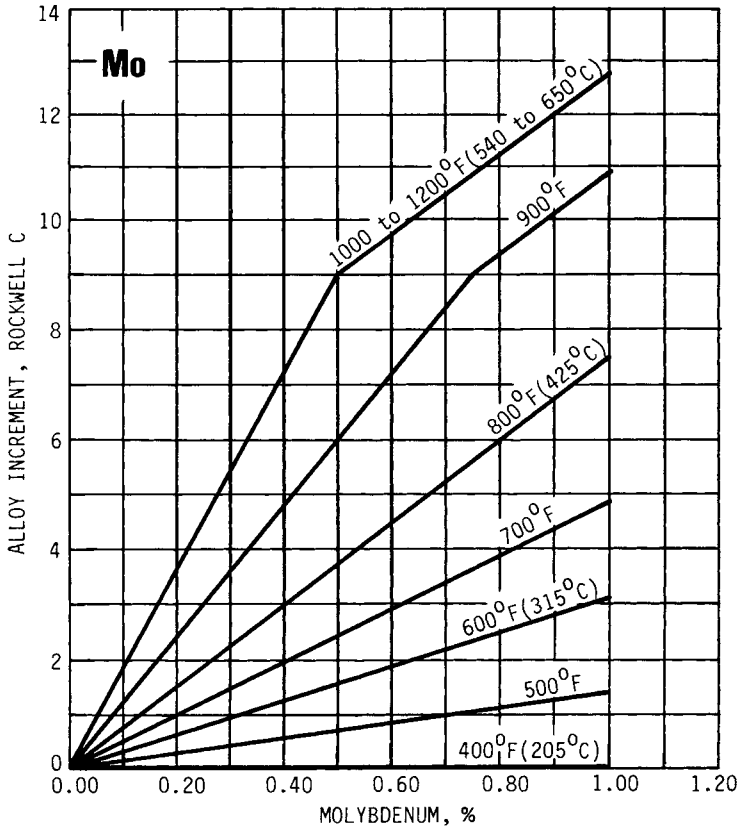

FIGURE 33.19 Effect of molybdenum on resistance to softening at various tempering temperatures. *(From [33.4] with permission of Pitman Publishing Ltd., London.)*

TABLE 33.13 Tempered Hardness and Ultimate Strength at Jominy Distances Due to Softening after Tempering 8640 Steel 2 Hours at 1000°F

Distance	R_Q	R_T	H_B	S_u, kpsi
1	56.0	33.4	314.2	157.1
4	54.3	32.9	310.2	155.1
8	45.0	29.7	283.9	142.0
12	38.4	27.5	267.5	133.8
16	33.6	25.8	257.0	128.5
20	30.7	24.8	252.4	126.2
				←Transition
24	29.2	23.9	246.6	123.3
28	28.0	22.7	241.2	120.6
32	27.4	22.1	237.6	118.8

TABLE 33.14 Surface Ultimate Strength of 8640 Steel Tempered for 2 Hours at 1000°F as a Function of Diameter of Round

Diameter, in	Equivalent Jominy distance, $\frac{1}{16}$ in	S_u, kpsi
0.5	2.7	156.0
1	5.1	151.5
2	8.2	141.6
3	10.0	137.3
4	11.4	135.0

TABLE 33.15 Ultimate and Yield Strength Traverse of a 4-in-Diameter Round of 8640 Steel Tempered 2 Hours at 1000°

Location r, in	Equivalent Jominy distance, $\frac{1}{16}$ in	S_u, kpsi	S_y, kpsi
2	11.4	135.0	110.8
1.6	18.0	127.4	99.0
1	23.5	123.7	94.1
0	29.7	119.8	89.9

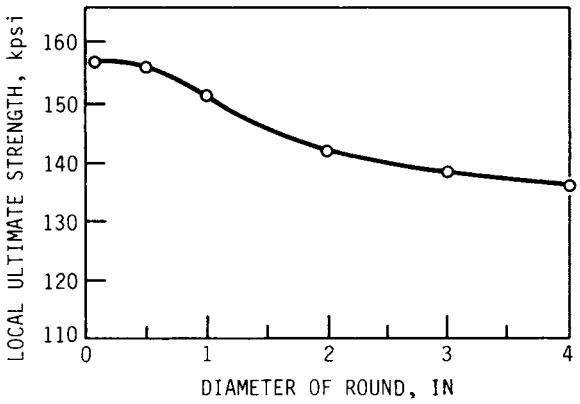

FIGURE 33.20 Variation on surface ultimate strength for 8640 steel oil-quenched (H = 0.35) from 1575°F and tempered for 2 hours at 1000°F as a function of diameter of round.

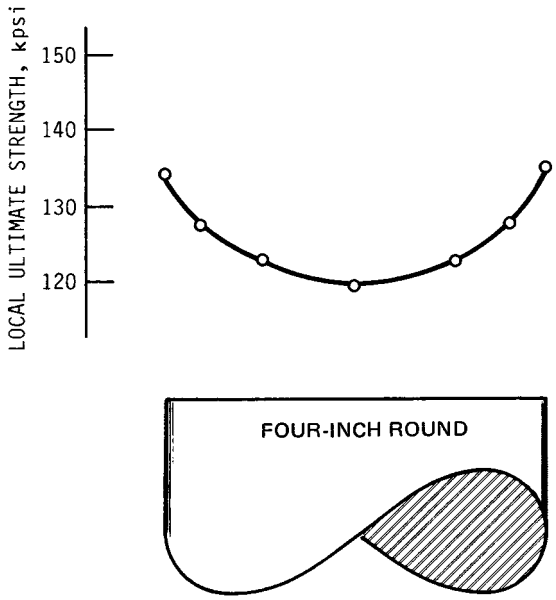

FIGURE 33.21 Variation in surface ultimate strength across a section of a 4-in round of 8640 steel oil-quenched ($H = 0.35$) from 1575°F and tempered for 2 hours at 1000°F as a function of radial position.

TABLE 33.16 Summary of Strength and Hardness Estimates for a 4-in Round of 8640 Steel Quenched in Oil ($H = 0.35$) from 1575°F and Tempered 2 Hours at 1000°F

Property	Estimate
Surface hardness	270 Brinell
Surface ultimate strength	135 kpsi
Surface yield strength	110.8 kpsi
Surface R. R. Moore endurance limit	67.5 kpsi
Contact endurance strength ($0.4H_B - 10$)	98 kpsi†
Central hardness	239.6 Brinell
Central ultimate strength	119.8 kpsi
Central yield strength	89.9 kpsi

† 10^8 cycles.

THE STRENGTH OF COLD-WORKED AND HEAT-TREATED STEELS

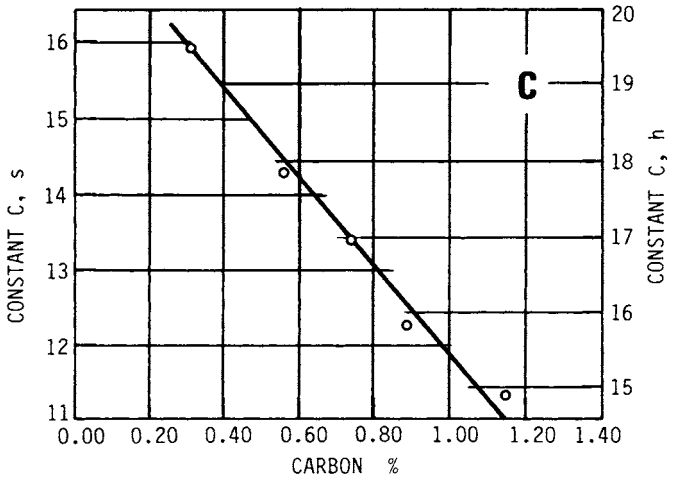

FIGURE 33.22 Variation with carbon content of constant C in time-temperature tradeoff equation for tempered, fully quenched plain carbon steels. *(From [33.4] with permission of Pitman Publishing Ltd., London.)*

33.7 TEMPERING TIME AND TEMPERATURE TRADEOFF RELATION

The tempering-temperature/time tradeoff equation is

$$(459 + F_1)(C + \log_{10} t_1) = (459 + F_2)(C + \log_{10} t_2) \tag{33.4}$$

where C is a function of carbon content determinable from Fig. 33.22. For 8640 steel, the value of C is 18.85 when the time is measured in hours. For a tempering temperature of 975°F, the tempering time is

$$(459 + 1000)(18.85 + \log_{10} 2) = (459 + 975)(18.85 + \log_{10} t_2)$$

from which $t_2 = 4.3$ h.

Since steel is bought in quantities for manufacturing purposes and the heat from which it came is identified as well as the ladle analysis, once such an estimation of properties procedure is carried out, the results are applicable for as long as the material is used. It is useful to employ a worksheet and display the results. Such a sheet is depicted in Fig. 33.23.

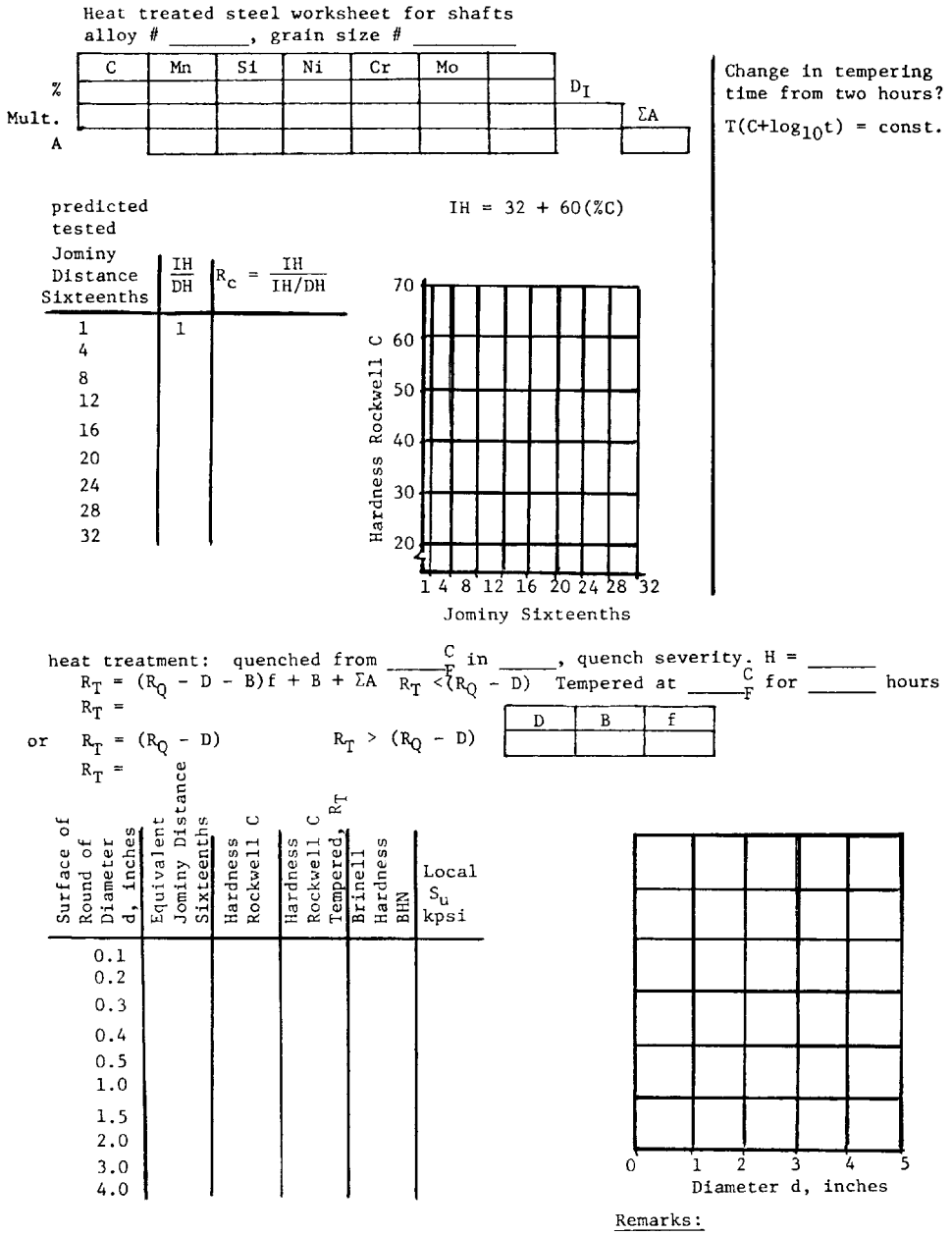

FIGURE 33.23 Heat-treated-steel worksheet for shafts.

THE STRENGTH OF COLD-WORKED AND HEAT-TREATED STEELS

REFERENCES

33.1 J. Datsko, *Materials in Design and Manufacturing,* published by the author, Ann Arbor, Mich., 1977.

33.2 M. P. Borden, "Multidimensional Tensile Properties of Materials Subjected to Large Cyclic Strains," Ph.D. thesis, University of Michigan, Ann Arbor, 1975.

33.3 R. W. Hertzberg, *Deformation and Fracture Mechanics of Engineering Materials,* John Wiley & Sons, New York, 1976.

33.4 W. Crafts and J. L. Lamont, *Hardenability and Steel Selection,* Pitman & Sons, London, 1949.

33.5 *Modern Steels and Their Properties,* Bethlehem Steel Corporation, 1972.

33.6 *Bethlehem Alloy Steel Hardenability Calculator, Calc 96,* Bethlehem Steel Corporation, 1966.

33.7 D. V. Doane and J. J. Kirkaldy (eds.), *Hardenability Concepts with Applications to Steel,* American Institute of Mining, Metallurgical and Petroleum Engineers, Warrendale, Pa., 1978.

33.8 C. A. Siebert, D. V. Doane, and D. H. Breen, *The Hardenability of Steels,* American Society for Metals, Metals Park, Ohio, 1977.

33.9 T. K. Ho, "Probabilistic Prediction of the Jominy Curve of Low Alloy Steels from Composition and Grain Size," Ph.D. thesis, Iowa State University, Ames, 1978.

RECOMMENDED READING

C. S. Brady and H. R. Clauser, *Metals Handbook,* 11th ed., McGraw-Hill, New York, 1977.

E. A. Brandes (ed.), *Smithells Metal Reference Book,* 6th ed., Butterworths, London, 1983.

C. R. Brooks, *Heat Treatment, Structure and Properties of Non Ferrous Alloys,* American Society for Metals, Metals Park, Ohio, 1982.

P. Harvey (ed.), *Engineering Properties of Steel,* American Society for Metals, Metals Park, Ohio, 1982.

G. Krauss, *Principles of Heat Treatment of Steel,* American Society for Metals, Metals Park, Ohio, 1980.

Metals Handbook, 9th ed., Vol. 1: *Properties and Selection: Irons and Steels;* Vol. 4: *Heat Treating,* American Society for Metals, Metals Park, Ohio, 1981.

CHAPTER 34
WEAR

Kenneth C. Ludema
Professor of Mechanical Engineering
Department of Mechanical Engineering and Applied Mechanics
The University of Michigan
Ann Arbor, Michigan

There is no shorthand method of designing machinery for a specified wear life. Thus a step-by-step method is given for designers to follow. The method begins with an examination of worn parts of the type to be improved. The next step is an estimate of stresses, temperatures, and likely conditions of operation of the redesigned machinery. Material testing for wear resistance is discussed, and finally, a procedure is given for selecting materials for wear resistance.

34.1 GENERAL PRINCIPLES IN DESIGN FOR WEAR RESISTANCE

The wear life of mechanical components is affected by nearly as many variables as human life. Wearing surfaces are composed of substrate material, oxide, absorbed gas, and dirt. They respond to their environment, method of manufacture, and conditions of operation. They suffer acute and/or progressive degeneration, and they can often be partially rehabilitated by either a change in operating conditions or some intrusive action.

The range of wearing components and devices is endless, including animal teeth and joints, cams, piston rings, tires, roads, brakes, dirt seals, liquid seals, gas seals, belts, floors, shoes, fabrics, electrical contacts, disks and tapes, tape heads, printer heads, tractor tracks, cannon barrels, rolling mills, dies, sheet products, forgings, ore crushers, conveyors, nuclear machinery, home appliances, sleeve bearings, rolling-element bearings, door hinges, zippers, drills, saws, razor blades, pump impellers, valve seats, pipe bends, stirring paddles, plastic molding screws and dies, and erasers. There is not a single universal approach to designing all these components for an acceptable wear life, but there are some rational design steps for some. There are no

equations, handbooks, or material lists of broad use, but there are guidelines for some cases. Several will be given in this section.

34.1.1 Types, Appearances, and Mechanisms of Wear

Wear is a loss or redistribution of surface material from its intended location by definition of the ASTM. Using this definition, we could develop a simple explanation for wear as occurring either by chemical reaction (that is, corrosion), by melting, or by mechanical straining. Thus to resist wear, a material should be selected to resist the preceding individual causes of wear or else the environment should be changed to reduce surface stress, temperature, or corrosiveness.

The preceding three natural processes are too broad to be useful for material selection in light of the known properties of materials. A more detailed list of material properties appropriate to the topic of wear is given in Table 34.1.

The preceding methods of material removal are usually not classified among the "mechanisms" of wear. Usually a *mechanism* is defined as a fundamental cause. Thus a fundamental argument might be that wear would not occur if there were no contact. If this were so, then mere contact could be called a mechanism of wear. However, if we define a *mechanism* as that which is capable of explanation by the laws of physics, chemistry, and derivative sciences, then mere contact becomes a statement of the condition in which surfaces exist and not a mechanism. But if stresses, lattice order, hydrogen-ion concentration, fugacity, or index of refraction were known, *and if* the effect of these variables on the wear rate were known, then a mechanism of wear has been given. Most terms used to describe wear therefore do not suggest a mechanism. Rather, most terms describe the condition under which wearing occurs or they describe the appearance of a worn surface. Terms of the former type include dry wear, metal-to-metal wear, hot wear, frictional wear, mechanical wear, and impact wear. Closer observation may elicit descriptions such as erosion, smooth

TABLE 34.1 Material Properties Involved in Wear

Chemical action
1. Chemical dissolution
2. Oxidation (corrosion, etc.)
Mechanical straining
3. Brittle fracture (as in spalling; see below)
4. Ductile deformation: a. To less than fracture strain (as in indentation) b. To fracture (as in cutting, galling, transfer, etc.)
5. High-cycle fatigue (as occurs in rolling contacts)
6. Low-cycle fatigue (as in scuffing, dry wear, etc.)
7. Melting

SOURCE: From Ludema [34.2].

wear, polishing wear, cavitation, corrosive wear, false brinelling, friction oxidation, chafing fatigue, fretting, and chemical wear. Still closer observation may reveal spalling, fatigue wear, pitting corrosion, delamination, cutting wear, deformation wear, gouging wear, galling, milling wear, plowing wear, scratching, scouring, and abrasion. The latter is often subdivided into two-body or three-body abrasion and low-stress or high-stress abrasion. Finally, some of the terms that come from the literature on "lubricated" wear include scuffing, scoring, and seizure. Most of these terms have specific meanings in particular products and in particular industries, but few find wide use.

Valiant attempts are continuously being made to define wear terms in the professional societies, but progress is slow. Researchers have attempted to classify most of the terms as either abrasive or adhesive mechanisms primarily, with a few terms classified as a fatigue mechanism. It is interesting that adhesiveness or abrasiveness is not often proven in real problems. Rather, a given wear process is simply modeled as abrasive *or* adhesive and often considered as exclusively so. Some authors attempt to escape such categories by separating wear into the mild and severe categories, which introduces value judgments on wear rates not inherently found in the other terms. Mechanisms of wear will be discussed at greater length below.

34.1.2 Design Philosophy

Most wearing surfaces are redesigned rather than designed for the first time. Thus designers will usually have access to people who have experience with previous products. Designing a product for the first time requires very mature skills, not only in materials and manufacturing methods, but also in design philosophy for a particular product.

The philosophy by which wear resistance or wear life of a product is chosen may differ strongly within and between various segments of industry. Such considerations as acceptable modes of failure, product repair, controllability of environment, product cost, nature of product users, and the interaction between these factors receive different treatment for different products. For example, since automobile tires are easier to change than is an engine crankshaft, the wear life of tires is not a factor in discussions of vehicle life. The opposite philosophy must apply to drilling bits used in the oil-well industry. The cone teeth and the bearing upon which the cone rotates must be designed for equal life, since both are equally inaccessible while wearing.

In some products or machines, function is far more important than manufacturing costs. One example is the sliding elements in nuclear reactors. The temperature environment of the nuclear reactor is moderate, lubricants are not permitted, and the result of wear is exceedingly detrimental to the function of the system. Thus expensive metal-ceramic coatings are frequently used. This is an example of a highly specified combination of materials and wearing conditions. Perhaps a more complex example is that of artificial teeth. The surrounding system is very adaptable, a high cost is relatively acceptable, but durability may be strongly influenced by body chemistry and choice of food, all beyond the range of influence by the designers.

Thus there is no general rule whereby designers can quickly proceed to select a wear-resisting material for a product. One often heard but misleading simple method of reducing wear is to increase the hardness of the material. There are, unfortunately, too many exceptions to this rule to have high confidence in it except for some narrowly defined wearing systems. One obvious exception is the case of

bronzes, which are more successful as a gear material against a hardened-steel pinion than is a hardened-steel gear. The reason usually given for the success of bronze is that dirt particles are readily embedded into the bronze and therefore do not cut or wear the steel away, but this is more of an intuitive argument than fact. Another exception to the hardness rule is the cams in automotive engines. They are hardened in the range of 50 Rockwell C instead of to the maximum available, which may be as high as 67 R_C. A final example is that of buckets and chutes for handling some ores. Rubber is sometimes found to be superior to very hard white cast iron in these applications.

We see in the preceding examples the possibility of special circumstances requiring special materials. The rubber offers resilience, and the cam material resists fatigue failure if it is not fully hardened. It is often argued that special circumstances are rare or can be dealt with on a case-by-case basis. This attitude seems to imply that most wearing systems are "standard," thus giving impetus to specifying a basic wear resistance of a material as one of its intrinsic properties. Little real progress has been made in this effort, and very little is likely to be made in the near future. Wear resistance is achieved by a balance of several very separate properties, not all of them intrinsic, that are different for each machine component or wear surface. Selecting material for wear resistance is therefore a complex task, and guidelines are needed in design. Such guidelines will be more useful as our technology becomes more complex, but some guidelines are given in the next section.

34.2 STEPS IN DESIGN FOR WEAR LIFE WITHOUT SELECTING MATERIALS

34.2.1 The Search for Standard Components

Designers make most of the decisions concerning material selection. Fortunately, for many cases and for most designers, the crucial components in a machine in which wear may limit useful machine life are available as separate packages with fairly well specified performance capabilities. Examples are gear boxes, clutches, and bearings. Most such components have been well tested in the marketplace, having been designed and developed by very experienced designers. For component designers, very general rules for selecting materials are of little value. They must build devices with a predicted wear life of ±10 percent accuracy or better. They know the range of capability of lubricants, they know the reasonable range of temperature in which their products will survive, and they know how to classify shock loads and other real operating conditions. Their specific expertise is not available to the general designer except in the form of the shapes and dimensions of hardware, the materials selected, and the recommended practices for use of their product. Some of these selections are based on tradition, and some are based on reasoning, strongly tempered by experience. The makers of specialized components usually also have the facilities to test new designs and materials extensively before risking their product in real use. General designers, however, must often proceed without extensive testing.

General designers must then decide whether to avail themselves of standard specialized components or to risk designing every part. Sometimes the choice is based on economics, and sometimes desired standard components are not available. In such cases, components as well as other machine parts must be designed in-house.

34.2.2 In-House Design

If a designer is required to design for wear resistance, it is logical to follow the methods used in parallel activities, such as in determining the strength and vibration characteristics of new machinery. This is often done by interpolating within or extrapolating beyond experience, if any, using

1. Company practice for similar items
2. Vendors of materials, lubricants, and components
3. Handbooks

Company Practice. If good information is available on similar items, a prediction of the wear life of a new product can be made with ± 20 percent accuracy unless the operating conditions of the new design are much beyond standard experience. Simple scaling of sizes and loads is often successful, but usually this technique fails after a few iterations. Careless comparison of a new design with "similar" existing items can produce very large errors for reasons discussed below.

When a new product must be designed that involves loads, stresses, or speeds beyond those previously experienced, it is often helpful to examine the worn surface of a well-used previous model in detail. It is also helpful to examine unsuccessful prototypes or wear-test specimens, as will be discussed below. An assessment should be made of the modes or mechanisms of wear of each part of the product. For this purpose, it is also useful to examine old lubricants, the contents of the lubricant sump, and other accumulations of residue.

Vendors of Materials. Where a new product requires bearings or materials of higher capacity than now in use, it is frequently helpful to contact vendors of such products. When a vendor simply suggests an existing item or material, the wear life of a new product may not be predictable to an accuracy of better than ± 50 percent of the desired life. This accuracy is worse than the ± 20 percent accuracy given earlier, especially where there is inadequate communication between the designer and the vendor. Accuracy may be improved where an interested vendor carefully assesses the needs of a design, supplies a sample for testing, and follows the design activity to the end.

Contact with vendors, incidentally, often has a general beneficial effect. It encourages designers to revise their thinking beyond the logical projection of their own experience. Most designers need a steady flow of information from vendors to remain informed on both the new products and the changing capability of products.

Handbooks. There are very few handbooks on selecting materials for wear resistance. Materials and design handbooks usually provide lists of materials, some of which are highlighted as having been successfully used in wearing parts of various products. They usually provide little information on the rates of wear of products, the mode of wear failure, the limits on operating conditions, or the method by which the wear-resisting parts should be manufactured or run in (if necessary).

Some sources will give wear coefficients, which are purported to be figures of merit, or rank placing of materials for wear resistance. A major limitation of wear coefficients of materials as given in most literature is that there is seldom adequate information given on how the data were obtained. Usually this information is taken from standard laboratory bench tests, few of which simulate real systems. The final result of the use of handbook data is a design which will probably not perform to an accuracy of better than ±95 percent.

34.3 WEAR EQUATIONS

There is a great need for wear equations. Ideally, a wear equation would provide a numerical value for material loss or transfer for a wide range of materials and operating conditions of the wearing parts.

Useful equations derived from fundamental principles are not yet available. Some empirical equations are available for very special conditions. The strictly empirical equations usually contain very few variables and are of the form

$$VT^n = f^a d^b K \tag{34.1}$$

which applies to metal cutting, and in which V = cutting speed, T = tool life, f = feed rate, and d = depth of cut. Experiments are done, measuring T over a range of f while holding V and d fixed at some arbitrary values, from which a can be obtained. The experiments are repeated over ranges of d and V to obtain b and K. It is generally assumed that the results will not depend on the selection of the variables to hold constant, which therefore assumes that there is neither any limit to the range of valid variables nor any interdependence between variables, which ultimately means that there is no change of wearing mechanisms over any chosen range of the variables. Wear equations built by strictly empirical methods are therefore seen to be limited to the case under present study; they have limited ability to predict conditions beyond those of the tests from which they were derived, and they have little applicability to other sliding systems.

A common method of building equations from fundamental principles is to assume that wearing will take place in direct proportion to the real (microscopic) contact area. These equations omit such important considerations as the presence of oxides and adsorbed gases on surfaces, and few of them recognize the role of repeated contact on sliding surfaces, which may lead to fatigue modes of material loss (wear).

In a recent study [34.1], over 180 wear equations were analyzed as to content and form. Though the authors collectively cited over 100 variables to use in these equations, few authors cited more than 5. The fact, then, that quantities such as hardness are found in the numerator of some equations and in the denominator of others leads to some confusion. Overall, no way was found to harmonize any selected group of equations, nor was there any way to determine which material properties are important to the wearing properties.

The parameters that may be included in the equation are of three types, as listed in Table 34.2. It may be readily seen from Table 34.2 that many of the parameters are difficult to quantify, and yet these (and perhaps several more) are known to affect the wear rate. Further complexity is added in cases where wear mechanisms, and therefore wear rates, change with time of sliding.

This state of affairs seems incomprehensible to designers who are steeped in mathematical methods that promise precise results. To use a specific example: For calculating the deflections of beams, simple equations are available that require only one material property, namely, Young's modulus. All other quantities in these equations are very specific; that is, they are measured in dimensions which not only seem available in four or five significant figures, but have compatible units.

Wear is far more complex, involving up to seven basic mechanisms that are operative in different balances or ratios under various conditions. Moreover, many of the mechanisms produce wear rates that are not linear in the simple parameters, such as applied load, sliding speed, surface finish, etc. Thus, in summary, there are at this time

TABLE 34.2 Parameters Often Seen in Wear Equations

a. Operational parameters
1. Surface topography
2. Contact geometry
3. Applied load
4. Slide/role speed
5. Coefficient of friction
6. Etc.
b. Material parameters
1. Hardness, cold and hot
2. Ductility
3. Fracture toughness
4. Strength
5. Work hardenability
6. Elastic moduli
7. Material morphology
8. Type and thickness of surface film
9. Thermal properties
10. Etc.
c. Environmental parameters
1. Type and amount of lubricant
2. Type and amount of dirt and debris
3. Rigidity of supporting structure
4. Ambient temperature
5. Multiple pass of continuous contact
6. Continuous, stop-start, reciprocating
7. Clearance, alignment, and fit
8. Matched or dissimilar material pair
9. Etc.

SOURCE: From Ludema [34.2].

no complete first principles or models available to use in selecting materials for wear resistance. However, there are good procedures to follow in selecting materials for wear resistance.

34.4 STEPS IN SELECTING MATERIALS FOR WEAR RESISTANCE

When designing for wear resistance, it is necessary to ascertain that wear will proceed by the same mechanism throughout the substantial portion of the life of the product. Only then is some reasonable prediction of life possible.

Certain considerations are vital in selecting materials, and these may be more important than selecting a material for the best wear resistance. These considerations are

1. The restriction on material use
2. Whether the sliding surface can withstand the expected static load
3. Whether the materials can withstand the sliding severity
4. Whether a break-in procedure is necessary or prohibited
5. The acceptable modes of wear failure or surface damage
6. The possibility of testing candidate materials in bench tests or in prototype machines

These considerations are discussed in detail in the next several pages.

34.4.1 Restrictions on Material Use

The first step in selecting materials for wear resistance is to determine whether there are any restrictions on material use. In some industries it is necessary for economic and other purposes to use, for example, a gray cast iron, or a material that is compatible with the human body, or a material with no cobalt in it such as is required in a nuclear reactor, or a material with high friction, or a selected surface treatment applied to a low-cost substrate. Furthermore, there may be a limitation on the surface finish available or the skill of the personnel to manufacture or assemble the product. Finally, there may be considerations of delivery or storage of the item before use, leading to corrosion, or false brinelling, or several other events that may befall a wear surface.

34.4.2 Static Load

The second step is to determine whether the sliding surface can withstand the expected static load without indentation or excessive distortion. Generally, this would involve a simple stress analysis.

34.4.3 Sliding Severity

The materials used must be able to withstand the severity of sliding. Factors involved in determining sliding severity include the contact pressure or stress, the temperature due to ambient heating and frictional temperature rise, the sliding speed, misalignment, duty cycle, and type of maintenance the designed item will receive. These factors are explained as follows.

Contact Stress. Industrial standards for allowable contact pressure vary considerably. Some specifications in the gear and sleeve bearing industries limit the average contact pressures for bronzes to about 1.7 MPa, which is about 1 to 4 percent of the yield strength of bronze. Likewise, in pump parts and valves made of tool steel, the contact pressures are limited to about 140 MPa, which is about 4 to 6 percent of the yield strength of the hardest state of tool steel.

However, one example of high contact pressure is the sleeve bearings in the landing gear of modern commercial aircraft. These materials again are bronzes and have yield strengths up to 760 MPa. The design bearing stress is 415 MPa but with expectations of peak stressing up to 620 MPa. Another example is the use of tool steel in lubricated sheet-metal drawing. Dies may be expected to be used for 500 000 parts with contact pressures of about 860 MPa, which is half the yield strength.

Temperature. The life of some sliding systems is strongly influenced by temperature. Handbooks often specify a material for "wear" conditions without stating a range of temperature within which the wear-resistance behavior is satisfactory. The influence of temperature may be its effect on the mechanical properties of the sliding parts. High temperatures soften most materials and low temperatures embrittle some. High temperature will produce degradation of most lubricants, but low temperature will solidify a liquid lubricant.

Ambient temperature is often easy to measure, but the temperature rise due to sliding may have a larger influence. For a quick view of the factors that influence temperature rise ΔT of asperities on rubbing surfaces, we may reproduce one simple equation:

$$\Delta T = \frac{fWV}{2a(k_1 + k_2)J} \tag{34.2}$$

where f = coefficient of friction, W = applied load, V = sliding speed, and k_1 and k_2 = thermal conductivities of the sliding materials. The quantity a is related to junction size, that is, the few, widely scattered points of contact between sliding parts.

From Eq. (34.2) it may seem that thermal conductivity of the materials could be influential in controlling temperature rise in some cases, but a more important factor is f, the coefficient of friction. If a temperature-sensitive wear mechanism is operative in a particular case, then high friction may contribute to a high wear rate, if not cause it. There is at least a quantitative connection between wear rate and the coefficient of friction when one compares dry sliding with adequately lubricated sliding, but there is no formal way to connect the coefficient of friction with the temperature rise.

Sliding Speed. Both the sliding speed and the PV limits are involved in determining the sliding severity. Maximum allowable loads and sliding speeds for materials are often specified in catalogs in the form of PV limits. In the PV product, P is the calculated average contact pressure (in psi) and V is the sliding speed (in ft/min). Plastics to be used in sleeve bearings and bronze bushings are the most common material to have PV limits assigned to them. A common range of PV limits for plastics is from 500 to 10 000, and these data are usually taken from simple laboratory test devices. The quantity P is calculated from W/A, where W = applied load and A = projected load-carrying area between sliding members. Thus PV could be written as WV/A. Returning to Eq. (34.2) for the temperature rise, it may be seen that the product WV influences ΔT directly, and it would seem that a PV limit might essentially be a limit on surface-temperature rise. This is approximately true, but not useful. That is, wear resistance of materials cannot be related in a simple way to the melting point or softening temperature of materials. The wide ranges of f, k, and other properties of materials prevent formulating a general rule on the relationship between PV limits and melting temperature. Indeed, a PV limit indicates nothing about the actual rate of wear of materials; it indicates only that

above a given *PV* limit a very severe form of wear may occur. However, the *PV* limit for one material has meaning relative to that of other materials, at least in test machinery.

Misalignment. The difficulty with misalignment is that it is an undefined condition other than that for which contact pressure between two surfaces is usually calculated. Where some misalignment may exist, it is best to use materials that can adjust or accommodate themselves, that is, break in properly.

Misalignment arises from manufacturing errors or from a deflection of the system-producing loading at one edge of the bearing, or it may arise from thermal distortion of the system, etc. Thus a designer must consider designing a system such that a load acts at the expected location in a bearing under all conditions. This may involve designing a flexible bearing mount, or several bearings along the length of a shaft, or a distribution of the applied loading, etc.

Designers must also consider the method of assembly of a device. A perfectly manufactured set of parts can be inappropriately or improperly assembled, producing misalignment or distortion. A simple tapping of a ball bearing with a hammer to seat the race may constitute more severe service than occurs in the lifetime of the machine and often results in early failure.

Misalignment may result from wear. If abrasive species can enter a bearing, the fastest wear will occur at the point of entry of the dirt. In that region, the bearing will wear away and transfer the load to other locations. A successful design must account for such events.

Duty Cycle. Important factors in selecting materials for wear resistance are the extent of shock loading of sliding systems, stop-start operations, oscillatory operation, etc. It is often useful to determine also what materials surround the sliding system, such as chemical or abrasive particles.

Maintenance. A major consideration that may be classified under sliding severity is maintenance. Whereas most phosphor bronze bushings are allowed a contact stress of about 1.4 to 7 MPa, aircraft wheel bushings made of beryllium bronze are allowed a maximum stress of 620 MPa, as mentioned before. The beryllium bronze has a strength only twice that of the phosphor bronze, but the difference between industrial and aircraft use includes different treatment of bearings in maintenance. Industrial goals are to place an object into service and virtually ignore it or provide infrequently scheduled maintenance. Aircraft maintenance, however, is more rigorous, and each operating part is under regular scrutiny by the flight crew and ground crew. There is scheduled maintenance, but there is also careful continuous observation of the part and supplies. Thus it is easier for an error to be made in selection of the lubricant in industry than with aircraft, for example. Second, the aircraft wheel bearing operates in a much more standard or narrowly defined environment. Industrial machinery must operate in the dirtiest and hottest of places and with the poorest care. These must be considered as severity conditions by the designer.

34.4.4 Break-In Procedure

Another vital consideration in the selection of materials is to determine whether or not a break-in procedure is necessary or prohibited. It cannot be assumed that the

sliding surfaces made to a dimensional accuracy and specified surface finish are ready for service. Sliding alters surfaces. Frequently, sliding under controlled light loads can prepare a surface for a long life of high loading, whereas immediate operation at moderate loads may cause early failure.

It is useful here to distinguish between two surface-altering strategies. The first we refer to as *break-in,* where a system is immediately loaded or operated to its design load. The incidence of failure of a population of such parts decreases with time of operation as the sliding surfaces change, and frequently the ability of the system to accommodate an overload or inadequate lubricant increases in the same time. The surfaces have changed in some way during running, and this is *break-in. Run-in,* however, is the deliberate and planned action that is necessary to prepare surfaces for normal service.

The wear that occurs during run-in or break-in can be considered a final modification to the machine surface. This leads to the possibility that a more careful specification of manufacturing practice may obviate the need for run-in or break-in. This has been the case with the automobile engine in particular, although part of a successful part surface-finish specification often includes the exact technique for making the surface. Only 30 years ago it was necessary to start and run an engine carefully for the first few thousand miles to ensure a reasonable engine life. If run-in were necessary today, one would not see an engine survive the short trip from the assembly plant to the haul-away trucks.

It is difficult to determine whether or not some of the present conservative industrial design practices result from the impracticality of effecting a run-in of some products. For example, a gear box on a production machine is expected to function immediately without run-in. If it were run in, its capacity might be greatly increased. But it is also well known that for each expected severity of operation of a device, a different run-in procedure is necessary. Thus a machine that has been operating at one level of severity may be no more prepared for a different state of severity than if it had never been run. A *safe* procedure, therefore, is to operate a device below the severity level at which run-in is necessary, but the device could actually be overdesigned simply to avoid run-in.

34.4.5 Modes of Wear Failure

The fifth consideration is to determine acceptable modes of wear failure or surface damage of machinery. To specify a wear life in terms of a rate of loss of material is not sufficient. For example, when an automotive engine seizes up, there is virtually no loss of material, only a rearrangement such that function is severely compromised. Thus in an engine, as well as on other precision slideways of machines, surface rearrangement or change in surface finish is less acceptable than attrition or loss of material from the system. Again, in metal-working dies, loss of material from the system is less catastrophic than is scratching of the product.

In truck brakes, some abrasiveness of brake linings is desirable, even though it wears brake drums away. This wear removes microcracks and avoids complete thermal fatigue cracking. However, in cutting tools, ore-crushing equipment, and amalgam filling in teeth, surface rearrangement is of little consequence, but material loss is to be avoided.

A final example of designing for an acceptable wear failure is a sleeve bearing in engines. Normally it should be designed against surface fatigue. However, in some applications corrosive conditions may seriously accelerate fatigue failure. This may

require the selection of a material that is less resistant to dry fatigue than is the best bearing material, and this applies especially to two-layer bearing materials. In all these examples a study of acceptable modes of wear may result in a different selection of material than if the goal were simply to minimize wear.

34.4.6 Testing Materials

Finally, it is necessary to consider the possibility of testing candidate materials in bench tests or in prototypes. After some study of worn parts from a device or machine that most nearly approximates the new or improved product, one of several conclusions could be reached:

1. The same design and materials in the wearing parts of the example device will perform adequately in the redesign, in terms of function, cost, and all other attributes.
2. A slight change in size, lubrication, or cooling of the example parts will be adequate for the design.
3. A significant change in size, lubrication, or cooling of the example parts will be necessary for the redesign.
4. A different material will be needed in the redesign.

The action to be taken after reaching one of the preceding conclusions will vary. The first conclusion can reasonably be followed by production of a few copies of the redesign. These should be tested and minor adjustments made to ensure adequate product life. The second conclusion should be followed by cautious action, and the third conclusion should invoke the building and exhaustive testing of a prototype of the redesign. The fourth conclusion may require tests in bench-test devices in conjunction with prototypes.

It is usually costly and fruitless to purchase bench-test machinery and launch into testing of materials or lubricants without experience and preparation. It is doubly futile for the novice to run accelerated wear tests with either bench tests, prototypes, or production parts.

Experience shows time after time that simple wear tests complicate the prediction of product life. The problem is correlation. For example, automotive company engineers have repeatedly found that engines on dynamometers must be run in a completely unpredictable manner to achieve the same type of wear as seen in engines of cars in suburban service. Engines turned by electric motors, though heated, wear very differently from fired engines. Separate components such as a valve train can be made to wear in a separate test rig nearly the same way as in a fired engine, with some effort, but cam materials rubbing against valve-lifter materials in a bench test inevitably produce very different results from those in a valve-train test rig.

Most machines and products are simpler than engines, but the principles of wear testing are the same; namely, the wear mechanisms must be very similar in each of the production designs, the prototype test, the subcomponent test, and the bench test. The wear rate of each test in the hierarchy should be similar, the worn surfaces must be nearly identical, and the transferred and loose wear debris should contain the same range of particle sizes, shapes, and composition. Thus it is seen that the prototype, subcomponent, and bench tests must be designed to correlate with the wear results of the final product. This requires considerable experience and confidence where the final product is not yet available. This is the reason for studying the worn

parts of a product nearest to the redesign and a good reason for retaining resident wear expertise in every engineering group.

A clear indication of the problem with bench tests may be seen in some results with three test devices. These are:

1. Pin-V test in which a ¼-in-diameter pin of AISI 3135 steel rotates at 200 rpm with four-line contact provided by two V blocks made of AISI 1137 steel.
2. Block-on-ring test where a rectangular block of a chosen steel slides on the outer (OD) surface of a ring of hard case-carburized AISI 4620 steel.
3. The four-ball test where a ball rotates in contact with three stationary balls, all of hardened AISI 52100 steel.

The four-ball test and the ring-on-block test were run over a range of applied loads and speeds. The pin-V test was run over a range of loads only. All tests were run continuously, that is, not in an oscillating or stop-start sequence mode. All tests were run with several lubricants.

Results from the ring-block test were not sufficiently reproducible or consistent for reliable analysis. Results from the other two tests were adequate for the formulation of a wear equation from each, as follows:

Pin-V test: $\text{Wear rate} \propto (\text{load})^2$

Four-ball test: $\text{Wear rate} \propto (\text{load})^{4.75} \times (\text{speed})^{2.5}$

These results may be compared with linear laws of wear discussed frequently in the literature, which would be of the form

Linear law: $\text{Wear rate} \propto (\text{load})^{1.0} \times (\text{speed})^{1.0}$

There are several points about the usefulness of published wear data to be derived from these results:

1. Practical wear rates are probably not linear in any parameter or variable of operation.
2. If three standard wear tests respond differently to changes in load and speed, then a practical part will probably respond differently again. Furthermore, an accelerated test with a standard wear tester will likely be misleading, since the influence of doubling load or speed would most likely be different between the test device and the product. In fact, the effect of variation in load and speed produces very irregular results with the block-on-ring test machine, which renders extrapolated values of tests useless.
3. It is not known whether the different results from the three wear testers are due to the use of different specimen materials or different specimen shapes or both. Thus rank ordering of materials from wear tests is likely to change among test devices and different testing conditions.

The point of the preceding discussion is that wear testing of materials and components must be done, but it must be done carefully. Testing should be done by experienced engineers and with a strong insistence upon close analysis of worn surfaces and wear debris. It would be useful to be able to compare one's observations with a large and comprehensive atlas of photographs of surfaces in various

stages of wear, but none is available. Photographs are scattered through published papers and handbooks and are of some value only when properly described and understood.

Engineers must therefore solve most wear problems themselves by analysis of worn surfaces and wear debris from existing machinery and wear testers. Guidelines for selecting wear-resisting materials and for indirectly selecting lubricants are given in the next section using the methods of product analysis.

34.5 MATERIAL-SELECTION PROCEDURE

The previous sections have established the important point that selecting materials for wear resistance requires a study of the details of wear in order to determine which of the several conventional properties of material can best resist a particular mode of wear. The best way to proceed, therefore, is to examine the most appropriate wear system (including the solids, the lubricant, and all the wear debris), such as an old product being redesigned or a wear tester. The best tools to use are microscopes, with some photography. The most useful microscope is a stereozoom type with a magnification range of 1× to 7×, with 5× or 10× eyepieces and a 100-W movable external light source. Stereo viewing gives a perspective on the shapes of surface features, such as grooves, folds, flakes, etc. The next most useful tool is the scanning (reflecting) electron microscope (SEM). The novice should use this instrument in conjunction with optical microscopes because the SEM and optical devices produce very different pictures of surfaces. Frequently the most useful SEM observations are those done at low magnification, between 20× and 200×, although it is fun to "see" surfaces at 20 000×. The virtue of the SEM is that very rough surfaces can be seen without the high regions and low regions being out of focus, as occurs in optical microscopy. The major problem is that the SEM usually accepts only small specimens [for example, ½ in (12.5 mm) thick by 2 in (50 mm) in diameter], and the surfaces must be clean because the SEM requires a vacuum (about 10^{-5} torr).

For a more detailed analysis of surface chemistry and substrate composition, an SEM with an x-ray dispersion (EDAX, etc.) attachment can be used. The operation of these instruments requires some combination of skill and expensive automation. Optical metallurgical microscopes may be useful as well, but usually not in the conventional bright-field, reflected-light mode. These microscopes often have several special objectives for phase contrast, polarized light, interference, and dark field, all requiring skill in use and in the interpretation of results.

Sometimes it is useful to obtain a topographic profile of worn surfaces. This can be done with the stylus tracer used in conventional surface-finish measurement, but it should be connected to a strip-chart recorder. It is the surface shape rather than a numerical value of surface finish that is most useful. Traces should be made in several places and in several directions during the progression of wearing, if possible. A major precaution to observe in analysis of the strip-chart data is that the representation of the height of surface shapes is often magnified from 10 to 1000 times greater than is the "horizontal" dimension. This leads to the sketching of surfaces as very jagged peaks upon which no one would care to sit. Actually, solid surfaces are more like the surfaces of a body of water in a 10-mi/h breeze.

Having examined a wear system, the designer can proceed through Table 34.3 and make a first attempt to select a material for wear resistance.

TABLE 34.3 Guide for Determining the Material Properties that Resist Wear

How to use the table:

1. Observe the nature of wear in existing equipment or of similar materials from appropriate wear-testing machines.
2. Check the lists in Section A for an applicable general description of worn surfaces or type of service and note the code that follows the selected term.
3. Proceed to Section B which lists 6 terms† that describe three scales of superimposed surface changes. Verify that the code listing is an adequate description of the worn surface. (It is possible to use Section B without reference to Section A.) From Section B, find the major term (capitalized).
4. In Section C, find the detailed description of the capitalized term from Section B and note which material-loss mechanism is applicable and confirm from the nature or description of wear debris.
5. Find the material-loss mechanism in Section D, note the material characteristics and microstructure that should influence wear resistance of material, and note the precautions in material selection to prevent failure.
6. Select materials in conjunction with materials specialists.

Section A Description of worn surfaces and type of service with code for use in Section B

General surface appearance‡	Some types of service‡
Stained: *f*	Surface corrosion or Erosion/corrosion: in solid machinery: *a*1 + *c*; in fluids: *a*2 + *d*2
Polished or smooth wear: *a*1 + *c* + *e* or *a*2 + *c* + *e*	
Scratched (short grooves): *b*3 + *c* + *e*	Abrasive wear (multiple scratches): *b*3 + *c*
Gouged: *b*3 + *d*1	
Scuffed: *a*1 + initiated and periodically perpetuated by *d*3 + *e*	Gouging: *b*1 + *d*1 + *e*
Galled: *b*1 + *d*3 + *3* (usually very rough)	Dry wear or unlubricated sliding: *b*1 + *d*3 + *e* or *a*1 + *c* + *e*
Grooved (smooth or rough): *a*1 + periodically advanced by *d*1 + *e*	Metal-to-metal wear or adhesive wear: *b*1 + *d*3 + *e*
Hazy: *b*2	Erosion at high angle: *b*2 + *d*4
Exfoliated or delaminated: *d*4 + *e*	Erosion at low angle: *b*3 + *d*1 or *d*2
Pitted: *b*2 and/or *d*5	
Spalled: *d*4	
Melted: *a*3	
Fretted: *a*1 + *d*5 + *f*	Fretting: *a*1 + *d*5 + *f*

†Surface geometries can usually be described in three scales, namely, macro-, micro-, and submicro. The first two scales can describe roughness; the third describes reflectivity. The worn surfaces in Section A may be described in terms of the three scales; e.g., polished surfaces are usually microsmooth (a), macrosmooth (c), and shiny (e). The numbers following the code letters explain how the suggested scale of surface geometry wa achieved, i.e., by abrasion which left a very thin film on the surface. Thus the code, polished wear—*a*1 + *c* + *e*, etc. Where a scale of geometry is not given, that scale may not be of consequence in the description of the worn surface.

‡Rigorous connection cannot always be made between the terms in the two columns in Section A because of the wide diversity of use and meaning of terms.

TABLE 34.3 Guide for Determining the Material Properties that Resist Wear *(Continued)*

Section B Code listing

a. Microsmooth, caused by 1. Progressive loss and reformation of surface films by fine *abrasion* and/or by tractive stresses imposed by *adhesive* or viscous interaction, or by 2. Very fine *abrasion*, with loss of substrate in addition to loss of surface film, if any, or 3. From *melting.* *c.* Macro-smooth, caused by, abrasive particles held on or between solid, smooth backing *e.* Shiny, due to very thin (<25nm?) surface films of oxide, hydroxide, sulfide, chloride, or other species	*b.* Microrough, caused by 1. Tractive stresses resulting from *adhesion*, or by 2. Micropitting by *fatigue*, or by 3. *Abrasion* by medium-coarse particles *d.* Macrorough, caused by 1. *Abrasion* with coarse particles, including carbide and other hard inclusions in the sliding materials that are removed by sliding action as the wear of matrix progresses, or by 2. *Abrasion* by fine particles in turbulent fluid, producing scallops, waves, etc., or by 3. Severe *adhesion* in early stages of damage, or by 4. Local *fatigue* failure resulting in pits or depressions due to repeated rolling-contact stress, repeated thermal gradients, high-friction sliding, or impact by hard particles as in erosion, or in 5. Advanced stages of microroughening, where little unaffected surface remains between pits. *f.* Dull or matte, due to films of perhaps greater than 25-nm thickness (resulting from aggressive environments, including high temperatures), i.e., due to *corrosion*

Section C Material-loss mechanisms and nature of debris

Material-loss mechanisms (italic)	Nature of debris
Corrosion (of surface): Chemical combination of material surface atoms with passing or deposited active species to form a new compound, i.e., oxide, etc.	Newly formed chemical compound, usually agglomerated and sometimes mixed with fragments of the original surface material
Abrasion: Involves particles (or acute angular shapes but mostly obtuse) that produce wear debris, some of which forms ahead of the abrasive particle, which mechanism is called *cutting*, but most of which is material that has been plowed aside repeatedly by passing particles, and breaks off by *low-cycle fatigue.*	Long, often curly chips or strings

TABLE 34.3 Guide for Determining the Material Properties that Resist Wear *(Continued)*

Section C Material-loss mechanisms and nature of debris (*Continued*)

Material-loss mechanisms (italic)	Nature of debris
Adhesion: A strong bond that develops between two surfaces (either between coatings and/or substrate materials) that, with relative motion, produces tractive stress that may be sufficient to deform materials to fracture. The mode of fracture will depend on the property of the material, involving various amounts of energy loss or ductility to fracture, that is,	
Low energy and ductility → *brittle fracture*	Solid particles, often with cleavage surfaces
High energy and ductility → *ductile fracture*	Severly deformed solids, sometimes with oxide clumps mixed in
Fatigue: Due to cyclic strains, usually at stress levels below the yield strength of the material, also called *high-cycle fatigue*	Solid particles, often with cleavage surfaces and ripple pattern
Melting: From very high-speed sliding	Spheres, solid or hollow, and "splat" particles

Section D Material-selection characteristics

Material-loss mechanisms	Appropriate material characteristics to resist wear	Precautions to be observed when selecting a material†
Corrosion	Reduce corrosiveness of surrounding region; increase corrosion resistance of material by alloy addition or by selection of soft, homogeneous material	Total avoidance of new surface species can result in high adhesion of contacting surfaces; soft materials tend to promote galling and seizure.
Cutting	Use material of high hardness, with very hard particles or inclusions, such as carbides, nitrides, etc., and/or overlaid or coated with materials that are hard or contain very hard particles	All methods of increasing cutting resistance cause brittleness or lower fatigue resistance.
Ductile fracture	High strength achieved by any method other than cold working or heat treatments that produce internal cracks and large, poorly bonded intermetallic compounds	
Brittle fracture	Minimize tensile residual stress for cold temperature; ensure low-temperature brittle transition; temper all martensites; use deoxidized metal; avoid carbides such as in pearlite, etc.; effect good bond between fillers and matrix to deflect cracks	In essence, soft materials will not fail through brittleness and will not resist cutting.
Low-cycle fatigue	Use homogeneous and high-strength materials that do not strain-soften; avoid overaged materials and two-phase systems with poor adhesion between filler and matrix	

TABLE 34.3 Guide for Determining the Material Properties that Resist Wear *(Continued)*

Section D Material-selection characteristics

Material-loss mechanisms	Appropriate material characteristics to resist wear	Precautions to be observed when selecting a material†
High-cycle fatigue	For steel and titanium, use stresses less than half the tensile strength (however achieved); for other materials to be load-cycled less than 10^8 times, allow stresses less than one-fourth the tensile strength (however achieved); avoid retained austenite; use spherical pearlite rather than plate structure; avoid poorly bonded second phases; avoid decarburization of surfaces; avoid platings with cracks; avoid tensile residual stresses or form-compressive residual stresses by carburizing or nitriding	Calculation of stress should include the influence of tractive stress.
Melting	Use material of high melting point and/or high thermal conductivity	

†Materials of high hardness or strength usually have decreased corrosion resistance, and all materials with multiple and carefully specified properties and structures are expensive.

SOURCE: From Ludema [34.2].

REFERENCES

34.1 H. C. Meng and K. C. Ludema, "Wear Models and Predictive Equations: Their Form and Content," *Wear,* vol. 181–183, pp. 443–457, 1995.

34.2 K. C. Ludema, "Selecting Materials for Wear Resistance," Conference on Wear of Materials, San Francisco, 1981, ASME, New York.

BIBLIOGRAPHY

The previous sections are composite views of many authors, so that a reference list would be very long. Interested readers could consult the many journals containing papers on wear, but that literature is potentially very confusing. The most useful journals are

Wear, Elsevier, Lausanne, starting in 1957.

Tribology International, Butterworth Scientific, Ltd., London, starting in 1968.

Tribology Transactions of the Society of Tribologists and Lubrication Engineers (formerly *Transactions* of the American Society of Lubrication Engineers).

Journal of Tribology, also identified as *Transactions F,* American Society of Mechanical Engineers.

CHAPTER 35
CORROSION

Milton G. Wille, Ph.D., P.E.
Professor of Mechanical Engineering
Brigham Young University
Provo, Utah

35.1 INTRODUCTION

Corrosion removal deals with the taking away of mass from the surface of materials by their environment and other forms of environmental attack that weaken or otherwise degrade material properties. The complex nature of corrosion suggests that the designer who is seriously concerned about corrosion review a good readable text such as *Corrosion Engineering* by Fontana and Greene [35.1].

Included in this chapter are many corrosion data for selected environments and materials. It is always hazardous to select one material in preference to another based only on published data because of inconsistencies in measuring corrosion, lack of completeness in documenting environments, variations in test methods, and possible publishing errors. These data do not generally indicate how small variations in temperature or corrosive concentrations might drastically increase or decrease corrosion rates. Furthermore, they do not account for the influence of other associated materials or how combinations of attack mechanisms may drastically alter a given material's behavior. Stray electric currents should be considered along with the various attack mechanisms included in this chapter. Brevity has required simplification and the exclusion of some phenomena and data which may be important in some applications.

The data included in this chapter are but a fraction of those available. *Corrosion Guide* by Rabald [35.2] can be a valuable resource because of its extensive coverage of environments and materials.

Again, all corrosion data included in this chapter or published elsewhere should be used only as a guide for weeding out unsuitable materials or selecting potentially acceptable candidates. Verification of suitability should be based on actual experience or laboratory experimentation. The inclusion or exclusion of data in this chapter should not be interpreted as an endorsement or rejection of any material.

35.2 CORROSION RATES

The vast majority of metal corrosion data in the United States are expressed in terms of surface regression rate *mpy* (mils, or thousands of an inch, per year). Multiply *mpy* by 0.0254 to obtain millimeters per year (mm/yr). To convert to mass-loss rate, multiply the surface regression rate by surface area and material density, using consistent units.

Polymer attack typically involves volume changes, usually increases, caused by liquid absorption; reductions in mechanical properties such as yield strength, tensile strength, flexure strength, and tensile modulus; discoloration; and/or changes in surface texture. Certain plastics are degraded by ultraviolet light, which limits their usefulness in sunlight unless they are pigmented with an opaque substance such as lamp-black carbon.

35.3 METAL ATTACK MECHANISMS

The attack on metals involves oxidation of neutral metal atoms to form positively charged ions which either enter into solution or become part of an oxide layer. This process generates electrons, which must be consumed by other atoms, reducing them, or making them more negatively charged. Conservation of electrons requires that the rate of metal oxidation (corrosion) equal the rate of reduction (absorption of electrons by other atoms).

35.3.1 General Attack

In general attack, oxidation and reduction occur on the same metal surface, with a fairly uniform distribution. Most of the corrosion data in this chapter are for selected materials subject to uniform attack in a given environment.

Once a suitable material is selected, further control of uniform attack can be achieved by coatings, sacrificial anodes (see Galvanic Corrosion), anodic protection (see Passivation), and inhibitors. Coatings are many times multilayered, involving both metallic and polymer layers. Inhibitors are additions to liquid environments that remove corrosives from solution, coat metal surfaces to decrease surface reaction rates, or otherwise alter the aggressiveness of the environment.

Chemically protective metallic coatings for steels are usually zinc (galvanized) or aluminum (aluminized). Aluminized steel is best for elevated temperatures up to 675°C and for severe industrial atmospheres. Both may be deposited by hot dipping, electrochemistry, or arc spraying. Common barrier-type metallic platings are those of chromium and nickel. The Environmental Protection Agency has severely limited or prohibited the use of lead-bearing and cadmium platings and cyanide plating solutions.

Polymer coatings (such as paints) shield metal surfaces from electron-receiving elements, such as oxygen, reducing corrosion attack rates. Under mild conditions, even "decorative paints" can be effective. Under more severe conditions, thicker and tougher films are used which resist the effects of moisture, heat, chlorides, and/or other undesirable chemicals. Acrylics, alkyds, silicones, and silicone-modified alkyds are the most commonly used finishes for industrial equipment, including farm equipment. The silicones have higher heat resistance, making them useful for heaters, engines, boilers, dryers, furnaces, etc.

35.3.2 Galvanic Corrosion and Protection

When two dissimilar metals are electrically connected and both are exposed to the same environment, the more active metal will be attacked at a faster rate than if there had been no electrical connection between the two. Similarly, the less active metal will be protected or suffer less attack because the surface areas of both metals can be used to dissipate the electrons generated by oxidation of the more active metal. The net flow of electrons from the more active to the less active metal increases the attack rate of the more active metal and decreases that of the less active metal.

An *adverse area ratio* is characterized by having a larger surface area of less active metal than that of the more active metal. Cracks in a barrier protective coating (i.e., polymers) applied to the more active metal in a galvanic-couple situation can create an extremely adverse area ratio, resulting in rapid localized attack in the cracks. The standard electromotive force (emf) series of metals (Table 35.1) lists

TABLE 35.1 Standard EMF Series of Metals

Metal–metal ion equilibrium (unit activity)	Electrode potential vs. normal hydrogen electrode at 25°C, V
$Au\text{-}Au^{3+}$	+1.498
$Pt\text{-}Pt^{2+}$	+1.2
$Pd\text{-}Pd^{2+}$	+0.987
$Ag\text{-}Ag^{+}$	+0.799
$Hg\text{-}Hg_2^{2+}$	+0.788
$Cu\text{-}Cu^{2+}$	+0.337
$H_2\text{-}H^{+}$	0.000
$Pb\text{-}Pb^{2+}$	−0.126
$Sn\text{-}Sn^{2+}$	−0.136
$Ni\text{-}Ni^{2+}$	−0.250
$Co\text{-}Co^{2+}$	−0.277
$Cd\text{-}Cd^{2+}$	−0.403
$Fe\text{-}Fe^{2+}$	−0.440
$Cr\text{-}Cr^{3+}$	−0.744
$Zn\text{-}Zn^{2+}$	−0.763
$Al\text{-}Al^{3+}$	−1.662
$Mg\text{-}Mg^{2+}$	−2.363

metals in order of increasing activity, starting with gold (Au), which is the least active. If two of the metals listed were joined in a galvanic couple, the more active one would be attacked and plating or deposition of the less active one would occur. This is based on the fact that solutions contain only unit activity (concentration) of ions of each of the two metals.

The standard EMF series is valid only for pure metals at 25°C and in equilibrium with a solution containing unit activity (concentration) of its own ions. If ion concentrations are greater than unit activity, the potentials are more positive; if less, the opposite is true.

TABLE 35.2 Galvanic Series of Some Commercial Metals and Alloys in Seawater

↑	Platinum
	Gold
Noble or	Graphite
cathodic	Titanium
	Silver
	Chlorimet 3 (62 Ni, 18 Cr, 18 Mo)
	Hastelloy C (62 Ni, 17 Cr, 15 Mo)
	18-8 Mo stainless steel (passive)
	18-8 stainless steel (passive)
	Chromium stainless steel 11-30% Cr (passive)
	Inconel (passive) (80 Ni, 13 Cr, 7 Fe)
	Nickel (passive)
	Silver solder
	Monel (70 Ni, 30 Cu)
	Cupronickels (60-90 Cu, 40-10 Ni)
	Bronzes (Cu-Sn)
	Copper
	Brasses (Cu-Zn)
	Chlorimet 2 (66 Ni, 32 Mo, 1 Fe)
	Hastelloy B (60 Ni, 30 Mo, 6 Fe, 1 Mn)
	Inconel (active)
	Nickel (active)
	Tin
	Lead
	Lead-tin solders
	18-8 Mo stainless steel (active)
	18-8 stainless steel (active)
	Ni-Resist (high Ni cast iron)
	Chromium stainless steel, 13% Cr (active)
	Cast iron
	Steel or iron
	2024 aluminum (4.5 Cu,. 1.5 Mg, 0.6 Mn)
Active or	Cadmium
anodic	Commercially pure aluminum (1100)
	Zinc
↓	Magnesium and magnesium alloys

SOURCE: M. G. Fontana and N. D. Greene, *Corrosion Engineering,* 2d ed., McGraw-Hill, New York, 1978. Used by permission.

The galvanic series (Table 35.2) shows a similar relationship, except that impure metals such as alloys are also included and the medium is seawater. Other media, other concentrations, and other temperatures can further alter the order of the list. Therefore, care should be exercised in applying these data to a given galvanic corrosion situation except as a general, loose guide.

35.3.3 Passivation

Certain common engineering materials, such as iron, nickel, chromium, titanium, and silicon as well as their alloys (i.e., stainless steels), exhibit a characteristic of being able to behave both as a more active and as a less active (passive) material.

Note in the galvanic series (Table 35.2) that several stainless steels are listed twice, once as passive and once as active. Some common metals other than those mentioned also exhibit passivity, but to a lesser extent.

A graphical representation of passivity is shown in Fig. 35.1. The three regions—active, passive, and transpassive—help to explain seemingly inconsistent behavior of active-passive materials under various degrees of attack severity.

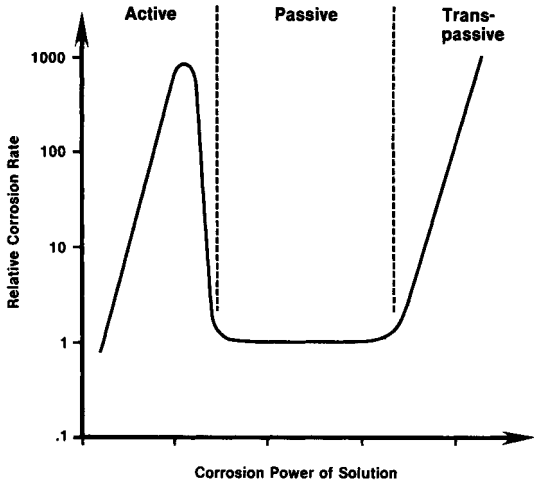

FIGURE 35.1 Corrosion characteristics of an active-passive metal.

There are both advantages and disadvantages to be gained or suffered because of active-passive behavior. In very aggressive environments, a method called anodic protection can be used whereby a *potentiostat* is utilized to electrochemically maintain a passive condition and hence a low rate of corrosion. However, accelerated corrosion test results may be useless because increasing the corrosion power of the medium may cause a shift from a high active corrosion rate to a low passive condition, producing the invalid conclusion that corrosion is not a problem. Another example involves inhibitors which function by maintaining a passive condition. If the concentration of these inhibitors were allowed to decrease, high corrosion could result by passing from a passive to an active condition.

Active-passive materials have a unique advantage in the area of corrosion testing and corrosion rate prediction. *Potentiodynamic polarization* curves can be generated in a matter of hours, which can provide good quantitative insights into corrosion behavior and prediction of corrosion rates in a particular environment. Most other corrosion testing involves months or years of testing to obtain useful results.

35.3.4 Crevice Corrosion and Pitting

Crevice corrosion is related to active-passive materials which are configured such that crevices exist. Mated screw threads, gaskets, packings, and bolted or lapped joints

are common examples of crevices. Inside the crevice, oxygen or other corrosives required for passivation have restricted entrance, resulting in reduced concentration as they are consumed by corrosion in the crevice. When the concentration of these corrosives is low enough to fail to maintain passivity, the metal in the crevice becomes active. The large electrically connected, passivated surface outside the crevice completes a galvanic couple with a large adverse-area ratio, providing high attack rates within the crevice. Welding or forming can be used to avoid crevices. However, intergranular corrosion may occur in welded stainless steels (see Sec. 35.3.9).

Pitting is a very localized attack that results in holes, or voids, on a metal surface. Although not restricted to active-passive metals, pitting is commonly related to these. With active-passive metals, pieces of dirt, scale, or other solid particles may rest on the bottom of a pipe or tank where velocities are not sufficient to move them. These particles form crevices, resulting in a localized attack similar to crevice corrosion.

35.3.5 Sacrificial Anodes

Magnesium rods are placed in steel glass-lined hot-water tanks, and zinc is used to coat sheet steel (galvanized steel) to provide protection to the steel against corrosion. As the more active magnesium rod is attacked, the electrons generated are conveyed to the electrically connected steel tank, which needs protection only for regions where cracks or flaws exist in the glass lining. Similarly, for galvanized steel, protection is required only for regions of scratches or where steel edges are exposed.

35.3.6 Stress Corrosion Cracking

In stress corrosion cracking (SCC), most of a metal's surface may show little attack, while fine intergranular or transgranular cracks may penetrate deeply into the surface. There may be a single continuous crack or a multibranched crack, or the entire surface may be covered with a lacy network of cracks. Usually dye penetrants and sectioning are needed to reveal the extent and depth of cracking.

Certain classes of alloys and environments are susceptible to this phenomenon, and usually tensile stresses are involved, with crack penetration rates increasing with increasing tensile stress. The higher the strength condition of a given alloy, the greater seems to be the tendency to suffer SCC. Table 35.3 lists some materials and environments that have been known to produce SCC.

Frequently, a difference in color or texture is noticeable between a stress corrosion crack and an adjacent region of overstress when the fracture is completed by mechanical means. Scanning electron micrographs are frequently useful in identifying SCC.

35.3.7 Selective Leaching

Selective leaching refers to the chemical removal of one metal from an alloy, resulting in a weak, porous structure. Brass sink traps suffer this type of attack by zinc being leached out of the yellow brass, leaving behind a porous structure of reddish copper. Aluminum and silicon bronzes and other alloys are also subjected to selective leaching.

TABLE 35.3 Environments That May Cause Stress Corrosion of Metals and Alloys

Material	Environment	Material	Environment
Aluminum alloys	$NaCl-H_2O_2$ solutions	Ordinary steels	NaOH solutions
	NaCl solutions		$NaOH-Na_2SiO_2$ solutions
	Seawater		Calcium, ammonium, and sodium nitrate solutions
	Air, water vapor		Mixed acids (H_2SO_4-HNO_3)
	Ammonia vapors and		HCN solutions
Copper alloys	solutions		Acidic H_2S solutions
	Amines		Seawater
	Water, water vapor		Molten Na-Pb alloys
Gold alloys	$FeCl_3$ solutions	Stainless steels	Acid chloride solutions
	Acetic acid-salt solutions		such as $MgCl_2$ and $BaCl_2$
Inconel	Caustic soda solutions		$NaCl-H_2O_2$ solutions
Lead	Lead acetate solutions		Seawater
Magnesium alloys	$NaCl-K_2CrO_4$ solutions		H_2S
	Rural and coastal atmospheres		$HaOH-H_2S$ solutions
	Distilled water		Condensing steam from chloride waters
Monel	Fused caustic soda	Titanium alloys	Red fuming nitric acid, seawater, N_2O_4, methanol-HCl
	Hydrofluoric acid		
	Hydrofluosilicic acid		
Nickel	Fused caustic soda		

SOURCE: M. G. Fontana and N. D. Greene, *Corrosion Engineering,* 2d ed., McGraw-Hill, New York, 1978. Used by permission.

35.3.8 Hydrogen Embrittlement

In any electrochemical process where hydrogen ions are reduced, monatomic hydrogen atoms are created prior to their joining in pairs to form diatomic hydrogen gas (H_2). Monatomic hydrogen, being small, can diffuse into metals, causing embrittlement. Corrosion of metals by acids, including cleaning by pickling, can produce hydrogen embrittlement. Heating can drive out monatomic hydrogen, reversing the process. If monatomic hydrogen diffuses into voids in a metal, high-pressure pockets of H_2 gas are formed which are not eliminated by heating, but rather may form hydrogen blisters.

35.3.9 Intergranular Corrosion

In some alloys, frequently related to prior heating, grain boundaries can experience localized variations in composition that can result in corrosion attack along or immediately adjacent to grain boundaries. The 18-8 stainless steels (such as type 304), when heated in the approximate range of 500 to 790°C, experience the precipitation of chromium carbides in grain boundaries, removing chromium from the regions adjacent to grain boundaries. This process is called *sensitization.* It is theorized that intergranular attack proceeds in the chromium-depleted regions of the grain boundaries, since these lack the protection provided by chromium alloying. When this class of stainless steels is welded, regions a bit removed from the weld axis are heated sufficiently to become sensitized and hence become subject to subsequent intergranular

(continued on page 35.28)

TABLE 35.4 Corrosion Data by Environment and Material†

Acetone

Nonmetallics. ABS — satis. **Acetal copolymer**—after 6 mos at 120 F: yld str −19%, tens mod −48%, length +2.1%, weight +4.5%, appearance no change. **Acetal homopolymer**—1 yr at 120 F: tens mod −40%, tens str −7%, length +1.1%, weight +2.6%. **Acrylic**—unsatis in 90% at 100 F. **Butyl rubber**—70 hrs at r.t.: +2% vol change. **Chlorinated polyether**—res at 80 F. **Chlorosulfonated polyethylene rubber**—minor to moderate effect at r.t. **Ethylene-propylene rubbers**—at r.t. after 70 hrs retain 81-83% ten str, vol changes −17 to +4%. **Fluorocarbon**—res to boiling. **Fluorocarbon (PVF_2)**—fair at 70 F, NR at 120 F. **Fluoroelastomer**—severe effect at r.t. **Glass (borosilicate)**—satis at 150 F. **Graphite (impervious)**—res 100% boiling. **Hydrocarbon rubber**—little or no effect at r.t. **Natural rubber**—satis. **Neoprene**—minor to moderate effect at r.t. **Nylon**—satis at 120 F. Polyacrylate rubber—after 70 hrs at r.t.: +201% vol change. **Polycarbonate**—not resistant after 6 mos at r.t. **Polyester (glass reinf)**—NR. **Polyethylene (hi-D)**—unsatis after 1 yr at 70 F. **Polyimide (glass reinf)**—after 7 days exp retains 100% of flex mod and 98% of r.t. flex str. **Polystyrene**—not res. **PVC**—plast and unplast unsatis at 68 F. **PVC-acrylic alloy**—attacked at 73 F. **SBR rubber**—after 70 hrs at r.t.: +18% vol change. **Silicone rubber**—after 7 days at 75 F: ten str −85%, volume +180%. **Styrene-acrylonitrile**—not resistant at 73 F. **Urethane rubber**—severe effect at r.t. **Vinyl ester (glass reinf)**—NR in 100%.

Ammonia

Metals. Aluminum—res. to dry gas even at elevated temp. If moist, attack low for all con. up to 120 F. **Copper and alloys**—generally res. if dry, rapidly attacked if moist. **Iron and steels**—good res. to aqueous and anhydrous sol. **Lead**—res. to dry gas. After 2 days in 1.7% sol. at r.t.: 1.9 mpy under quiet conditions, 1.1 mpy under aerated cond. **Magnesium**—res. to dry gas at r.t.; presence of water vapor may cause attack. **Nickel and alloys**—nickel res. to anhydrous, and to aqueous up to about 1% sol. Nickel alloys generally res., except Ni-Cu. Ni-Cu res. anhydrous ammonia, but readily attacked by aqueous ammonia and ammonium hydroxide. **Stainless steels**—high res. under certain contions, severely attacked in others, depending on con., temp and pressure. After 2 mos in 99% NH_3 vapor at 932 F, 7 to 54 mpy for type 310, more severe attack on 304, 309, 316 and 446 grades. **Tin**—res. to gaseous ammonia, even if heated, but ammonia may become decomposed. Res. liquid ammonia, but readily attacked if sodium in sol.

Nonmetallics. ABS—satis in gas. **Chlorinated polyether**—res to gas at 220 F. Acrylic—satis in gas at 100 F. **Chlorosulfonated polyethylene rubber**—minor to moderate effect by anhydrous at r.t. **Fluorocarbon (PVF_2)**—exc to 275 F. **Fluorocarbon (TFE, FEP)**—res liquid at 78 F. **Fluoroelastomer**—severe effect by anhydrous at r.t. **Hydrocarbon rubber**—no data, likely to be compatible at r.t. **Neoprene**—little or no effect by anhydrous at r.t. **Nylon**—satis in gas at r.t. **Polyethylene (Hi-D)**—satis after 180 days at 122 F. **PVC**—dry: unplast shows some att or absorp at 68 F and unsatis at 140 F, plast unsatis at 68 F. **Silicone rubber**—no change in vol after 7 days at 75 F. **Urethane rubber**—no data, likely to be compatible with anhydrous.

†A footnote on the last page of the table supplies spelled-out forms for the abbreviations used.

TABLE 35.4 Corrosion Data by Environment and Material (*Continued*)

Ammonium hydroxide

Metals. Aluminum—low rate of attack in all con. up to 120 F. **Cobalt**—good res. in dilute sol. at r.t.; 0.8 mpy in 5% con. at 77 F under static conditions. **Copper and alloys**—rapidly attacked if more than a few ppm ammonia present, cupronickels being the most resistant. **Irons and steels**—good res.; moderately attacked in hot con. **Lead**—"satisfactory" with liquid or gas at most con. and temps. **Nickel and alloys**—nickel has high res. in very dilute sol., but rapidly attacked in increasing con.; < 1 mpy in 1% sol., over 500 mpy in 13% sol. after 20 hrs at r.t. Aeration may increase res. in low con., but increases attack in high con. Except for Ni-Cu alloys, which are readily attacked, nickel alloys have high res. in all con. to boil. pt. **Stainless steels**—good res. in all con. up to boil. pt; rapid attack likely above atmospheric boil. pt. **Tin**—0.1 to 0.3 mpy in IN sol. at 68 F after 24 hrs. **Titanium**—good res.; 0.2 mpy in 5% sol., 0.1 mpy in 28% sol. at r.t. **Tungsten**—good res., only slightly attacked. **Zinc**—12 mpy in quiet (28 mpy for air agitated) 3.4% sol. after 2 days. **Zirconium**—res. in 28% solution, r.t. to 212 F.

Nonmetallics. ABS—satis. **Acetal copolymer**—after 6 mos at 180 F in 10%: yld str −0.3%, tens mod −12%, length · +0.4%, weight +0.74%, discoloration. **Acetal homopolymer**—90 days at 73 F at 10%: unsatis. **Acrylic**—satis in 30% at 100 F. **Acrylic-PVC alloy**—no change in 10% after 7 days at 73 F. **Alumina (porous)**—res 28% at r.t. **Chlorosulfonated rubber**—little or no effect at 200 F. **Fluorocarbon (PVF_2)**—exc to 275 F. **Fluoroelastomer**—little or no effect at r.t. **Graphite (impervious)**—res in all conc at boiling. **Hydrocarbon rubber**—little or no effect at r.t. **Natural rubber**—satis. **Neopene**—little or no effect at 158 F. **Nitrile rubber**—rec in 28%. **Nylon**—satisfactory at r.t. **Phenolic**—varies with grade, some show little weight change in 10% and exc appearance after 1 yr. **Polyester (glass reinf)**—rec in 5% to 160 F. **Polyethylene (hi-D)**—satis in 28% after 90 days at 70 F. **Polyimide (glass reinf)**— 7 days in 10%: retains 81% of flex mod and 77% of r.t. flex str. **Modified polyphenylene oxide**—no effect in 10% after 3 days at 185 F. **Polypropylene**—satis for 30 days at r.t. **Polystyrene**—res conc; heat reduces res. **Silicone rubber**—after 7 days at 75 F in sat'd: ten str −45%, volume +5%. **Styrene-acrylonitrile**—resistant in 30% at 122 F. **Thermoplastic rubber**—satis in 3% after 2 weeks at r.t. **Urethane rubber**—little or no effect at r.t. **Vinyl ester (glass reinf)**—rec in 20% at 150 F, 29% at 100 F.

TABLE 35.4 Corrosion Data by Environment and Material (*Continued*)

Atmosphere — General outdoors except marine

Metals. Aluminum and alloys—high res.; weathering rate is self-limiting, decreasing with time. Alloys tend to acquire light gray patina. In clean atmos away from seacoast, transformation is slow, surface may retain some sheen even after many years. Depth of attack ranges from virtually nil in dry rural atmos (Phoenix) to 5 mils max. after 20 yrs in severe industrial atmos (New Kensington, Pa.). **Beryllium**—information limited, but commercially pure grade develops tough, stable, oxide coating which inhibits attack under normal conditions. **Cadmium**—fair to good res.; 0.4 mpy after 1 yr for 0.8 in thk plate in urban indus atmos (N.Y.C.); 0.2 mpy for 3 mos, 0.6 mpy for 9 mos in London. 60 to 90% rusting in severe indus atmos (Altoona, Pa). 4 to 12% in rural (State College, Pa.) after 1 yr. **Carbon steels**—rust rapidly, but rust may be more or less protective depending on steel composition and contaminants in atmos. Rust most protective if surface washed by rain and dries periodically. Plain carbon steel (0.02Cu) attacked to depth of 4 mils after 2 yrs, 13 mils after 10 yrs in severe indus atmos (Pittsburgh). **Cast irons**—fair to good res. depending on type. Austenitic grades generally best; not rust-free, but superior to gray iron and far superior to plain carbon steel. **Chromium**—high res. **Cobalt and alloys**—high res. **Columbium**—high res.; expected to acquire only slight tarnish after 15 yrs in indus atmos. **Copper and alloys**—high res.; copper tarnishes to a brown color which gradually turns black and, after a few yrs, the characteristic green patina starts to form and lasts indefinitely. Some alloys react similarly; but high-zinc brasses and nickel silvers are more resistant to tarnishing than copper. Rate of attack for copper is 0.01 to 0.02 mpy in rural atmos (State College and Phoenix), 0.05 mpy in severe indus atmos (Altoona) after 20 yrs. High-copper alloys (over 70% Cu) have similar res. in above rural areas, somewhat less (0.06 to 0.12 mpy) in Altoona. **Lead**—high res.; 0.01 mpy in rural atmos (State College and Phoenix), 0.01 to 0.02 mpy in urban indus (N.Y.C.) after 20 yrs.; 0.02 to 0.03 mpy in severe indus atmos (Altoona) after 10 yrs. **Low alloy steels**—rust rapidly, but rust may be more or less protective depending on steel composition and contaminants in atmos. Copper structural steel (0.24 Cu) about twice as resistant as plain carbon steel (0.04 Cu) for 0 to 12 yrs in indus atmos (Kearney, N.J.). "High strength low alloy" steels, which include "weathering" grades, at least twice as resistant as copper steel. For 0.2 Cu-0.2 Ni steel, 1.8 mpy after 1 yr and 0.8 mpy after 3 yrs in indus atmos (Bayonne, N.J.). For 5 Ni steel, 1.3 and 0.6 mpy, resp, at same site. **Magnesium**—Good res, may be superior to aluminum in certain atmos. Highly protective oxide film forms upon exposure to atmos. **Molybdenum**—High res; tarnishes quickly in indus atmos (Bayonne, N.J.) but attacked very slowly (0.03 mpy after 2.2 yrs). **Nickel and alloys**—good to excellent res. Nickel stays bright in clean, dry atmos, tarnishes if relative humidity exceeds about 70%. Tarnishes to faint gray in rural atmos; green corrosion products may form if sheltered from rain. Rate of attack very low in rural areas (State College and Phoenix). Pollutants in severe industrial (Altoona) and urban industrial (N.Y.C.) increase attack markedly. Nickel alloys have high resistance to almost all atmos, 67Ni-33Cu roofing in N.Y.C. shows no measurable loss in thickness after 44 yrs; however, slight pitting (2 to 4 mils) and tarnishing may occur over 20 yrs in Altoona and N.Y.C. **Precious metals**—high res, although some may tarnish under certain conditions. **Stainless steels**—high res for most grades; "300" grades best and will retain brightness for many yrs in most urban and rural atmos; but slight staining occurs in sulfur-bearing industrial atmos. **Tantalum**—should have high res. **Tin**—high res; corrosion rates (mpy) for 20 yrs: 0.02 in rural atmos (State College and Phoenix); 0.07 in severe indus (Altoona); **Titanium and alloys**—high res; 0.0008 mpy in an indus atmos. **Tungsten**—high res. **Zinc and alloys**—good res; rate of attack after 10 to 20 yrs $<$ 0.01 mpy in dry rural atmos (Phoenix), 0.20 to 0.23 mpy in urban-indus (N.Y.C.) and 0.19 to 0.31 mpy in severe indus (Altoona). Rate of attack is roughly similar whether in form of galvanized steel, die castings or rolled sheet. **Zirconium and alloys**—high res.

Nonmetallics. Acetal copolymer and homopolymer—special UV stabilized and black pigmented grades prevent little loss in prop. **Acrylic**—satis up to 20 yrs. **Epoxy (glass reinf)**—after 1 yr retains 98+% flex str. **Fluorocarbon (PVF_2)**—exc after 8 yrs. **Polyethylene**—not normally res but can be made to produce satis service for 5-20 yrs.

TABLE 35.4 Corrosion Data by Environment and Material (*Continued*)

Atmosphere — Marine

Metals. Aluminum and alloys—1000, 3000, 5000 and 6000 series alloys have high res. with 5000 grades generally the most suitable. In severe atmos; initial attack may be as high as 4 mpy, but usually tapers off to as low as 0.1 mpy after first yr. After 5 yrs 80 ft and 800 ft from tide at Kure Beach, attack ranged from 0.007 to 0.025 mpy. Most widely used are 5083, 5086, 5154, 5052 and 6061. Many alloys apt to pit but tapers off in time. Above alloys also have good res. in splash zone, where pitting tendency may be less, but attack rate high if pits develop. Corrosion rate higher in mean-tide than splash zone, but less than if fully immersed. **Beryllium**—information very limited, but believed apt to pit. **Cadmium**—very good res. based on tests at Kure Beach. **Carbon steels**—rapidly attacked in splash zone, rates ranging to 50 mpy, which may be 10 times higher than for same steel submerged. Attack decreases with distance from tide: 47 mpy 80 ft from mean tide, 1.3 to 1.6 mpy 800 ft from tide, at Kure Beach. 2.3 to 2.8 mpy 300 ft from tide at Cristobal, Canal Zone. **Cast irons**—Austenitic cast irons have good res. and plain cast iron is about twice as res. as 0.2% copper steel, based on 7½ yrs exposure at Kure Beach. **Cobalt and alloys**—very good res. 0.1 mpy 80 ft from tide and 0.2 mpy 800 ft from tide after 3 yrs at Kure Beach for cobalt. At same site, 67Co-30Cr-2W, a wear-resistant alloy, lost none of its reflectivity after 1½ yrs. **Columbium**—should be res. to attack. **Copper and alloys**—good to high res.; 0.01 to 0.17 mpy for copper, various brasses, and cupronickels exposed for up to 20 yrs at Cristobal, Kure Beach, Key West, La Jolla, Calif. and Sandy Hook, N.J. Rate of attack somewhat higher in tropical zones than in temperate climates. Alloying with aluminum, nickel, zinc tend to increase, silicon and tin decrease, res. over pure copper, but differences slight. In general, alloy with 15% or more zinc susceptible to dezincification, but can be controlled by small additions of arsenic, antimony or phosphorus. Performance in splash zone more similar to that in atmos than in immersion. Generally, alloys having good res. in severe atmos (Cristobal) also good in splash zone. At mean tide, attack about 20 to 60% that for fully immersed. **Lead**—very good res. 0.02 mpy for chemical and antimonial lead after 20 yrs at La Jolla and Sandy Hook; 0.08 mpy after 8 yrs at Cristobal. Even better res. if atmos polluted. **Low alloy steels**—substantially greater res. than plain carbon steels: 0.7 to 0.9 mpy for low alloy steels, 1.8 mpy for copper steel, at Cristobal; in general, total alloy content of 2% seems to provide maximum return in performance. At Kure Beach, 800 ft from tide, 0.350 mpy for nickel-copper-molybdenum steel having alloy content of 2%, 0.582 mpy for 1.1%. **Magnesium and alloys**—fair; 1 mpy fairly typical. For AZ31 alloy: 0.94 mpy after 16 yrs at Cristobal; about 0.9 mpy after 32 mos. at Daytona Beach; 0.57 mpy 80 ft from tide after 4 yrs at Kure Beach. Oxide film which form upon exposure to normal atmos tends to break down in salt-laden atmos, especially salt spray. **Molybdenum and alloys**—high res. in atmos; 0.1 mpy (max pit 2.4 mils) after 7 yrs, 80 ft and 800 ft from tide at Kure Beach. Alloys TZM and Mo30W should behave similarly. **Nickel and alloys**—generally high res.; 0.01 mpy or less for nickel (0.0095 mpy after 7 yrs 80 ft from tide at Kure Beach, 0.0075 mpy and negligible pitting after 16 yrs at Cristobal). Ni-Cu, "Monel 400," will tarnish, but attack rate low (0.014 mpy after 7 yrs at Kure Beach and 16 yrs at Cristobal; other tests show lower rates). Ni-Cr, "Inconel 600": 0.0016 mpy (1.3 mils max pit depth) after 7 yrs 80 ft from tide at Kure Beach. Ni-Cr-Fe, "Incoloy 800" and "825": 0.006 mpy (0.9 and 0.7 mil max pit depths, resp.) after 7 yrs at Kure Beach. Ni-15/22Cr-3/7Mo alloys such as "Hastelloys F" and "G", "Inconel 700" and "718", "Illium R" and "Elgiloy" are even more res. Most res. of all (only titanium alloys have comparable res.) are Ni-16/22Cr-9/18Mo alloys like "Hastelloy C", "C-276" and "X", "Inconel 625", "MP35N" (based on preliminary tests), "Chlorimet 3" and "Rene 41". Res. in splash zone is virtually as good as in atmos, but may be somewhat reduced in tide zone. **Precious metals**—except for silver, which tarnishes, especially if sulfur compounds present, major noble metals, e.g. platinum, palladium and gold, virtually immune to attack, platinum being the most resistant. **Stainless steel**—good to high res.; austenitic grades generally preferred because of greater res. to staining. Type 304: < 0.1 mpy 800 ft from tide at Kure Beach (somewhat more staining but also negligible attack 80 ft from tide). Type 316 even more resistant. Types 301, 316 and 321 free from pitting and weight loss after 8 yrs at Cristobal. Martensitic grades, typified by 410, may resist after few months, pit on long term (up to 5 mils deep after 8 yrs at Cristobal, but negligible weight loss, e.g., 0.007 mpy). Ferritic 430 subject to partial rusting after about 1 yr at Christobal, but weight loss negligible. Resistance in splash zone also good (austenitic grades again superior). However, subject to some attack in tide zone, e.g., 0.02 mpy for 316 stainless, 0.11 mpy for 304 after 8 yrs in Pacific off Canal Zone. **Tantalum**—should be res. **Tin**—good res.; 0.07 mpy at Sandy Hook, 0.11 mpy at La Jolla, after 20 yrs 0.09 mpy after 10 yrs at Key West. **Titanium and alloys**—excellent res.; immune to crevice attack, pitting and general corrosion at ambient temperatures. Corrosion rate nil for commercially pure titanium after 5 yrs 80 ft and 800 ft from tide at Kure Beach. Also virtually immune to corrosion in splash and tide zones. **Tungsten**—

TABLE 35.4 Corrosion Data by Environment and Material (*Continued*)

Atmosphere — Marine (Continued)			
should be res. **Wrought iron**—somewhat similar res. to carbon steel. 1.2 mpy at Halifax, Nova Scotia; 2.2 mpy, Aukland, New Zealand; 4.7 mpy, Plymouth, England; 11 mpy, Colombo, Ceylon; 2.1 to 3.5 mpy,	300 ft from tide at Cristobal. **Zinc and alloys**—good res.; 0.02 to 0.03 mpy at Key West; 0.06 to 0.07 mpy, Sandy Hook; 0.05 to 0.08 mpy, La Jolla, Calif; for various grades of rolled zinc after 10	to 20 yrs. At Kure Beach, rolled zinc contaminated with traces of iron: 0.4 to 0.5 mpy 80 ft from tide (0.3 mpy at 800 ft) after 6 mos.; 0.3 to 0.4 mpy, 80 ft (0.2 at 800 ft) after 1 yr.	**Ref.** Fink, F. W.; Boyd, W. K.; "The Corrosion of Metals in Marine Environments," DMIC Report 245, Battelle (Columbus), May '70. Published by: Bayer & Co., Col., Ohio.
Carbon tetrachloride			
Nonmetallics. ABS—unsatis. **Acetal copolymer**—after 6 mos at 120 F: yld str −11%, ten mod −32%, length +1.2%, weight +5.2%, appearance no change. **Acetal homopolymer**—365 days at 120 F: ten mod −44%, ten str −7%, length −0.3%, weight +5.7%. **Butyl rubber**—70 hrs at r.t.: +214% vol change. **Chlorinated polyether**—res at 80 F. **Chlorosulfonated polyethylene rubber**—severe effect at r.t. **Fluorocarbon (PVF_2)**—exc to 275 F. **Fluoroelastomer**—little or no effect at 158 F. **Fluorosilicone rubber**—after 7 days at 75 F: ten str. −45%, volume +20%. **Graphite (impervious)**—res 100% boiling. **Hydrocarbon rubber**—severe effect at r.t. **Neoprene**—severe effect at r.t. **Nitrile rubber**—rec. **Nylon**—little or no att. **Phenolic**—varies with grade,	some show little weight change and exc appearance after 1 yr. **Polycarbonate**—not res after 6 mos at r.t. **Polyester (glass reinf)**—NR. **Polyethylene (hi-D)**—marginal after 7 days at 70 F. **Polyimide (glass reinf)**—after 7 days exp retains 92% of flex mod and 76% of flex str. **Polypropylene**—unsatis after 100 days at 140 F. **Polystyrene**—soluble. **Polysulfone**—7 days at 72 F: weight	+0.2%. **PVC-acrylic: alloy**—very slightly whitened after 7 days at 73 F. **Silicone rubber**—after 5 days at 120 F: t.s. −45%, volume +20%. **Styrene-acrylonitrile**—moderately resistant at 73 F. **SBR rubber**—after 70 hrs at r.t.: +207% vol change. **Urethane rubber**—severe effect at 122 F. **Vinyl ester (glass reinf)**—rec at 80 F.
Chlorine			
Metals. Aluminum—res. to normal amounts (10 ppm or less) used to treat water. **Carbon steels**—res. to dry, liquid or gaseous at r.t. **Columbium**—little or no attack in wet at 205 F. **Lead**—res. to dry; attacked, but suitable for use if moist up to 230 F; res. to amounts used to treat water. **Magnesium**—res. to dry at r.t., attacked if moist. **Molybdenum**—attacked by wet at r.t. and by dry above 480 F (but little weight loss up to 1470 F). **Nickel and alloys**—res. to dry, liquid or gaseous at r.t., and at elevated temps. under certain conditions. **Precious metals**—gold	and palladium rapidly attacked; platinum, rhodium and ruthenium slightly attacked, iridium unaffected by dry or moist at moderate temp. Silver has good res. at r.t. **Stainless steels**—austenitic grades have good res. to dry gas at r.t., severely attacked at high temps. or by wet gas. Rate of attack in dry gas about 10 mpy at 400 F, 60 mpy at 600 F, 400 mpy at 800 F. **Tantalum**—no appreciable attack in wet or dry below 300 F. **Tin**—severely attacked. **Titanium**—exc. res. in moist; < 0.1 mpy at r.t. if more than 0.1% water present; rapid attack if dry (< 0.1%	water). **Tungsten**—attacked by dry at about 480 F. **Zinc**—res. to dry gas. **Zirconium**—res. to dry gas, attacked if moist. **Nonmetallics. Chlorinated polyether**—res to wet or dry at 80 F. **Chlorosulfonated polyethylene rubber**—dry and wet at r.t.: severe effect. **Fluorocarbon (PVF_2)**—exc in dry and wet to 212 F. **Fluorcarbon (TFE, FEP)**—res at 200 F. **Fluoroelastomer**—dry at 212 F and wet at r.t.: little or no effect. **Graphite (impervious)**—res 100% dry at r.t. **Hydrocarbon rubber**—dry at r.t.: no data, not likely to be compatible; wet at r.t.: severe	effect. **Neoprene**—dry at r.t.: minor to moderate effect; wet at r.t.: severe effect. **Nylon**—unsatis in gas at r.t. **Polyethylene (Hi-D)**—unsatis at 70 F. **Polypropylene**—unsatis in gas and marginal in liquid at 68 F. **PVC**—100% dry: unplast satis at 68 F, some att or absorp at 140 F. **Silicon carbide**—at 390 F: dry −0.1 mpy, wet +0.1 mpy. **Urethane rubber**—dry and wet at r.t.: no data, not likely to be compatible. **Vinyl ester** (glass reinf)—rec in wet and dry at 210 F.

TABLE 35.4 Corrosion Data by Environment and Material (*Continued*)

Citric acid

Metals. Aluminum—generally res. **Beryllium**—initially attacked, but res. in time. **Cast irons**—rapidly attacked. Even austenitic grades have poor res., 90 mpy in 5% solution at 60 F. **Chromium**—good res. in dilute sol. at r.t.; no attack in 10% sol. at 54 F, 7 mpy at 136 F. **Copper**—moderate res.; 2.2 mpy in 0.2% sol. at 70 F after 5 days. **Nickel**—good res. in dilute sol. at r.t., 0.8 mpy after 5 days in 2% sol. Moderately attacked in higher con. and temps; 5 mpy in 5% sol. at r.t. after 7 days, 20 mpy at 140 F after 7 days. Aeration increases attack. **Silver**—good res. **Stainless steels**—high to moderate res., some pitting may occur. In 10% sol. at 210 to 215 F after 4 hrs: 0.5 mpy for 316, 0.8 mpy for 430, 8 mpy for 302 and 304, 10 mpy for 410. In 60 to 78% sol. at 125 F after 5 wks: 0.1 mpy for 304 and 316. **Tin**—good res. in dilute, air-free sol.; 0.12 mpy in 0.75% sol. after 9 days. Poor res. in hot, con. or aerated sol. **Titanium**—high res.; 0.5 mpy in all con. at 212 F. **Zinc**—attacked. **Zirconium**—high res.; 0.5 mpy and 0.2 mpy max at 140 and 212 F resp. for all con.

Nonmetallics. Acetal copolymer—after 12 mos at 73 F at 10%: yld str +3%, tens and mod −10%, length +0.2%, weight +1.9%, appearance NC. **Acrylic**—limited service in 80% at 220 F. **Chlorinated polyether**—res at 250 F. **Chlorosulfonated polyethylene rubber**—little or no effect at r.t. **Fluorocarbon (PVF_2)**—exc to 250 F. **Fluoroelastomer**—little or no effect at r.t. **Graphite (impervious**—res to all conc at boiling. **Hydrocarbon rubber**—little or no effect at r.t. **Neoprene**—little or no effect at r.t. **Nylon**—little or no att to some att in 10% at r.t. **Polyethylene (hi-D)**—satis after 180 days at 122 F. **Polyester (glass reinf)**—rec in all conc to 200 F. **Polypropylene**—satis after 30 days at 140 F. **Polystyrene**—res to 10%, heat reduces res; slight att in 20%; heat reduces res. **Polysulfone**—7 days at 72 F at 40%: weight +0.4%. **PVC**—unplasticized satis at 140 F, plast at 68 F. **PVC-acrylic alloy**—no change in 10% after 7 days at 73 F. **Styrene-acrylonitrile**—res in 10% at 122 F. **Urethane rubber**—little or no effect at r.t. **Vinyl ester (glass reinf)**—rec at 210 F.

Detergents

Nonmetallics. ABS—satis. **Acetal copolymer**—after 6 mos at 180 F: yld str +3%, tens mod −15%, length +0.3%, weight +1%, slight discoloration. **Acetal homopolymer**—1 yr at 73 F in Lestoil: ten str −4%, weight +0.2%. **Ethylene-propylene rubber**—at r.t. after 70 hrs ten str is 100-105% of original, vol changes −1 to −2%. **Fluorocarbon (TFE, FEP)**—res to boiling. **Nylon**—no att. **Phenolic**—varies with grade, some show little weight change and exc appearance after 1 yr. **Polyester (glass reinf)**—rec in sulfonated to 140 F. **Polyethylene (hi-D)**—satis at 70 F. **Polypropylene**—satis after 30 days at 140 F. **Polysulfone**—7 days in Lestoil: weight +0.3%. **Styrene-acrylonitrile**—resistant at 73 F.

TABLE 35.4 Corrosion Data by Environment and Material (*Continued*)

Ethyl alcohol

Nonmetallics. ABS—satis in 50%. **Chlorosulfonated polyethylene rubber**—little or no effect at 200 F. **Fluorocarbon (TFE, (FEP)**—res at 400 F. **Fluoroelastomer**—little or no effect at r.t. **Fluorosilicone rubber**—after 7 days at 75 F: t.s. −30%, volume +5%. **Graphite (impervious)**—res 100% boiling. **Hydrocarbon rubber**—little or no effect at r.t. **Neoprene**— little or no effect at 158 F. **Nitrile rubber**—rec. **Polycarbonate**—res in 96% after 6 mos at r.t. **Polyester (glass reinf)**—rec. **Polypropylene**—satis after 100 days at 140 F. **Polystyrene**—slight att; heat reduces res. **Polysulfide rubber**—exc (0-20% vol swell) for 30 days at 80 F. **PVC**—unplast satis at 68 F, some att or absorp at 140 F, plast satis at 68 F. **PVC-acrylic alloy**—no change in 95% after 7 days at 73 F. **Silicone rubber**—after 7 days at 75 F: t.s. −30%, volume +5%. **Urethane rubber**—severe effect at r.t.

Ethylene glycol

Metals. Aluminum—res.; attack may occur if less than 0.01% water present, and at elevated temps. **Cast irons**—gray irons have good res.; austenitic and high-silicon irons even more res. **Copper and alloys**—res.

Magnesium—res. at r.t. **Nickel and alloys**—res. **Stainless steel**—exc. res.; < 0.1 mpy for 302 and 316 at 70 to 160 F.

Nonmetallics. ABS—satis. **Acetal copolymer**—after 6 mos at 180 F at 50%: yld str 0% change, ten mod −18%, length +0.4%, weight +1.3%, slight discoloration. **Acrylic**—satis at 100 F. **Butyl rubber**—70 hrs at 212 F: −1% vol change. **Chlorinated polyether**—res at 220 F. **Chlorosulfonated polyethylene rubber**—little or no effect at 200 F. **Epoxy (glass reinf)**—after 30 days little weight change, retains 100% flex str. **Ethylene-propylene rubber**—at r.t. after 70 hrs t.s. is 87-102% of original, vol change negligible. **Fluorocarbon (PVF_2)**—exc to 275 F. **Fluoroelastomer**—little or no effect at 250 F. **Fluorosilicone rubber**—after 7 days at 180 F: t.s. −5%, volume no change. **Graphite (impervious)**—res all conc at 338 F. **Hydrocarbon rubber**—little or no effect at r.t. **Natural rubber**—satis. **Neoprene**—little or no effect at 158 F. **Nitrile rubber**—rec. **Polyacrylate rubber**—after 70 hrs at 212 F: +37% vol change. **Nylon**—satis at 90% at r.t. **Polyester (glass reinf)**—rec to 200 F. **Polyethylene (Hi-D)**—satis after 180 days at 122 F. **Polypropylene**—satis after 1 yr at 73 F. **Polysulfide rubber**—exc (0-20% vol swell) for 30 days at 80 F. **PVC**—unplast satis at 140 F, plast satis at 68 F. **SBR rubber**—after 70 hrs at 212 F: +4% vol change. **Silicone rubber**—after 7 days at 180 F: t.s. −5%, vol no change. **Styrene-acrylonitrile**—resistant at 73 F. **Urethane rubber**—minor to moderate effect.

TABLE 35.4 Corrosion Data by Environment and Material (*Continued*)

Ferric chloride

Metals. Aluminum—attacked. **Cobalt**—negligible attack after 1 day in 2% sol. for 50Co-20Cr-15W-10Ni alloy; 0.2 to 10 mpy for various Co-Cr-W alloys. **Columbium**—high res. No attack in 10% sol. after 1 mo. **Chromium**—high res. in dilute sol. at r.t.; no attack in 10% sol. at 54 F; 16 mpy at 136 F. **Copper and alloys**—moderate to severe attack. **Lead**—rapidly attacked. **Magnesium**—rapidly attacked. **Nickel and alloys**—nickel rapidly attacked except in very dilute sol. Most nickel alloys also readily attacked; however, high-molybdenum and chromium alloys, e.g., 54Ni-16Mo-16Cr, may be exception. **Precious metals**—platinum has high res.; 0.01 mpy to 10% sol. at r.t. Hot sol. attacks gold, palladium, platinum and the rhodium-and-iridium-platinum alloys. Iridium, rhodium and ruthenium resist hot sol. **Stainless steels**—most grades apt to pit, some very severely. Molybdenum-bearing grades, e.g., 316, 329, generally most res. **Tantalum**—high res. **Tin**—rapidly attacked. **Titanium**—exc. res.; < 0.5 mpy in 1 to 30% con. at 212 F, 0.7 mpy in 50% con. at 235 F. **Zinc**—attacked. **Zirconium**—exc. res. in very dilute sol. at r.t. and moderately elevated temps. Moderate to severe attack with increasing con. and temps. Based on 6-day tests: 0.1 mpy at 95 F, 0.2 mpy (140 F), 0.4 mpy (212 F) in 1% sol., 1 mpy (95 F), 0.7 mpy (140 F), 31 mpy (212 F) in 5% sol., 3.9 mpy (95 F), 5.4 mpy (140 F), 145 mpy (212 F) in 10% sol.

Nonmetallics. Acetal homopolymer—1 yr at 73 F at 5%: ten str −4%, weight −0.9%. **Chlorinated polyether**—res at 250 F. **Chlorosulfonated polyethylene rubber**—little or no effect at 200 F. **Fluorocarbon (PVF$_2$)**—exc in 50% to 275 F. **Fluoroelastomer**—little or no effect at r.t. **Graphite (impervious)**—res all conc at boiling. **Hydrocarbon rubber**—little or no effect at r.t. **Natural rubber**—ebonite is satis; soft is limited. **Neoprene**—little or no effect at r.t. **Nylon**—unsatis at r.t. **Polyester (glass reinf)**—rec to 200 F. **Polyethylene (hi-D)**—satis at 70 F. **Polypropylene**—satis at 73 F **Polystyrene**—res; heat reduces res. **PVC**—satis at 140 F. **Silicone rubber**—unaffected in 60% after 7 days at 212 F. **Styrene-acrylonitrile**—resistant at 122 F. **Urethane rubber**—little or no effect at r.t. **Vinyl ester (glass reinf)**—rec at 210 F.

Freon

Metals. Aluminum—res. to most types, slight attack in others. **Carbon steel**—should be satisfactory. **Copper and alloys**—res. **Magnesium**—res. if dry at r.t.; attacked if moist and at elevated temps.

Nonmetallics. ABS—varies with type: satis in 12, unsatis in 11. **Chlorinated polyether**—res at 150 F. **Chlorosulfonated polyethylene rubber**—little or no effect by 11, 12, 22, 113, 114 at r.t. **Fluoroelastomer**—no to moderate effect by 11, 12 at r.t.; severe effect by 22 at r.t.; little or no effect by 113, 114 at r.t. **Graphite (impervious)**—res 11, 12 at r.t. **Hydrocarbon rubber**—severe effect by 11, 22, 113, 114 at r.t.; minor to moderate effect by 12 at r.t. **Neoprene**—little or no effect by 12, 22, 113, 114 at r.t. **Nitrile rubber**—rec in 11, 12, 13, 32, 113. **Polyethylene (hi-D)**—satis at 70 F. **Polypropylene**—satis at 73 F. **Polysulfide rubber**—exc (0-20% vol swell) in 11, 12, 13, 32, 112, 114, 115, 218; fair (40-80% vol swell) in 22 and 31; unsatis in 21; all values 30 days, 80 F. **Silicone rubber**—varies with type: in Freon 12 vol changes +45 to +150% after 3 days at 75 F. **Styrene-acrylonitrile**—at r.t. not resistant to 11, res. to 12. **Urethane rubber**—minor-moderate effect by 11 at r.t.; little or no effect by 12, 113 at r.t.; severe effect by 22 at r.t.

TABLE 35.4 Corrosion Data by Environment and Material (*Continued*)

Gasoline		
Metals. Aluminum—high res. to refined and anhydrous, attacked in sour. **Copper and alloys**—high res. to refined, fair to poor res. in sour. **Nickel alloy**—"Monel" has high res. to refined, poor res. to sour. **Stainless steels**—high res. for most grades to refined; in sour, 302, 304, 316 have high res.; 410, 416, 430 fair res. **Tin**—high res. if moisture- and sulfur-free. **Nonmetallics. ABS**—unsatis. **Acetal copolymer**—after 6 mos at 120 F: yld str −12%, ten mod −12%, length +0.7%, weight +1.5%, appearance no change. **Acetal homopolymer**—820 days at 73 F in Texaco: ten mod −17%, ten str −7%, length +0.7%, weight +1.6%. **Acrylic**—unsatis at 100 F. **Chlorinated polyether**—res at 220 F. **Chlorosulfonated polyethylene rubber**—minor to moderate effect at r.t. **Fluorocarbon (TFE, FEP)**—res at 200 F. **Fluoroelastomer**—little or no effect at r.t. **Graphite (impervious)**—res boiling. **Hydrocarbon rubber**—minor-severe effect at r.t. **Neoprene**—minor-moderate effect at r.t. **Nitrile rubber**—rec. **Nylon**—no att. **Polyester (glass reinf)**—rec at ambient. **Polyethylene (hi-D)**—marginal after 365 days at 68 F. **Polypropylene**—satis after 100 days at 140 F, marginal after 1 yr at 73 F. **Polystyrene**—not res. **Polysulfide rubber**—exc (0-20% vol swell) for 30 days at 80 F. **Polysulfone**—7 days at 72 F: weight +0.1%. **PVC-acrylic alloy**—no change after 30 days at 73 F except very sl staining. **PVC**—unplast satis at 140 F. **Silicone rubber**—after 7 days at 75 F, volume +165%. **Styrene-acrylonitrile**—resistant at 122 F. **Urethane rubber**—minor-moderate effect at r.t. **Vinyl ester (glass reinf)**—rec at 100 F.	
Grease		
Nonmetallics. Acetal copolymer—after 6 mos at 180 F: yld str +4%, tens mod +3%, length +0.2%, weight −0.03%, appearance NC. **Acetal homopolymer**—240 days at 200 F in chassis lubricant: ten str 0% change, weight −0.3%. **Polypropylene**—satis at 68 F. **Silicone rubber**—after 3 days at 300 F: no change in ten str, volume +20%. **Styrene-acrylonitrile**—moderately resistant at 73 F.		

TABLE 35.4 Corrosion Data by Environment and Material (*Continued*)

Hydraulic fluid

Nonmetallics. ABS—unsatis in Skydrol-500, 700. **Acetal copolymer**—after 6 mos at 180 F in Lockheed 21: yld str −11%, ten mod −41%, length +1.4%, weight +3.6%, appearance no change. **Acetal homopolymer**—after 310 days at 160 F in Lockheed 21: ten str −23%, length +0.3%, weight +0.9%. **Butyl rubber**—70 hrs at 212 F: +3% vol change. **Chlorosulfonated polyethylene rubber**—severe effect by Skydrol-500 at r.t. **Epoxy (glass reinf)**—after 30 days little weight change, retains 100% flex str. **Ethylene-propylene rubbers**—after 70 hrs at 212 F in Skydrol-500A retain 87-99% of ten str, vol changes −24 to +11%. **Fluoroelastomer**—severe effect by Skydrol-500 at r.t. **Fluorosilicone rubber**—after 7 days at 120 F in Skydrol-500A; ten str −35%, volume +10%. **Hydrocarbon rubber**—little or no effect by Skydrol-500 at 250 F. **Neoprene**—severe effect by Skydrol-500 at r.t. **Nitrile rubber**—rec. **Polyacrylate rubber**—after 70 hrs at 212 F: +116% vol change. **Polyimide (glass reinf)**—after 60 days in Skydrol-500 flex mod is 95% of r.t. value. **Polysulfide rubber**—good (20-40% vol swell) in Skydrol for 30 days at 80 F. **Polysulfone**—3 days at 250 F in Skydrol 500A: dissolves. **Silicone rubber**—after 7 days in Skydrol-500A at 160 F: ten str −10 to −80%, volume +10 to +30%. **Styrene-acrylonitrile**—moderately resistant at 73 F. **SBR rubber**—after 70 hrs at 212 F: +10% vol change. **Urethane rubber**—severe effect by Skydrol-500 at 122 F.

Hydrochloric acid

Metals. Aluminum—rapidly attacked. **Beryllium**—rapidly attacked at r.t. **Carbon steels**—rapidly attacked. **Cast irons**—unalloyed and low alloy grades rapidly attacked. High-silicon irons, especially those containing molybdenum, have good res. (up to 5 mpy) under most conditions. **Chromium**—rapidly attacked. **Cobalt alloys**—certain Co-Cr-W and Co-Cr-W-Ni alloys attacked at 9 to 52 mpy in 5% con. at r.t. after 24 hrs; may be more rapidly attacked in 10% to con. sol. at moderately elevated temps. **Columbium**—virtually immune to attack (0 to 0.1 mpy) in 18.37% con. at r.t.; 4 mpy in 37% solution at 230 F. **Copper and alloys**—rapidly attacked in con. sol. and moderately elevated temps. For copper, attack at r.t. may range from 4 mpy in 0.03% sol. to over 160 mpy in 37% con. For more res. alloys, rates may vary from 4 to 32 mpy at r.t. to 256 mpy for con. sol. at higher temps. Aeration accelerates corrosion. **Lead**—attacked at about 10 to 13 mpy in con. < 1%, 20 mpy in 5 to 20% sol. at r.t. Antimonial lead fairly resistant in con. below 18% up to 212 F. **Low alloy steels**—generally similar to carbon steels. **Magnesium**—rapidly attacked. **Molybdenum**—high res. to hot or cold sol.; 1.1 mpy for 1 to 20% con. at 160 F after 2 days, appreciably higher attack for longer periods; 0.3 mpy in con. sol. at 230 F. Presence of oxidizing agents accelerates attack. **Nickel and alloys**—nickel is only moderately attacked (1-10 mpy) in air-free, dilute (up to 10%) sol. at r.t. Rate of attack increases with increasing con.; 70 mpy for 30% air-free sol. at r.t. Substantially greater attack (50 to 90 mpy) in air saturated solutions up to 30% con. at r.t. Certain alloys have better res. (62Ni-

TABLE 35.4 Corrosion Data by Environment and Material (*Continued*)

Hydrochloric acid (Continued)

28Mo considered best, 54Ni-16Mo-16Cr second best). Rates for 62Ni-28Mo: 0.3 to 2 mpy for 2 to 37% con. at r.t.; 6 to 9 mpy for 2 to 15% con. at 150 F; 3 mpy for boil. (214 F) 2% sol. **Precious metals**—generally exc res. in absence of oxidizing agents. No appreciable attack for gold, iridium, osmium, palladium, platinum, rhodium and ruthenium in 36% con. at r.t. after 1 week. At 212 F, iridium, ruthenium and rhodium unattacked; gold and platinum slightly attacked; palladium and osmium attacked at 2 and 6.1 mpy resp. Silver is res. under certain conditions, but subject to attack with increasing con. and temps. **Stainless steels**—rapidly attacked. Higher nickel alloys are less susceptible to attack, but are res. only in very dilute sol. **Tantalum**—high res.; < 1 mpy in 18% solution at 75 F, no attack in 37% solution at 230 F. **Tin**—moderate res., 2 to 14 mpy, in dilute (up to 6%); air-free sol. r.t. Poor res. in high con. or aerated sol. **Titanium**—rapidly attacked; addition of 0.15 Pd to Ti or nitriding improves res. in dilute sol. **Tungsten**—generally res.; no attack in dilute (10%) sol. at r.t., moderate attack (18 mpy) at elevated temps. **Zinc**—rapidly attacked. **Zirconium**—high res.; < 1 mpy in boiling 20% sol. and 37% sol. at 212 F.

Nonmetallics. ABS—in 50% satis after 30 days at r.t., unsatis in 140 F. **Acetal copolymer**—not rec in 10%. **Acetal homopolymer**—90 days at 73 F at 10%: unsatis. **Acrylic**—satis in 40% at 150 F, limited service in 30% at 212 F. **Acrylic-PVC alloy**—no change in 10% after 7 days at 73 F. **Alumina (porous)**—res 35% at 212 F. **Butyl rubber**—70 hrs at r.t. in conc: no change. **Chlorinated polyether**—res to 35% at 250 F. **Chlorosulfonated polyethylene rubber**—varies from little or no effects to 37% at 122 F to minor-moderate effect at 200 F. **Epoxy (glass reinf)**—after 30 days in 10% little weight change, retains 60% flex str. **Ethylene-propylene rubber**—after 70 hrs in 30% at r.t. retains 94-99% of ten str, vol change −1 to +4 %. **Fluoroelastomer**—varies from little or no effect to 37% at 158 F, to minor-moderate effect at 230 F. **Fluorocarbon (TFE, FEP)**—res to 0-100% at boiling. **Fluorocarbon (PVF_2)**—exc in conc to 275 F. **Glass-ceramic**—exc in 37% at 194 F. **Graphite (impervious)**—res to all conc at boiling. **Hydrocarbon rubber**—no effect to moderate effect at r.t. **Natural rubber**—satis. **Nitrile rubber**—variable in 20, 30%; not res in 37%. **Nylon**—unsatis in 10% at r.t. **Phenolic**—varies with grade, some show little weight change and exc appearance in 10% after 1 week. **Polyacrylate rubber**—after 70 hrs at r.t. in conc: 4% vol change. **Polyester (glass reinf)**—rec in 37% to 140 F, 20% to 160 F, 10% to 200 F. **Polyethylene (hi-D)**—satis in 37% after 90 days at 70 F. **Modified polyphenylene oxide**—no effect in conc after 3 days at 185 F. **Neoprene**—varies from little or no effect to 37% at r.t. to severe effect at 200 F. **Polysulfide rubber**—varies from exc (0-20% vol swell) in 10%, to good (20-40% vol swell) in 50%, to unsatis in 100%; all values for 30 days, 80 F. **Polysulfone**—7 days at 72 F at 20%: weight +0.4%. **Polypropylene**—satis in 35% after 180 days at r.t., marginal after 100 days at 140 F. **Polystyrene**—res 10%, heat reduces res.; slight att in 38%, heat reduces res. **PVC**—plasticized and unplast satis in 22% at 140 F; in conc HCl plast and unplast satis at 68 F, plast satis at 140 F, unplast some att at 140 F. **Silicon carbide**—minus 0.1 mpy in 25% at boiling temp. **Silicone rubber**—after 3 days at 150 F: t.s. −35%, volume +10%. **Styrene-acrylonitrile**—at 122 F res in 25%, moderately res in 37%. **SBR rubber**—after 70 hrs at r.t. in conc: +3% vol change. **Urethane rubber**—severe effect at r.t. **Vinyl ester (glass reinf)**—rec in 37% at 210 F.

TABLE 35.4 Corrosion Data by Environment and Material (*Continued*)

Motor oil			
Nonmetallics. ABS—satis. Acetal copolymer—after 6 mos at 180 F: yld str +5%, ten mod 0% change, length −0.1%, weight −0.1%, appearance no change. **Acetal homopolymer**—1 yr at 160 F: ten mod +2%, ten str +3%, length −0.3%, weight −0.2%. **Chlorosulfonated polyethylene rubber**—severe effect at r.t. **Fluorelastomer**—little or no effect at r.t. **Hydrocarbon rubber**—severe effect at r.t. **Neoprene**—severe effect at r.t. **Polypropylene**—satis after 100 days at 140 F. **Polystyrene**—slight att; heat does not reduce res. **Polysulfide rubber**—exc (0-20% vol swell) for 30 days at 80 F. **Polysulfonate**—7 days at 72 F: weight unchanged. **Silicone rubber**—after 3 days at 300 F: t.s. −5%, vol no change. **Urethane rubber**—little or no effect at 158 F.			
Nitric acid			
Metals. Aluminum—good res. at con. above 82% at r.t. and slightly elevated temps. **Beryllium**—good res. to con. sol. if cold (violent reaction upon heating). Slow attack in dilute sol. **Carbon steels**—attacked by dilute and intermediate sol. **Cast irons**—high-silicon and high-chromium grades generally res.; others rapidly attacked. **Chromium**—attacked; 12 mpy after 1 day in 32% sol. at 60 F. **Cobalt alloys**—certain Co-Cr-W and Co-Cr-W-Ni alloys have good res. based on 24 hr tests (0.5 to 6 mpy in boil. 10% sol, 0.5 to 32 mpy in 40% con. at 150 F). **Columbium**—high res.; no attack in 70% con. at 75 F and 212 F. **Copper and alloys**—rapidly attacked except by very dilute (0.1% max) sol. **Lead**—moderately attacked in high con. (48 mpy in 95% sol at r.t.). Severely attacked in con. below 80%. **Low alloy steels**—generally similar to carbon steels. **Magnesium**—rapidly attacked. **Molybdenum**—res. attack in con. sol. at r.t; rapidly attacked by boil. con. sol. and dilute (about 25%) sol. at r.t. **Nickel and alloys**—nickel rapidly attacked except possibly in very dilute (less than 0.5%) cold sol. Of the alloys, 47Ni-22Cr-17Fe-6Mo and 42Ni-30Fe-22Cr-3Mo are most res. For 42Ni alloy: 0.5 mpy after 1 mo. in white fuming acid at r.t. (43 mpy after 1 wk at 160 F). For 47Ni alloy: 0.1 mpy in 10 to 70% con. at r.t.; 0.1 to 1 mpy at 150 F and 0.4 to 16 mpy at boil., under same conditions. **Precious metals**—exc. res in 60% and 95% con at r.t. for iridium, platinum, rhodium and ruthenium. These metals also highly res. to 95% concentrations at 212 F. Poor res. for osmium and palladium under these conditions. Gold highly res. to 70% con. at r.t., but subject to some attack in 95% sol. Silver rapidly attacked. **Stainless steels**—austenitic grades generally have high res.; < 0.1 mpy for 304, 321 and 347 in all con. at r.t., and up to 200 F in dilute sol. These grades have high to moderate res (0.1 to 50 mpy) in 10 to 95% sol from r.t. to boil. pt. (210 to 240 F); rate of attack increasing with con. and temp. Type 430 also has good res.; < 0.1 to 0.4 mpy in con. up to 80% at 0 to about 125 F. In general, all grades are attacked (45 to 400 mpy) by fuming nitric. **Tantalum**—only slightly attacked by con. sol. at r.t. and mod-			

TABLE 35.4 Corrosion Data by Environment and Material (*Continued*)

Nitric acid (Continued)

erately elevated temps.; < 1 mpy in 70% sol at 75 and 185 F. Negligible attack in red fuming acid at 250 to 300 F. **Tin**—poor res.; 150 mpy in aerated or air-free 3% sol. at r.t. **Titanium**—exc res. to all con. including fuming at r.t. and at least up to 70% con. at 95 F. However, under certain conditions (e.g. less than 1.34% H_2O or more than 6% NO.) in fuming nitric, pyrophoric reactions may occur. Moderate res., 0.2 to 8 mpy in 5 to 65% sol. at 212 F; < 50 mpy in all con. up to 345 F. **Tungsten**—generally res. in dilute (10%) sol. at r.t. **Zinc**—attacked. **Zirconium**—high res. in con. up to 69.5% at boil. pt.; < 1 mpy at 95 F. in White fuming, < 1 mpy at 160 F. in red fuming, < 5 mpy at 60 F.

Nonmetallics. ABS—unsatis in conc; in 20% satis after 30 days at r.t., unsatis at 140 F. **Acetal copolymer**—not rec in 10%. **Acetal homopolymer**—275 days at 75 F at 10%: unsatis. **Acrylic**—lim service at r.t. **Acrylic-PVC alloy**—no change in 70% after 7 days at 73 F. **Alumina (porous)**—res 70% at 212 F. **Butyl rubber**—70 hrs at r.t.; excessive softening in conc. **Chlorinated polyether**—res to 10% at 180 F, 70% at 80 F, 100% not rec. **Chlorosulfonated polyethylene rubber**—little or no effect by 10% at r.t., severe effect by 30% at 158 F, minor-moderate effect by 60-70% at r.t. **Ethylene-propylene rubbers**—after 70 hrs at r.t. in 10% t.s. is 87-109% of original, vol changes −3 to +10%. **Epoxy (glass reinf)**—after 30 days in 10% little weight change, retains 50% flex str. **Fluorocarbon (TFE, FEP)**—res to 0-100% at b.p. **Fluorocarbon (PVF_2)**—exc in conc to 120F. **Fluoroelastomer**—little or no effect by 10-70% at r.t. **Fluorosilicone rubber**—after 7 days at 75 F in 70%: t.s. −40%, volume +5%. **Glass (borosilicate)**—satis at 150 F. **Glass-ceramic**—exc in 70% at 194 F, 98% at 77 F. **Graphite (impervious)**—res 0-10% at 185 F, 10-20% at 140 F, NR over 20%. **Hydrocarbon rubber**—minor-moderate effect by 10-30% at r.t., severe effect by 30% at 158 F and 60-70% at r.t. **Natural rubber**—not generally rec in 20%. **Neoprene**—minor to moderate effect by 10% at r.t., severe effect by 30%. **Nitrile rubber**—varies in 20, 30%; not rec in 40%. **Nylon**—unsatis in 10% at r.t. **Phenolic**—Varies with grade, some show little weight change and exc appearance in 10% after 1 week. **Polyacrylate rubber**—after 70 days at r.t.: +52% vol change in conc. **Polyester (glass reinf)**—rec in 5% to 140 F. **Polyethylene (hi-D)**—satis in 25% at 70 F, marginal in 50% at 70 F. **Polyimide (glass reinf)**—7 days in 10%: retains 94% of flex mod and 80% of r.t. flex str. **Modified polyphenylene oxide**—no effect in 10% after 3 days at 185 F. **Polypropylene**—satis in 75% after 180 days at 68 F, unsatis after 100 days at 100 F. **Polystyrene**—not res to 20%. **Polysulfide rubber**—unsatis in 10% for 30 days at 80 F. **Polysulfone**—7 days at 72 F at 71%: weight +3.8%, surface attacked, discolored. **PVC**—varies from satis at 5% at 140 F to unsatis in 95% at 68 F. **Silicon carbide**—at boiling temp, 0.0 mpy in 50%, −0.2 mpy in 70%. **Silicone rubber**—little change in 10% at 75 F; after 3 days at 150 F in 50% ten str −80%, volume +5%; after 7 days at 75 F in 70% t.s. −40%, volume +5%. **Styrene-acrylonitrile**—at 122 F resistant in 10%, not res in 25%. **SBR rubber**—after 70 hrs in conc at r.t. disintegrates. **Thermoplastic rubber**—after 2 weeks at r.t. 4-5% wt gain, 90+% decrease in ten str. **Urethane rubber**—severe effect by 10-70% at r.t. **Vinyl ester (glass reinf)**—rec in 20% at 150 F.

TABLE 35.4 Corrosion Data by Environment and Material (*Continued*)

Sea water

Metals. Aluminum alloys—tend to pit, rate of penetration generally decreasing with increasing oxygen content. Pitting rate highest first yr, tapering off to much lower rate in time. In well-aerated waters pitting not a serious problem for certain alloys; "2000" and "7000" series alloys most susceptible; "5000" alloys relatively immune. Depth of pitting generally increases with increasing ocean depths; even 5000 alloys may show severe pitting at great depths. Alloys most susceptible to pitting also generally most susceptible to crevice attack, and vice versa. Crevice attack also more severe at greater ocean depths than in surface waters. **Beryllium**—will pit, rate of pitting being most intense during first 2 mos. **Carbon steels**—chloride ion (sea salt is about 55% chloride) very corrosive to carbon steels, rate of attack increasing with increasing velocity, available oxygen, temperature and pollutants. Certain biofouling, mineral deposits and film formations tend to reduce attack. Rate of attack tends to be less at greater ocean depths than in surface waters. Average penetration rates generally 2 to 5 mpy. **Cast iron**—res. about half that of carbon steel. **Chromium**—should be res. in sheet form and local attack apt to be less than for stainless steel. **Cobalt and alloys**—electrolytic cobalt moderately attacked: 0.7 mpy after 2 yrs; may tend to pit in quite sea water. Co-Cr-Mo alloys have high res. **Columbium**—should be resistant; no measurable attack after 6 mos. **Copper and alloys**—for copper: 0.5 to 2 mpy typical in shallow and deep ocean; lower rates reported, e.g., 0.38 mpy after 16 yrs in shallow depths of Pacific off Panama Canal. **Single phase brasses, silicon and phosphor bronzes are generally similar. Beryllium-copper slightly** more res. Res. of iron-modified alloy 194 seems to be considerably greater than for copper. Brasses vary res.; high zinc grades tend to fail by dezincafication, especially those of two or more phases. Alloys with 15% Zn or less not as apt to fail in this manner. Red brass, Alloy 230, similar to copper (0.5 to 2 mpy) in deep and shallow waters. Arsenic inhibited admiralty brass also resistant (0.6 mpy after 3 yrs in both shallow and deep waters). Aluminum brass (Alloy 687) has very high res.; 0.7 mpy after 5 mos., 0.2 mpy after 3 yrs at 6000 ft. Silicon bronze similar to copper in rate of attack. 5% aluminum bronze has high res. (< 1 mpy after several mos., 0.3 mpy after 3 yrs). 7% aluminum bronze prone to dealuminumization. Cupronickels have high res.; 0.1 to 1.3 mpy after several mos., about 0.8 mpy after 3 yrs. **Lead**—0.4 to 1.2 mpy at shallow depths (6 mos. to 4 yrs); 0.3 to 1.1 mpy (after 6 mos.) at 2000 to 6000 ft. **Low alloy steels—generally similar to carbon steels. Magnesium and alloys**—poor res.; highly purified distilled grade attacked at rate of 10 mpy; commercial grade often corrodes at 100 times this rate, largely because of impurity content. **Molybdenum**—slight attack; 0.3 mpy, in synthetic ocean water at r.t. Attack increases at moderately elevated temps.; 2.1 mpy (140 F), 3.5 mpy (212 F). **Nickel and alloys**—relatively poor res. for nickel; 5 mpy in rapidly flowing water, greater attack with severe pitting in quiet waters. Ni-Cu "Monel 400" and "K500", have high res. in high velocity waters, but tend to pit in quiet waters. Cupronickels are more resistant than "400." Molybdenum imparts virtual immunity to nickel alloys as evidenced by exc res. of "Hastelloy B" (Ni-28Mo-5Fe) and Ni-Cr-Mo alloys like "Hastelloy C", "Inconel 625", others. "Inconel 600" and "X750" resist well-aerated sea water, but apt to pit. "Inconel 718" (3% Mo) much more res. Overall, "Hastelloy C" and "Inconel 625" are best (based on extensive data); among common metals, their res. to sea water is said to be equalled only by titanium. **Precious metals**—platinum and gold have exc. res. Palladium also res., but less so than platinum. **Stainless steels**—In general, all grades susceptible to local attack, highly alloyed grades being most res. Although 304 and 316 will pit, satisfactory service is possible in moderate to high velocity waters. Alloy 20Cb superior to 304 and 316, especially in high velocity waters, but will also pit under low velocity conditions. Ferritic and martensitic grades generally not recommended. 17-4PH can be used effectively under high velocity conditions. **Tantalum**—tantalum and 90Ta-10W alloy virtually immune at ambient conditions. **Tin**—tends to pit, severely at times. **Titanium alloys**— virtually immune to attack at all depths and velocities, including polluted, diluted and hot waters as well as waters containing chlorine, ammonia, hydrogen sulfide gases or excess carbon dioxide. **Tungsten**—subject only to slight attack at ambient and moderately elevated temps., e.g., 0.3 mpy after 6 months in sea water; 0.2 mpy (95 F), 0.3 mpy (140 F), 0.7 mpy (212 F) in synthetic sea water.

TABLE 35.4 Corrosion Data by Environment and Material (*Continued*)

Sea water (Continued)			
Wrought iron—somewhat more res. than carbon steel. **Zinc**—generally attacked at rates of 1 to 2 mpy; higher rates have been reported. **Zirconium**—normally high res.; however, presence of free chlorine will cause attack.	**Ref.** Fink, F. W.; Boyd, W. K.; "The Corrosion of Metals in Marine Environments", DMIC Report 245, Battelle (Columbus), May '70. Published by: Bayer & Co., Columbus, Ohio.	**Nonmetallics. Chlorosulfonated polyethylene rubber**—little or no effect at r.t. **Fluorocarbon (PVF)**—exc to 275 F. **Fluoroelastomers**—little or no effect at r.t. **Glass (borosilicate)**—satis at 150 F. **Hydrocarbon rubber**—little or no effect at r.t. **Neoprene**—little or no effect at r.t. **Polyethylene (hi-D)**—satis at 70 F. **Polypropylene**—satis at 212 F. **PVC**—satis at 140 F. **Urethane rubber**—little or no effect at r.t.	
Sodium chloride			
Metals. Aluminum—attacked. **Copper**—moderate res., aeration accelerates attack. After 2 days in 1N sol. at r.t., 2.6 mpy (unagitated), 4.6 mpy (air-agitated). Up to 12 mpy reported after 3 days under strong aeration and agitation in 3% sol. **Chromium**—high res. in dilute sol.; no attack in 10% sol. at 54 F and 136 F. **Lead**—good to moderate res. in dilute sol.; 0.2 to 1.2 mpy in 0.25 to 5.7% con. at 46 F after 200 days. 4 to 5 mpy in 5.5% sol. after 2 days. **Magnesium**—rapidly attacked. **Nickel and alloys**—generally good res. **Tantalum**—res. **Tin**—good res. in very dilute sol.; 0.3 mpy after 1 wk, 0.6 after 1 mo., in 1.3% sol. at 68 F. **Titanium**—exc. res., 0.01 mpy in 3% boil. sol., 0.1 mpy in 29% sol. at 230 F, 0.05 mpy in boil. saturated con. under unaerated conditions. **Zinc**—moderate res. in very dilute sol.; 5 to 10 mpy after 1 mo. in 3.5% sol. at r.t. **Zirconium**—high res. in 3% sol. at r.t.	**Nonmetallics. ABS**—satis after 30 days at 140 F. **Acetal copolymer**—after 6 mos at 180 F at 10%: yld str +4%, tens mod −10%, length +0.2%, weight +0.49%, slight discoloration. **Acrylic**—satis in 30% at 200 F. **Acrylic-PVC alloy**—no change in 10% after 7 days at 73 F. **Butyl rubber**—70 hrs at 212 F: no change in sol'n. **Chlorinated polyether**—res at 250 F. **Chlorosulfonated polyethylene rubber**—little or no effect at r.t. **Epoxy (glass reinf)**—after 30 days in 10%, little weight change, retains 90+% flex str. **Fluorocarbon (PVF_2)**—exc to 275 F. **Fluoroelastomer**—little or no effect at r.t. **Glass (borosilicate)**—satis at 150 F. **Graphite (impervious)**—res all conc at boiling. **Hydrocarbon rubber**—little or no effect at r.t. **Modified polyphenylene oxide**—no effect after 3 days at 185 F. **Neoprene**—little or no effect at r.t. **Nitrile rubber**—rec **Nylon**—satis at r.t. **Phenolic**—varies with grade, some show little weight change and exc appearance in 10% after 1 yr. **Polyacrylate rubber**—after 70 days at 212 F: 2% vol change in sol'n. **Polyester (glass reinf)**—rec to 200 F. **Polypropylene**—satis in 10% after 30 days at 140 F. **Polystyrene**—slight att in 20%; heat does not reduce res. **Polysulfide rubber**—exc (0-20% vol swell) in 10% for 30 days ae 80 F. **PVC**—satis at 140 F. **SBR rubber**—after 70 hrs in sol'n at 212 F: no change. **Silicone rubber**—no vol change in 2% after 7 days at 75 F. **Styrene-acrylonitrile**—resistant at 122 F. **Thermoplastic rubber**—satis in 10% after 2 weeks at r.t. **Urethane rubber**—little or no effect at r.t. **Vinyl ester (glass reinf)**—rec at 210 F.	

TABLE 35.4 Corrosion Data by Environment and Material (*Continued*)

Sodium hydroxide

Metals. Aluminum—rapidly attacked. **Beryllium**—attack not as severe as on many other materials, but use is not recommended for extended periods over 1000F. **Carbon steels**—res. in dilute sol., attacked in hot con. sol. **Cast irons**—moderately res.; $\leqq$ 5 mpy for gray cast iron up to 70% con. and up to about 180 F. Austenitic cast irons attacked at rate of $<$ 5 mpy at temps. up to boil. pt. in con. up to 70%. Rate of attack increases rapidly above 70% con. at temps. near boil. **Cobalt**—certain Co-Cr-W and Co-Cr-W-Ni alloys have high res.; negligible attack to 0.6 mpy in 50% con. at 150 F after 1 day. **Columbium**—embrittled by boil. sol. of even low con. **Copper and alloys**—both copper and alloys are moderately attacked in dilute sol. For copper, 14 mpy in 3.9% sol. at 86 F after 2 days under static conditions (20 mpy under air-agitated cond.); lower rates have been reported. Of alloys, cupronickels most resistant. **Iron and carbon steels**—moderate to good res. in very dilute sol.; 1 mpy for mild steel in 50% sol. at 100 F after 7 mos.; rapid attacks in 73% sol. after 4 mos. **Lead**—moderate res. in very dilute unaerated sol.; 9.4 mpy in quiet (47 mpy air-agitated) 3.8% sol. after 2 days at r.t. Poor res. in hot or con. sol. **Molybdenum**—severely attacked in fused at 1000 F. **Nickel and alloys**—exc. res.; 0.01 mpy for nickel, 67Ni-33Cu and 76Ni-16Cr-7Fe in 50% con. at 100 F after 7 mos.; 0.1 mpy for 67Ni-33Cu, 1 mpy for nickel and 76Ni-16Cr-7Fe alloy, in 73% con. at 265 F after 7 mos. In fused 100% con., 0.9 to 2.5 mpy for nickel at 750 to 1075 F. **Precious metals**—silver has high res., even at elevated temps. Gold and platinum metals also have good res. **Stainless steels**—exc. res. for both chromium and chromium-nickel grades in dilute sol. up to moderately elevated temps. High to moderate res. in high con. at moderately elevated temps. Cracking may occur near boil. pt. After 3 to 4 mos.: in 20% con. at 120 to 140 F, $<$ 0.1 mpy for 302, 304, 309, 310; 0.1 mpy for 410, 430. In 72% con. at 245 to 255 F, under moderate aeration, 0.1 mpy for 21Cr-34Ni-0.5Cu alloy, 0.3 mpy for 329, 3.1 mpy for 316, 3.7 mpy for 304, 6 mpy for 410, 32 mpy for 430. In 73% nonaerated sol. at 212 to 248 F, 38 mpy for 302, 45 mpy for 304. **Tantalum**—res. to 5% boil. sol., but attacked in fused at 605 F, severely attacked at 1000 F. **Tin**—severely attacked. **Titanium**—high to moderate res.; 0.8 mpy in 10% boil. sol.; 0.1 mpy in 28% sol. at r.t.; 5 mpy in 40% sol. at 176 F. In molten, attacked at 1000 F. **Tungsten**—slight attack in hot alkaline sol.: severely attacked at 1000 F. **Zinc**—attacked; after 2 days in 3.9% sol. at r.t. 18 mpy under quiet conditions, 35 mpy under air-agitated con. **Zirconium**—res.

Nonmetallics. ABS—satis in 25%. **Acetal copolymer**—after 6 mos at 180 F at 60%: yld str −3%, ten mod −6%, length −0.1%, weight −0.18%, slight discoloration. **Acrylic**—limited service in 10% at 120 F. **Acrylic-PVC alloy**—no change in 10% after 7 days at 73 F. **Alumina (porous)**—edges rounded in 10% at 212 F. **Chlorinated polyether**—res to 70% at 250 F. **Chlorosulfonated polyethylene rubber**—little or no effect by 73% at 280 F. **Ethylene-propylene rubbers**—after 70 hrs at r.t. in 50% t.s. is 99-118% of original, vol changes 0 to −1%. **Fluorocarbon (PVF$_2$)**—exc in 50% to 275 F. **Fluorocarbon (TFE, FEP)**—res to 0-100% at boiling. **Fluoroelastomer**—little or no effect by 47% at r.t., severe effect by 50% at r.t. **Fluorosilicone rubber**—after 7 days at 75 F in 50%: ten str −10%, volume no change. **Glass (borosilicate)**—satis at 150 F. **Glass-ceramic**—good (less than 20 mpy) in 1% at 194 F, satis (20-25 mpy) in 7% at 194 F. **Graphite (impervious)**—res 6-67% at boiling, 67-80% at 275 F. **Hydrocarbon rubber**—little or no effect by 20-73%. **Modified polyphenylene oxide**—no effect in conc after 3 days at 185 F. **Neoprene**—little or no effect by 20, 73% at r.t. and 47% at 158 F. **Nitrile rubber**—rec in 50%. **Nylon**—satis at r.t. **Phenolic**—generally poor res in 10% after 1 week. **Polyester (glass reinf)**—rec in 10 and 25% to 130 F, 5% to 160 F, NR in 50%. **Polyethylene (hi-D)**—satis at 70 F. **Polyimide (glass reinf)**—7 days in 10%: retains 93% of flex mod and 82% of r.t. flex str. **Polypropylene**—satis in 60% after 30 days at 140 F. **Polystyrene**—slight att in 1-50%; heat does not reduce res. **Polysulfide rubber**—exc (0-20% vol swell) in 20% for 30 days at 80 F. **Polysulfone**—110 days at 72 F at 5%: weight −0.03%. **PVC**—unplasticized satis at 140 F, plast some att or absorp at 140 F. **Silicon carbide**—+73 mpy in 25% at boiling temp. **Silicone rubber**—after 7 days at 75 F: t.s. −10%, vol no change. **Styrene-acrylonitrile**—resistant in sat at 122 F. **Urethane rubber**—at r.t. little or no effect by 20%, severe effect by 50%. **Vinyl ester (glass reinf)**—rec in 50% at 210 F.

TABLE 35.4 Corrosion Data by Environment and Material (*Continued*)

Sulfuric acid

Metals. Aluminum—res. attack in very dilute (1% or less) or very high con. (98 to 100%) at r.t. Rapidly attacked at other con. and higher temps. **Beryllium**—rapidly attacked at r.t. **Carbon steels**—moderately res. at con. above 70% (5 to 20 mpy at 75 F, 20 to 50 mpy at 125 F, 50 to 200 mpy at 175 F in static tests; higher rates likely in service); more res. at 100% con. Rapidly attacked by con. below 70%. **Cast irons**—good res. in certain con. and temps. High-silicon irons generally best, followed by austenitic grades. For gray iron < 5 mpy in con. above 65% at r.t., but rapid attack at lower con. **Chromium**—attacked; 28 mpy after 1 day in 17% sol. at 60 F. **Cobalt and alloys**—cobalt has moderate res.; 9 mpy in 5% con. at r.t. under static conditions. Certain Co-Cr-W and Co-Cr-W-Ni alloys suffer negligible attack in high con. (77 to 96%) at r.t., but may be attacked by 25% sol. at moderately elevated temps. (150 F). **Columbium**—virtually immune to attack in 20% con. at 200 F and 40% and 95% con. at 75 F. Slight attack (0.1 mpy) in 98% con. at 75 F. Slight attack (0.1 mpy) in 98% con. at r.t. At high con. (95%) rate of attack increases with temp.; 0.8 mpy at 120 F, 19 mpy at 212 F, 180 mpy at 290 F. **Copper and alloys**—copper has high res.; up to 2 mpy in 10 to 80% con. at r.t.; decreasing temps. increase attack (6 to 15 mpy at 140 F). In 60 to 70% sol., attack moderate (3 to 12 mpy) up to 176 F. Rates roughly similar for Si-Mn bronze and 70Cu-30Ni cupronickel. Aeration increases attack. **Lead**—good res.; < 5 mpy in 5 to 50% con. Attack markedly increased in con. below 5%. Attack up to 50 mpy at 50 to 97% con. up to boil. temp. Antimonial lead superior to chemical lead at high con. **Low alloy steels**—generally similar to carbon steels. **Magnesium**—rapidly attacked. **Molybdenum**—high res.; 0.15 mpy to cold sol. up to about 96% con. Good res. to boil. sol. up to 50% con. Increasing con. and temps. increase attack severely. **Nickel and alloys**—Nickel has moderate res.; 2 to 9 mpy in unaerated, dilute (1 to 20%) sol. at r.t. Aeration increases attack appreciably (50 to 60 mpy for 1% and 5% sol.) Con. sol. more aggressive: 30 and 70 mpy for 70% and 95% con. Attack 10 to 30 mpy for 5 to 48% sol. at 140 to 180 F. Among nickel alloys, Ni-Mo, Ni-Mo-Cr and Ni-Si grades are best overall (< 5 mpy for virtually all con. to about 200 F to 250 F). 67Ni-33Cu also has moderate res. (< 5 mpy) in con. up to 80%. **Precious metals**—gold, iridium, osmium, palladium, platinum, rhodium and ruthenium have exc. res. in 98% con. at r.t. and all but rhodium (moderately attacked) and palladium (excessively attacked) have high res. at 212 F. Iridium and ruthenium also have high res. at 570 F for 7 hrs. in 98% sol.; gold only slightly attacked (0.7 mpy). Silver res. dilute sol. at r.t. and is only slightly attacked (0.7 mpy) in boil. 10% and 20% sol. **Stainless steels**—several austenitic grades have high res. in aerated sol. at low and moderately elevated temps. In general, increasing con. and temps. and absence of air-accelerate attack. In nitrogen-saturated 5% sol. at 86 F, < 0.1 mpy for 317, 0.6 mpy (316), 1.2 mpy (310 and 321), 9 mpy (301), 12 mpy (347) and 57 mpy (304); 201, 302, 430 rapidly attacked. In aerated dilute sol. (up to about 10%), 304, 310, 316 and 317 have high res.; < 0.1 mpy at temps. of 0 to 160 F. These grades about equally res. at all con. in aerated sol. at temps up to 70 to 125 F. Types 310 and 317 also have high res. in intermediate (20 to 60%) aerated sol. at 125 to 150 F, 310 being somewhat superior. **Tantalum**—high res.; 0 to 0.1 mpy in 20 to 95% con. at 75 to 350 F. Some attack in 95% sol. at higher temp.; 1.5 mpy at 390 F, 29 mpy at 480 F. In fuming acid: 0.3 mpy at 75 F, 9 mpy at 160 F. **Tin**—moderate res., 2 to 10 mpy in dilute (up to 10%), air-free sol. at r.t. Poor res. in high con.; 70 mpy in air-free 20% sol. at r.t. **Titanium**—high res. in very dilute sol. at r.t.; 0.1 mpy in 1% sol. Moderate to poor res. with increasing con. (75 to 80% sol. being most corrosive) and temps.; 4 mpy in 1% sol. at 100 F, 9 mpy in 5% sol. at r.t. and 30 mpy at 100 F, 60 mpy in 40% sol. at r.t., 250 mpy in 50% sol. at 100 F. Addition of 0.15 Pd increases res. in dilute sol., anodizing improves res. in 40% sol. **Zinc**—attacked. **Zirconium**—high res. < 1 mpy in con. up to 70% up to boil. pt. Severe attack in con. above 80%, especially with increasing temp.

Nonmetallics. ABS—in 50% after 30 days satis at r.t., unsatis at 140 F. **Acetal copolymer**—NR in 30%. **Acetal homopolymer**—316 days at 95 F at 10%: unsatis. **Acrylic**—limited service in 10% at 180 F, 50% at 100 F, unsatis in 50% at 150 F. **Acrylic-PVC alloy**—no change in 30% after 7 days at 73 F. **Alumina (porous)**—res 96% at 212 F. **Butyl rubber**—70 hrs at r.t.: +1% vol change in 50%. **Chlorinated poly-**

TABLE 35.4 Corrosion Data by Environment and Material (*Continued*)

Sulfuric acid (Continued)

ether—res to 80% at 250 F, 90% at 180 F, 96% at 80 F, NR in 98%. **Chlorosulfonated polyethylene rubber**—little or no effect by up to 50% at 250 F, 50-80% at 158 F, 95% at r.t. **Diallyl phthalate**—retains 80% of flex str in 3% after 1 yr. **Epoxy (glass reinf)**—in 3% after 30 days little weight change, retains 75% flex str. **Ethylene-propylene rubber**—after 70 hrs in 98% at r.t. retains 23-80% of ten str, vol change +5 to +8%; in 10% at 212 F t.s. is 96-111% of original, vol change 0 to −2.5%. **Fluorocarbon (TFE, FEP)**—in 0-100% TFE res to 500 F, FEP to 400 F. **Fluoroelastromer**—little or no effect up to 80% at r.t., 60% at 250 F, 90% at 158 F. **Fluorocarbon (PVF_2)**—exc in 60% to 230 F, 85% to 150 F. **Glass-ceramic**—exc in 98% at 194 F. **Graphite (impervious)**—res 0-70% at boiling, 70-85% at 338 F, 85-90% at 300 F, 90-93% at 160 F, 93-96% at r.t., NR over 96%. **Hydrocarbon rubber**—at r.t. little or no effect to 50%, severe effect 60-95%. **Natural rubber**—satis in 50%. **Neoprene**—little or no effect up to 50% at 158 F, generally severe effect over 50% at r.t. **Nitrile rubber**—rec in 17, 30%; varies in 42, 56%; not rec in 70%. **Nylon**—unsatis at r.t.. **Phenolic**—varies with grade, some show little weight change and exc appearance in 30% after 1 yr. **Polyacrylate rubber**—after 70 days at r.t.: disintegrates in conc, +3% vol change in 50%. **Polyester (glass reinf)**—rec in 70% to 140 F, 50% to 200 F. **Polyethylene (hi-D)**—at 70 F satis in 70%, marginal in 95%. **Polymide (glass reinf)**—7 days in 10%: retains 88% of flex mod and 88% of r.t. flex str. **Modified polyphenylene oxide**—no effect in 90% after 3 days. **Polypropylene**—satis in 97% after 30 days at 140 F. **Polystyrene**—slight att in 10-50%; heat reduces res, NR in conc. **Polysulfide rubber**—varies from exc (0-20% vol swell)in 10%, to fair (40-80% vol swell) in 20%, to unsatis in 50% and 100%; all values 30 days, 80 F. **Polysulfone**—69 days at 72 F at 95%: dissolves. **PVC**—unplast satis to 80% at 140 F, plast satis to 45% at 140 F; check perf at higher conc. **Silicone carbide**—+0.1 mpy in 80% at boiling temp. **Silicone rubber**—after 3 days at 150 F in 50% ten str −35%, volume no change; decomposes in 95% after 7 days at 75 F. **SBR rubber**—after 70 hrs at r.t.: disintegrates in conc, +3% vol change in 50%. **Styrene-acrylonitrile**—at 122 F resistant in 25%, not res in conc. **Thermoplastic rubber**—satis in 10% after 2 weeks at r.t. **Urethane rubber**—severe effect at r.t. **Vinyl ester (glass reinf)**—rec in 70% at 210 F.

TABLE 35.4 Corrosion Data by Environment and Material (*Continued*)

Waters other than sea water

Metals. Aluminum and alloys—high res. in high purity (distilled or deionized) or water vapor up to about 400 F. In general, good res. to most neutral or nearly neutral waters providing waters do not contain compounds other than salts of alkaline earth metals. Acid waters containing chlorides can cause severe pitting; sulfate waters of low pH also aggressive. Compounds of Cu, Pb, Sn, Ni and Co in waters promote pitting of alloys ("alclad" aluminum coatings help reduce attack). **Beryllium**—high res. at ambient temps. in neutral waters, even under static conditions. Under aeration and flowing cond., good res. at moderately elevated temps. Protection required above 500 F. Presence of chloride ions in water markedly increases attack. Sulfate, cupric or ferric ions also increase attack. **Carbon steels**—fresh waters: normally pit in neutral solutions since protection afforded by rust is usually irregular; supply of dissolved oxygen and deposited protective films being most critical factors governing attack. 2 to 5 mpy avg rate of attack in quiet waters free of salts and containing dissolved air. Agitation or aeration usually increase attack; deposition of compounds usually supresses attack. Presence of various salts or other substances may either increase or decrease attack. Boiler water: supply of dissolved oxygen again critical factor; deaeration common corrosion preventative. Mine waters: can cause severe attack. **Cast irons**—res. generally similar to carbon steels for plain cast irons. **Cobalt**—good res. in distilled water, 0.2 mpy at 77 F under static conditions. Wear resistant alloys undergo little attack in mine and boiler waters at ordinary temps. **Columbium**—good resistance to 500 F in oxygenated water. Res. seems good under both static and dynamic conditions. **Copper and alloys**—copper has good res. to all fresh waters, attack ranging from 0.2 to 1 mpy, sometimes less. Hard waters seldom corrosive, but soft waters, especially with substantial amounts of free carbon dioxide, may be sufficiently corrosive to cause green stains on plumbing fixtures by reacting with soap. Distilled water not very corrosive, but will pick up trace of copper on long standing. Carbonated water much more corrosive, after 20 hrs at r.t. in water saturated with air and carbon dioxide: 2 to 10 mpy in city water, 2 to 6 mpy in distilled water. Some copper alloys, e.g., red brass, better than pure copper for fresh water plumbing. Silicon and phosphor bronzes, cupronickels, cast bronzes and nickel silvers also have high res. Tin-bearing copper alloys, e.g., 88Cu-10Zn-2Sn, most res. to river waters containing acid-mine drainage. **Lead**—not attacked by pure distilled water free of dissolved gases, but aerated distilled water free of carbon dioxide can be corrosive. Also resists non-potable water, except possibly acid mine waters. Soft waters attack lead sufficiently to have discontinued its use for potable soft water systems (toxicity problem). Fresh waters may also be corrosive if containing carbon dioxide or small amounts of organic acids. Small amounts of nitrates in ground water also increase corrosivity. **Low alloy steels**—more or less similar to carbon steels for fresh waters, with variations in attack more likely under short-term submergence, e.g., over long-term no significant difference in attack of copper structural steels and plain carbon steels. In partly stagnant waters corrosion rate of low alloy steel similar to carbon steel, i.e., about ½ rate in aerated waters. Nickel additions may be marginally beneficial, e.g., in Pittsburgh water at 140 to 145 F: 14.6 mpy for mild steel, 13.2 mpy for 1.65Ni steel, 12.2 mpy for 3.61Ni steel, 12.6 mpy for 5.20Ni steel. In simulated reactor boiling water, essentially no difference between carbon steels and steels of up to 5% alloy content. **Magnesium and alloys**—good res. in stagnant distilled water at r.t. Pitting may occur if small amounts of chlorides, heavy metal salts or carbon dioxide present. Agitation or constant replenishment of water may lead to attack, e.g., little attack on AZ31 alloy after 35 days in stagnant distilled water at 125 F; when water continuously replenished to maintain 6.8pH, rate of attack 7 mpy. Corrosion rates in water at different temperatures: MIA—13.2 mpy (95 F), 6.0 mpy (150 F), 13.2 mpy (180 F), 72 mpy (212 F); AZ92A—0.8 mpy (95 F), 16.3 mpy (212 F); AM100A—0.8 mpy (95 F), 26.9 mpy (212 F). **Molybdenum**—tranished but not attacked by fresh waters up to moderately elevated temps. Poor res. to oxygenated water at 600 F and to water vapor at 1200 F. **Nickel**—high res. to most natural, fresh, distilled, deionized and high purity waters; attack usually < 0.1 mpy. Attack usually < 0.02 mpy in domestic hot water up to 200 F. Res. to carbonated fresh water also good, 0.2 mpy after 10 days at r.t. and 200 psig. Nickel may be attacked in polluted (acid drainage) rivers, e.g., 3.8 mpy in Monongahela River at 5pH (0.3 mpy, 6.5pH), and severely attacked by acid mine waters. **Stainless steels**—high res. to distilled, tap and other fresh waters, including relatively polluted lake and river waters, cold or hot; e.g., after 490 days in Monongahela containing coal mine drainage and spent pickling acid, attack rate < 0.1 mpy for 304, 316, 410 and 430 steels; 2 mpy for 502. In general negligible attack from boiler, high purity and mine waters under most conditions. **Tantalum**—tarnishes in oxygenated water at 500 F. **Tin**—will tarnish, but virtually immune to distilled water and only slightly attacked by carbonated waters. Attacked by drinking waters purified by addition

TABLE 35.4 Corrosion Data by Environment and Material (*Continued*)

Waters other than sea water (Continued)

of strong oxidizing agents which produce nascent oxygen. **Titanium and alloys**—high res. even to brackish river waters, and distilled, degassed-distilled or oxygenated-distilled waters at 500 F. **Tungsten**—no attack from cold or hot water. **Wrought iron**—more or less similar to carbon steels, but may be more res. to pitting under certain conditions. **Zinc**—good res., but only in narrow pH range around neutral point. Can provide good galvanic protection to steel in fresh waters. Moderate attack in aerated distilled water up to about 120 F, severe attack from 120 to 200 F. Aeration increases attack in distilled water, especially if trace amounts of carbon dioxide present. Some rates: 2.0 mpy for plain water at 54 F after 2 months; 4.8 mpy in quiet distilled water. **Zirconium and alloys**—good res. to high temperature waters and steam to 900 F.

Nonmetallics. ABS—satis. **Acetal copolymer**—rec for continuous use at 180 F, retains nearly original tens str in boiling after 22 weeks. **Acetal homopolymer**—not rec for long-term service over 150 F. **Acrylic**—satis after 5 yrs. **Butyl rubber**—disintegrated after 70 hrs at 212 F. **Chlorinated polyether**—res at 250 F. **Chlorosulfonated polyethylene rubber**—little or no effect at 212 F. **Epoxy (glass reinf)**—after 5 yrs immersion minor weight change. **Ethylene-propylene rubber**—after 70 hrs at 212 F t.s. is 76-110% of original, vol change +2%. **Fluorocarbon (PVF)**—in brine exc to 275 F. **Fluoroelastomer**—little or no effect at 212 F. **Fluorosilicone rubber**—in steam after 1 day at 100 psi: t.s. −20%, volume no change. **Graphite (impervious)**—res boiling. **Hydrocarbon rubber**—little or no effect at 212 F. **Neoprene**—little or no effect at 212 F. **Nitrile rubber**—rec in distilled. **Nylon**—no att in cold, little or no att in hot. **PVC-acrylic alloy**—no change after 7 days at 140 F except slight staining (none at 73 F). **Phenolic**—varies in distilled with grade, some show little weight change and exc appearance after 1 yr. **Polyacrylate rubber**—after 70 days at 212 F: +23% vol change. **Polyester (glass reinf)**—rec to 200 F. **Polyethylene (hi-D)**—satis after 1 yr at 70 F. **Polyimide (glass reinf)**—in boiling after 7 days flex mod is +3% and flex str is +12% over r.t. values. **Polypropylene**—satis in distilled after 160 days at 140 F. **Polystyrene**—in distilled—res; heat reduces res. **Polysulfide rubber**—exc (0-20% vol swell) after 30 days at 80 F. **Polysulfone**—7 days at 72 F: weight +0.6%. 7 days at 210 F: weight +0.9%. **SBR rubber**—after 70 hrs at 212 F: +10% vol change. **Silicone rubber**—no change after 3 days at 212 F. **Styrene-acrylonitrile**—in distilled res at 122 F. **Thermoplastic rubber**—in distilled satis after 2 weeks at r.t. **Urethane rubber**—little or no effect at 212 F.

†Abbreviations used in this table: ABS = acrylonitrile-butadiene-styrene; att = attack; atmos = atmosphere; boil pt = boiling point; con, connc = concentrated; exc = excellent; flex mod = flexural modulus; flex str = flexural strength; indus = industrial; max = maximum; mos = months; mpy = mils per year; plast = plasticized; ppm = parts per million; PVC = polyvinyl chloride; res = resistance; resp = respectively; r.t. = room temperature; satis = satisfactory; SBR = styrene butadiene; sol = soluble; ten mod = tensile modulus; tens str = tensile stress; unsatis = unsatisfactory; unplast = unplasticized; vol = volume; yld str = yield stress or strength; yrs = years.

SOURCE: R. J. Fabian and J. A. Vaccari, eds., "How Materials Stand Up to Corrosion and Chemical Attack," *Materials Engineering*, vol. 73, no. 2, p. 36, 1971. Reprinted with permission of Penton/IPC.

corrosion (weld decay). Heating to higher temperatures, 1060 to 1120°C, followed by water quenching will redissolve the precipitated carbides and keep them in solution. Appropriate alloying changes can reduce carbide precipitation.

35.3.10 Mechanical Contributions

Fluid flow or mechanical rubbing can cause removal of or damage to a protective oxide, increasing the proximity of the bare metal and the attacking medium. This can result in increased attack rates because a stable oxide layer is frequently a corrosion rate limiter. An example is *erosion corrosion* caused by high flow rates of domestic hot water in copper pipes, especially around fittings, which can generate turbulence. Another example involves the press fit of gears, wheels, pulleys, etc., onto shafts that experience elastic torsion, or bending. Small relative motions occur at the contacting surfaces which mechanically break up protective oxide layers. This type of corrosion is known as *fretting corrosion.*

35.4 CORROSION DATA FOR MATERIALS SELECTION†

Subject to the limitations mentioned at the beginning of this chapter, the corrosion data in Table 35.4 can be used as a guide in selecting materials for the environments listed. The organization is first by environments and then by materials, metals followed by nonmetals. The abbreviation NR means not recommended.

REFERENCES

35.1 M. G. Fontana and N. D. Greene, *Corrosion Engineering,* 2d ed., McGraw-Hill, New York, 1978.

35.2 E. Rabald, *Corrosion Guide,* 2d ed., rev., Elsevier Scientific Publishing, Amsterdam, 1968.

35.3 R. J. Fabian and J. A. Vaccari (eds.), "How Materials Stand Up to Corrosion and Chemical Attack," *Materials Engineering,* vol. 73, no. 2, February 1971, p. 36.

P · A · R · T · 9

CLASSICAL STRESS AND DEFORMATION ANALYSIS

CHAPTER 36
STRESS

Joseph E. Shigley
Professor Emeritus
The University of Michigan
Ann Arbor, Michigan

36.1 DEFINITIONS AND NOTATION

The general two-dimensional stress element in Fig. 36.1*a* shows two normal stresses σ_x and σ_y, both positive, and two shear stresses τ_{xy} and τ_{yx}, positive also. The element is in static equilibrium, and hence $\tau_{xy} = \tau_{yx}$. The stress state depicted by the figure is called *plane* or *biaxial stress.*

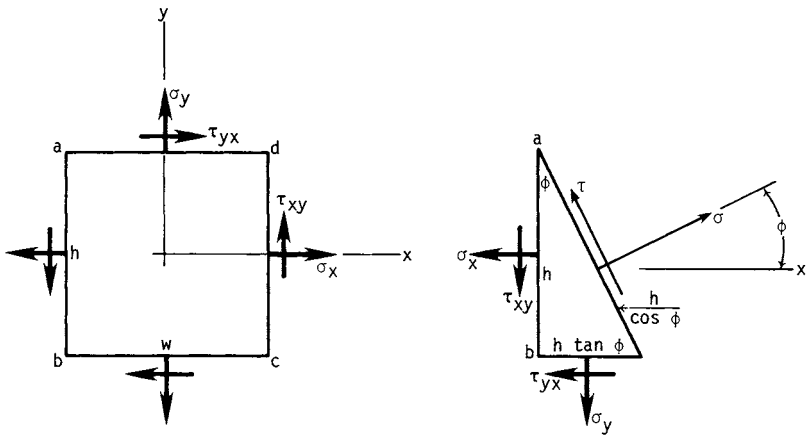

FIGURE 36.1 Notation for two-dimensional stress. (*From* Applied Mechanics of Materials, *by Joseph E. Shigley. Copyright © 1976 by McGraw-Hill, Inc. Used with permission of the McGraw-Hill Book Company.*)

Figure 36.1*b* shows an element face whose normal makes an angle ϕ to the x axis. It can be shown that the stress components σ and τ acting on this face are given by the equations

$$\sigma = \frac{\sigma_x + \sigma_y}{2} + \frac{\sigma_x - \sigma_y}{2} \cos 2\phi + \tau_{xy} \sin 2\phi \tag{36.1}$$

$$\tau = -\frac{\sigma_x - \sigma_y}{2} \sin 2\phi + \tau_{xy} \cos 2\phi \tag{36.2}$$

It can be shown that when the angle ϕ is varied in Eq. (36.1), the normal stress σ has two extreme values. These are called the *principal stresses,* and they are given by the equation

$$\sigma_1, \sigma_2 = \frac{\sigma_x + \sigma_y}{2} \pm \left[\left(\frac{\sigma_x - \sigma_y}{2} \right)^2 + \tau_{xy}^2 \right]^{1/2} \tag{36.3}$$

The corresponding values of ϕ are called the *principal directions.* These directions can be obtained from

$$2\phi = \tan^{-1} \frac{2\tau_{xy}}{\sigma_x - \sigma_y} \tag{36.4}$$

The shear stresses are always zero when the element is aligned in the principal directions.

It also turns out that the shear stress τ in Eq. (36.2) has two extreme values. These and the angles at which they occur may be found from

$$\tau_1, \tau_2 = \pm \left[\left(\frac{\sigma_x - \sigma_y}{2} \right)^2 + \tau_{xy}^2 \right]^{1/2} \tag{36.5}$$

$$2\phi = \tan^{-1} - \frac{\sigma_x - \sigma_y}{2\tau_{xy}} \tag{36.6}$$

The two normal stresses are equal when the element is aligned in the directions given by Eq. (36.6).

The act of referring stress components to another reference system is called *transformation of stress.* Such transformations are easier to visualize, and to solve, using a *Mohr's circle diagram.* In Fig. 36.2 we create a $\sigma\tau$ coordinate system with normal stresses plotted as the ordinates. On the abscissa, tensile (positive) normal stresses are plotted to the right of the origin *O,* and compression (negative) normal stresses are plotted to the left. The sign convention for shear stresses is that clockwise (cw) shear stresses are plotted *above* the abscissa and counterclockwise (ccw) shear stresses are plotted *below.*

The stress state of Fig. 36.1*a* is shown on the diagram in Fig. 36.2. Points *A* and *C* represent σ_x and σ_y, respectively, and point *E* is midway between them. Distance *AB* is τ_{xy} and distance *CD* is τ_{yx}. The circle of radius *ED* is *Mohr's circle.* This circle passes through the principal stresses at *F* and *G* and through the extremes of the shear stresses at *H* and *I.* It is important to observe that an extreme of the shear stress may *not* be the same as the maximum.

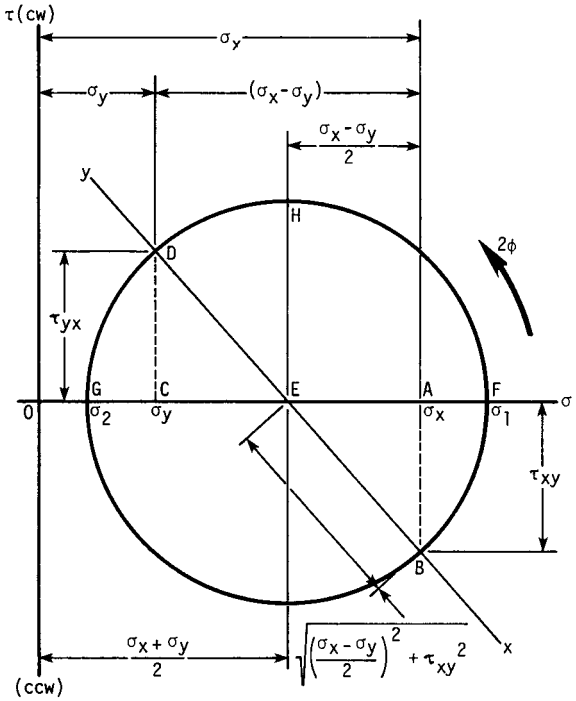

FIGURE 36.2 Mohr's circle diagram for plane stress. (*From* Applied Mechanics of Materials, *by Joseph E. Shigley. Copyright © 1976 by McGraw-Hill, Inc. Used with permission of the McGraw-Hill Book Company.*)

36.1.1 Programming

To program a Mohr's circle solution, plan on using a rectangular-to-polar conversion subroutine. Now notice, in Fig. 36.2, that $(\sigma_x - \sigma_y)/2$ is the base of a right triangle, τ_{xy} is the ordinate, and the hypotenuse is an extreme of the shear stress. Thus the conversion routine can be used to output both the angle 2ϕ and the extreme value of the shear stress.

As shown in Fig. 36.2, the principal stresses are found by adding and subtracting the extreme value of the shear stress to and from the term $(\sigma_x + \sigma_y)/2$. It is wise to ensure, in your programming, that the angle ϕ indicates the angle *from* the x axis *to* the direction of the stress component of interest; generally, the angle ϕ is considered positive when measured in the ccw direction.

36.2 TRIAXIAL STRESS

The general three-dimensional stress element in Fig. 36.3*a* has three normal stresses σ_x, σ_y, and σ_z, all shown as positive, and six shear-stress components, also shown as positive. The element is in static equilibrium, and hence

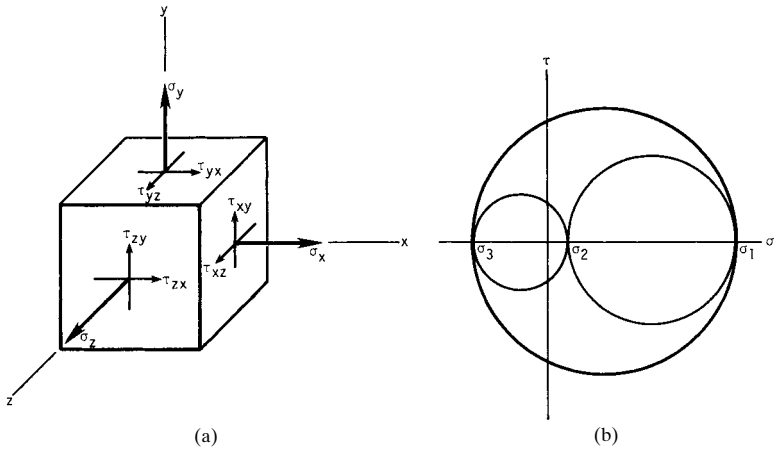

FIGURE 36.3 (*a*) General triaxial stress element; (*b*) Mohr's circles for triaxial stress.

$$\tau_{xy} = \tau_{yx} \qquad \tau_{yz} = \tau_{zy} \qquad \tau_{zx} = \tau_{xz}$$

Note that the first subscript is the coordinate normal to the element face, and the second subscript designates the axis parallel to the shear-stress component. The negative faces of the element will have shear stresses acting in the opposite direction; these are also considered as positive.

As shown in Fig. 36.3*b*, there are three principal stresses for triaxial stress states. These three are obtained from a solution of the equation

$$\sigma^3 - (\sigma_x + \sigma_y + \sigma_z)\sigma^2 + (\sigma_x\sigma_y + \sigma_x\sigma_z + \sigma_y\sigma_z - \tau_{xy}^2 - \tau_{yz}^2 - \tau_{zx}^2)\sigma$$
$$- (\sigma_x\sigma_y\sigma_z + 2\tau_{xy}\tau_{yz}\tau_{zx} - \sigma_x\tau_{yz}^2 - \sigma_y\tau_{zx}^2 - \sigma_z\tau_{xy}^2) = 0 \qquad (36.7)$$

In plotting Mohr's circles for triaxial stress, arrange the principal stresses in the order $\sigma_1 > \sigma_2 > \sigma_3$, as in Fig. 36.3*b*. It can be shown that the stress coordinates $\sigma\tau$ for any arbitrarily located plane will always lie on or *inside* the largest circle or on or *outside* the two smaller circles. The figure shows that the maximum shear stress is always

$$\tau_{max} = \frac{\sigma_1 - \sigma_3}{2} \qquad (36.8)$$

when the normal stresses are arranged so that $\sigma_1 > \sigma_2 > \sigma_3$.

36.3 STRESS-STRAIN RELATIONS

The stresses due to loading described as *pure tension, pure compression,* and *pure shear* are

$$\sigma = \frac{F}{A} \qquad \tau = \frac{F}{A} \qquad (36.9)$$

where F is positive for tension and negative for compression and the word *pure* means that there are no other complicating effects. In each case the stress is assumed to be uniform, which requires that

- The member is straight and of a homogeneous material.
- The line of action of the force is through the centroid of the section.
- There is no discontinuity or change in cross section near the stress element.
- In the case of compression, there is no possibility of buckling.

Unit engineering strain ϵ, often called simply *unit strain,* is the elongation or deformation of a member subjected to pure axial loading per unit of original length. Thus

$$\epsilon = \frac{\delta}{l_0} \tag{36.10}$$

where δ = total strain
l_0 = unstressed or original length

Shear strain γ is the change in a right angle of a stress element due to pure shear.

Hooke's law states that, within certain limits, the stress in a material is proportional to the strain which produced it. Materials which regain their original shape and dimensions when a load is removed are called *elastic materials.* Hooke's law is expressed in equation form as

$$\sigma = E\epsilon \qquad \tau = G\gamma \tag{36.11}$$

where E = the *modulus of elasticity* and G = the *modulus of ridigity,* also called the *shear modulus of elasticity.*

Poisson demonstrated that, within the range of Hooke's law, a member subjected to uniaxial loading exhibits both an axial strain and a lateral strain. These are related to each other by the equation

$$\nu = -\frac{\text{lateral strain}}{\text{axial strain}} \tag{36.12}$$

where ν is called *Poisson's ratio.*

The three constants given by Eqs. (36.11) and (36.12) are often called *elastic constants.* They have the relationship

$$E = 2G(1 + \nu) \tag{36.13}$$

By combining Eqs. (36.9), (36.10), and (36.11), it is easy to show that

$$\delta = \frac{Fl}{AE} \tag{36.14}$$

which gives the total deformation of a member subjected to axial tension or compression.

A solid round bar subjected to a *pure* twisting moment or torsion has a shear stress that is zero at the center and maximum at the surface. The appropriate equations are

$$\tau = \frac{T\rho}{J} \qquad \tau_{max} = \frac{Tr}{J} \tag{36.15}$$

where T = torque
ρ = radius to stress element
r = radius of bar
J = second moment of area (polar)

The total angle of twist of such a bar, in radians, is

$$\theta = \frac{Tl}{GJ} \tag{36.16}$$

where l = length of the bar. For the shear stress and angle of twist of other cross sections, see Table 36.1.

36.3.1 Principal Unit Strains

For a bar in uniaxial tension or compression, the principal strains are

$$\epsilon_1 = \frac{\sigma_1}{E} \qquad \epsilon_2 = -\nu\epsilon_1 \qquad \epsilon_3 = -\nu\epsilon_1 \tag{36.17}$$

Notice that the stress state is uniaxial, but the strains are triaxial.

For triaxial stress, the principal strains are

$$\epsilon_1 = \frac{\sigma_1}{E} - \frac{\nu\sigma_2}{E} - \frac{\nu\sigma_3}{E}$$

$$\epsilon_2 = \frac{\sigma_2}{E} - \frac{\nu\sigma_1}{E} - \frac{\nu\sigma_3}{E} \tag{36.18}$$

$$\epsilon_3 = \frac{\sigma_3}{E} - \frac{\nu\sigma_1}{E} - \frac{\nu\sigma_2}{E}$$

These equations can be solved for the principal stresses; the results are

$$\sigma_1 = \frac{E\epsilon_1(1-\nu) + \nu E(\epsilon_2 + \epsilon_3)}{1 - \nu - 2\nu^2}$$

$$\sigma_2 = \frac{E\epsilon_2(1-\nu) + \nu E(\epsilon_1 + \epsilon_3)}{1 - \nu - 2\nu^2} \tag{36.19}$$

$$\sigma_3 = \frac{E\epsilon_3(1-\nu) + \nu E(\epsilon_1 + \epsilon_2)}{1 - \nu - 2\nu^2}$$

The biaxial stress-strain relations can easily be obtained from Eqs. (36.18) and (36.19) by equating one of the principal stresses to zero.

TABLE 36.1 Torsional Stress and Angular Deflection of Various Sections†

Sectional shape	Shape constant	Shear stress
1. Solid round 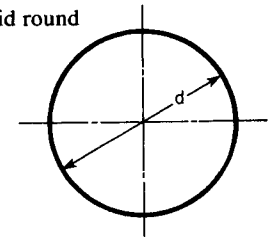	$K = \dfrac{\pi d^4}{32}$	$\tau_{max} = \dfrac{16T}{\pi d^3}$
2. Round tube 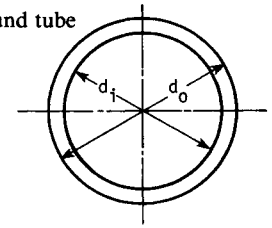	$K = \dfrac{\pi(d_o^4 - d_i^4)}{32}$	$\tau_{max} = \dfrac{16Td_o}{\pi(d_o^4 - d_i^4)}$
3. Square [36.1] 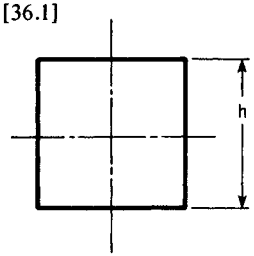	$K = \dfrac{h^4}{7.2}$	$\tau_{max} = \dfrac{4.8T}{h^3}$

TABLE 36.1 Torsional Stress and Angular Deflection of Various Sections† (*Continued*)

4. Square tube, generous fillets [36.2] 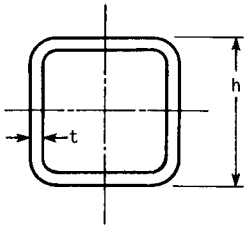 	$K = t(h - t)^3$	$\tau \cong \dfrac{T}{2t(h - t)^2}$
5. Rectangle [36.1] 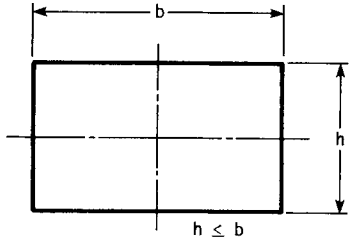 	$K = \dfrac{bh^3}{A}$ $A = 3 + 1.462\dfrac{h}{b} + 2.976\left(\dfrac{h}{b}\right)^2 - 0.238\left(\dfrac{h}{b}\right)^3$	$\tau_{max} = \dfrac{T(3b + 1.8h)}{b^2h^2}$
6. Rectangular tube, generous fillets [36.2] 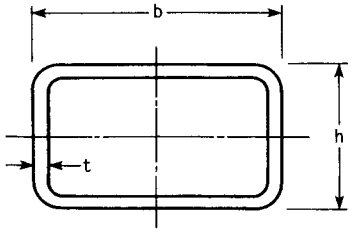 	$K = \dfrac{2t(b - t)^2(h - t)^2}{b + h - 2t}$	$\tau \cong \dfrac{T}{2t(b - t)(h - t)}$

TABLE 36.1 Torsional Stress and Angular Deflection of Various Sections† (*Continued*)

Sectional shape	Shape constant	Shear stress
7. Hexagon [36.1] 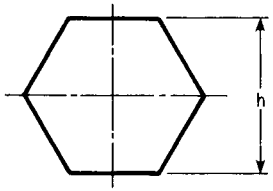	$K = \frac{h^4}{8.8}$	$\tau_{max} = \frac{5.7T}{h^3}$

† Deflection is $\theta = Tl/KG$ in rad, where T = torque, l = length, K = shape constant, and G = modulus of rigidity. See [36.2] for additional shapes in torsion.

36.3.2 Plastic Strain

It is important to observe that all the preceding relations are valid only when the material obeys Hooke's law.

Some materials (see Sec. 32.9), when stressed in the plastic region, exhibit a behavior quite similar to that given by Eq. (36.11). For these materials, the appropriate equation is

$$\bar{\sigma} = K\varepsilon^n \tag{36.20}$$

where $\bar{\sigma}$ = true stress
K = strength coefficient
ε = true plastic strain
n = strain-strengthening exponent

The relations for the true stress and true strain are

$$\bar{\sigma} = \frac{F_i}{A_i} \qquad \varepsilon = \ln \frac{l_i}{l_0} \tag{36.21}$$

where A_i and l_i are, respectively, the instantaneous values of the area and length of a bar subjected to a load F_i. Note that the areas in Eqs. (36.9) are the original or unstressed areas; the subscript zero was omitted, as is customary. The relations between true and engineering (nominal) stresses and strains are

$$\bar{\sigma} = \sigma \exp \epsilon \qquad \varepsilon = \ln(\epsilon + 1) \tag{36.22}$$

36.4 FLEXURE

Figure 36.4*a* shows a member loaded in flexure by a number of forces F and supported by reactions R_1 and R_2 at the ends. At point C a distance x from R_1, we can write

$$\Sigma M_C = \Sigma M_{\text{ext}} + M = 0 \tag{36.23}$$

where $\Sigma M_{\text{ext}} = -xR_1 + c_1F_1 + c_2F_2$ and is called the *external moment* at section C. The term M, called the *internal* or *resisting moment,* is shown in its positive direction in both parts *b* and *c* of Fig. 36.4. Figure 36.5 shows that a positive moment causes the top surface of a beam to be concave. A negative moment causes the top surface to be convex with one or both ends curved downward.

A similar relation can be defined for shear at section C:

$$\Sigma F_y = \Sigma F_{\text{ext}} + V = 0 \tag{36.24}$$

where $\Sigma F_{\text{ext}} = R_1 - F_1 - F_2$ and is called the *external shear force* at C. The term V, called the *internal shear force,* is shown in its positive direction in both parts *b* and *c* of Fig. 36.4.

Figure 36.6 illustrates an application of these relations to obtain a set of shear and moment diagrams.

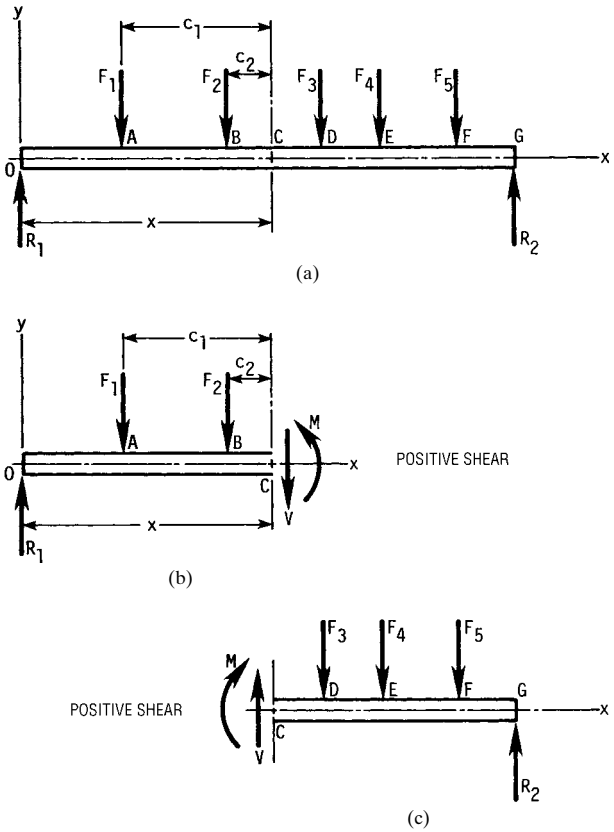

FIGURE 36.4 Shear and moment. (*From* Applied Mechanics of Materials, *by Joseph E. Shigley. Copyright © 1976 by McGraw-Hill, Inc. Used with permission of the McGraw-Hill Book Company.*)

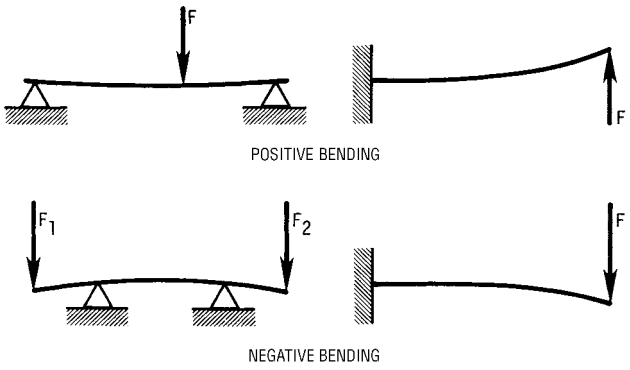

FIGURE 36.5 Sign conventions for bending. (*From* Applied Mechanics of Materials, *by Joseph E. Shigley. Copyright © 1976 by McGraw-Hill, Inc. Used with permission of the McGraw-Hill Book Company.*)

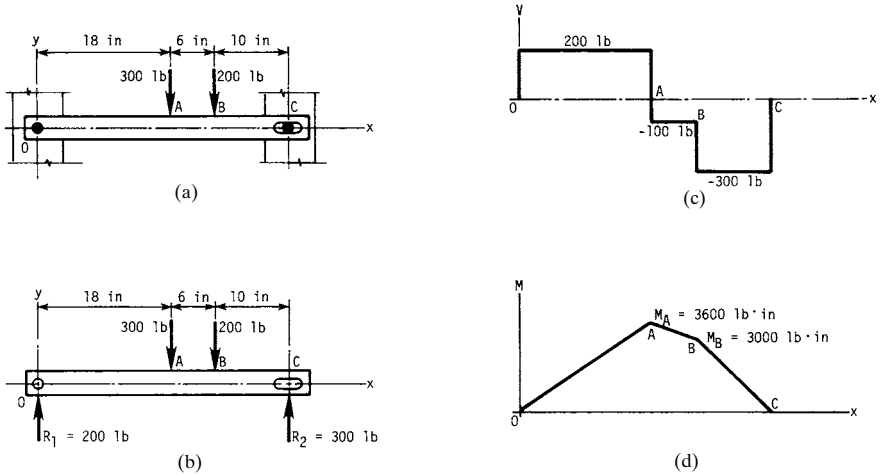

FIGURE 36.6 (*a*) View showing how ends are secured; (*b*) loading diagram; (*c*) shear-force diagram; (*d*) bending-moment diagram. (*From* Applied Mechanics of Materials, *by Joseph E. Shigley. Copyright © 1976 by McGraw-Hill, Inc. Used with permission of the McGraw-Hill Book Company.*)

The previous relations can be expressed in a more general form as

$$V = \frac{dM}{dx} \tag{36.25}$$

If the flexure is caused by a distributed load,

$$\frac{dV}{dx} = \frac{d^2M}{dx^2} = -w \tag{36.26}$$

where w = a downward-acting load in units of force per unit length. A more general load distribution can be expressed as

$$q = \lim_{\Delta x \to 0} \frac{\Delta F}{\Delta x}$$

where q is called the *load intensity;* thus $q = -w$ in Eq. (36.26). Two useful facts can be learned by integrating Eqs. (36.25) and (36.26). The first is

$$\int_{V_A}^{V_B} dV = \int_{x_A}^{x_B} q\, dx = V_B - V_A \tag{36.27}$$

which states that *the area under the loading function between x_A and x_B is the same as the change in the shear force from A to B.* Also,

$$\int_{M_A}^{M_B} dM = \int_{x_A}^{x_B} V\, dx = M_B - M_A \tag{36.28}$$

which states that *the area of the shear-force diagram between x_A* and *x_B is the same as the change in moment from A to B.*

Figure 36.7 distinguishes between the *neutral axis of a section* and the *neutral axis of a beam,* both of which are often referred to simply as the *neutral axis.* The assumptions used in deriving flexural relations are

- The material is isotropic and homogeneous.
- The member is straight.
- The material obeys Hooke's law.
- The cross section is constant along the length of the member.
- There is an axis of symmetry in the plane of bending (see Fig. 36.7).
- During pure bending (zero shear force), plane cross sections remain plane.

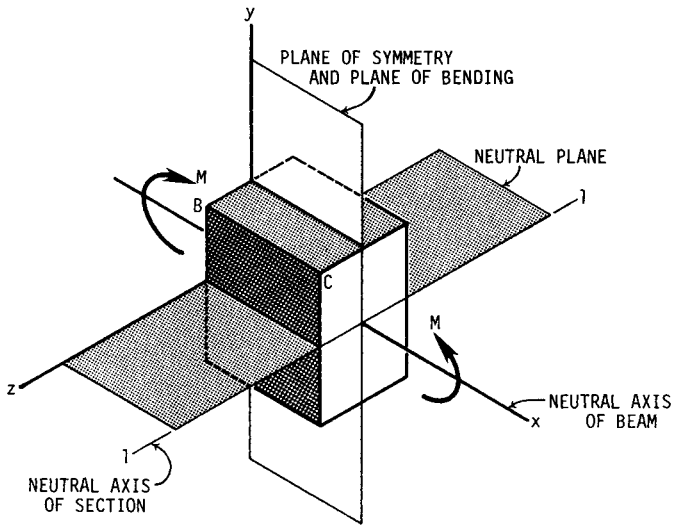

FIGURE 36.7 The meaning of the term *neutral axis.* Note the difference between the *neutral axis of the section* and the *neutral axis of the beam.* (*From* Applied Mechanics of Materials, *by Joseph E. Shigley. Copyright © 1976 by McGraw-Hill, Inc. Used with permission of the McGraw-Hill Book Company.*)

The *flexural formula* is

$$\sigma_x = -\frac{My}{I} \tag{36.29}$$

for the section of Fig. 36.7. The formula states that a normal compression stress σ_x occurs on a fiber at a distance y from the neutral axis when a *positive moment M* is applied. In Eq. (36.29), I is the *second moment of area.* A number of formulas are listed in the Appendix.

The maximum flexural stress occurs at $y_{max} = c$ at the outer surface of the beam. This stress is often written in the three forms

$$\sigma = \frac{Mc}{I} \qquad \sigma = \frac{M}{I/c} \qquad \sigma = \frac{M}{Z} \tag{36.30}$$

where Z is called the *section modulus*. Equations (36.30) can also be used for beams having unsymmetrical sections provided that the plane of bending coincides with one of the two principal axes of the section.

When shear forces are present, as in Fig. 36.6*c*, a member in flexure will also experience shear stresses as given by the equation

$$\tau = \frac{VQ}{Ib} \tag{36.31}$$

where b = section width, and Q = first moment of a vertical face about the neutral axis and is

$$Q = \int_{y_1}^{c} y\, dA \tag{36.32}$$

For a rectangular section,

$$Q = \int_{y_1}^{c} y\, dA = b \int_{y_1}^{c} y\, dy = \frac{b}{2}(c^2 - y_1^2)$$

Substituting this value of Q into Eq. (36.31) gives

$$\tau = \frac{V}{2I}(c^2 - y_1^2)$$

Using $I = Ac^2/3$, we learn that

$$\tau = \frac{3V}{2A}\left(1 - \frac{y_1^2}{c^2}\right) \tag{36.33}$$

The value of b for other sections is measured as shown in Fig. 36.8.

In determining shear stress in a beam, the dimension b is not always measured parallel to the neutral axis. The beam sections shown in Fig. 36.8 show how to measure b in order to compute the static moment Q. It is the tendency of the shaded area to slide relative to the unshaded area which causes the shear stress.

Shear flow q is defined by the equation

$$q = \frac{VQ}{I} \tag{36.34}$$

where q is in force units per unit length of the beam at the section under consideration. So shear flow is simply the shear force per unit length at the section defined by $y = y_1$. When the shear flow is known, the shear stress is determined by the equation

$$\tau = \frac{q}{b} \tag{36.35}$$

36.5 STRESSES DUE TO TEMPERATURE

A *thermal stress* is caused by the existence of a *temperature gradient* in a member. A *temperature stress* is created in a member when it is *constrained* so as to prevent expansion or contraction due to temperature change.

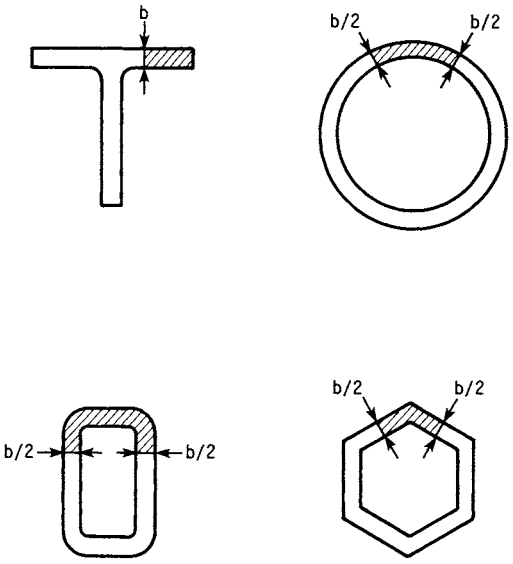

FIGURE 36.8 Correct way to measure dimension b to determine shear stress for various sections. (*From* Applied Mechanics of Materials, *by Joseph E. Shigley. Copyright © 1976 by McGraw-Hill, Inc. Used with permission of the McGraw-Hill Book Company.*)

36.5.1 Temperature Stresses

These stresses are found by assuming that the member is not constrained and then computing the stresses required to cause it to assume its original dimensions. If the temperature of an unrestrained member is uniformly increased, the member expands and the normal strain is

$$\epsilon_x = \epsilon_y = \epsilon_z = \alpha(\Delta T) \tag{36.36}$$

where ΔT = temperature change and α = *coefficient of linear expansion.* The coefficient of linear expansion increases to some extent with temperature. Some mean values for various materials are shown in Table 36.2.

Figure 36.9 illustrates two examples of temperature stresses. For the bar in Fig. 36.9*a,*

$$\sigma_x = -\alpha(\Delta T)E \qquad \sigma_y = \sigma_z = -\nu\sigma_x \tag{36.37}$$

The stresses in the flat plate of Fig. 36.9*b* are

$$\sigma_x = \sigma_y = -\frac{\alpha(\Delta T)E}{1-\nu} \qquad \sigma_z = -\nu\sigma_x \tag{36.38}$$

TABLE 36.2 Coefficients of Linear Expansion

Material	Celsius scale		Fahrenheit scale	
	$10^6\alpha$	°C	$10^6\alpha$	°F
Aluminum	24.0	20–100	13.4	68–212
Aluminum	26.7	20–300	14.9	68–572
Brass (cast)	18.75	0–100	10.4	32–212
Brass (wire)	19.3	0–100	10.7	32–212
Brass (spring)	19.8	25–300	11.0	77–572
Cast iron	10.6	40	5.9	104
Carbon steel	10.8	40	6.0	104
Carbon steel	11.5	100–200	6.4	212–392
Carbon steel	15	300–400	8.3	572–752
Magnesium (cast)	27.0	20–100	15.0	68–212
Nickel steel (10%)	13.0	20	7.2	68
Stainless steel (hardened)	9.6	20–100	5.3	68–212
Stainless steel (hardened)	9.8	20–200	5.5	68–392
Stainless steel (annealed)	10.3	20–100	5.7	68–212
Stainless steel (annealed)	10.7	20–200	6.0	68–392

36.5.2 Thermal Stresses

Heating of the top surface of the restrained member in Fig. 36.10*a* causes end moments of

$$M = \frac{\alpha(\Delta T)EI}{h} \tag{36.39}$$

and maximum bending stresses of

$$\sigma_x = \pm\frac{\alpha(\Delta T)E}{2} \tag{36.40}$$

with compression of the top surface. If the constraints are removed, the bar will curve to a radius

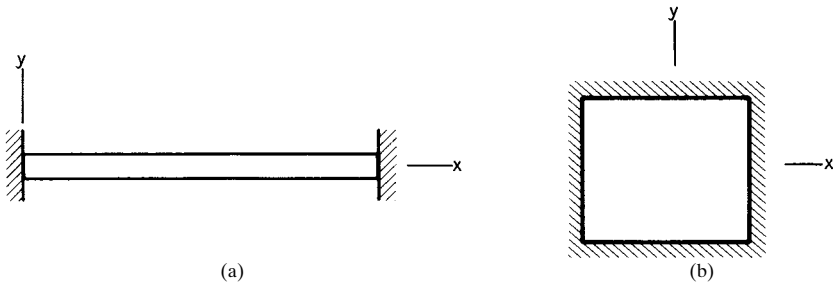

FIGURE 36.9 Examples of temperature stresses. In each case the temperature rise ΔT is uniform throughout. (*a*) Straight bar with ends restrained; (*b*) flat plate with edges restrained.

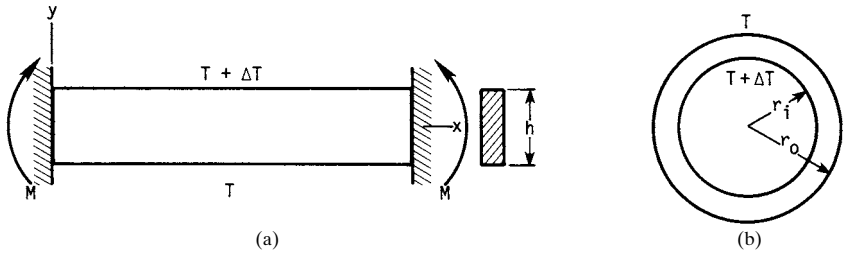

(a) (b)

FIGURE 36.10 Examples of thermal stresses. (*a*) Rectangular member with ends restrained (temperature difference between top and bottom results in end moments and bending stresses); (*b*) thick-walled tube has maximum stresses in tangential and longitudinal directions.

$$r = \frac{h}{\alpha(\Delta T)}$$

The thick-walled tube of Fig. 36.10*b* with a hot interior surface has tangential and longitudinal stresses in the outer and inner surfaces of magnitude

$$\sigma_{lo} = \sigma_{to} = \frac{\alpha(\Delta T)E}{2(1-\nu)\ln(r_o/r_i)}\left[1 - \frac{2r_i^2 \ln(r_o/r_i)}{r_o^2 - r_i^2}\right] \tag{36.41}$$

$$\sigma_{li} = \sigma_{ti} = \frac{-\alpha(\Delta T)E}{2(1-\nu)\ln(r_o/r_i)}\left[1 - \frac{2r_o^2 \ln(r_o/r_i)}{r_o^2 - r_i^2}\right] \tag{36.42}$$

where the subscripts *i* and *o* refer to the inner and outer radii, respectively, and the subscripts *t* and *l* refer to the tangential (circumferential) and longitudinal directions. Radial stresses of lesser magnitude will also exist, although not at the inner or outer surfaces.

If the tubing of Fig. 36.10*b* is thin, then the inner and outer stresses are equal, although opposite, and are

$$\sigma_{lo} = \sigma_{to} = \frac{\alpha(\Delta T)E}{2(1-\nu)}$$
$$\sigma_{li} = \sigma_{ti} = -\frac{\alpha(\Delta T)E}{2(1-\nu)} \tag{36.43}$$

at points not too close to the tube ends.

36.6 CONTACT STRESSES

When two elastic bodies having curved surfaces are pressed against each other, the initial point or line of contact changes into area contact, because of the deformation, and a three-dimensional state of stress is induced in both bodies. The shape of the contact area was originally deduced by Hertz, who assumed that the curvature of the

two bodies could be approximated by second-degree surfaces. For such bodies, the contact area was found to be an ellipse. Reference [36.3] contains a comprehensive bibliography.

As indicated in Fig. 36.11, there are four special cases in which the contact area is a circle. For these four cases, the maximum pressure occurs at the center of the contact area and is

$$p_o = \frac{3F}{2\pi a^2} \tag{36.44}$$

where a = the radius of the contact area and F = the normal force pressing the two bodies together.

In Fig. 36.11, the x and y axes are in the plane of the contact area and the z axis is normal to this plane. The maximum stresses occur on this axis, they are principal stresses, and their values for all four cases in Fig. 36.11 are

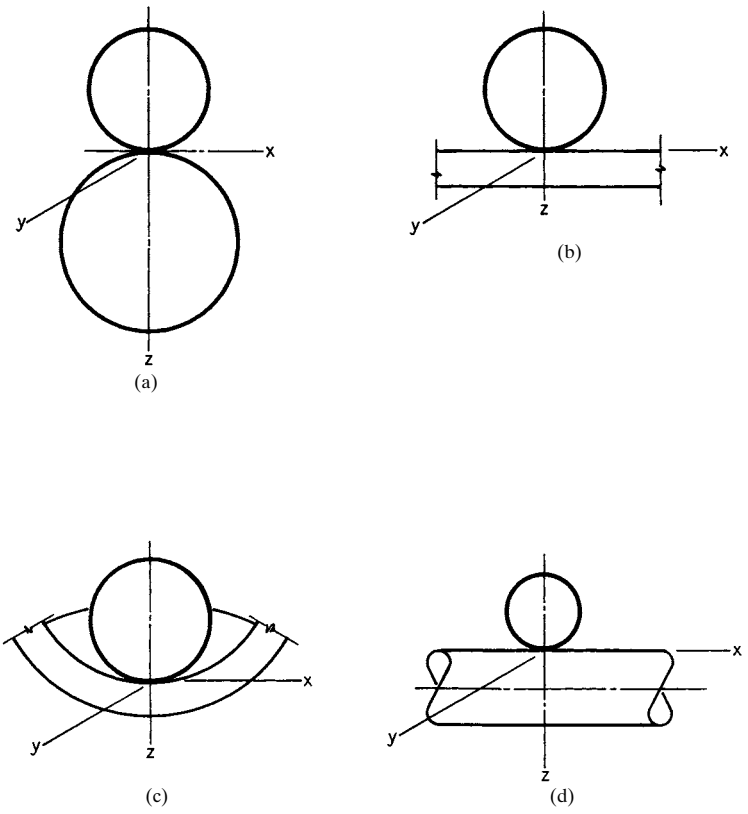

FIGURE 36.11 Contacting bodies having a circular contact area. (*a*) Two spheres; (*b*) sphere and plate; (*c*) sphere and spherical socket; (*d*) crossed cylinders of equal diameters.

$$\sigma_x = \sigma_y = -p_o \left\{ \left(1 - \frac{z}{a} \tan^{-1} \frac{1}{z/a}\right)(1+\nu) - \frac{1}{2(1+z^2/a^2)} \right\} \tag{36.45}$$

$$\sigma_z = \frac{-p_o}{1+z^2/a^2} \tag{36.46}$$

These equations are plotted in Fig. 36.12 together with the two shear stresses τ_{xz} and τ_{yz}. Note that $\tau_{xy} = 0$ because $\sigma_x = \sigma_y$.

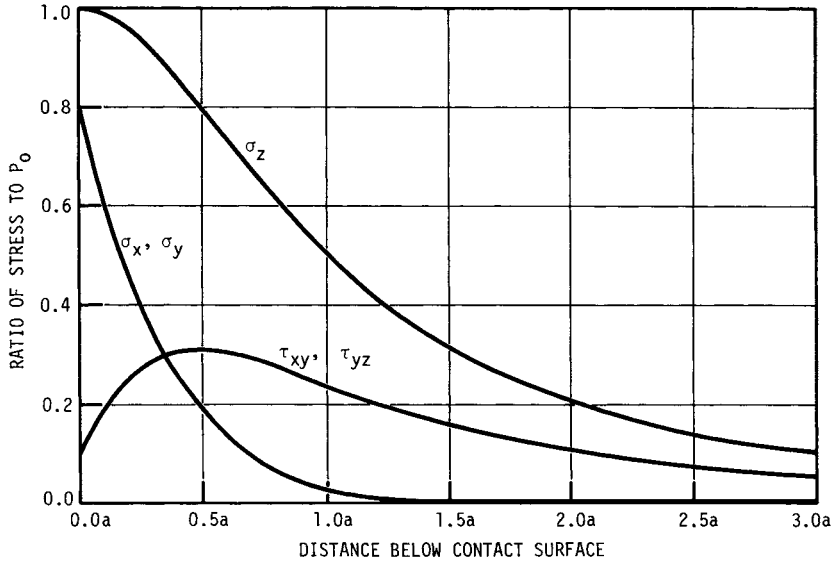

FIGURE 36.12 Magnitude of the stress components on the z axis below the surface as a function of the maximum pressure. Note that the two shear-stress components are maximum slightly below the surface. The chart is based on a Poisson's ratio of 0.30.

The radii a of the contact circles depend on the geometry of the contacting bodies. For two spheres, each having the same diameter d, or for two crossed cylinders, each having the diameter d, and in each case with like materials, the radius is

$$a = \left(\frac{3Fd}{8} \frac{1-\nu^2}{E}\right)^{1/3} \tag{36.47}$$

where ν and E are the elastic constants.

For two spheres of unlike materials having diameters d_1 and d_2, the radius is

$$a = \left[\frac{3F}{8} \frac{d_1 d_2}{d_1 + d_2} \left(\frac{1-\nu_1^2}{E_1} + \frac{1-\nu_2^2}{E_2}\right)\right]^{1/3} \tag{36.48}$$

For a sphere of diameter d and a flat plate of unlike materials, the radius is

$$a = \left[\frac{3Fd}{8}\left(\frac{1-\nu_1^2}{E_1} + \frac{1-\nu_2^2}{E_2}\right)\right]^{1/3} \tag{36.49}$$

For a sphere of diameter d_1 and a spherical socket of diameter d_2 of unlike materials, the radius is

$$a = \left[\frac{3F}{8}\frac{d_1 d_2}{d_2 - d_1}\left(\frac{1-\nu_1^2}{E_1} + \frac{1-\nu_2^2}{E_2}\right)\right]^{1/3} \tag{36.50}$$

Contacting cylinders with parallel axes subjected to a normal force have a rectangular contact area. We specify an xy plane coincident with the contact area with the x axis parallel to the cylinder axes. Then, using a right-handed coordinate system, the stresses along the z axis are maximum and are

$$\sigma_x = -2\nu p_o\left[\left(1 + \frac{z^2}{b^2}\right)^{1/2} - \frac{z}{b}\right] \tag{36.51}$$

$$\sigma_y = -p_o\left[\left(2 - \frac{1}{1 + z^2/b^2}\right)\left(1 + \frac{z^2}{b^2}\right)^{1/2} - \frac{2z}{b}\right] \tag{36.52}$$

$$\sigma_z = \frac{-p_o}{(1 + z^2/b^2)^{1/2}} \tag{36.53}$$

where the maximum pressure occurs at the origin of the coordinate system in the contact zone and is

$$p_o = \frac{2F}{\pi b l} \tag{36.54}$$

where l = the length of the contact zone measured parallel to the cylinder axes, and b = the half width. Equations (36.51) to (36.53) give the principal stresses. These equations are plotted in Fig. 36.13. The corresponding shear stresses can be found from a Mohr's circle; they are plotted in Fig. 36.14. Note that the maximum is either τ_{xz} or τ_{yz} depending on the depth below the contact surface.

The half width b depends on the geometry of the contacting cylinders. The following cases arise most frequently: Two cylinders of equal diameter and of the same material have a half width of

$$b = \left(\frac{2Fd}{\pi l}\frac{1-\nu^2}{E}\right)^{1/2} \tag{36.55}$$

For two cylinders of unequal diameter and unlike materials, the half width is

$$b = \left[\frac{2F}{\pi l}\frac{d_1 d_2}{d_1 + d_2}\left(\frac{1-\nu_1^2}{E_1} + \frac{1-\nu_2^2}{E_2}\right)\right]^{1/2} \tag{36.56}$$

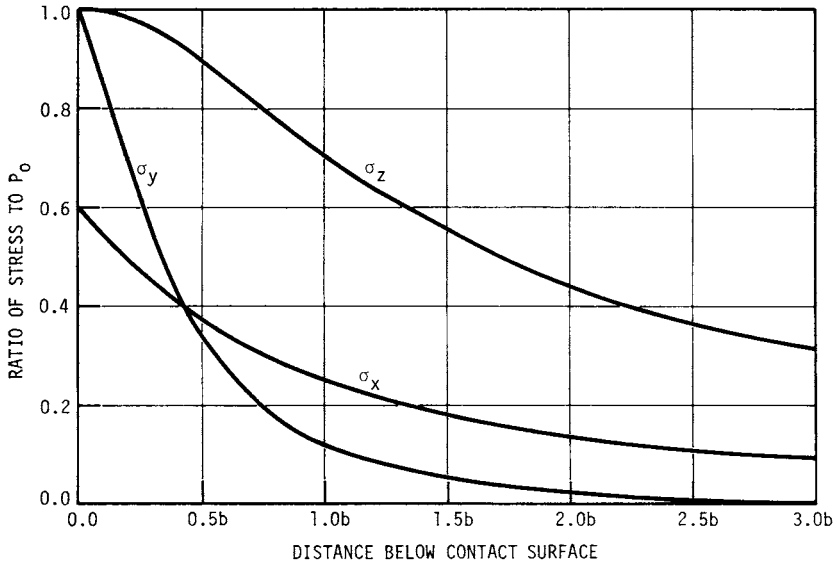

FIGURE 36.13 Magnitude of the principal stresses on the z axis below the surface as a function of the maximum pressure for contacting cylinders. Based on a Poisson's ratio of 0.30.

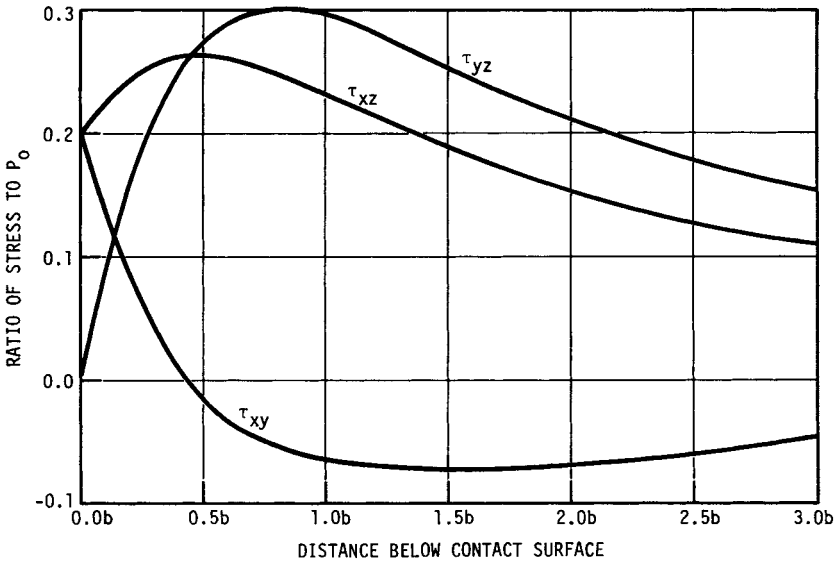

FIGURE 36.14 Magnitude of the three shear stresses computed from Fig. 36.13.

For a cylinder of diameter d in contact with a flat plate of unlike material, the result is

$$b = \left[\frac{2Fd}{\pi l}\left(\frac{1-\nu_1^2}{E_1}+\frac{1-\nu_2^2}{E_2}\right)\right]^{1/2} \tag{36.57}$$

The half width for a cylinder of diameter d_1 pressing against a cylindrical socket of diameter d_2 of unlike material is

$$b = \left[\frac{2F}{\pi l}\frac{d_1 d_2}{d_2-d_1}\left(\frac{1-\nu_1^2}{E_1}+\frac{1-\nu_2^2}{E_2}\right)\right]^{1/2} \tag{36.58}$$

REFERENCES

36.1 F. R. Shanley, *Strength of Materials,* McGraw-Hill, New York, 1957, p. 509.

36.2 W. C. Young, *Roark's Formulas for Stress and Strain,* 6th ed., McGraw-Hill, 1989, p. 348–359.

36.3 J. L. Lubkin, "Contact Problems," in W. Flugge (ed.), *Handbook of Engineering Mechanics,* McGraw-Hill, New York, 1962, pp. 42-10 to 42-12.

CHAPTER 37
DEFLECTION

Joseph E. Shigley
Professor Emeritus
The University of Michigan
Ann Arbor, Michigan

Charles R. Mischke, Ph.D., P.E.
Professor Emeritus of Mechanical Engineering
Iowa State University
Ames, Iowa

GLOSSARY OF SYMBOLS

a	Dimension
A	Area
b	Dimension
C	Constant
D, d	Diameter
E	Young's modulus
F	Force
G	Shear modulus
I	Second moment of area
J	Second polar moment of area
k	Spring rate
K	Constant
ℓ	Length
M	Moment
N	Number

q	Unit load
Q	Fictitious force
R	Support reaction
T	Torque
U	Strain energy
V	Shear force
w	Unit weight
W	Total weight
x	Coordinate
y	Coordinate
δ	Deflection
θ	Slope, torsional deflection

37.1 STIFFNESS OR SPRING RATE

The *spring rate* (also called *stiffness* or *scale*) of a body or ensemble of bodies is defined as the partial derivative of force (torque) with respect to colinear displacement (rotation). For a helical tension or compression spring,

$$F = \frac{d^4 G y}{8D^3 N} \qquad \text{thus} \qquad k = \frac{\partial F}{\partial y} = \frac{d^4 G}{8D^3 N} \tag{37.1}$$

where D = mean coil diameter
d = wire diameter
N = number of active turns

In a round bar subject to torsion,

$$T = \frac{GJ\theta}{\ell} \qquad \text{thus} \qquad k = \frac{\partial T}{\partial \theta} = \frac{GJ}{\ell} \tag{37.2}$$

and the tensile force in an elongating bar of any cross section is

$$F = \frac{AE\delta}{\ell} \qquad \text{thus} \qquad k = \frac{\partial F}{\partial \delta} = \frac{AE}{\ell} \tag{37.3}$$

If k is constant, as in these cases, then displacement is said to be linear with respect to force (torque). For contacting bodies with all four radii of curvature finite, the approach of the bodies is proportional to load to the two-thirds power, making the spring rate proportional to load to the one-third power. In hydrodynamic film bearings, the partial derivative would be evaluated numerically by dividing a small change in load by the displacement in the direction of the load.

37.2 DEFLECTION DUE TO BENDING

The relations involved in the bending of beams are well known and are given here for reference purposes as follows:

$$\frac{q}{EI} = \frac{d^4y}{dx^4} \tag{37.4}$$

$$\frac{V}{EI} = \frac{d^3y}{dx^3} \tag{37.5}$$

$$\frac{M}{EI} = \frac{d^2y}{dx^2} \tag{37.6}$$

$$\theta = \frac{dy}{dx} \tag{37.7}$$

$$y = f(x) \tag{37.8}$$

These relations are illustrated by the beam of Fig. 37.1. Note that the x axis is *positive* to the right and the y axis is *positive* upward. All quantities—loading, shear force, support reactions, moment, slope, and deflection—have the same sense as y; they are positive if upward, negative if downward.

37.3 PROPERTIES OF BEAMS

Table 37.1 lists a number of useful properties of beams having a variety of loadings. These must all have the same cross section throughout the length, and a linear relation must exist between the force and the deflection. Beams having other loadings can be solved using two or more sets of these relations and the principle of superposition.

In using Table 37.1, remember that the deflection at the center of a beam with off-center loads is usually within 2.5 percent of the maximum value.

37.4 ANALYSIS OF FRAMES

Castigliano's theorem is presented in Chap. 38, and the energy equations needed for its use are listed in Table 38.2. The method can be used to find the deflection at any point of a frame such as the one shown in Fig. 37.2. For example, the deflection δ_C at C in the direction of F_2 can be found using Eq. (38.2) as

$$\delta_C = \frac{\partial U}{\partial F_2} \tag{37.9}$$

where U = the strain energy stored in the entire frame due to all the forces. If the deflection is desired in another direction or at a point where no force is acting, then a fictitious force Q is added to the system at that point and in the direction in which

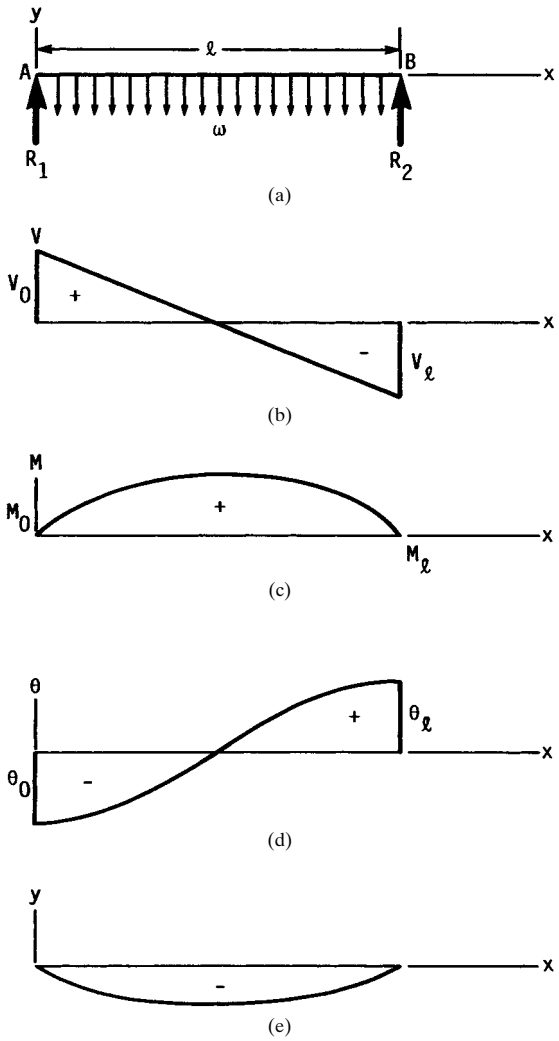

FIGURE 37.1 (*a*) Loading diagram showing beam supported at A and B with uniform load w having units of force per unit length, $R_1 = R_2 = w\ell/2$; (*b*) shear-force diagram showing end conditions; (*c*) moment diagram; (*d*) slope diagram; (*e*) deflection diagram.

the deflection is desired. After the partial derivatives have been found, Q is equated to zero, and the remaining terms give the wanted deflection.

The first step in using the method is to make a force analysis of each member of the frame. If Eq. (*a*) is to be solved, then the numerical values of F_1 and F_2 can be used in the force analysis, but the value of F_2 must *not* be substituted until after each

TABLE 37.1 Properties of Beams

1. Cantilever—intermediate load

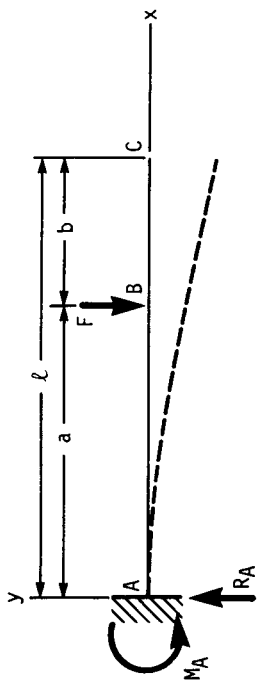

$R_A = F \quad M_A = -Fa$

$y_B = -\dfrac{Fa^3}{3EI} \quad y_C = -\dfrac{Fa^3}{3EI}\left(1 + \dfrac{3b}{2a}\right)$

2. Cantilever—intermediate couple

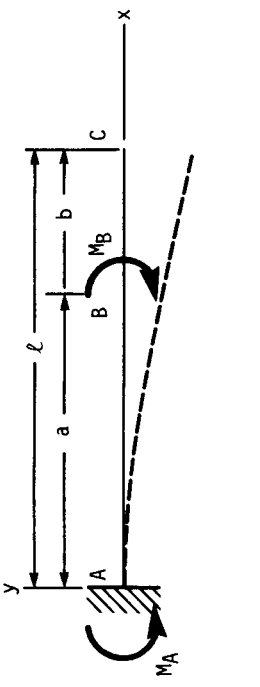

$V = 0 \quad M_A = M$

$y_B = -\dfrac{Ma^2}{2EI} \quad y_C = -\dfrac{Ma^2}{2EI}\left(1 + \dfrac{2b}{a}\right)$

TABLE 37.1 Properties of Beams (*Continued*)

3. Cantilever—distributed load

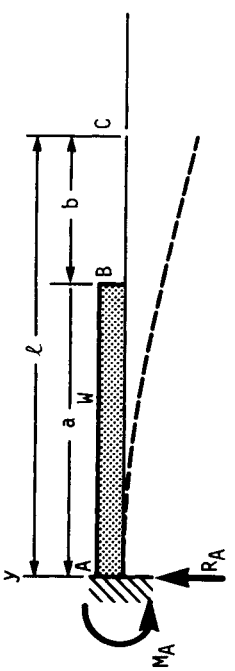

$$R_A = W \qquad M_A = -\frac{Wa}{2}$$

$$y_B = -\frac{Wa^3}{8EI} \qquad y_C = -\frac{Wa^3}{8EI}\left(1 + \frac{4b}{3a}\right)$$

4. Cantilever—partial distributed load

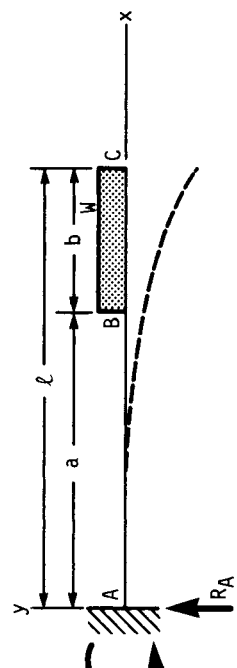

$$R_A = W \qquad M_A = -W\left(a + \frac{b}{2}\right)$$

$$y_C = -\frac{W}{24EI}(8a^3 + 18a^2b + 12ab^2 + 3b^3)$$

TABLE 37.1 Properties of Beams (*Continued*)

5. Cantilever—partial distributed load

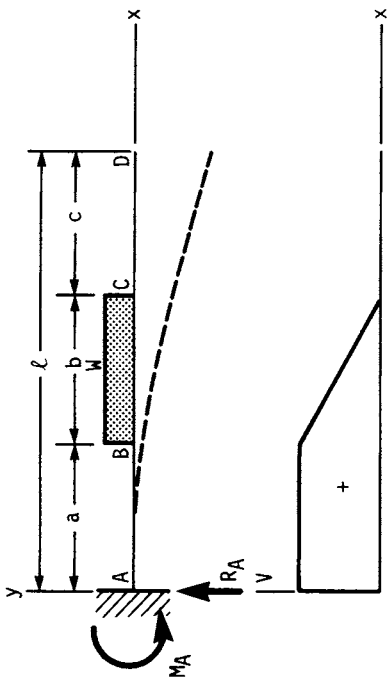

$$R_A = W \qquad M_A = -W\left(a + \frac{b}{2}\right)$$

$$y_D = -\frac{W}{24EI}(8a^3 + 18a^2b + 12ab^2 + 3b^3 + 12a^2c + 12abc + 4b^2c)$$

6. Simple support—intermediate load

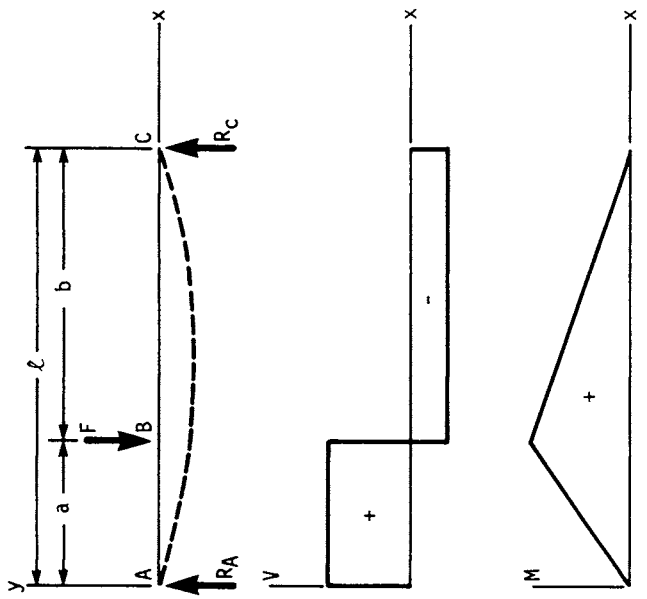

$$R_A = \frac{Fb}{\ell} \qquad R_B = \frac{Fa}{\ell} \qquad M_B = \frac{Fab}{\ell}$$

At center $y = -\dfrac{F\ell^3}{48EI}\left(\dfrac{3a}{\ell} - \left(\dfrac{4a}{\ell}\right)^3\right)$

TABLE 37.1 Properties of Beams (*Continued*)

7. Simple support—intermediate couple

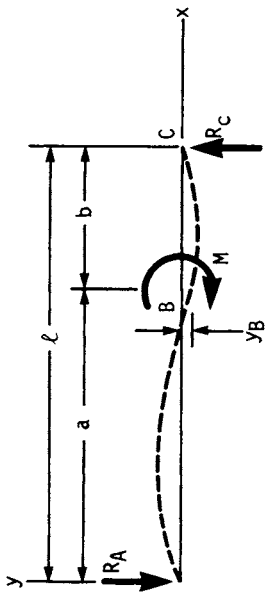

$$R_A = -R_C = -\frac{M}{\ell} \qquad M_{AB} = R_A x$$

$$y_B = -\frac{Mab}{3EI\ell}(a - b) \qquad a > b$$

8. Simple support—end moments

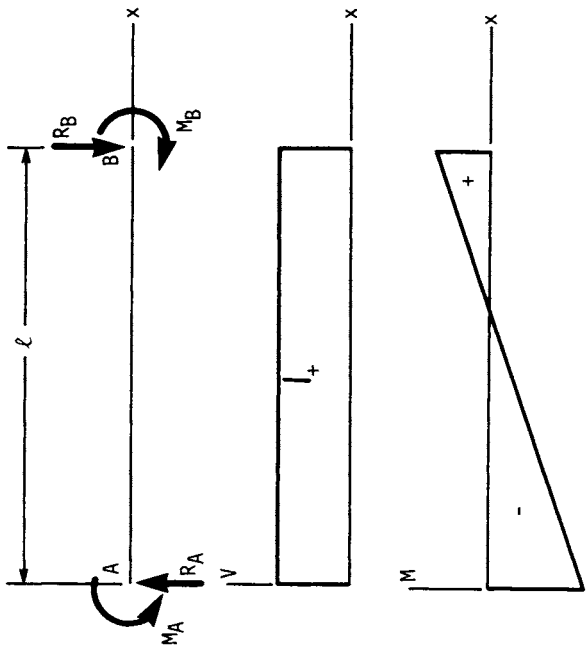

M_B positive, M_A negative, $|M_A| > |M_B|$

$$R_A = -R_B = -\frac{M_A + M_B}{\ell}$$

when $|M_A| = |M_B|$ $\qquad y_{max} = \frac{M\ell^2}{8EI}$

TABLE 37.1 Properties of Beams (*Continued*)

9. Simple support—overhung load

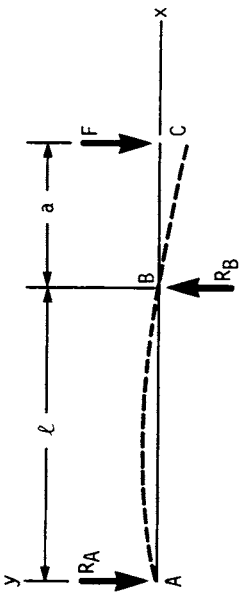

$$R_A = -\frac{Fa}{\ell} \qquad R_B = \frac{F}{\ell}(\ell + a)$$

$$M_B = -Fa$$

$$y_C = -\frac{Fa^2}{3EI}(\ell + a)$$

10. Simple support— uniform loading

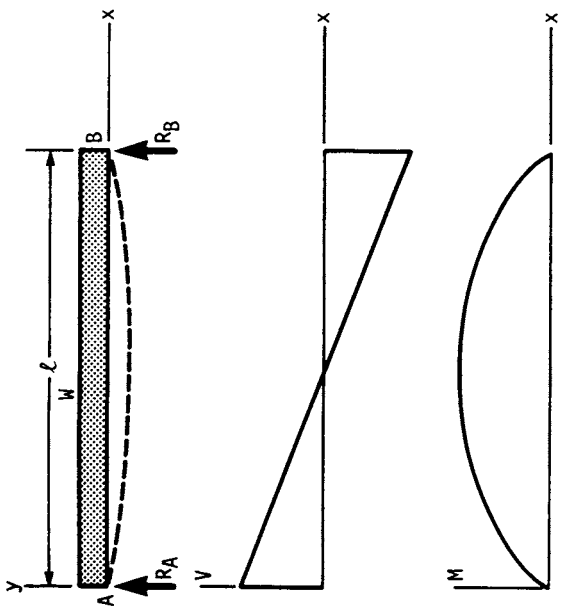

$$R_A = R_B = \frac{W}{2} \qquad M_{max} = \frac{W\ell}{8}$$

$$y_{max} = -\frac{5W\ell^3}{384EI}$$

TABLE 37.1 Properties of Beams (*Continued*)

11. Simple support—partial uniform loading

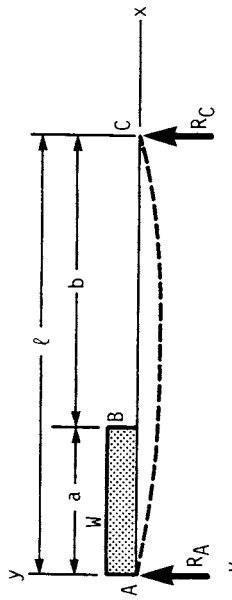

$$R_A = \frac{W}{2\ell}(2\ell - a) \qquad R_B = \frac{Wa}{2\ell} \qquad x_1 = \frac{a}{2\ell}(2\ell - a)$$

At center $y = -\dfrac{Wa}{48EI}(a^2 + 2\ell^2) \qquad a < \dfrac{\ell}{2}$

12. Simple support—uniform loading, overhung

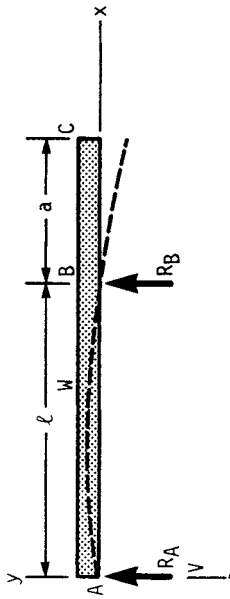

$$R_A = \frac{W}{2\ell}(\ell - a) \qquad R_B = \frac{W}{2\ell}(\ell + a) \qquad x_1 = \frac{1}{2\ell}(\ell^2 - a^2)$$

$$M_1 = \frac{W}{8\ell^2}(\ell + a)(\ell - a)^2 \qquad M_B = -\frac{Wa^2}{2(\ell + a)}$$

$$y_C = \frac{Wa}{24EI}(3a^2 + a\ell - \ell^2)$$

TABLE 37.1 Properties of Beams (*Continued*)

13. Simple support—overhung uniform load

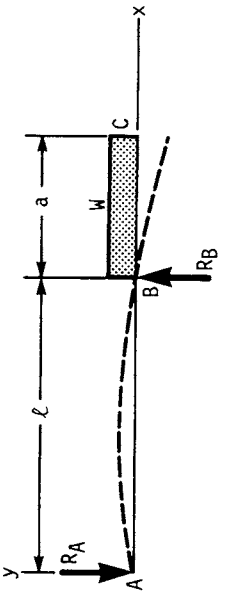

$$R_A = -\frac{Wa}{2\ell} \qquad R_B = \frac{W}{2\ell}(2\ell + a) \qquad M_{max} = -\frac{Wa}{2}$$

$$y_{max} = \frac{0.032Wa\ell^2}{EI} \quad \text{between supports}$$

$$y_C = -\frac{Wa^2}{24EI}(4\ell + 3a)$$

14. Fixed and simple support—intermediate load

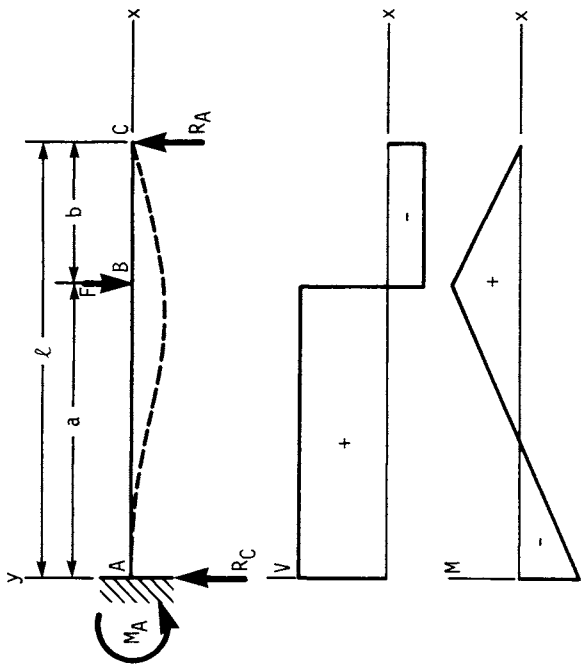

$$R_A = \frac{Fb}{2\ell^3}(3\ell^2 - b^2) \qquad R_C = \frac{Fa^2}{2\ell^3}(3\ell - a)$$

$$M_A = \frac{Fb}{2\ell^2}(b^2 - \ell^2) \qquad M_B = \frac{Fa^2b}{2\ell^3}(3\ell - a)$$

$$y_B = \frac{Fba^2}{12EI\ell^3}(3b^2\ell - 3\ell^3 + 3a\ell^2 - ab^2)$$

TABLE 37.1 Properties of Beams (*Continued*)

15. Fixed and simple support—uniform load

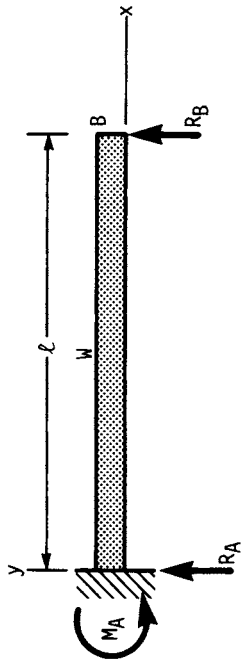

$$R_A = \frac{5W}{8} \qquad R_B = \frac{3W}{8}$$

$$M_A = -\frac{W\ell}{8} \qquad M_1 = \frac{9W\ell}{128}$$

$$y_{max} = -\frac{W\ell^3}{185EI}$$

16. Fixed supports—intermediate load

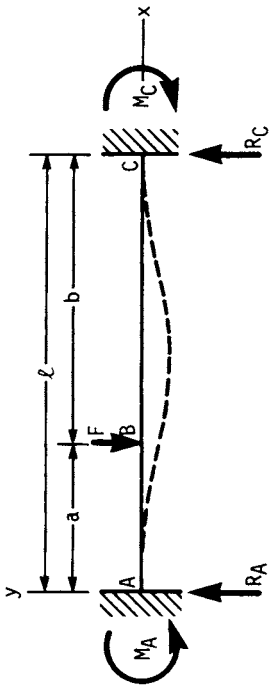

$$R_A = \frac{Fb^2}{\ell^3}(3a + b) \qquad R_B = \frac{Fa^2}{\ell^3}(3b + a)$$

$$M_A = -\frac{Fab^2}{\ell^2} \qquad M_B = \frac{Fab^2}{\ell^3}(3a + b - \ell)$$

$$M_C = -\frac{Fa^2b}{\ell^2} \qquad y_B = \frac{Fa^3b^2}{6EI\ell^3}(3a + b - 3\ell)$$

TABLE 37.1 Properties of Beams (*Continued*)

17. Fixed supports—uniform load

$$R_A = R_B = \frac{W}{2} \qquad M_A = M_B = -\frac{W\ell}{12}$$

$$\text{At } x = \frac{\ell}{2} \qquad M = \frac{W\ell}{24}$$

$$y_{max} = -\frac{W\ell^3}{384EI}$$

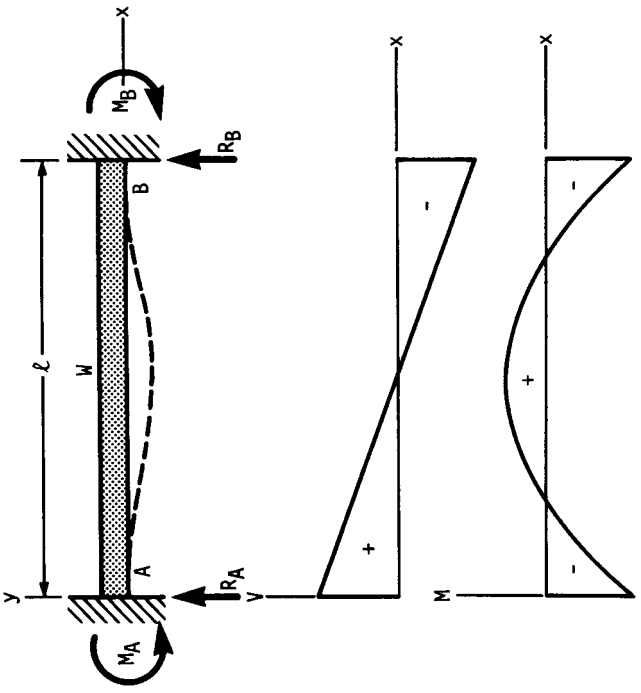

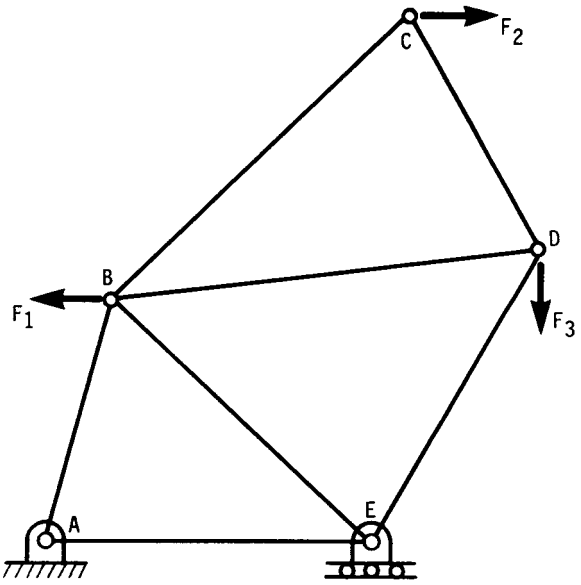

FIGURE 37.2 Frame loaded by three forces.

member has been analyzed and the partial derivatives obtained. The following example demonstrates the technique.

Example 1. Find the downward deflection of point D of the frame shown in Fig. 37.3.

Solution. A force analysis of the system gives an upward reaction at E of $R_E = 225 + 3F_2$. The reaction at A is downward and is $R_A = 75 - 2F_2$.

The strain energy for member CE is

$$U_{CE} = \frac{R_A^2 \ell}{2AE} \tag{1}$$

The partial deflection is taken with respect to F_2 because the deflection at D in the direction of F_2 is desired. Thus

$$\frac{\partial U_{CE}}{\partial F_2} = \frac{2R_A \ell}{2AE} \frac{\partial R_A}{\partial F_2} \tag{2}$$

Also,

$$\frac{\partial R_A}{\partial F_2} = -2$$

Thus Eq. (2) becomes

$$\frac{\partial U_{CE}}{\partial F_2} = \frac{(75 - 2F_2)(30)}{0.2E}(-2) = \frac{37\,500}{E} \tag{3}$$

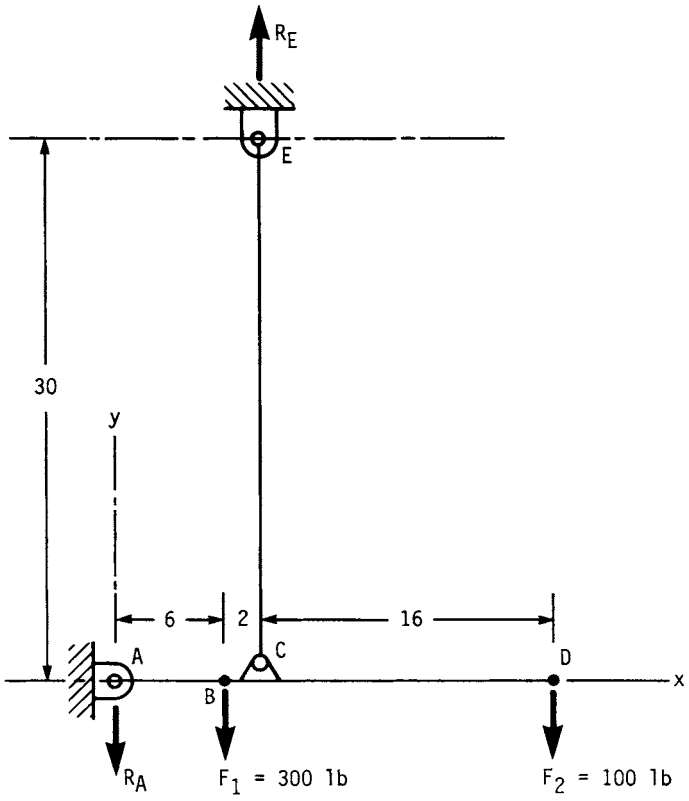

FIGURE 37.3 Frame loaded by two forces. Dimensions in inches: $A_{CE} = 0.20$ in^2; $I_{AD} = 0.18$ in^4; $E = 30 \times 10^6$ psi.

Note that we were able to substitute the value of F_2 in Eq. (3) because the partial derivative had been taken.

The strain energy stored in member $ABCD$ will have to be computed in three parts because of the change in direction of the bending moment diagram at points B and C. For part AB, the moment is

$$M_{AB} = R_A x = (75 - 2F_2)x$$

The strain energy is

$$U_{AB} = \int_0^6 \frac{M_{AB}^2}{2EI}\, dx \tag{4}$$

Taking the partial derivative with respect to F_2 as before gives

$$\frac{\partial U_{AB}}{\partial F_2} = \int_0^6 \frac{2M_{AB}}{2EI} \frac{\partial M_{AB}}{\partial F_2}\, dx \tag{5}$$

But

$$\frac{\partial M_{AB}}{\partial F_2} = -2x \tag{6}$$

Therefore, Eq. (5) may be written

$$\frac{\partial U_{AB}}{\partial F_2} = \frac{1}{EI}\int_0^6 x(75 - 2F_2)(-2x)\,dx$$

$$= \frac{1}{0.18E}\int_0^6 250x^2\,dx = \frac{100\,000}{E} \tag{7}$$

where the value of F_2 again has been substituted after taking the partial derivative.

For section BC, we have

$$M_{BC} = R_A x - F_1(x - 6) = 1800 - 225x - 2F_2x$$

$$\frac{\partial M_{BC}}{\partial F_2} = -2x$$

$$\frac{\partial U_{BC}}{\partial F_2} = \int_6^8 \frac{2M_{BC}}{2EI}\frac{\partial M_{BC}}{\partial F_2}\,dx$$

$$= \frac{1}{EI}\int_6^8 (1800 - 225x - 2F_2x)(-2x)\,dx$$

$$= \frac{1}{0.18E}\int_6^8 (-3600x + 850x^2)\,dx = \frac{145\,926}{E}$$

Finally, section CD yields

$$M_{CD} = -(24 - x)F_2 \qquad \frac{\partial M_{CD}}{\partial F_2} = -(24 - x)$$

$$\frac{\partial U_{CD}}{\partial F_2} = \int_8^{24} \frac{2M_{CD}}{2EI}\frac{\partial M_{CD}}{\partial F_2}\,dx$$

$$= \frac{1}{EI}\int_8^{24} F_2(24 - x)^2\,dx$$

$$= \frac{1}{0.18E}\int_8^{24} (57\,600 - 4800x + 100x^2)\,dx$$

$$= \frac{758\,519}{E}$$

Then

$$y_D = \frac{\partial U_{CE}}{\partial F_2} + \frac{\partial U_{AB}}{\partial F_2} + \frac{\partial U_{BC}}{\partial F_2} + \frac{\partial U_{CD}}{\partial F_2}$$

$$= \frac{1}{30(10)^6}(37\,500 + 100\,000 + 145\,926 + 758\,519)$$

$$= 0.0347 \text{ in} \qquad \text{(when rounded)}$$

37.4.1 Redundant Members

A frame consisting of one or more redundant members is statically indeterminate because the use of statics is not sufficient to determine all the reactions. In this case, Castigliano's theorem can be used first to determine these reactions and second to determine the desired deflection.

Let R_1, R_2, and R_3 be a set of three indeterminate reactions. The deflection at the supports must be zero, and so Castigliano's theorem can be written three times. Thus

$$\frac{\partial U}{\partial R_1} = 0 \qquad \frac{\partial U}{\partial R_2} = 0 \qquad \frac{\partial U}{\partial R_3} = 0 \tag{37.10}$$

and so the number of equations to be solved is the same as the number of indeterminate reactions.

In setting up Eqs. (37.10), *do not* substitute the numerical value of the particular force corresponding to the desired deflection. This force symbol must appear in the reaction equations because the partial derivatives must be taken with respect to this force when the deflection is found. The method is illustrated by the following example.

Example 2. Find the downward deflection at point D of the frame shown in Fig. 37.4.

Solution. Choose R_B as the statically indeterminate reaction. A static force analysis then gives the remaining reactions as

$$R_A = R_C = 0.625(F - R_B) \tag{1}$$

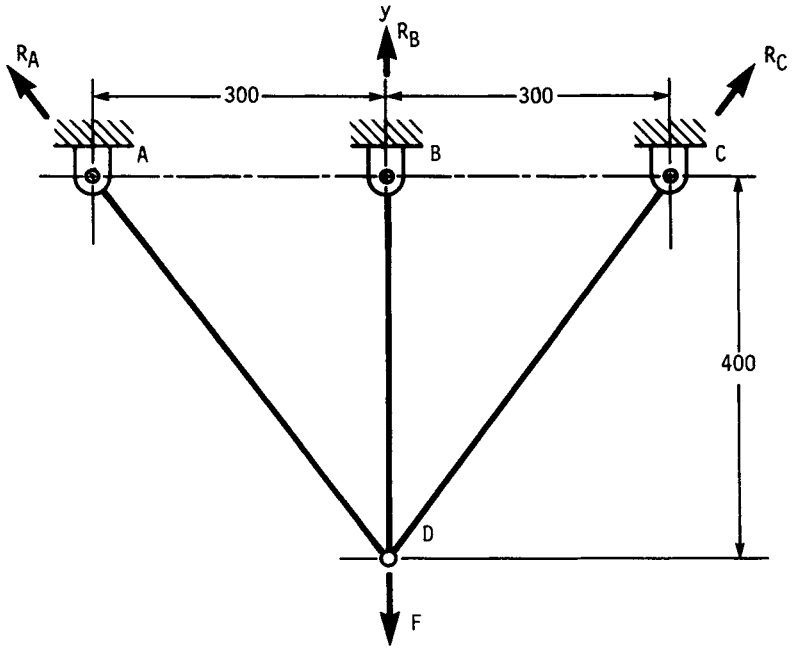

FIGURE 37.4 Frame loaded by a single force. Dimensions in millimeters: $A_{AD} = A_{CD} = 2$ cm^2, $A_{BD} = 1.2$ cm^2, $E = 207$ GPa, $F = 20$ kN.

The frame consists only of tension members, so the strain energy in each member is

$$U_{AD} = U_{DC} = \frac{R_A^2 \ell_{AD}}{2A_{AD}E} \qquad U_{BD} = \frac{R_B^2 \ell_{BD}}{2A_{BD}E} \tag{2}$$

Using Eq. (37.10), we now write

$$0 = \frac{\partial U}{\partial R_B} = \frac{2R_A \ell_{\mathrm{AD}}}{A_{AD}E} \frac{\partial R_A}{\partial R_B} + \frac{R_B \ell_{BD}}{A_{BD}E} \frac{\partial R_B}{\partial R_B} \tag{3}$$

Equation (1) gives $\partial R_A/\partial R_B = -0.625$. Also, $\partial R_B/\partial R_B = 1$. Substituting numerical values in Eq. (3), except for F, gives

$$\frac{2(0.625)(F - R_B)(500)(-0.625)}{2(207)} + \frac{R_B(400)(1)}{1.2(207)} = 0 \tag{4}$$

Solving gives $R_B = 0.369F$. Therefore, from Eq. (1), $R_A = R_C = 0.394F$. This completes the solution of the case of the redundant member. The next problem is to find the deflection at D.

Using Eq. (2), again we write

$$y_D = \frac{\partial U}{\partial F} = \frac{2R_A \ell_{AD}}{A_{AD}E} \frac{\partial R_A}{\partial F} + \frac{R_B \ell_{BD}}{A_{BD}E} \frac{\partial R_B}{\partial F} \tag{5}$$

For use in this equation, we note that $\partial R_A/\partial F = 0.394$ and $\partial R_B/\partial F = 0.369$. Having taken the derivatives, we can now substitute the numerical value of F. Thus Eq. (5) becomes†

† In general, when using metric quantities, prefixed units are chosen so as to produce number strings of not more than four members. Thus some preferred units in SI are MPa (N/mm^2) for stress, GPa for modulus of elasticity, mm for length, and, say, cm^4 for second moment of area.

People are sometimes confused when they encounter an equation containing a number of mixed units. Suppose we wish to solve a deflection equation of the form

$$y = \frac{64F\ell^3}{3\pi d^4 E}$$

where $F = 1.30$ kN, $\ell = 300$ mm, $d = 2.5$ cm, and $E = 207$ GPa. Form the equation into two parts, the first containing the numbers and the second containing the prefixes. This converts everything to base units, including the result. Thus,

$$y = \frac{64(1.30)(300)^3}{3\pi(2.5)^4(207)} \frac{(\text{kilo})(\text{milli})^3}{(\text{centi})^4(\text{giga})}$$

Now compute the numerical value of the first part and substitute the prefix values in the second. This gives

$$y = (29.48 \times 10^3)\left[\frac{10^3(10^{-3})^3}{(10^{-2})^4(10^9)}\right] = 29.48 \times 10^{-4} \text{ m}$$

$$= 2.948 \text{ mm}$$

Note that we multiplied the result by 10^3 mm/m to get the answer in millimeters. When this approach is used with Eq. (5), it is found that the result must be multiplied by $(10)^{-2}$ to get y in millimeters.

DEFLECTION

$$y_D = \left\{ \frac{2[0.394(20)](500)(0.394)}{2(207)} + \frac{[0.369(20)](400)(0.369)}{1.2(207)} \right\} 10^{-2}$$

$$= 0.119 \text{ mm}$$

If care is taken to refrain from substituting numerical values for reactions or forces until after partial derivatives are taken, Castigliano's theorem is applicable to statically indeterminate frames containing redundant members.

DEFLECTION

CHAPTER 38
CURVED BEAMS AND RINGS

Joseph E. Shigley
Professor Emeritus
The University of Michigan
Ann Arbor, Michigan

NOTATION

A	Area, or a constant
B	Constant
C	Constant
E	Modulus of elasticity
e	Eccentricity
F	Force
G	Modulus of rigidity
I	Second moment of area (Table A.1)
K	Shape constant (Table 36.1), or second polar moment of area
M	Bending moment
P	Reduced load
Q	Fictitious force
R	Force reaction
r	Ring radius
$\bar{r}$	Centroidal ring radius
T	Torsional moment
U	Strain energy
V	Shear force
W	Resultant of a distributed load
w	Unit distributed load
X	Constant

Y Constant
y Deflection
Z Constant
γ Load angle
ϕ Span angle, or slope
σ Normal stress
θ Angular coordinate or displacement

Methods of computing the stresses in curved beams for a variety of cross sections are included in this chapter. Rings and ring segments loaded normal to the plane of the ring are analyzed for a variety of loads and span angles, and formulas are given for bending moment, torsional moment, and deflection.

38.1 BENDING IN THE PLANE OF CURVATURE

The distribution of stress in a curved member subjected to a bending moment in the plane of curvature is hyperbolic ([38.1], [38.2]) and is given by the equation

$$\sigma = \frac{My}{Ae(r - e - y)} \tag{38.1}$$

where r = radius to centroidal axis
y = distance from neutral axis
e = shift in neutral axis due to curvature (as noted in Table 38.1)

The moment M is computed about the *centroidal axis,* not the neutral axis. The maximum stresses, which occur on the extreme fibers, may be computed using the formulas of Table 38.1.

In most cases, the bending moment is due to forces acting to one side of the section. In such cases, be sure to add the resulting axial stress to the maximum stresses obtained using Table 38.1.

38.2 CASTIGLIANO'S THEOREM

A complex structure loaded by any combination of forces, moments, and torques can be analyzed for deflections by using the elastic energy stored in the various components of the structure [38.1]. The method consists of finding the total strain energy stored in the system by all the various loads. Then the displacement corresponding to a particular force is obtained by taking the partial derivative of the total energy with respect to that force. This procedure is called *Castigliano's theorem.* General expressions may be written as

$$y_i = \frac{\partial U}{\partial F_i} \qquad \theta_i = \frac{\partial U}{\partial T_i} \qquad \phi_i = \frac{\partial U}{\partial M_i} \tag{38.2}$$

where U = strain energy stored in structure
y_i = displacement of point of application of force F_i in the direction of F_i

$\theta_i =$ angular displacement at T_i
$\phi_i =$ slope or angular displacement at moment M_i

If a displacement is desired at a point on the structure where no force or moment exists, then a fictitious force or moment is placed there. When the expression for the corresponding displacement is developed, the fictitious force or moment is equated to zero, and the remaining terms give the deflection at the point where the fictitious load had been placed.

Castigliano's method can also be used to find the reactions in indeterminate structures. The procedure is simply to substitute the unknown reaction in Eq. (38.2) and use zero for the corresponding deflection. The resulting expression then yields the value of the unknown reaction.

It is important to remember that the displacement-force relation must be linear. Otherwise, the theorem is not valid.

Table 38.2 summarizes strain-energy relations.

38.3 RING SEGMENTS WITH ONE SUPPORT

Figure 38.1 shows a cantilevered ring segment fixed at *C*. The force *F* causes bending, torsion, and direct shear. The moments and torques at the fixed end *C* and at any section *B* are shown in Table 38.3. The shear at *C* is $R_C = F$. Stresses in the ring can be computed using the formulas of Chap. 36.

To obtain the deflection at end *A*, we use Castigliano's theorem. Neglecting direct shear and noting from Fig. 38.1*b* that $l = r\,d\theta$, we determine the strain energy from Table 38.2 to be

$$U = \int_0^{\phi} \frac{M^2 r\,d\theta}{2EI} + \int_0^{\phi} \frac{T^2 r\,d\theta}{2GK} \tag{38.3}$$

Then the deflection y at A and in the direction of F is computed from

$$y = \frac{\partial U}{\theta F} = \frac{r}{EI}\int_0^{\phi} M\frac{\partial M}{\partial F}\,d\theta + \frac{r}{GK}\int_0^{\phi} T\frac{\partial T}{\partial F}\,d\theta \tag{38.4}$$

The terms for this relation are shown in Table 38.3. It is convenient to arrange the solution in the form

$$y = \frac{Fr^3}{2}\left(\frac{A}{EI} + \frac{B}{GK}\right) \tag{38.5}$$

where the coefficients A and B are related only to the span angle. These are listed in Table 38.3.

Figure 38.2*a* shows another cantilevered ring segment, loaded now by a distributed load. The resultant load is $W = wr\phi$; a shear reaction $R = W$ acts upward at the fixed end *C*, in addition to the moment and torque reactions shown in Table 38.3.

A force $W = wr\theta$ acts at the centroid of segment *AB* in Fig. 38.2*b*. The centroidal radius is

$$\bar{r} = \frac{2r\sin(\theta/2)}{\theta} \tag{38.6}$$

TABLE 38.1 Eccentricities and Stress Factors for Curved Beams†

1. Rectangle

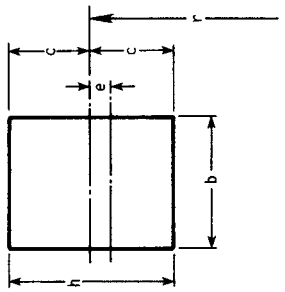

$$e = r - \frac{h}{\ln\left(\frac{r+c}{r-c}\right)} \qquad K_i = \frac{c(c-e)}{3e(r-c)} \qquad K_o = \frac{c(c+e)}{3e(r+c)}$$

2. Solid round

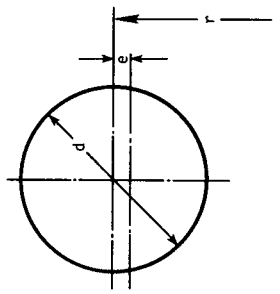

$$e = r - \frac{d^2}{4(2r - \sqrt{4r^2 - d^2})} \qquad K_i = \frac{d(d-2e)}{8e(2r-d)} \qquad K_o = \frac{d(d+2e)}{8e(2r+d)}$$

TABLE 38.1 Eccentricities and Stress Factors for Curved Beams† (*Continued*)

3. Hollow round

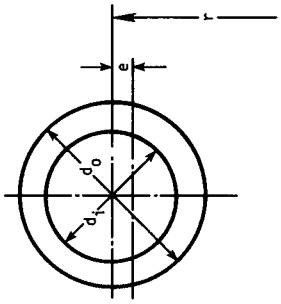

$$e = r - \frac{d_o^2 - d_i^2}{4(\sqrt{4r^2 - d_i^2} - \sqrt{4r^2 - d_o^2})} \qquad K_i = \frac{2I(d_o - 2e)}{Ad_oe(2r - d_o)}$$

$$K_o = \frac{2I(d_o + 2e)}{Ad_oe(2r + d_o)}$$

4. Hollow rectangle

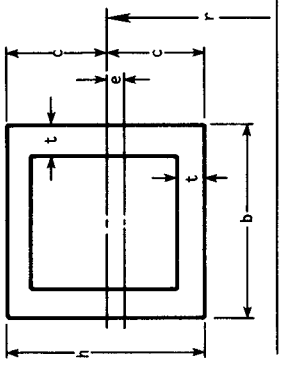

$$e = r - \frac{A}{b \ln\left(\frac{r + t - c}{r - c}\right) + 2t \ln\left(\frac{r + c - t}{r + t - c}\right) + b \ln\left(\frac{r + c}{r + c - t}\right)}$$

$$K_i = \frac{I(c - e)}{Aec(r - c)} \qquad K_o = \frac{I(c + e)}{Aec(r + c)}$$

TABLE 38.1 Eccentricities and Stress Factors for Curved Beams† (*Continued*)

5. Trapezoid

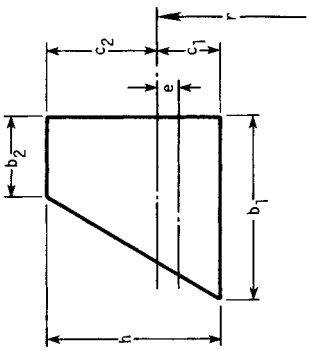

$$e = r - \frac{A}{\dfrac{b_1(r + c_2) - b_2(r - c_1)}{h} \ln\left(\frac{r + c_2}{r - c_1}\right) - (b_1 - b_2)}$$

$$K_i = \frac{I(c_1 - e)}{Aec_1(r - c_1)} \qquad K_o = \frac{I(c_2 + e)}{Aec_2(r + c_2)}$$

6. T Section

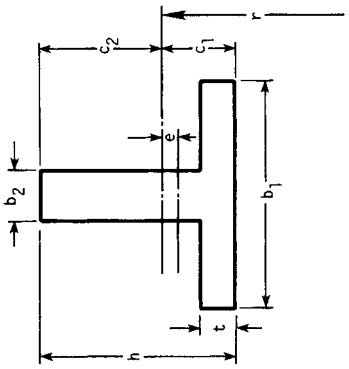

$$e = r - \frac{A}{b_1 \ln\left(\dfrac{r + t - c_1}{r - c_1}\right) + b_2 \ln\left(\dfrac{r + c_2}{r + t - c_1}\right)}$$

$$K_i = \frac{I(c_1 - e)}{Aec_1(r - c_1)} \qquad K_o = \frac{I(c_2 + e)}{Aec_2(r + c_2)}$$

TABLE 38.1 Eccentricities and Stress Factors for Curved Beams† (*Continued*)

7. U Section

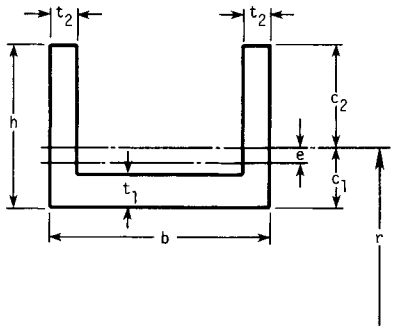

$$e = r - \frac{A}{b \ln\left(\frac{r + t_1 - c_1}{r - c_1}\right) + 2t_2 \ln\left(\frac{r + c_2}{r + t_1 - c_1}\right)}$$

$$K_i = \frac{I(c_1 - e)}{Aec_1(r - c_1)} \qquad K_o = \frac{I(c_2 + e)}{Aec_2(r + c_2)}$$

†Notation: r = radius of curvature to centroidal axis of section; A = area; I = second moment of area; e = distance from centroidal axis to neutral axis; $\sigma_i = K_i\sigma$ and $\sigma_o = K_o\sigma$ where σ_i and σ_o are the normal stresses on the fibers having the smallest and largest radii of curvature, respectively, and σ are the corresponding stresses computed on the same fibers of a straight beam. (Formulas for A and I can be found in Table A.1.)

TABLE 38.2 Strain-Energy Formulas

Loading	Formula
1. Axial force F	$U = \dfrac{F^2 l}{2AE}$
2. Shear force F	$U = \dfrac{F^2 l}{2AG}$
3. Bending moment M	$U = \displaystyle\int \dfrac{M^2\,dx}{2EI}$
4. Torsional moment T	$U = \dfrac{T^2 l}{2GK}$

To determine the deflection of end A, we employ a fictitious force Q acting down at end A. Then the deflection is

$$y = \frac{\partial U}{\partial Q} = \frac{r}{EI}\int_0^{\phi} M\,\frac{\partial M}{\partial Q}\,d\theta + \frac{r}{GK}\int_0^{\phi} T\,\frac{\partial T}{\partial Q}\,d\theta \tag{38.7}$$

The components of the moment and torque due to Q can be obtained by substituting Q for F in the moment and torque equations in Table 38.3 for an end load F; then the total of the moments and torques is obtained by adding this result to the equations for M and T due only to the distributed load. When the terms in Eq. (38.7) have

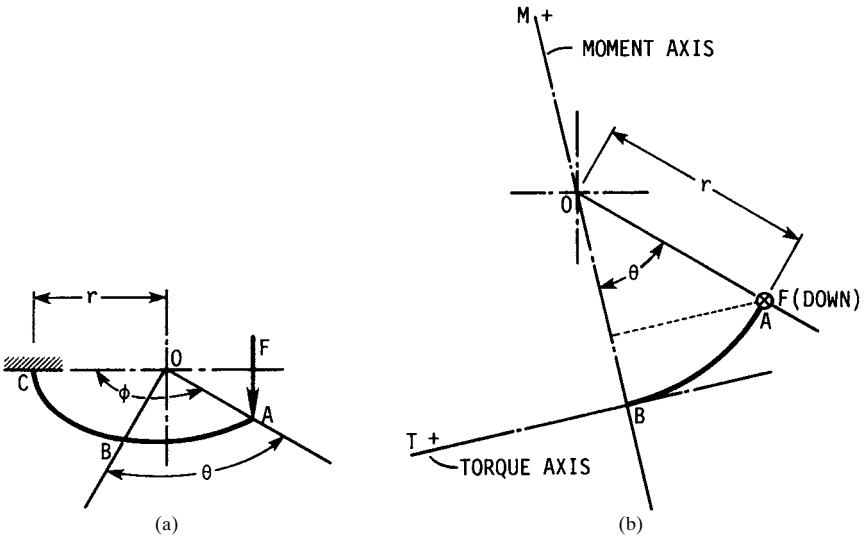

FIGURE 38.1 (*a*) Ring segment of span angle ϕ loaded by force F normal to the plane of the ring. (*b*) View of portion of ring AB showing positive directions of the moment and torque for section at B.

TABLE 38.3 Formulas for Ring Segments with One Support

Loading	Term	Formula
End load F	Moment Torque	$M = Fr \sin\theta \quad M_C = Fr \sin\phi$ $T = Fr(1 - \cos\theta) \quad T_C = Fr(1 - \cos\phi)$
	Derivatives	$\frac{\partial M}{\partial F} = r \sin\theta \quad \frac{\partial T}{\partial F} = r(1 - \cos\theta)$
	Deflection coefficients	$A = \phi - \sin\phi \cos\phi$ $B = 3\phi - 4 \sin\phi + \sin\phi \cos\phi$
Distributed load w; fictitious load Q	Moment Torque	$M = wr^2(1 - \cos\theta) \quad M_C = wr^2(1 - \cos\phi)$ $T = wr^2(\theta - \sin\theta) \quad T_C = wr^2(\phi - \sin\phi)$
	Derivatives	$\frac{\partial M}{\partial Q} = r \sin\theta \quad \frac{\partial T}{\partial Q} = r(1 - \cos\theta)$
	Deflection coefficients	$A = 2 - 2 \cos\phi - \sin^2\phi$ $B = \phi^2 - 2\phi \sin\phi + \sin^2\phi$

been formed, the force Q can be placed equal to zero prior to integration. The deflection equation can then be expressed as

$$y = \frac{wr^4}{2}\left(\frac{A}{EI} + \frac{B}{GK}\right) \tag{38.8}$$

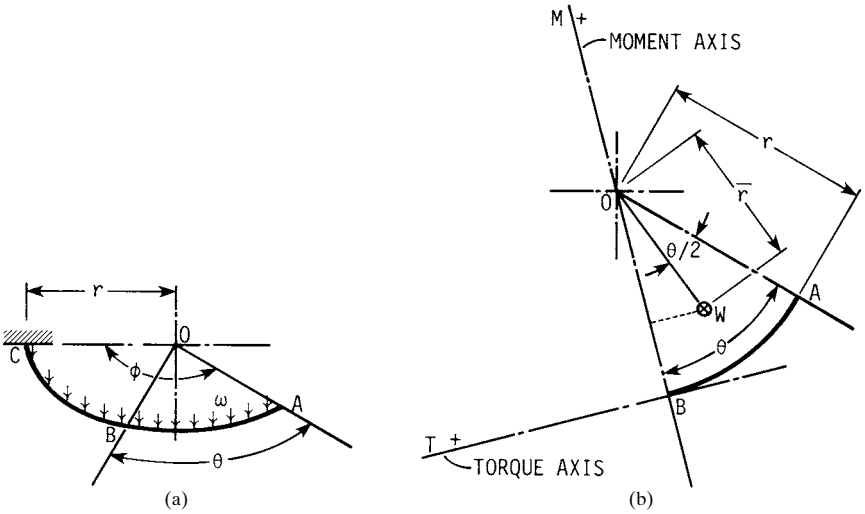

FIGURE 38.2 (*a*) Ring segment of span angle ϕ loaded by a uniformly distributed load w acting normal to the plane of the ring segment; (*b*) view of portion of ring AB; force W is the resultant of the distributed load w acting on portion AB of ring, and it acts at the centroid.

38.4 RINGS WITH SIMPLE SUPPORTS

Consider a ring loaded by any set of forces F and supported by reactions R, all normal to the ring plane, such that the force system is statically determinate. The system shown in Fig. 38.3, consisting of five forces and three reactions, is statically determinate and is such a system. By choosing an origin at any point A on the ring, all forces and reactions can be located by the angles ϕ measured counterclockwise from A. By treating the reactions as negative forces, Den Hartog [38.3], pp. 319–323, describes a simple method of determining the shear force, the bending moment, and the torsional moment at any point on the ring. The method is called *Biezeno's theorem.*

A term called the *reduced load P* is defined for this method. The reduced load is obtained by multiplying the actual load, plus or minus, by the fraction of the circle corresponding to its location from A. Thus for a force F_i, the reduced load is

$$P_i = \frac{\phi_i}{360^\circ} F_i \tag{38.9}$$

Then Biezeno's theorem states that the shear force V_A, the moment M_A, and the torque T_A at section A, all statically indeterminate, are found from the set of equations

$$\begin{aligned} V_A &= \sum_n P_i \\ M_A &= \sum_n P_i r \sin \phi_i \\ T_A &= \sum_n P_i r(1 - \cos \phi_i) \end{aligned} \tag{38.10}$$

where n = number of forces and reactions together. The proof uses Castigliano's theorem and may be found in Ref. [38.3].

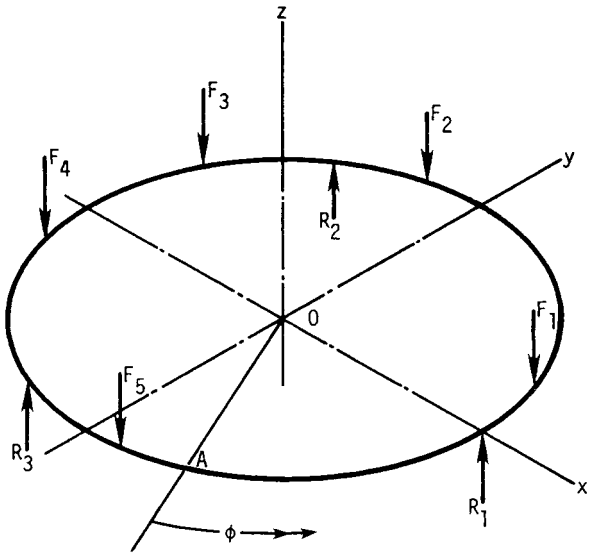

FIGURE 38.3 Ring loaded by a series of concentrated forces.

Example 1. Find the shear force, bending moment, and torsional moment at the location of R_3 for the ring shown in Fig. 38.4.

Solution. Using the principles of statics, we first find the reactions to be

$$R_1 = R_2 = R_3 = \frac{2}{3} F$$

Choosing point A at R_3, the reduced loads are

$$P_0 = -\frac{0°}{360°} R_3 = 0 \qquad P_1 = \frac{30}{360} F = 0.0833F$$

$$P_2 = -\frac{120}{360} R_1 = -\frac{120}{360}\frac{2}{3} F = -0.2222F$$

$$P_3 = \frac{210}{360} F = 0.5833F$$

$$P_4 = -\frac{240}{360} R_2 = -\frac{240}{360}\frac{2}{3} F = -0.4444F$$

Then, using Eqs. (38.10), we find $V_A = 0$. Next,

$$M_A = \sum_5 P_i r \sin \phi_i$$

$$= Fr\,(0 + 0.0833 \sin 30° - 0.2222 \sin 120° + 0.5833 \sin 210°$$

$$- 0.4444 \sin 240°)$$

$$= -0.0576Fr$$

In a similar manner, we find $T_A = 0.997Fr$.

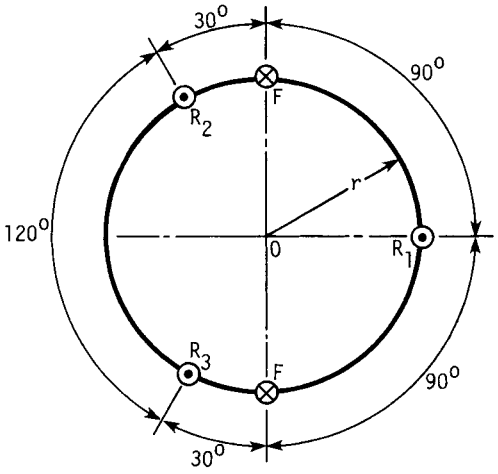

FIGURE 38.4 Ring loaded by the two forces F and supported by reactions R_1, R_2, and R_3. The crosses indicate that the forces act downward; the heavy dots at the reactions R indicate an upward direction.

The task of finding the deflection at any point on a ring with a loading like that of Fig. 38.3 is indeed difficult. The problem can be set up using Eq. (38.2), but the resulting integrals will be lengthy. The chances of making an error in signs or in terms during any of the simplification processes are very great. If a computer or even a programmable calculator is available, the integration can be performed using a numerical procedure such as Simpson's rule. Most of the user's manuals for programmable calculators contain such programs in the master library. When this approach is taken, the two terms behind each integral should not be multiplied out or simplified; reserve these tasks for the computer.

38.4.1 A Ring with Symmetrical Loads

A ring having three equally spaced loads, all equal in magnitude, with three equally spaced supports located midway between each pair of loads, has reactions at each support of $R = F/2$, $M = 0.289Fr$, and $T = 0$ by Biezeno's theorem. To find the moment and torque at any location θ from a reaction, we construct the diagram shown in Fig. 38.5. Then the moment and torque at A are

$$\begin{aligned} M &= M_1 \cos\theta - R_1 r \sin\theta \\ &= Fr\,(0.289\cos\theta - 0.5\sin\theta) \end{aligned} \tag{38.11}$$

$$\begin{aligned} T &= M_1 \sin\theta - R_1 r\,(1 - \cos\theta) \\ &= Fr\,(0.289\sin\theta - 0.5 + 0.5\cos\theta) \end{aligned} \tag{38.12}$$

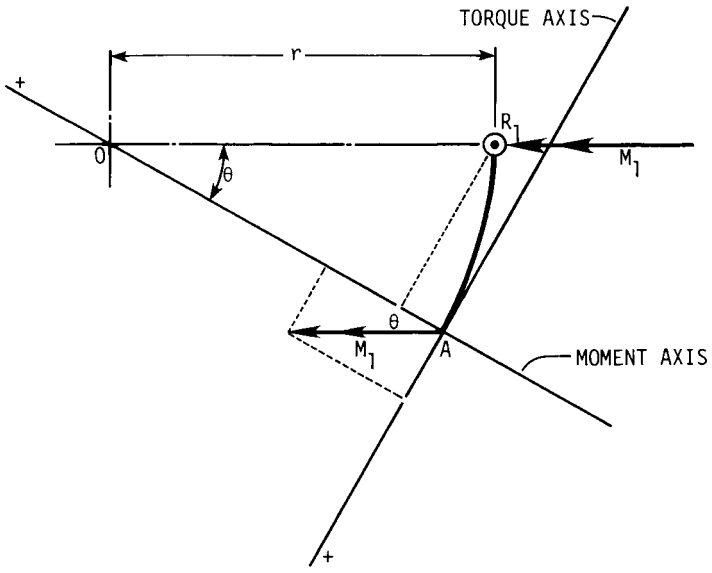

FIGURE 38.5 The positive directions of the moment and torque axes are arbitrary. Note that $R_1 = F/2$ and $M_1 = 0.289Fr$.

Neglecting direct shear, the strain energy stored in the ring between any two supports is, from Table 38.2,

$$U = 2\int_0^{\pi/3} \frac{M^2 r\, d\theta}{2EI} + 2\int_0^{\pi/3} \frac{T^2 r\, d\theta}{2GK} \tag{38.13}$$

Castigliano's theorem states that the deflection at the load F is

$$y = \frac{\partial U}{\partial F} = \frac{2r}{EI}\int_0^{\pi/3} M\frac{\partial M}{\partial F}\, d\theta + \frac{2r}{GK}\int_0^{\pi/3} T\frac{\partial T}{\partial F}\, d\theta \tag{38.14}$$

From Eqs. (38.11) and (38.12), we find

$$\frac{\partial M}{\partial F} = r(0.289\cos\theta - 0.5\sin\theta)$$

$$\frac{\partial T}{\partial F} = r(0.289\sin\theta - 0.5 + 0.5\cos\theta)$$

When these are substituted into Eq. (38.14), we get

$$y = \frac{Fr^3}{2}\left(\frac{A}{EI} + \frac{B}{GK}\right) \tag{38.15}$$

which is the same as Eq. (38.5). The constants are

$$A = 4\int_0^{\pi/3} (0.289\cos\theta - 0.5\sin\theta)^2\, d\theta$$

$$B = 4\int_0^{\pi/3} (0.289\sin\theta - 0.5 + 0.5\cos\theta)^2\, d\theta \tag{38.16}$$

These equations can be integrated directly or by a computer using Simpson's rule. If your integration is rusty, use the computer. The results are $A = 0.1208$ and $B = 0.0134$.

38.4.2 Distributed Loading

The ring segment in Fig. 38.6 is subjected to a distributed load w per unit circumference and is supported by the vertical reactions R_1 and R_2 and the moment reactions M_1 and M_2. The zero-torque reactions mean that the ring is free to turn at A and B. The resultant of the distributed load is $W = wr\phi$; it acts at the centroid:

$$\bar{r} = \frac{2r\sin(\phi/2)}{\phi} \tag{38.17}$$

By symmetry, the force reactions are $R_1 = R_2 = W/2 = wr\phi/2$. Summing moments about an axis through BO gives

$$\Sigma M(BO) = -M_2 + W\bar{r}\sin\frac{\phi}{2} - M_1\cos(\pi - \phi) - \frac{wr^2\phi}{2}\sin\phi = 0$$

Since M_1 and M_2 are equal, this equation can be solved to give

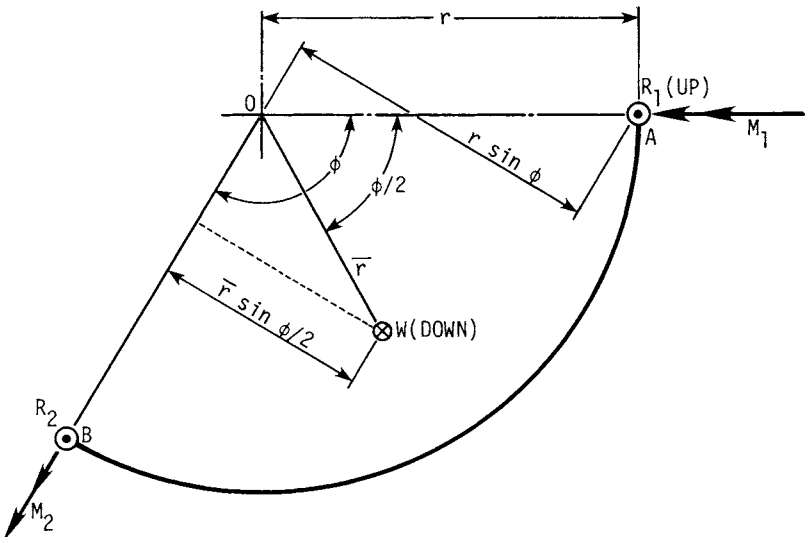

FIGURE 38.6 Section of ring of span angle ϕ with distributed load.

$$M_1 = wr^2 \left[\frac{1 - \cos\phi - (\phi/2)\sin\phi}{1 - \cos\phi} \right] \tag{38.18}$$

Example 2. A ring has a uniformly distributed load and is supported by three equally spaced reactions. Find the deflection midway between supports.

Solution. If we place a load Q midway between supports and compute the strain energy using half the span, Eq. (38.7) becomes

$$y = \frac{\partial U}{\partial Q} = \frac{2r}{EI}\int_0^{\phi/2} M\frac{\partial M}{\partial Q}\,d\theta + \frac{2r}{GK}\int_0^{\phi/2} T\frac{\partial T}{\partial Q}\,d\theta \tag{38.19}$$

Using Eq. (38.18) with $\phi = 2\pi/3$ gives the moment at a support due only to w to be $M_1 = 0.395\ wr^2$. Then, using a procedure quite similar to that used to write Eqs. (38.11) and (38.12), we find the moment and torque due only to the distributed load at any section θ to be

$$\begin{aligned} M_w &= wr^2\left(1 - 0.605\cos\theta - \frac{\pi}{3}\sin\theta\right) \\ T_w &= wr^2\left(\theta - 0.605\sin\theta - \frac{\pi}{3} + \frac{\pi}{3}\cos\theta\right) \end{aligned} \tag{38.20}$$

In a similar manner, the force Q results in additional components of

$$\begin{aligned} M_Q &= \frac{Qr}{2}(0.866\cos\theta - \sin\theta) \\ T_Q &= \frac{Qr}{2}(0.866\sin\theta - 1 + \cos\theta) \end{aligned} \tag{38.21}$$

Then
$$\frac{\partial M_Q}{\partial Q} = \frac{r}{2}(0.866\cos\theta - \sin\theta)$$
$$\frac{\partial T_Q}{\partial Q} = \frac{r}{2}(0.866\sin\theta - 1 + \cos\theta)$$

And so, placing the fictitious force Q equal to zero, Eq. (38.19) becomes

$$y = \frac{wr^4}{EI}\int_0^{\pi/3}\left(1 - 0.605\cos\theta - \frac{\pi}{3}\sin\theta\right)(0.866\cos\theta - \sin\theta)\,d\theta$$
$$+\frac{wr^4}{GK}\int_0^{\pi/3}\left(\theta - 0.605\sin\theta - \frac{\pi}{3} + \frac{\pi}{3}\cos\theta\right)(0.866\sin\theta - 1 + \cos\theta)\,d\theta \qquad (38.22)$$

When this expression is integrated, we find

$$y = \frac{wr^4}{2}\left(\frac{0.141}{EI} + \frac{0.029}{GK}\right) \qquad (38.23)$$

38.5 RING SEGMENTS WITH FIXED ENDS

A ring segment with fixed ends has a moment reaction M_1, a torque reaction T_1, and a shear reaction R_1, as shown in Fig. 38.7*a*. The system is indeterminate, and so all three relations of Eq. (38.2) must be used to determine them, using zero for each corresponding displacement.

38.5.1 Segment with Concentrated Load

The moment and torque at any position θ are found from Fig. 38.7*b* as

$$M = T_1\sin\theta + M_1\cos\theta - R_1 r\sin\theta + Fr\sin(\theta - \gamma)$$
$$T = -T_1\cos\theta + M_1\sin\theta - R_1 r(1 - \cos\theta) + Fr[1 - \cos(\theta - \gamma)]$$

These can be simplified; the result is

$$M = T_1\sin\theta + M_1\cos\theta - R_1 r\sin\theta + Fr\cos\gamma\sin\theta - Fr\sin\gamma\cos\theta \qquad (38.24)$$
$$T = -T_1\cos\theta + M_1\sin\theta - R_1 r(1 - \cos\theta) - Fr\cos\gamma\cos\theta - Fr\sin\gamma\sin\theta + Fr \qquad (38.25)$$

Using Eq. (38.3) and the third relation of Eq. (38.2) gives

$$\frac{\partial U}{\partial M_1} = \frac{r}{EI}\int_0^{\phi} M\frac{\partial M}{\partial M_1}\,d\theta + \frac{r}{GK}\int_0^{\phi} T\frac{\partial T}{\partial M_1}\,d\theta = 0 \qquad (38.26)$$

Note that
$$\frac{\partial M}{\partial M_1} = \cos\theta$$
$$\frac{\partial T}{\partial M_1} = \sin\theta$$

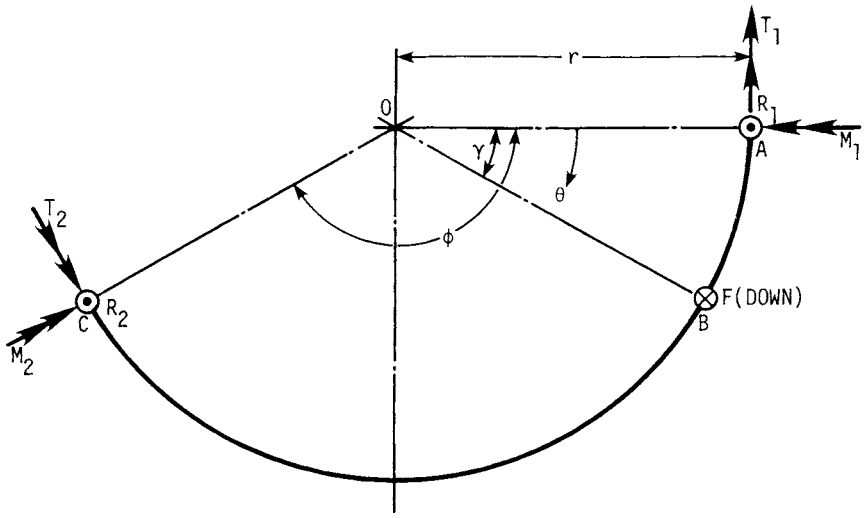

(a)

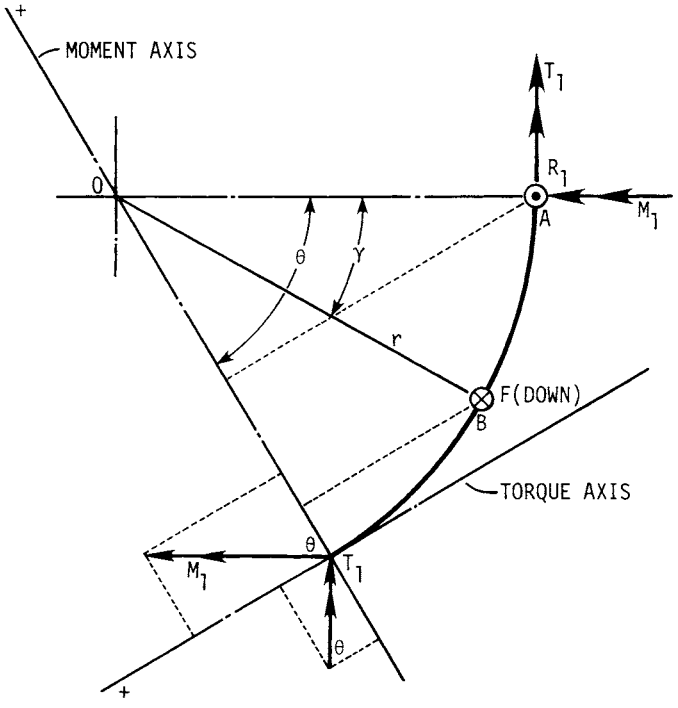

(b)

FIGURE 38.7 (*a*) Ring segment of span angle ϕ loaded by force *F*. (*b*) Portion of ring used to compute moment and torque at position θ.

Now multiply Eq. (38.26) by EI and divide by r; then substitute. The result can be written in the form

$$\int_0^{\phi} (T_1 \sin\theta + M_1 \cos\theta - R_1 r \sin\theta) \cos\theta \, d\theta$$

$$+ Fr \int_{\gamma}^{\phi} (\cos\gamma \sin\theta - \sin\gamma \cos\theta) \cos\theta \, d\theta$$

$$+ \frac{EI}{GK} \left\{ \int_0^{\phi} [-T_1 \cos\theta + M_1 \sin\theta - R_1 r(1 - \cos\theta)] \sin\theta \, d\theta \right.$$

$$\left. - Fr \int_{\gamma}^{\phi} (\cos\gamma \cos\theta + \sin\gamma \sin\theta - 1) \sin\theta \, d\theta \right\} = 0 \tag{38.27}$$

Similar equations can be written using the other two relations in Eq. (38.2). When these three relations are integrated, the results can be expressed in the form

$$\begin{bmatrix} a_{11} & a_{12} & a_{13} \\ a_{21} & a_{22} & a_{23} \\ a_{31} & a_{32} & a_{33} \end{bmatrix} \begin{bmatrix} T_1/Fr \\ M_1/Fr \\ R_1/F \end{bmatrix} = \begin{bmatrix} b_1 \\ b_2 \\ b_3 \end{bmatrix} \tag{38.28}$$

where

$$a_{11} = \sin^2\phi - \frac{EI}{GK} \sin^2\phi \tag{38.29}$$

$$a_{21} = (\phi - \sin\phi \cos\phi) + \frac{EI}{GK} (\phi + \sin\phi \cos\phi) \tag{38.30}$$

$$a_{31} = (\phi - \sin\phi \cos\phi) + \frac{EI}{GK} (\phi + \sin\phi \cos\phi - 2 \sin\phi) \tag{38.31}$$

$$a_{12} = (\phi + \sin\phi \cos\phi) + \frac{EI}{GK} (\phi - \sin\phi \cos\phi) \tag{38.32}$$

$$a_{22} = a_{11} \tag{38.33}$$

$$a_{32} = \sin^2\phi + \frac{EI}{GK} [2(1 - \cos\phi) - \sin^2\phi] \tag{38.34}$$

$$a_{13} = -a_{32} \tag{38.35}$$

$$a_{23} = -a_{31} \tag{38.36}$$

$$a_{33} = -(\phi - \sin\phi \cos\phi) - \frac{EI}{GK} (3\phi - 4 \sin\phi + \sin\phi \cos\phi) \tag{38.37}$$

$$b_1 = \sin\gamma \sin\phi \cos\phi - \cos\gamma \sin^2\phi + (\phi - \gamma) \sin\gamma + \frac{EI}{GK} [\cos\gamma \sin^2\phi$$

$$- \sin\gamma \sin\phi \cos\phi + (\phi - \gamma)\sin\gamma + 2 \cos\phi - 2 \cos\gamma] \tag{38.38}$$

$$b_2 = (\gamma - \phi)\cos\gamma - \sin\gamma + \cos\gamma\sin\phi\cos\phi + \sin\gamma\sin^2\phi$$
$$+ \frac{EI}{GK}[(\gamma - \phi)\cos\gamma - \sin\gamma + 2\sin\phi - \cos\gamma\sin\phi\cos\phi - \sin\gamma\sin^2\phi] \quad (38.39)$$

$$b_3 = (\gamma - \phi)\cos\gamma - \sin\gamma + \cos\gamma\sin\phi\cos\phi + \sin\gamma\sin^2\phi$$
$$+ \frac{EI}{GK}[(\gamma - \phi)\cos\gamma - \sin\gamma - \cos\gamma\sin\phi\cos\phi - \sin\gamma\sin^2\phi$$
$$+ 2(\sin\phi - \phi + \gamma + \cos\gamma\sin\phi - \sin\gamma\cos\phi)] \quad (38.40)$$

For tabulation purposes, we indicate these relations in the form

$$a_{ij} = X_{ij} + \frac{EI}{GK}Y_{ij} \qquad b_k = X_k + \frac{EI}{GK}Y_k \quad (38.41)$$

Programs for solving equations such as Eq. (38.28) are widely available and easy to use. Tables 38.4 and 38.5 list the values of the coefficients for a variety of span and load angles.

TABLE 38.4 Coefficients a_{ij} for Various Span Angles

Coefficients		Span angle ϕ						
		$3\pi/2$	π	$3\pi/4$	$2\pi/3$	$\pi/2$	$\pi/3$	$\pi/4$
a_{11}	X_{11}	1	0	0.5	0.75	1	0.75	0.5
	Y_{11}	−1	0	−0.5	−0.75	−1	−0.75	−0.5
a_{21}	X_{21}	4.7124	π	2.8562	2.5274	1.5708	0.6142	0.2854
	Y_{21}	4.7124	π	1.8562	1.6614	1.5708	1.4802	1.2854
a_{31}	X_{31}	4.7124	π	2.8562	2.5274	1.5708	0.6142	0.2854
	Y_{31}	6.7124	π	0.4420	−0.0707	−0.4292	−0.2518	−0.1288
a_{12}	X_{12}	4.7124	π	1.8562	1.6614	1.5708	1.4802	1.2854
	Y_{12}	4.7124	π	2.8562	2.5274	1.5708	0.6142	0.2854
a_{22}	X_{22}	1	0	0.5	0.75	1	0.75	0.5
	Y_{22}	−1	0	−0.5	−0.75	−1	−0.75	−0.5
a_{32}	X_{32}	1	0	0.5	0.75	1	0.75	0.5
	Y_{32}	1	4	2.9142	2.25	1	0.25	0.0858
a_{13}	X_{13}	−1	0	−0.5	−0.75	−1	−0.75	−0.5
	Y_{13}	−1	−4	−2.9142	−2.25	−1	−0.25	−0.0858
a_{23}	X_{23}	−4.7124	$-\pi$	−2.8562	−2.5274	−1.5708	−0.6142	−0.2854
	Y_{23}	−6.7124	$-\pi$	−0.4420	0.0707	0.4292	0.2518	0.1288
a_{33}	X_{33}	−4.7124	$-\pi$	−2.8562	−2.5274	−1.5708	−0.6142	−0.2854
	Y_{33}	−18.1372	-3π	−3.7402	−2.3861	−0.7124	−0.1105	−0.0277

TABLE 38.5 Coefficients b_k for Various Span Angles ϕ and Load Angles γ in Terms of ϕ

Coefficients, load angles γ			Span angle ϕ						
			$3\pi/2$	π	$3\pi/4$	$2\pi/3$	$\pi/2$	$\pi/3$	$\pi/4$
$\frac{\phi}{4}$	b_1	X_1	2.8826	1.6661	0.2883	−0.0806	−0.4730	−0.4091	−0.2780
		Y_1	2.8826	−1.7481	−1.4019	1.0806	−0.4730	−0.1162	−0.0396
	b_2	X_2	−1.3525	−2.3732	−2.1628	−1.8603	−1.0884	−0.4051	−0.1849
		Y_2	−5.2003	−2.3732	−0.4727	−0.1283	0.1462	0.1022	0.0535
	b_3	X_3	−1.3525	−2.3732	−2.1628	−1.8603	−1.0884	−0.4051	−0.1849
		Y_3	−13.0342	−5.6714	−2.0455	−1.2699	−0.3622	−0.0544	−0.0135
$\frac{\phi}{3}$	b_1	X_1	3.1416	1.8138	0.4036	0.0446	−0.3424	−0.3179	−0.2180
		Y_1	3.1416	−1.1862	−1.0106	−0.7817	−0.3424	−0.0839	−0.0286
	b_2	X_2	0	−1.9132	−1.8178	−1.5620	−0.9069	−0.3346	−0.1522
		Y_2	−4	−1.9132	−0.4036	−0.1307	0.0931	0.0706	0.0373
	b_3	X_3	0	−1.9132	−1.8178	−1.5620	−0.9069	−0.3346	−0.1522
		Y_3	−10.2832	−4.3700	−1.5452	−0.9536	−0.2692	−0.0401	−0.0099
$\frac{\phi}{2}$	b_1	X_1	2.3732	1.5708	0.4351	0.1569	−0.1517	−0.1712	−0.1203
		Y_1	2.3732	−0.4292	−0.4379	−0.3431	−0.1517	−0.0372	−0.0127
	b_2	X_2	1.6661	−1	−1.1041	−0.9566	−0.5554	−0.2034	−0.0922
		Y_2	−1.7481	−1	−0.2311	−0.0906	0.0304	0.0286	0.0154
	b_3	X_3	1.6661	−1	−1.1041	−0.9566	−0.5554	−0.2034	−0.0922
		Y_3	−5.0463	−2.1416	−0.7395	−0.4529	−0.1262	−0.0186	−0.0046

38.5.2 Deflection Due to Concentrated Load

The deflection of a ring segment at a concentrated load can be obtained using the first relation of Eq. (38.2). The complete analytical solution is quite lengthy, and so a result is shown here that can be solved using computer solutions of Simpson's approximation. First, define the three solutions to Eq. (38.28) as

$$T_1 = C_1 Fr \qquad M_1 = C_2 Fr \qquad R_1 = C_3 F \tag{38.42}$$

Then Eq. (38.2) will have four integrals, which are

$$A_F = \int_0^{\phi} [(C_1 - C_3)\sin\theta + C_2\cos\theta]^2\, d\theta \tag{38.43}$$

$$B_F = \int_0^{\phi} (\cos\gamma\sin\theta - \sin\gamma\cos\theta)^2\, d\theta \tag{38.44}$$

$$C_F = \int_0^{\phi} [(C_3 - C_1)\cos\theta + C_2\sin\theta - C_3]^2\, d\theta \tag{38.45}$$

$$D_F = \int_0^{\phi} [1 - (\cos\gamma\cos\theta + \sin\gamma\sin\theta)]^2\, d\theta \tag{38.46}$$

The results of these four integrations should be substituted into

$$y = \frac{Fr^3}{EI}\left[A_F + B_F + \frac{EI}{GK}(C_F + D_F)\right] \tag{38.47}$$

to obtain the deflection due to F and at the location of the force F.

It is worth noting that the point of maximum deflection will never be far from the middle of the ring, even though the force F may be exerted near one end. This means that Eq. (38.47) will not give the maximum deflection unless $\gamma = \phi/2$.

38.5.3 Segment with Distributed Load

The resultant load acting at the centroid B' in Fig. 38.8 is $W = wr\phi$, and the radius $\bar{r}$ is given by Eq. (38.6), with ϕ substituted for θ. Thus the shear reaction at the fixed end A is $R_1 = wr\phi/2$. M_1 and T_1, at the fixed ends, can be determined using Castigliano's method.

We use Fig. 38.9 to write equations for moment and torque for any section, such as the one at D. When Eq. (38.6) for $\bar{r}$ is used, the results are found to be

$$M = T_1\sin\theta + M_1\cos\theta - \frac{wr^2\phi}{2}\sin\theta + wr^2(1 - \cos\theta) \tag{38.48}$$

$$T = -T_1\cos\theta + M_1\sin\theta - \frac{wr^2\phi}{2}(1 - \cos\theta) + wr^2(\theta - \sin\theta) \tag{38.49}$$

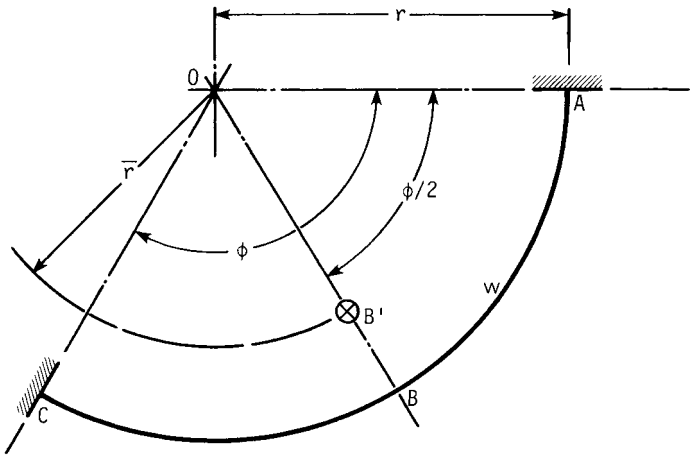

FIGURE 38.8 Ring segment of span angle ϕ subjected to a uniformly distributed load w per unit circumference acting downward. Point B' is the centroid of the load. The ends are fixed to resist bending moment and torsional moment.

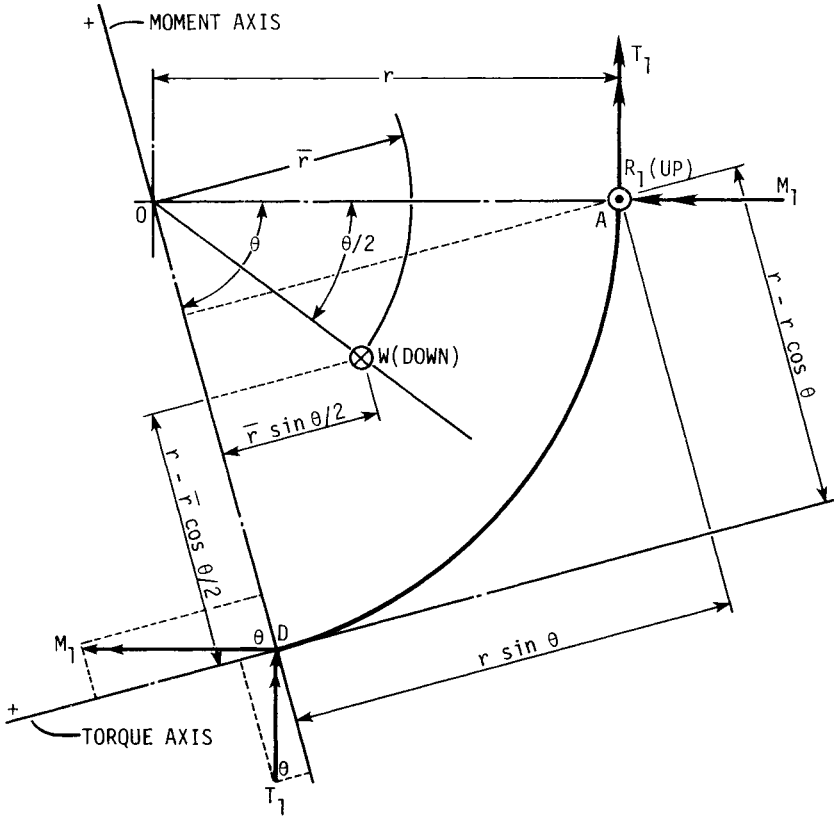

FIGURE 38.9 A portion of the ring has been isolated here to determine the moment and torque at any section D at angle θ from the fixed end at A.

These equations are now employed in the same manner as in Sec. 38.5.1 to obtain

$$\begin{bmatrix} a_{11} & a_{12} \\ a_{21} & a_{22} \end{bmatrix} \begin{bmatrix} T_1/wr^2 \\ M_1/wr^2 \end{bmatrix} = \begin{bmatrix} b_1 \\ b^2 \end{bmatrix} \tag{38.50}$$

It turns out that the a_{ij} terms in the array are identical with the same coefficients in Eq. (38.28); they are given by Eqs. (38.29), (38.30), (38.32), and (38.33), respectively. The coefficients b_k are

$$b_k = X_k + \frac{EI}{GK} Y_k \tag{38.51}$$

where

$$X_1 = \frac{\phi}{2} \sin^2 \phi + \sin \phi \cos \phi + \phi - 2 \sin \phi \tag{38.52}$$

$$Y_1 = \phi - 2 \sin \phi - \frac{\phi}{2} \sin^2 \phi - \sin \phi \cos \phi + \phi(1 + \cos \phi) \tag{38.53}$$

TABLE 38.6 Coefficients b_k for Various Span Angles and Uniform Loading

Coefficients		Span angle ϕ						
		$3\pi/2$	π	$3\pi/4$	$2\pi/3$	$\pi/2$	$\pi/3$	$\pi/4$
b_1	X_1	9.0686	3.1416	1.0310	0.7147	0.3562	0.1409	0.0675
	Y_1	9.0686	3.1416	1.5430	1.0572	0.3562	0.0602	0.0156
b_2	X_2	10.1033	0.9348	0.4507	0.3967	0.2337	0.0716	0.0263
	Y_2	8.1033	0.9348	−1.7274	−2.0102	−1.7663	−0.9750	−0.5810

$$X_2 = \frac{\phi^2}{2} - 2(1 - \cos\phi) - \frac{\phi}{2}\sin\phi\cos\phi + \sin^2\phi \tag{38.54}$$

$$Y_2 = \frac{\phi^2}{2} - 2(1 - \cos\phi) + \frac{\phi}{2}\sin\phi\cos\phi - \sin^2\phi + \phi\sin\phi \tag{38.55}$$

Solutions to these equations for a variety of span angles are given in Table 38.6.

A solution for the deflection at any point can be obtained using a fictitious load Q at any point and proceeding in a manner similar to other developments in this chapter. It is, however, a very lengthy analysis.

REFERENCES

38.1 Raymond J. Roark and Warren C. Young, *Formulas for Stress and Strain,* 6th ed., McGraw-Hill, New York, 1984.

38.2 Joseph E. Shigley and Charles R. Mischke, *Mechanical Engineering Design,* 5th ed., McGraw-Hill, New York, 1989.

38.3 J. P. Den Hartog, *Advanced Strength of Materials,* McGraw-Hill, New York, 1952.

CHAPTER 39
PRESSURE CYLINDERS

Sachindranarayan Bhaduri, Ph.D.
Associate Professor
Mechanical and Industrial Engineering Department
The University of Texas at El Paso
El Paso, Texas

39.1 INTRODUCTION

The pressure vessels commonly used in industrial applications consist basically of a few closed shells of simple shape: spherical or cylindrical with hemispherical, conical, ellipsoidal, or flat ends. The shell components are joined together mostly by welding and riveting; sometimes they are bolted together using flanges.

Generally, the shell elements are axisymmetrical surfaces of revolution formed by rotation of a straight line or a plane curve known as a *meridian* or a *generator* about an axis of rotation. The plane containing the axis of rotation is called the *meridional plane.* The geometry of such simple shells is specified by the form of the midwall surface, usually two radii of curvature and the wall thickness at every point. The majority of pressure vessels are cylindrical.

In practice, the shell is considered thin if the wall thickness t is small in comparison with the circumferential radius of curvature R_θ and the longitudinal radius of curvature R_ℓ. If the ratio $R_\theta/t > 10$, the shell is considered to be thin shell. This implies that the stresses developed in the shell wall by external loads can be considered to be uniformly distributed over the wall thickness. Many shells used in pressure-vessel construction are relatively thin ($10 < R_\theta/t < 500$), with the associated uniform distribution of stresses throughout the cylinder wall. Bending stresses in the walls of such membrane shells due to concentrated external loads are of higher intensity near the area of application of the load. The attenuation distance from the load where the stresses die out is short. The radial deformation of a shell subjected to internal pressure is assumed smaller than one-half the shell thickness. The shell thickness is designed to keep the maximum stresses below the yield strength of the material.

39.2 DESIGN PRINCIPLES OF PRESSURE CYLINDERS

In the design of a pressure vessel as a unit, a number of criteria should be considered. These are (1) selection of the material for construction of the vessel based on a working knowledge of the properties of the material, (2) determination of the magnitude of the induced stress in conformity with the requirements of standard codes, and (3) determination of the elastic stability. To simplify the design and keep the cost of fabrication low, the components of a vessel should be made in the form of simple geometric shapes, such as spherical, cylindrical, or conical. A spherical geometry provides minimum surface area per unit volume and requires minimum wall thickness for a given pressure. From the point of view of material savings and uniform distribution of induced stresses in the shell wall, a spherical shape is favorable. However, the fabrication of spherical vessels is more complicated and expensive than that of cylindrical ones. Spherical vessels are used commonly for storage of gas and liquids. For large-volume, low-pressure storage, spherical vessels are economical. But for higher-pressure storage, cylindrical vessels are more economical.

The most common types of vessels can be classified according to their

1. Functions: Storage vessels, reactors, boilers, mixers, and heat exchangers
2. Structural materials: Steel, cast iron, copper, plastics, etc.
3. Method of fabrication: Welded, cast, brazed, flanged, etc.
4. Geometry: Cylindrical, spherical, conical, combined
5. Scheme of loading: Working under internal or external pressure
6. Wall temperatures: Heated, unheated
7. Corrosion action: Moderate or high corrosion effects
8. Orientation in space: Vertical, horizontal, sloped
9. Method of assembly: Detachable, nondetachable
10. Wall thickness: Thin-walled ($d_o/d_i < 1.5$); thick-walled ($d_o/d_i \geq 1.5$)

Most vessels are designed as cylindrical shells fabricated of rolled sheet metal or as cylindrical shells that are cast. From the point of view of simplified structural design, the stressed state of the material of a thin-wall shell is considered biaxial. This is permissible because the magnitude of the radial stress in such a vessel wall is very small. The stressed state of the shell wall is generally the sum of the two basic components: (1) stressed state due to uniformly distributed forces on the surface as a result of fluid pressure, and (2) stressed state due to the action of the forces and moments distributed around the contour.

The stressed condition due to uniform pressure of fluid on the surface of the shell can be determined either by the membrane or moment theory. The *membrane theory* yields accurate enough results for most engineering applications and is widely used for structural designs. The *moment theory* is not usually applied for the determination of stresses due to uniformly distributed fluid forces on a surface. The equations resulting from the application of the moment theory are complex and the design process is quite involved.

End forces and moments are calculated in sections where a sudden change in load, wall thickness, or the properties of the shell material occurs. The stressed state induced by the applied end forces and moments are determined by application of the moment theory [39.1]. The induced stress and deformations due to end effects

influence mostly the zones where the end forces and moments are applied. In general, end stresses should be carefully evaluated, and design measures must be taken to keep them within the safe limit. High values of end stresses are to be avoided, especially for brittle materials and vessels operating under high alternating loads.

The structural reliability of the equipment parts is determined by two different approaches. The *theory of elasticity* requires that the strength be determined by the ultimate stress which the part can withstand without rupture, whereas the *theory of plasticity* suggests that the strength be determined by the ultimate load the part can withstand without residual deformation. The elastic theory is based on the assumption that the material of the component parts of the vessel is in an elastic state everywhere and nowhere does the state of stress exceed the yield point.

The parts of a pressure vessel are not generally bonded uniformly. When the structural design is based on the ultimate stress occurring at the most loaded region of the construction, the required material consumption could be excessive. In design works using the membrane theory, only average stresses are assumed, and no efforts are made to include the local stresses of significant magnitude. However, the designer should consider the probable adverse effects of very high local stress intensities and modify the design accordingly.

In heavily loaded parts of pressure vessels made of plastic materials, partial transition to the elastic-plastic state occurs. The plastic design method permits a realistic evaluation of the maximum load this vessel can withstand without failure.

39.3 DESIGN LOADS

The principal loads (i.e., forces) applied in actual operations to a vessel or its structural attachments to be considered in the design of such a vessel are

1. Design pressure (internal or external or both)
2. Dead loads
3. Wind loads
4. Thermal loads
5. Piping load
6. Impact load
7. Cyclic loads

Several loading combinations are often possible. The designer should consider them carefully for a particular situation and select the most probable combination of simultaneous loads for an economical and reliable design. Failure of a pressure vessel may be due to improper selection of materials, defects in materials due to inadequate quality control, incorrect design conditions, computational errors in design, improper or faulty fabrication procedures, or inadequate inspection and shop testing.

Design pressure is the pressure used to determine the minimum thickness of each of the vessel components. It is the difference between the internal and external pressures. A suitable margin above the operating pressure (usually 10 percent of operating pressure and a minimum of 10 psi) plus a static head of operating liquid must be included. The minimum design pressure for a "code" nonvacuum vessel is 15 psi. Vessels with negative gauge operating pressures are designed for full vacuum. In

determining the design load, the designer must consult the *ASME Boiler and Pressure Vessel Code,* Sec. VIII, Pressure Vessels, Division I. The maximum operating pressure is, according to code definition, the maximum gauge pressure permissible at the top of the completed vessel in its operating condition at the designated temperature. It is based on the nominal thickness, exclusive of the corrosion allowance, and the thickness required for loads other than fluid pressure.

The *required thickness* is the minimum thickness of the vessel wall, computed by code formula. The *design thickness* is the minimum required thickness plus an allowance for corrosion. The *nominal thickness* is the design thickness of the commercially available material actually used in making the vessel.

The vessel shell must be designed to withstand the combined effect of the pressure and temperature under the anticipated operating conditions. One has to use the pressure-vessel code and standard engineering analysis whenever applicable to determine the nominal stress at any part of the vessel. The stresses cannot in general exceed the allowable stress obtained by the code guidelines.

Design temperature is really more a design environmental condition than a load. *Thermal loads* originate from temperature changes combined with body restraints or existing temperature gradients. Reduction in structural strength due to rising temperature, increase in brittleness with rapidly falling temperature, and the associated changes in the vessel dimensions should be taken into careful consideration for the design. The code design temperature must not be less than the mean vessel-wall temperature under operating conditions. It can be determined by the standard heat-transfer methods. Generally, the standard vessel design temperature is equal to the maximum operating temperature of the fluid in the vessel plus 50°F for safety considerations. For low-temperature operation, the minimum fluid temperature is used for the design temperature. The designer should consult the *ASME Boiler and Pressure Vessel Codes* and the excellent books by Bednar [39.2] and Chuse [39.3].

Dead loads are the forces due to the weight of the vessel and the parts permanently connected with the vessel. The *piping loads* acting on the vessel must be evaluated carefully. They consist of the weight of the pipe sections supported by the nozzles into the vessel shell, as well as operating forces due to thermal expansion of the pipes.

If the pressure vessel is exposed to the environment, the dynamic pressure forces due to the turbulent flow of air and associated gustiness must be evaluated for structural stability of the vessel support system. Determination of *wind load* is outlined in the SEI/ASCE 7-02 standard, and the designer must follow the guidelines to determine the effective dynamic load due to wind speed past the vessel and support-structure system. The same code provides guidelines for evaluation of seismic loads on flexible tall vessels.

In actual design situations, many combinations of loads are possible. Consequently, the designer should use discretion to determine the important ones and select only certain sets of design loads which can most probably occur simultaneously.

39.4 CYLINDRICAL SHELLS—STRESS ANALYSIS

Cylindrical shells are widely used in the manufacture of pressure vessels. They can be easily fabricated and have great structural strength. Depending on their function, they may be vertical or horizontal. Vertical pressure vessels are often preferred, especially for a thin-walled vessel operating under low internal pressure.

The design of a vertical cylindrical vessel becomes simple because the additional bending stresses due to weight of the vessel itself and of the fluid can be eliminated.

Cylindrical shells of malleable materials, such as steels, nonferrous metals, and their alloys, operating under internal pressures up to 10 MPa are fabricated mostly of rolled and welded sheets of corrosion-resistant material (see Ref. [39.1]). The minimum thickness of a shell rolled from low-carbon sheet metal and welded is 4.0 mm. The minimum thickness for an austenitic steel shell is 3.4 mm; for copper shells, 2.5 to 30 mm; and for cast shells, 20 to 25 mm.

39.4.1 Cylindrical Storage Vessel

Before the actual design calculation of a vertical cylindrical vessel is done, the relationship between the optimum height and the diameter should be determined. The volume of the sheet metal needed to make a vertical cylindrical storage tank (Fig. 39.1) is determined by the following formula:

$$V_s = \pi d_o H t_1 + \frac{\pi d_o^2}{4}(t_k + t_a)$$

$$= \pi d_o H t_1 + \frac{\pi d_o^2}{4} t_2 \tag{39.1}$$

Vessel capacity is

$$V = \frac{\pi d_i^2}{4} H \tag{39.2}$$

The inside diameter of the vessel is

$$d_i = \sqrt{\frac{4V}{\pi H}} \tag{39.3}$$

Since thickness t_1 is very small in comparison with d_o and d_i, we may consider $d_i \approx d_o$. Substitution of Eq. (39.3) into Eq. (39.1) gives

$$V_s = 2t_1\sqrt{\pi V H} + \frac{V t_2}{H} \tag{39.4}$$

The minimum volume of sheet metal is obtained by differentiating Eq. (39.4) with respect to H and equating the derivative to zero. Thus

$$\frac{dV_s}{dH} = t_1\sqrt{\pi V/H} - \frac{V t_2}{H^2} = 0 \tag{39.5}$$

The optimum height and the optimum diameter of the tank are given by

$$H_{\text{opt}} = \left[\frac{V}{\pi}\left(\frac{t_2}{t_1}\right)^2\right]^{1/3} \tag{39.6}$$

and

$$d_{\text{opt}} = 2\left[\frac{V t_1}{\pi t_2}\right]^{1/3} \tag{39.7}$$

The shell thickness is given by

$$t_1 = \frac{H_{\text{opt}} \gamma d_{\text{opt}}}{2\sigma_a} \tag{39.8}$$

where γ = specific weight of the fluid in the tank, and σ_a = allowable stress. Substituting the optimum values of height and outside diameter in Eq. (39.8), the tank capacity V is recovered as

$$V = \pi t_1^2 \sqrt{\frac{\sigma_a^3}{\gamma^3 t_2}} \tag{39.9}$$

Considering a minimum shell thickness of $t_1 = 4$ mm and top and bottom thicknesses of 4 mm, we find $t_2 = 8$ mm. The specific weight of the liquid can be obtained from appropriate property tables. The allowable stress for low-carbon steel is 137 MPa. Using this information in Eq. (39.9), one can easily find the corresponding tank volume.

Pressure vessels subjected to internal and/or external pressures require application of the theoretical principles involved in shell analysis. The structural configurations of relatively simple geometric shapes such as cylinders and spheres have been studied extensively in the theories of plates and shells (see Refs. [39.2], [39.4], and [39.5]). In fact, no single chapter or even an entire textbook can cover all the advancements in the field, particularly where internal pressure, external pressure, and other modes of loading are present. Therefore, attempts will be made here only to cover the materials which are pertinent for design of simple pressure vessels and piping. The majority of piping and vessel components are designed for internal pressure and have been analyzed to a great degree of sophistication. Numerous cases involve application of external pressure as well, where stresses, elastic stability, and possible structural failure must be analyzed and evaluated.

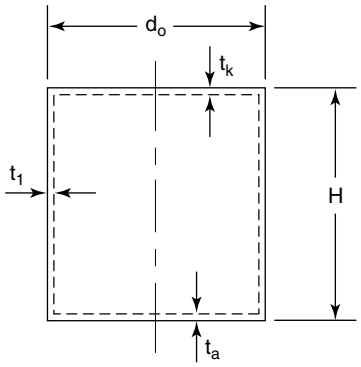

FIGURE 39.1 Cylindrical storage vessel.

39.4.2 Membrane Theory

The common geometric shapes of pressure vessels used in industrial processes are spheres, cylinders, and ellipsoids. Conical and toroidal configurations are also used. Membrane theory can be applied to determine the stresses and deformations of such vessels when they have small thicknesses compared with other dimensions and have limited and small bending resistance normal to their surface. The stresses are considered to be average tension or compression over the thickness of the pipe or vessel wall acting tangential to the surface subjected to normal pressure. The imaginary surface passing through the middle of the wall thickness, however, extends in two directions and calls for rather complicated mathematical analysis, particularly when more than one expression for the curvature is necessary to describe the displacement of a point in the shell wall. In fact, in the more general sense it is neces-

sary to define a normal force, two transverse shear forces, two bending moments, and a torque in order to evaluate the state of stress at a point. Membrane theory simplifies this analysis to a great extent and permits one to ignore bending and twisting moments when shell thickness is small. In many practical cases, consideration of equilibrium of the forces allows us to develop necessary relations for stresses and displacements in terms of the shell parameters for adequate design.

39.4.3 Thin Cylindrical Shells under Internal Pressure

When a thin cylinder is subjected to an internal pressure, three mutually perpendicular principal stresses—hoop stress, longitudinal stress, and radial stress—are developed in the cylinder material. If the ratio of thickness t and the inside diameter of the cylinder d_i is less than 1:20, membrane theory may be applied and we may assume that the hoop and longitudinal stresses are approximately constant across the wall thickness. The magnitude of radial stress is negligibly small and can be ignored. It is to be understood that this simplified approximation is used extensively for the design of thin cylindrical pressure vessels. However, in reality, radial stress varies from zero at the outside surface to a value equal to the internal pressure at the inside surface. The ends of the cylinder are assumed closed. Hoop stress is set up in resisting the bursting effect of the applied pressure and is treated by taking the equilibrium of half of the cylindrical vessel, as shown in Fig. 39.2. Total force acting on the half cylinder is

$$F_h = p_i d_i L \tag{39.10}$$

where d_i = inside diameter of cylinder, and L = length of cylinder. The resisting force due to hoop stress σ_h acting on the cylinder wall, for equilibrium, must equal the force F_h. Thus

$$F_h = 2\sigma_h t T \tag{39.11}$$

Substituting for F_h from Eq. (39.10) into Eq. (39.11), one obtains the following relation:

$$\sigma_h = \frac{p_i d_i}{2t} \qquad \text{or} \qquad \sigma_h = \frac{p_i r_i}{t} \tag{39.12}$$

Despite its simplicity, Eq. (39.12) has wide practical applications involving boiler drums, accumulators, piping, casing chemical processing vessels, and nuclear pressure vessels. Equation (39.12) gives the maximum tangential stress in the vessel wall on the assumption that the end closures do not provide any support, as is the case with long cylinders and pipes. Hoop stress can also be expressed in terms of the radius of the circle passing through the midpoint of the thickness. Then we can write

$$\sigma_h = \frac{p_i(r_i + 0.5t)}{t} \tag{39.13}$$

The shell thickness is then expressed as

$$t = \frac{p_i r_i}{\sigma_h - 0.5p_i} \tag{39.14}$$

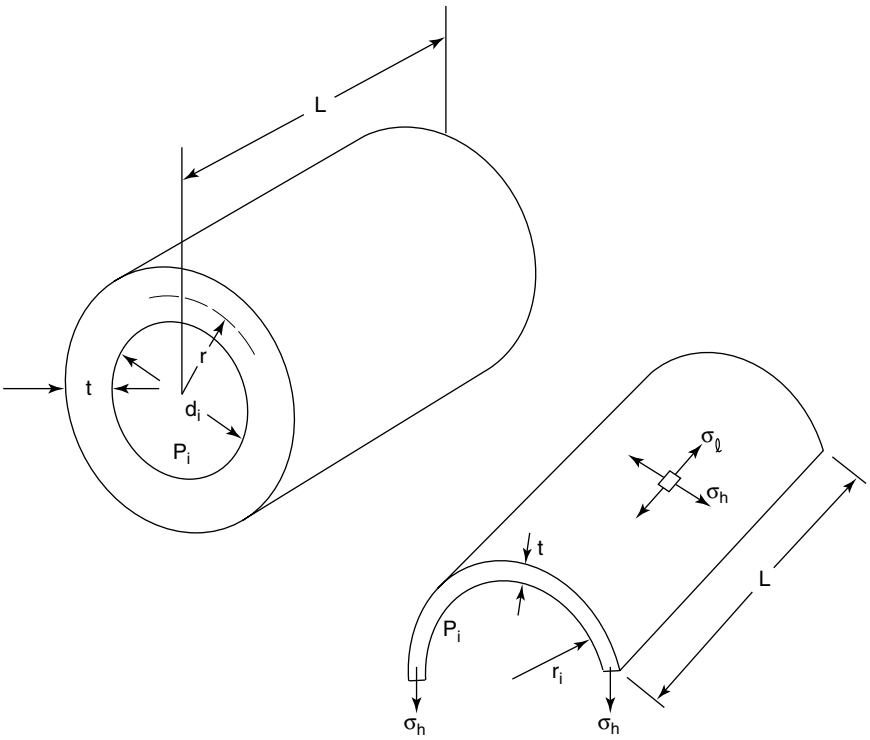

FIGURE 39.2 Thin cylindrical shell under internal pressure.

The code stress and shell thickness formulas based on inside radius approximate the more accurate thick-wall formula of Lamé, which is

$$t = \frac{p_i r_i}{Se - 0.6p_i} \tag{39.15}$$

where e = code weld-joint efficiency, and S = allowable code stress.

Consideration of the equilibrium forces in the axial direction gives the longitudinal stress as

$$\sigma_\ell = \frac{p_i d_i}{4t}$$

or

$$\sigma_\ell = \frac{p_i r_i}{2t} \tag{39.16}$$

Equations (39.12) and Eqs. (39.16) reveal that the efficiency of the circumferential joint needs only be one-half that of the longitudinal joint. The preceding relations are good for elastic deformation only. The consequent changes in length, diameter, and intervolume of the cylindrical vessel subjected to inside fluid pressure can be determined easily.

The change in length is determined from the longitudinal strain ε_ℓ given by

$$\varepsilon_\ell = \frac{1}{E}(\sigma_\ell - \nu\sigma_h) \tag{39.17}$$

where E = modulus of elasticity, and ν = Poisson's ratio. The change in length ΔL is then given by

$$\Delta L = \frac{L}{E}(\sigma_\ell - \nu\sigma_h)$$

or

$$\Delta L = \frac{p_i d_i}{4Et}(1 - 2\nu)L \tag{39.18}$$

Radial growth or dilatation under internal pressure is an important criterion in pipe and vessel analysis. For a long cylindrical vessel, the change in diameter is determined from consideration of the change in the circumference due to hoop stress. The change in circumference is obtained by multiplying hoop strain ε_h by the original circumference. The changed, or new, circumference is found to be equal $(\pi d_i + \pi d_i \varepsilon_h)$. This is the circumference of the circle of diameter $d_i(1 + \varepsilon_h)$. It can be shown easily that the diametral strain equals the hoop or circumferential strain. The change in diameter Δd_i is given by

$$\Delta d_i = \frac{d_i}{E}(\sigma_h - \nu\sigma_\ell)$$

or

$$\Delta d_i = \frac{p_i d_i^2}{4Et}(2 - \nu) \tag{39.19}$$

The change in the internal volume ΔV of the cylindrical vessel is obtained by multiplying the volume strain by the original volume of the vessel and is given by

$$\Delta V = \frac{p_i d_i}{4Et}(5 - 4\nu)V_o \tag{39.20}$$

where ΔV = change in volume, and V_o = original volume.

39.4.4 Thin Spherical Shell under Internal Pressure

A sphere is a symmetrical body. The internal pressure in a thin spherical shell will set up two mutually perpendicular hoop stresses of equal magnitude and a radial stress. When the thickness-to-diameter ratio is less than 1:20, membrane theory permits us to ignore the radial stress component. The stress system then reduces to one of equal biaxial hoop or circumferential stresses.

Considering the equilibrium of the half sphere, it can be seen that the force on the half sphere (Fig. 39.3) due to internal pressure p_i is

$$F = \frac{\pi}{4} d_i^2 p_i \tag{39.21}$$

The resisting force due to hoop stress is given by

$$F_h = \pi d_i t \sigma_h \tag{39.22}$$

For equilibrium, the resistive force must be equal to the force due to pressure. Therefore,

$$\frac{\pi}{4} d_i^2 p_i = \pi d_i t \sigma_h$$

$$\sigma_h = \frac{p_i d_i}{4t} \quad \text{or} \quad \sigma_h = \frac{p_i r_i}{2t} \tag{39.23}$$

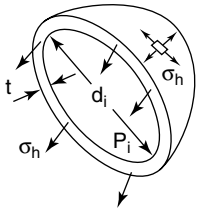

FIGURE 39.3 Spherical shell under internal pressure.

Equation (39.23) gives the relevant maximum stress in a spherical shell. The expression for hoop stress for a thin cylindrical shell and that for a thin spherical shell are similar. This simple deduction is of great importance in the design of pressure vessels because the thickness requirement for a spherical vessel of the same material strength and thickness-to-diameter ratio is only one-half that required for a cylindrical shell.

The change in internal volume ΔV of a spherical shell can be evaluated easily from consideration of volumetric strain and the original volume. Volumetric strain is equal to the sum of three equal and mutually perpendicular strains. The change in internal volume due to internal pressure is given by

$$\Delta V = \frac{3 p_i d_i}{4Et} (1 - \nu) V_o \tag{39.24}$$

39.4.5 Vessels Subjected to Fluid Pressure

During the process of pressurization of a vessel, the fluid used as the medium changes in volume as the pressure is increased, and this must be taken into account when determining the amount of fluid which must be pumped into a cylinder in order to increase the pressure level in the vessel by a specified amount. The cylinder is considered initially full of fluid at atmospheric pressure. The necessary change in volume of the pressurizing fluid is given by

$$\Delta V_f = \frac{p V_o}{K} \tag{39.25}$$

where K = bulk modulus of fluid
p = pressure
V_o = original volume

The additional amount of fluid necessary to raise the pressure must take up the change in volume given by Eq. (39.25) together with the increase in internal volume of the cylinder. The amount of additional fluid V_a required to raise the cylinder pressure by p is given by

$$V_a = \frac{p d_i}{4Et} [5 - 4\nu] V + \frac{pV}{K} \tag{39.26}$$

It can be shown by similar analysis that the additional volume of fluid V_a required to pressurize a spherical vessel is given by

$$V_a = \frac{3pd_i}{4Et}(1-\nu)V + \frac{pV}{K} \tag{39.27}$$

39.4.6 Cylindrical Vessel with Hemispherical Ends

One of the most commonly used configurations of pressure vessels is a cylindrical vessel with hemispherical ends, as shown in Fig. 39.4. The wall thickness of the cylindrical and hemispherical parts may be different. This is often necessary because the hoop stress in the cylinder is twice that in a sphere of the same inside diameter and wall thickness. The internal diameters of both parts are generally considered equal. In order that there should be no distortion or mismatch of hoop stress at the junction, the hoop stresses for the cylindrical part and the hemispherical part must be equal at the end junctions. Therefore,

$$\frac{pd_i}{4Et_c}[2-\nu] = \frac{pd_i}{4Et_s}[1-\nu] \tag{39.28}$$

where t_c = thickness of the cylinder, and t_s = thickness of the hemisphere. Simplification of Eq. (39.28) gives

$$\frac{t_s}{t_c} = \frac{(1-\nu)}{(2-\nu)} \tag{39.29}$$

39.4.7 Effects of Joints and End Plates in Vessel Fabrication

The preceding sections have assumed homogeneous materials and uniform material properties of the components. The effects of the end plates and joints will be the reduction of strength of the components due to characteristic fabrication techniques, such as riveted joints, welding, etc. To some extent, this reduction is taken into account by using a parameter, joint efficiency, in the equation of the stresses. For a thin cylindrical vessel as depicted in Fig. 39.5 the actual hoop and longitudinal stresses are given by the following equations:

$$\sigma_h = \frac{pd_i}{2t\eta_l} \tag{39.30}$$

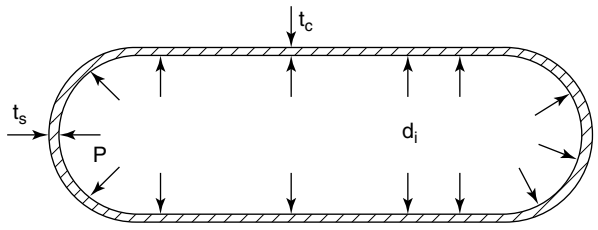

FIGURE 39.4 Thin cylindrical shell with hemispherical ends.

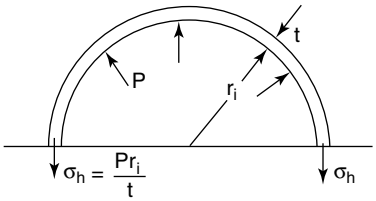

FIGURE 39.5 Thin cylindrical shell subjected to internal pressure.

$$\sigma_l = \frac{pd_t}{4t\eta_c} \tag{39.31}$$

where η_l = efficiency of longitudinal joint, and η_c = efficiency of the circumferential joints. Similarly, for a thin sphere, hoop stress is given by

$$\sigma_h = \frac{pd_l}{4t\eta} \tag{39.32}$$

where η = the joint efficiency.

39.5 THICK CYLINDRICAL SHELLS

The theoretical treatment of thin cylindrical shells assumes that hoop stress is constant across the thickness of the shell wall and also that there is no pressure gradient across the wall. The Lamé theory for determination of the stresses in the walls of thick cylindrical shells considers a mutually perpendicular, triaxial, principal-stress system consisting of the radial, hoop or tangential, and longitudinal stresses acting at any element in the wall. For the case of the shell depicted in Fig. 39.6, subjected to internal pressure only, radial stress σ_r, and hoop stress σ_h are given by

$$\sigma_r = \frac{pr_i^2}{(r_0^2 - r_i^2)}\left(\frac{r^2 - r_0^2}{r^2}\right) \tag{39.33}$$

and

$$\sigma_h = \frac{pr_i^2}{(r_0^2 - r_i^2)}\left(\frac{r^2 + r_0^2}{r^2}\right) \tag{39.34}$$

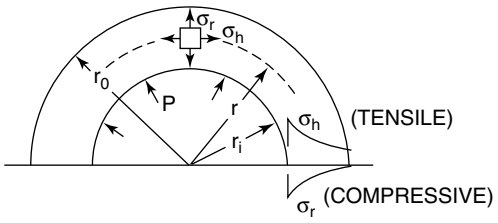

FIGURE 39.6 Thick cylindrical shell subjected to internal pressure.

where r_l and r_o = inside and outside radii of the shell, respectively, and r = any radius such that $r_l < r < r_o$.

In order to get an expression for the longitudinal stress σ_l, the shell is considered closed at both ends, as shown in Fig. 39.7. Simple consideration of the force equilibrium in the longitudinal direction yields

$$\sigma_l = \frac{pr_i^2}{r_0^2 - r_i^2} \tag{39.35}$$

The changes in the dimensions of the cylindrical shell can be determined by the folloing strain formulas:
Hoop strain:

$$E_h = \frac{1}{E}[\sigma_h - \nu\sigma_r - \nu\sigma_l] \tag{39.36}$$

Longitudinal strain:

$$E_l = \frac{1}{E}[\sigma_l - \nu\sigma_r - \nu\sigma_h] \tag{39.37}$$

It can be shown easily that diametral stress and the circumferential or hoop stress are equal. It is seen that the inside diameter-to-thickness ratio d_i/t is an important parameter in the stress formulas. For d_i/t values greater than 15, the error involved in using the thin-shell theory is within 5 percent. If, however, the mean diameter d_m is used for calculation of the thin-shell values instead of the inside diameter, the error reduces from 5 percent to approximately 0.25 percent at $d_m/t = 15.0$.

When the cylindrical shell is subjected to both the external pressure p_o and the internal pressure p_i, the radial and hoop stresses can be expressed by

$$\sigma_r = \frac{r_i^2 p_i - r_o^2 p_o}{r_o^2 - r_i^2} - \frac{(p_i - p_o) r_i^2 r_o^2}{r^2(r_o^2 - r_i^2)} \tag{39.38}$$

and

$$\sigma_h = \frac{r_i^2 p_i - r_o^2 p_o}{r_o^2 - r_i^2} + \frac{(p_i - p_o) r_i^2 r_o^2}{r^2(r_o^2 - r_i^2)} \tag{39.39}$$

It is observed from the preceding equations that the maximum value of σ_h occurs at the inner surface. The maximum radial stress σ_r is equal to the larger of the two pressures p_i and p_o. These equations are known as the *Lamé solution.* The sum of the two stresses remains constant, which indicates that the deformation of all elements in the

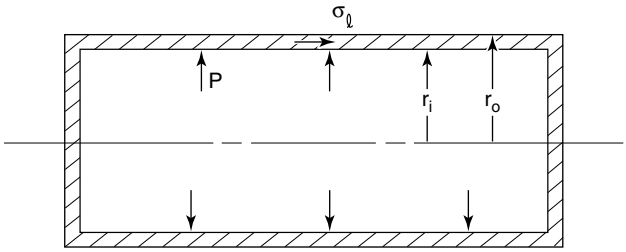

FIGURE 39.7 Thick cylindrical shell closed at both ends and subjected to internal pressure.

axial direction is the same, and the cross sections of the cylinder remain plane after deformation.

The maximum shearing stress at any point in the wall of a cylinder is equal to one-half the algebraic difference between the maximum and minimum principal stresses at that point. The axial or longitudinal stress is usually small compared with the radial and tangential stresses. The shear stress τ at any radial location in the wall is given by

$$\tau = \frac{\sigma_h - \sigma_r}{2}$$

or

$$\tau = \frac{(p_i - p_o) r_i^2 r_o^2}{(r_o^2 - r_i^2) r^2} \tag{39.40}$$

39.5.1 Compound Cylinders

Equation (39.34) indicates that there is a large variation in hoop stress across the wall of a cylindrical shell subjected to internal pressure p_i. In order to obtain a more uniform hoop-stress distribution, cylindrical shells are often fabricated by shrinking one onto the outside of another. When the outer cylinder contracts on cooling, the inner tube is brought into a state of compression. The outer cylinder will be in tension. If the compound cylinder is subjected to an internal pressure, the resultant hoop stresses will be the algebraic sum of those resulting from the internal pressure and those resulting from the shrinkage. The net result is a small total variation in hoop stress across the wall thickness. A similar effect is realized when a cylinder is wound with wire or steel tape under tension. Comings [39.4] gives a complete analysis for such systems. In order to obtain a favorable stress pattern, an analogous technique can be used by applying a sufficiently high internal pressure to produce plastic deformation in the inner part of the cylinder. On removal of this internal pressure, the residual stress persists, with the net effect of compression in the inner part and tension in the outer part of the cylinder. This process is called *autofrettage.* Harvey [39.5] discusses stress analysis for autofrettage in detail.

39.6 THERMAL STRESSES IN CYLINDRICAL SHELLS

Thermal stresses in the structure are caused by the temperature gradient in the wall and accompanying dimensional changes. In order to develop the thermal stresses, the structural member must be restrained in some way. The constraints in the thermal-stress problems in the design of vessels are usually divided into external and internal constraints. Whenever there is a significant temperature gradient across the vessel wall, thermal expansion takes place. Generally, the effects of the externally applied loads and the effects of thermal expansion or contraction are independently analyzed, and the final effects of the total combined stresses are considered additive when comparisons are made with maximum allowable stresses. It is usually assumed that thermal stresses are within the elastic range on the stress-strain curve of the vessel material. If the temperature is very high, the creep may become significant and must be considered. The induced thermal stresses often exceed the yield strength of the vessel material. Since thermal stresses are self-limiting, local plastic relaxation will tend to reduce the acting load.

The basic equations for thermal stresses can be developed by considering that a body is composed of unit cubes of uniform average temperature T. If the temperature of the unit cube is changed to T_1 such that $T_1 > T$ and is restricted, then there are three distinct cases according to the nature of restriction. If a cartesian coordinate system x, y, z is considered, then restrictions can be imagined in (1) the x direction, (2) in the x and y directions, and (3) in all three directions, i.e., in the $x, y,$ and z directions. The corresponding thermal stresses are given by the following expressions:

$$\sigma_x = -\alpha E(T_1 - T) \tag{39.41}$$

$$\sigma_x = \sigma_y = \frac{-\alpha E}{(1 - \nu)} (T_1 - T) \tag{39.42}$$

$$\sigma_x = \sigma_y = \sigma_z = \frac{-\alpha E}{(1 - \nu)} (T_1 - T) \tag{39.43}$$

where α = coefficient of thermal expansion
ν = Poisson's ratio
E = modulus of elasticity

The equations are basic for direct thermal stresses under external or internal constraints and give the maximum thermal stress for the specific constraint.

The internal constraint is due to nonuniform temperature distribution in the body of the structure such that it does not allow free expansion of the individual body elements according to the local temperatures. In such a case, stresses are induced in the body in the absence of any external constraints. A thick cylindrical shell may be assumed to consist of thin, mutually connected, concentric cylindrical shells. Whenever a temperature gradient exists in the vessel wall due to heat transfer, the cylindrical elements will be at different average temperatures and will expand at different rates. The individual cylindrical elements will be constrained by each other, and consequently, thermal stresses will be induced in the otherwise nonrestrained cylinder wall. Detailed treatments of the general analytical methods for solving thermal stresses caused by internal constraints are given by Gatewood [39.6], Bergen [39.7], and Goodier [39.8].

Most cylindrical shell and pressure-vessel problems can be reduced to two-dimensional stress problems. Generally, analytical solutions are possible for relatively simpler cases.

39.6.1 Thermal Stresses in Thin Cylindrical Vessels

Consider a hollow, thin cylindrical vessel (Fig. 39.8) subjected to a linear radial temperature gradient. The temperature at the inner wall is T_1 and is greater than temperature T_2 at the outer wall. If the vessel is long and restrained at the ends, then the longitudinal stress σ_z is given by

$$\sigma_z = \frac{E\alpha(T_1 - T_2)}{2(1 - \nu)} \tag{39.44}$$

where α = coefficient of thermal expansion, and ν = Poisson's ratio.

Estimation of thermal stresses in composite cylinders is quite involved. Faupel and Fisher [39.10] consider the thermal stresses in a multishell laminate of different materials with thermal gradients through each shell.

39.6.2 Thermal Stresses in Thick Cylindrical Vessels

When a thick-walled cylindrical vessel is subjected to a thermal gradient, nonuniform deformations are induced, and consequently, thermal stresses are developed. Fluids under high pressure and temperature are generally transported through structures such as boilers, piping, heat exchangers, and other pressure vessels. Owing to the presence of a large temperature gradient between the inner and outer walls, thermal stresses are produced in these structures. Radial, hoop, and longitudinal stresses in thick, hollow cylinders with a thermal gradient across the wall may be estimated analytically, but generally the computations are lengthy, tedious, and time-consuming. Bhaduri [39.9] developed a set of dimensionless graphs from computer solutions, and they can be used to find the thermal-stress components with a few simple calculations.

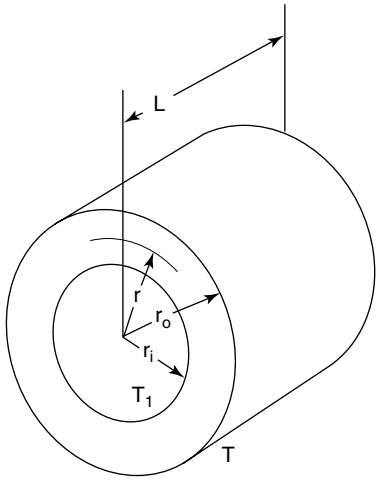

FIGURE 39.8 Hollow cylinder subjected to a temperature gradient.

In this technique, the temperature of the shell's inner surface at radius r_i and outer surface at radius r_o are considered to be T_i and T_o, respectively. The ends of the cylindrical shell are considered unrestrained. The longitudinal strain developed as a result of the thermal stresses is assumed to be uniform and constant. The temperature distribution in the shell wall is given by

$$T = T_i \left(\frac{\ln r_o/r}{\ln r_o/r_i} \right)$$

when the outer surface temperature $T_o = 0$, that is, when the temperature differences are measured relative to the outer surface temperature. The dimensionless hoop-stress function F_h, radial stress function F_r, and longitudinal stress function F_z are obtained analytically for cylindrical shells of various thickness ratios. The stress functions are given by the following equations:

$$F_h = \frac{2(1-\nu)\sigma_h}{\alpha E T_i} = \frac{1}{\ln R_o} \left[1 - \ln \frac{R_o}{R} - \frac{(R_o/R)^2 + 1}{R_o^2 - 1} \ln R_o \right]$$

$$F_r = \frac{2(1-\nu)\sigma_r}{\alpha E T_i} = \frac{1}{\ln R_o} \left[\ln \frac{R}{R_o} + \frac{(R_o/R)^2 - 1}{R_o^2 - 1} \ln R_o \right] \tag{39.45}$$

$$F_z = \frac{2(1-\nu)\sigma_z}{\alpha E T_i} = \frac{1}{\ln R_o} \left(1 - 2 \ln \frac{R_o}{R} - \frac{2}{R_o^2 - 1} \ln R_o \right)$$

where σ_h = hoop stress
σ_r = radial stress
σ_z = longitudinal stress
ν = Poisson's ratio

α = coefficient of thermal expansion
E = Young's modulus
R = r/r_i
R_o = r_o/r_i

The stress functions are shown graphically for the radii ratios $r_o/r_i = 2.0$, 2.5, and 3.00, respectively, in Fig. 39.9. These curves are general enough to compute the hoop, radial, and shear stresses produced by temperature gradients encountered in most cylindrical-shell designs.

The procedure is simple. The value of R_o must be known to select the appropriate curve. For a particular value of R, the corresponding values of the stress functions can be read from the ordinate. The stresses at any radial location of the shell wall can be easily calculated from the known values of the stress function, property values of the shell material, and temperature of the inside surface of the shell.

39.7 FABRICATION METHODS AND MATERIALS

Welding is the most common method of fabrication of pressure-vessel shells. Structural parts such as stiffening rings, lifting lugs, support clips for piping, internal trays, and other parts are also attached to the vessel wall by welding. Welded joints are used for pipe-to-vessel connections to ensure optimum leak-proof design, particularly when the vessel contains hazardous fluid at a very high temperature. A structure whose parts are joined by welding is called a *weldment.* The most widely used industrial welding method is arc welding. It is any of several fusion welding processes wherein the heat of fusion is generated by electric arc. Residual stresses in a weld and in the adjoining areas cannot be avoided. They are quite complex. If the weld residual stress is superposed on the stress due to external loads and the resultant stress exceeds the yield point of the material, local plastic yielding will result in redistribution of the stress in ductile materials. A good weld requires a highly ductile material. In order to prevent loss of ductility in the welded region, low-carbon steels with less than 0.35 percent carbon content are used as construction materials. Carbon itself is a steel hardener. However, in the presence of a manganese content of 0.30 to 0.80 percent, carbon does not cause difficulties when present in steel up to 0.30 percent. Welding is a highly specialized manufacturing process. In pressure-vessel fabrication, the designer has to follow the code developed by the American Society of Mechanical Engineers. Chuse [39.3] provides simplified guidelines for designing welding joints for pressure vessels. For design purposes, welding is classified into three basic types: groove, fillet, and plug welds. Welding joints are described by the position of the pieces to be joined and are divided into five basic types: butt, tee, lap, corner, and edge. Bednar [39.2] describes various types of welds and outlines methods for stress calculation.

39.7.1 Construction Materials

A designer of a cylindrical pressure vessel should be familiar with commonly used construction materials to be able to specify them correctly in the design and in material specification. The selection of materials for code pressure vessels has to be made from the code-approved material specifications.

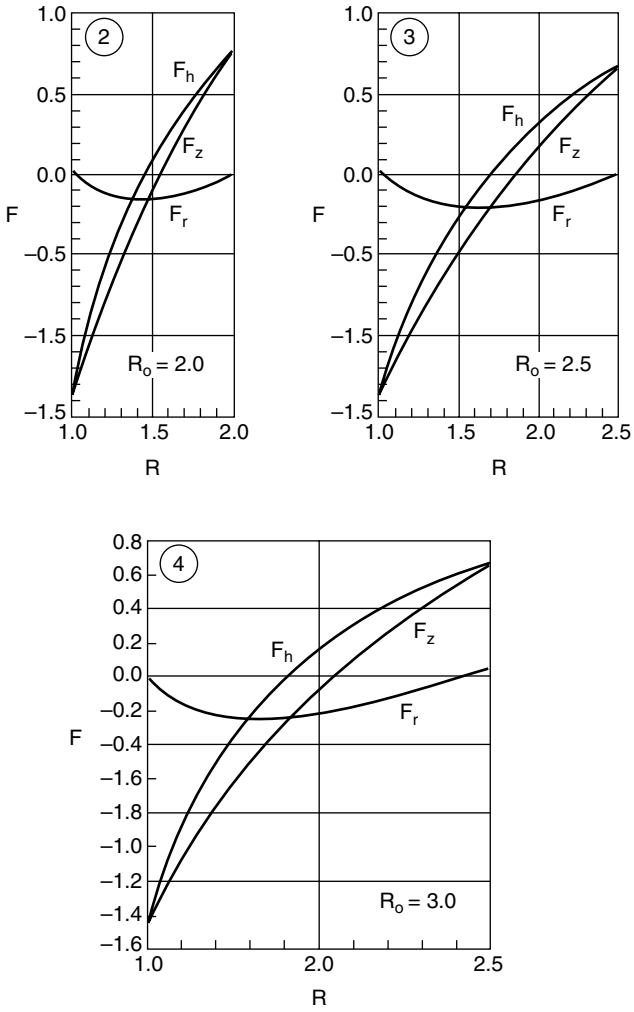

FIGURE 39.9 Thermal stress functions for thick cylindrical shell. *(From Ref. [39.9].)*

39.8 DESIGN OF PRESSURE CYLINDERS

Cylindrical shells are commonly used in industrial applications for their adequate structural strength, ease of fabrication, and economical consumption of material. The vessels, depending on their function, can be vertical or horizontal. A vertical orientation is often preferred for thin-walled vessels operating under low internal pressure because of the additional bending stresses resulting from the weights of the vessel itself and the fluid in the vessel.

Cylindrical shells of such elastic materials as steels, nonferrous metals, and most alloys that operate under internal pressures up to 10 MPa are fabricated mostly of rolled and subsequently welded sheets. The joint connections of cylindrical shells made of copper or brass sheets are made by soldering with suitable solders. Cylindrical vessels of steel operating under pressures greater than 10 MPa are commonly fabricated of forged pieces that are heat-treated. Cylindrical shells of brittle materials for vessels operating under low internal pressures (approximately up to 0.8 MPa) are molded. Cast shells are usually fabricated with a bottom. In some cases, cast shells are made of elastic metals and their alloys.

The fabrication of the cylindrical vessels by the rolling of sheets is a very common method of manufacturing low- and medium-pressure (1.75 to 10.0 MPa) vessels.

Azbel and Cheremisinoff [39.1] give the following general guidelines for designing welded and soldered cylindrical shells:

1. The length of the seams should be minimized.
2. The minimum number of longitudinal seams should be provided.
3. Longitudinal and circumferential seams must be butt welded.
4. All joints should be accessible for inspection and repair.
5. It is not permissible to provide holes, access holes, or any opening on the seams, especially on longitudinal seams.

Shell thicknesses of vessels operating under very low pressures are not designed; they are selected on the basis of manufacturing considerations. Durability is estimated from the available information regarding corrosion resistance of the material. The minimum thicknesses of a shell rolled from sheet metals are given as follows: carbon and low-alloy steel, 4 mm; austenite steel, 3.0 to 4.0 mm; copper, 2.5 to 3.0 mm; and cast materials, 2.0 to 2.5 mm.

39.8.1 Design of Welded Cylindrical Shells

The structural design of cylindrical shells is based on membrane theory. In order to express the design relations in convenient form, it is necessary to (1) select the strength theory best reflecting the material behavior, (2) consider the weakening of the construction induced by welding and other connections, (3) consider wall thinning as a result of corrosion effects, and (4) establish a factor of safety and allowable stresses.

The distortion-energy theory (see Chap. 28) gives the basic design stress as

$$\sigma_d = [\sigma_t^2 + \sigma_\ell^2 + \sigma_r^2 - 2(\sigma_t\sigma_\ell + \sigma_t\sigma_r + \sigma_\ell\sigma_r)]^{1/2} \tag{39.46}$$

where σ_t, σ_ℓ, and σ_r = principal circumferential, longitudinal, and radial stresses, respectively. For a thin-walled cylindrical shell operating under an internal pressure p_i, the radial stress is assumed to be equal to zero, and the longitudinal stress induced in the shell is given by

$$\sigma_\ell = \frac{p_i d_i}{4t} \tag{39.16}$$

where d_i = inside diameter, and t = the thickness of the shell. The circumferential stress induced in the shell is given by

$$\sigma_t = \frac{p_i d_i}{2t} \tag{39.12}$$

When the deformation reaches plastic state, a definite amount of deformation energy is assumed (see Ref. [39.1]), and the value of the Poisson's coefficient v is taken as equal to 0.5.

Substituting Eqs. (39.16) and (39.12) into Eq. (39.46) and assuming the value of Poisson's coefficient $v = 0.5$, the design stress can be expressed as

$$\sigma_d = 0.87 \frac{p_i r_o}{t} \tag{39.47}$$

where r_o = external radius of the shell. The external radius $r_o = d_o/2$, where d_o = external diameter of the shell.

It is observed that according to the distortion-energy theory, considering the combined effect of the longitudinal and tangential stresses, the design stress for plastic material is 13.0 percent less compared with the maximum value of the main stress. The allowable stress σ_a is therefore given by

$$\sigma_a = \frac{p_i d_o}{2.3t} \tag{39.48}$$

And the thickness of the shell t is given by

$$t = \frac{p d_o}{2.3\sigma_a} \tag{39.49}$$

Introducing the joint efficiency factor η_j and allowance factor t_c for corrosion, erosion, and negative tolerance of the shell thickness, the following relation for design thickness is obtained:

$$t_d = \frac{p d_o}{2.3\sigma_a \eta_j} + t_c \tag{39.50}$$

Azbel and Cheremisinoff [39.1], on the basis of similar analysis, give the following design formula for the determination of shell thickness:

$$t_d = \frac{p_i d_i}{2.3\eta_j \sigma_a - p_i} + t_c \tag{39.51}$$

where $d_o/d_i \leq 1.5$.

The proper selection of allowable stress to provide safe operation of a vessel is an important design consideration. The allowable stress value is influenced by a number of factors, such as (1) the strength and ductility of the material, (2) variations in load over time, (3) variations in temperature and their influence on ductility and strength of the material, and (4) the effects of local stress concentration, impact loading, fatigue, and corrosion.

In shell design, the criterion of determining the allowable stresses in an environmentally moderate temperature is the *ultimate tensile strength.* The pressure-vessel codes [39.3] use a safety factor of 4 based on the yield strength S_y for determining the allowable stresses for pressure vessels. The safety factor η_y is defined as

$$\eta_y = \frac{S_y}{\sigma_a} \tag{39.52}$$

It is known that for ductile metals, an increase in temperature results in an increase in ductility and a decrease in the yield-strength value. The allowable stress at higher temperatures can be estimated by using the following relation:

$$\sigma_a = \frac{S_y^T}{\eta_y} \tag{39.53}$$

where S_y^T = yield strength of the material at a given operating temperature.

Implied in the preceding analysis is an assumption that no creeping of the shell material is involved. This is generally a valid assumption for ferrous metals under load at temperatures less than 360°C. However, at higher operating temperatures, the material creeps under load, and an increase in stress takes place with time. The resulting stresses do not exceed the yield-strength values. It is to be noted that the yield point at high temperatures cannot generally be used as a criterion for allowance of the stressed state because creep of the material may induce failures as a result of the increased deformation over a long period of time. The basic design criterion for shells operating at moderate temperatures is the stability of size and dimensional integrity of the loaded elements. For a shell operating at higher temperatures, increase in size, which ensures that creep does not exceed a tolerable limit, should be considered. When a loaded material is under creep, there is an associated relaxation of stress. The stress decreases over time as a result of plastic deformation. The creep rate is dependent on temperature and state of stress in the metal. Azbel and Cheremisinoff [39.1] discuss the effects of creep and stress relaxation on loaded shells and give a formula for determining the allowable stresses and safety factors on the basis of fatigue stress.

REFERENCES

39.1 D. S. Azbel and N. P. Cheremisinoff, *Chemical and Process Equipment Design—Vessel Design and Selection,* Ann Arbor Science Publishers, Ann Arbor, Michigan, 1982.

39.2 H. H. Bednar, *Pressure Vessel Design Handbook,* Van Nostrand Reinhold, New York, 1981.

39.3 R. Chuse, *Pressure Vessel—The ASME Code Simplified,* 5th ed., McGraw-Hill, New York, 1977.

39.4 E. W. Comings, *High Pressure Technology,* McGraw-Hill, New York, 1956.

39.5 J. F. Harvey, *Pressure Vessel Design: Nuclear and Chemical Applications,* D. Van Nostrand, Princeton, N.J., 1963.

39.6 B. L. Gatewood, *Thermal Stresses,* McGraw-Hill, New York, 1957.

39.7 D. Bergen, *Elements of Thermal Stress Analysis,* C. P. Press, Jamaica, N.Y., 1971.

39.8 J. N. Goodier, "Thermal Stress in Pressure Vessel and Piping Design, Collected Papers," *ASME,* New York, 1960.

39.9 S. Bhaduri, "Thermal Stresses in Cylindrical Sheels," *Machine Design,* vol. 52, no. 7, April 10, 1980.

39.10 J. H. Faupel and F. E. Fisher, *Engineering Design,* Wiley, New York, 1981.